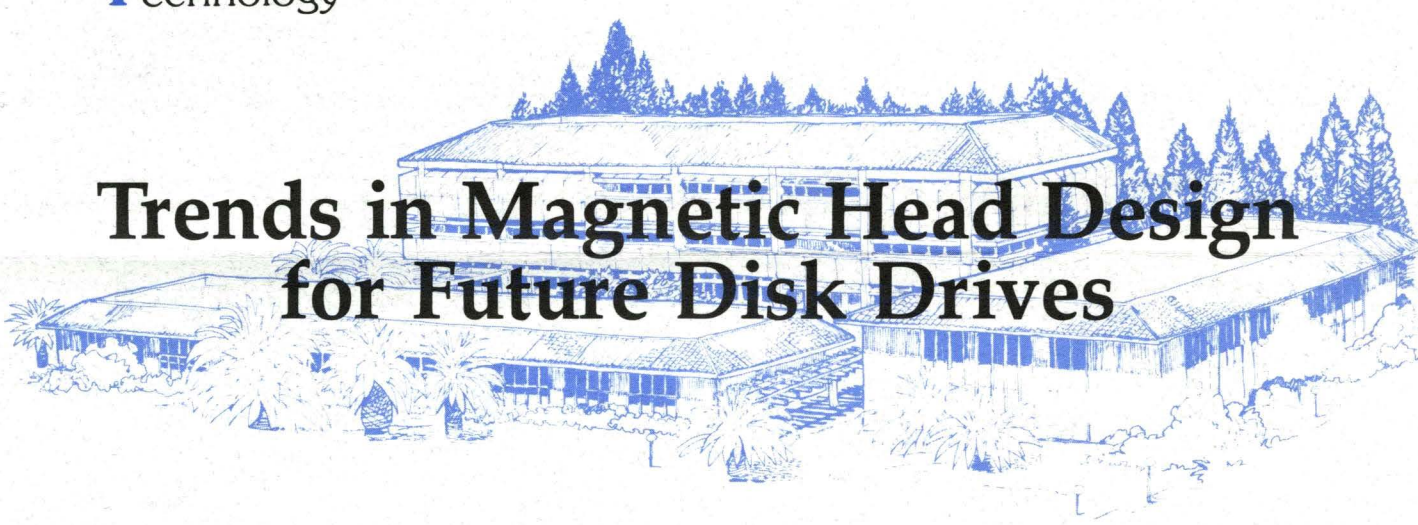


Institute For
Information
Storage
Technology



Trends in Magnetic Head Design for Future Disk Drives

A Short Course

OVERVIEW

This short course is designed to provide an insight and greater understanding of the dramatic progress being made in magnetic head technology, the head/disk interface and the role these play in the accelerating pressure for higher areal density and disk drive miniaturization. The opportunities presented by new advances such as the MR head and in micro-mechanics will be covered as well as the challenges the move to gigabit per square inch densities raise for design, test and manufacturing of disk drives.

AUDIENCE

This course is intended for engineers involved in disk drive design, the design or manufacture of their magnetic head/media components as well as scientists, technical managers, planners and consultants in the magnetic data storage industry.

SANTA CLARA UNIVERSITY

SESSIONS

Overview: Where We Are and Where We Are Going

... Edgar Williams

This session will review progress in magnetic recording heads, disks and channel electronics and will indicate directions for improvements which allow increased areal densities in tomorrow's disk drives. Conventional ferrite, MIG and thin film inductive heads will be compared with newer components such as double MIG, multiple yoke thin film heads, and MR detectors. Improvements in preamplifiers, write drivers, media properties and in head air bearings will also be addressed in this session.

Inductive Thin-Film Heads

... Erich Valstyn

Miniaturization of disk drives and the demand for higher areal density dictate changes in the design of inductive thin-film heads, particularly an increase in the number of turns and in the number of layers of the coil, as well as a reduction in pole-tip width. On the other hand, standard-size drives are moving toward higher data rates. The ramifications and challenges of these design changes will be addressed. Novel designs will be discussed.

Magnetoresistive Heads

... Mason L. Williams

Basic concepts of magnetoresistive head operation, description of published design alternatives, techniques for biasing and stabilizing the magnetoresistive element, and examples of the results of micromagnetic modelling of sensor elements.

Silicon Planar Heads

... J. P. Lazzari

Silicon planar heads based on microelectronic processing were developed five years ago. This lecture is a review of today's status and potentialities. The new 57 turns design will be described and performances in recording will be given (electrical and start stop). MR silicon planar head design will be discussed. As gate arrays in microelectronics, silicon planar heads are personalized just at the end of the process fabrication. The head design has been optimized for full automatic assembly. Finally, we will show how, with silicon planar heads the head industry may move into the IC's maker's world.

High Density Vertical Recording Heads

... Eric Katz

The subject of this talk will be the heads which are used with perpendicular recording media to increase storage densities in disk drives. The relevant background on perpendicular recording will be presented, including a discussion of the important similarities and differences between longitudinal and perpendicular recording.

Scaling Suspension System Designs

... Celia Yeack-Scranton

Disk drives are evolving toward smaller physical devices with closer head to disk spacings and tighter tolerances on those spacings. This represents a challenge to suspension design since the air bearing requirements do not scale with suspension size reduction and there are practical constraints on materials and dimensions. Simple scaling examples will be given with a discussion of the current industry solutions and challenges for the future.

Head Positioning and Tracking for High Track Densities

... John S. Heath

This session sets out to explain why bits are not square! The session reviews the operation of actuators and various servo systems in positioning and tracking. The dependence of track density on errors in head positioning is explained, and how the various sources of position error depend on the servo architecture and mechanical design. Finally, the ways in which these errors have been reduced to enable higher track densities are described, and the factors limiting track density are identified.

Low Flying/Contact Recording

... James U. Lemke

Since the dominant losses in recording and reproducing are exponentially dependent upon the ratio of the spacing and the inverse wave-length, high recording densities of current and projected recorders/drives dictate near-contact between the head and medium. Inevitable asperity contacts generally limit the durability of the interface in current disk applications. Efforts to prevent contact while achieving acceptable small interface spacings will be reviewed with emphasis on new liquid interfaces using non-Newtonian liquids. Other approaches to contact recording will also be discussed.

Magnetic Head Testing

... Ralph Simmons

The advances in recording density and in drive performance must be matched by advances in the characterization of the read/write heads. In this session, a brief overview of the specifications for a typical head tester will be followed by detailed discussions of signal to noise and pulse shape characterizations. Particular attention is paid to measuring the matched filter SNR and to issues involved with high transfer rate applications. The discussions will cover both inductive and magnetoresistive heads.

Signal to Noise and Equalization Issues

... Tom Howell

As recording densities increase, the amount of magnetic material representing each recorded symbol decreases, and the signal to noise ratio decreases. In order to maintain and even improve reliability, system designers must use better coding and signal processing techniques. Write precompensation can counteract nonlinear transition shifts. Adaptive equalization can reduce distortion in readback signals. Maximum likelihood detection and new codes can improve the system's immunity to noise and distortion.

Small Form Factor Drive Design Tradeoffs

... Bob Kobliska

The advanced magnetic recording technologies required for small form factor drives will be reviewed. The design process consists of the optimization of the head and disk characteristics, the tailoring of the flying height profile, and the verification of the tribological performance. The proper selection of read/write detection and error correction chips will be discussed. The design considerations for a 1.8 and 1.3 inch drive will be highlighted.

Case Study: 1.3 inch "Kittyhawk" Drive

... Carol Schwiebert

In June 1992, Hewlett-Packard announced the first 1.3" drive aimed at the mobile computing market. This session will discuss the actual head/media system design tradeoffs that were made to meet the program goals of ruggedness, performance, cost and schedule.

FACULTY

Edgar M. Williams, Read-Rite, is Vice President of Advanced Technology where he is responsible for the design and analysis of new devices and concepts in magnetic recording transducers. Ed has worked 27 years in magnetic recording and in xerographic technologies. He has published numerous technical papers, a book on xerography and co-founded Gemini Magnetics, Inc. in 1983 where he developed thin film magnetic disks for small disk drive applications.

Erich P. Valstyn, Read-Rite, received his Ph.D. in E.E. from the University of Minnesota. He has worked in the field of magnetics and magnetic recording the last 30 years and is now Director of Device Analysis at Read-Rite.

Mason L. Williams, IBM, received his Ph.D. in E.E. from U.S.C. He has been at IBM in San Jose since 1970, where his work on thin film media recording with R.L. Comstock led to the Williams/Comstock recording model in 1971. In 1982 he joined the IBM Magnetic Recording Institute and its current successor, the IBM Advanced Magnetic Recording Laboratory. Presently he is manager of Head Physics in the Research Division, IBM-Almaden and has interests in recording head design and micromagnetics.

J.P. Lazzari, Silmag, is CEO of Silmag and is the inventor of planar silicon heads. He obtained his Ph.D. degree at Grenoble University in 1970 where he was responsible for developing the first thin film heads. From 1971 to 1981, he worked for CII Honeywell Bull where he was Director of the Research Center. He returned to LETI in 1981 to manage the Microelectronic Department. Jean Pierre Lazzari holds more than 100 international patents.

Eric R. Katz, Censtor, received his Ph.D. in Physics from U.C. Berkeley in 1969. Since then he has worked in many areas within magnetic recording, including particulate media development, ferrite and thin film head development and component evaluation and optimization for floppy disk drives. Currently Principal Scientist at Censtor, he is working on advanced perpendicular recording components. He has published a number of papers and holds several patents.

Celia Yeack-Scranton, IBM-Almaden, is a Research Staff Member and has worked in the disk drive business for over 13 years. Her areas of expertise include glide test, ultrasonic transducers and contact recording. Her broader research interests are in overall HSA design, head process technology nonvolatile RAM and micromotors for DASD. She is a senior member of the IEEE and has a Ph.D. in Applied Physics from Stanford.

John S. Heath, IBM, since joining IBM in 1968 has been involved in or has lead the mechanical and servo design and development of disk products from 14 to 2.5 inches. Inventor of the rotary actuator, he holds many patents and is currently in the Adstar Advanced Magnetic Recording Lab. He is a Fellow of the I Mech E and a member of the IBM Academy of Technology.

James U. Lemke, Recording Physics, has been active in magnetic recording R&D most of his professional life. He received a Ph.D. in theoretical physics from U.C. San Diego, and has published numerous papers on the theory and practice of magnetic recording. He holds several patents in this field. He is an IEEE Magnetics Society Distinguished Lecturer for 1991-1992.

Ralph Simmons, Hewlett Packard, is responsible for characterization of advanced head/media systems for Hewlett Packard's Disk Memory Division. Since 1979, he has worked on the design and characterization of magnetoresistive heads, of sputtered thin film media and on error rate budgeting for various head/media systems. He received his Ph.D. in Physics from Washington State University in 1979.

Tom Howell, Quantum, is Director of Advanced Recording Technology. He spent 13 years in the IBM Research Division where he worked on application of coding and signal processing techniques to magnetic recording systems. In 1990, he joined Quantum where he is responsible for the development of advanced technology in the areas of heads, media and channels. He received his Ph.D. from Cornell University.

Bob Kobliska, Aura Associates, received his Ph.D. in Physics from the University of Chicago. He joined the research staff at IBM in 1973 and has managed groups concentrating on magnetic bubbles, lithography, magnetic materials and tribology. From 1985 to 1991 he was V.P. of Engineering and Chief Technical Officer at Akashic Memories. In 1991 he joined Aura Associates as V.P. of Technology to design small form factor disk drives.

Carol Schwiebert, Hewlett Packard, is the research and development head/media manager for 5.25" and small form factor drives at Hewlett-Packard's Disk Memory Division in Boise, Idaho. Carol has a B.S. in Electrical Engineering and Mathematics and an M.S. in Physical Chemistry from Oregon State University.

REGISTRATION FORM

Yes, please enroll me in "Trends in Magnetic Head Design for Future Disk Drives"

Name: _____

Company: _____

Address: _____ (MS) _____

Phone: (_____) _____

Registration Fee: \$835 Please make check out to IIST
Send both completed form and check to:

Phone: (408) 554-6853

IIST
School of Engineering
Santa Clara University
Santa Clara, CA 95053

**"Where We Are
&
Where We Are Going"**

Edgar M. Williams

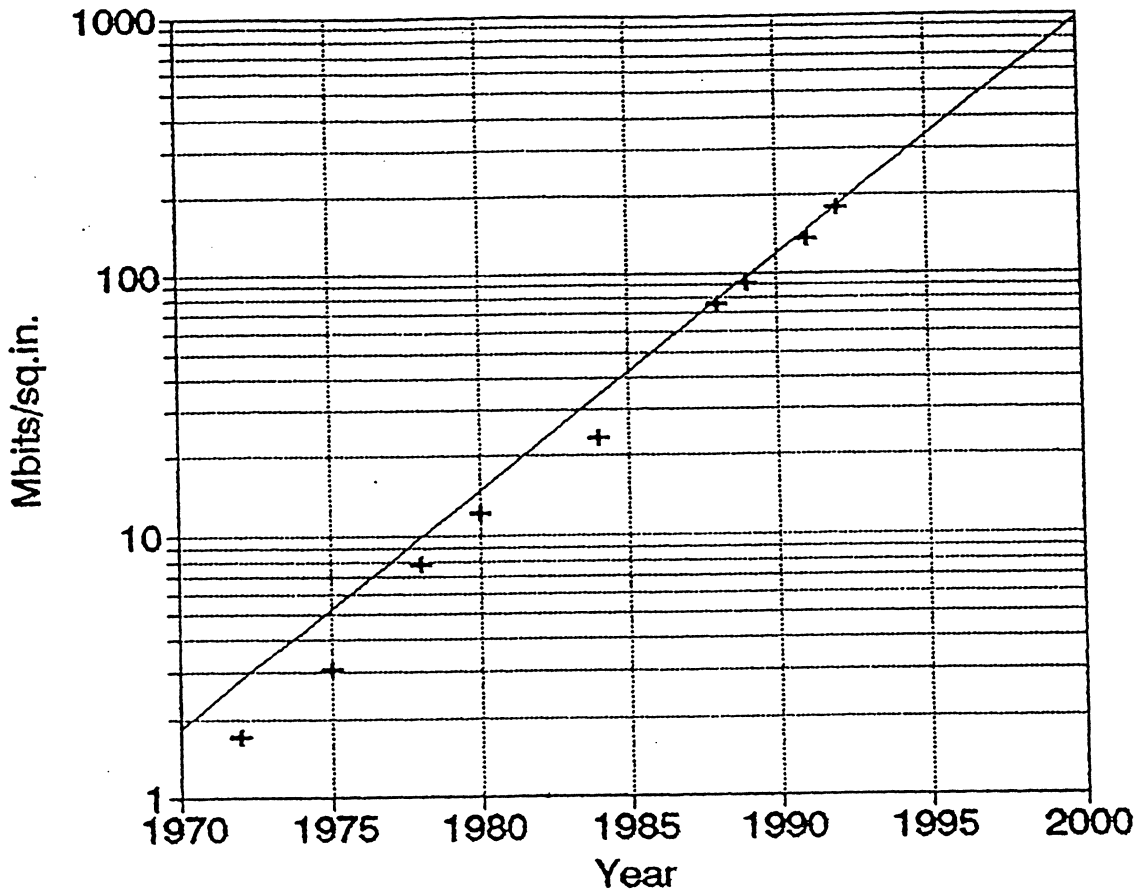
Read-Rite Corp.

Institute for Information **S**torage **T**echnology

Santa Clara University, California

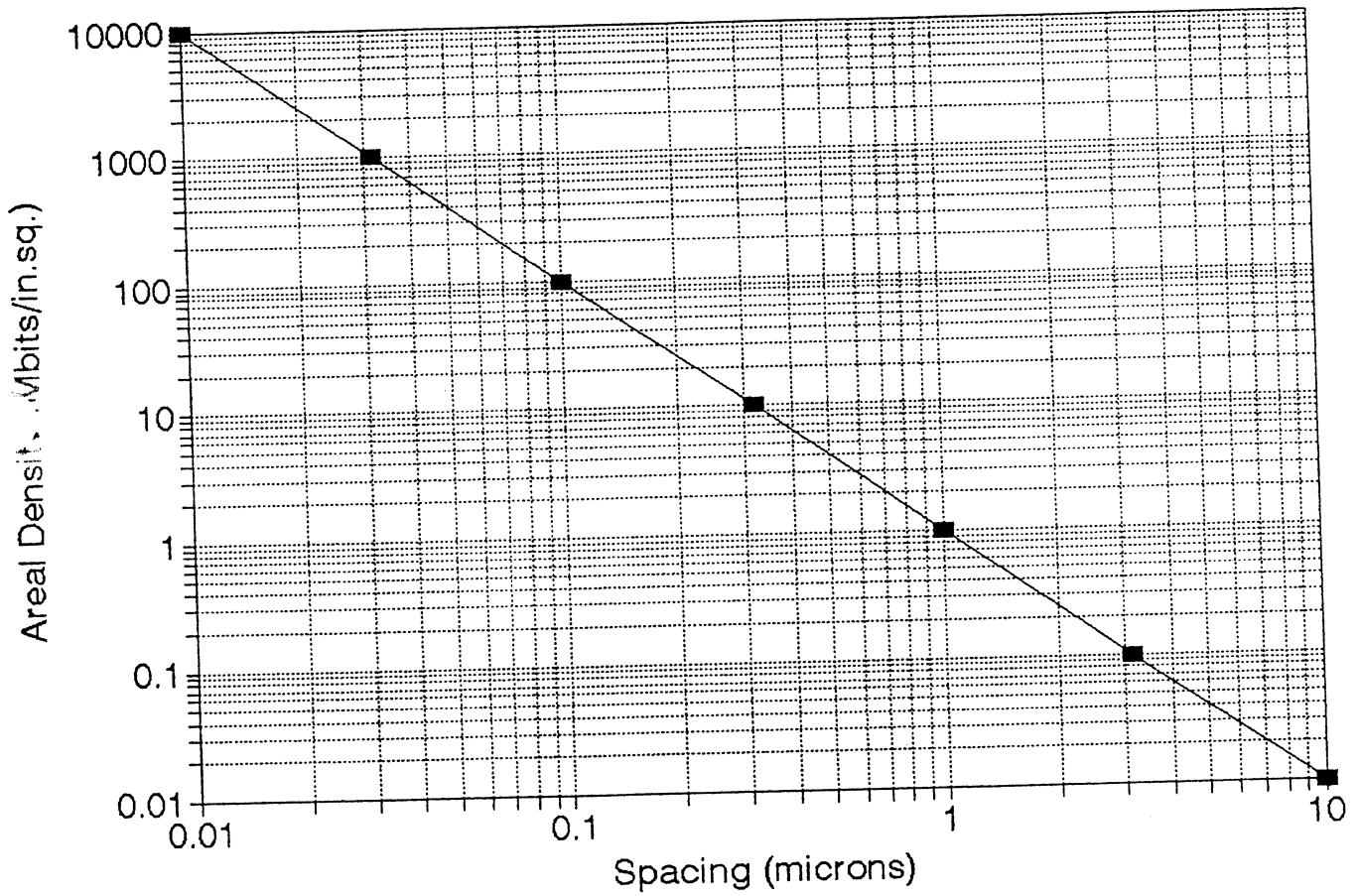
December 14 - 16, 1992

Areal Density (Mb/sq.in.) vs Year

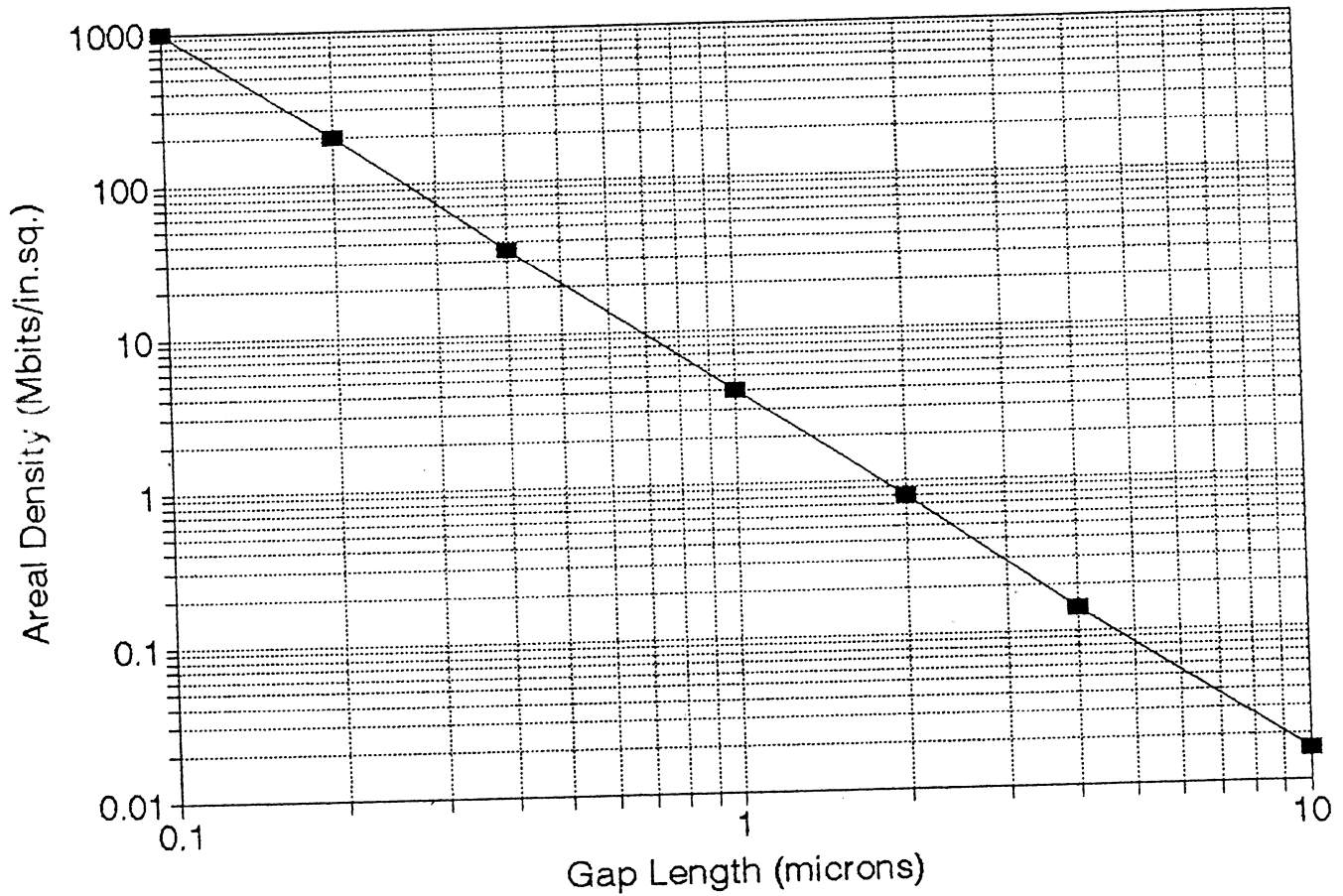


Heads	NiZn Ferrite	NiZn Ferrite	MnZn Ferr. + TFH	MIG + TFH	DMIG & TFH + MR	TFH + MR
Disks	Fe ₂ O ₃ Particles	Fe ₂ O ₃ Particles	CoFe ₂ O ₃ + TF Disks	TF Disks	TF Disks	TF Disks
Electronics	2nV/√Hz LPF + PK.Det	2nV/√Hz LPF + PK.Det	1.5nV/√Hz LPF + PK.Det	1.0nV/√Hz Cosine + Kost + PK. Det.	0.6nV/√Hz PrML Kost + Cosine	0.4V/√Hz PrML Kost + Cosine
Code	2f & MFM	MFM	MFM + RLL + RLL (2,7)	RLL (2,7) + RLL (1,7)	RLL (1,7) RLL (8,9)	RLL (8,9) + ?

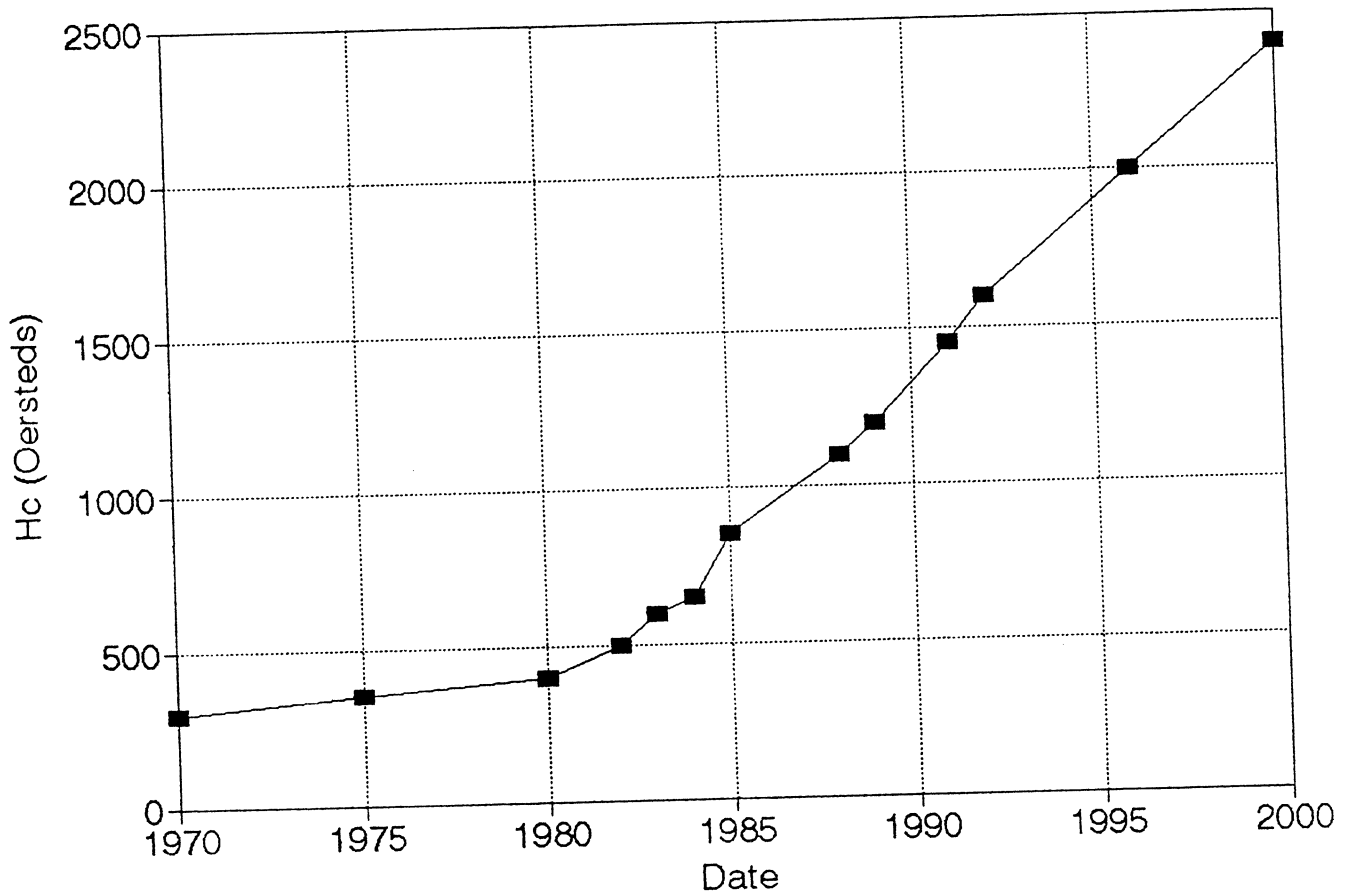
Areal Density vs Head-Medium spacing



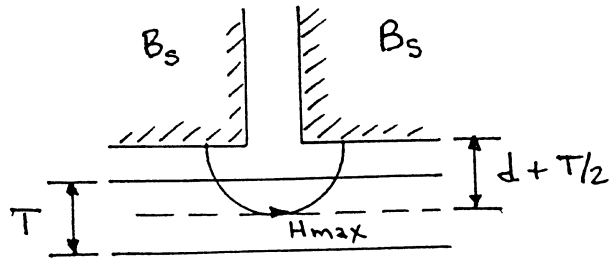
Areal Density vs Head Gap Length



Disk Coercivity vs Date

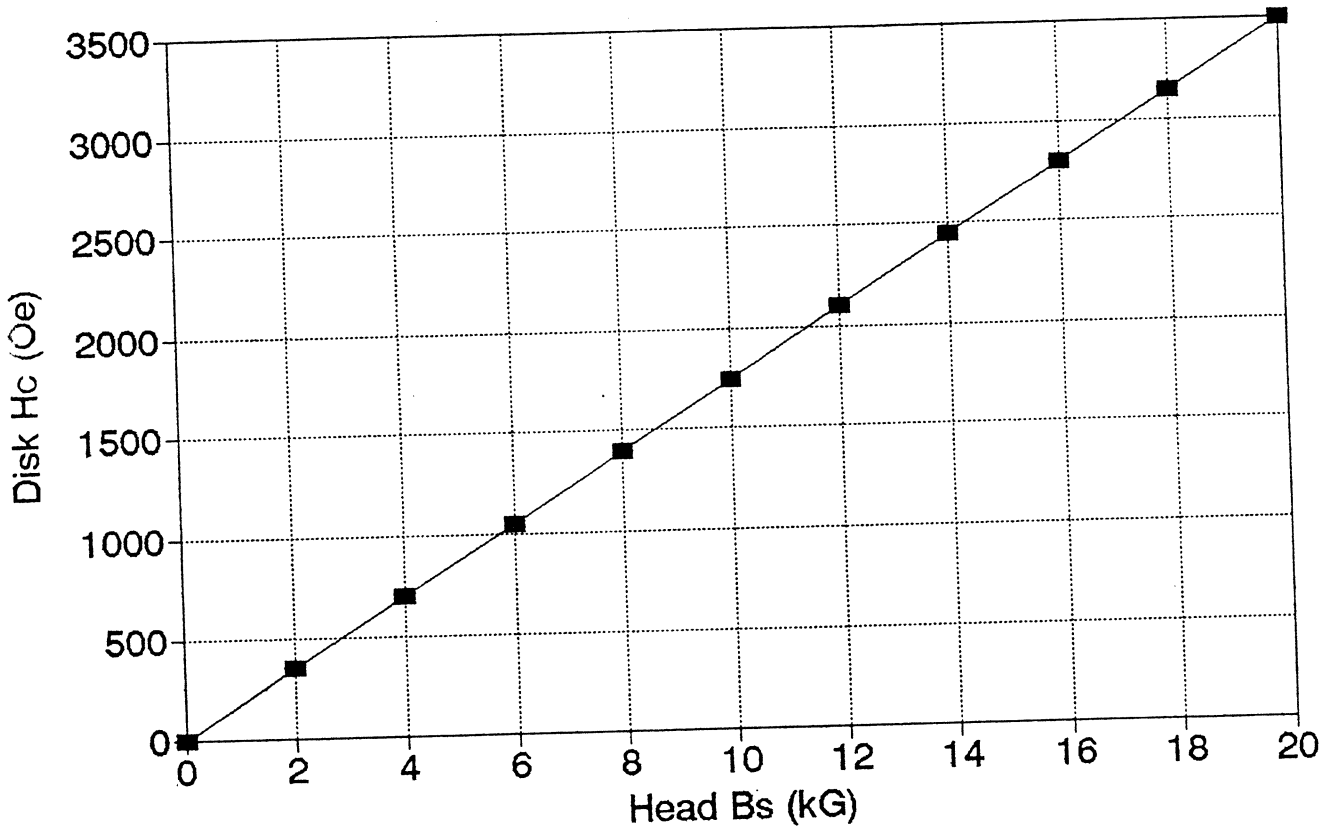


*stretched
near oxide
too long - gives
drop to curve.*



Disk Hc vs Head Bs

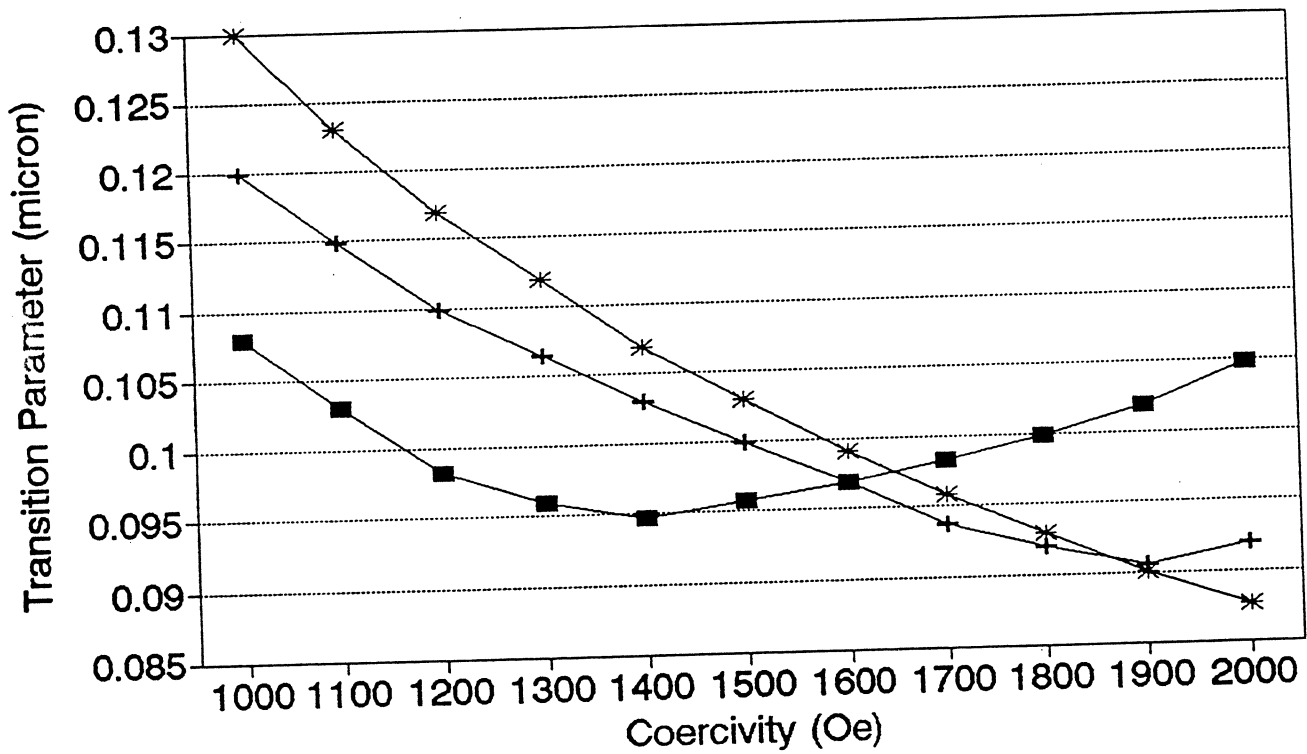
(assumes $H_{max} = 3.0 H_c$)



<i>Hand</i>	Material	B_s (kG)
	NiZn Ferrite	3
<i>high</i>	MnZn Ferrite	4-6
<i>TF</i>	NiFe (82/18)	10
<i>Silicon (super)</i>	FeAlSi	11-13
<i>Super Miller</i>	FeAlN	20

Transition Parameter vs Coercivity

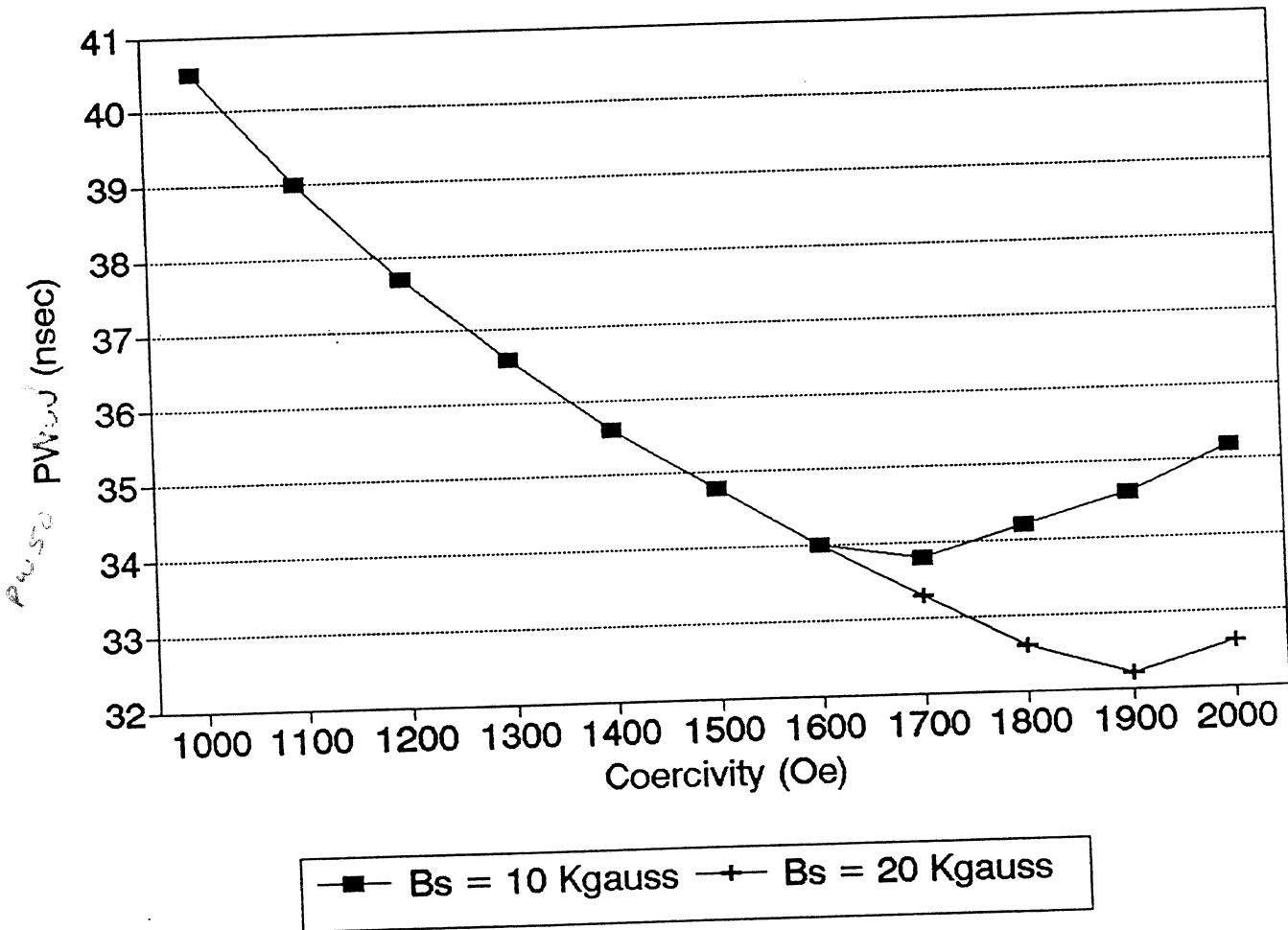
Write Gradient and Medium-limited



Bs = 10 Kgauss
 Bs = 20 Kgauss
 Medium-limited

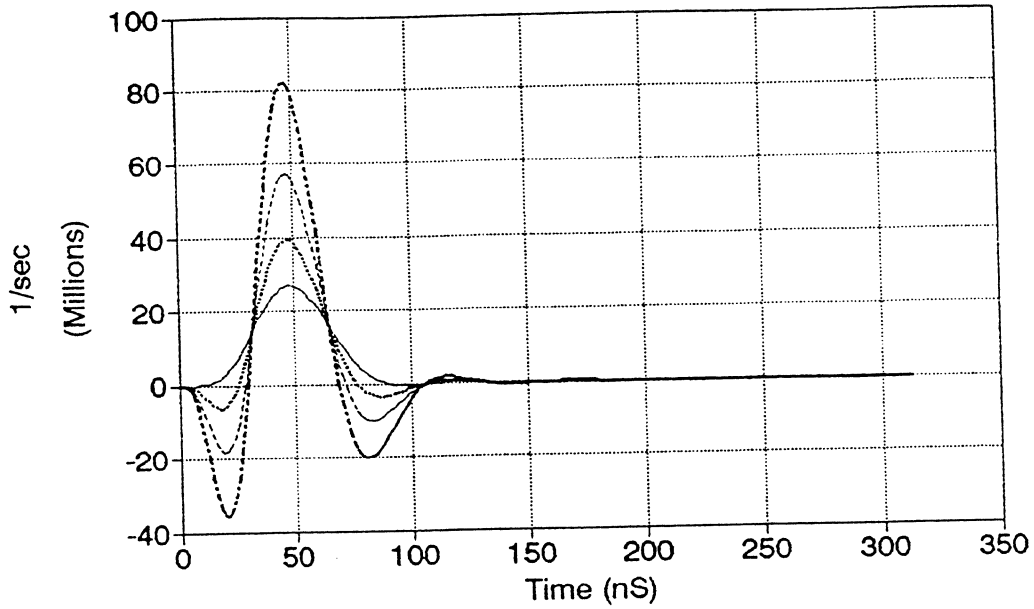
*Head limited
need minimum
transition*

Pulse Width vs Coercivity

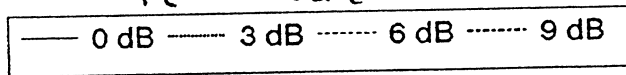


*Velocity
900 em/s
3 1/2 - 3600
ID*

Kost Filter Impulse Response

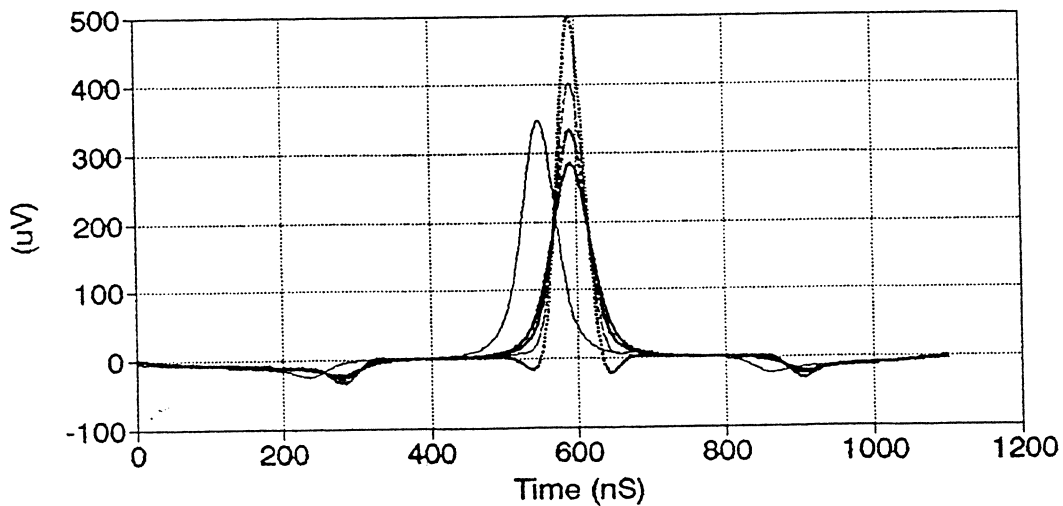


$$f_c = 10 \text{ MHz}$$

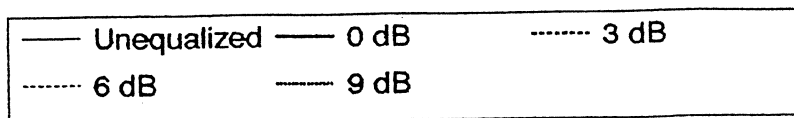


Isolated Pulses vs Time

Unequalized and Equalized

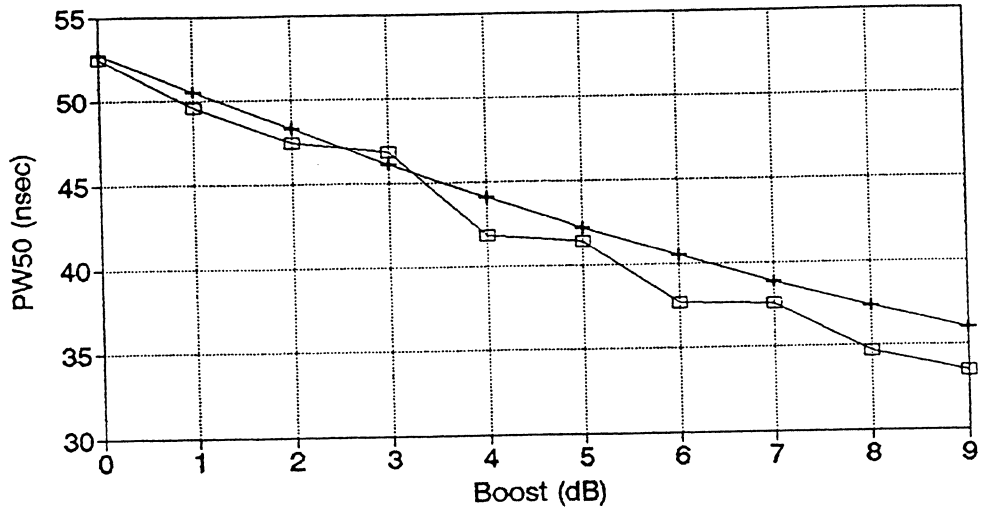


$$11.9 \text{ m/sec} ; f_c = 10 \text{ MHz}$$



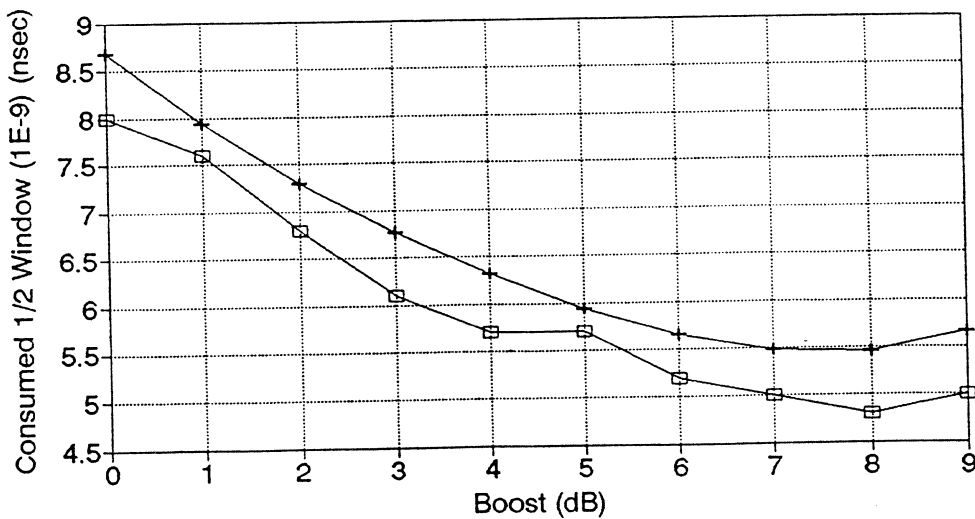
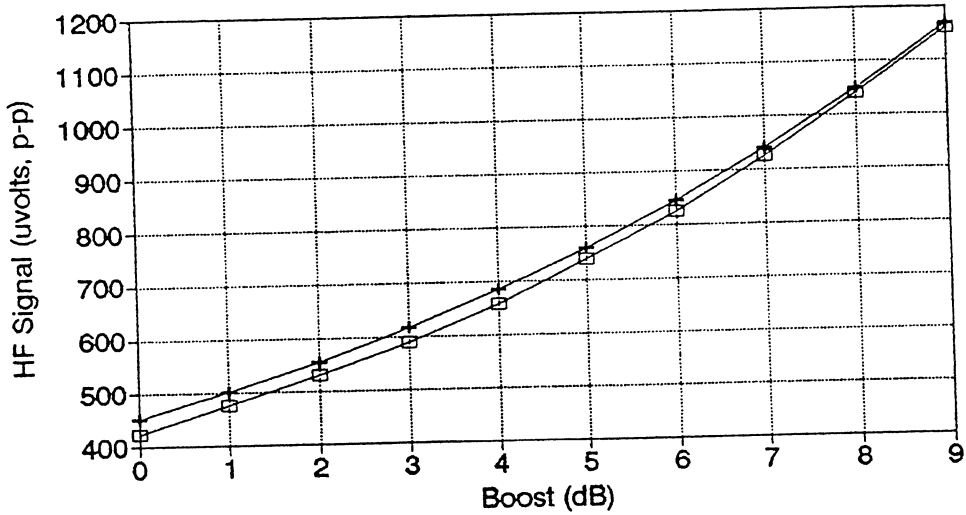
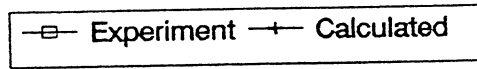
Equalized Signals: R24 Head & SD Disk

SSI 32F8011 with 13.69 MHz cutoff



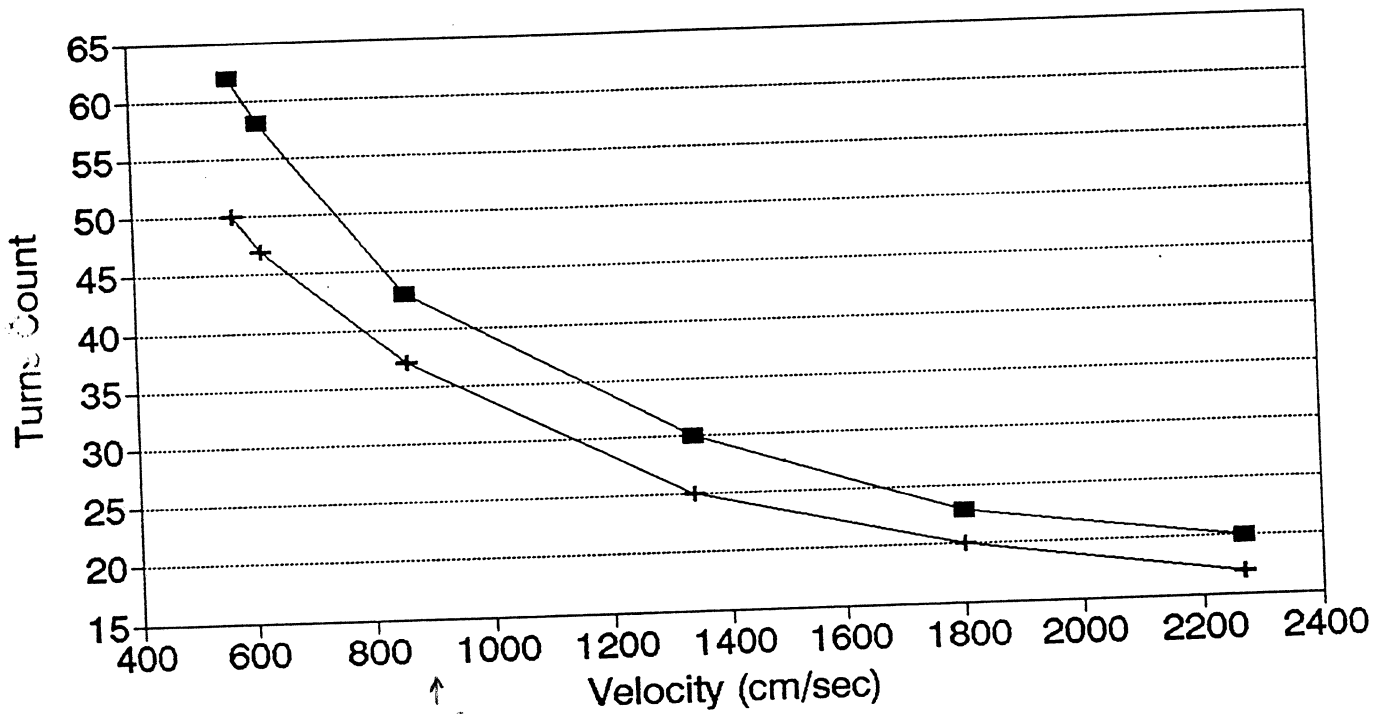
$v = 19.9 \text{ m/sec}$

35.0 Kfci



Turns vs Surface Velocity

0% Margin (1E-10) @ 400 Mb/sq.in.

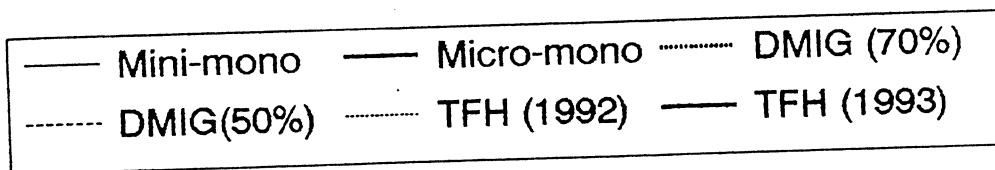
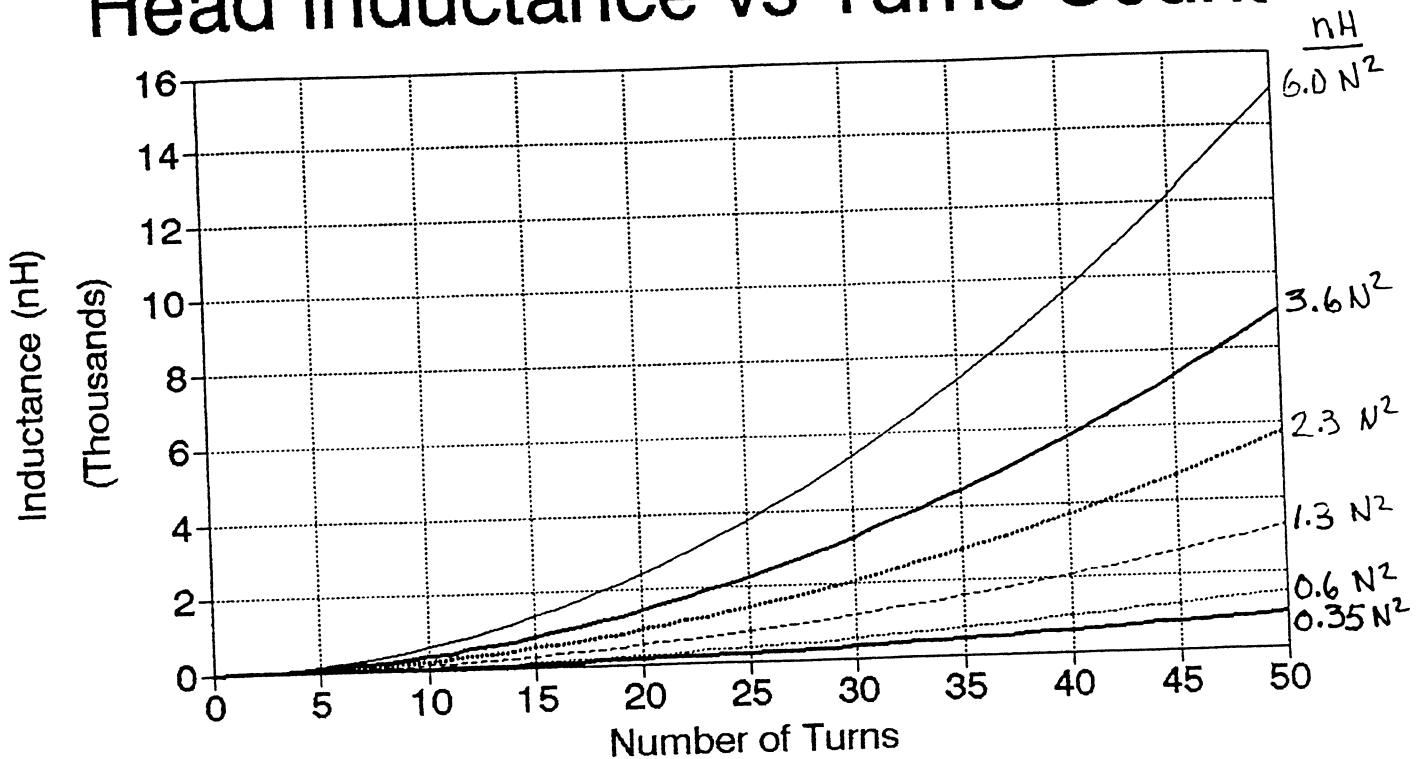


1.0 ohm/turn
 0.5 ohm/turn

$L = 0.6 N^2 \text{ (nH)}$

↑
 x 3600
 RPM

Head Inductance vs Turns Count



Problems of High Inductance

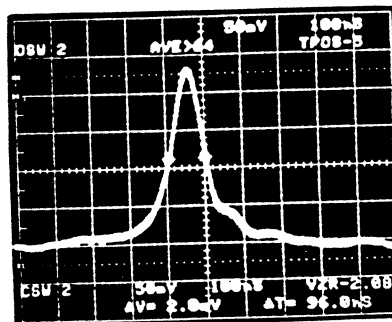
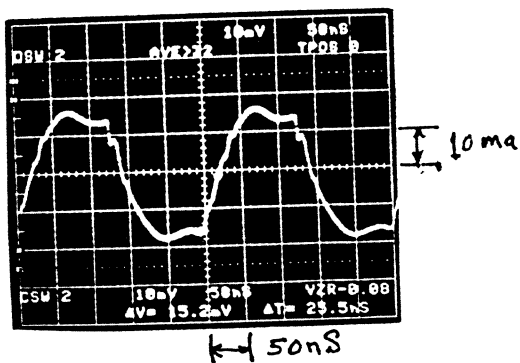
MIG (70%)

$N = 24 + 24$ Turns

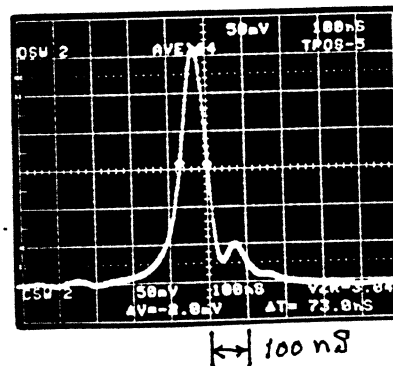
$L \approx 7 \mu H$; Write Driver $V \approx 4.0V$

$\Delta T(0.50\%) \approx \frac{L \Delta I}{V}$; Writing $I(t)$

is $\Delta T \approx 25 nS$ at $\Delta I = 15ma(0-p)$



Isolated Pulse at 9.5 m/sec



Isolated Pulse at 16.6 m/sec (VM214 Preamp)

Noise Impedance ($\text{Re}[Z]$) vs Frequency

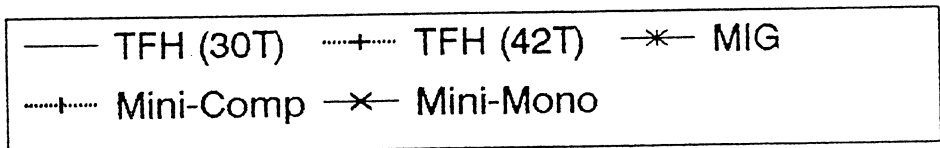
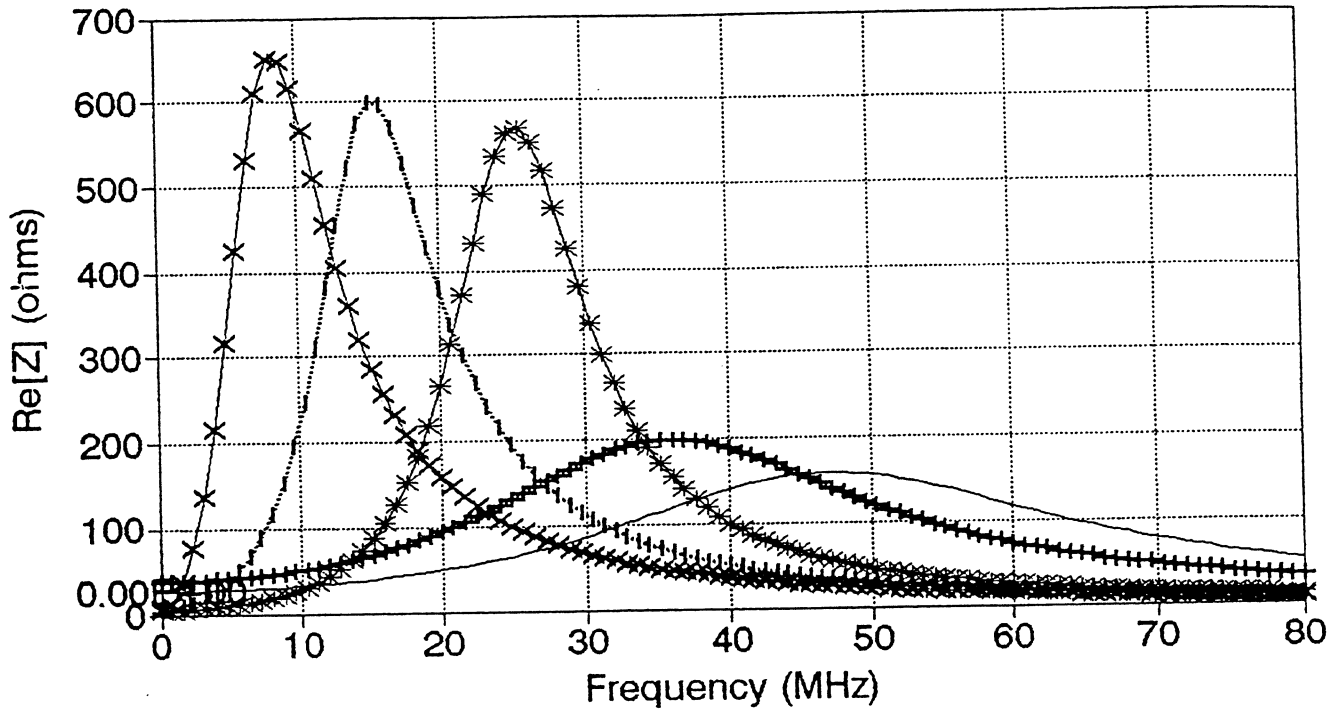


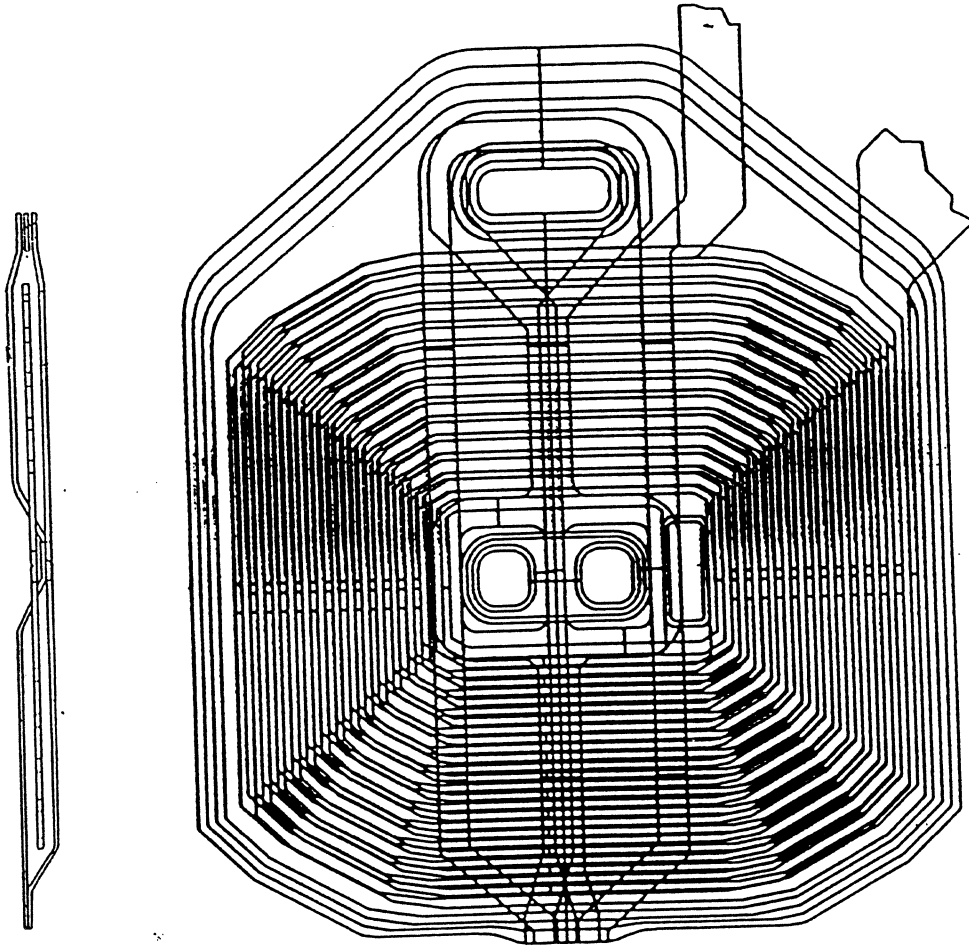
Table 1: Electrical Properties of Inductive Heads

Head Type	$R_H(\Omega)$	$R_S(\Omega)$	L(nH)	C(pF)	$f_r(\text{MHz})$
TFH (30-turn)	31.0	292	475	5.2	101.3
TFH (42-turn)	45.0	417	825	5.0	78.4
MIG (34-turn)	4.4	2805	1580	5.0	56.8
Mini-Composite	6.0	3410	4200	5.2	33.9
Mini-Monolithic	6.0	5410	14000	6.0	17.4

(Ref: Arnoldussen and Nunnolley, eds., "Noise in Digital magnetic Recording." chap.7, World Scientific (1992).)

DOUBLE YOKE TFH

TYPE I



READ-RITE Corporation

DG-01 DOUBLE YOKE HEAD

ZONE 1: LR = 0.61 inch; 230 in/sec; HF = 5.07 MHz; LF = 1.27 MHz
 Density = 44.1 Kfci (58.6 Kbpi)
 Flying Height \approx 3.7 μ inches
 Test Disk: 1400 Oe Komag

P1/G/P2 = 3.3/0.35/3.3 μ m; P1W/P2W = 9.5/7.5 μ m
 27 Turns, 2 layers

equivalent to 54 turns

75% efficiency

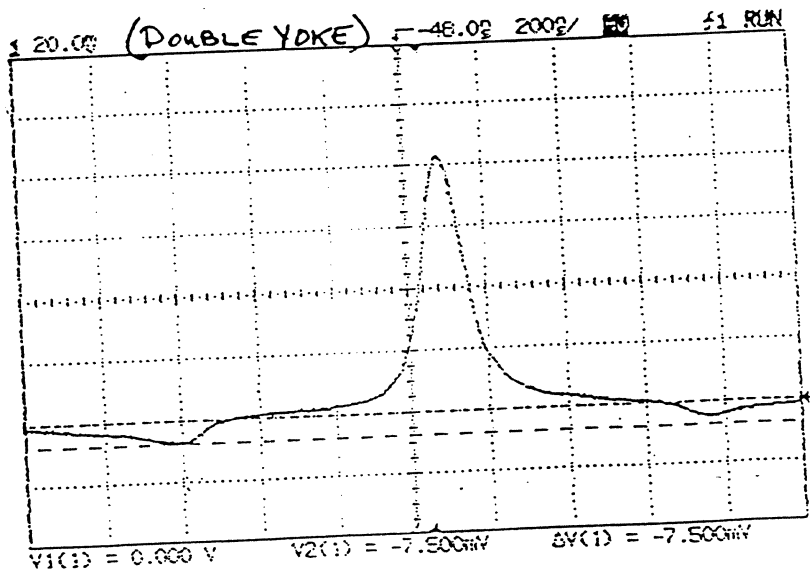
HF Signal = 199 μ volts
 Resolution = 76.7%
 PW50 = 14.7 nsec
 Overwrite = -30.9 dB
 Consumed Window = 15.9 nsec
 Window Margin = 36%

Control Heads: R93 (42 turns)

P1/G/P2 = 3.5/0.35/3.5 μ m; P1W/P2W = 9.5/7.5 μ m
 Flying Height \approx 4.1 μ inches

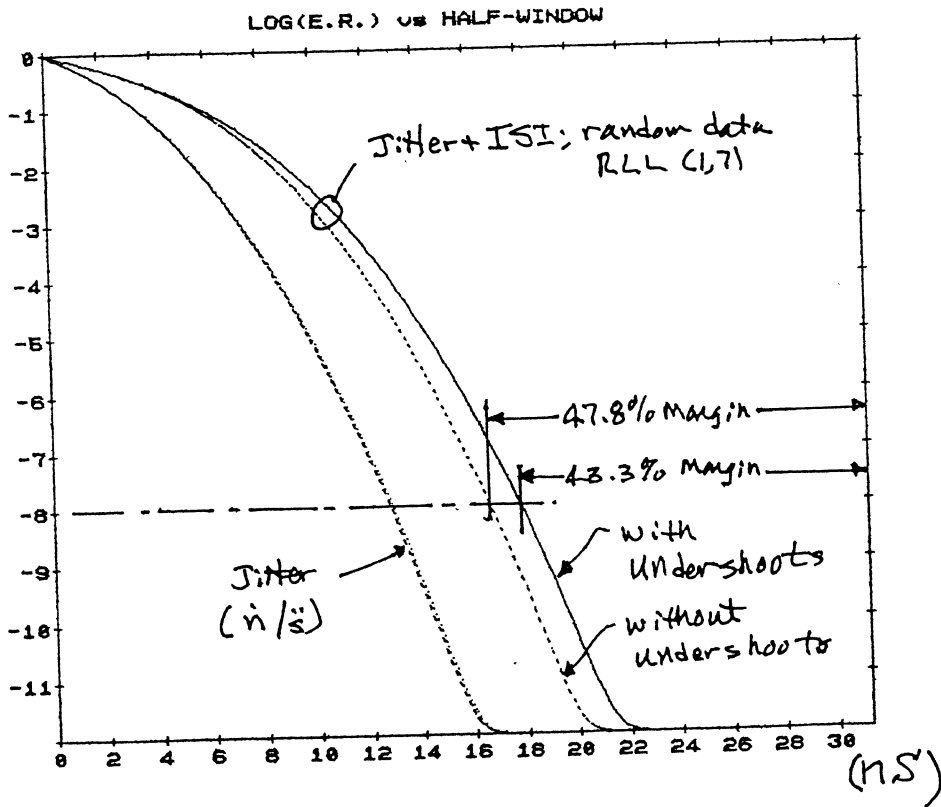
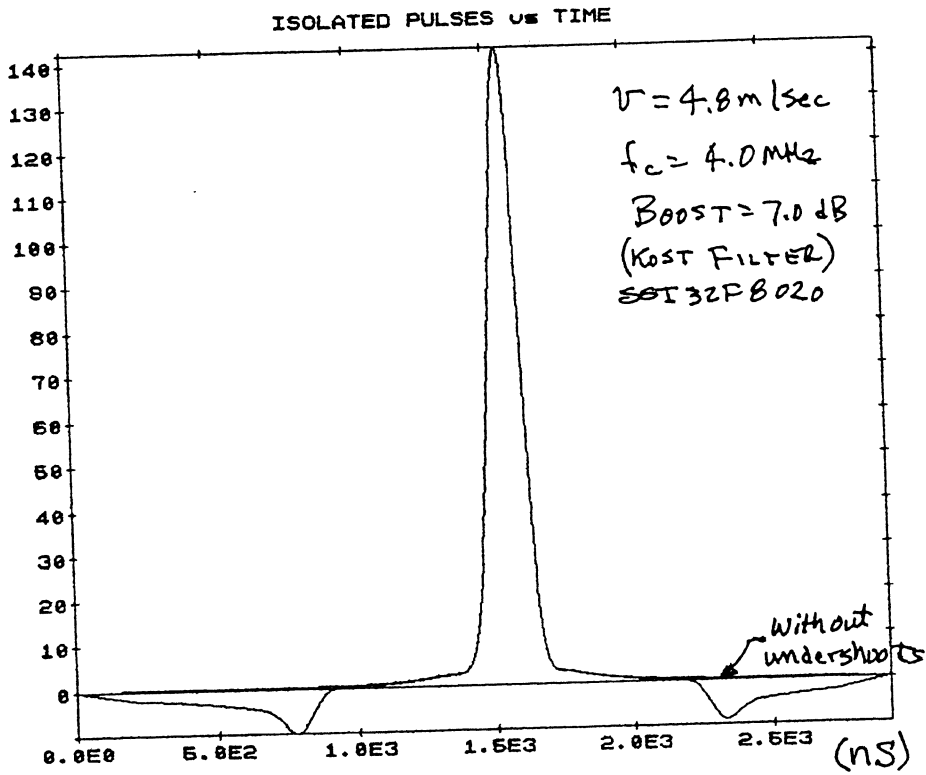
HF Signal = 214 μ volts
 Resolution = 71.4%
 PW50 = 104.0 nsec
 Overwrite = -28.4 dB
 Consumed Window = 17.9 nsec
 Window Margin = 28%

85%

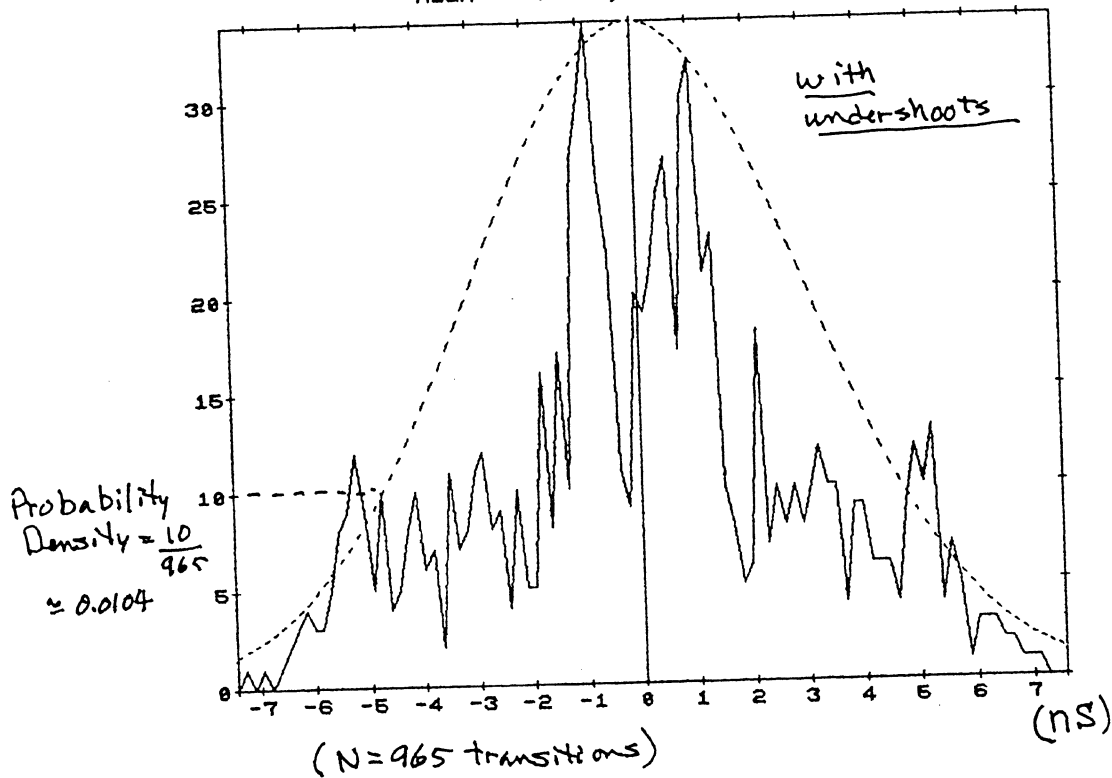


INFLUENCE of UNDERSHOOTS on ERROR RATE

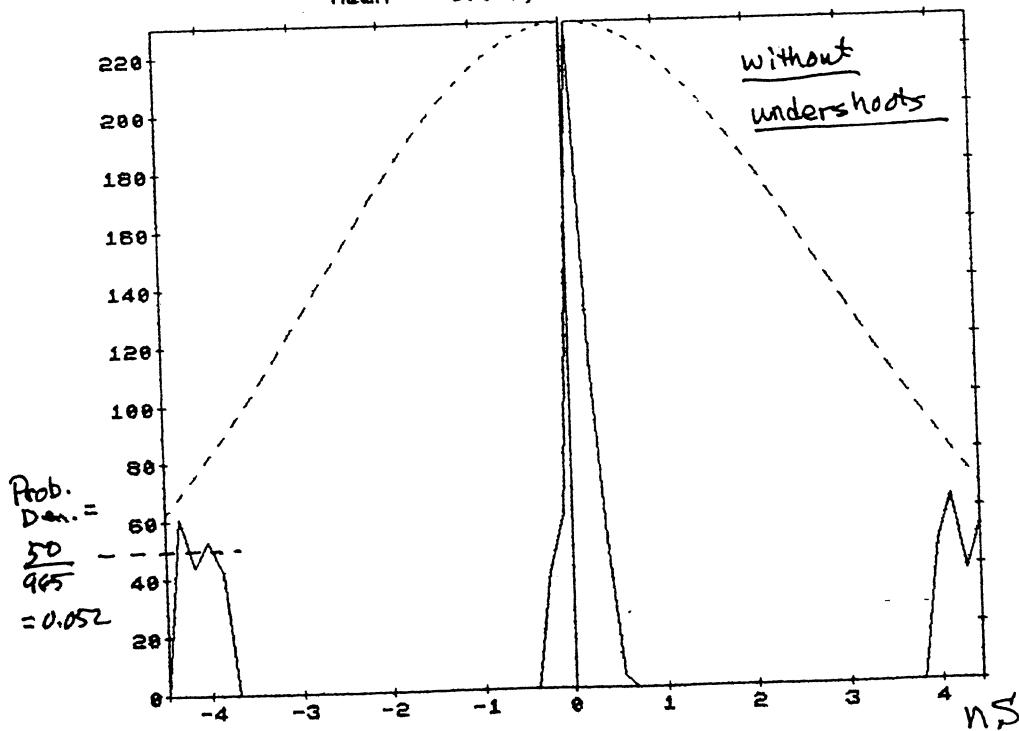
(μV)



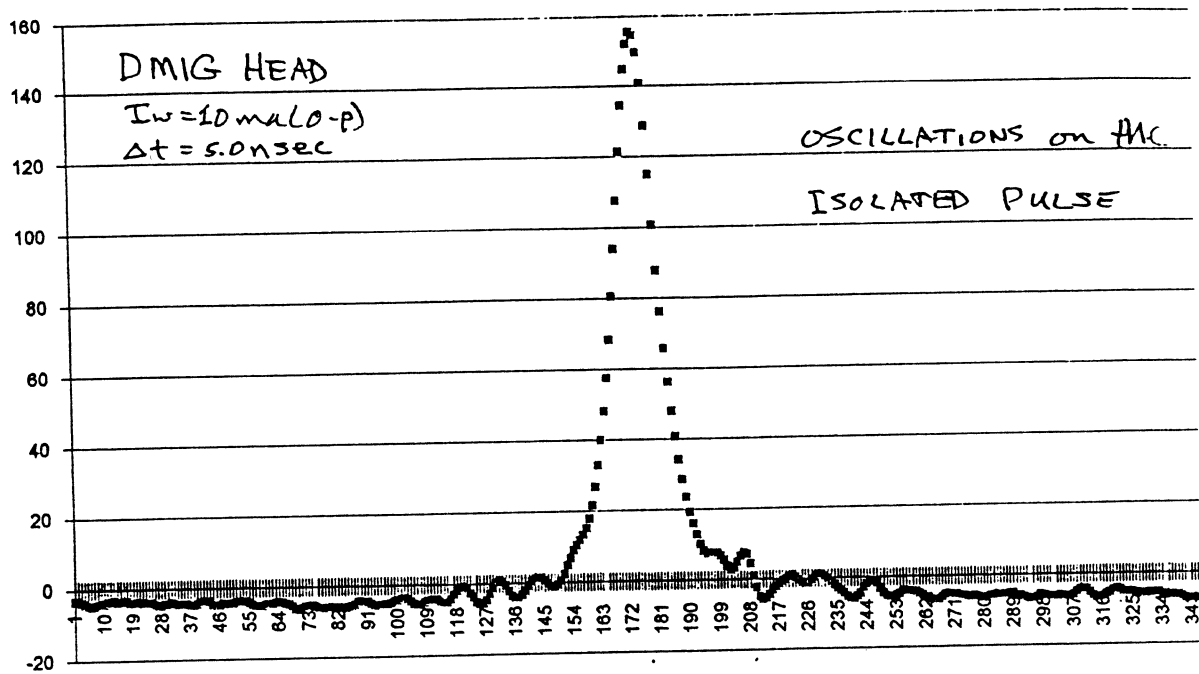
HISTOGRAM OF (1,7) PEAKSHIFT VALUES
 Mean = -0.834; SD = 3.01 ns



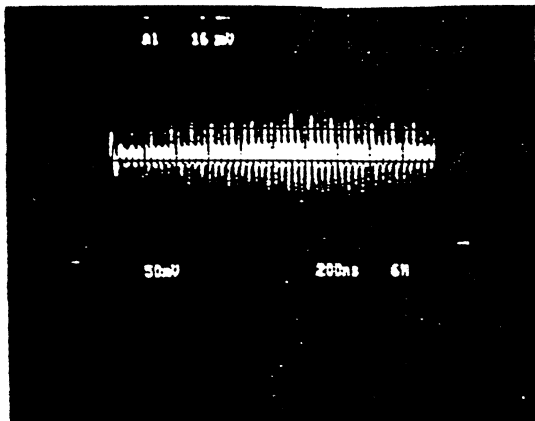
HISTOGRAM OF (1,7) PEAKSHIFT VALUES
 Mean = 0.051; SD = 2.81 ns



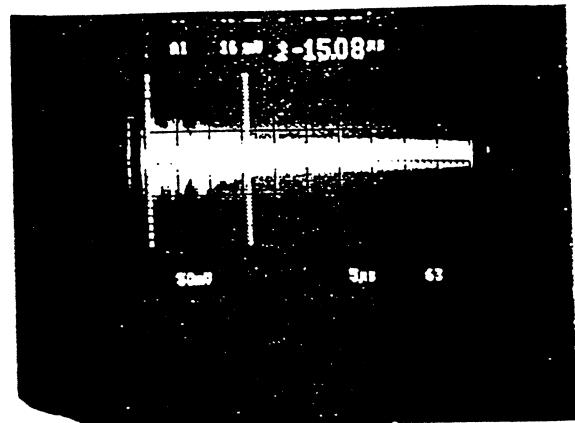
DMIG and TFH APPLICATION ISSUES



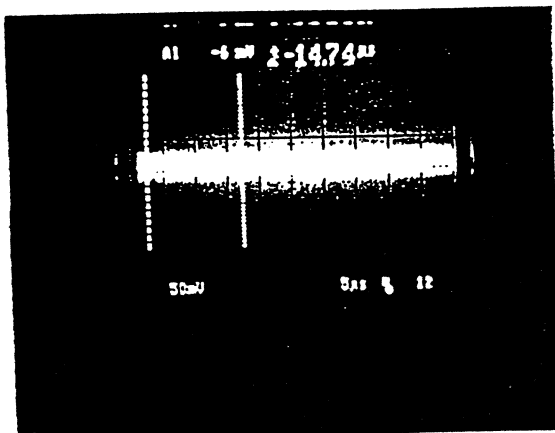
READ-AFTER-WRITE OSCILLATIONS &/OR RELAXATION NOISE :



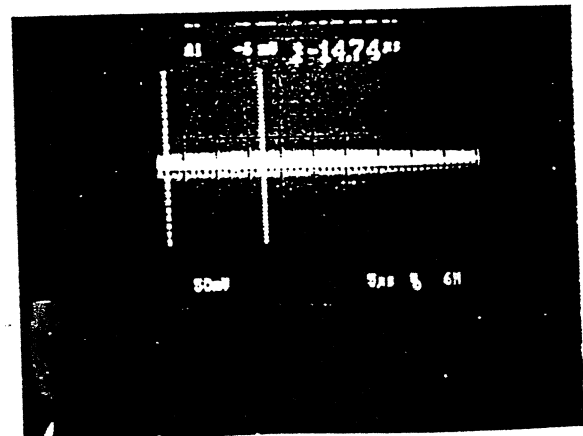
DMIG #11



DMIG #11



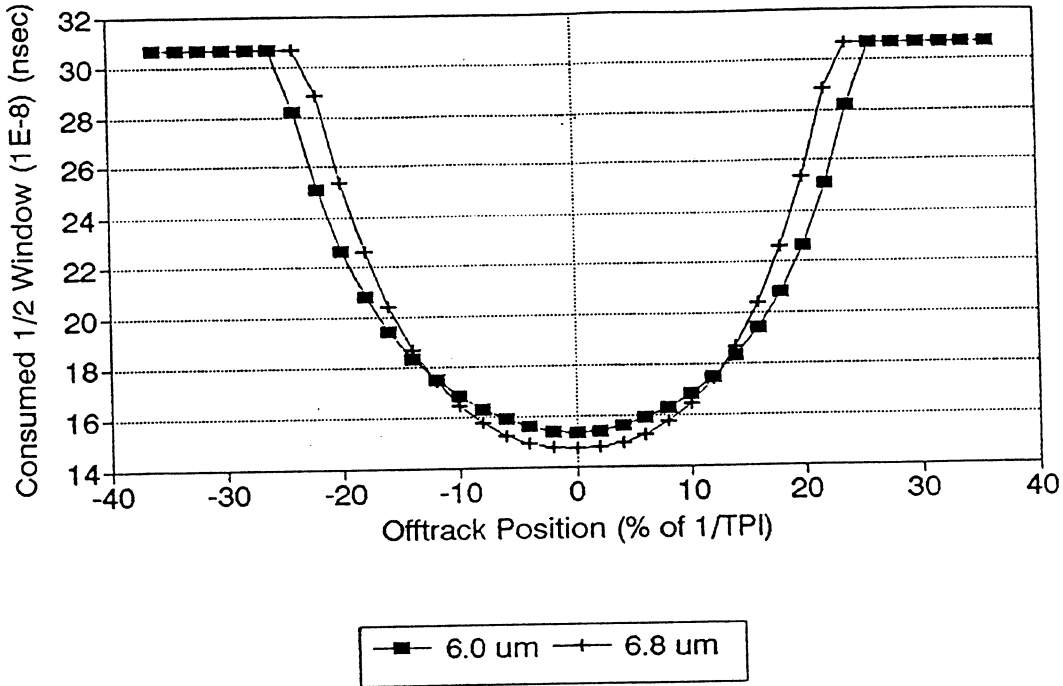
TFH



TFH #161

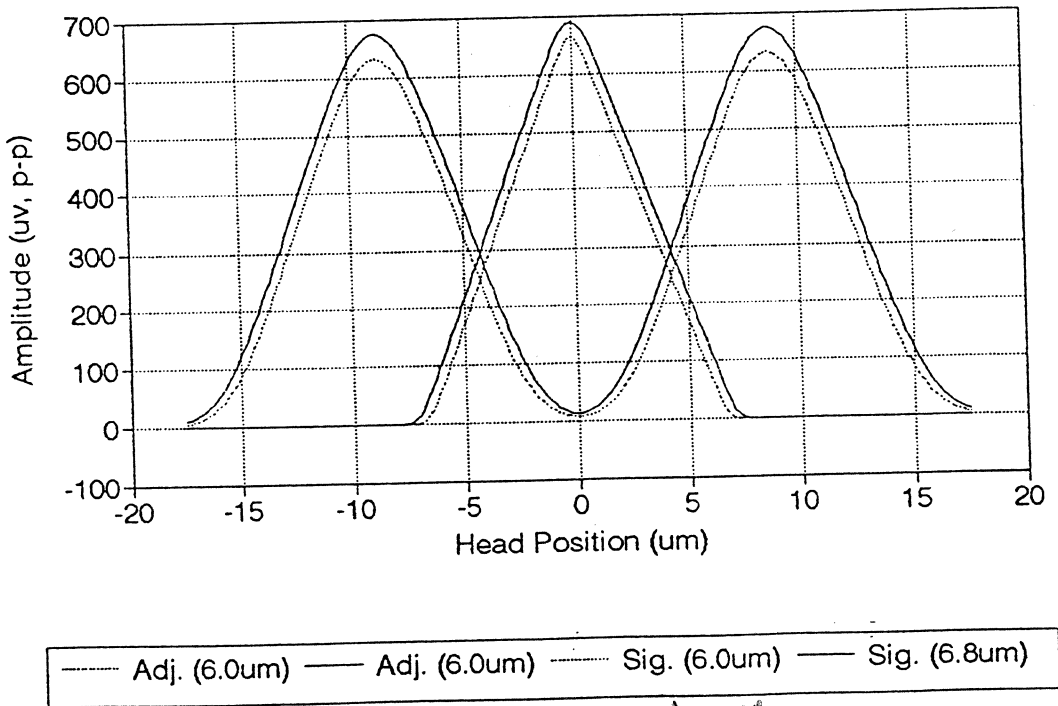
Pole Trimming (P2W = 6.0 μm)

3200 TPI: Written Width = 6.0; 6.8 μm



Track Profiles

Written Width = 6.0 ; 6.8 μm



trimmed head.

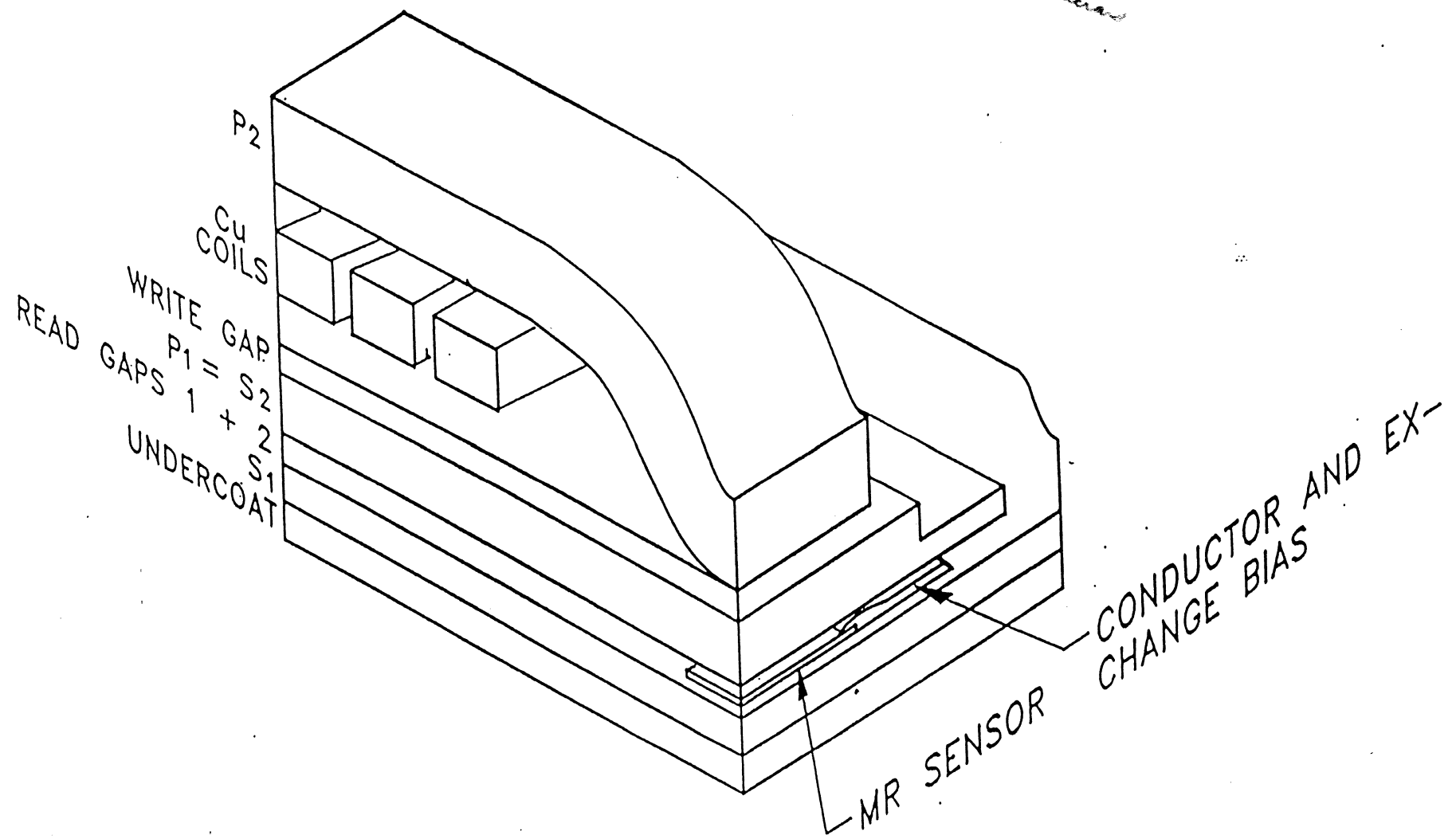
READ-RITE

Corporation

MR HEAD DESIGN

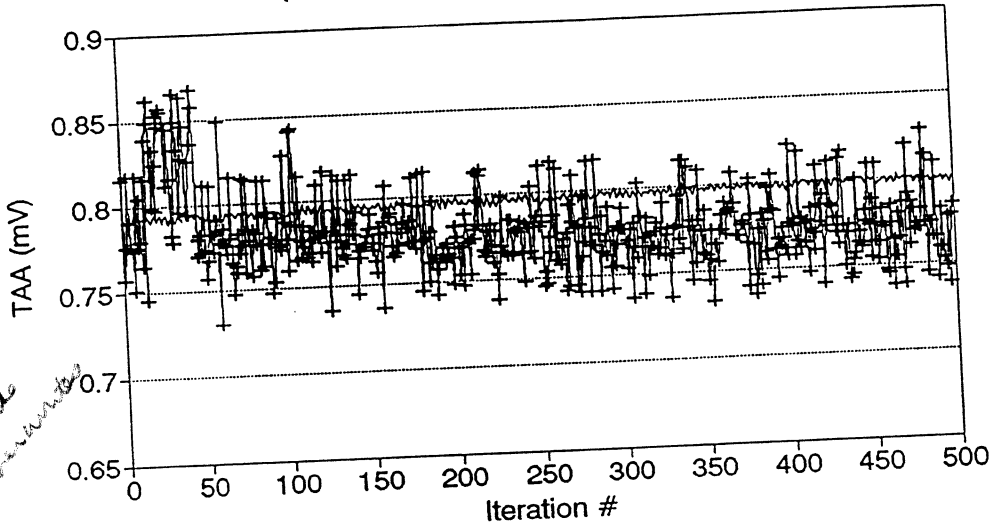
*write well
head narrow
requires biasing*

*15 teeth
3 - .35 micras*

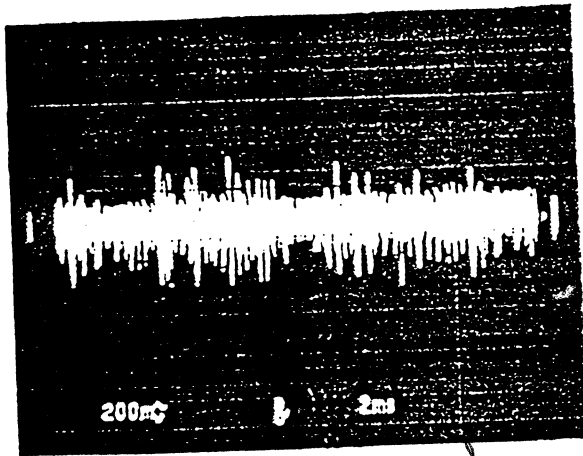


MR HEADS: APPLICATION ISSUES

stability: TAA isolated pulse.
(With and without rewrite).

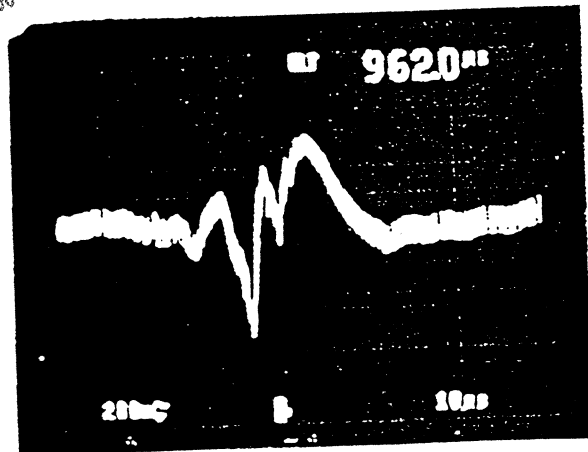


Variation in amplitude due to temperature



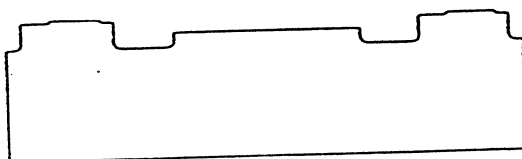
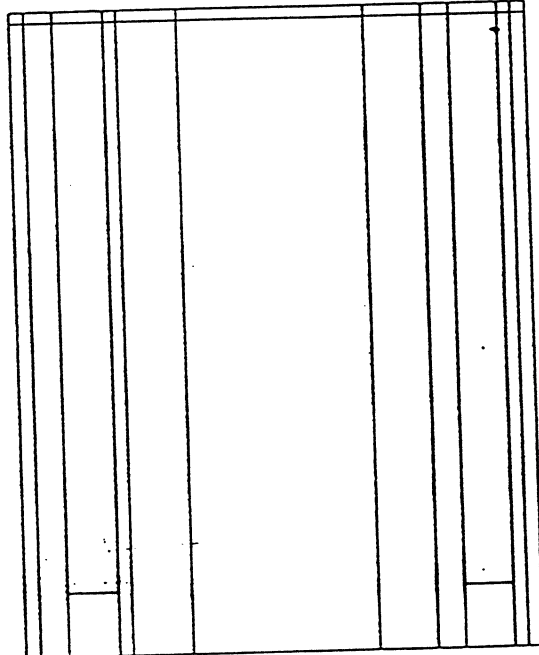
thermal

Disparity effect



CONSTANT FLY HEIGHT DESIGNS

REVISIONS					
ZONE	ECN NO.	REV	DESCRIPTION	DATE	APPROVED

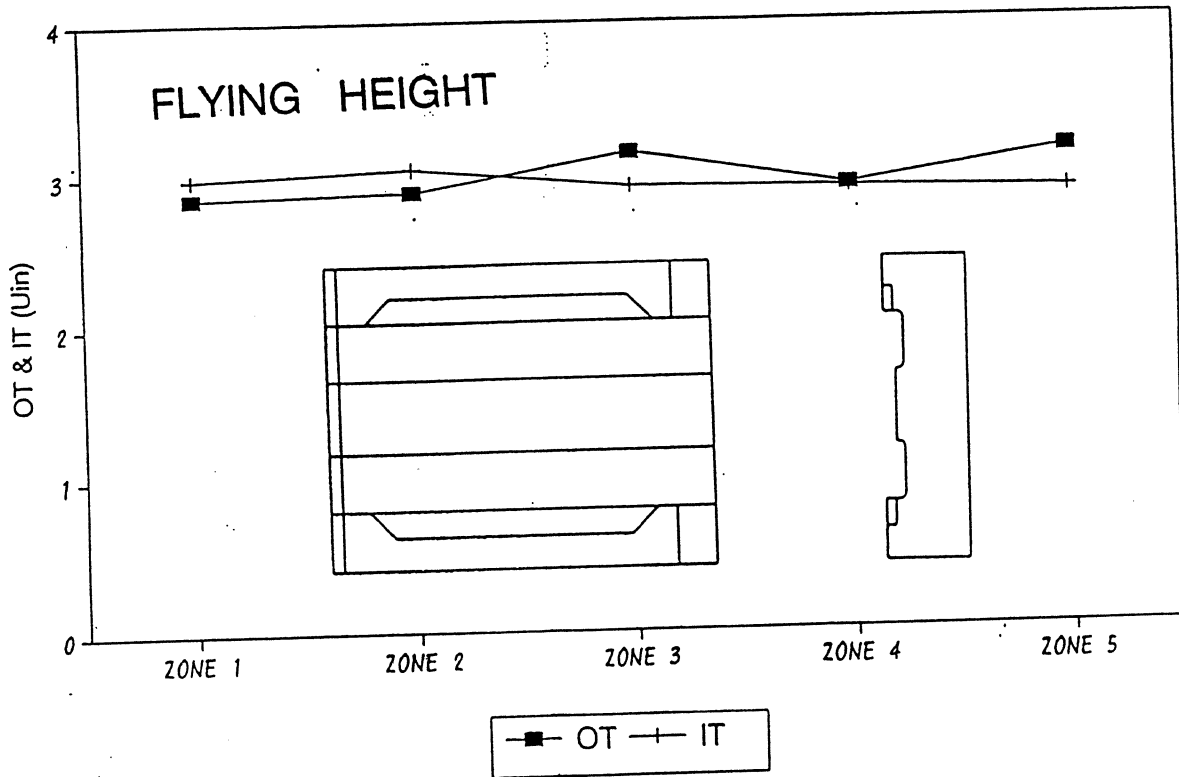


Constant flying height

2 real hard.

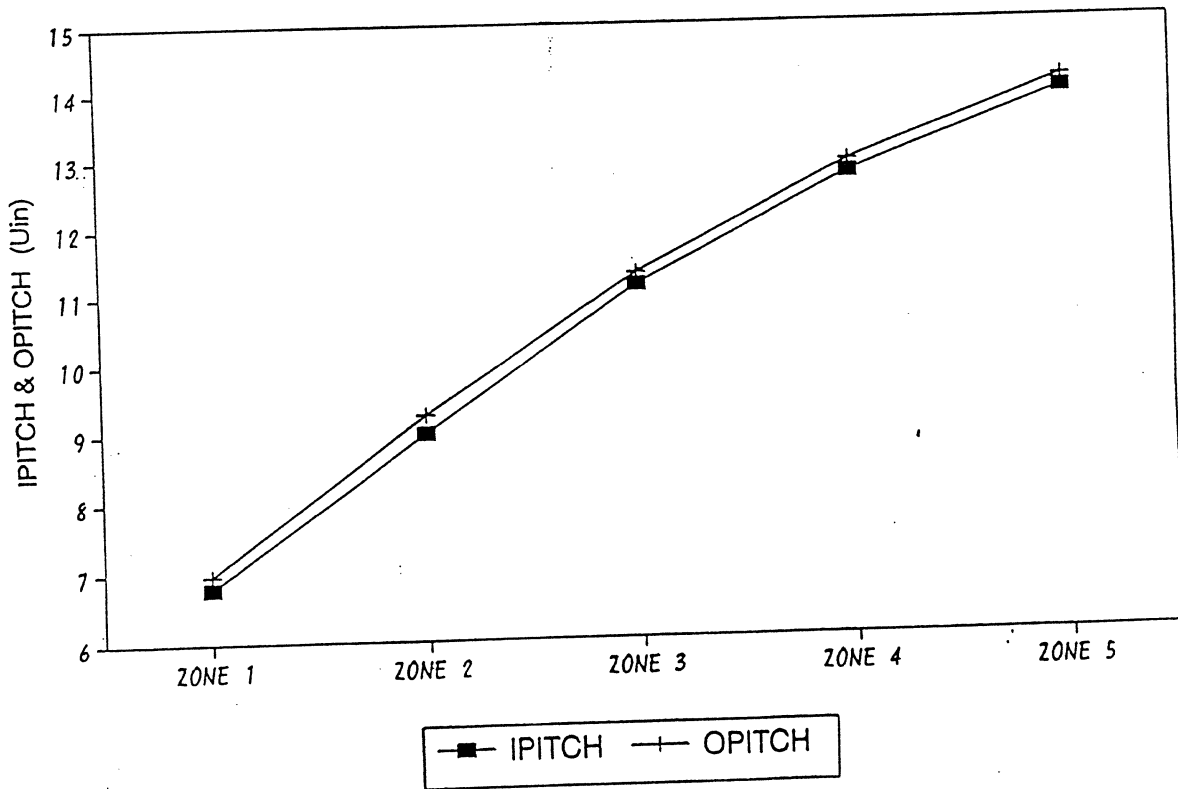


ITEM NO.	QTY REQ'D	NOMENCLATURE OR DESCRIPTION	MATERIAL SPECIFICATION	PART OR IDENTIFYING NO.		
PARTS LIST						
<small>UNLESS OTHERWISE SPECIFIED DIMENSIONS ARE IN INCHES.</small> <small>TOLERANCES:</small> <small>FRACTIONS DECIMALS ANGLES</small> <small>± .001 ± .0005 ±</small>		<small>MATERIAL AND COMMENT</small> <div style="text-align: right; font-weight: bold; font-size: 1.2em;"> READ-RITE Corporation Milpitas, California. </div>				
<small>INFORMATION CONTAINED IN THIS DOCUMENT IS CONFIDENTIAL AND PROPRIETARY TO READ-RITE. REPRODUCTION OR TRANSMITTAL OF ITS CONTENTS IN WHOLE OR IN PART WITHOUT WRITTEN PERMISSION FROM READ-RITE IS PROHIBITED.</small>		<small>APPROVALS</small> DRAWN <i>J. Chen</i> 5/19/92 CHECKED APPROVED APPROVED		TITLE: MICROSLIDER, TPC 22		
		SIZE	FSCM NO.	DWG NO.	REV	
		SCALE 30X			SHEET 1 OF 1	
		APPLICATION DO NOT SCALE DRAWING				



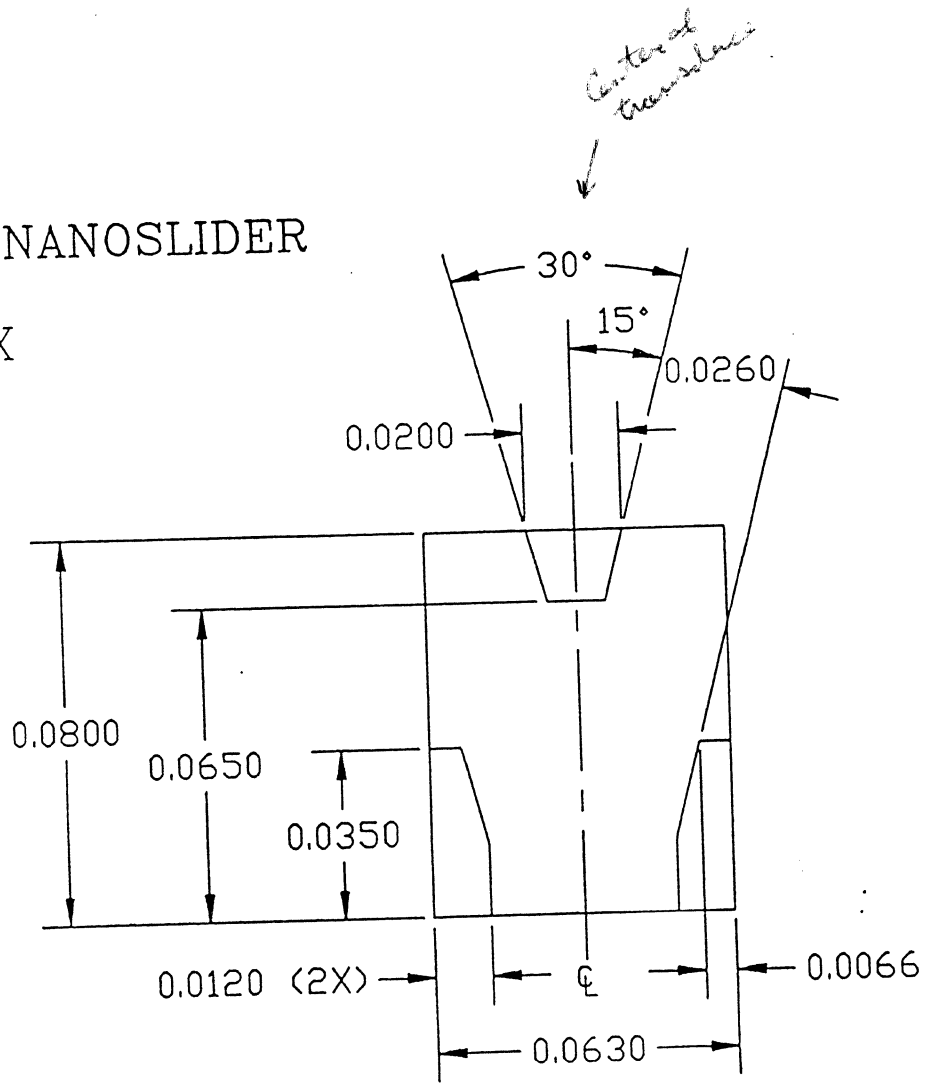
Stable flying height

Steel angles



READ-RITE Corporation
 Milpitas, California.
 TITLE: NANOSLIDER, ABLATED ABS

TRI-PAD NANOSLIDER
VER. 12
SCALE:30X



*low grow
level 1-2g
machining
instead
of laser etching*

"Inductive Thin-Film Heads"

Erich Valstyn

Read-Rite Corp.

Institute for Information Storage Technology

Santa Clara University, California

December 14 - 16, 1992

TWO CHALLENGES:

1. SMALL DRIVES: LOW VELOCITIES + HIGH TPI
2. LARGER DRIVES (3.5"): HIGHER DATA RATES + HIGH TPI

SOLUTION:

INCREASE NUMBER OF TURNS N .

PROBLEM: SIGNAL-TO-NOISE RATIO

N increased by factor k - S/N not increased by factor k

impedance
DC

$$Z = R + j\omega L = R + j\omega (L_m + L_c)$$

inductance

$$L_m = KN^2 \mu_e = KN^2 (\mu_e' - j\mu_e'')$$

$$L_c = 7 N^2 r \times 10^{-7} \text{ H}$$

$$Z = (R + KN^2 \omega \mu_e'') + j\omega (KN^2 \mu_e' + L_c)$$

$$\overline{\Delta v_N^2} = 4kT \operatorname{Re}(Z) \Delta f$$

$$(V_N)_{rms} = \sqrt{4kT \int_{f_1}^{f_2} \operatorname{Re}(Z) df}$$

Skin Effect

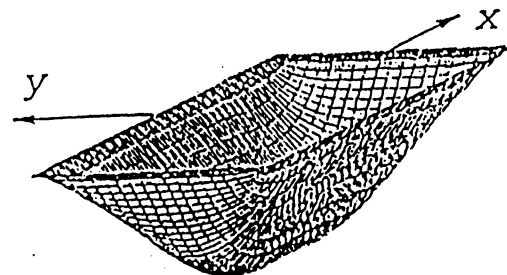
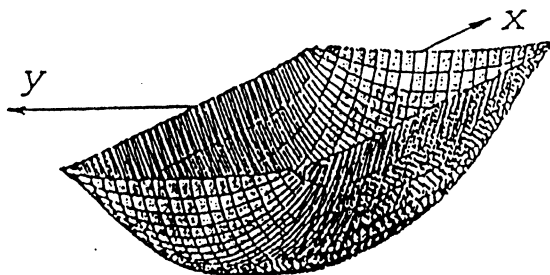
$$\frac{\partial^2 H_z}{\partial x^2} + \frac{\partial^2 H_z}{\partial y^2} = j\omega\sigma\mu H_z$$

$$H_z(x, y) = \frac{4H_0}{\pi} \sum_{n=1}^{\infty} \frac{(-1)^{n+1}}{2n-1} \left(\frac{\cosh b_n x \cos(2n-1) \frac{\pi y}{t}}{\cosh \frac{b_n w}{2}} + \frac{\cosh d_n y \cos(2n-1) \frac{\pi x}{w}}{\cosh \frac{d_n t}{2}} \right)$$

$$b_n^2 = (2n-1)^2 \frac{\pi^2}{t^2} + j \frac{2}{\delta^2}$$

$$d_n^2 = (2n-1)^2 \frac{\pi^2}{w^2} + j \frac{2}{\delta^2} \quad (2)$$

where δ is the skin depth: $\delta^2 = \frac{2}{\omega\sigma\mu}$.



$$\mu_e = \frac{\Phi}{H_0 w t} = \frac{16 \mu}{\pi^2 w t} \sum_{n=1}^{\infty} \frac{1}{(2n-1)^2} \left(\frac{t}{b_n} \tanh \frac{b_n w}{2} + \frac{w}{d_n} \tanh \frac{d_n t}{2} \right).$$

$$\mu_e = \mu \frac{2}{\tau t} \tanh \frac{\tau t}{2}, \quad \tau = \frac{1+j}{\delta}.$$

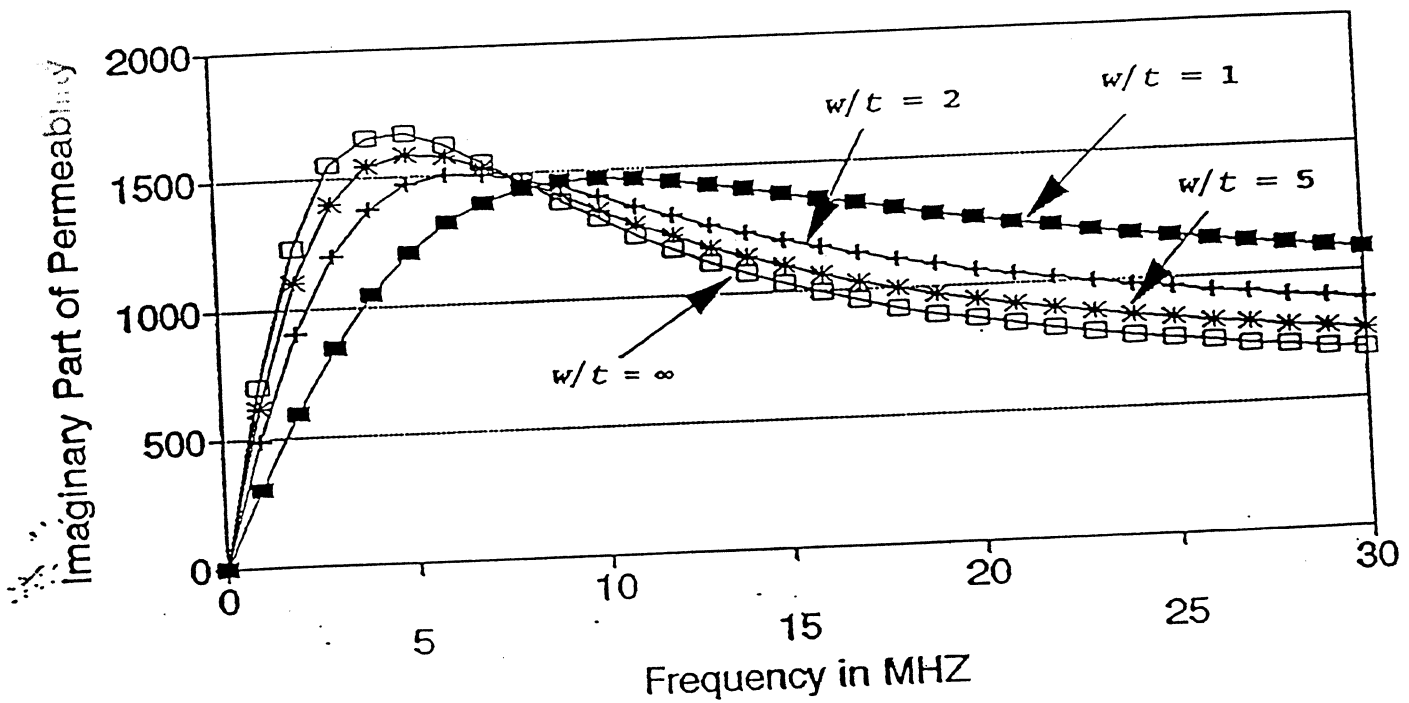
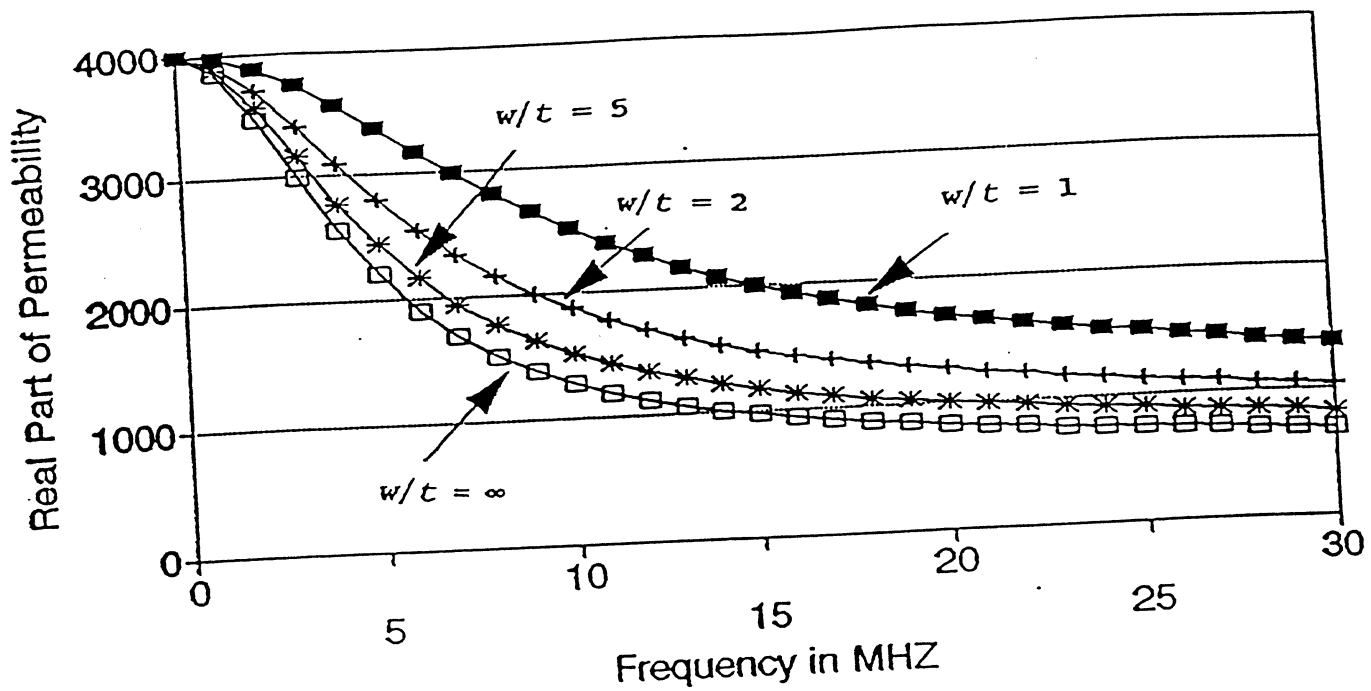


Figure 4. Real and imaginary part of permeability vs. frequency..
 $t = 3.5 \mu\text{m}$, $\mu = 4000$, $\rho = 17.5 \times 10^{-8} \Omega\cdot\text{m}$.

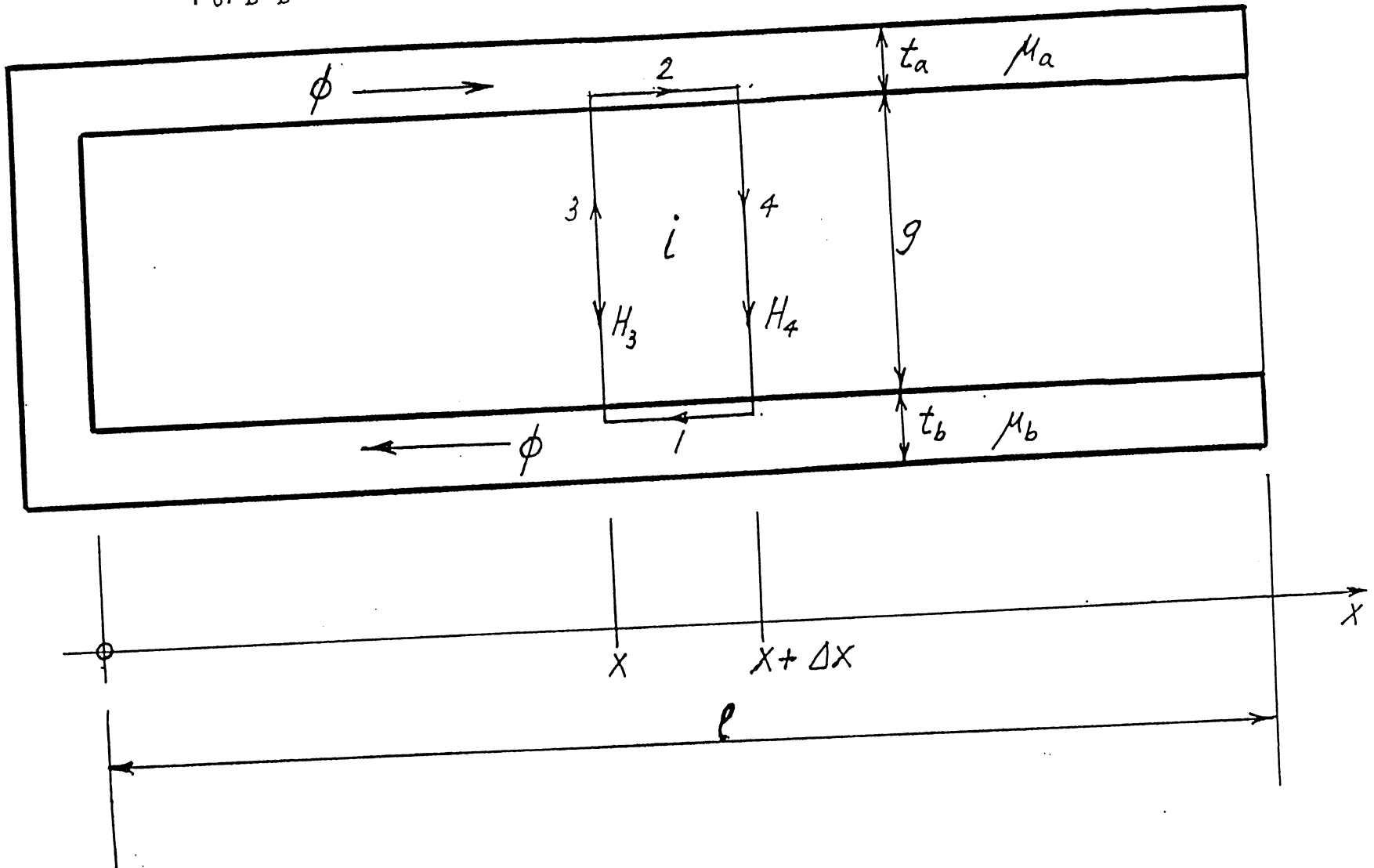
$$i = \oint \vec{dl}$$

$$i = H_1 \Delta x + H_2 \Delta x - H_3 g + H_4 g$$

$$i = \frac{I \Delta x}{l}$$

$$H_1 = \frac{\Phi(x)}{\mu_0 \mu_b t_b w} \quad H_2 = \frac{\Phi(x)}{\mu_0 \mu_a t_a w} \quad H_3 = \frac{-1}{\mu_0 w} \cdot \frac{d\Phi}{dx}(x) \quad H_4 = \frac{-1}{\mu_0 w} \cdot \frac{d\Phi}{dx}(x + \Delta x)$$

transmission line model.
let's consider
D's



$$i = \oint \vec{H} \cdot d\vec{\ell}$$

$$i = H_1 \Delta x + H_2 \Delta x - H_3 g + H_4 g$$

$$H_1 = \frac{\Phi(x)}{\mu_0 \mu_b t_b w} \quad H_2 = \frac{\Phi(x)}{\mu_0 \mu_a t_a w} \quad H_3 = \frac{-1}{\mu_0 w} \cdot \frac{d\Phi}{dx}(x) \quad H_4 = \frac{-1}{\mu_0 w} \cdot \frac{d\Phi}{dx}(x + \Delta x)$$

$$i = \frac{I \Delta x}{\ell}$$

$$H_4 = -\frac{1}{\mu_0 w} \cdot \frac{d\Phi}{dx}(x + \Delta x)$$

$$H_4 = -\frac{1}{\mu_0 w} \left[\frac{d\Phi}{dx}(x) + \frac{d}{dx} \left(\frac{d\Phi}{dx} \right) \Delta x \right]$$

$$H_4 = -\frac{1}{\mu_0 w} \left[\frac{d\Phi}{dx}(x) + \frac{d^2\Phi}{dx^2} \Delta x \right]$$

$$\frac{I \Delta x}{\ell} = \frac{\Phi(x) \Delta x}{\mu_0 w} \left(\frac{1}{\mu_a t_a} + \frac{1}{\mu_b t_b} \right) + \frac{g}{\mu_0 w} \cdot \frac{d\Phi}{dx}(x) - \frac{g}{\mu_0 w} \left[\frac{d\Phi}{dx}(x) + \frac{d^2\Phi}{dx^2} \Delta x \right]$$

$$\frac{1}{t} \equiv \frac{1}{\mu_a t_a} + \frac{1}{\mu_b t_b} \quad \text{Simplify} \rightarrow$$

$$\frac{I \Delta x}{\ell} = \frac{\Phi(x) \Delta x}{\mu_0 w t} - \frac{g \Delta x}{\mu_0 w} \cdot \frac{d^2\Phi}{dx^2}$$

Final equation

$$\frac{d^2\Phi}{dx^2} - \frac{\Phi}{gt} = -\frac{\mu_0 w I}{g \ell}$$

$$\alpha \equiv \frac{1}{\sqrt{gt}}$$

$$\Phi'' = \alpha^2 \Phi - \frac{\mu_0 w I}{g \ell}$$

$$V'' = \gamma^2 V$$

$$\Phi'' = \alpha^2 \Phi - \frac{\mu_0 w I}{g \ell}$$

$$\Phi(x) = A \sinh \alpha x + B \cosh \alpha x + \frac{\mu_0 w t I}{\ell}$$

$$\frac{d\Phi}{dx} = \alpha A \cosh \alpha x + \alpha B \sinh \alpha x$$

$$\left[\frac{d\Phi}{dx} \right]_{x=0} = 0, \quad A = 0$$

$$[\Phi]_{x=\ell} = 0, \quad B = -\frac{\mu_0 w t I}{\ell \cosh \alpha \ell}$$

$$\Phi(x) = \frac{\mu_0 I w t}{\ell} \left[1 - \frac{\cosh \alpha x}{\cosh \alpha \ell} \right]$$

$$H_g = -\frac{1}{\mu_0 w} \left[\frac{d\Phi}{dx} \right]_{x=\ell} = \frac{I t \alpha}{\ell} \tanh \alpha \ell = \frac{I}{\ell} \sqrt{\frac{t}{g}} \tanh \frac{\ell}{\sqrt{g t}}$$

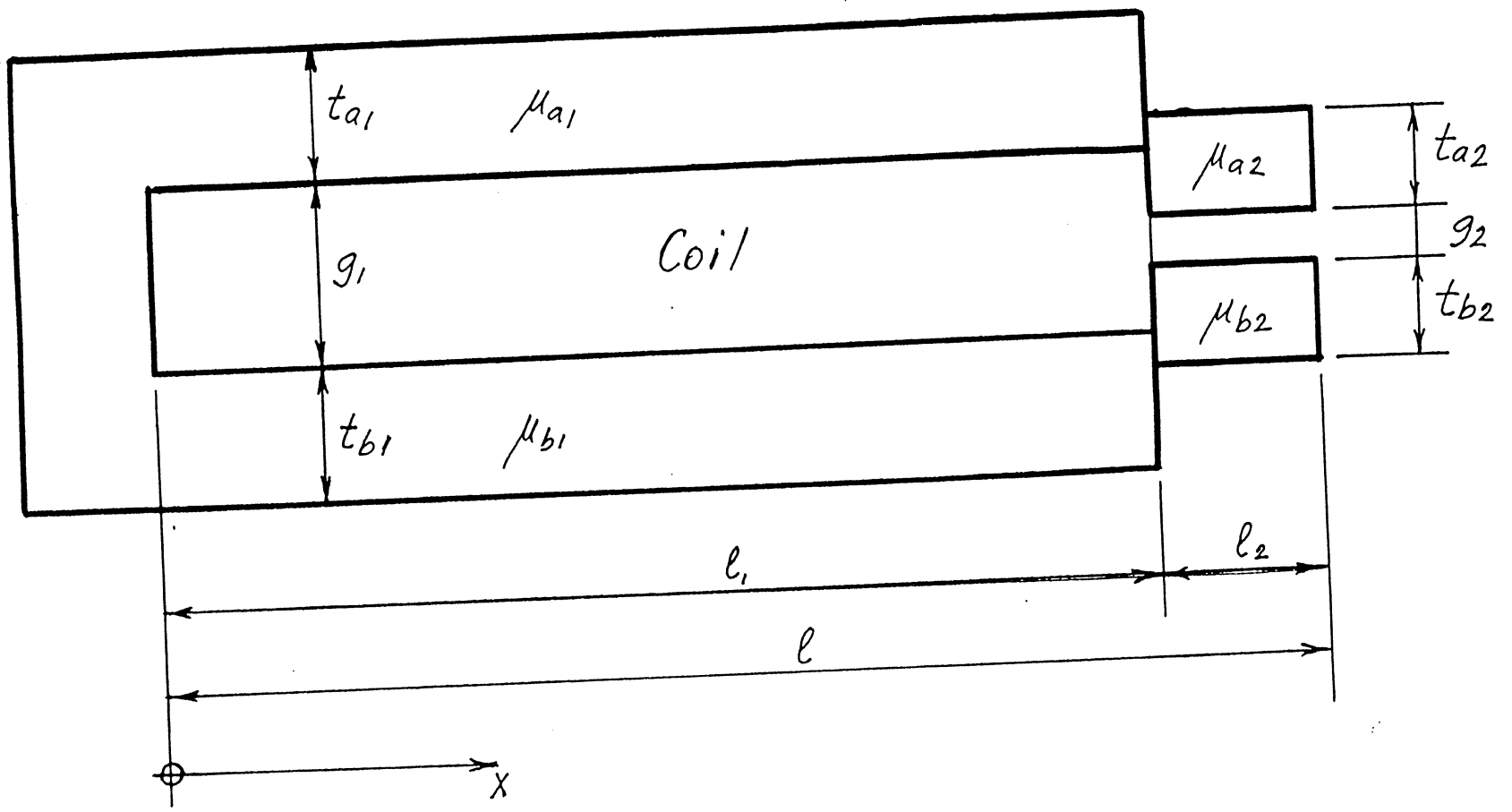
$$\epsilon = \frac{H_g g}{I} = \frac{\sqrt{g t}}{\ell} \tanh \frac{\ell}{\sqrt{g t}}$$

*transfer
model
used to be called
efficiency.*

$$L = \frac{1}{I \ell} \int_0^{\ell} \Phi(x) dx = \frac{\mu_0 w t}{\ell} \left(1 - \frac{\sqrt{g t}}{\ell} \tanh \frac{\ell}{\sqrt{g t}} \right) = \frac{\mu_0 w t}{\ell} (1 - \epsilon)$$

$$\text{For } \frac{\ell}{\sqrt{g t}} = 0 \quad \epsilon = 1$$

$$l = l_1 + l_2, \quad \alpha_1 = \frac{1}{\sqrt{g_1 l_1}}, \quad \alpha_2 = \frac{1}{\sqrt{g_2 t_2}}$$



$$\Phi_1(x) = A_1 \sinh \alpha_1 x + B_1 \cosh \alpha_1 x + Q, \quad 0 < x < \ell_1$$

$$\Phi_2(x) = A_2 \sinh \alpha_2 x + B_2 \cosh \alpha_2 x, \quad \ell_1 < x < \ell$$

$$\left[\frac{d\Phi_1}{dx} \right]_{x=0} = 0, \quad A_1 = 0$$

$$\Phi_1(x) = B_1 \cosh \alpha_1 x + Q$$

$$[\Phi_2]_{x=\ell} = 0, \quad B_2 = -A_2 \tanh \alpha_2 \ell$$

$$\Phi_2(x) = A_2 (\sinh \alpha_2 a - \tanh \alpha_2 \ell \cosh \alpha_2 x) = -\frac{A_2 \sinh \alpha_2 (\ell - x)}{\cosh \alpha_2 \ell}$$

$$x = \ell_1, \quad \Phi_1 = \Phi_2, \quad \frac{d\Phi_1}{dx} = \frac{d\Phi_2}{dx}$$

$$\Phi_1 = \Phi_2 : \quad B_1 \cosh \alpha_1 \ell_1 + Q = -A_2 \frac{\sinh \alpha_2 \ell_2}{\cosh \alpha_2 \ell}$$

$$\frac{d\Phi_1}{dx} = \frac{d\Phi_2}{dx} : \quad \alpha_1 B_1 \sinh \alpha_1 \ell_1 = \alpha_2 A_2 \frac{\cosh \alpha_2 \ell_2}{\cosh \alpha_2 \ell}$$

$$\Phi_1(x) = \mathcal{Q} \left(1 - \frac{\alpha_2 \cosh \alpha_2 l_2 \cosh \alpha_1 x}{\alpha_1 \sinh \alpha_1 l_1 \sinh \alpha_2 l_2 + \alpha_2 \cosh \alpha_1 l_1 \cosh \alpha_2 l_2} \right)$$

$$\Phi_2(x) = \mathcal{Q} \frac{\alpha_1 \sinh \alpha_1 l_1 \sinh \alpha_2 (l-x)}{\alpha_1 \sinh \alpha_1 l_1 \sinh \alpha_2 l_2 + \alpha_2 \cosh \alpha_1 l_1 \cosh \alpha_2 l_2}$$

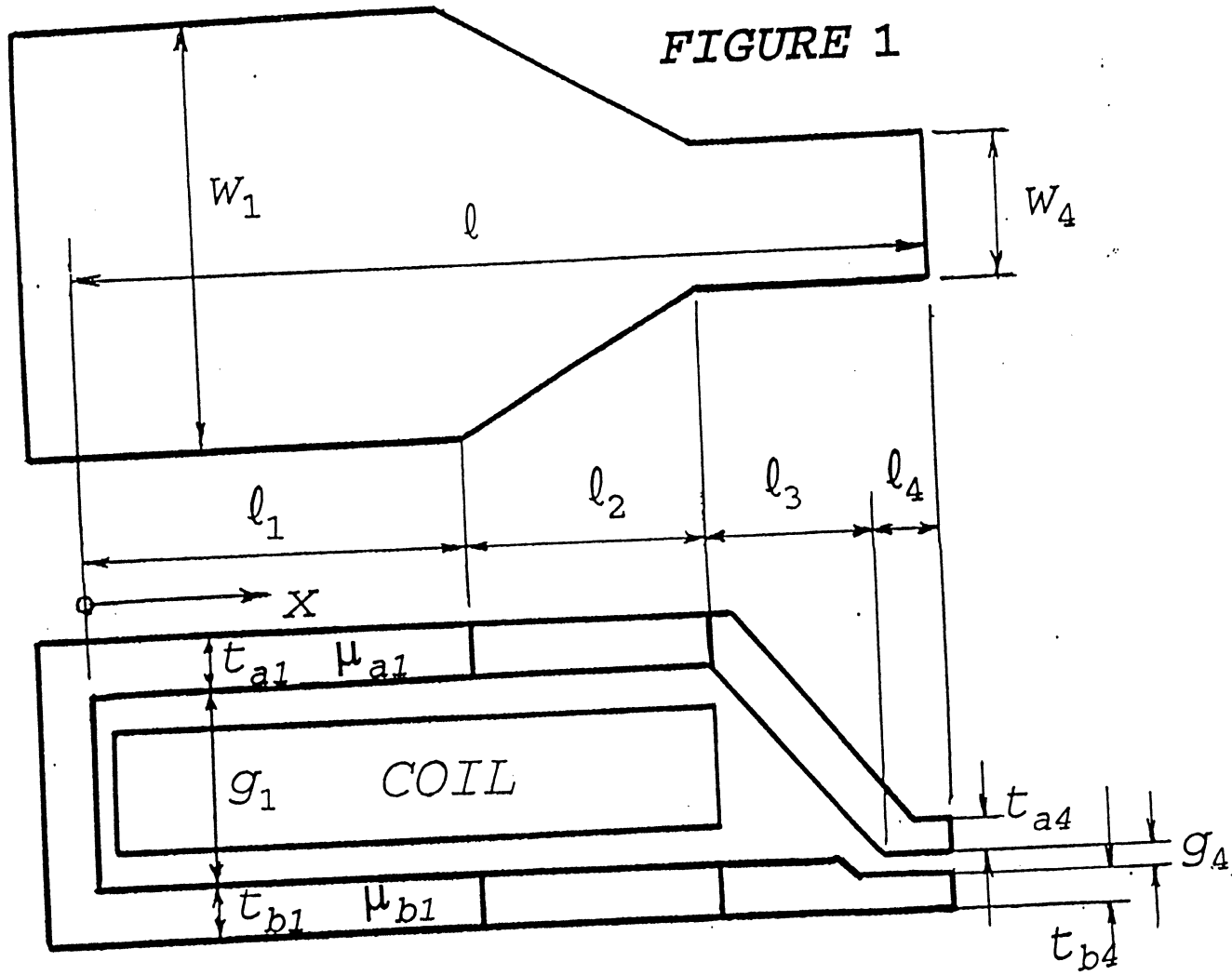
$$\epsilon = \frac{H_g g_2}{I} = - \frac{g_2}{\mu_0 w I} \left[\frac{d\Phi_2}{dx} \right]_{x=l}$$

$$\epsilon = \frac{g_2 t_1 \sinh \alpha_1 l_1}{l_1 (\sqrt{g_2 t_2} \sinh \alpha_1 l_1 \sinh \alpha_2 l_2 + \sqrt{g_1 t_1} \cosh \alpha_1 l_1 \cosh \alpha_2 l_2)}$$

$$L = \frac{1}{I l_1} \int_0^{l_1} \Phi_1(x) dx$$

$$L = \frac{\mu_0 w t_1}{l_1} \left(1 - \frac{\alpha_2 \tanh \alpha_1 l_1}{\alpha_1 l_1 (\alpha_2 + \alpha_1 \tanh \alpha_1 l_1 \tanh \alpha_2 l_2)} \right)$$

FIGURE 1

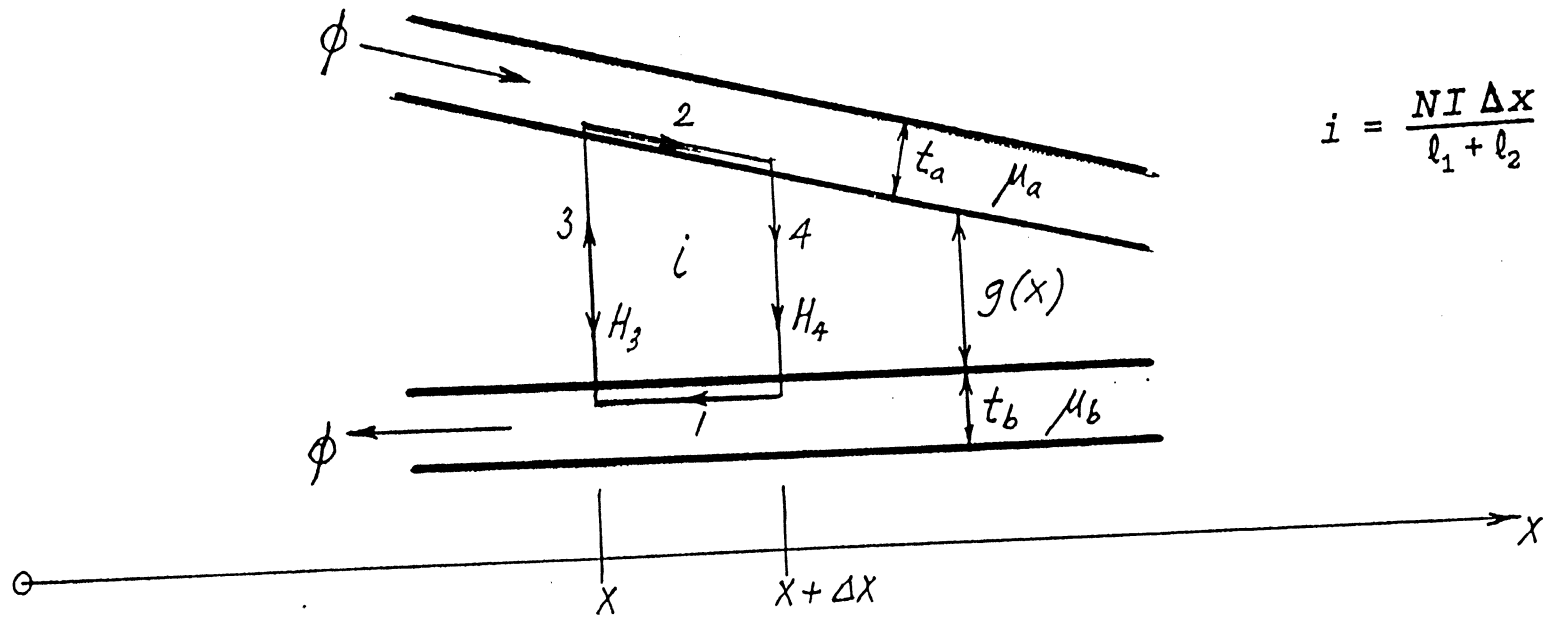


$$w = w_0 - k_w x \quad g = g_0 - k_g x$$

$$w_0 - k_w x$$

$$i = \oint \vec{H} \cdot d\vec{l}$$

$$i = H_1 \Delta x + H_2 \Delta x \sqrt{1+k_g^2} - H_3 g_3 + H_4 g_4$$



$$i = \frac{NI \Delta x}{l_1 + l_2}$$

$$H_1 = \frac{\Phi(x)}{\mu_0 \mu_b t_b w_3} \quad H_2 = \frac{\Phi(x)}{\mu_0 \mu_a t_a w_3} \quad H_3 = \frac{-1}{\mu_0 w_3} \cdot \frac{d\Phi}{dx}(x) \quad H_4 = \frac{-1}{\mu_0 w_4} \cdot \frac{d\Phi}{dx}(x + \Delta x)$$

$$w_3 = w(x) \quad w_4 = w(x) - k_w \Delta x$$

$$g_3 = g(x) \quad g_4 = g(x) - k_g \Delta x$$

$$i = \oint \vec{H} \cdot d\vec{l}$$

$$i = H_1 \Delta x + H_2 \Delta x \sqrt{1+k_g^2} - H_3 g_3 + H_4 g_4$$

$$H_1 = \frac{\Phi(x)}{\mu_0 \mu_b t_b w_3} \quad H_2 = \frac{\Phi(x)}{\mu_0 \mu_a t_a w_3} \quad H_3 = \frac{-1}{\mu_0 w_3} \cdot \frac{d\Phi}{dx}(x) \quad H_4 = -\frac{1}{\mu_0 w_4} \left[\frac{d\Phi}{dx}(x) + \frac{d^2\Phi}{dx^2} \Delta x \right]$$

$$\frac{NI \Delta x}{\ell_1 + \ell_2} = \frac{\Phi(x) \Delta x}{\mu_0 w_3} \left(\frac{\sqrt{1+k_g^2}}{\mu_a t_a} + \frac{1}{\mu_b t_b} \right) + \frac{g_3}{\mu_0 w_3} \cdot \frac{d\Phi}{dx}(x) - \frac{g_4}{\mu_0 w_4} \left[\frac{d\Phi}{dx}(x) + \frac{d^2\Phi}{dx^2} \Delta x \right]$$

$$\frac{1}{t} \equiv \frac{\sqrt{1+k_g^2}}{\mu_a t_a} + \frac{1}{\mu_b t_b}$$

$$\Phi'' + \frac{gk_w - wk_g}{wg} \Phi' - \frac{\Phi}{tg} = -\frac{\mu_0 NIW}{g(\ell_1 + \ell_2)}$$

Sections 1 and 4:

*constant width
& depth*

$$k_w = k_g = 0 \quad \Phi'' - \frac{\Phi}{tg} = -\frac{\mu_0 NIW}{g(\ell_1 + \ell_2)}$$

Section 1:

*Source
Current*

$$\Phi'' - \frac{\Phi}{t_1 g_1} = -\frac{\mu_0 NIW_1}{g_1(\ell_1 + \ell_2)}$$

Section 4:

*No
Source
Current*

$$i = 0 \quad \Phi'' - \frac{\Phi}{t_4 g_4} = 0$$

$$\Phi'' + \frac{gk_w - wk_g}{wg} \Phi' - \frac{\Phi}{tg} = -\frac{\mu_0 NIW}{g(\ell_1 + \ell_2)}$$

Section 2:

*width
decreases*

$$k_g = 0 \quad \Phi'' + \frac{k_w}{w(x)} \Phi' - \frac{\Phi}{t_2 g_1} = -\frac{\mu_0 NIW(x)}{g_1(\ell_1 + \ell_2)}$$

Section 3:

*depth
decreases*

$$k_w = 0, \quad i = 0 \quad g(x) \Phi'' - k_g \Phi' - \frac{\Phi}{t_3} = 0$$

*$\mu_0 NI$
decreases
Current*

$$\Phi(x) = \frac{NI\mu_0}{l_1+l_2} \left\{ a_1 \cosh \alpha_1 x + t_1 w_1 \right\} \quad 0 \leq x \leq l_1$$

$$\Phi(x) = \frac{NI\mu_0}{l_1+l_2} \left\{ a_2 \cdot (w_0 - k_w x) \cdot I_1[\alpha_2 (w_0 - k_w x)] + b_2 \cdot (w_0 - k_w x) \cdot K_1[\alpha_2 (w_0 - k_w x)] + Q(x) \right\}$$

$$Q(x) = - \frac{(w_0 - k_w x)^3}{g_1 k_w^2} \sum_{n=0}^{\infty} \frac{2^{2n+1} n! (n+1)!}{(2n+1)! (2n+3)!} [\alpha_2 (w_0 - k_w x)]^{2n} \quad l_1 \leq x \leq l_1 + l_2$$

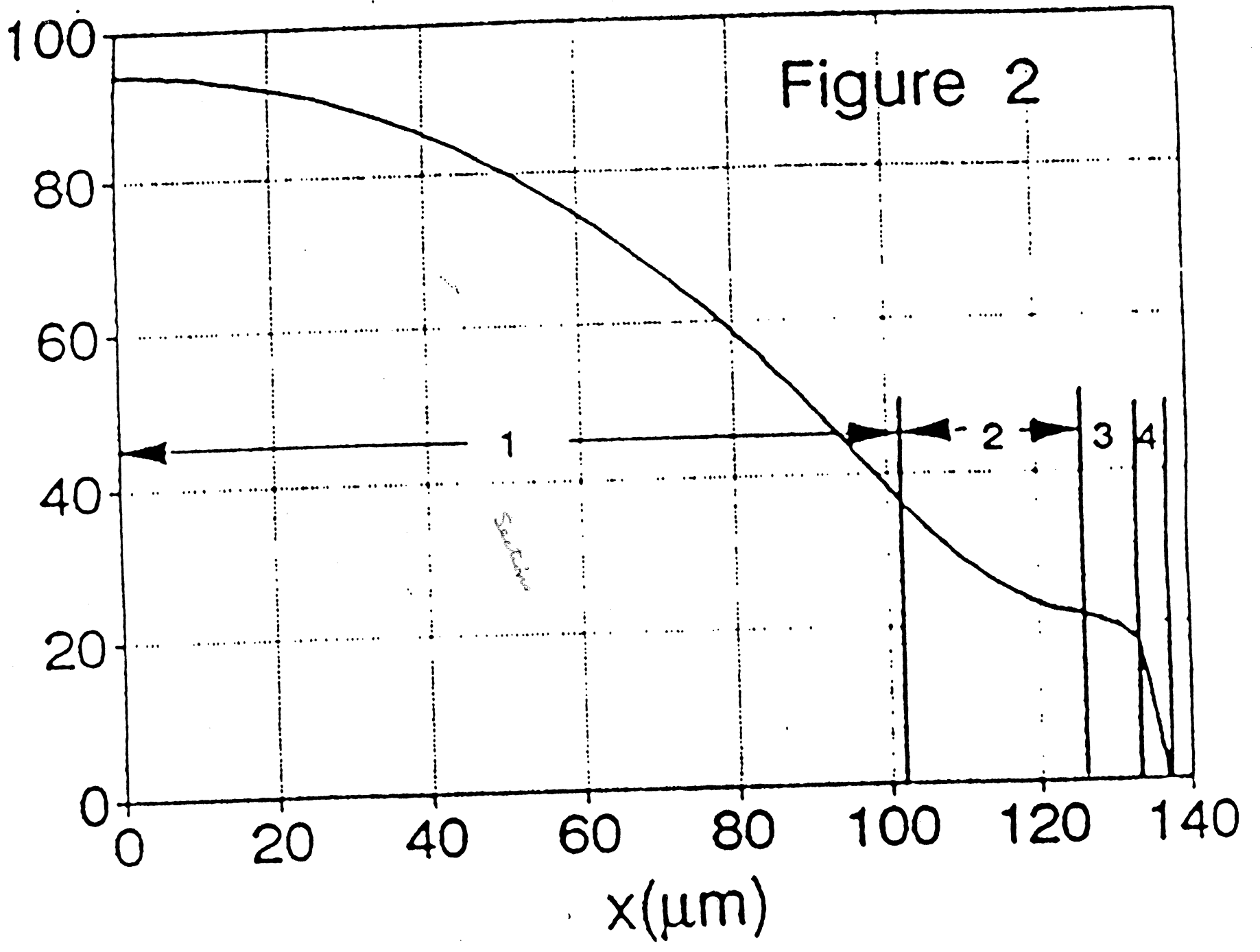
$$\Phi(x) = \frac{NI\mu_0}{l_1+l_2} \left\{ a_3 I_0(2\alpha_3 \sqrt{g_0 - k_g x}) + b_3 K_0(2\alpha_3 \sqrt{g_0 - k_g x}) \right\} \quad l_1 + l_2 \leq x \leq l_1 + l_2 + l_3$$

$$\Phi(x) = \frac{NI\mu_0}{l_1+l_2} \left\{ a_4 \sinh \alpha_4 (l-x) \right\} \quad l_1 + l_2 + l_3 \leq x \leq l$$

$$\alpha_1^2 = (t_1 g_1)^{-1}, \quad \alpha_2 = (t_2 g_1 k_w^2)$$

$$\alpha_3^2 = (t_3 k_g^2)^{-1}, \quad \alpha_4^2 = (t_4 g_4)^{-1}$$

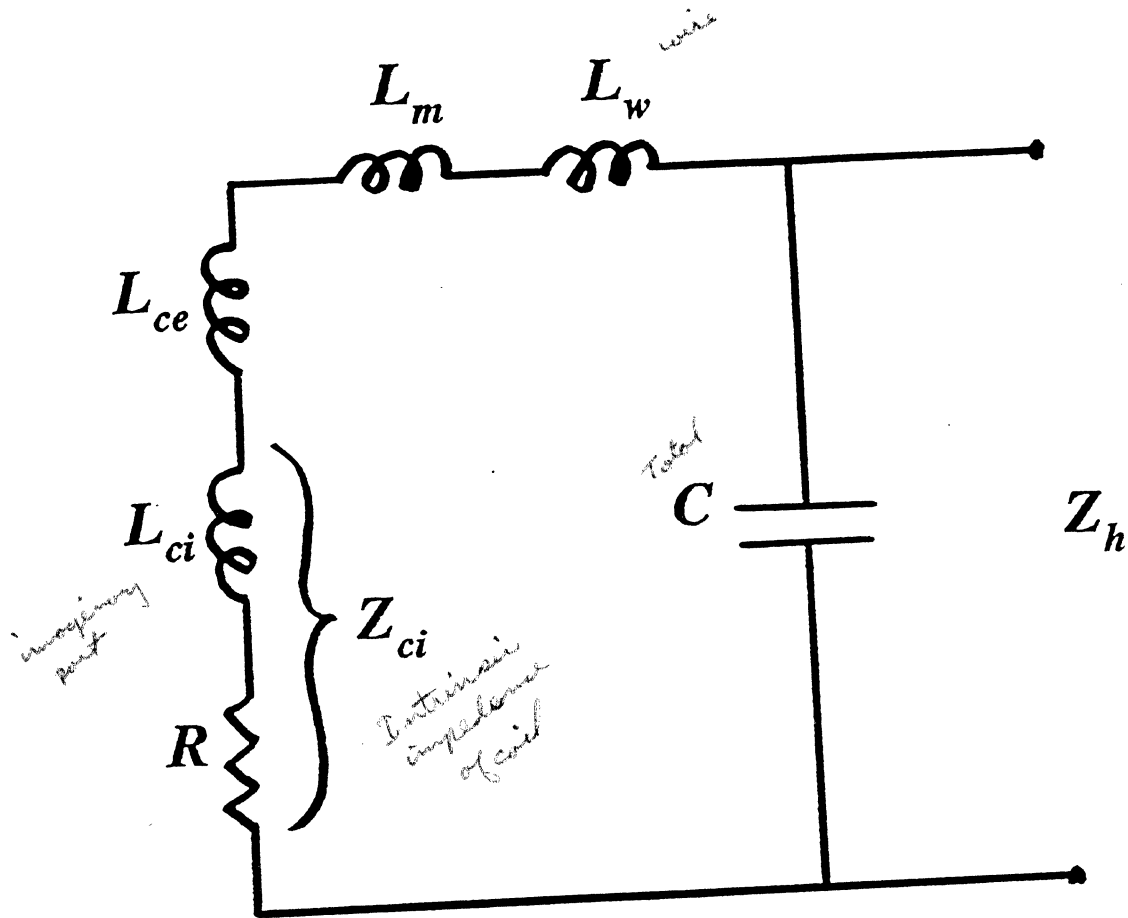
Figure 2



Induktions

$$L_m = \frac{N}{I(l_1+l_2)} \int_0^{l_1+l_2} \Phi(x) dx.$$

$$L_m = \frac{\mu_0 N^2}{(l_1+l_2)^2} \left\{ t_1 w_1 l_1 + \frac{b_2 l_2}{\alpha_2} + \frac{a_1}{\alpha_1} \sinh \alpha_1 l_1 \right. \\ \left. + \frac{1}{k_w} \sum_{n=0}^{\infty} \frac{\alpha_2^{2n+1} (w_1^{2n+3} - w_4^{2n+3})}{2^{2n+1} n! (n+1)! (2n+3)} \left[a_2 + b_2 \left(\gamma + \ln \frac{w_1}{w_4} - \frac{1}{2n+2} - \frac{1}{2n+3} - \sum_{m=1}^n \frac{1}{m} \right) \right] \right. \\ \left. - \frac{2^{2n+1} n! (n+1)! t_2 \alpha_2^{2n+2} (w_1^{2n+4} - w_4^{2n+4})}{(2n+1)! (2n+4)!} \right\}$$



$$L_m = L_m' - jL_m''$$

$$L_{ci} = L_{ci}' - jL_{ci}''$$

$$Z_h = \frac{Z_1}{1 + j\omega CZ_1}$$

$$Z_1 = j\omega(L_{ce} + L_m + L_w) + Z_{ci}$$

$$L_m = L'_m - jL''_m$$

$$Z_1 = j\omega(L_{ce} + L'_m + L_w) + \omega L''_m + Z_{ci}$$

$$L_{ce} = 7N^2 r \times 10^{-7} \text{ H}$$

$$L_w \approx 10^{-7} \text{ H}$$

$$Z_{ci} = R_{dc} \frac{\tau t}{2M} \cdot \frac{[2 + (M-1)(M+3)] \cosh^2 \frac{\tau t}{2} - M^2 + 1}{\sinh \tau t} \quad \text{for odd } M$$

$$Z_{ci} = R_{dc} \frac{\tau t}{2} \cdot \frac{(M+2) \cosh^2 \frac{\tau t}{2} - M}{\sinh \tau t} \quad \text{for even } M.$$

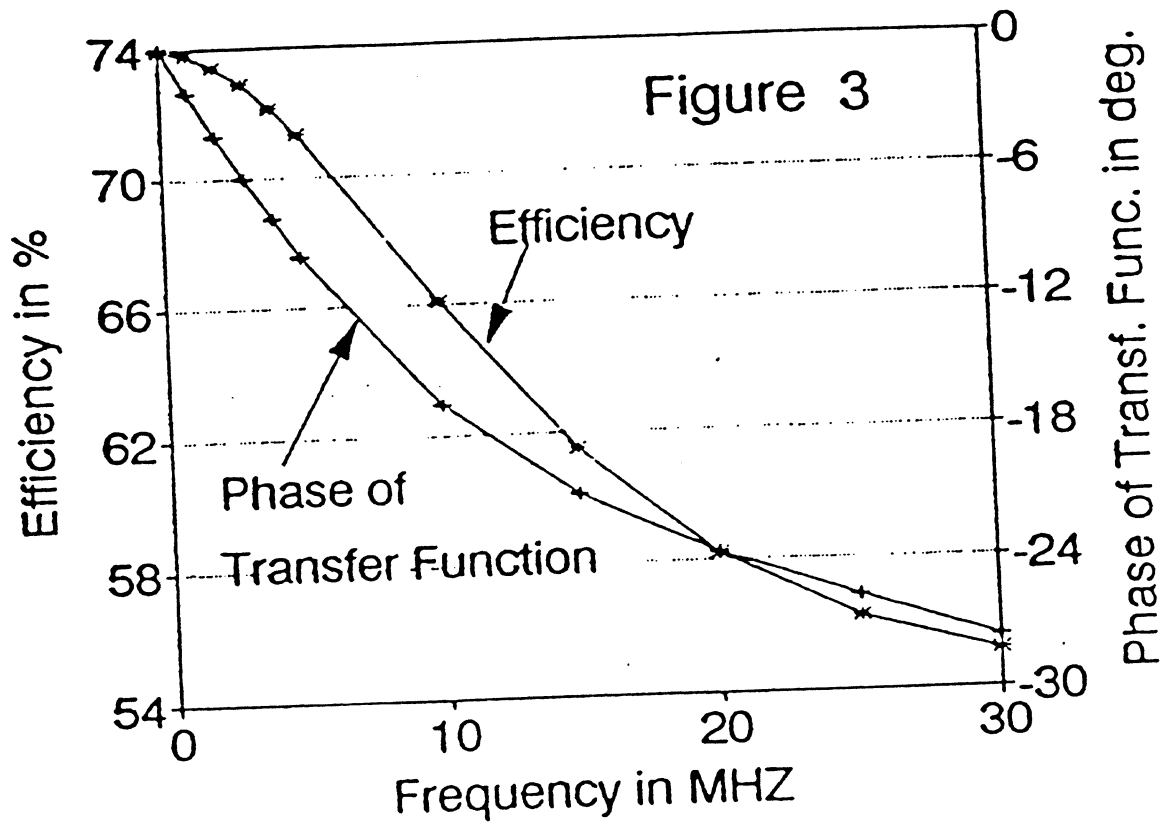
*Elly
Circuit
change*

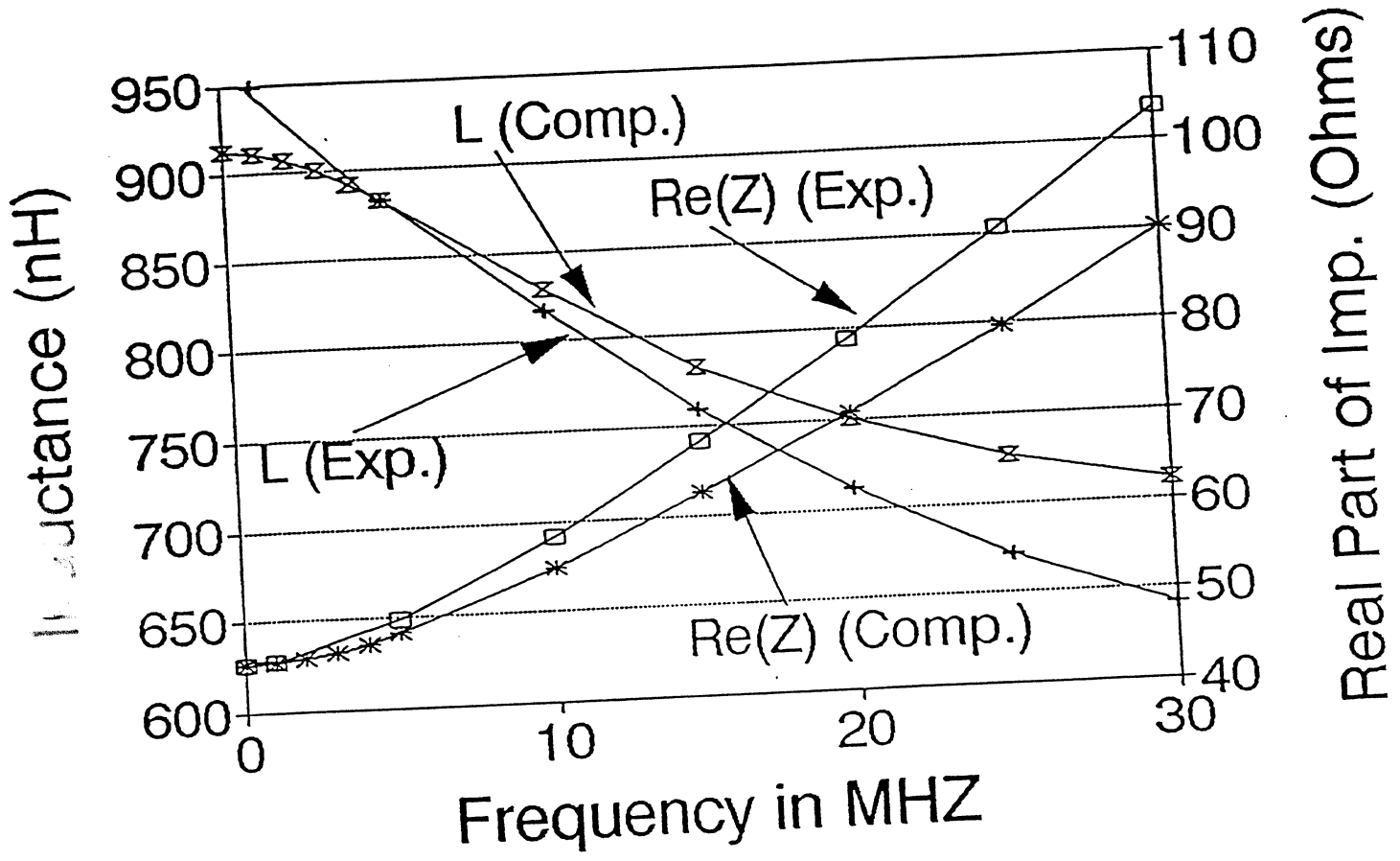
$$I = \frac{I_h}{1 + j\omega CZ_1}$$

$$H_g = \frac{NI\mu_0 a_4 \alpha_4}{w_4 (l_1 + l_2)} = \frac{NI_h \mu_0 a_4 \alpha_4}{w_4 (l_1 + l_2) (1 + j\omega CZ_1)}$$

$$T(\omega) = \frac{H_g g_4}{I_{h,y}} = \frac{N\mu_0 a_4 \alpha_4 g_4}{w_4 (l_1 + l_2) (1 + j\omega CZ_1)}$$

*Does this
make sense
anyway*





RECIPROCITY

$$e(\bar{x}) = -\mu_0 v \int_{-\frac{w}{2}}^{+\frac{w}{2}} dz \int_d^{d+\delta} dy \int_{-\infty}^{+\infty} \frac{dM_x(x-\bar{x})}{d\bar{x}} \cdot \frac{H_x(x, y, z)}{I} dx$$

$$\bar{x} = vt \qquad v = \frac{d\bar{x}}{dt}$$

$$e(t) = -\mu_0 \int_{-\frac{w}{2}}^{+\frac{w}{2}} dz \int_d^{d+\delta} dy \int_{-\infty}^{+\infty} \frac{dM_x(x-vt)}{dt} \cdot \frac{H_x(x, y, z)}{I} dx$$

Sinusoidal magnetization:

$$M_r = M_0 \sin kx, \quad k = \frac{2\pi}{\lambda}$$

$$e(\bar{x}) = -\mu_0 v w M_0 \frac{H_g g}{I} k \delta (e^{-k\delta}) \left(\frac{1 - e^{-k\delta}}{k\delta} \right) \left(\frac{\sin(kg/2)}{kg/2} \right) \cos k\bar{x}$$

$$k = \frac{2\pi}{\lambda}, \quad kv = \frac{2\pi v}{\lambda} = 2\pi f = \omega, \quad k\bar{x} = kv t = \omega t$$

$$(t) = -\mu_0 \omega w M_0 \frac{H_g g}{I} \delta (e^{-k\delta}) \left(\frac{1 - e^{-k\delta}}{k\delta} \right) \left(\frac{\sin(kg/2)}{kg/2} \right) \cos \omega t$$

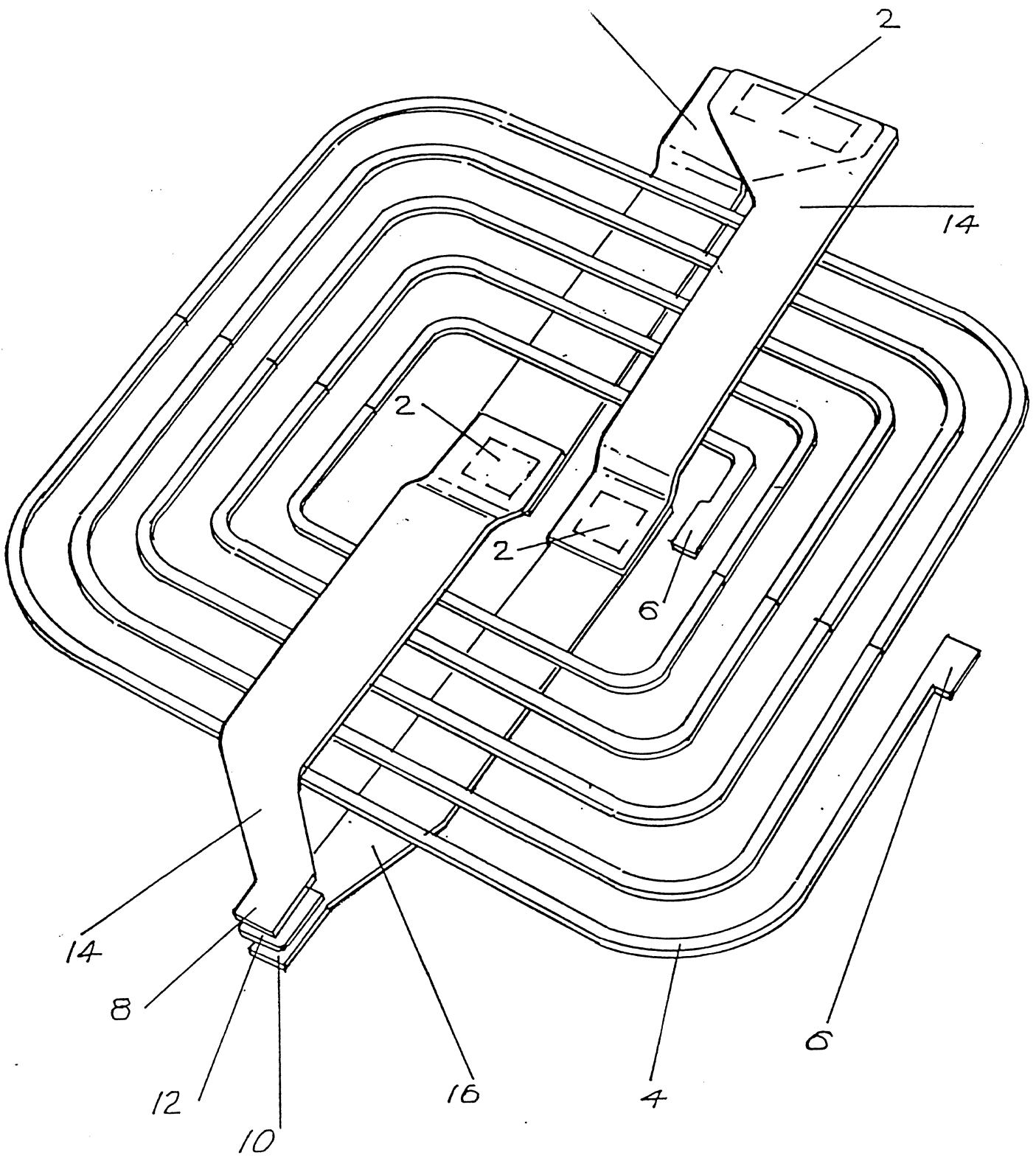


FIGURE 1

"Magnetoresistive Heads"

Mason L. Williams

IBM Corp.

Institute for Information Storage Technology

Santa Clara University, California

December 14 - 16, 1992

Outline

- Magnetoresistance phenomenon
- Unshielded MR read head
- Shielded MR read head
- Signal bias techniques
- Domain stabilization
- Signal and resolution models
- Head-media matching considerations
- Micromagnetic modeling
- State-of-the-art from publications
- References

Magnetoresistance phenomenon

Ordinary Magnetoresistance

Caused by curvature of electron paths by the Lorentz force when the mean free path is larger than the cyclotron radius, the ordinary magnetoresistance increases with the square of the magnetic field perpendicular to the current. This is not the dominant mechanism in NiFe at room temperature.

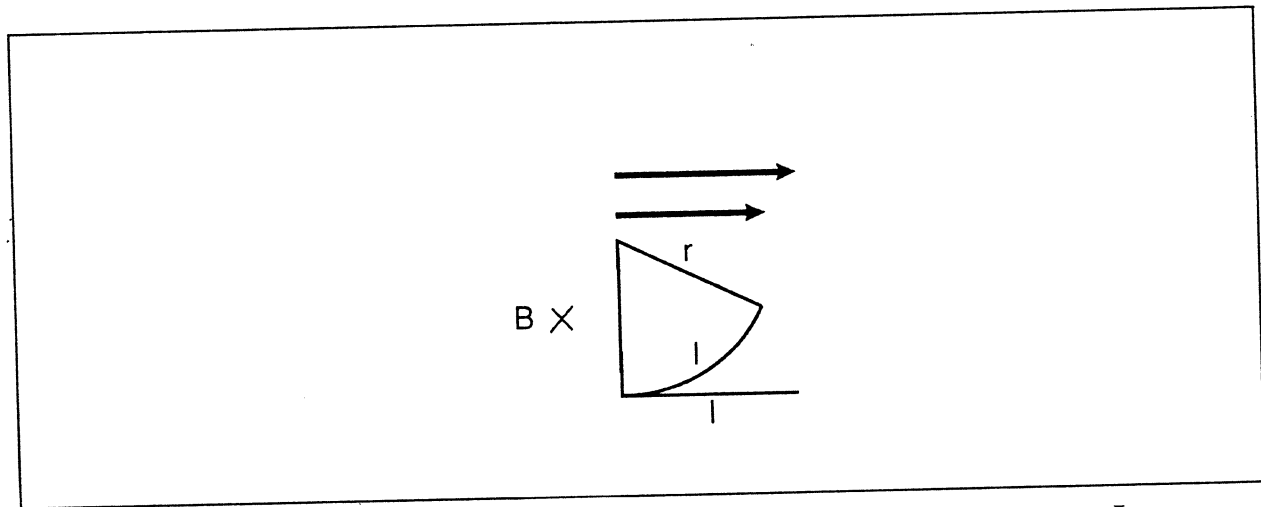


Figure 1. Ordinary resistance increases with square of B normal to J

$$F = qV \times B = mV^2/r$$

$$\frac{\sigma}{\sigma_0} = \frac{mV}{qBl} \sin\left(\frac{lqB}{mV}\right)$$

$$\frac{\sigma}{\sigma_0} \approx 1 - \frac{1}{3} \left(\frac{qB\tau}{m} \right)^2$$

Anisotropic Magnetoresistance in Ferromagnets

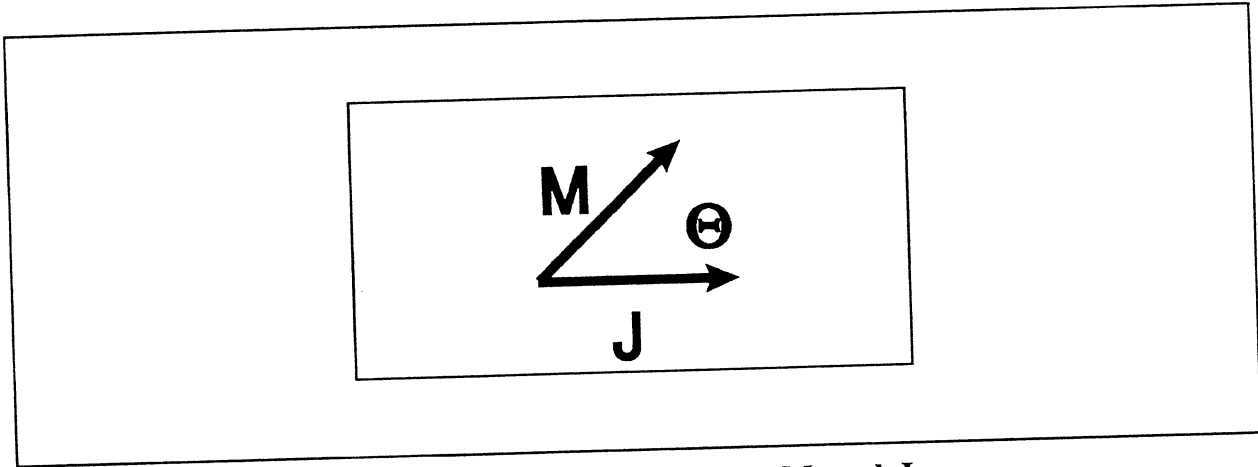


Figure 2. Resistance depends on angle between M and J

Origin In NiFe, conduction is mostly by 4s electrons. The resistance is largely determined by scattering to 3d states, because in the transition metals the 3d shell is not full. In the ferromagnetic state, the 3d up spin states are essentially fully occupied. Spin up 4s electrons (about half the conduction electrons) cannot scatter to 3d states and have longer mean free paths carrying most of the current. The spin-orbit interaction causes the d orbitals to prefer to line up in planes perpendicular to M. The spin down 4s electrons see more vacant d states to scatter into if the current is parallel to M, so the resistance is higher that way. It is almost as if the d electrons were an array of parallel conducting donuts¹.

Magnitude 2 to 4 percent in NiFe alloys, 3-6 percent in NiCo alloys², at room temperature. At liquid hydrogen temperature, 14K, 20 percent is observed.

Giant Magnetoresistance and Spin Valve effect

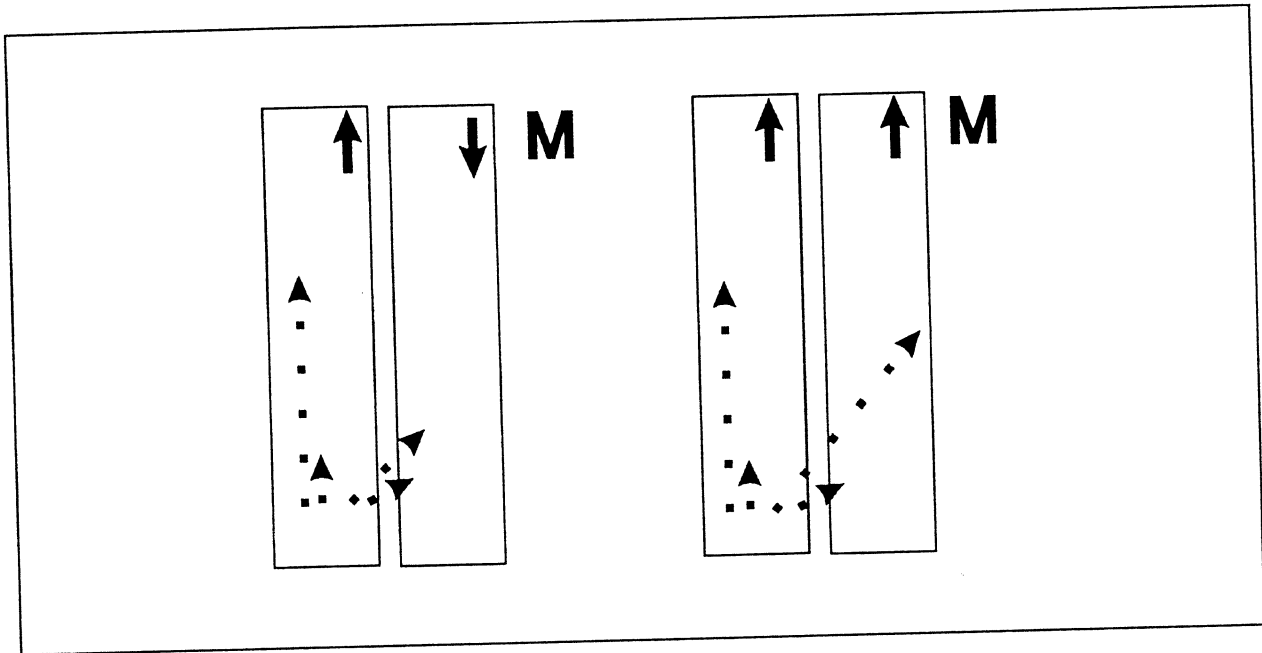


Figure 3. Giant magnetoresistance and spin valve effects

Origin When thicknesses of layers are comparable to the spin up and spin down mean free paths, the probability of 4s electrons crossing the boundaries without spin flipping can be high. The resistance of the sandwich then depends on whether the magnetization in the ferromagnetic films is parallel or anti-parallel. This effect has the highest magnetoresistance at room temperature, but has yet to find practical application in recording sensors.

Magnitude At room temperature, up to about 5 percent for NiFe/Cu/NiFe sandwiches, and 9 percent for Co/Cu/Co sandwiches. Investigation of physics and materials is ongoing.

Unshielded MR read head

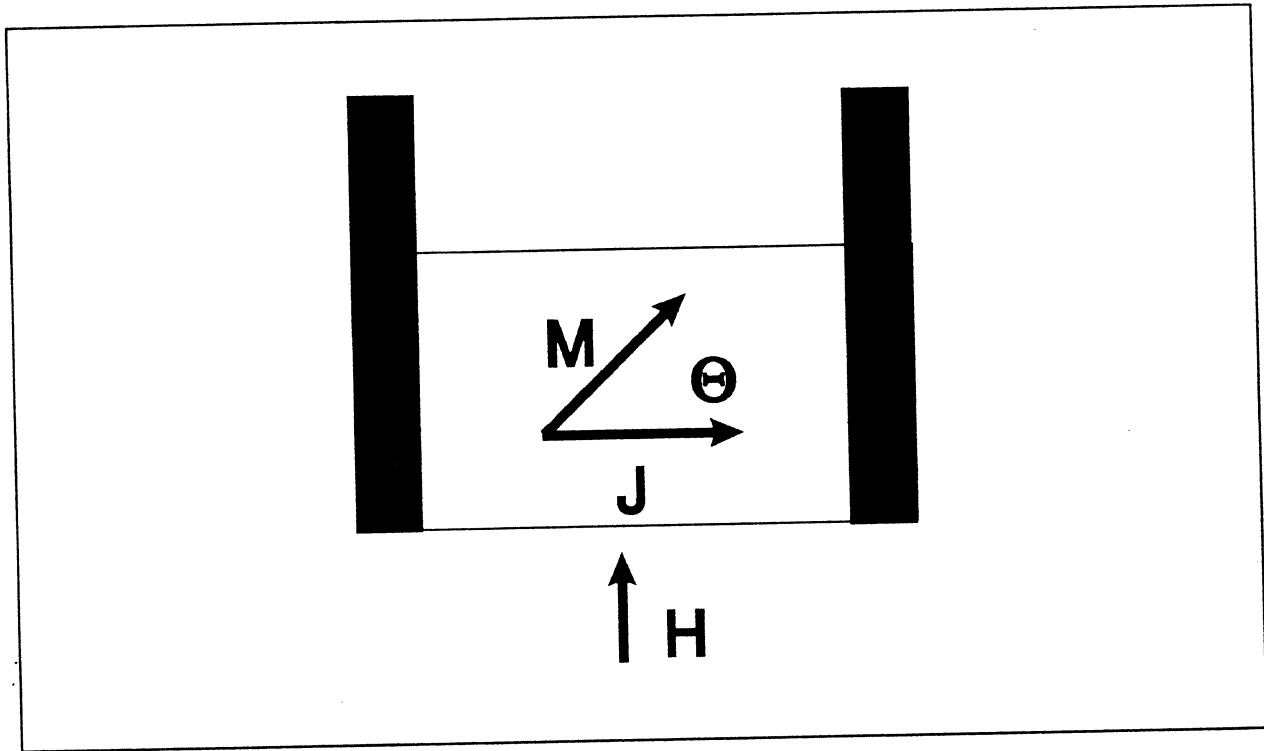


Figure 4. An unshielded MR head

The simplest MR head is just a stripe of NiFe with leads attached³, and perhaps some bias means to be discussed below. A constant current is applied, the field from the disk or tape rotates M and the signal voltage is observed across the sensor. Denoting the angle between M and J by Θ ,

$$\rho = \rho_0 + \Delta\rho \cos^2\Theta$$

- Advantages

- Simplicity
- Large signal
- Disadvantages
 - Resolution limited by size of the stripe. Although equalization can trade off the signal advantage for recovery of linear density¹⁰, adjacent track cross talk makes the approach only practical for low track densities.

Shielded MR read head

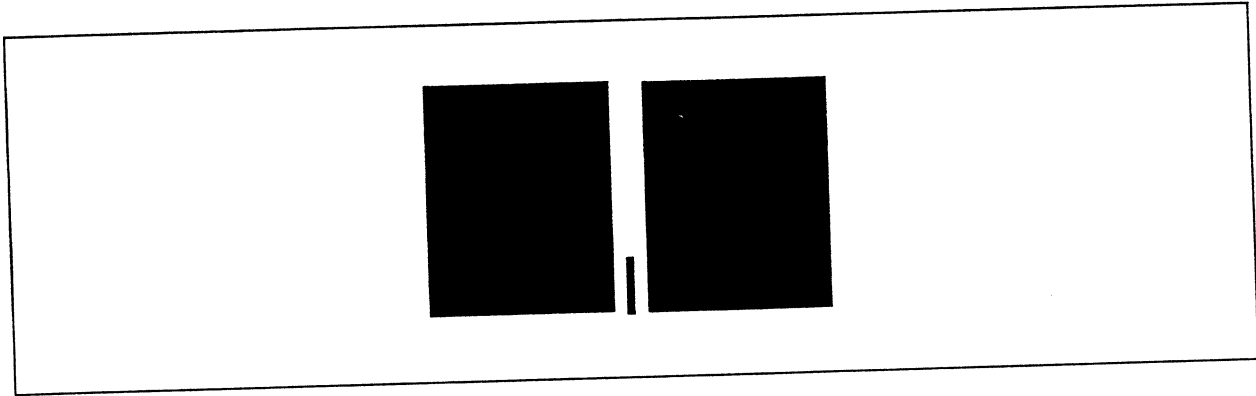


Figure 5. A shielded MR head

The shielded MR head was discussed by Potter⁴. In this head, the NiFe shields increase the resolution by preventing flux from transitions far from the gap from reaching the sensor element. The linear resolution of a shielded MR head is similar to that of an inductive ring head which has a gap about half of the shield to shield distance. Details below. Variations include

- Integrated head, in which the shields are the poles of a write head.
- Piggyback, or dual-element, head⁵, in which a write head is fabricated on top of the shielded head. At the cost of complexity, advantages are less disturbance of sensor by the write process and the ability to separately optimize read and write gaps and trackwidths.

- Recessed sensor fluxguide heads with vertical current routing were discussed by Sony⁸ at Intermag '88. Advantage is metal at gap may be grounded at a cost of read efficiency due to shorting of the lowest part of the sensor.

Yoke MR heads

The presence of an electrically active element at the head media interface introduces concerns about wear, corrosion, and shorting. Yoke MR heads⁶ locate the sense element in a second gap in the magnetic path of a ring head or pole head.

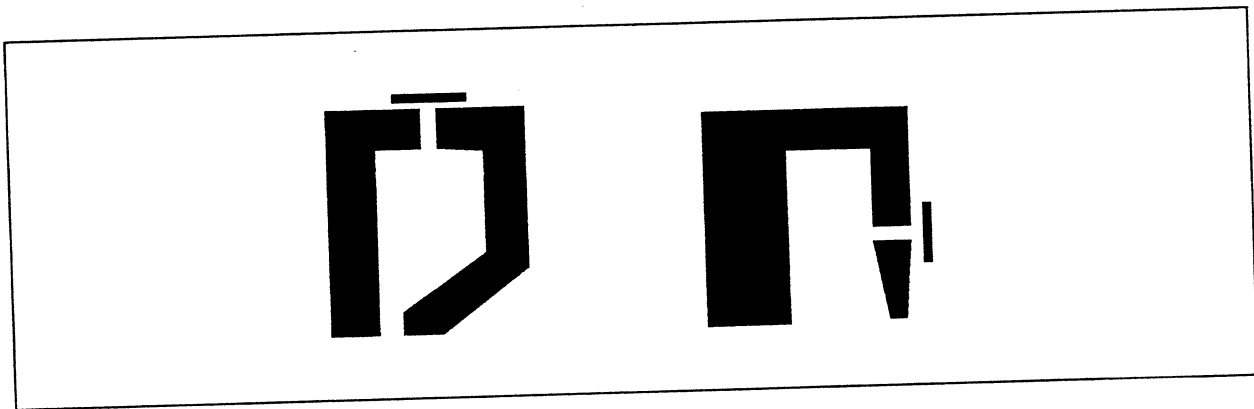


Figure 6. Yoke MR heads

- Advantages
 - Element safely encapsulated
 - Wider choice of materials
 - Element size decoupled from bit cell size somewhat

- Disadvantages
 - Lower efficiency (less signal)
 - Domain stabilization problems for yoke
 - Ring head may be sensitive to stray fields

Signal bias techniques

Recall that where Θ is the angle between M and J ,

$$\rho = \rho_0 + \Delta\rho \cos^2\Theta.$$

If the MR effect is only 1 or 2 percent, we can ignore the second changes in current density due to ρ variation, and write the power dissipation as

$$I^2\Delta R = \int J^2\Delta\rho \cos^2\Theta.$$

For uniform rotation, we can set the resistance nominal at $\Theta = 0$, note that $M_y = M_s \sin \Theta$, so that

$$\frac{\Delta R}{R} = - \left(\frac{M_y}{M_s} \right)^2 \left(\frac{\Delta\rho}{\rho} \right).$$

For roughly linear response from the sensor, some "transverse" bias must be provided. In practice, the parabola reverses curvature and breaks to lower slope before total saturation due to local saturation caused by non uniform excitation and biasing. Biasing at the inflection point provides minimum second harmonic distortion. Some of the transverse (signal direction) bias approaches are:

Conductor bias

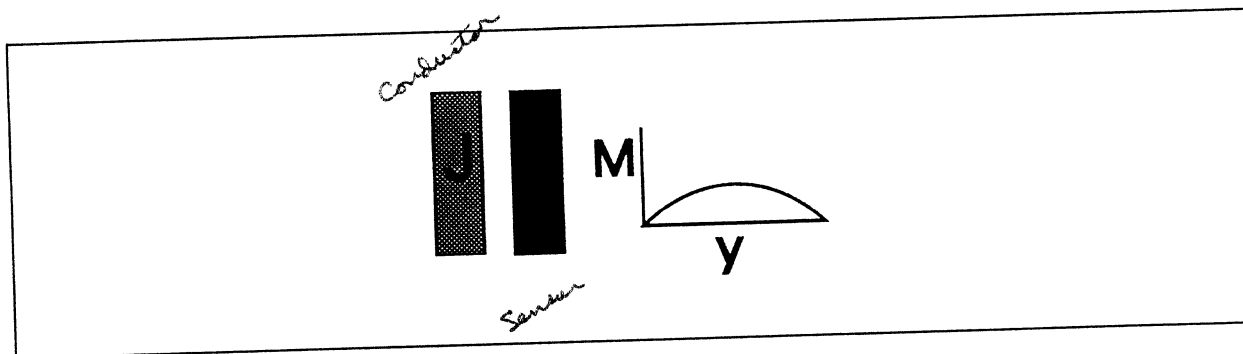


Figure 7. Conductor bias sensor cross section

Large current is required for effective bias. For close spacing, bias at bottom is less than half that in the center. May become shunt bias accidentally.

Shunt bias

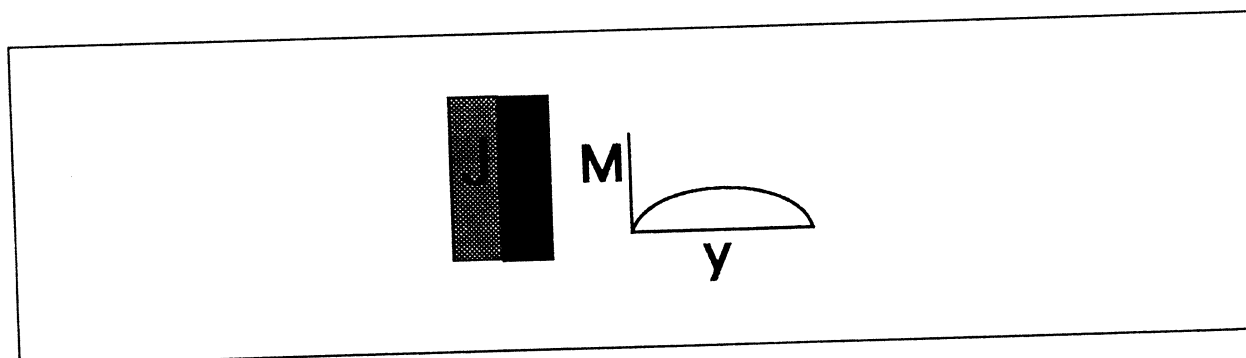


Figure 8. Shunt bias sensor cross section

This is current bias with electrical contact between the conductor and the sensor. Some of the sense current is shunted to one side of the sensor to break the symmetry and provide a net transverse bias. This has the problems of conductor bias with

an added loss of signal power due to the partial shorting of the sensor.

Soft film bias

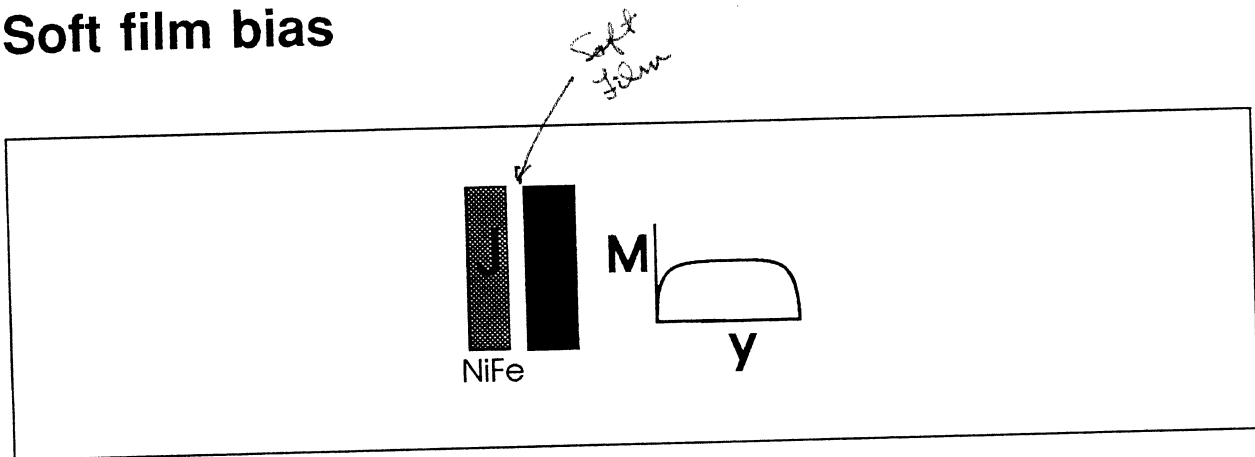


Figure 9. Soft film bias sensor cross section

More uniform and efficient biasing is provided by this scheme. The soft film acts to reduce demagnetization of the biased sensor by providing flux closure. The sandwich acts somewhat like a flat toroid with two air gaps. More exact analysis shows the bias flux roughly constant over the sensor except for top and bottom regions which have characteristic lengths of

$$\lambda = \sqrt{\mu st/2} ,$$

where t is the sensor thickness and s is the spacing between magnetic films. Best operation of this scheme is obtained by thinning the soft film so that it just saturates at the current which places the sensor film at the correct bias angle. This avoids most loss of signal flux to the soft film. Of course, high

resistivity in the soft film is desirable to minimize signal shunting.

Barber Pole bias

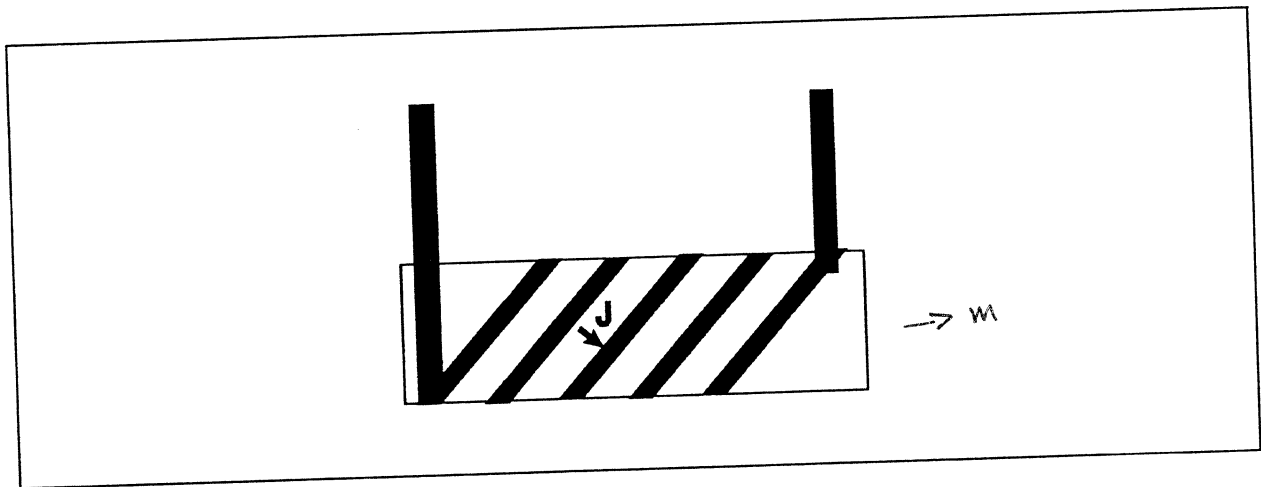


Figure 10. Barber Pole sensor geometry

In the barber pole scheme, rather than bias M at an angle to the stripe, one slants J by introducing an array of shunting conductor bars at a 45 degree angle to the stripe. The sensor current will be almost perpendicular to each conductor bar. The sense current flowing through the shunting bars also provides some longitudinal bias, which we will see is desirable for noise suppression. The disadvantages are loss of signal from the shorted areas, and tight lithography requirements.

Domain stabilization

For reliable data detection, it is important that the sensor always respond the same to the same flux excitation. Sensor linearity is desirable if equalization and maximum likelihood detection schemes are expected to work well. A few principles¹¹:

- Magnetization rotation is fast and linear
- Domain walls nucleate and move in complicated, irregular ways
- Reversal of Neel wall sense during remagnetization can be noisy
- Two domain patterns can carry the same vertical flux, differ in R
- It is best to ensure single domain behavior in the sensor region.

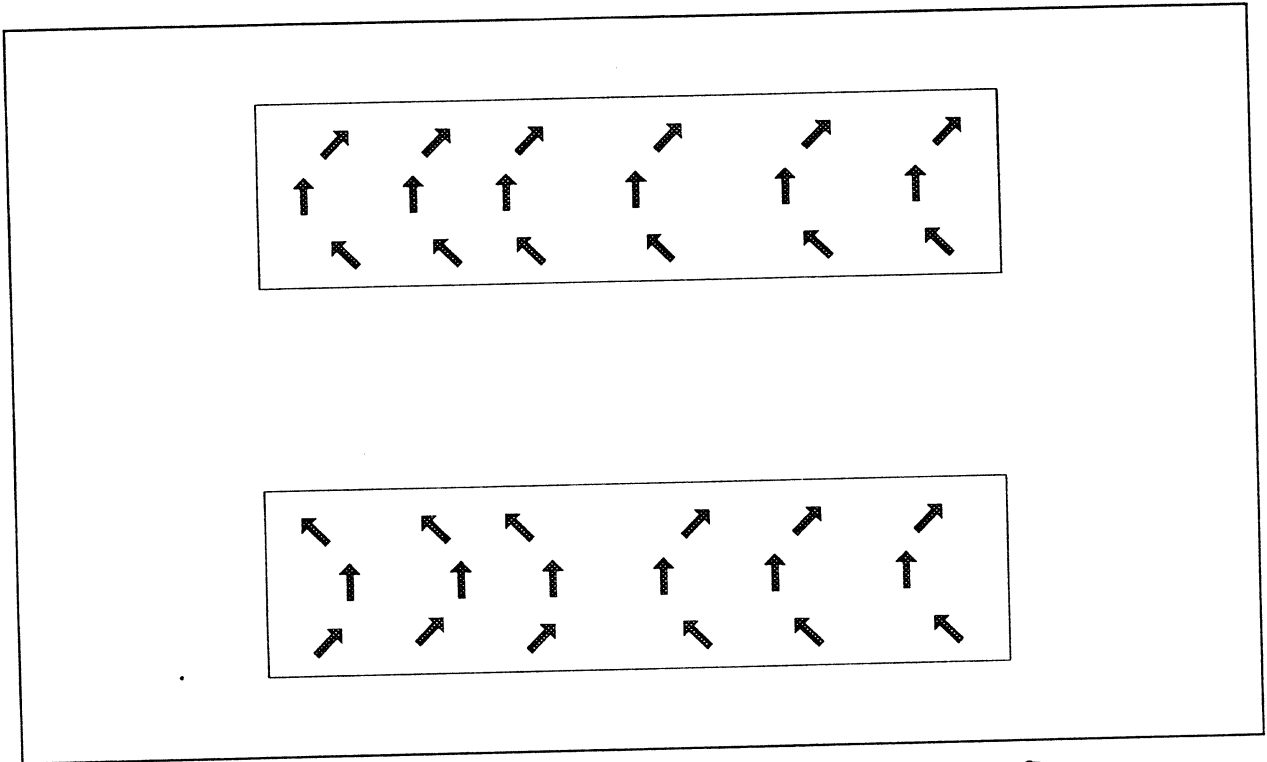


Figure 11. Undesirable multiple magnetic states for same disk flux

Methods for stabilizing domains:

- Longitudinal bias fields
- Reduce demagnetization that encourages domain formation
 - Long sensor with gradual taper to single domain width
 - Picture frame closure

- Exchange bias to an antiferromagnetic film (e.g. FeMn)
- Avoid over control- it results in loss of signal

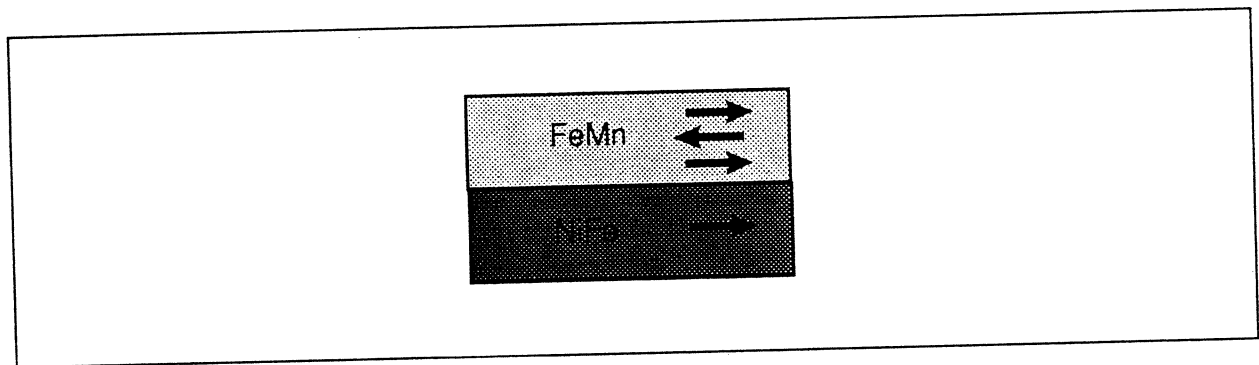


Figure 12. Exchange bias to an antiferromagnetic film

Signal and resolution models

With the assumption that biasing makes an MR sensor linear, a reciprocity relation can be used to simplify calculating the sense signal. The inductive head reciprocity equation gives the derivative of flux through the head coil as the integral of $\frac{dM}{dx}$ times the head field produced by a unit current. We are interested in the flux in the sense element, so we place a fictitious thin coil about the sense element and integrate once to get

$$\phi(x) = -W_t \int_{-\infty}^{\infty} \int_d^{d+\delta} \frac{dM}{dx} (x-x',y) \times mmf(x',y) dy dx'$$

where $mmf(x,y)$ is the scalar potential below the head with unit current in the imaginary coil. For improved accuracy, we can vary the current density in the coil in the same way that sensor bias varies with position.

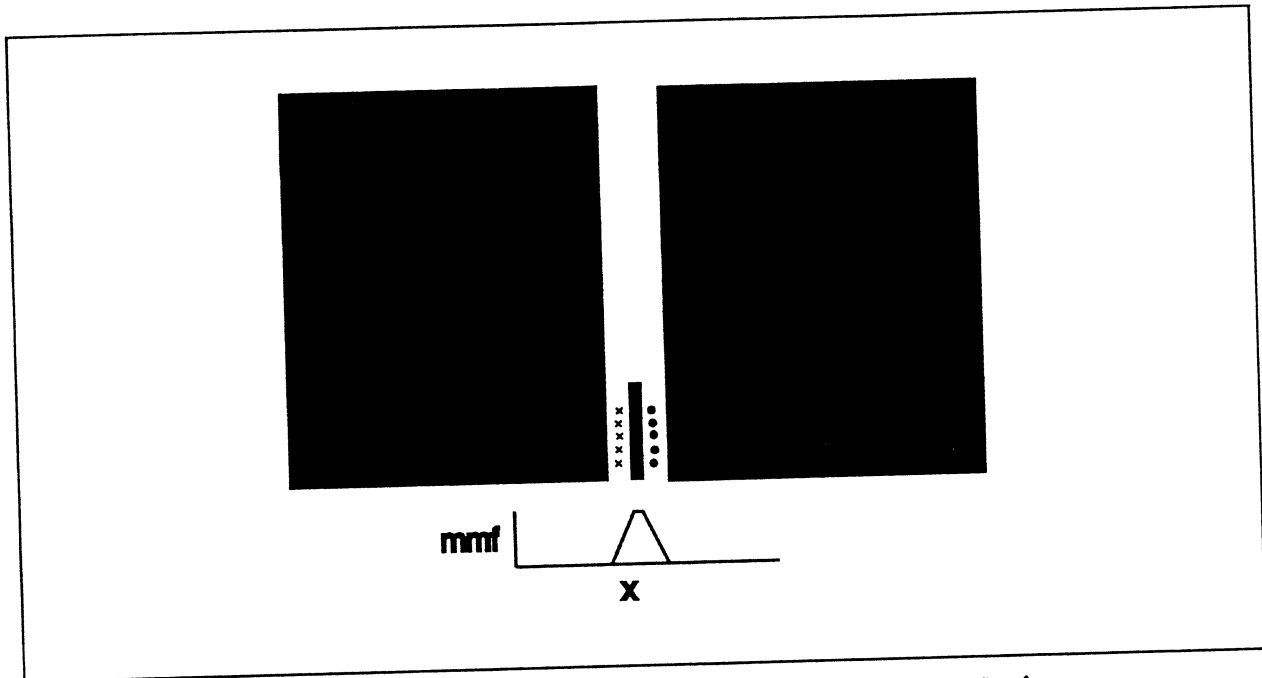


Figure 13. Fictitious coil and resultant mmf for signal calculation

For evaluation of peak detection margins, it is useful to be able to calculate the response of the head to a series of equally spaced transitions. That response is the convolution of the head mmf at the head surface (a trapezoid, roughly) with the closed form¹² of the sum of an alternating series of Lorentzians of half-amplitude width $p = 2(y + a)$, spaced s apart:

$$\frac{\left(\frac{\pi p}{2s}\right) \sinh\left(\frac{\pi p}{2s}\right) \cos\left(\frac{\pi x}{s}\right)}{\cosh^2\left(\frac{\pi p}{2s}\right) - \cos^2\left(\frac{\pi x}{s}\right)}$$

The convolution is easily done by multiplying the FFT's. The roll-off curve can be obtained by convolving the trapezoid with the preceding function and evaluating at $x=0$.

More exact results can be obtained using a two or three dimensional magnetics modeling program to directly calculate flux in the sensor from one or more transitions.

Sensor height considerations

In addition to the non-uniformity of bias applied to the sense element, signal is limited by the non-uniformity of signal flux which, applied at the bottom, leaks to the shields. It's worth looking in some detail at this because similar phenomena pop up often in MR heads. Note this effect is already taken care of if you use a magnetic modeling program and the reciprocity technique described above.

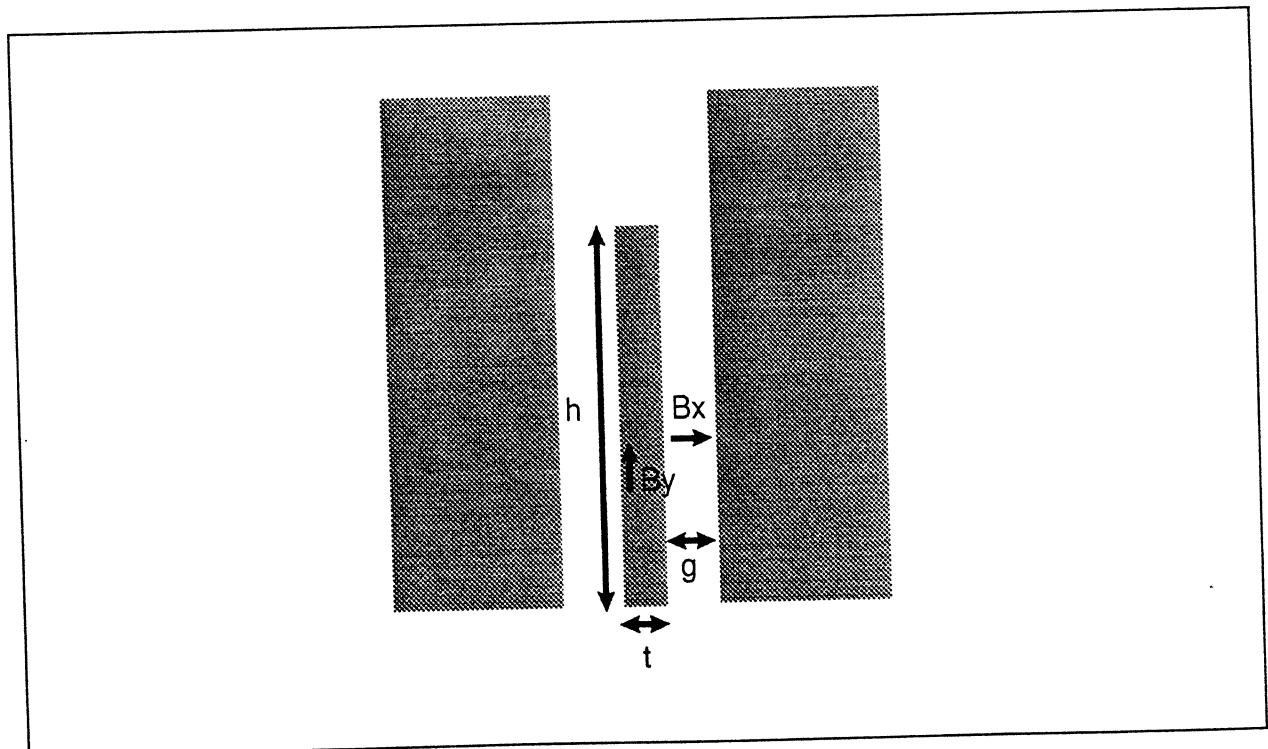


Figure 14. Leakage of flux from sensor to shield

$$B(y) = \mu H(y)$$

$$H_y = - \frac{d\phi}{dy}$$

$$H_x = \frac{\phi}{g} = B_x$$

$$t \frac{dB_y}{dy} = 2B_x = 2 \frac{\phi}{g}$$

$$B_y = - \mu \frac{d\phi}{dy} = - \frac{\mu g t}{2} \frac{d^2 B_y}{dy^2}$$

or

$$\frac{d^2 B_y}{dy^2} = - \frac{1}{\lambda^2} B_y$$

where

$$\lambda = \sqrt{(\mu g t / 2)}.$$

With the boundary condition $B_y = 0$ at $y = h$,

$$B_y = \frac{B_0 \sinh\left(\frac{h-y}{\lambda}\right)}{\sinh\left(\frac{h}{\lambda}\right)}$$

Sensors higher than λ are inefficient. For large lambda, there is at least a factor of two loss in resistance change due to this non uniform excitation compared to the saturation values, in addition to the loss due to non uniform bias.

Head-media matching considerations

With inductive heads, the linear response allows larger signals to be obtained from higher moment/area media, only limited by the tradeoff with linear density due to demagnetizing fields.

With magnetoresistive heads, it is necessary to design the head/medium system together to insure maximum signal while avoiding distortion from overdriving. Roughly, the moment per unit area of the medium should be matched to that of the sensor layer.

The signal power to noise power ratio is an important parameter for low on track error rates. The signal energy $\frac{V^2}{R} \tau_{bit}$ must be several times kT for reliable detection. Engineers usually refer to the noise voltage of a sensor being proportional to $\sqrt{RkT(\Delta f)}$. If we maintain saturated operation of the sensor, the energy signal to noise ratio goes like

$$\frac{\frac{V^2}{R} \tau}{kT} = \frac{I^2 R \left(\frac{\Delta R}{R} \right)^2}{kT \Delta f}.$$

Here, we see that in addition to $\frac{\Delta R}{R}$ being important, the signal to noise ratio is proportional to the total dc power dissipated. This means that a thicker sensor, requiring a thicker medium, can provide more signal power at the same current density, a similar result to the inductive situation, but not identical. Note that the signal power is proportional to the input power. One

must take into account the thermal design of a head as well as be careful of electromigration current density limits. Note that the sense current in many designs cannot be adjusted at the last minute without resultant non-optimum biasing of the sense element.

The lower limit to sensor thickness is found when the apparent resistivity rises due to dominance of surface scattering, and must be found experimentally.

Micromagnetic Modelling

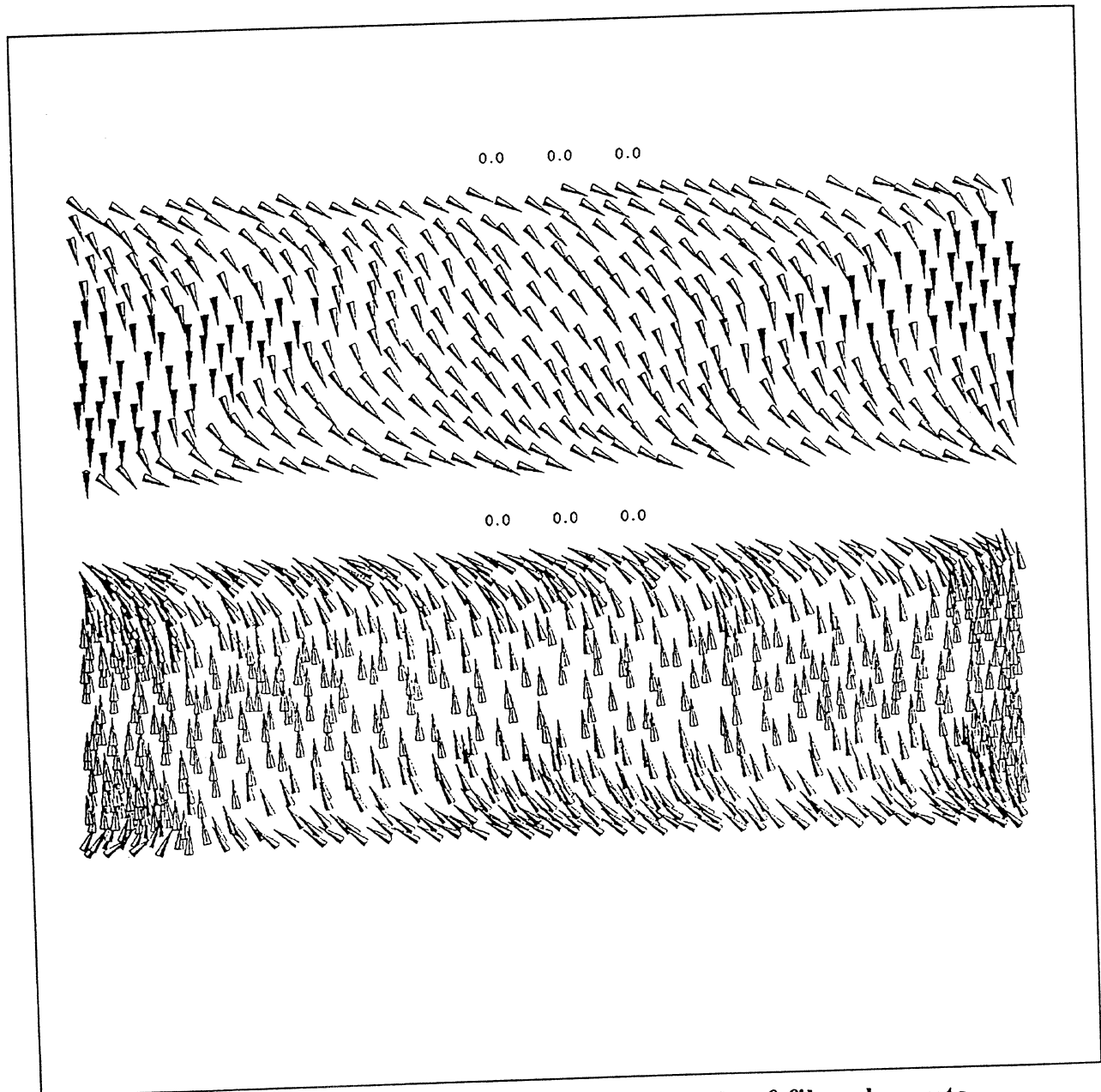


Figure 15. Micromagnetic modelling of sensor and softfilm elements

Micromagnetic modelling is possible on today's work station computers, and is necessary for detailed understanding of track profiles.

This figure by courtesy of T. R. Koehler, IBM Research Division

State of the art from publications

At Intermag '90, C. Tsang, *et al*, of IBM reported demonstration of Gigabit/ square inch recording with error rate testing as a function of off-track head positioning⁹. Signals were as high as 250-300 microvolts per micron of trackwidth. Some of the parameters were:

Trackwidths

2.5 to 4.5 micron

Write gap

0.4 micron

Write poles

4 micron thickness

Read gap

0.25 microns

Stripe height

1 micron or less

Current

5 ma

Flying

About 60 nm

Disk Moment

0.0007 emu/sq cm

Hc

1800 Oe

-3dB density

3900 fc/mm

-6 dB density

4900 fc/mm

At Intermag '91 Hitachi reported MR heads with density capability estimated to be 2 Gb/ sq inch.

Published Magnetoresistive Head Activity

Product Supplier	Activity
Read-Rite, Milpitas, CA	MR program for 250-450 Mb/sq.in.
Rocky Mountain Magnetics, Louisville, CO	MR head program for 300 Mb/sq.in.
AMC, Goleta, CA	Second generation (merged) MR head design
Seagate, Scotts Valley, CA	80 MB 2.5 inch disk drive product announced, MR heads at 160 Mb/sq.in.
IBM AdStaR, San Jose, CA	2.0 GB 3.5 inch disk drive with next generation MR heads at 260 Mb/sq. in.
Dastek, San Jose, CA	MR head development activity with H.P., Palo Alto, CA

This table by courtesy of R. A. Scranton, IBM Adstar¹³.

Next Generation Magneto-resistive Heads

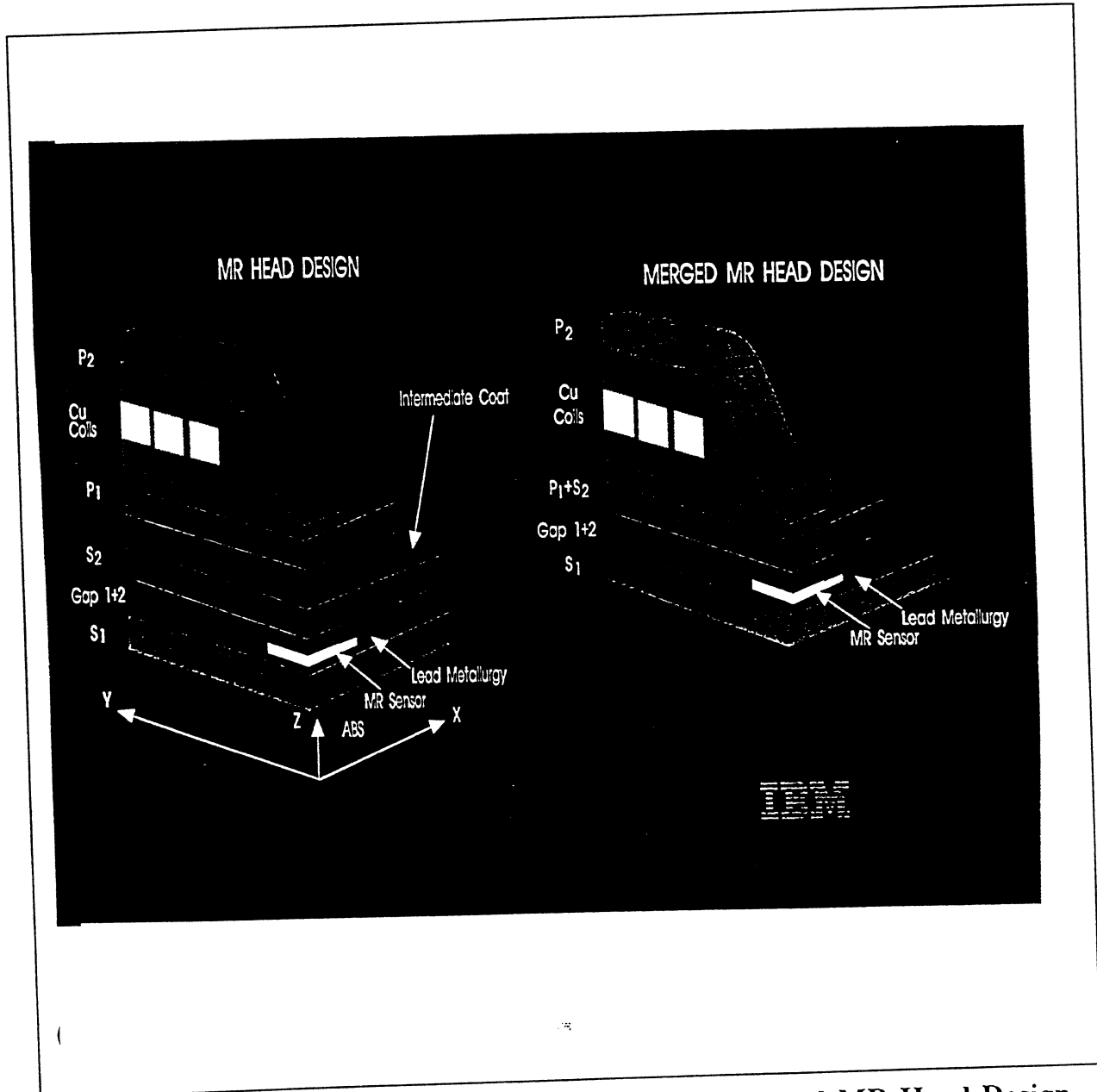


Figure 16. First generation MR Head Design and Merged MR Head Design

This information by courtesy of R. A. Scranton, IBM Adstar¹³.

Magnetic Head Perspective

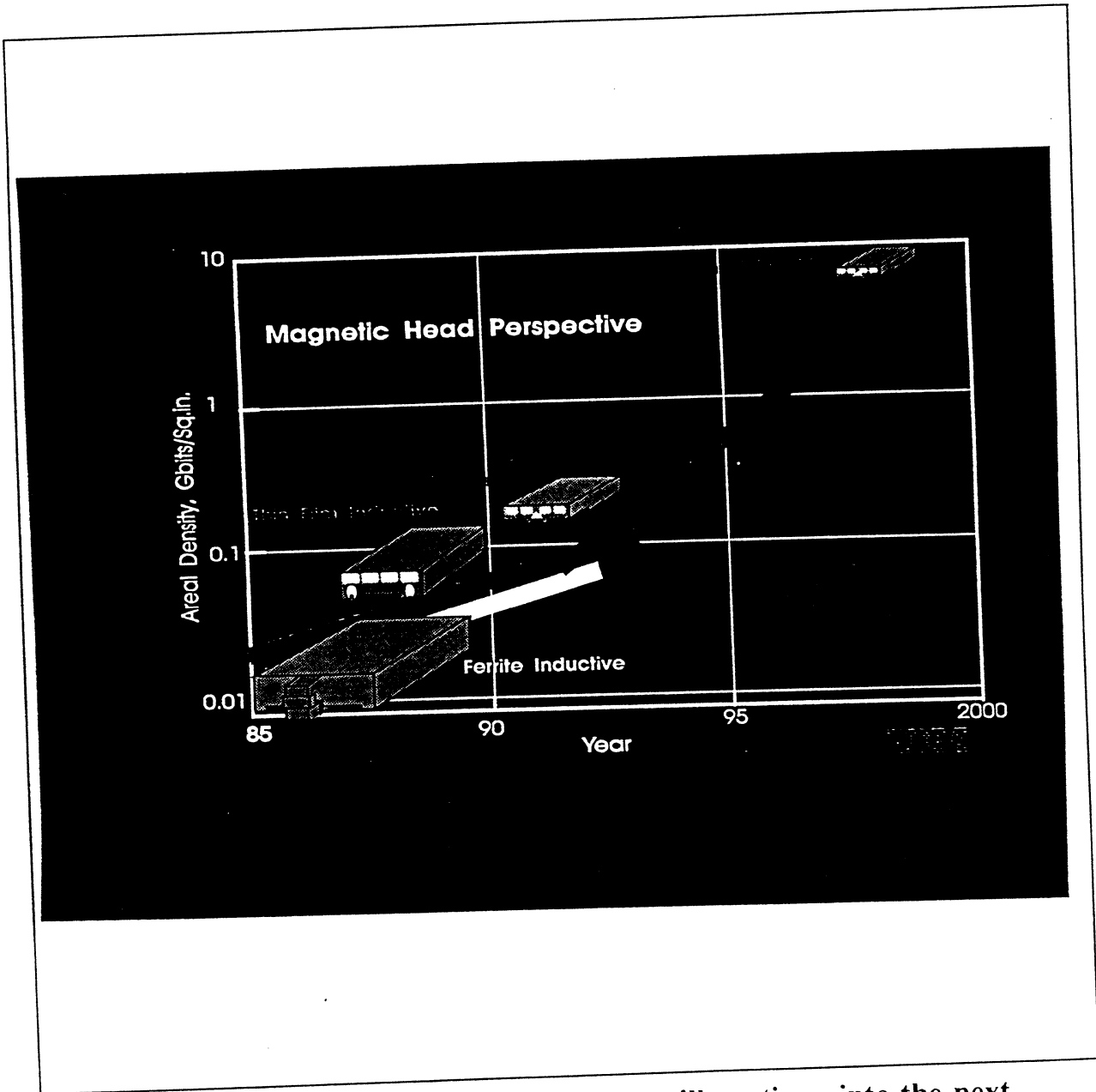


Figure 17. Magnetoresistive head technology will continue into the next century

This chart by courtesy of R. A. Scranton, IBM Adstar¹³.

Misc definitions

Parameter	Definition
H_k	The applied field necessary to rotate the magnetization to a right angle from the easy axis is called the anisotropy field.
M_s	The saturation magnetization is reached when large fields are applied
μ	The slope of the hard axis curve, $4\pi M_s/H_k$.
J	Current density in A/m^2

Reminder on units

- Magneticians like to use cgs-Gaussian units in which the unit of electrical potential is the abvolt (10 nV). Don't bother. Just use cgs-emu until you get to an electric circuit, then convert to SI as follows.
- All you need to know about units

CGS-emu Quantity	Equals
1.2566 Oe	1 A/cm (1.2566 is $4\pi/10$)
10 KGauss	1 Volt second/square meter
1 Oe	1 Gauss
1 <i>emu/cm³</i>	1 Gauss

All you need to know about Maxwell's equations (from a cgs viewpoint)

$$\vec{B} = \vec{H} + 4\pi\vec{M}$$

$$\nabla \cdot \vec{B} = 0$$

$$\nabla \times \vec{H} = \vec{J}$$

$$\vec{B} = \mu\vec{H}$$

General References

1. J. Smit, "Magnetoresistance of Ferromagnetic Metals and Alloys at Low Temperatures", *Physica*, vol 17, 612 (1951)
2. H. C. Van Elst, "The Anisotropy in the Magneto-resistance of some Nickel Alloys", *Physica*, vol 25, 708 (1959)
3. R. P. Hunt, "A Magnetoresistive Readout Transducer", *IEEE Transactions on Magnetics*, vol MAG-7, 150 (1971)
4. R. I. Potter, "Digital Magnetic Recording Theory", *IEEE Transactions on Magnetics*, vol MAG-10, 502 (1974)
5. C. H. Bajorek, *et al*, "An Integrated Magnetoresistive Read, Inductive Write High Density Recording Head", *20th Annual AIP Conf. Proceedings*, no 24. 548 (1974)
6. W. F. Druyvesteyn, *et al*, "Magnetoresistive Heads", *IEEE Transactions on Magnetics*, vol MAG-17, 2884 (1981)
7. C. Tsang, "Magnetics of small magnetoresistive sensors", *J. Appl. Phys.*, vol 55, 2226 (1984)

8. H. Suyama, *et al*, "Thin Film MR Head for High Density Rigid Disk Drive", *IEEE Transactions on Magnetics*, vol 24, 2612 (1988)
9. C. Tsang, *et al*, "Performance Study and Analysis of Dual-element Head on Thin-Film Disk for Gigabit-Density Recording", *IEEE Transactions on Magnetics*, vol 26, 2948 (1990)
10. F. Jeffers and H. Karsh, "Unshielded Magnetoresistive Heads in Very High Density Recording", *IEEE Transactions on Magnetics*, vol 20, 703 (1984)
11. C. Tsang and S. Decker, "The origin of Barkhausen noise in small permalloy magnetoresistive sensors", *J. Appl. Phys.*, vol 52, 2465 (1981)
12. R. Comstock and M. Williams, "Frequency Response in Digital Magnetic Recording", *IEEE Transactions on Magnetics*, vol MAG-9, 342 (1973)
13. R. A. Scranton, "MR Technology and Future Designs", *8th Annual Rigid Disk Head/Media Technology Review*, Spon-

sored by Peripheral Research Corporation and Don Mann
Magnetics, Las Vegas, Nevada, November 15, 1992

"Silicon Planar Heads"

Jean-Pierre Lazzari

Silmag

Institute for Information **S**torage **T**echnology

Santa Clara University, California

December 14 - 16, 1992



C.E.N.G. - B.P. 85 X
F 38041 Grenoble Cedex
Tél. (33) 76 88 58 92
Fax (33) 76 88 50 48

PLANAR SILICON HEADS

J.P. LAZZARI

SILMAG COMPANY





PLAN

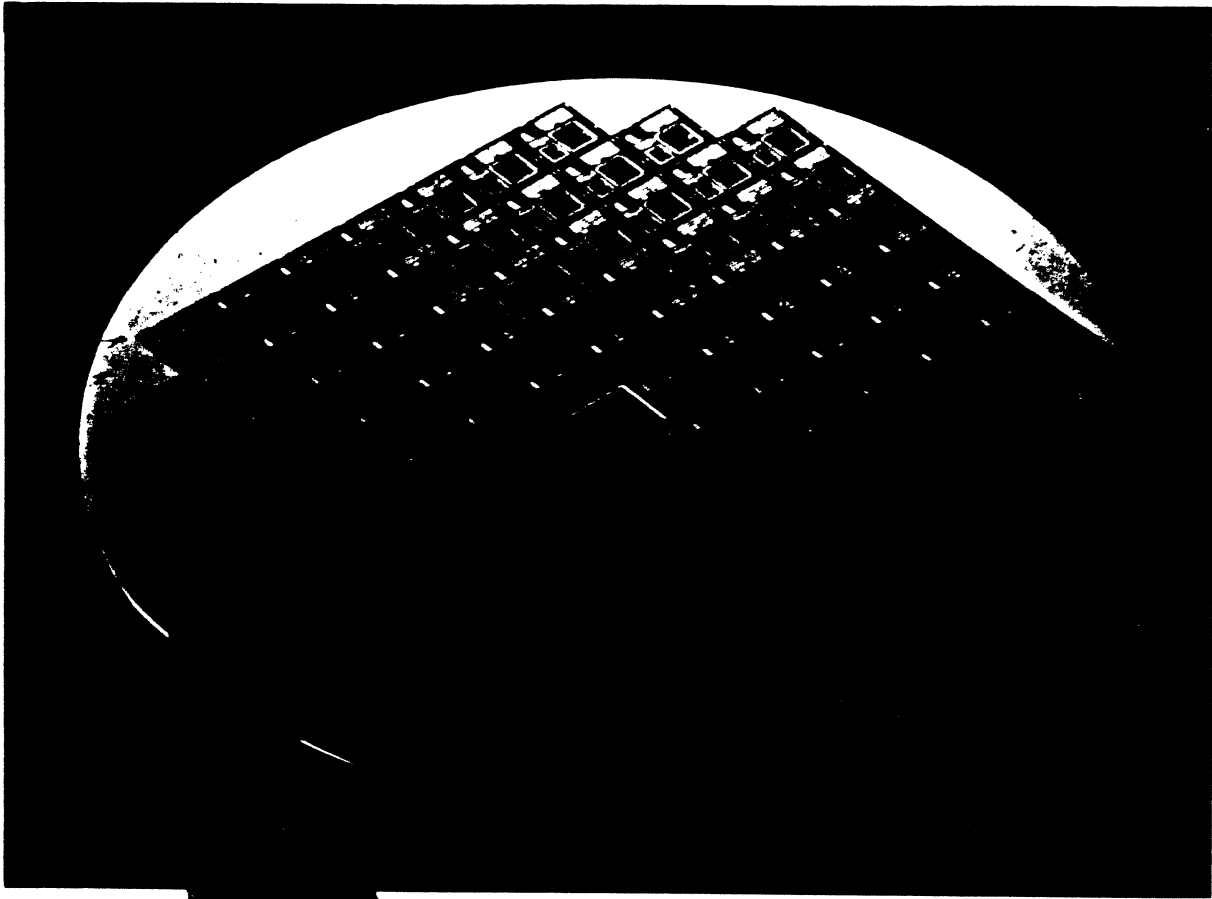
PART I : TECHNOLOGY

PART 2 : TH - MR - PSH



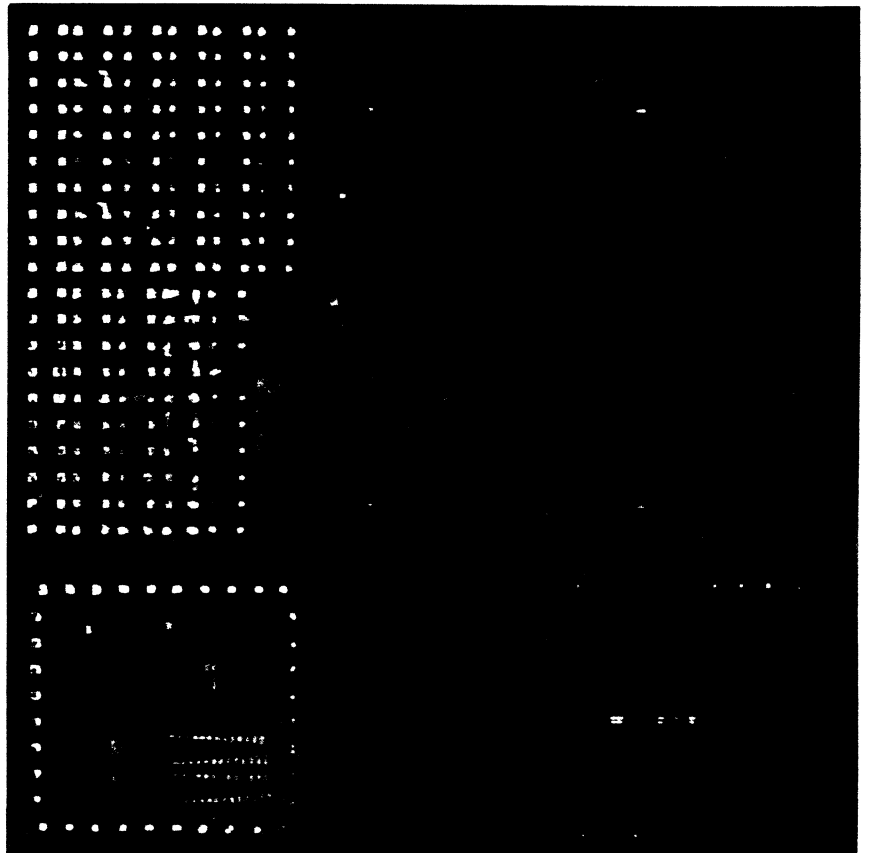
PART 1

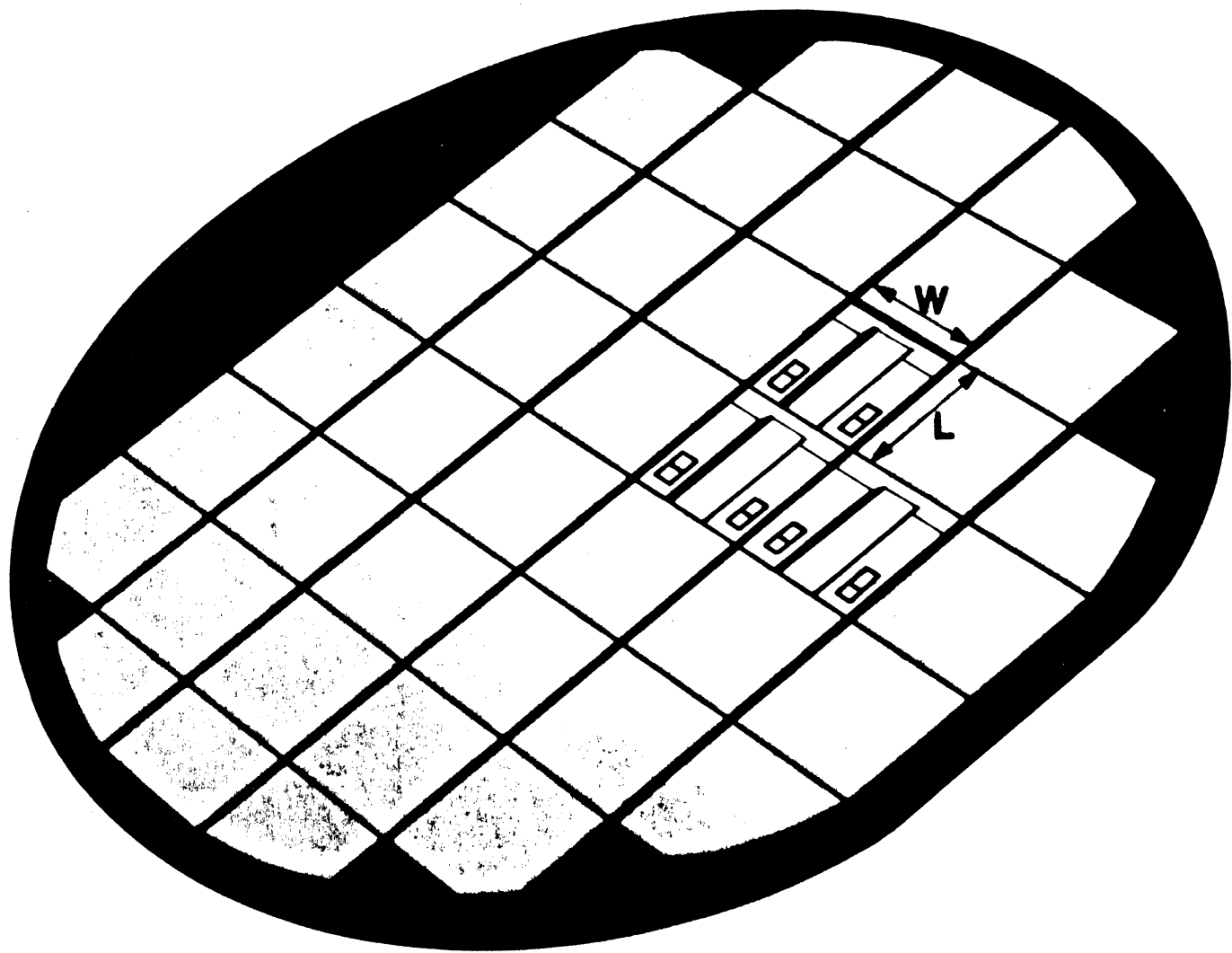
TECHNOLOGY



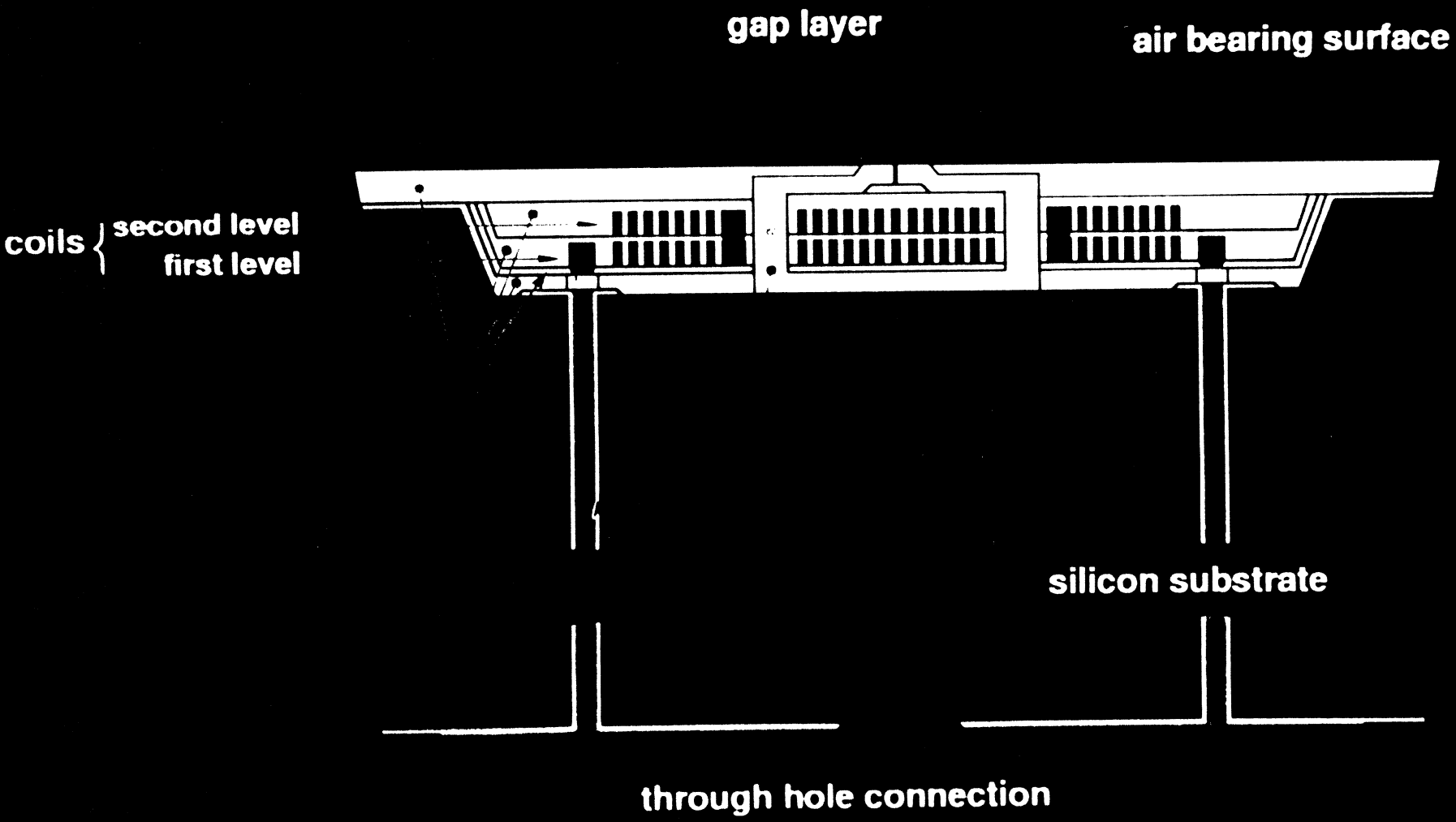
plaquette de silicium (WAFER)

circuit intégré ou "PUCE"

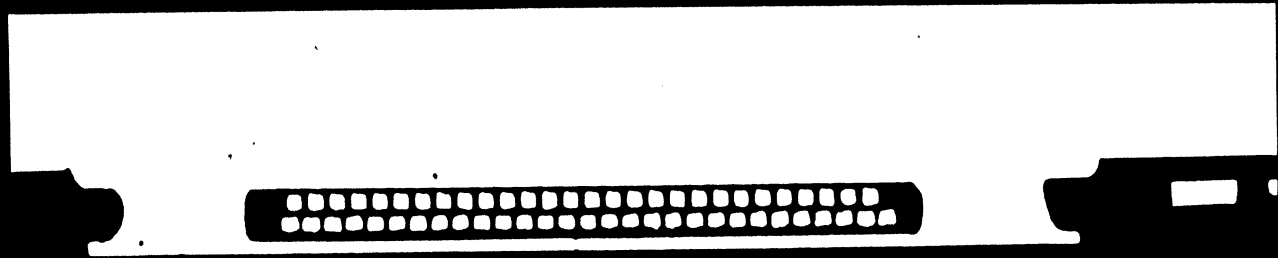




Schematic view of I.C. head

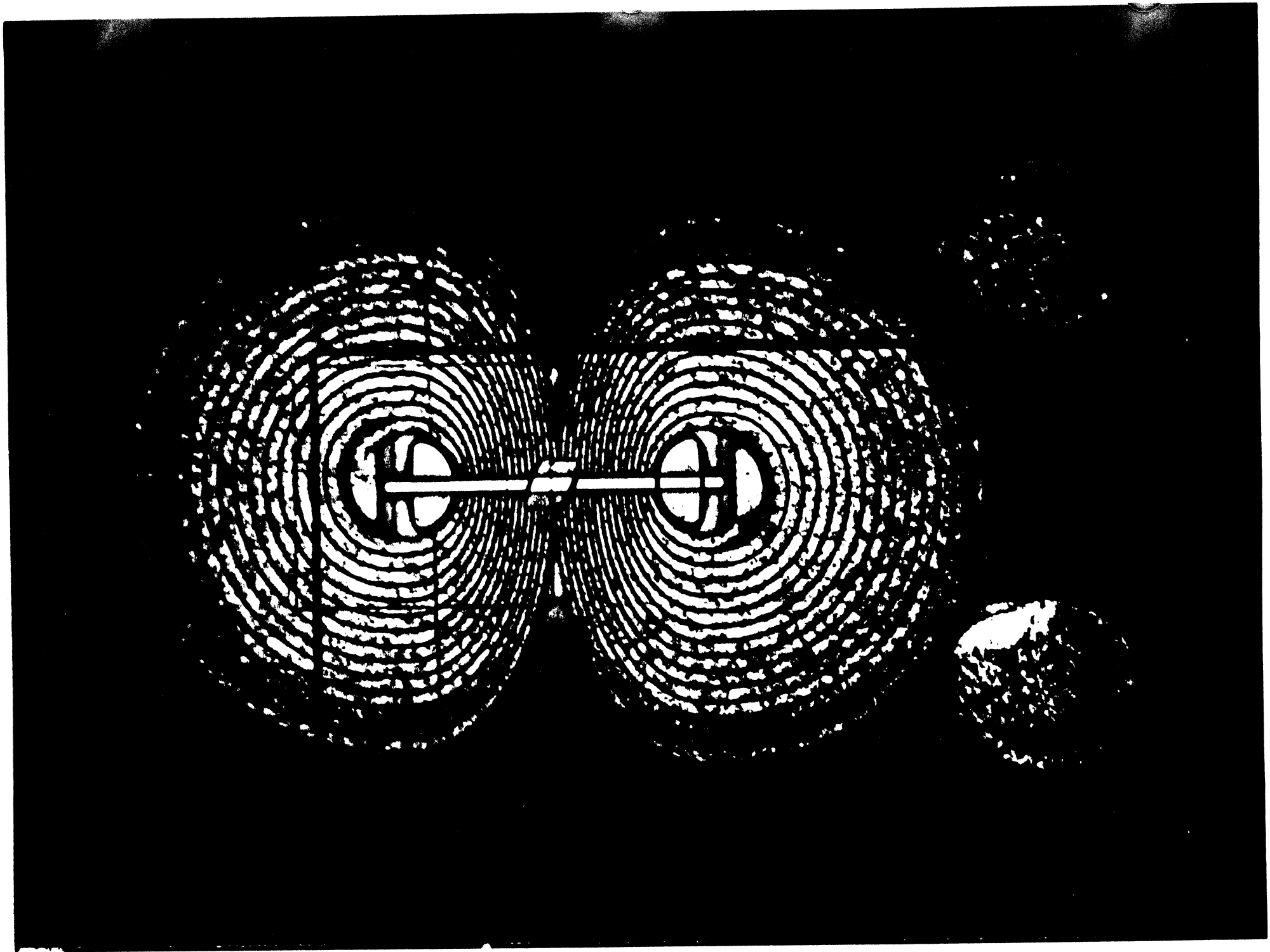


Cross section of planar silicon head

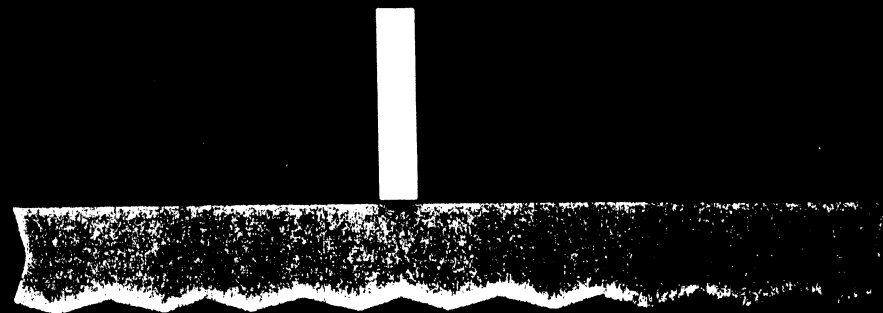
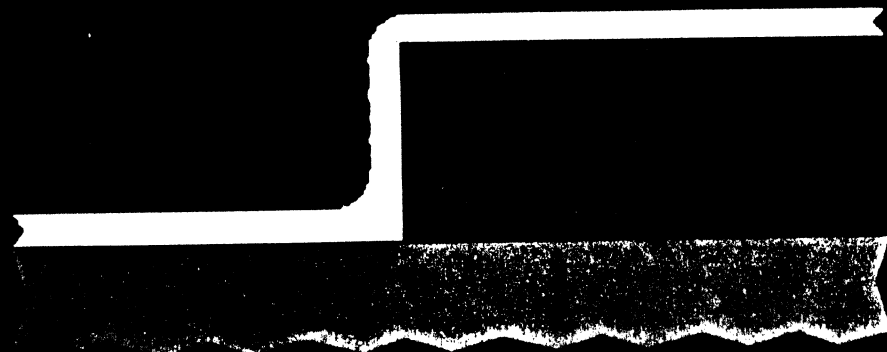


AT 16302

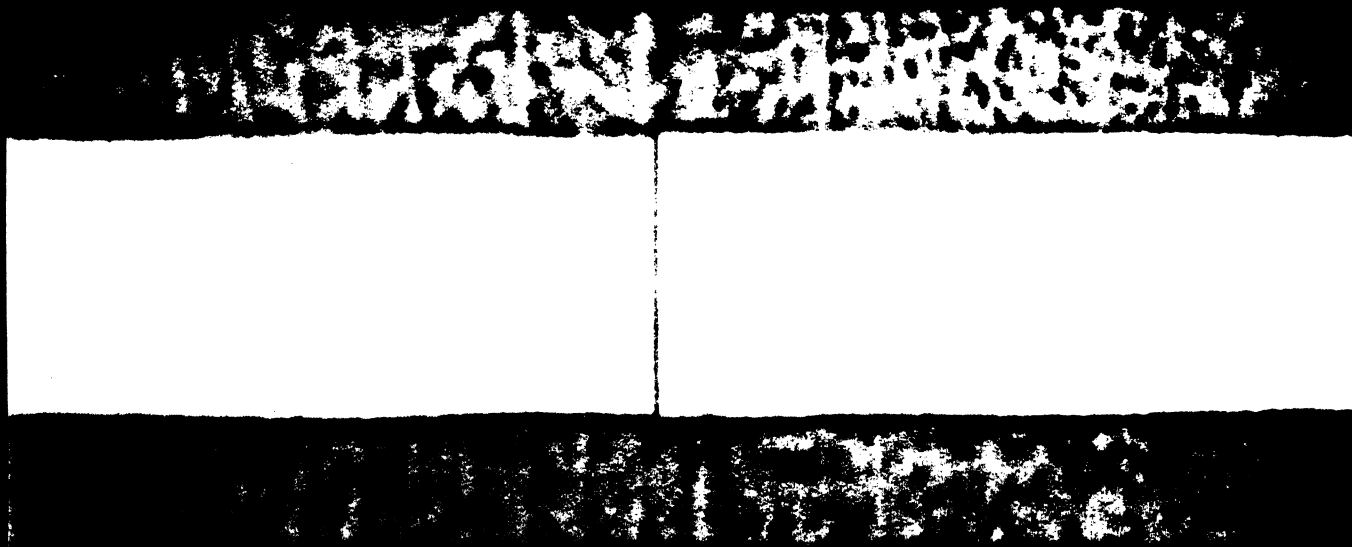




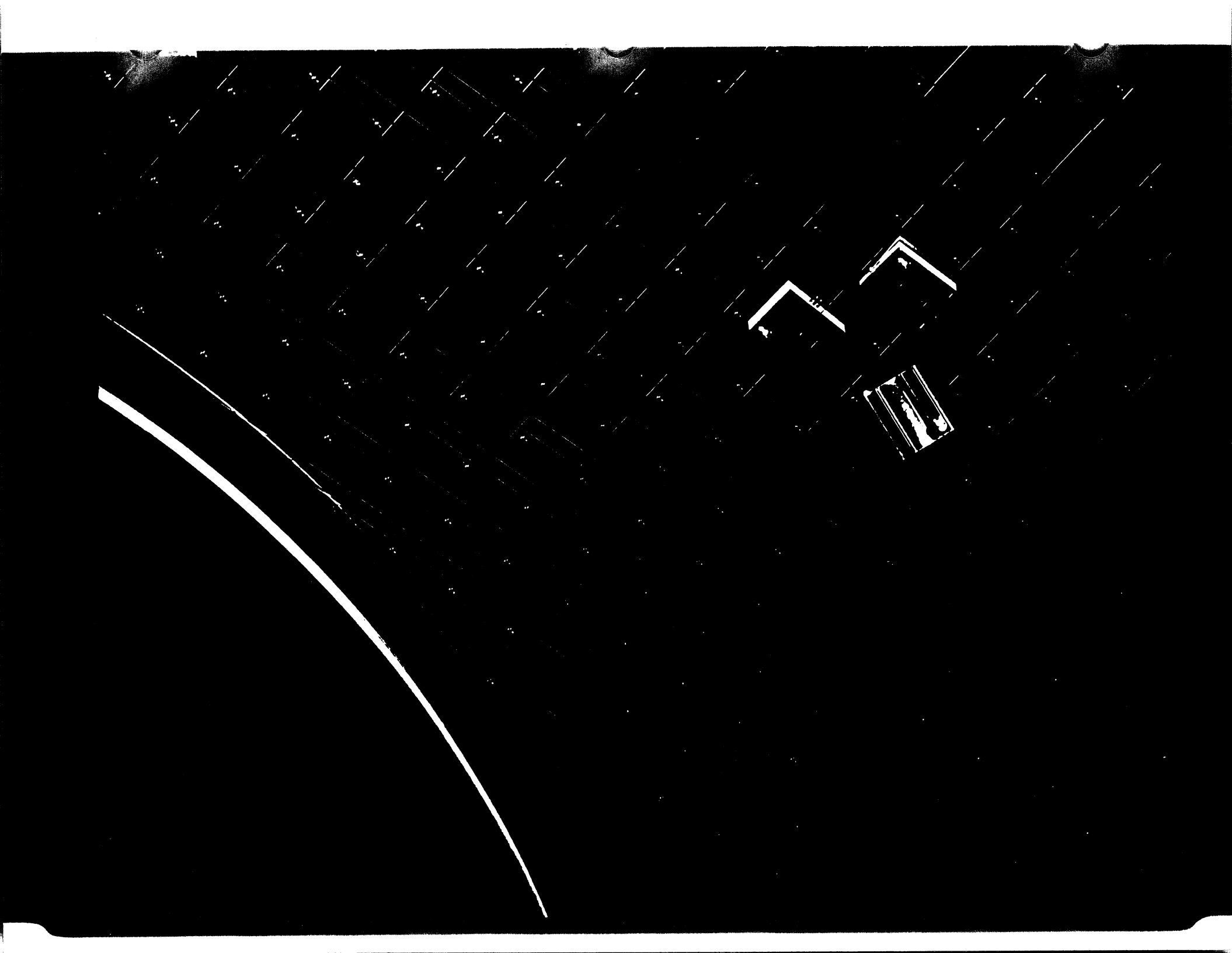
3 D gap process fabrication



IC head gap

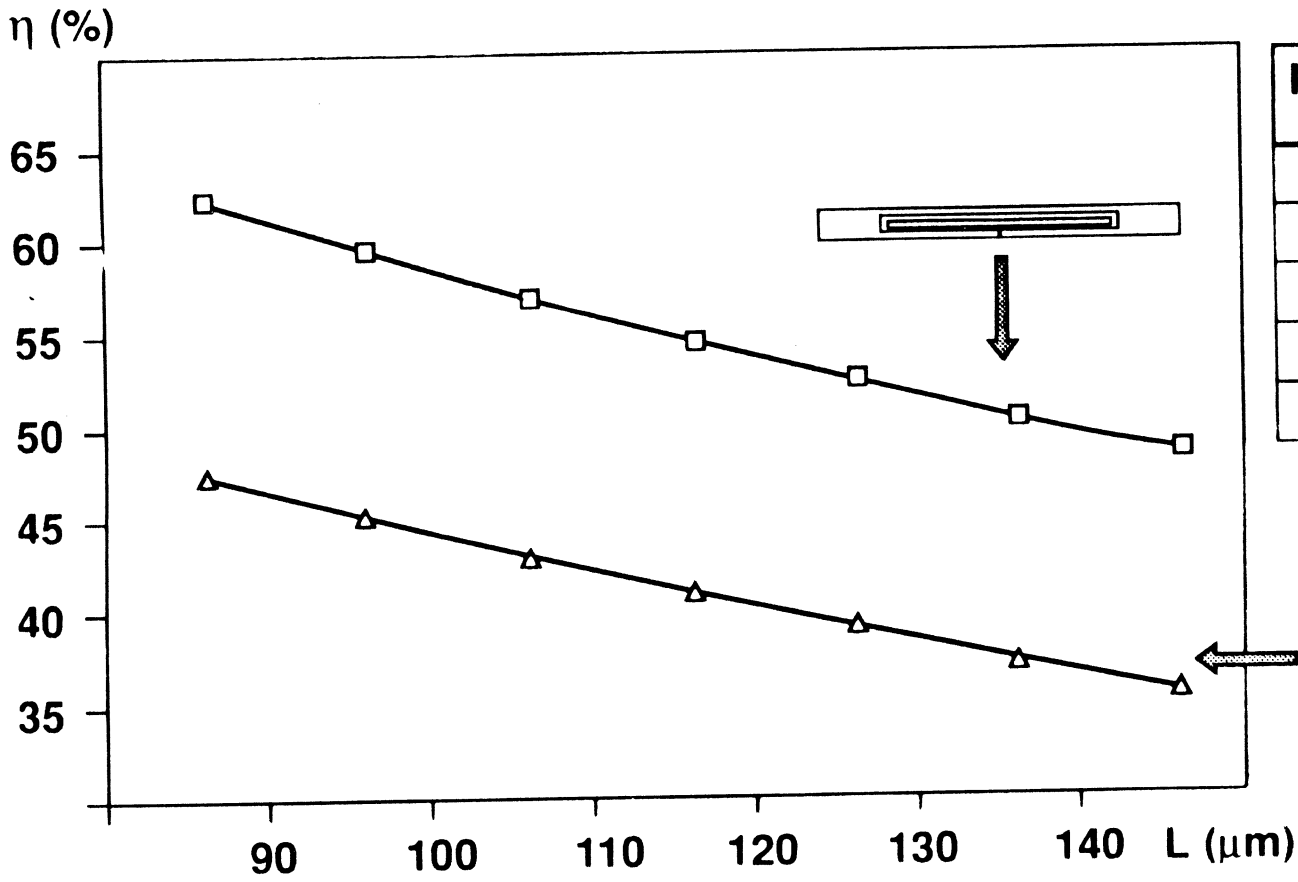


AT11143

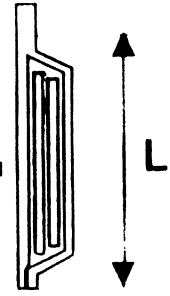


numerical calculations of thin film head

efficiency analysis (finite elements method - flux - 2D)

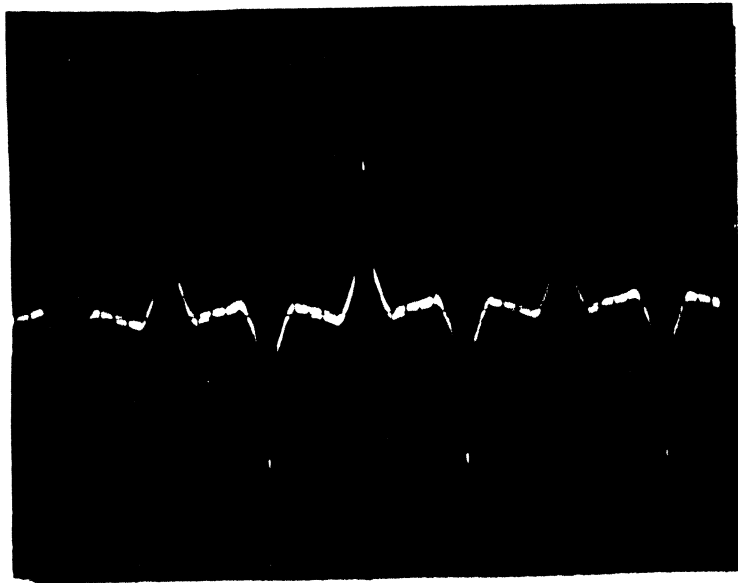


parameters	I.C head	conventional
hv	-	8
Ga	8	18
T layer	3	4.5
B layer	4	4.5 / 3.5
L gap	0.4	0.4

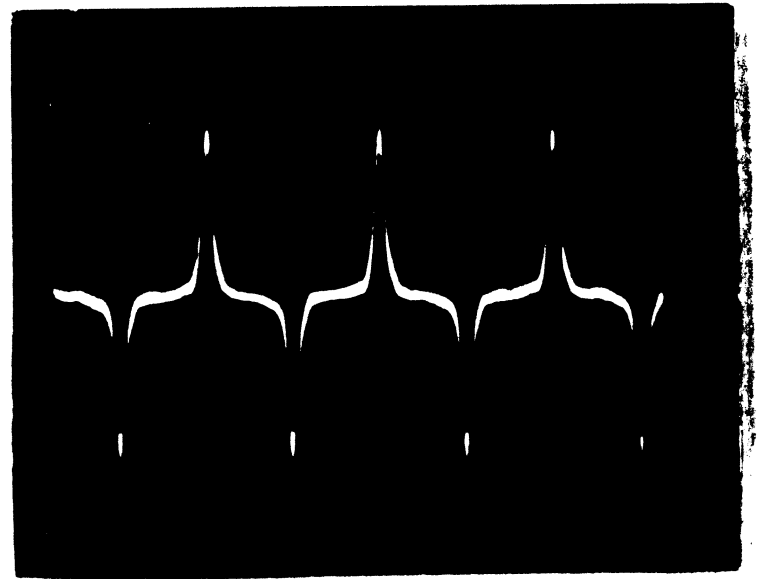


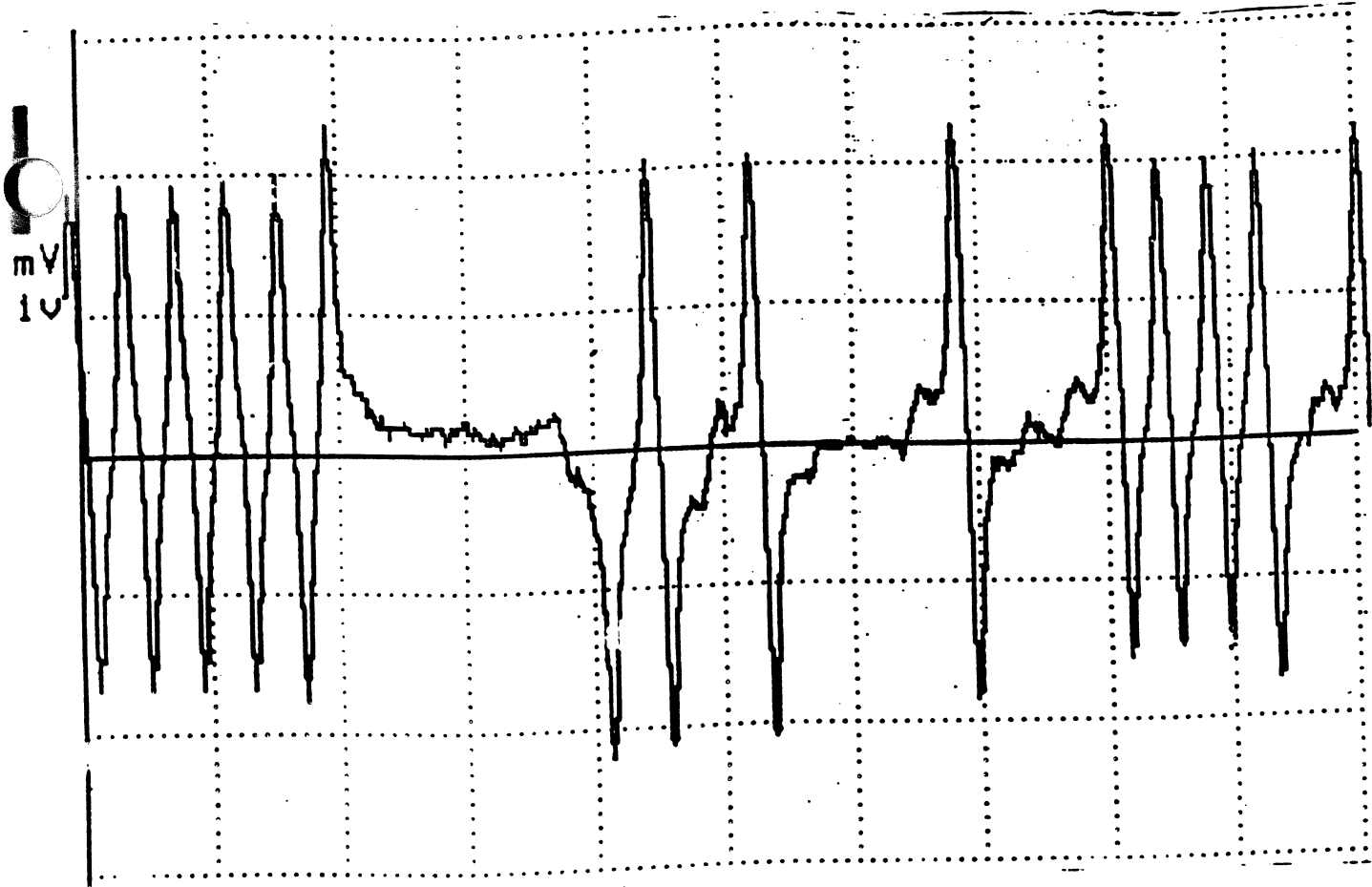
playback pulses:

**conventional
thin film head**



I.C. head

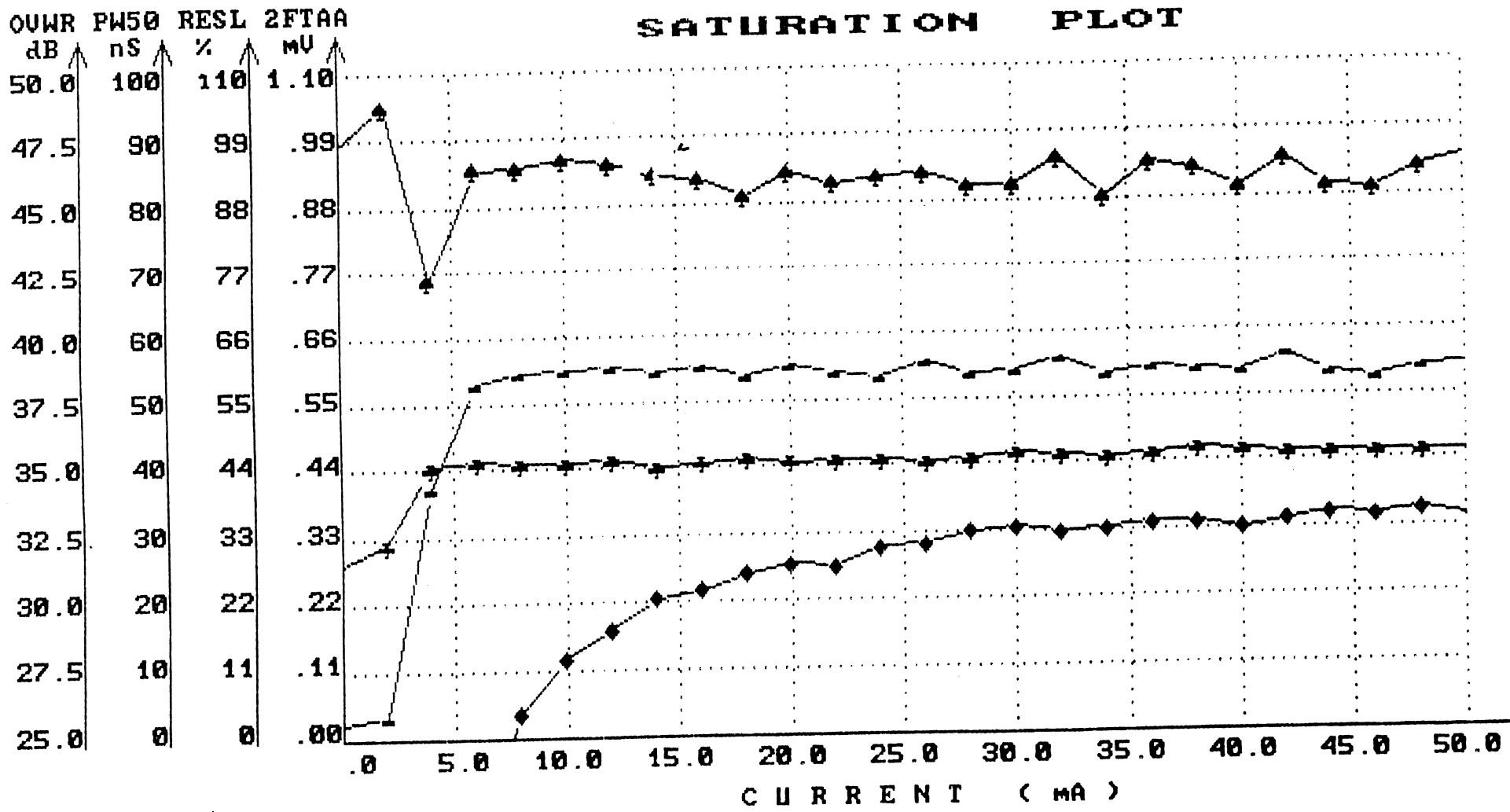


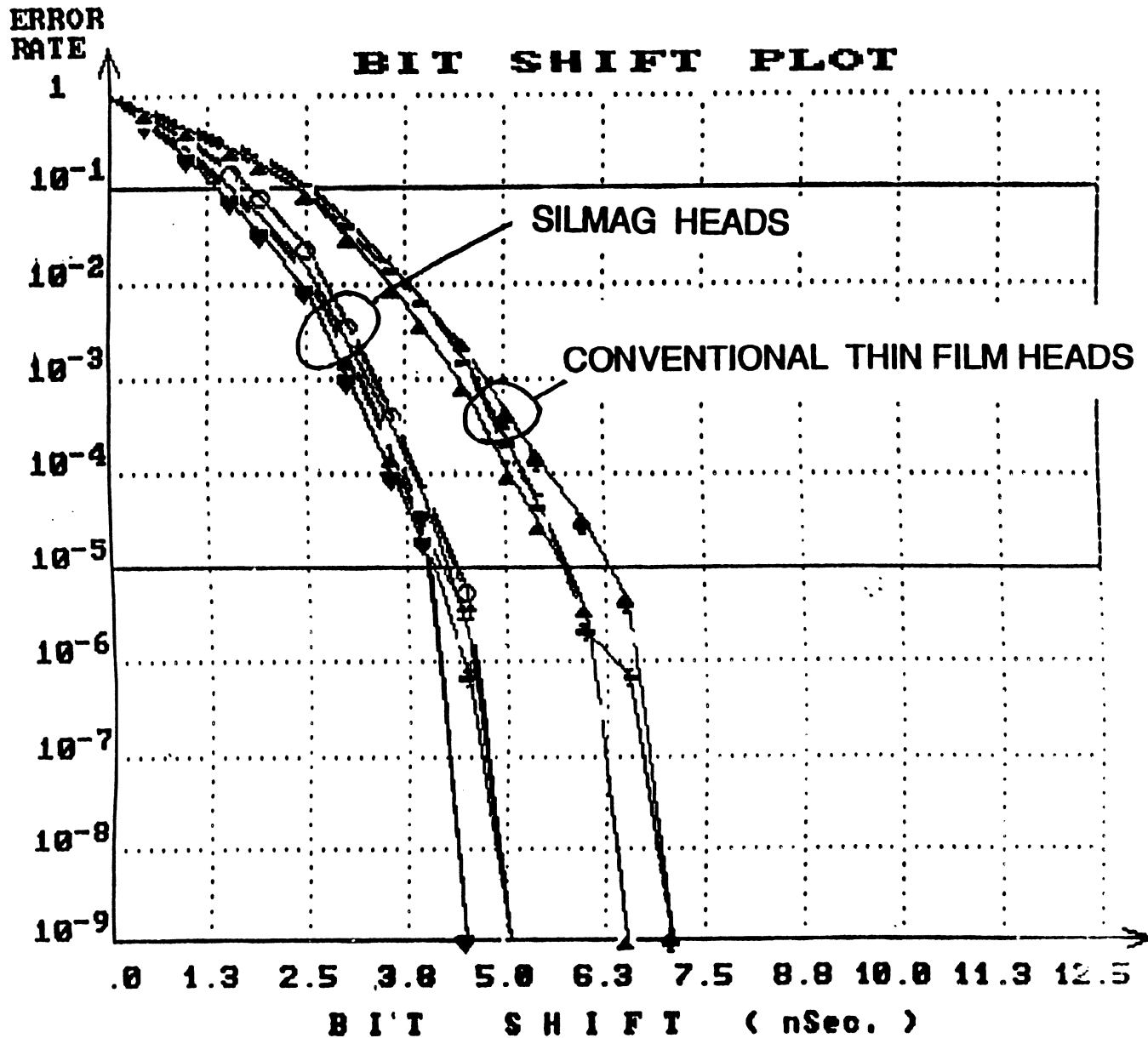


SILMAG HORIZONTAL SILICON HEADS



SATURATION PLOT





	TRAK	HD	PIRN	ZERO	S	THRS
▲	1	0	F232	6.5	I	50.0
	PARAM	C27	BOTH	15mA		50nS L
+	1	0	F232	5.1	I	50.0
	PARAM	C27	BOTH	15mA		50nS L
▲	1	0	F232	5.1	I	50.0
	PARAM	C27	BOTH	15mA		50nS L
-	1	0	F232	4.5	I	50.0
	PARAM	C27	BOTH	15mA		50nS L
▲	1	0	F232	4.5	I	50.0
	PARAM	C27	BOTH	15mA		50nS L
▼	1	0	F232	5.1	I	50.0
	PARAM	C27	BOTH	15mA		50nS L
▲	1	0	F232	5.1	I	50.0
	PARAM	C27	BOTH	15mA		50nS L
○	1	0	F232	5.1	I	50.0
	PARAM	C27	BOTH	15mA		50nS L
	1	0	F232	5.1	I	50.0
	PARAM	C27	BOTH	15mA		50nS L
▼	1	0	F232	4.5	I	50.0
	PARAM	C27	BOTH	15mA		50nS L
◆	1	0	F232	6.5	I	50.0
	PARAM	C27	BOTH	15mA		50nS L
+	1	0	F232	7.1	I	50.0
	PARAM	C27	BOTH	15mA		50nS L
▲	1	0	F232	7.1	I	50.0
	PARAM	C27	BOTH	15mA		50nS L
-	1	0	F232	6.5	I	50.0
	PARAM	C27	BOTH	15mA		50nS L



40 TURNS SILMAG HEADS PRELIMINARY SPECIFICATIONS 3 1/2 DRIVE

GENERAL CHARACTERISTICS		
Track Width	microns	10 ± 0.3
Gap Length	microns	0.4 ± 0.05
Number of turns	turns	40
Media Size	mm (inches)	90 (3.5)
Media Coercivity	Oe	1400
Rotational Speed	RPM	4500
Head Load Force	grams	5 ± 0.6
Flying Height	microns (µin.)	minimum 0.11 µm (4.5 µ inch)
MECHANICAL CHARACTERISTICS		
Slider sizes	mm	2.25 x 2.85 x 0.52
Material		Silicon
Rails		Thin film silicon oxyde
Crown	A	No neg crown (max 750 A)
Camber	A	No neg camber
Rugosity	A	10 < Ra < 30
TEST CONDITIONS		
Test Radius R1	mm (inches)	24 (0.95)
R2	mm (inches)	45 (1.78)
Skew R1	deg	- 6.3
R2	deg	- 15.5
Frequencies LF	MHz	2.5
HF	MHz	6.66
Write Current	mA OP	15
ELECTRICAL CHARACTERISTICS		
Amplitude (HF,R1)	microvolts	> 600
Isolated Pulse		No undershoot
Resolution (R1)	%	> 90
Overwrite (R2)	dB	> 30
Instability	%	< 2
PW 50 (R1)	ns	< 55
Signal to noise ratio	dB	≥32
Popcorn noise		0
Bit shift		< 6
Linear Density (D50)	FRPM (FCI)	>1400 (36.000)
Resistance	Ohms	< 38
Inductance (1 MHz)	nH	< 300
Resonant frequency	MHz	> 150
Number of C.S.S.		> 150 K
Stiction friction coeff.		< 0.2

Note :

- a) Specifications are based on tests with KOMAG media and Guzik 501 tester.
- b) All others specifications will be respected in regards to customers requests.



57 TURNS SILMAG HEADS PRELIMINARY SPECIFICATIONS 3 1/2 DRIVE

GENERAL CHARACTERISTICS		
Track Width	microns	8.5 ± 0.3
Gap Length	microns	0.4 ± 0.05
Number of turns	turns	57
Media Size	mm (inches)	1.8
Media Coercivity	Oe	1400
Rotational Speed	RPM	4500
Head Load Force	grams	5 ± 0.5
Flying Height	microns (µin.)	0.11 µm (4.5 µ minimum)
MECHANICAL CHARACTERISTICS		
Slider sizes	mm	2.25 x 2.85 x 0.52
Material		Silicon
Rails		Thin film silicon oxyde
Crown	A	No neg crown
Camber	A	No neg camber
Rugosity	A	10 < Ra < 30
TEST CONDITIONS		
Test Radius R1	mm (inches)	24 (0.95)
R2	mm (inches)	45 (1.78)
Skew R1	deg	- 6,3
R2	deg	- 15.5
Frequencies LF	MHz	2.25
HF	MHz	9
Write Current	mA OP	15
ELECTRICAL CHARACTERISTICS		
Amplitude (HF,R1)	microvolts	> 700
Isolated Pulse		No undershoot
Resolution (R1)	%	> 88
Overwrite (R2)	dB	> 30
Instability	%	< 2
PW 50 (R1)	ns	< 55
Signal to noise ratio	dB	> 31
Popcorn noise		0
Linear Density (D50)	FRPM (FCI)	> 45 k
Resistance	Ohms	< 40
Inductance (1 MHz)	nH	< 700
Resonant frequency	MHz	> 150
Stiction frictioncoefficient		< 0.2
Number of C.S.S.		> 150 K

Note :

- a) Specifications are based on tests with KOMAG media and Guzik 501 tester.
- b) All others specifications will be respected in regards to customers requests.

Test results

CFG:
Revision: 1.1
Chip Gain: 1
Operator: IRENE
RW Board: chip&rw

Grades: None
Tester: HTU285-1011
Date: 19921126
Time: 22:53:46

Record: 078

Head Name DOWN
Serial Number C023P033106
Disk ID KOMAG 1400
Cal OFF

*10 µm Track width
40 turns*

Amplitude	.673
Wobble	.976
F1 Ampl	.668
F2 Ampl	.663
Res	99.326
OW	35.576
F1 Ampl	.465
F2 Ampl	.428
Res	92.151
OW	36.764
PW	49.122

Grades Passed Disabled



High start - stop reliability



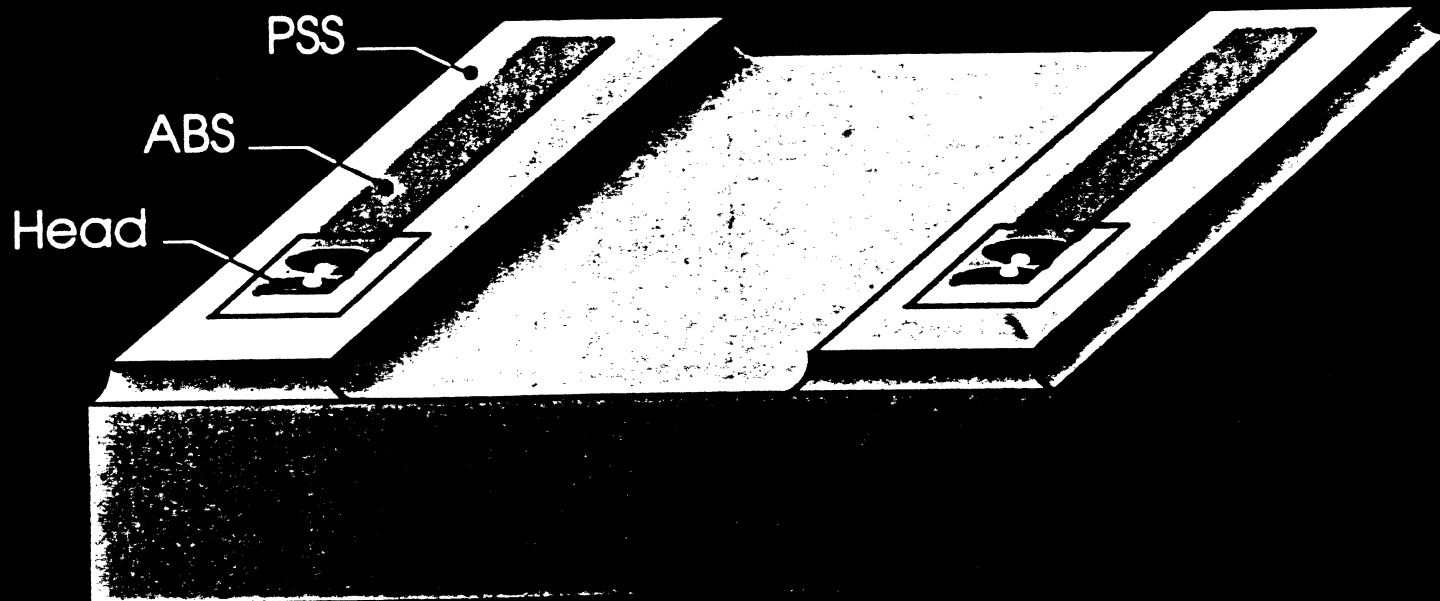
- Low thermal expansion

- Silica has high thermal conductivity

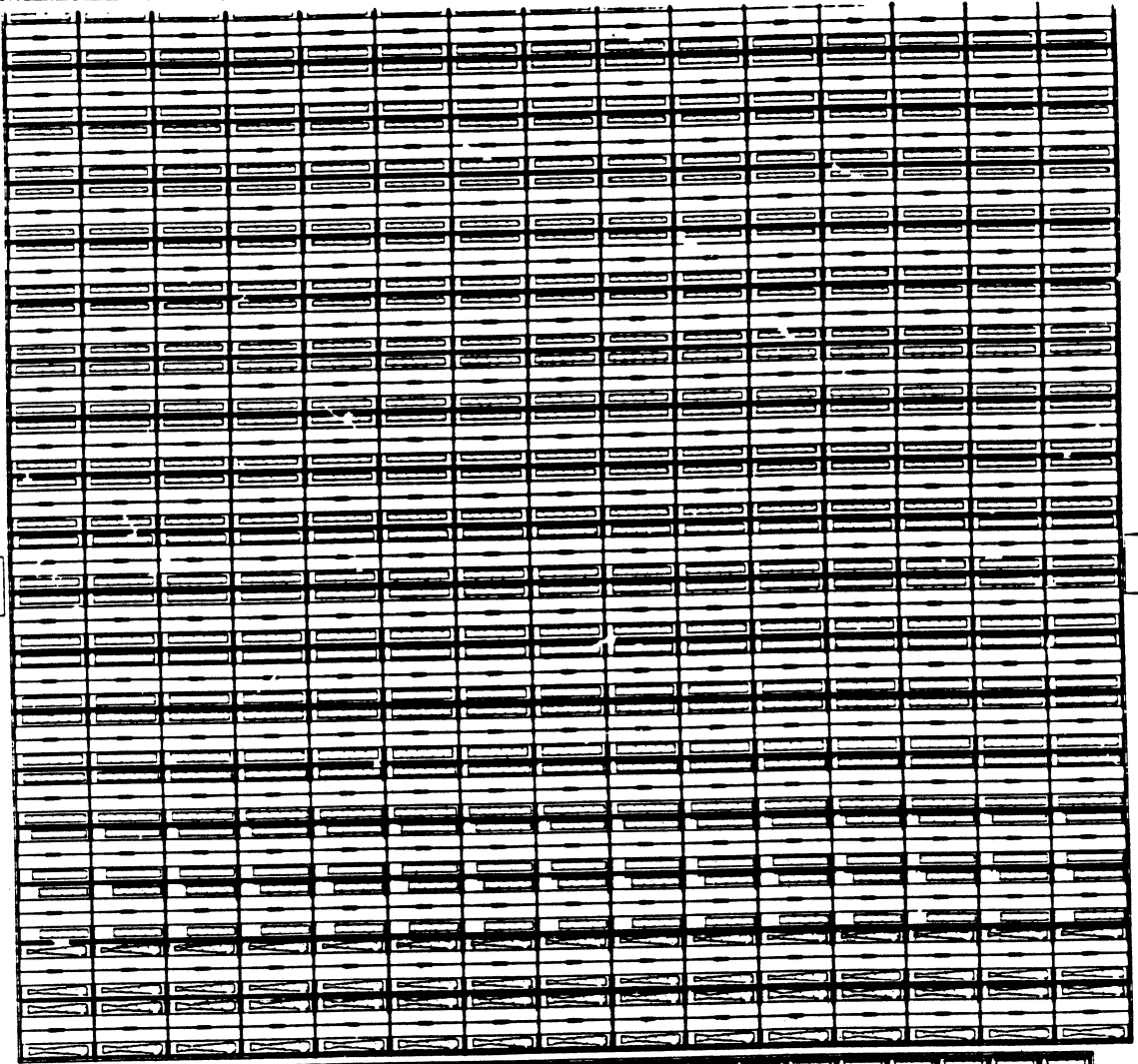
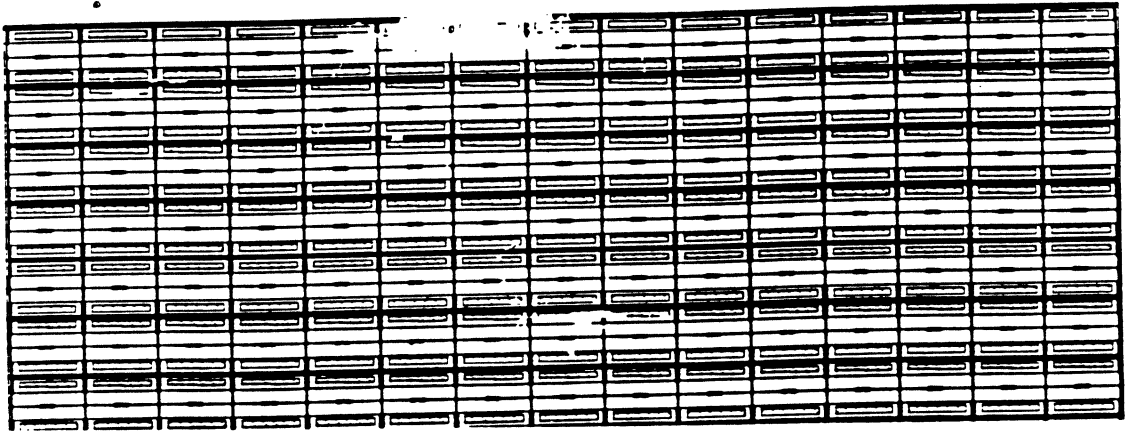
- SiO₂ protection is dense and material homogenous

Head description

-  The complete device (head, slider, ABS) is fabricated on silicon wafer, with micro electronic processes.
-  SiO_2 coats the rails and the head. SiO_2 is used by etching to shape and design ABS.
-  The Peripheral Secondary Surface (PSS) obtained, contributes to determine the flying parameters, on the entire disk radius.
-  PSS surrounds ABS including leading, trailing and lateral edges.



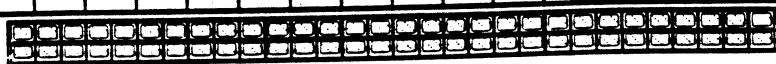
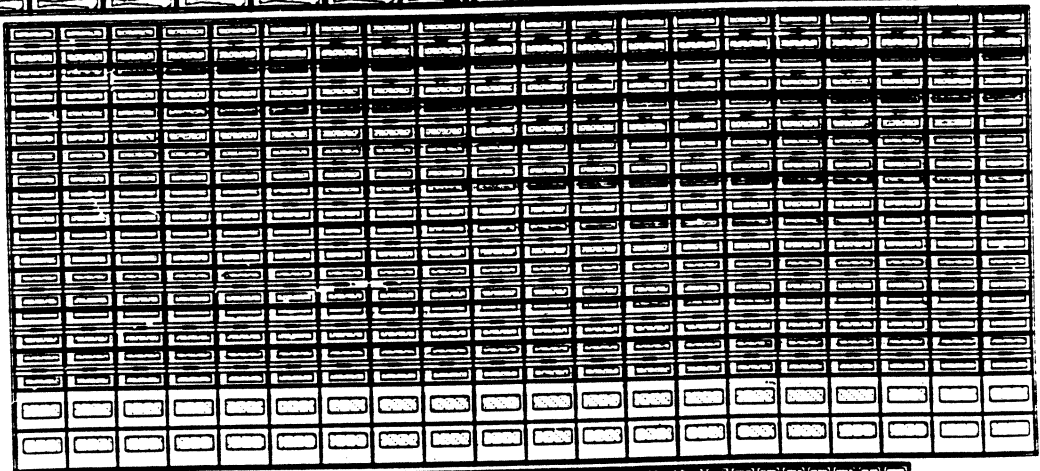
60
Alphabet
patterns
on six marks.



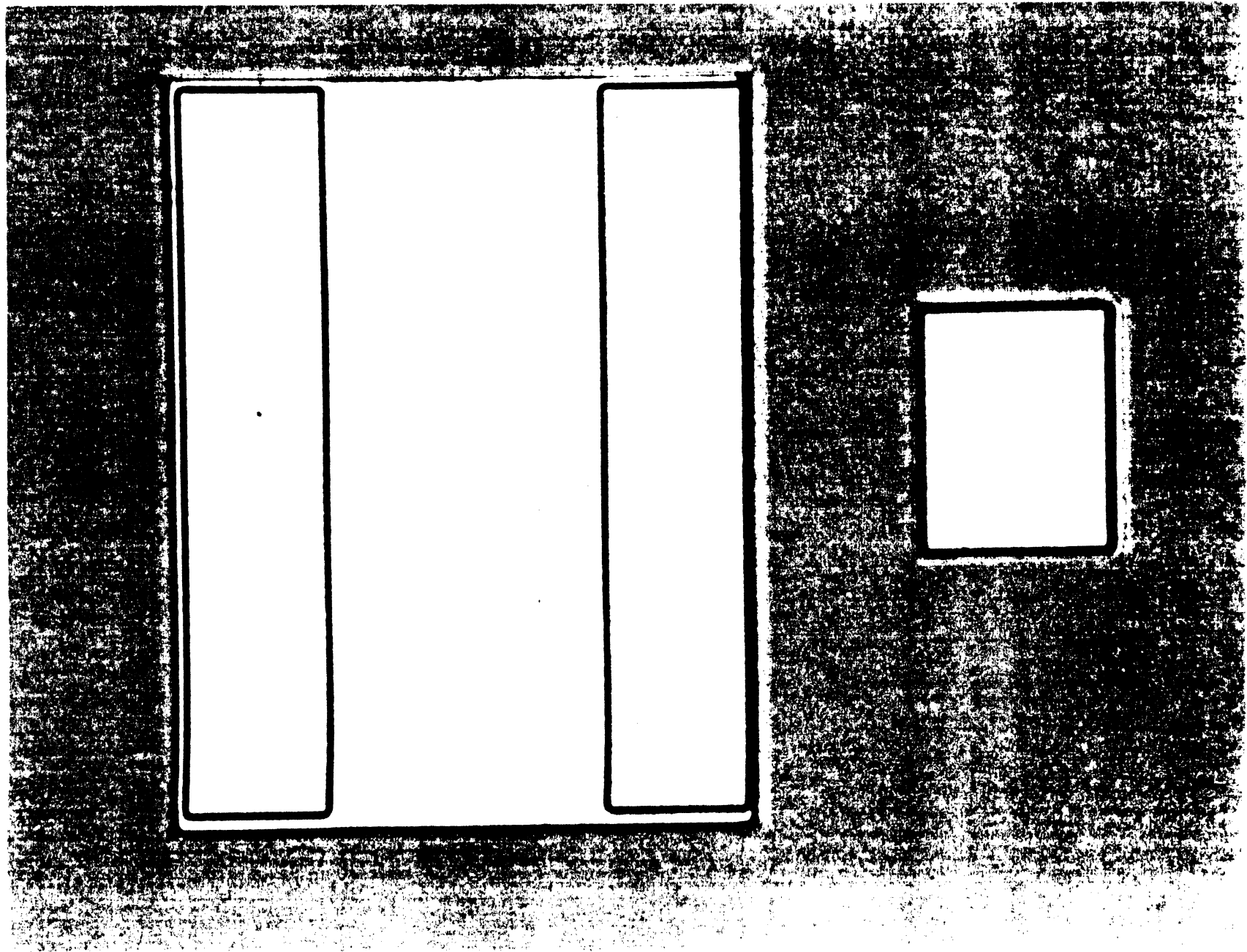
Micro

Pico

Nano



(n)





Natural mechanical resonance frequencies

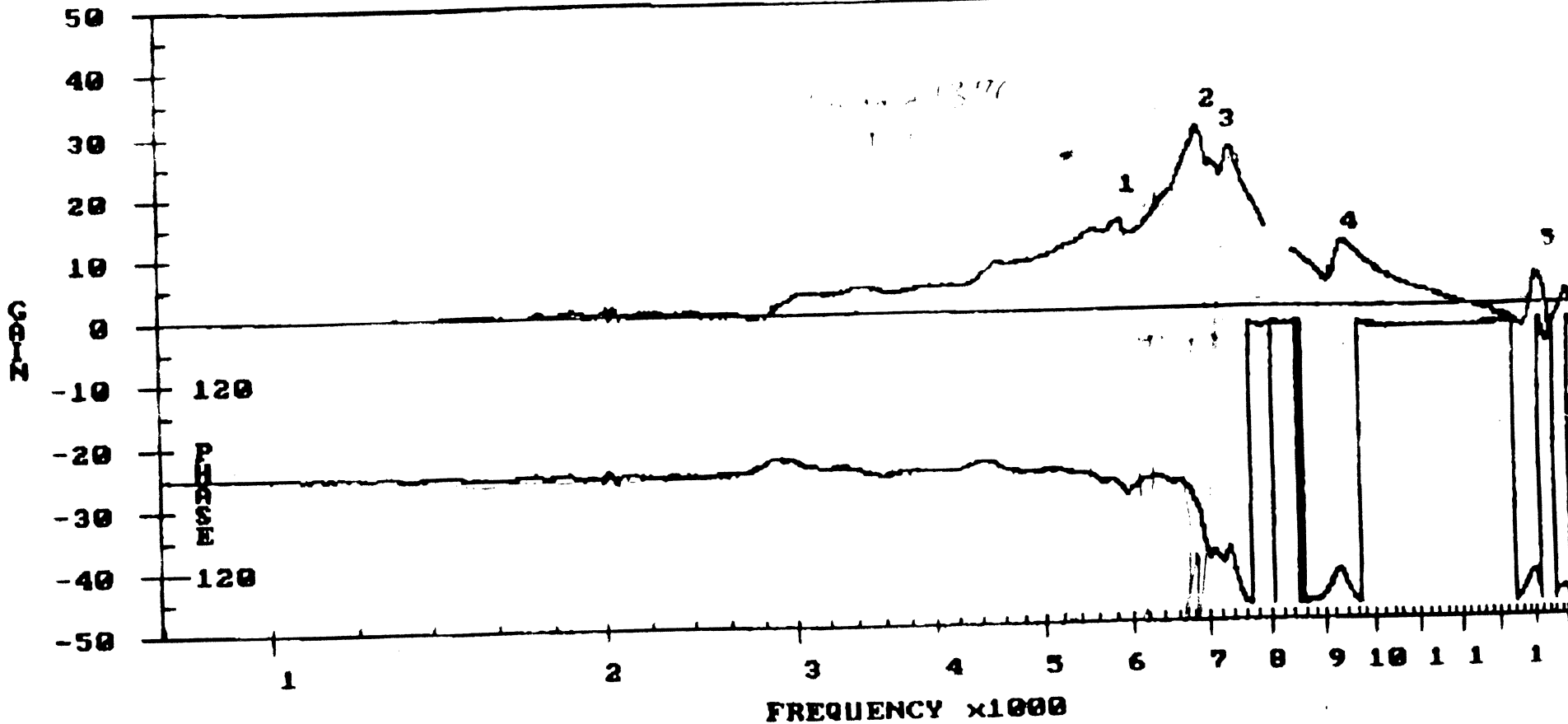


	Ceramics			
Dimensions (mm)	4 x 3	2.3 x 2.9	1.5 x 2	2.3 x 2.9
Vertical	16 KHz	22 KHz	47 KHz	45 KHz
Roll	35 KHz	18.5 KHz	30 KHz	37 KHz
Pitch	28 KHz	42 KHz	~ 58 KHz	48 KHz

HUTCHINSON TECHNOLOGY INC.
 FREQUENCY RESPONSE FUNCTION
 DATE: 12/04/98 TIME: 10:47:15 TEMP: 25 C.

FREQUENCY PEAKS	1	2	3	4	5
54.3037	149.1625	143.4822	140.9888	140.9888	140.9888
54.3037	149.1625	143.4822	140.9888	140.9888	140.9888
54.3037	149.1625	143.4822	140.9888	140.9888	140.9888
54.3037	149.1625	143.4822	140.9888	140.9888	140.9888

#97 #92 Resonance - Silmag slider PT.3

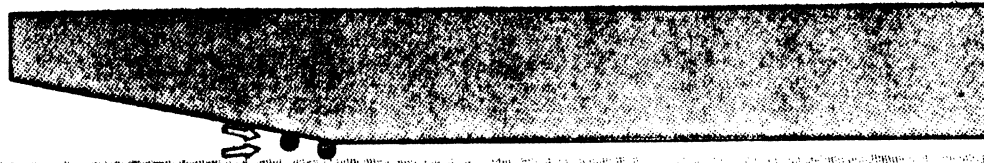




Protection against particle deterioration

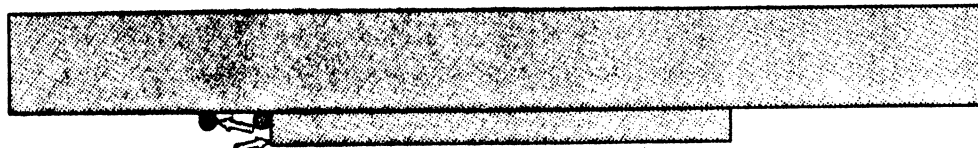


Conventional ABS

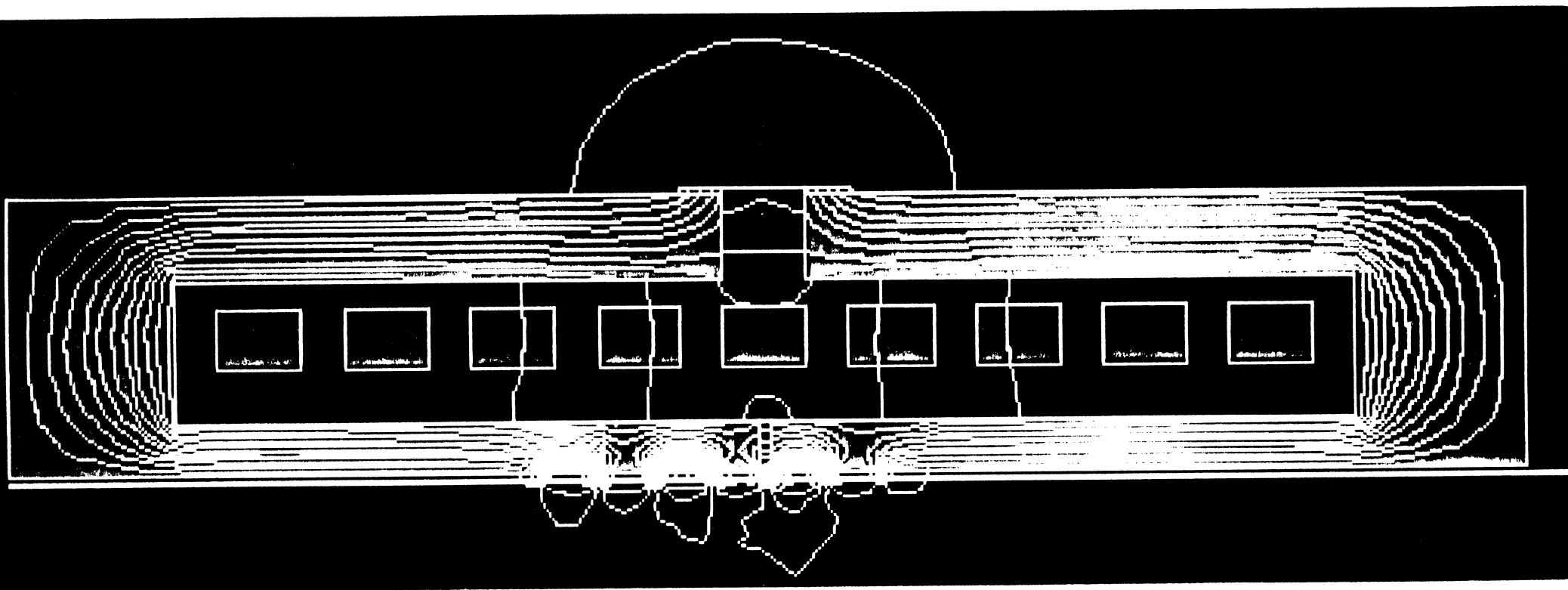


Particles increase pitch and can move under ABS

"Step" ABS



- *Particles don't change pitch*
- *Particles cannot move under ABS*

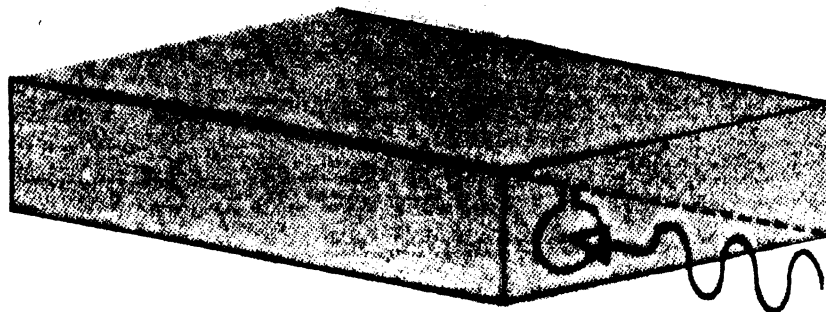




Protection against external magnetic field

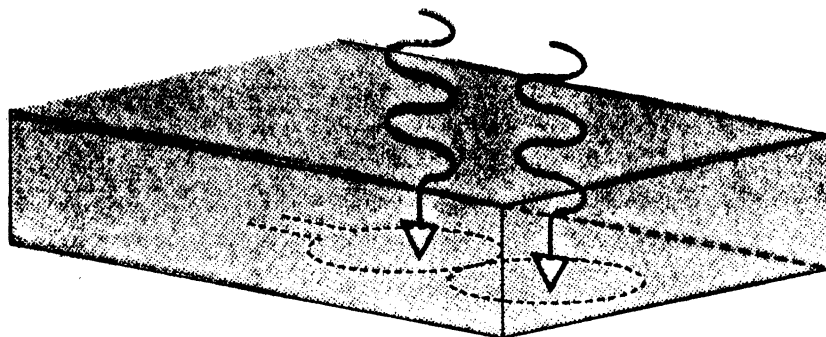


Conventional servo thin film heads



- Full sensitivity to external field

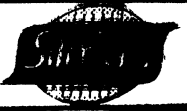
Servo planar silicon heads



- 1. Low sensitivity to external field due to common mode coil
- 2. The coil is shielded between conductive silicon and disk



SILMAG heads : 10 key issues



1 : Two coils design

- Less self inductance
- Good thermal link with silicon
- Good yield

2 : Semi infinite pole piece

- Pure output, no undershoot

3 : Microlithography and reactive ion etching for ABS

- Very high dimensional accuracy
- Any shape of ABS
- Very low flying height capabilities

4 : Outstanding tribology reliability

- Low mass slider (high mechanical resonance frequency)
- More than 100,000 start-stop, guaranteed

5 : No slider grinding



SILMAG heads : 10 key issues (cont'd)



6 : **Wafer base fabrication (like gate arrays in IC's)**

- **Mass production of standard wafer base**

- *Fine pole piece*

- *Coil*

- **Customization at the end of the process**

- *Track width/gap length*

- *ABS*

7 : **Automatic HGA assembly capabilities**

- **Alignment targets on the top slider surface done with output contacts**

8 : **Possible read amplifier in the slider**

9 : **Promise to good MR performances**

10 : **Under huge microelectronics industry (standard equipments & processes)**



PART 2

TH - PR - PSH



PSH - TF- LAM DESIGN CONSIDERATION



		PSH	TF	LAM
ABS	Roughness Recess ABS shape ABS precision	15 A° < 50 A° in situ high	40 A° 200 A° extra operation -	? ? ? -
POLE TIP	Throat Height Sensitivity Narrow track width Inductance Undershoot Wiggle Popcorn	No Sensitive Well adapted Very low No - 0	- Sensitive Difficult Low Yes - Yes	- Sensitive Possible Medium No Low 0



PSH - TH - LAM IN INDUCTANCE



	36 T	42 T	57 T	80 T	100 T
Planar Silicon Heads (0.6 Ω /T)		0.35	0.75	1.4	2.2
Thin Film Heads (0.9 Ω /T)		1.3	2.8	4.8	
LAM (0.12 Ω /T)	1.15	2.2	4,2		

(INDUCTANCE : μ H)

*good in 100 turns
to reach 2.2 μ H*



PSH NUMBER OF TURNS VS YEARS



	1993	1994	1995	1996
PSH COIL	57	80	80	100
(TURNS)	40	57	57	80
		40		



PSH FLYING HEIGHT VS YEARS



	1993	1994	1995	1996	1997
FH	3.5	3	2	< 2	1.5
(μ in)	4	3.5	3	2.5	2



PSH BPI VS YEARS



	1993	1994	1995	1996
KBPI	75	90 *	110 *	150 *
PSH	50	70	80	100

* WITH PRML



PSH TPI VS YEARS



	1993	1994	1995	1996
KTPI	3500	4000	4500	5000
PSH	3000	3200	3500	4000



PSH - TH - MR (Mbits - in2)



	1993	1994	1995	1996
T.H.	200	250	310	400
P.S.H.	250	350 *	500 *	720 *
M.R.	300	450	600	1000

- * - HIGHER NUMBER OF TURNS
- REDUCED TW
- REDUCED FH
- PRML CODING



PSH - TH MASS FABRICATION



FORECAST T.H.	1993	1994	1995
Munits	200	240	260

IC Manufacturing

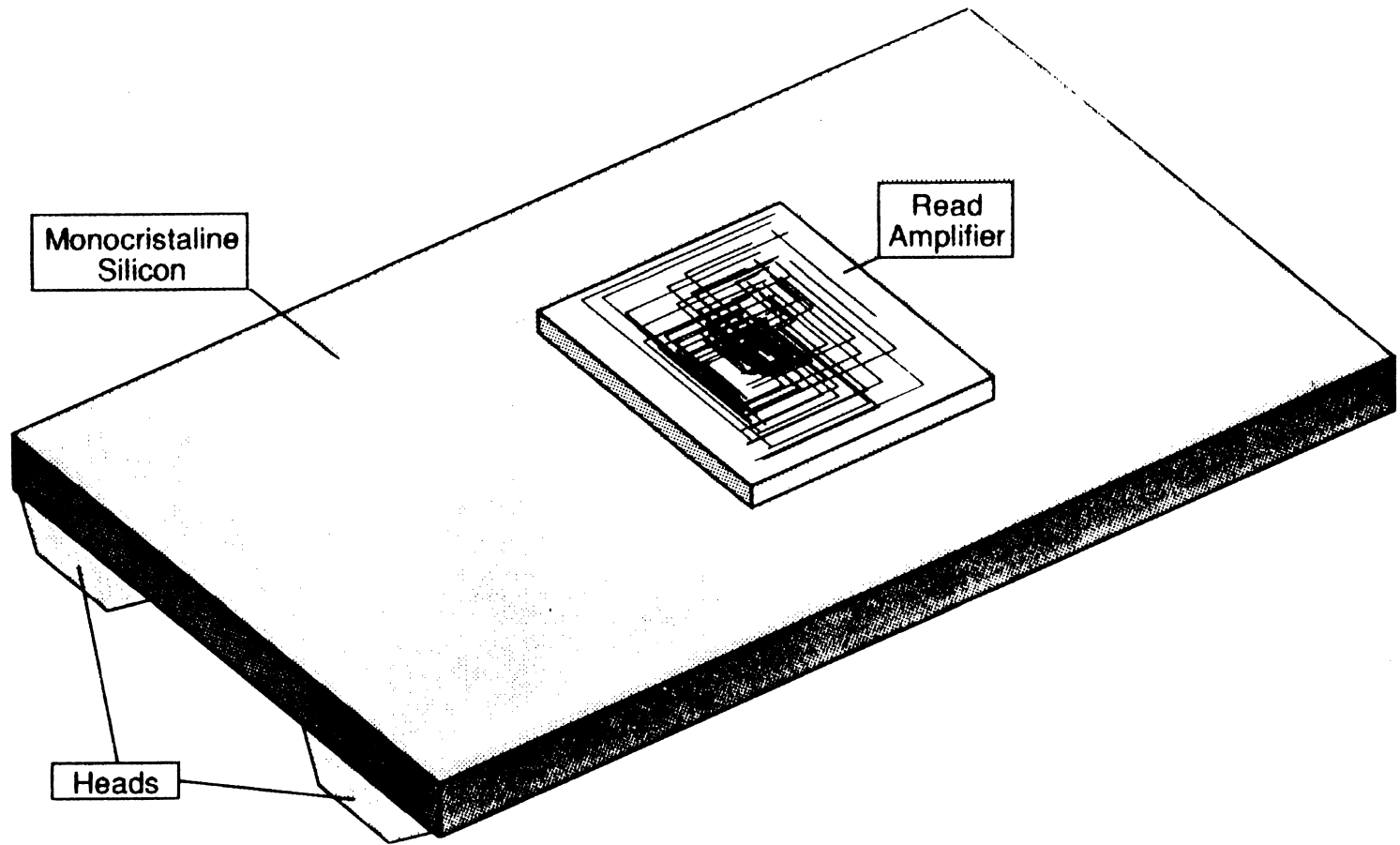
Ex : 4 inches - nano sliders

PILOTE LINE : 10 k wafers/Y x 1000 good sliders = 10 Munits/Y
(160 people)

MEDIUM IC FAB. : 10 k wafers/month x 12 x 1000 = 120 Munits/Y
(400 people)

PSH

MICROSYSTEM





HGA COST CONSIDERATION



PSH :

$$C = \frac{K}{\text{Slider area}}$$



FULLY AUTOMATED
HGA ASSEMBLY
(LIKE IC'S)

TF :

$$C = \frac{K}{\text{Slider section}} + \text{machine cost}$$



FULLY AUTOMATED
HGA ASSEMBLY
?
BECAUSE SPECIFIC



Hall effect + CMOS in the slider

HALL DETECTOR

Today :

=> 150 μm X 150 μm
=> 1 mv / G

END 1993:

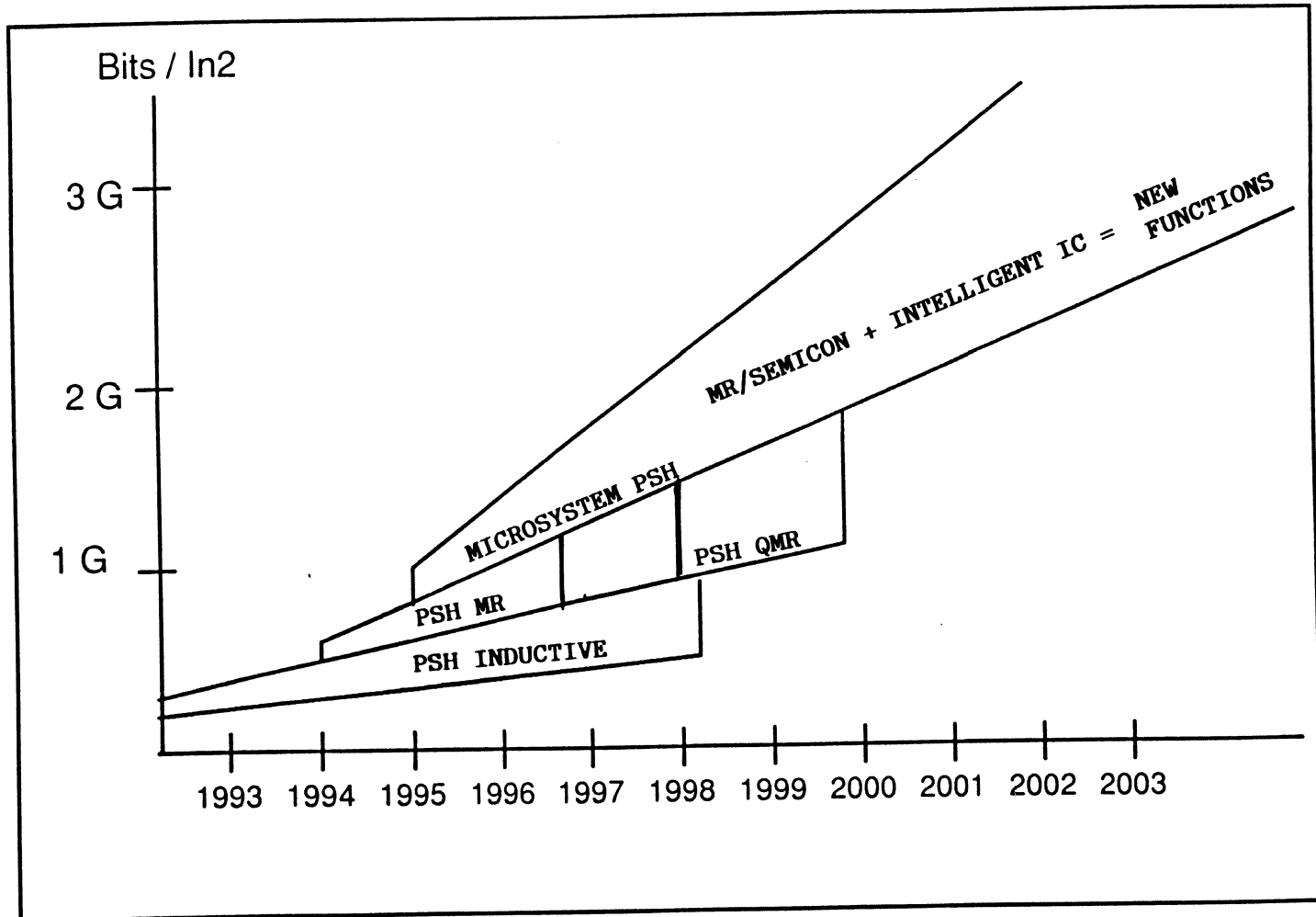
=> Reduced to 2 μm X 2 μm
=> 2 mv / G

CMOS

=> DC control
=> Signal processing



"SENSOR PSH TOWARD "MICROSYSTEM" PSH



"High Density Vertical Recording Heads"

Eric Katz

Censtor

Institute for Information Storage Technology

Santa Clara University, California

December 14 - 16, 1992

OVERVIEW

EARLY HISTORY AND EXAMPLES OF DESIGNS

THEORETICAL COMPARISON WITH LONGITUDINAL RECORDING

RESOLUTION RESPONSE AND PW50 FORMULA

AMPLITUDE RESPONSE Vs. OPERATING CHARACTERISTICS

EXAMPLES OF PERFORMANCE

WINCHESTER HEAD FORMAT

IN-CONTACT HEADS

DESCRIPTION OF THE HEAD

ELECTRICAL PERFORMANCE

DESIGN IMPROVEMENTS AND PERFORMANCE PROJECTIONS

MAGNETORESISTIVE HEADS

RESPONSE TO LONGITUDINAL MEDIA

RESPONSE TO PERPENDICULAR MEDIA

REDESIGNED HEAD FOR PERPENDICULAR MEDIA

BRIEF SUMMARY

INTRODUCTION
AND
EARLY HISTORY

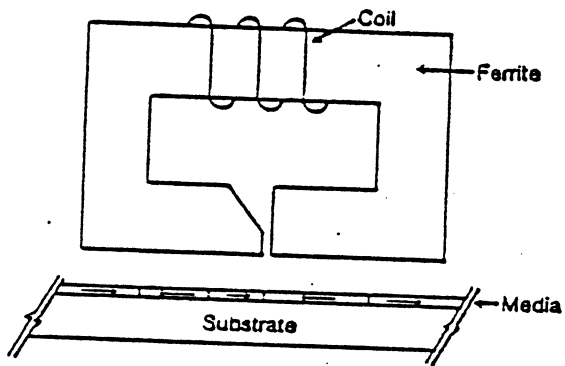


Figure 6A
FERRITE HEAD

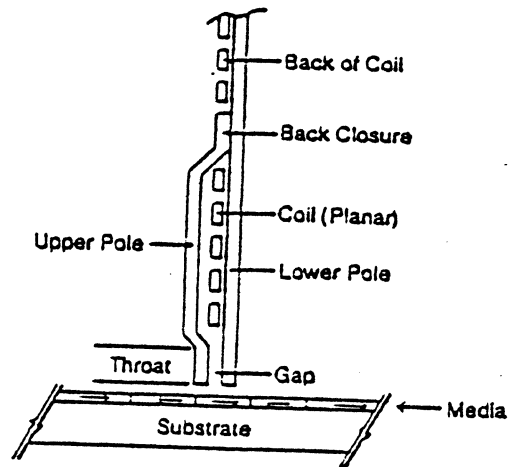


Figure 6B
THIN FILM HEAD

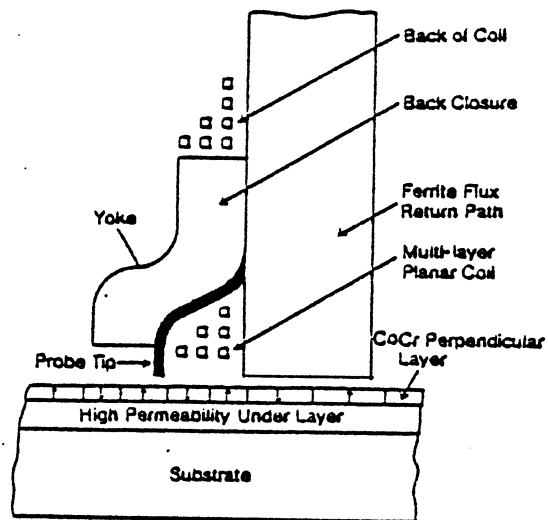
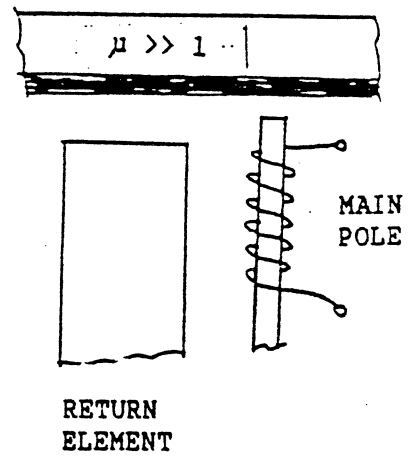
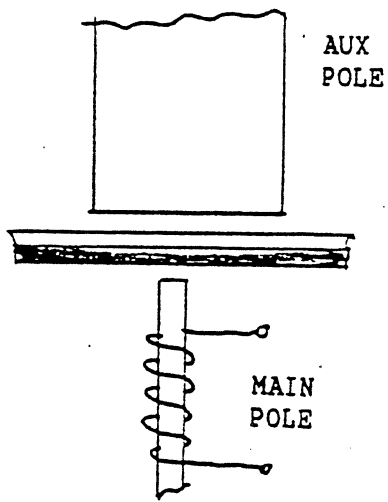
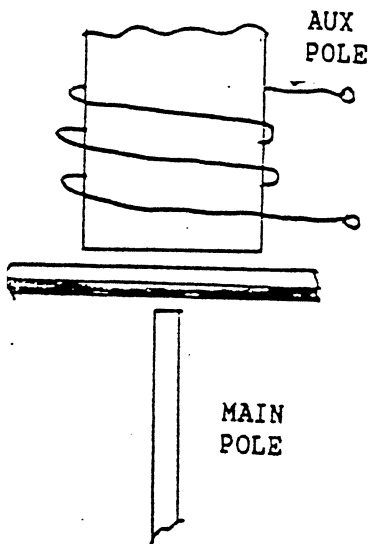
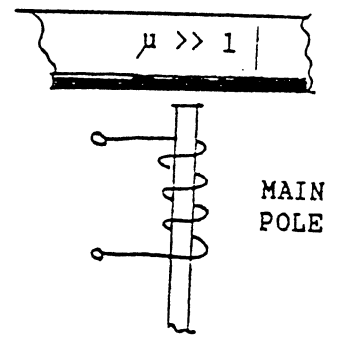
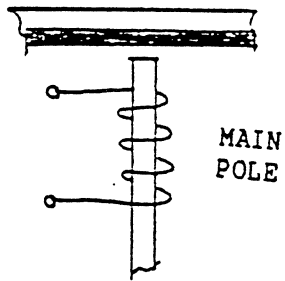
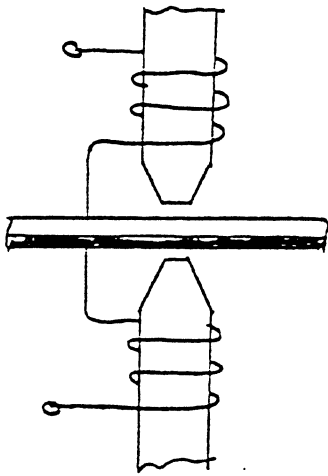
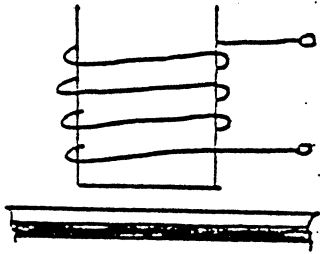


Figure 7
DIAGRAM OF PERPENDICULAR HEAD & DISC

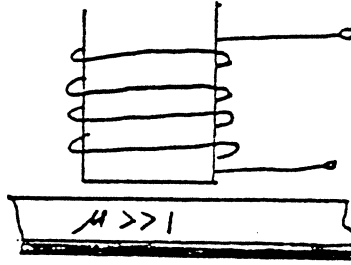
TYPES OF HEADS



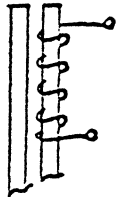
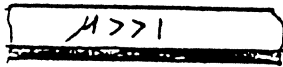
CONFIGURATIONS



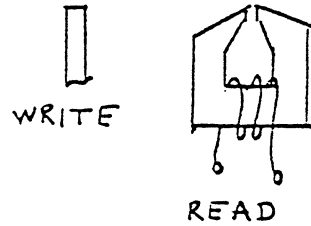
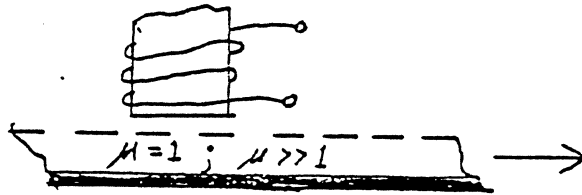
I
Iwasaki
1978



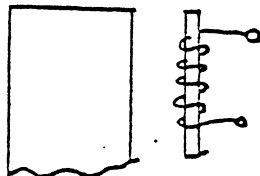
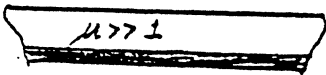
II
Iwasaki et al
1979 & 1980



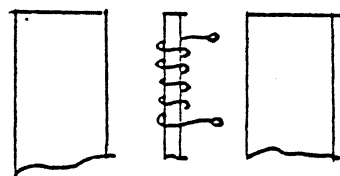
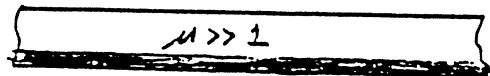
III
Fisher & Katz 1979
Langland et al 1981



IV
Yamamuri et al
1981



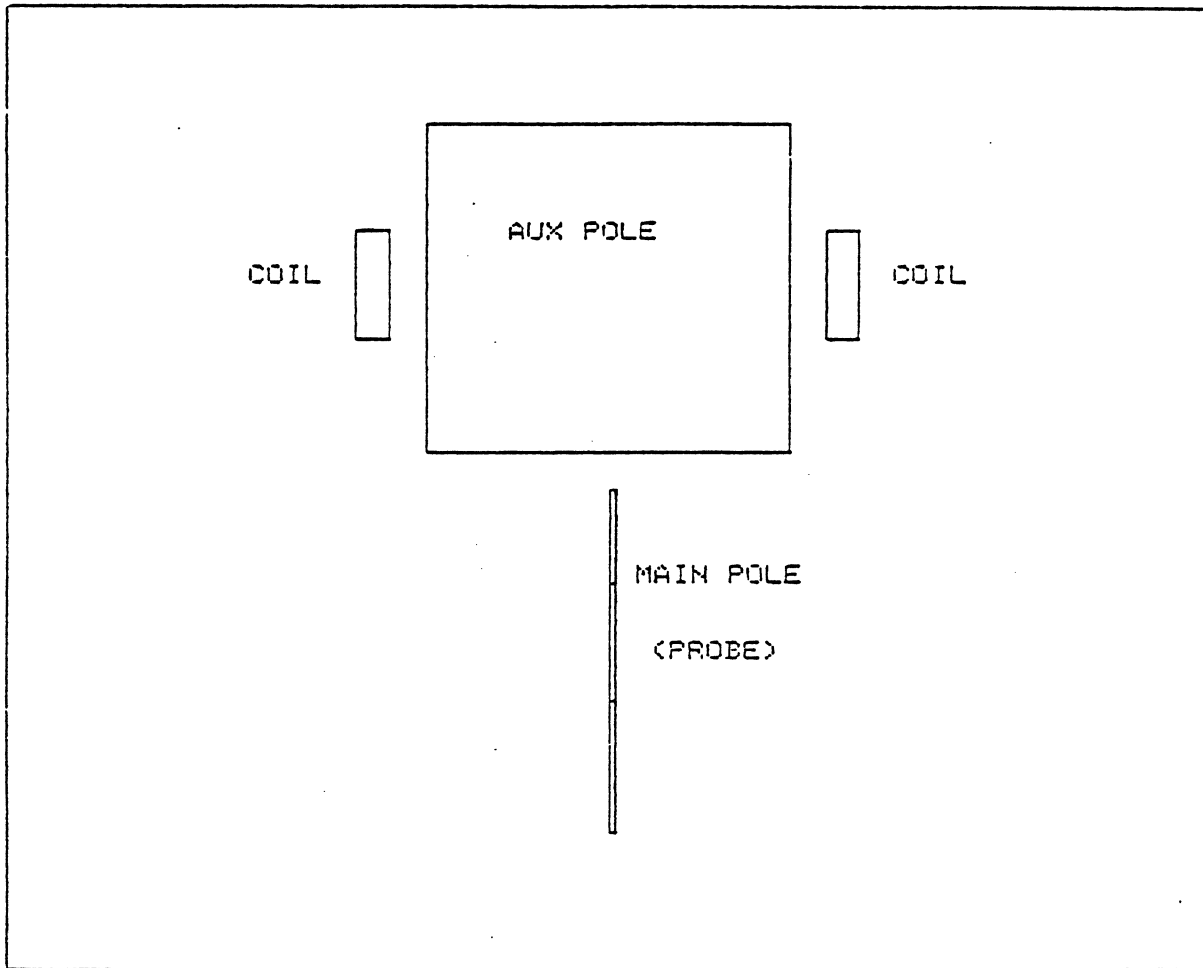
V
Lazzari et al 1981
Tsui (Censtor) 1985



"WSP" HEAD

VI
Hokkyo et al
1984

ANSOFT
Magnetostat
Version 4.03

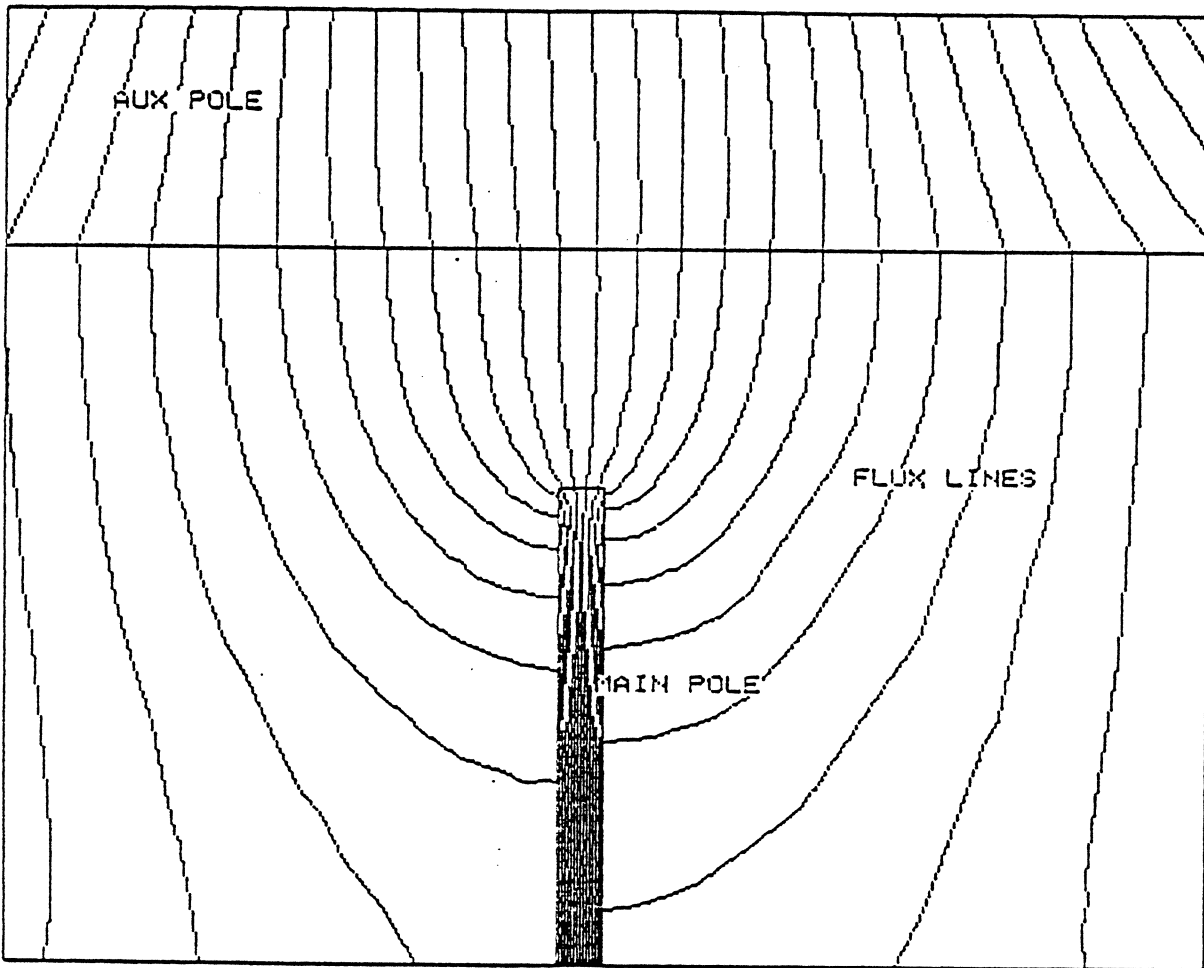
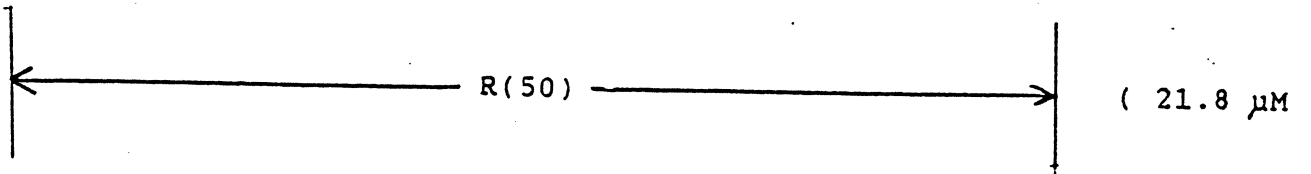


PROBE THICKNESS = 1 μM

POLE TO AUX POLE SPACING = 5 μM

SCALE = 10 X

PERMEABILITY = 1000



ANSOFT
Magnetostat
Version 4.83

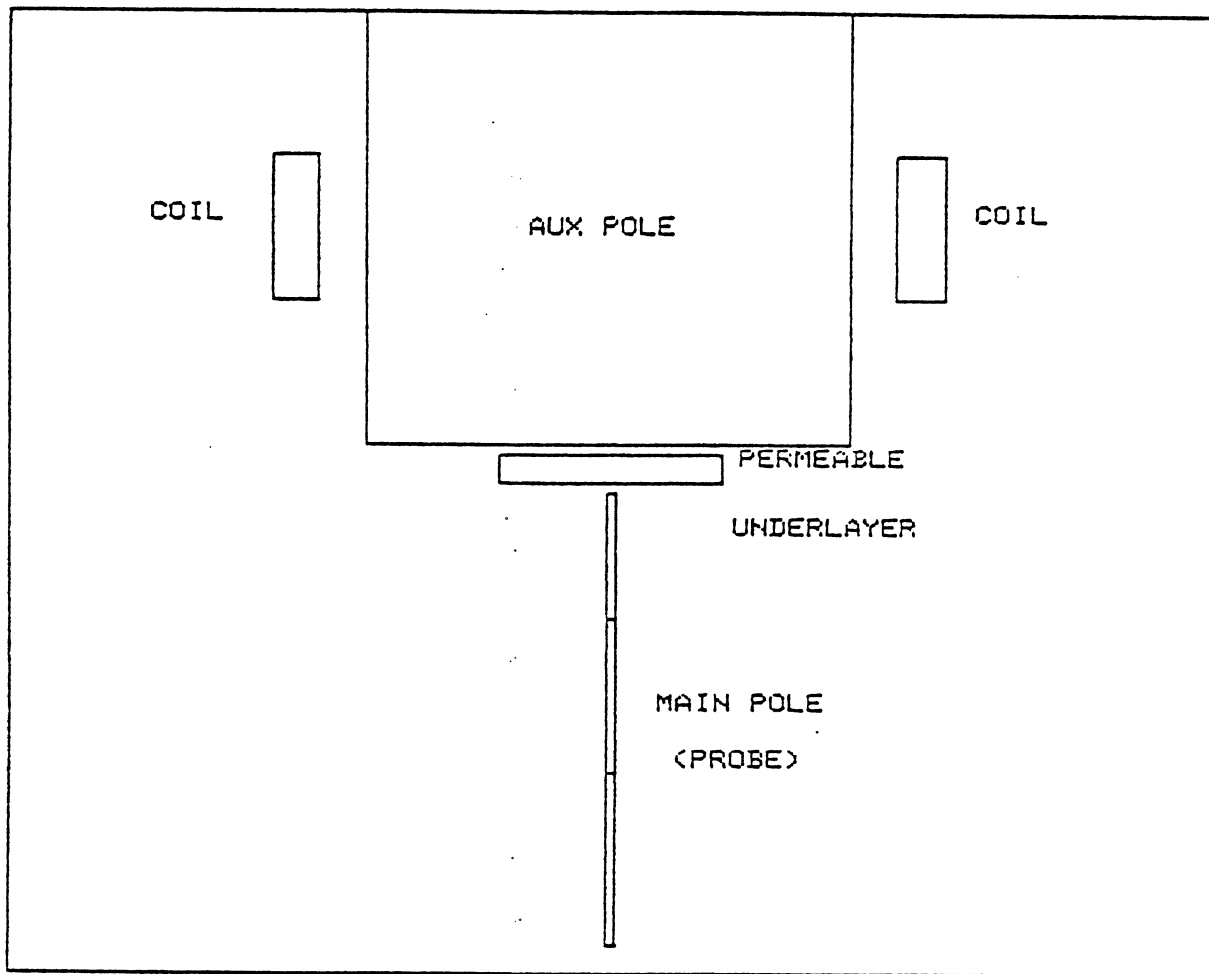
PROBE THICKNESS = 1 μM

POLE TO AUX POLE SPACING = 5 μM

PERMEABILITY = 1000

SCALE = 100 X

ANSOFT
Magnetostat
Version 4.03



PROBE THICKNESS = 1 μM

POLE TO UNDERLAYER SPACING = 1 μM

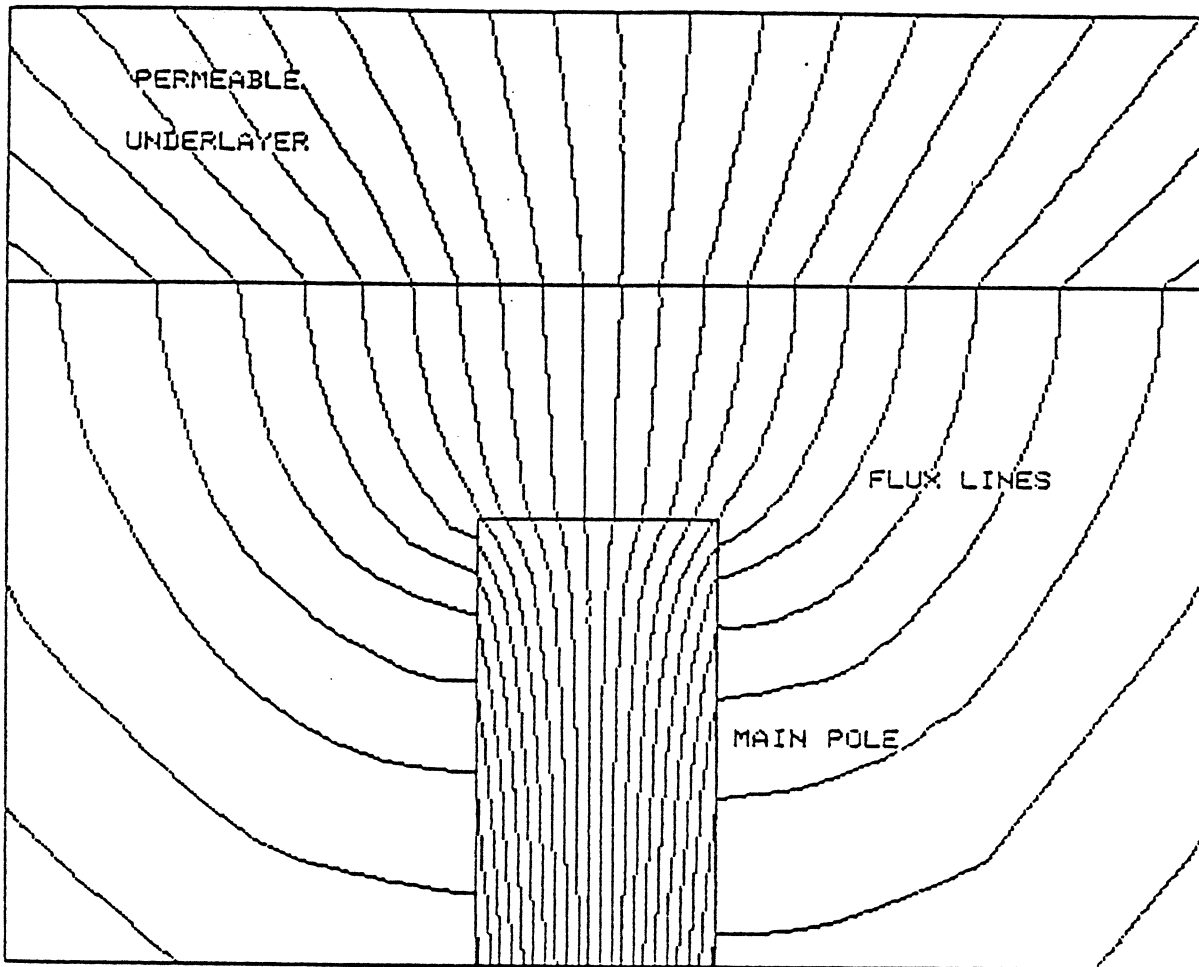
UNDERLAYER THICKNESS = 3 μM

SCALE = 10 X

UNDERLAYER TO AUX POLE SPACING = 1 μM

PERMEABILITY = 1000

← R(50) → (3.0 μM)



ANSOFT
Magnetostat
Version 4.03

PROBE THICKNESS = 1 μM

POLE TO UNDERLAYER SPACING = 1 μM

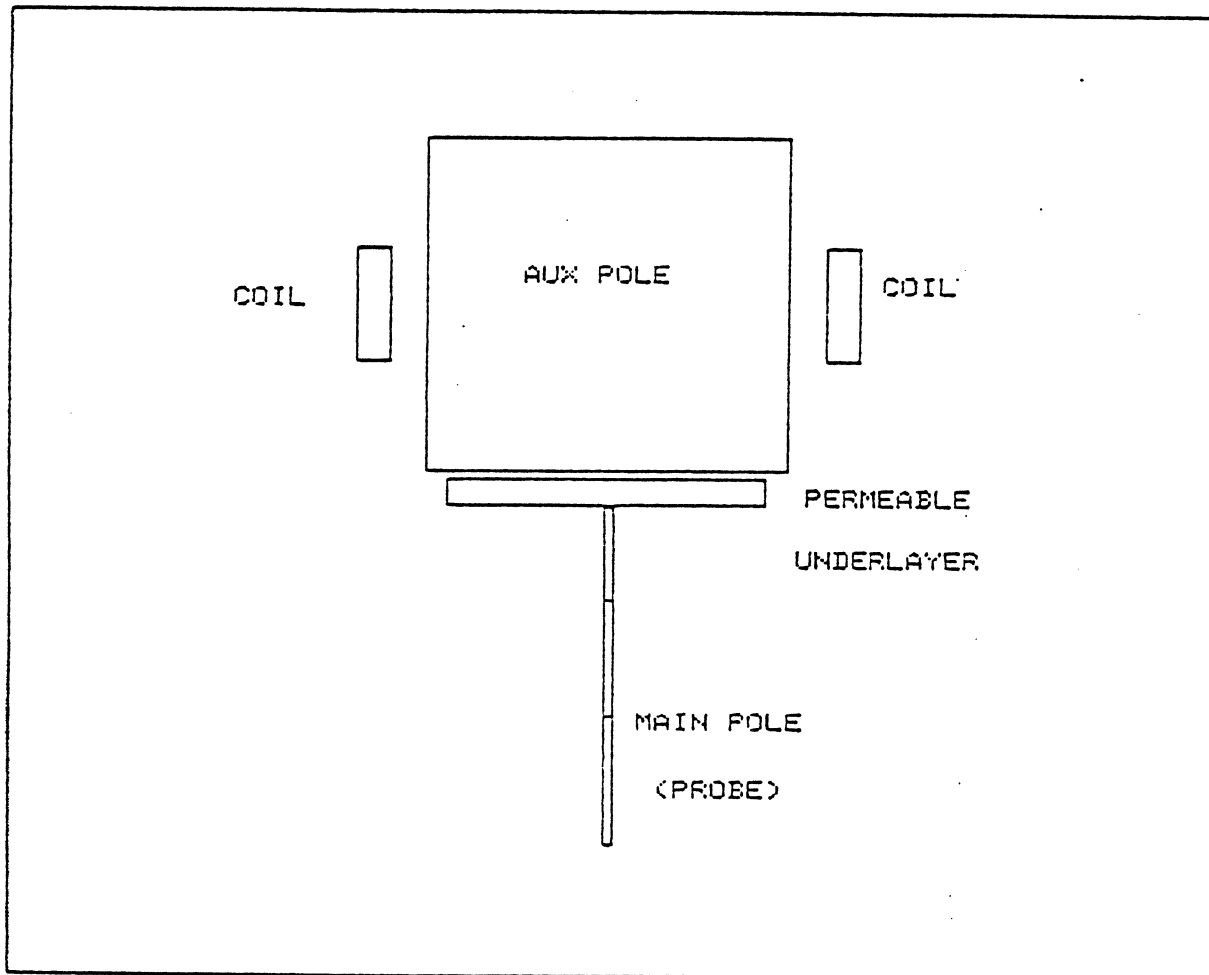
UNDERLAYER THICKNESS = 3 μM

UNDERLAYER TO AUX POLE SPACING = 1 μM

PERMEABILITY = 1000

SCALE = 500 X

ANSOFT
Magnetostat
Version 4.03



POLE THICKNESS = 1 μM

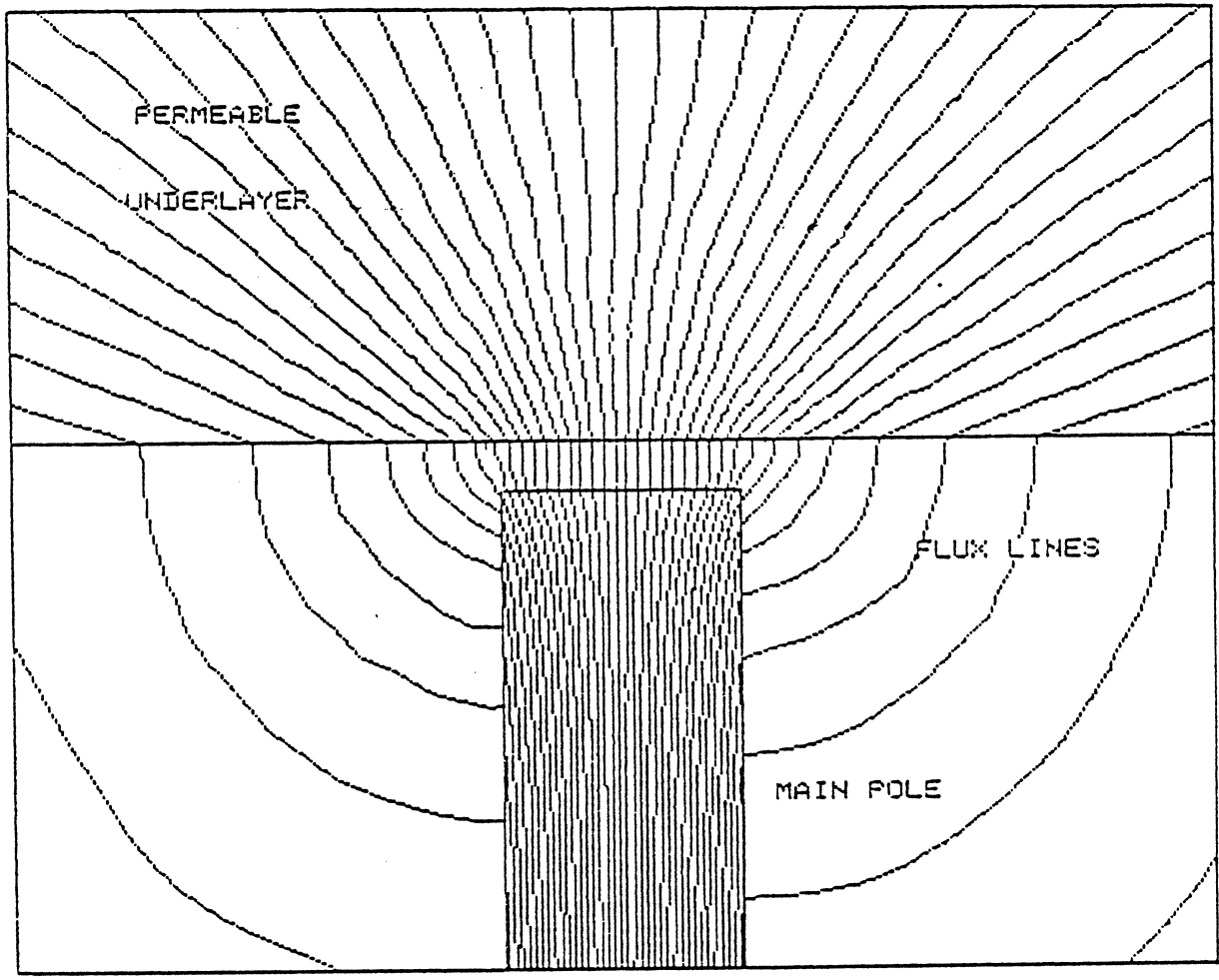
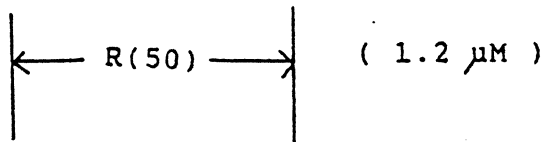
POLE TO UNDERLAYER SPACING = 0.2 μM

UNDERLAYER THICKNESS = 3.8 μM

SCALE = 10 X

UNDERLAYER TO AUX POLE SPACING = 1 μM

PERMEABILITY = 1000



ANSOFT
Magnetostat
Version 4.03

POLE THICKNESS = 1 μM

POLE TO UNDERLAYER SPACING = 0.2 μM

UNDERLAYER THICKNESS = 3.8 μM

SCALE = 500 X

UNDERLAYER TO AUX POLE SPACING = 1 μM

PERMEABILITY = 1000

THEORETICAL
BACKGROUND

Figure 8
 LONGITUDINAL RECORDING
 MAGNETOSTATICS

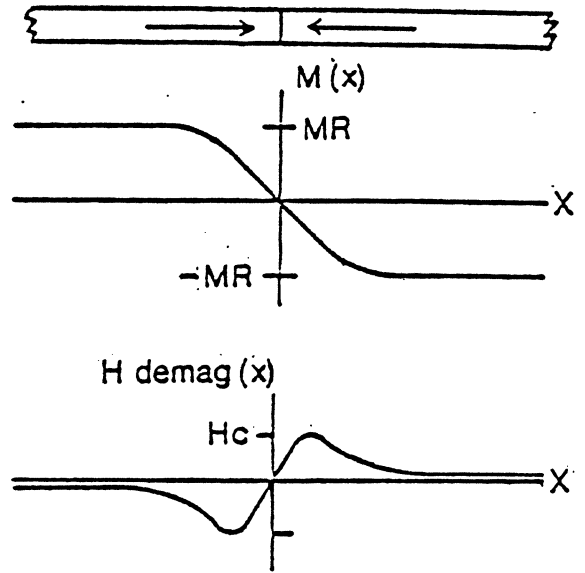
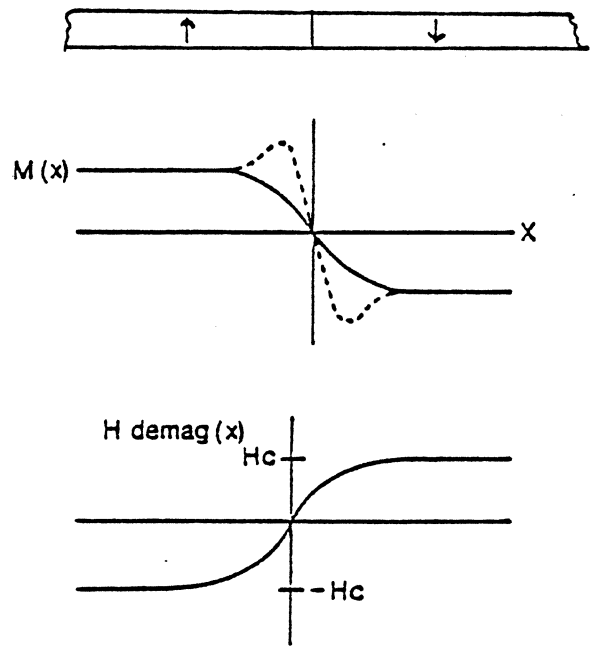
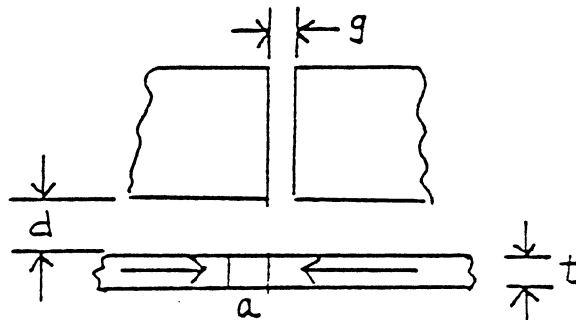


Figure 9
 PERPENDICULAR RECORDING
 MAGNETOSTATICS



SIMILARITIES BETWEEN LONGITUDINAL AND PERPENDICULAR RECORDING
- RESOLUTION DEPENDENCE

LONGITUDINAL



SIMPLIFYING ASSUMPTIONS

1. The longitudinal field of the head is described by the Karlquist field function
2. The media magnetization is completely longitudinal (no vertical component)
3. The transition region can be approximated by an arctangent function:

$$M(x) = M_0 \arctan((x-x_0)/a)$$

RESULTS

1. Isolated transitions result in a Lorentzian shaped pulse:

$$V(\tau) = V_0 \frac{1}{1+(\tau/\tau_0)^2}$$

2. The width of the pulse is given by:

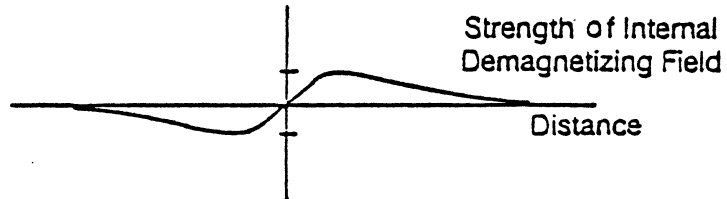
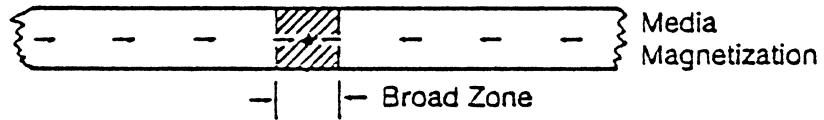
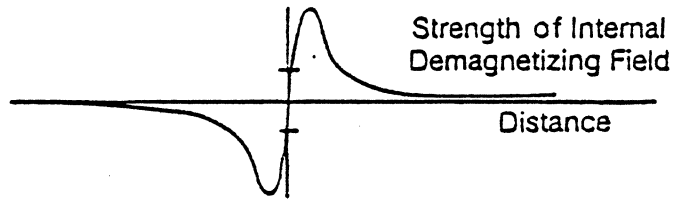
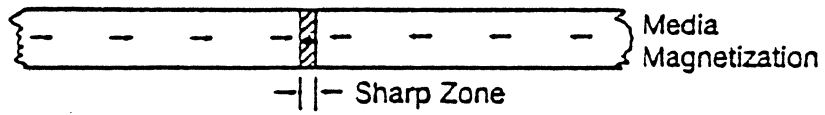
$$PW_{50} = 2\sqrt{(a+d)^2 + (g/2)^2}$$

3. For media of finite thickness, t , the effective flying height is measured to a point interior to the media. This increases PW_{50} slightly, as follows:

$$PW_{50} = 2\sqrt{(a+d)(a+d+t) + (g/2)^2}$$

4. The resolution performance characteristics of the head (bitshift, amplitude vs bit density) are determined by PW_{50}

SELF-DEMAGNETIZATION, TRANSITION ZONE BROADENING



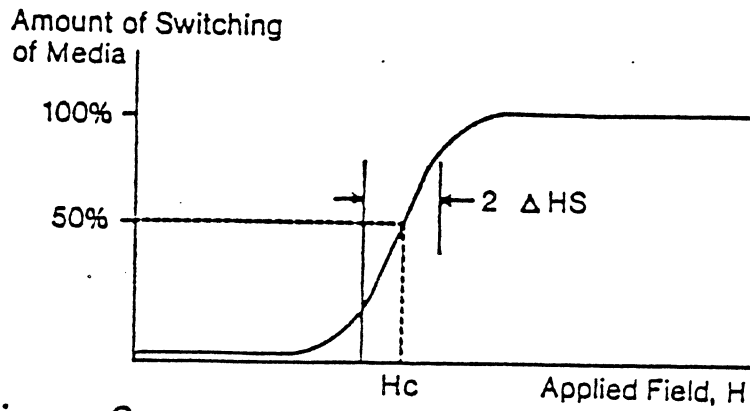


Figure 3
 DEGREE OF SWITCHING vs. APPLIED FIELD

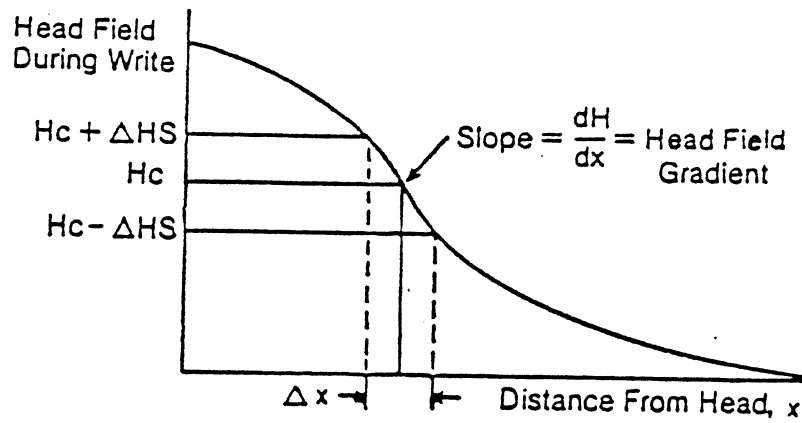
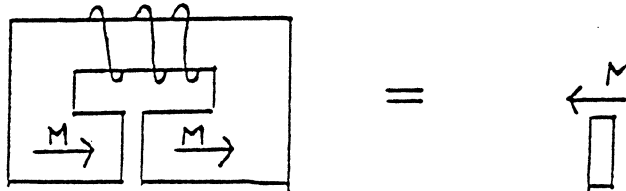


Figure 4
 HEAD FIELD vs. DISTANCE

APPLICATION OF LONGITUDINAL RESULTS
TO PERPENDICULAR CASE

THEOREM 1 - The write field of a gapped-ring head is the same as that of an oppositely magnetized slab with the same dimensions as the gap.

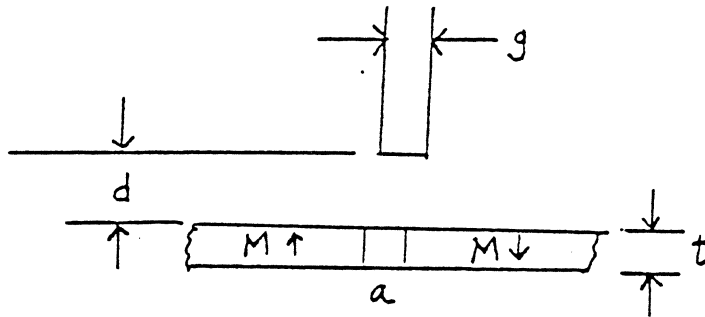


THEOREM 2 - Regarding the fringing field of a uniformly magnetized 2-dimensional body: if the magnetization of that body is rotated uniformly by any angle (say 90°), then at each point in space external to the body, the fringing field rotates in the opposite direction by the same angle (in our example, -90°).

THEOREMS 1 AND 2 CONVERT A GAPPED RING HEAD TO A PERPENDICULAR RECORDING PROBE HEAD, WITH PROBE THICKNESS EQUIVALENT TO THE ORIGINAL GAP LENGTH.

THEOREM 3 - CONVOLUTION THEOREM

- A. Applied to media which is magnetized purely longitudinally: the readback signal is given by the convolution of the longitudinal component of the head writing field function with the media magnetization function.
- B. Applied to media which is magnetized purely perpendicularly: the readback signal is given by the convolution of the perpendicular component of the head writing field function with the media magnetization function.



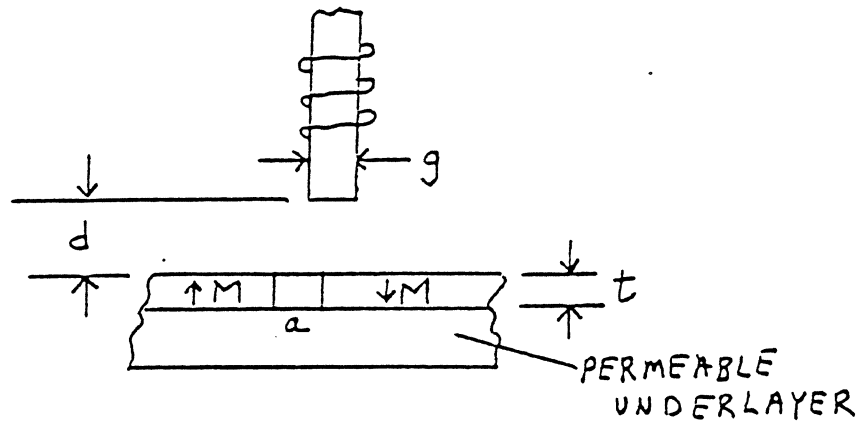
$$PW_{50} = 2 \sqrt{(a+d)^2 + (g/2)^2}$$

$$\rightarrow 2 \sqrt{(a+d)(a+d+t) + (g/2)^2}$$

PERPENDICULAR RECORDING - RESOLUTION

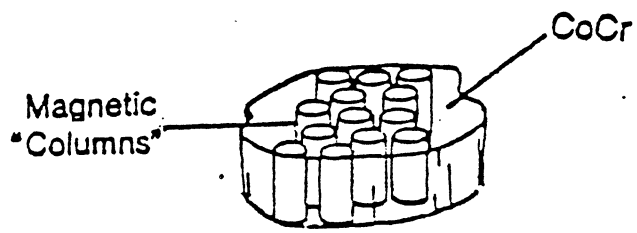
1. Probe tip thickness in perpendicular recording plays the same role as gap length in longitudinal recording.
2. Both have the same spacing loss (flying-height) sensitivity.
3. Both depend in a similar way on the transition length in the media:

$$PW_{50} = 2\sqrt{(a+d)(a+d+t) + (g/2)^2}$$



4. For a double layer media (permeable underlayer), the head "sees" images of magnetic structures located above the underlayer.
 - a. This doubles the effective thickness of the written media.
 - b. This doubles the perpendicular component of the head write field function at the position of the media, thereby increasing the amplitude response of the head.

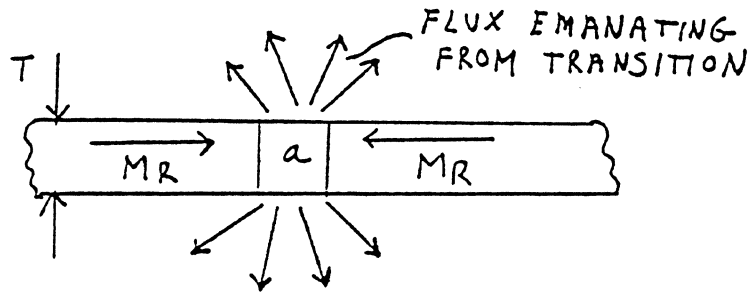
$$PW_{50} = 2\sqrt{(a+d)(a+d+2t) + (g/2)^2}$$



COLUMNAR STRUCTURE

SIGNAL AMPLITUDE - DEPENDENCE ON FLYING HEIGHT

LONGITUDINAL



1. SIGNAL AMPLITUDE $\propto \frac{\text{(TOTAL FLUX THROUGH COIL)}}{\text{(TIME REQ'D FOR FLUX TO REVERSE DIRECTION THROUGH THE COIL)}}$

2. TOTAL FLUX (PER UNIT OF TRACKWIDTH)

$\Phi_{\text{TOTAL}} = 2 \times 4\pi M_R \times T$

← Core links do field

3. FRACTION OF FLUX "CAPTURED" BY THE HEAD

$$f = \frac{\mu - 1}{\mu + 1}$$

4. HEAD EFFICIENCY (FRACTION OF FLUX ENTERING THE HEAD WHICH "LINKS" THROUGH THE COIL AND GENERATES SIGNAL).

$$\eta = \frac{R_g}{R_g + R_c}$$

$R_g = \text{gap reluctance}$
 $R_c = \text{core reluctance}$

SIGNAL AMPLITUDE - PERPENDICULAR

1. FLUX LINES ARE GENERATED EVERYWHERE IN THE MEDIA,
EXCEPT AT THE TRANSITIONS.

2. THE RELEVANT FLUX LINES ARE THE ONES IN THE MEDIA IN
THE IMMEDIATE VICINITY OF THE PROBE TIP.

3. THESE FLUX LINES ARE DIVIDED INTO TWO PATHS:
 - THROUGH THE HEAD
 - DEMAGNETIZING FIELDS INSIDE THE MEDIA

4. THE FRACTION OF THE FLUX LINES IN EACH OF THESE PATHS
DEPENDS ON THE MAGNETIC RELUCTANCES OF THE TWO PATHS.

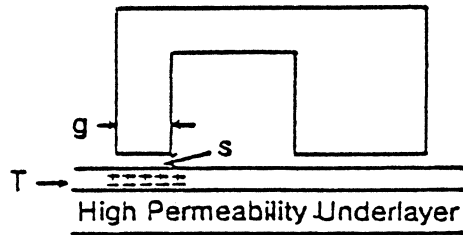


Figure 10A
 DIAGRAM OF HEAD ON DUAL LAYER MEDIA

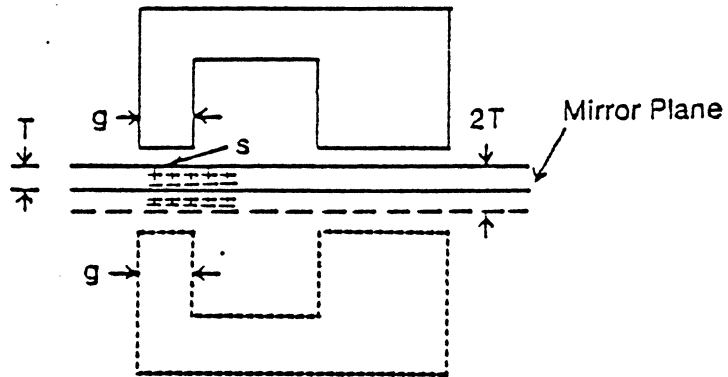


Figure 10B
 EQUIVALENT MAGNETICS, IMAGE CHARGES

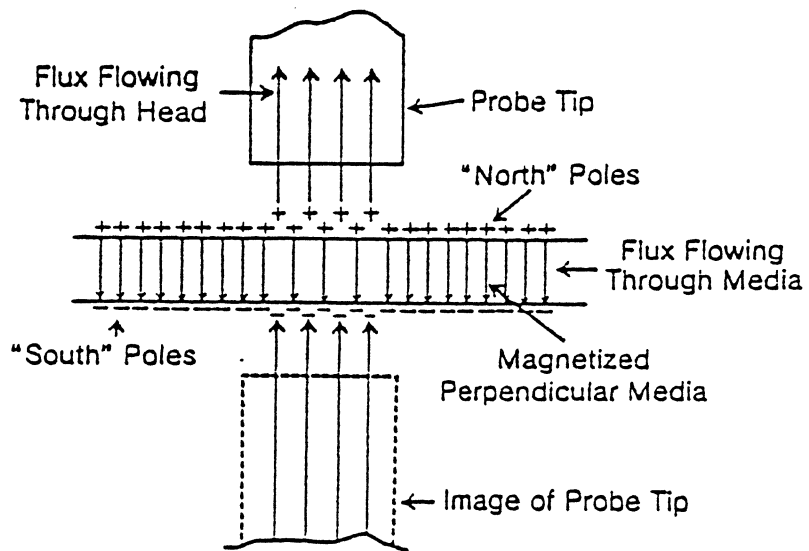


Figure 10C

FLUX DIVIDER ACTION IN
 PERPENDICULARLY RECORDED MEDIA
 NEAR READ HEAD

SIGNAL AMPLITUDE - PERPENDICULAR

1. TOTAL FLUX AVAILABLE (PER UNIT OF TRACKWIDTH)

$$\bar{\Phi}_{\text{TOTAL}} = 4\pi M_R g \longrightarrow H_c \times g$$

2. FRACTION OF FLUX "CAPTURED" BY THE HEAD

$$f = \frac{R_{\text{DEMAG}}}{R_{\text{HEAD PATH}} + R_{\text{DEMAG}}}$$
$$= \frac{T}{T + D + L_h}$$

T = CoCr Media Thickness

D = Flying height

L_h = Head reluctance, expressed as an equivalent magnetic path length through air

(Can be made negligible)

3. HEAD EFFICIENCY

$$\eta = \frac{R_g}{R_g + R_c}$$

RESULTS

$$\Phi_{\text{PERP}} = 2 H_c \cdot g \cdot \frac{T}{T+D} \cdot \eta$$

H_c = Media Coercivity
 g = probe tip thickness
 T = Media thickness
 D = Head/media spacing
 η = Core efficiency

$$\Phi_{\text{LONGIT}} = 2 \cdot B_r T \cdot \eta$$

B_r = Media remanance
 T = media thickness
 η = Core efficiency

1. Available flux is proportional to g rather than T .
2. Media remanance is proportional to coercivity.
3. Flux divider action term: Signal amplitude drops as D is increased past T (In addition to dropping due to the broadening of the pulse).
4. Design optimization for perpendicular recording is based on these considerations.

PERPENDICULAR RECORDING OVERALL SIGNAL EFFICIENCY

o FLUX AVAILABLE FOR THE SIGNAL

$$\bar{\Phi} \text{ PERP} = 2 H_c \cdot g \cdot \frac{T}{T + D} \cdot \eta$$

H_c = MEDIA COERCIVITY

g = PROBE TIP THICKNESS

T = MEDIA THICKNESS

D = HEAD / MEDIA SEPARATION

η = HEAD EFFICIENCY

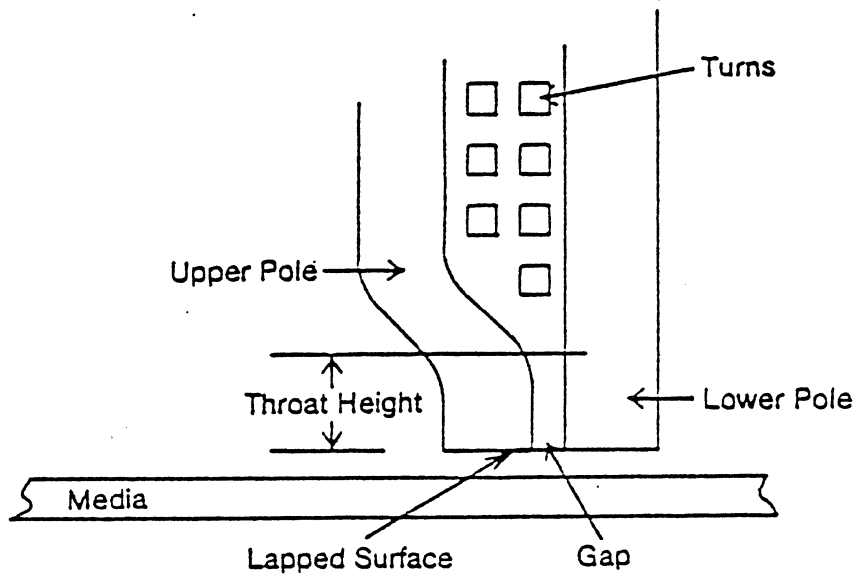
o SIGNAL

$$\text{SIGNAL} \propto \frac{d\bar{\Phi}}{dt} \propto \frac{\text{VELOCITY} \cdot \bar{\Phi} \text{ PERP}}{\text{PW}_{50}}$$

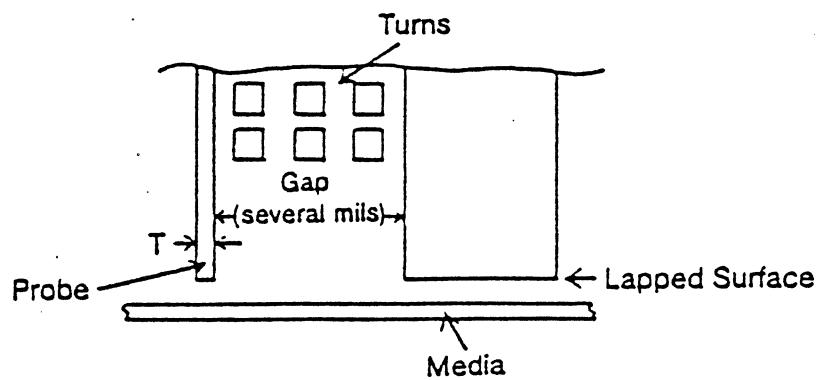
o PULSE WIDTH

$$\text{PW}_{50} = 2 \sqrt{(a+D)(a+D+2T) + (g/2)^2}$$

a = MEDIA TRANSITION ZONE



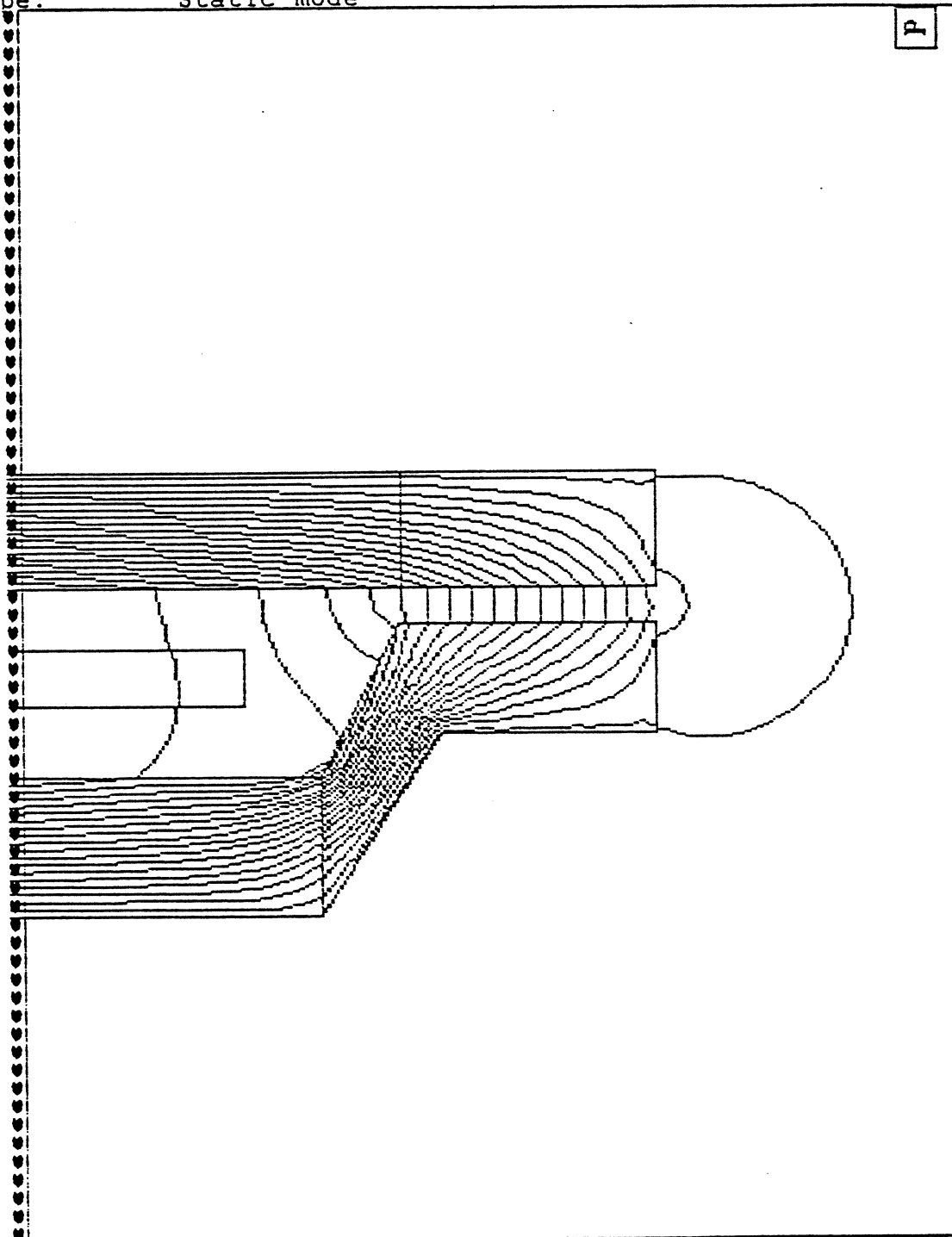
CROSS SECTION OF THIN FILM HEAD NEAR AIR-BEARING SURFACE



CROSS SECTION OF PERPENDICULAR RECORDED MEDIA NEAR READ HEAD

DATE = 11/12/1992 TIME= 15:55:26.72
Current database: dbase.ies
Current file: TFHEAD1
Mode of analysis: MAGNETO 2D Field analysis
Analysis type: Static mode

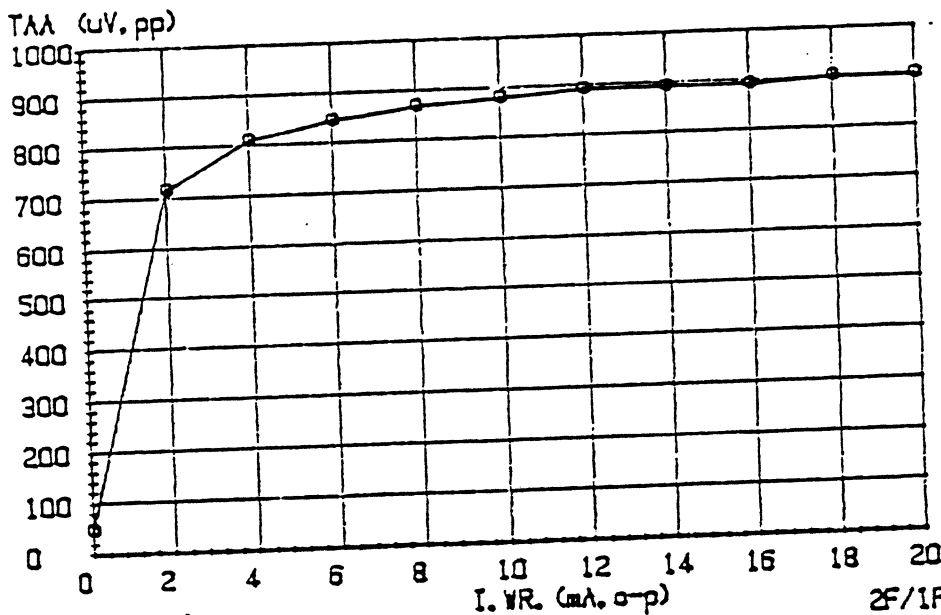
FLUX LINES IN POLE TIP REGION
OF THIN FILM HEAD



FLYING HEADS
- WINCHESTER FORMAT

DISK S/N BR8-518-16 B
 HEAD S/N 642-12-07 ON (1700 TPI) 50T
 F.H. = 6μ in. TPI = 1700
 I. WR. 12 mA FREQ. .25 MHz
 SPEED 3590 RPM 1000 IPS
 RADIUS 2.66 In

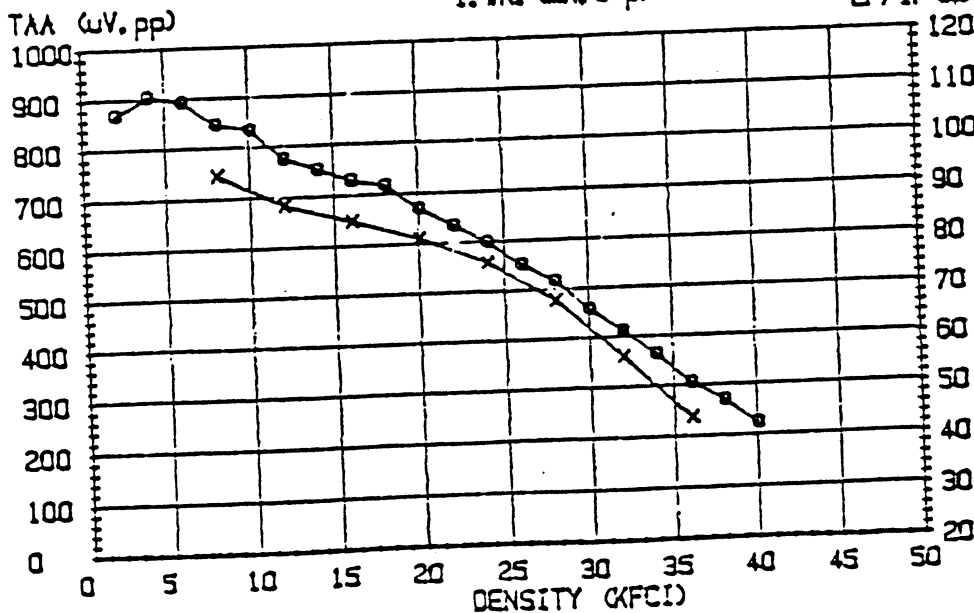
TAA (pp) 834.5 μ V MOD. 5.2 %
 Epp 870 μ V
 PW-50 56.65 ns 56.7 μ IN
 PW-20 107.4 ns 107.4 μ IN
 SYM-AREA 13.8 %
 NOISE Elec. 6.8 μ V. Mod. 4.3 μ V
 (20 MHz) Total 8 μ V



—SAT. CURVE—
 FREQ. WR. .25 MHz
 SPEED 1000 IPS
 RADIUS 2.66 IN

KFCI	20.0	25.0	30.0
BIT INTERVAL SHIFT			
tp (ns)	2.2	8.3	10

S/N (dB)			
Elect.	33.4	32.4	30.4
Media	37.3	36.3	34.3
Total	31.9	30.9	28.9

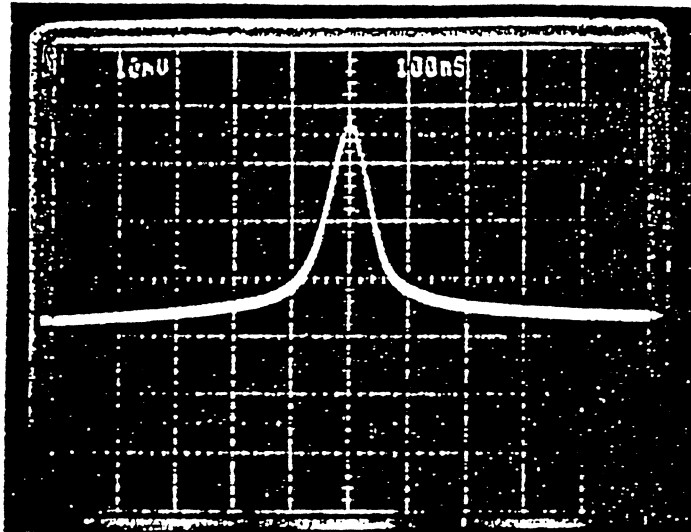


—RES. CURVE—
 o - Epp. x - Res. %
 I. WR. 12 mA
 SPEED 1000 IPS
 RADIUS 2.66 IN

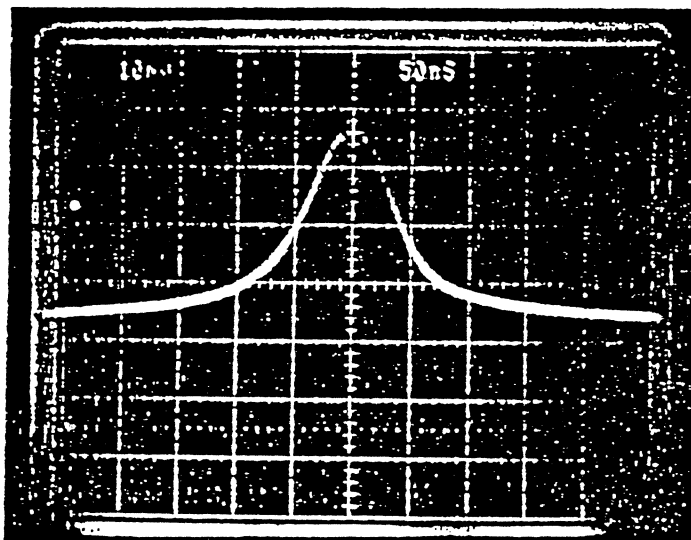
KFCI.	RES. %	TAA (pp)
25.7	70.0	538.2
20.0	80.4	664.1
30.0	61	457.7

Q. Y. 32.5 dB @ 8/4MHz

CPR. INIT. _____ #1



100 ns/div



50 ns/div

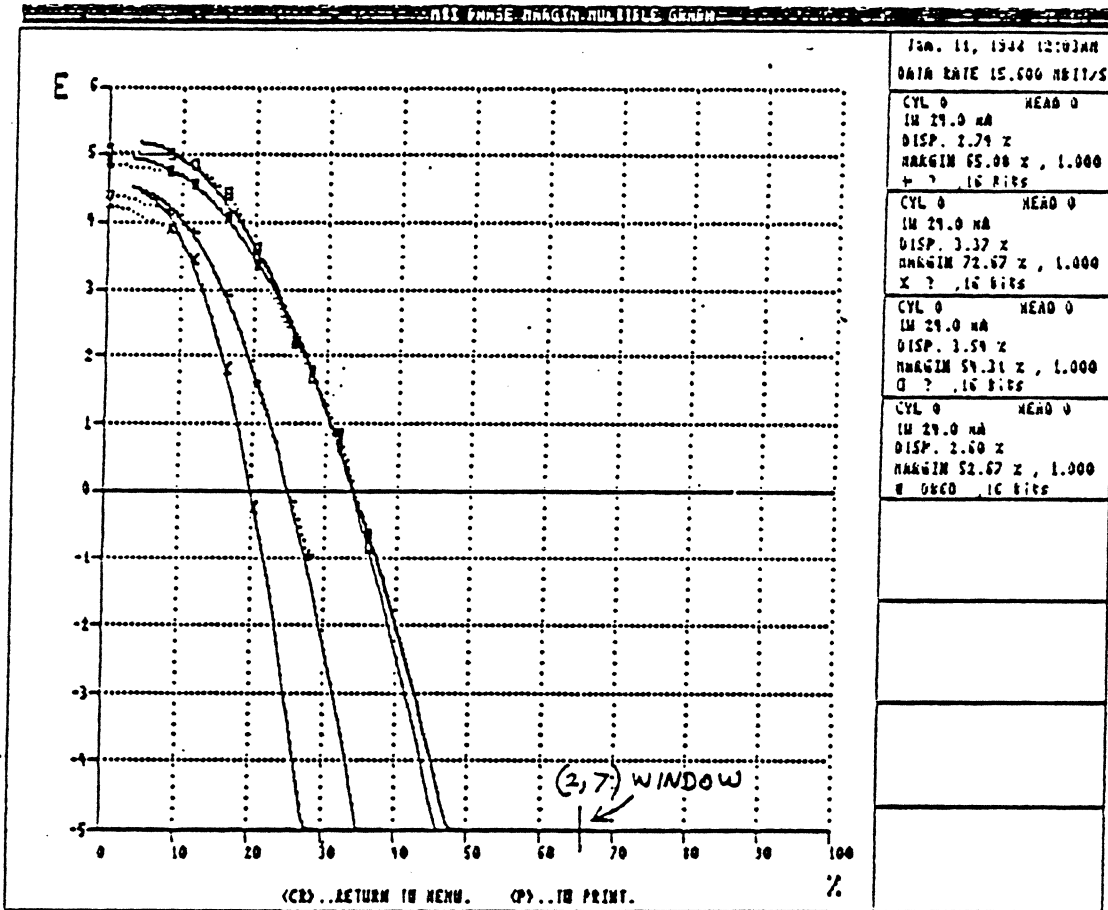
vel = 550 ips

9

HEAD 504-04-04U
 DISK MRF 25/35-50A
 PREAMP VTC VM114
 Rd = 1500 OHM
 2.66" r, 3600 RPM (1000 IPS)
 15.6 KFCI

MARGIN #
 1
 2
 3
 4

CONDITIONS
 1F
 2F
 110110...
 DB6D



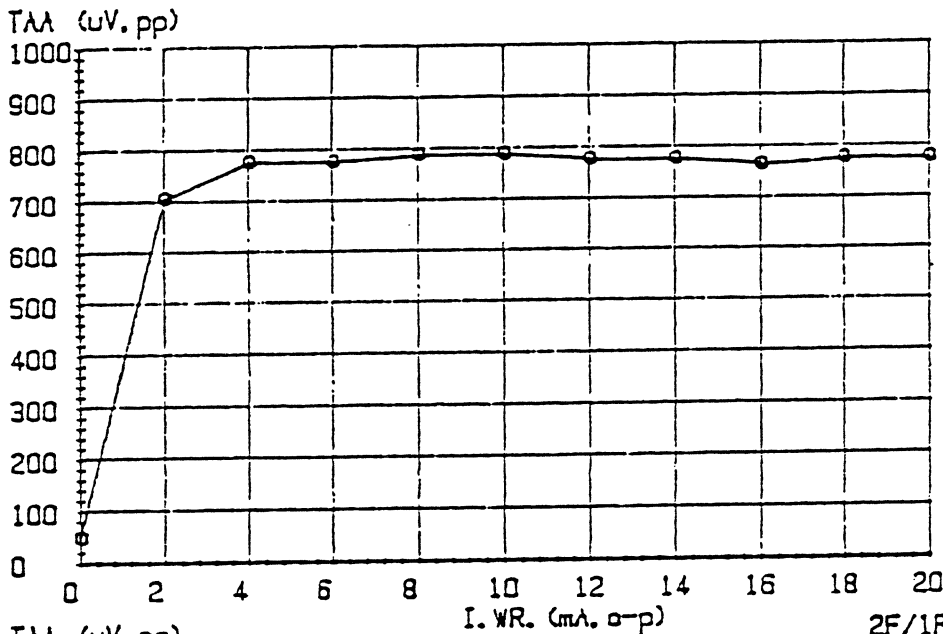
8" FORMAT 16 KFCI (2,7) CODE = 24 KBPI
 2200 TPI 52.8 bits/in²

6Y¹

DISK S/N RW158
 HEAD S/N 679-08-08 DN
 F.H. = 3.64" I.D. TPI = 1700 60T.
 I.WR. 10 mA FREQ. .25 MHz
 SPEED 2073 RPM 477.6 IPS
 RADIUS 2.2 In

TAA (pp) 752.3 uV MOD. 10 %
 Epp 775.3 uV
 PW-50 82.0400001 nS 39.2 uIN
 PW-20 156.3 nS 74.6 uIN
 SYM-AREA 11.7 %
 NOISE Elec. 7.4 uV, Mod. 4 uV
 (20 MHz) Total 8.4 uV

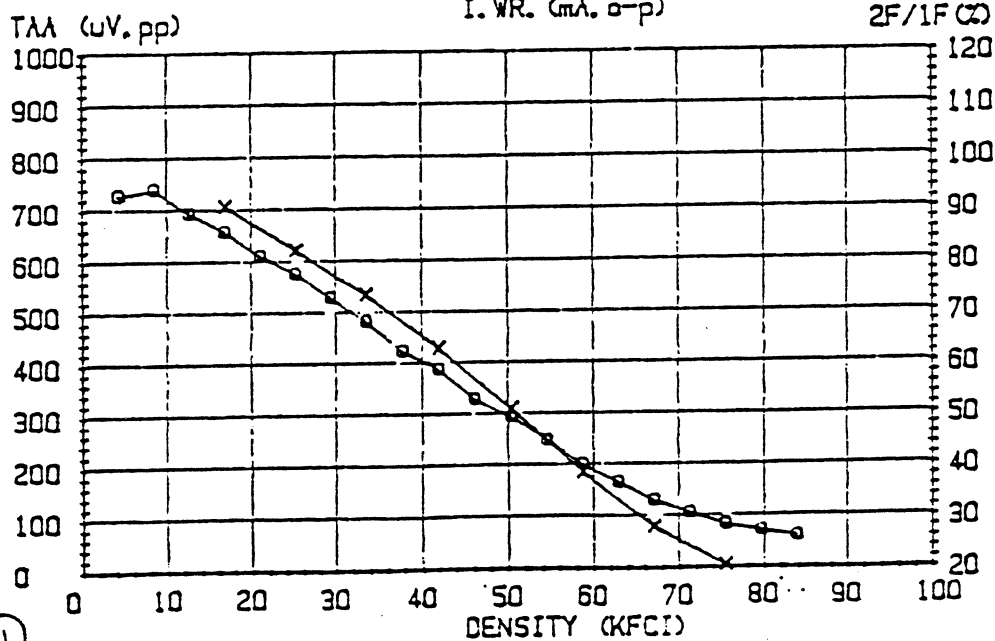
5 1/4"



—SAT. CURVE—
 FREQ. WR. .25 MHz
 SPEED 477.6 IPS
 RADIUS 2.2 IN

KFCI	20.0	25.0	30.0
BIT INTERVAL SHIFT			
tp (ns)	2.7	1.8	7.2

S/N (dB)			
Elect.	32.5	31.8	30.9
Media	37.7	37	36.1
Total	31.4	30.7	29.8

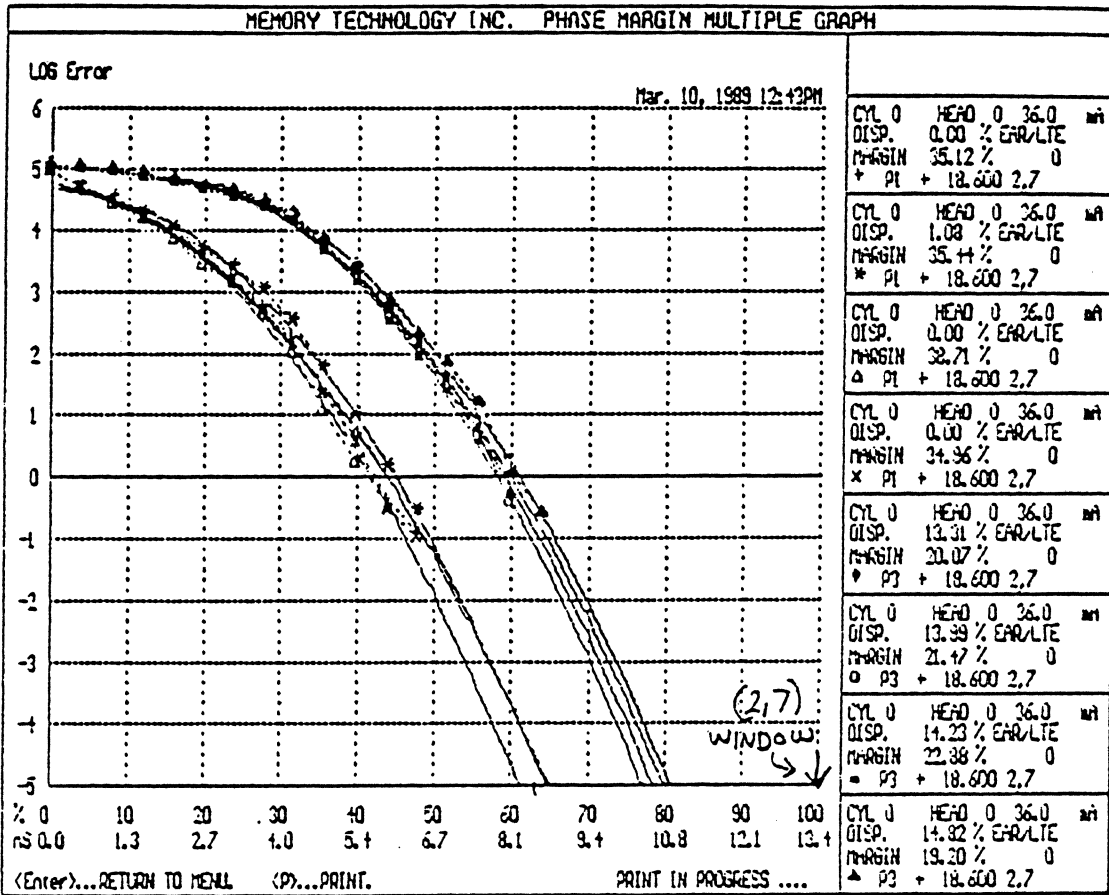


—RES. CURVE—
 o - Epp. x - Res. %
 I. WR. 10 mA
 SPEED 477.6 IPS
 RADIUS 2.2 IN

KFCI.	RES. %	TAA (pp)
35.6	70.0	453.5
20.0	88	619.8
30.0	76.9	515.8

O.V. -34.3 dB @ 8/4MHZ

OPR. INIT. _____ #1

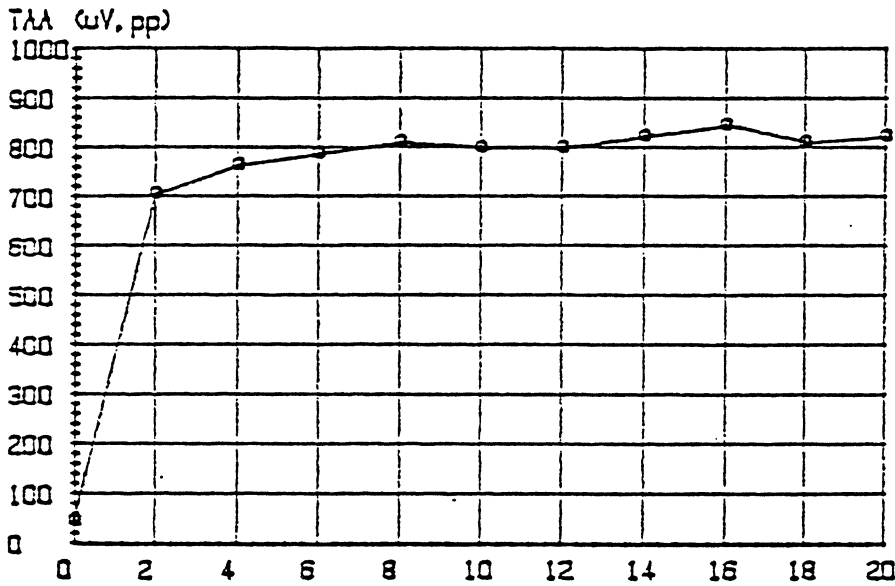


5 1/4" FORMAT 26 KFCI (2,7) CODE = 39 KBPI
 1700 TPI = 66.3 x 10⁶ bits/in²
 (60 TURNS)

DISK S/N 8-A
 HEAD S/N 1037-25-10 (UP)
 → F.H. = 3 1/2" uIn. TPI = 11 μm
 I. WR. 10 mA FREQ. .25 MHz (2000 TPI)
 SPEED 2575 RPM 377.5 IPS
 RADIUS 1.4 In

544

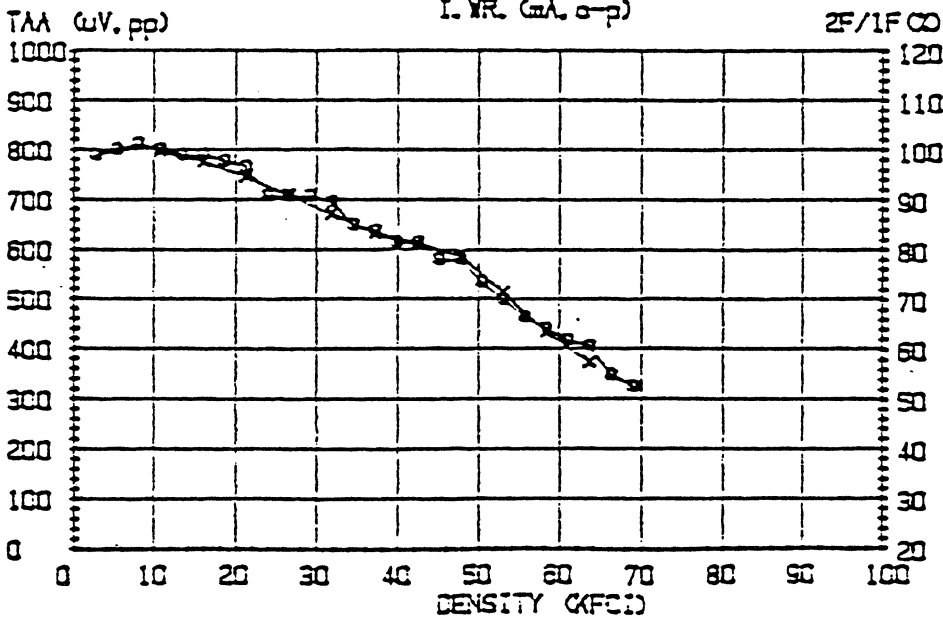
TAA (pp) 788.6 uV MOD. 9 %
 Epp 837.5 uV
 PY-50 72.2700001 nS 27.3 uIN
 PY-20 128.9 nS 48.7 uIN
 SYN-AREA 10.9 %
 NOISE Elec. 7 uV. Mod. 3 uV
 (20 MHz) Total 7.6 uV



—SAT. CURVE—
 FREQ. WR. .25 MHz
 SPEED 377.5 IPS
 RADIUS 1.4 IN

KFCI 20.0 25.0 30.0
 BIT SHIFT
 tp (ns) 2.8 3.4 4.3

S/N (dB)
 Elect. 34.7 34.5 33.8
 Media 42.1 41.8 41.1
 Total 34 33.7 33



—RESOL. CURVE—
 o - Epp. x - Res. %
 I. WR. 10 mA
 SPEED 377.5 IPS
 RADIUS 1.4 IN

KFCI. RES. % TAA (pp)
 20.0 70.0 496
 25.0 88.3 698.4

O. V. 31.8 dB @ 4/8MHz

OPR. INIT. _____ #1

PHASE MARGIN ANALYZER II

DISK - B-A (95 mm)

HEAD - 1037-26-10

CONDITIONS:

MICRO. READ. - 28.70 PERIOD - 28.30

SPEED - 2117 RPM, DETENT - 130 MM

RADIUS - 1.70", VELOCITY - 377 IPS

FREQUENCY - 18.6 VFO, 13CODE.RLL

P.O.

24 JULY 1990

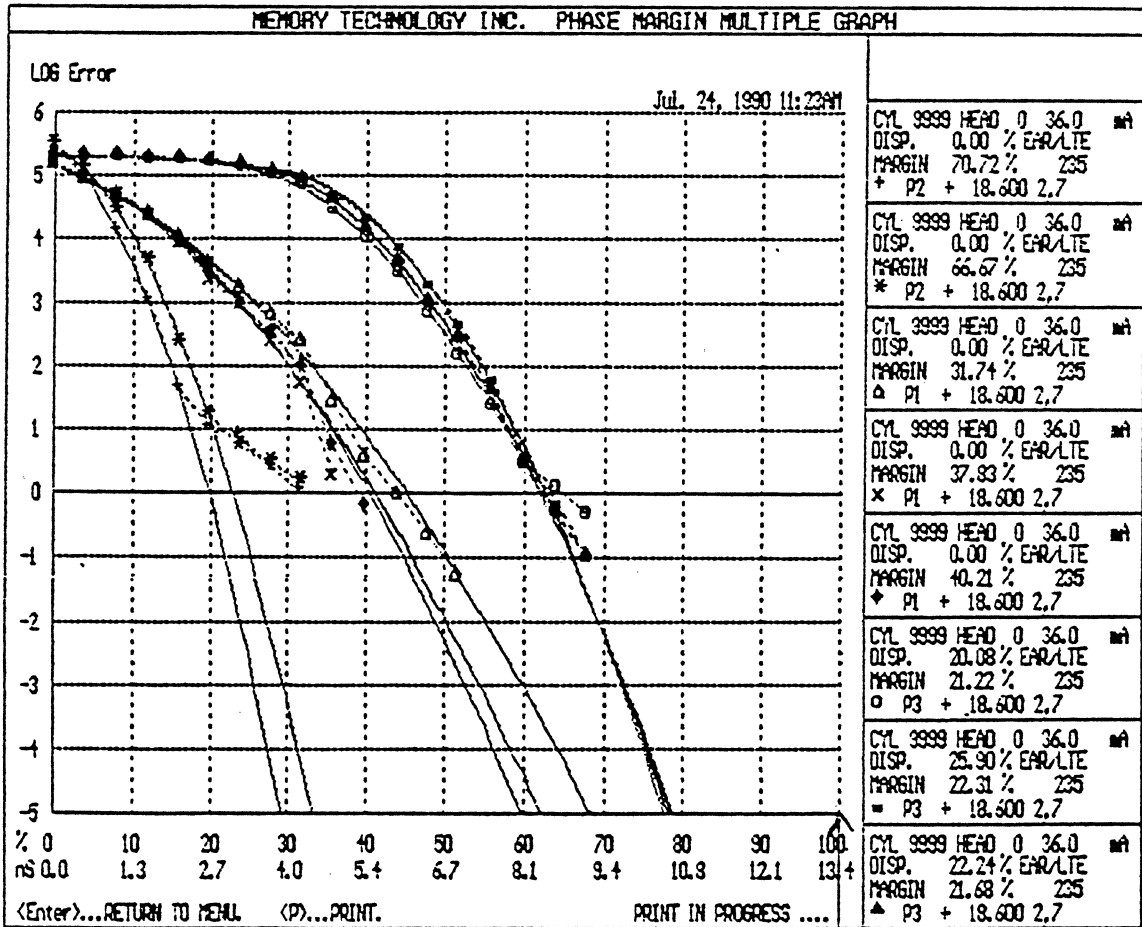
COMMENTS:

50.6 KFCI MFM 67 KBPI (1,7)

18.6 mb/s Read Channel

(Read channel 9.6 MHz)

PRECOMP K = 235 ON DIBIT



f *2f* *DIBITS*

67 KBPI
(1,7)

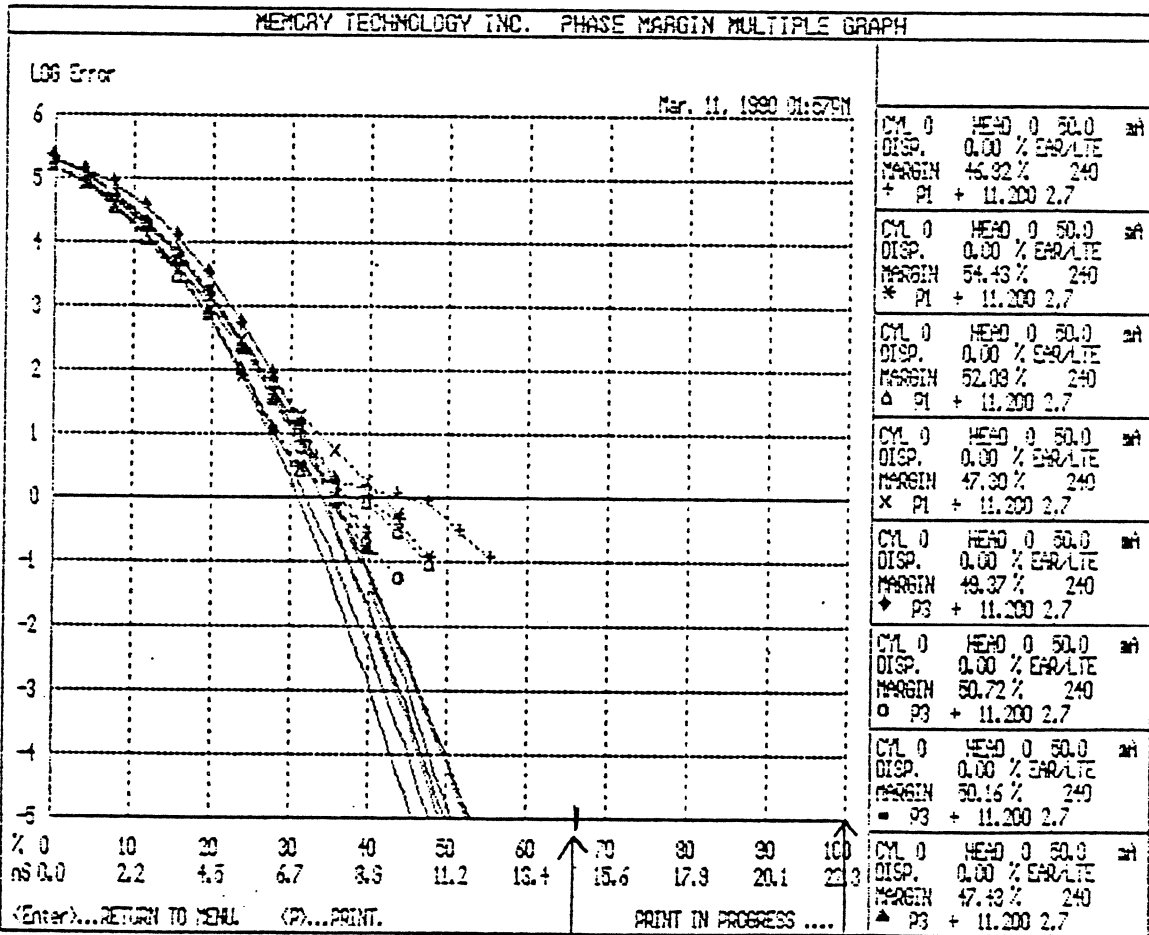
(110-130 mb/in²)

PHASE MARGIN ANALYZER II

DISK - RW5 283 4 A (CELL 4 DISK)
 HEAD - 826 03 10 UP 1700 TPI
 CONDITIONS :
 MICRO. READ... 16.03 PERIOD - 38.60
 DETENT - 130 MM
 RADIUS - 1.7" VELOCITY - 277 IPS
 FREQUENCY - 11.2 VFO , 13CODE.RLL
 ROMMEL (MEL) GARCIA
 12 MARCH 1990

TAA (F2) -
 FIRST 4 CURVES - F1
 NEXT 4 CURVES - DIBIT
 COMMENTS:
 1700 TPI HEADS 277 IPS
 40 KFCI MFM 60 KBPI (2,7)
 *** 11.2 READ CHANNEL ***
 PRECOMP K = 240 ON DIBIT

NOTE: USED NORMAL MACRO IN GETTING DIBIT. (223M)



60 KBPI
(2,7)

40 KBPI
MFM

(100-120 mb/in²
95 mm Disk)

CONTACT HEADS

DESIGN PHILOSOPHY AND RATIONALE

RUN HEAD IN CONTINUOUS CONTACT WITH DISK

High Areal Density

Better use of ZBR

MAKE MASS OF HEAD VERY SMALL

High Mechanical Frequencies

Low Inertial Forces

PRELOAD HEAD WITH SMALL FORCE

Maintain Compliance with Disk

Keep Pressure Low to Minimize Wear

MAKE CONTACT PAD VERY SMALL

Keep Pole Tip Close to Media in
Presence of Disk Runout

Waste Less of Data Band

FABRICATE HEAD ENTIRELY BY WAFER-FAB TECHNIQUES

Low Cost

Maintain Tolerances on Small Dimensions

DESIGN DETAILS - HEAD

FLEXURE - Flexible beam of pattern-defined sputtered ceramic material. 20 mils wide X 400 mils length X 2 mils thick

SLIDER - sputtered ceramic pad, approx. 1 mil square, reinforced with proprietary wear control material

PRELOAD - 40 milligrams, nom.

EFFECTIVE MASS - 400 micrograms

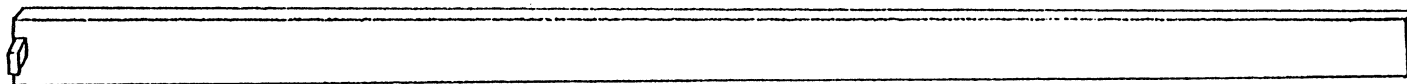
EQUIVALENT ACCELERATION - 100 g's

GIMBALING - not needed

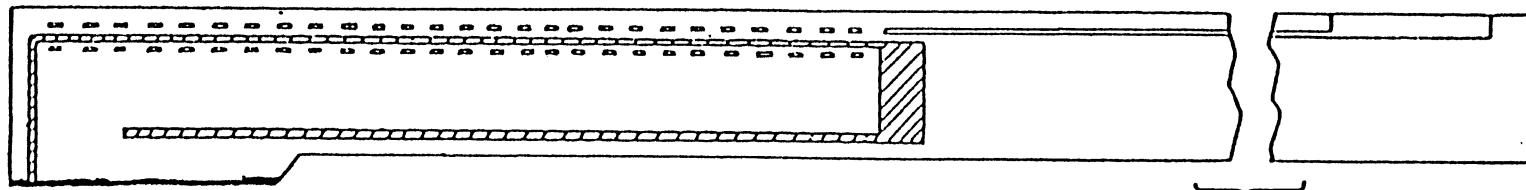
WEAR LIFE - 5 years, continuous duty

PHYSICAL DESCRIPTION OF THE HEAD

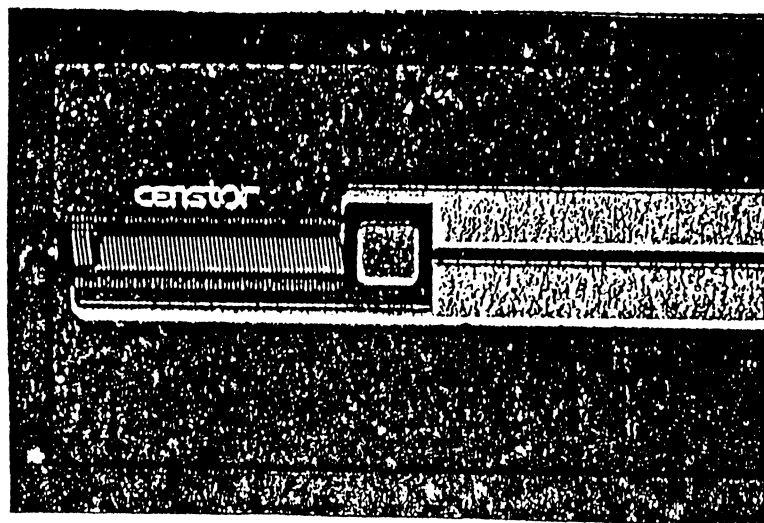
STRUCTURE OF CENSTOR'S MICRO FLEXHEAD™



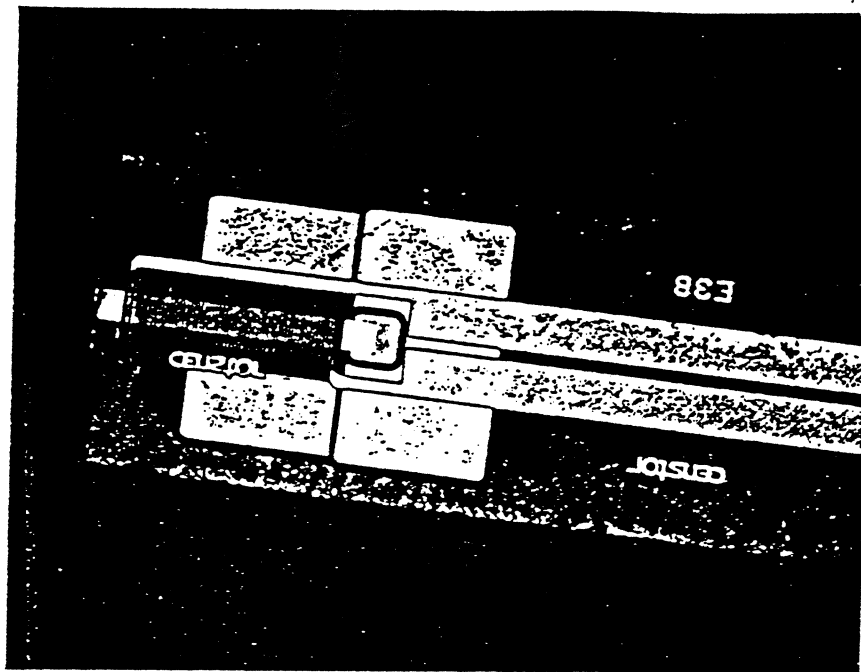
15X



CROSS-SECTION

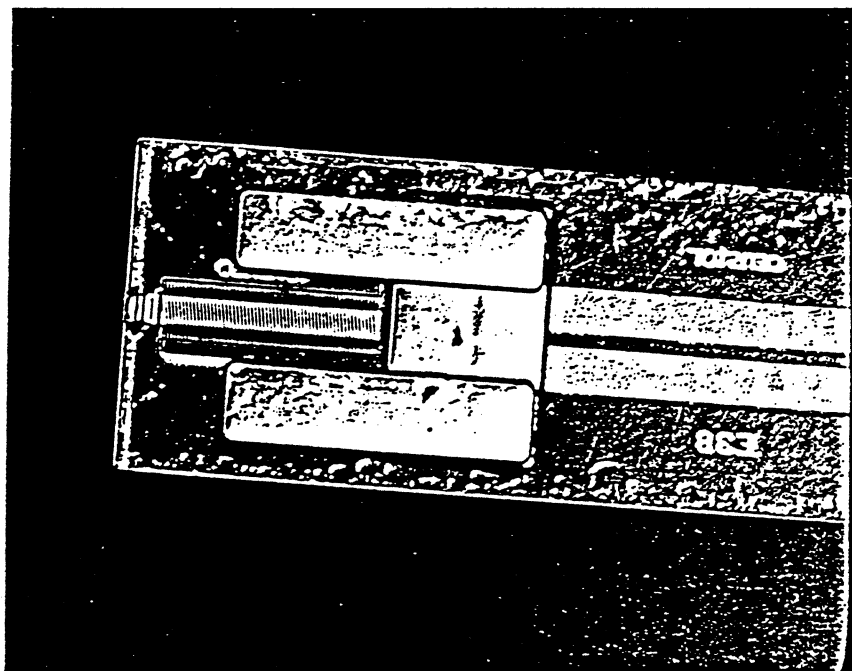


100X



get

AT ASSA CLW.



ELECTRICAL PERFORMANCE

Early version

STATIC ELECTRICAL CHARACTERISTICS

NUMBER OF TURNS 60

RESISTANCE 40 Ω

25 Ω

INDUCTANCE 0.6 μH

RESONANT FREQUENCY ~ 33 MHz

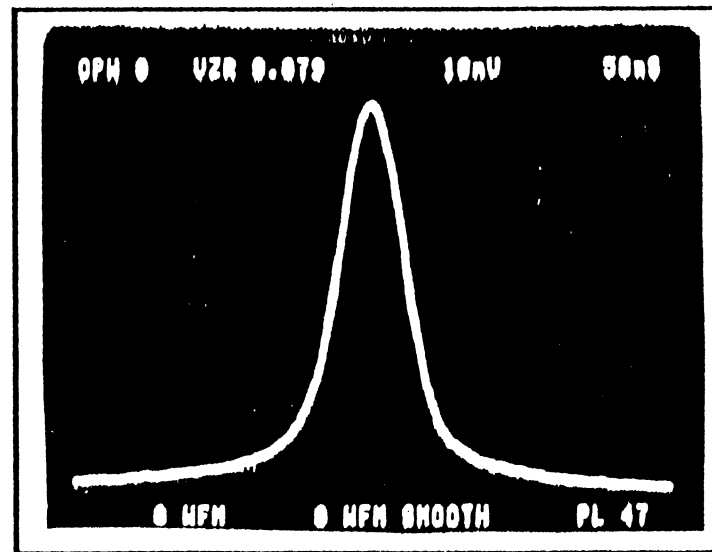
($C_s \sim 35$ pF)

TRACK WIDTH (early prototypes) 11 μM (440 μ'')

(2000 TPI)

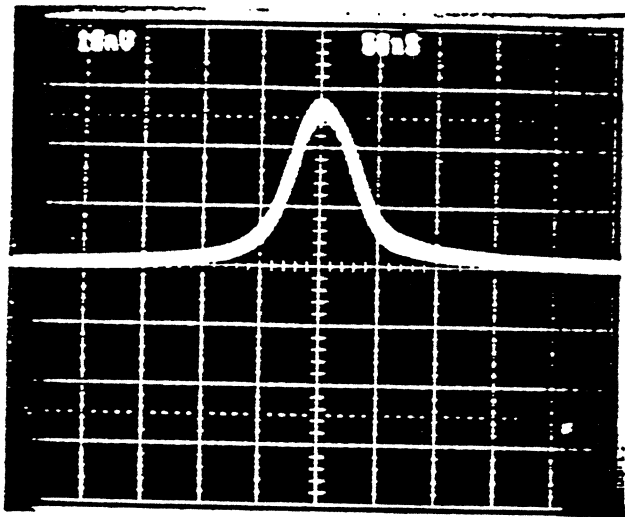
PROBE TIP THICKNESS (early prototypes) 0.3 μM (12 μ'')

Isolated Pulse

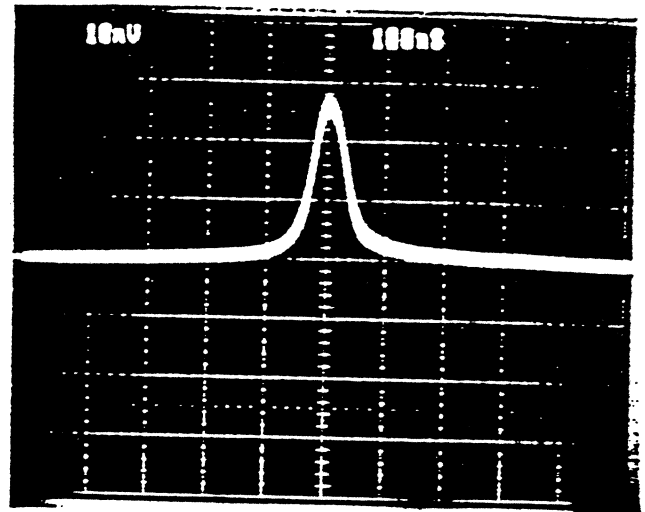


Amplitude 1000 μV pp

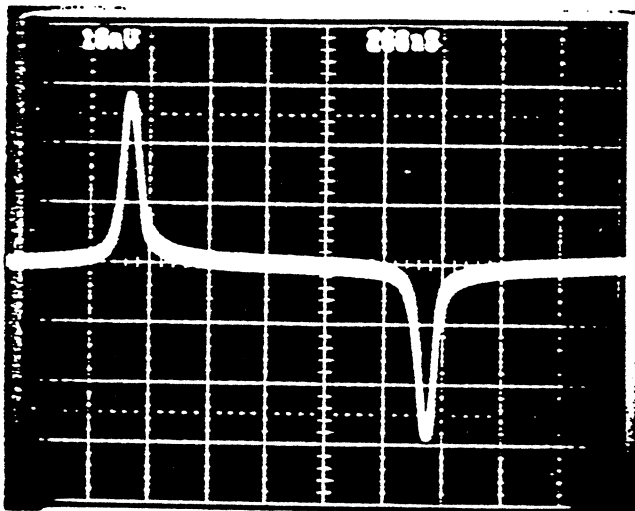
PW50 19 μs



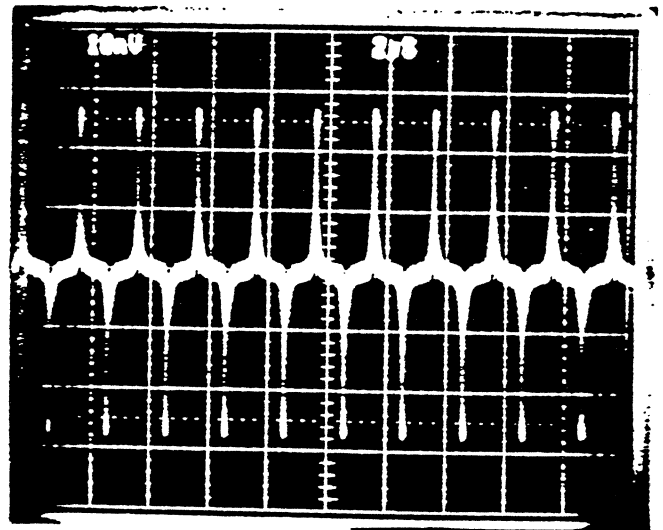
50 nS/div



100 nS/div



200 nS/div



2 uS/div

ISOLATED PULSE WAVEFORM

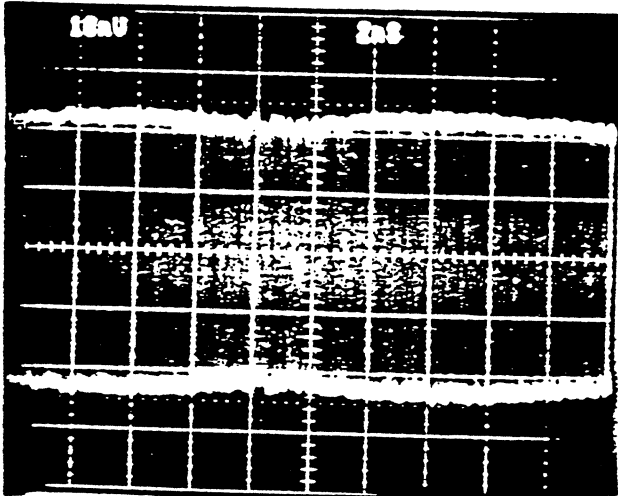
V = 300 IPS

FREQ = 1 MTRANSITION/SEC

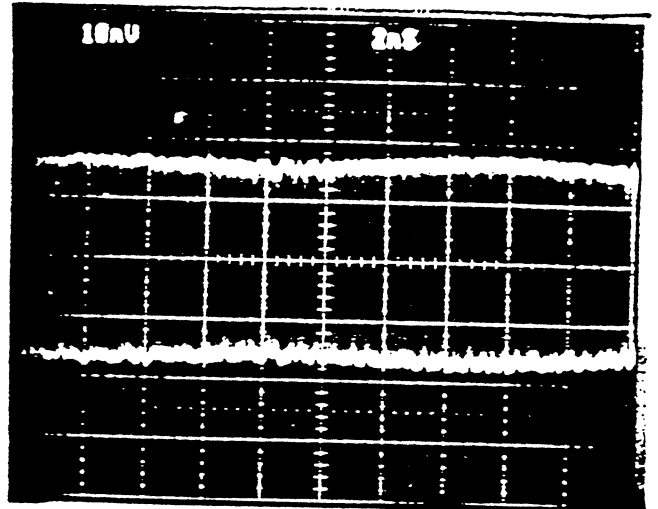
= 3.3 KFCI

HEAD: R2C1 (60 TURNS T.W. = 11 µM)

DISK: PL-706-57 A (95 mm 100 Å C)



33 KFCI



67 KFCI

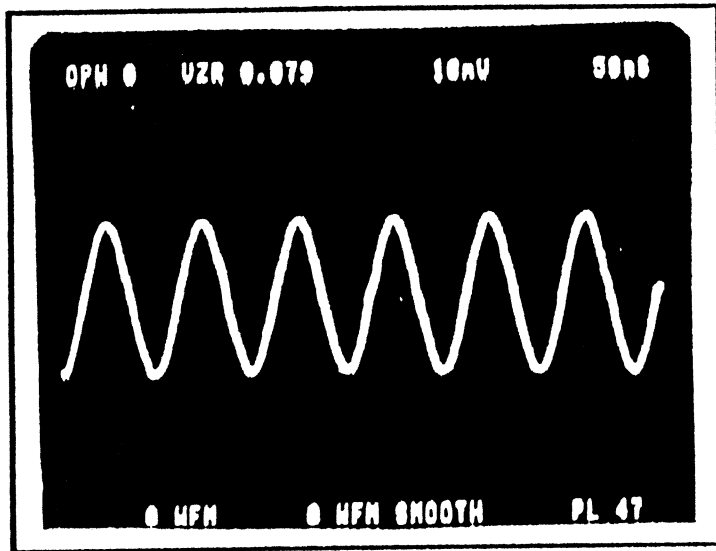
ONCE-AROUND ENVELOPE

V = 300 IPS @ 2400 RPM

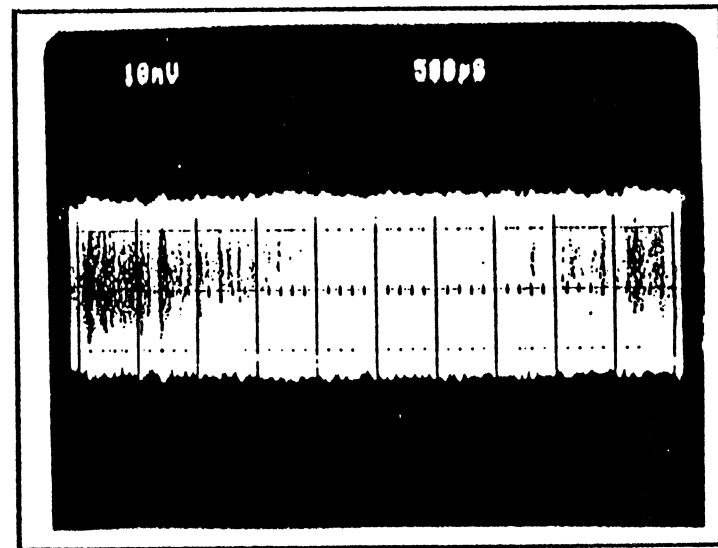
HEAD: R2C1 (60 TURNS T.W. = 11 μ M)

DISK: PL-706-57 A (95 mm 100 \AA C)

80 Kfci



Individual Pulses



Envelope

Amplitude $500 \mu\text{Vpp}$

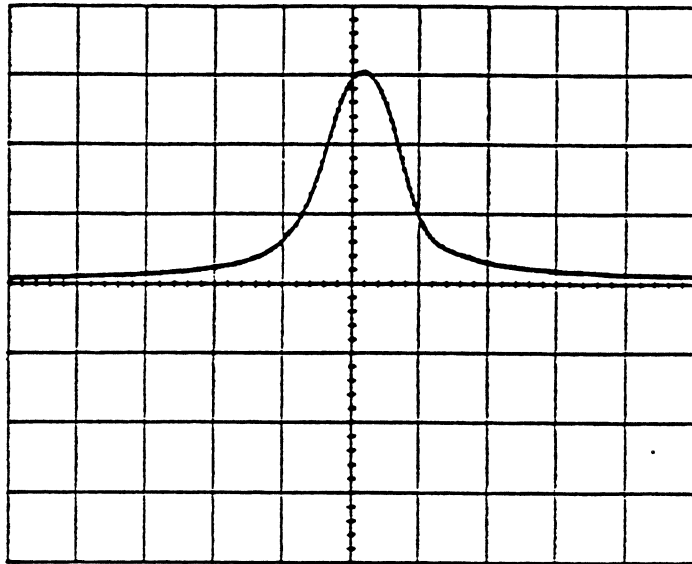
CENSTOR

FRI 08/07/90 09:14:04 Pg.

68.97E-03

165.8 uV

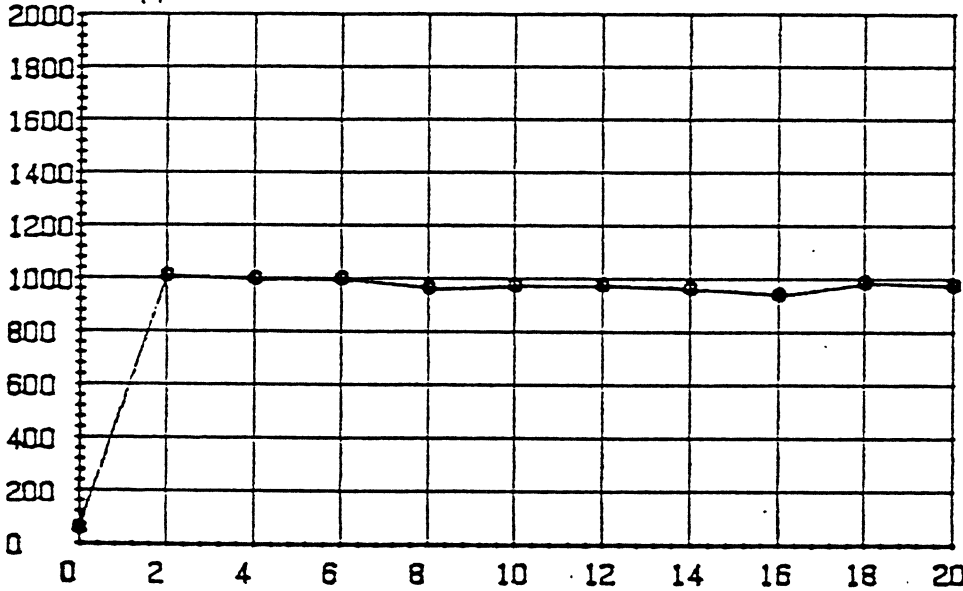
50E-09



DISK S/N PL-706-57-A
 HEAD S/N CONTACT HEAD S/N R2C3
 F.H. = uIn. TPI = 11 μm
 I. WR. 5 mA FREQ. .5 MHz
 SPEED 2390 RPM 300.3 IPS
 RADIUS 1.2 In

TAA (pp) 997.4 uV MOD. 9 %
 Epp 987.7 uV
 PV-50 66.41 nS 19.9 uIN
 PV-20 107.4 nS 32.3 uIN
 SYN-AREA 2 %
 NOISE Elec. 7.2 uV, Mod. 3.7 uV
 (20 MHz) Total 8.1 uV

TAA (uV, pp)

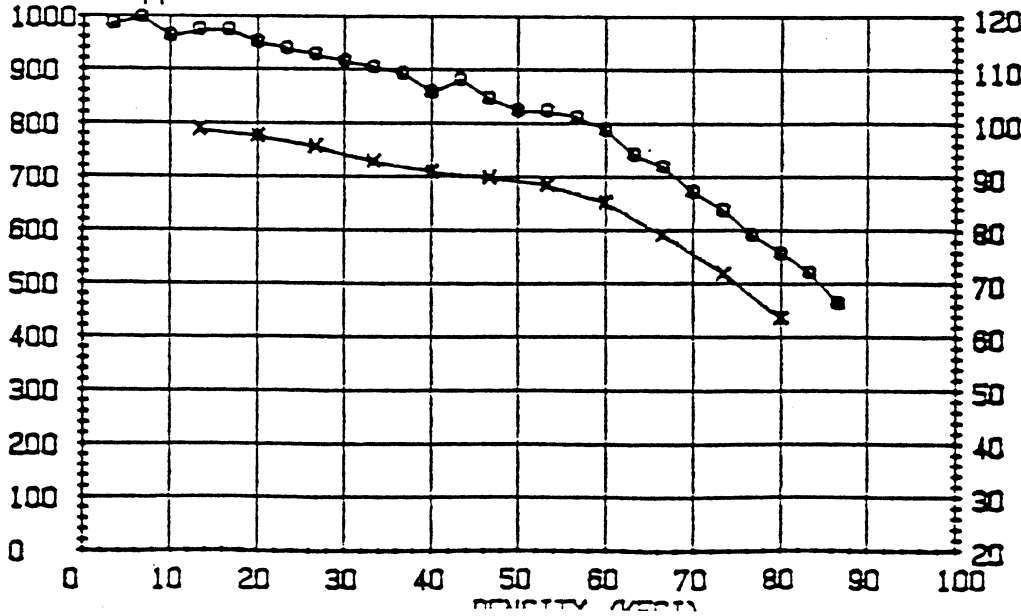


—SAT. CURVE—
 FREQ. WR. .5 MHz
 SPEED 300.3 IPS
 RADIUS 1.2 IN

20.0 40.0 60.0

EST Linear Density:
 ~ 80 KBPI
 EST. Track Density:
 3500
 areal Density:
 280 mb/in²

TAA (uV, pp)



—RESO. CURVE—
 o - Epp. x - Res. %
 I. WR. 5 mA
 SPEED 300.3 IPS
 RADIUS 1.2 IN

KFCI.	RES. %	TAA (pp)
74.3	70.0	622.1
20.0	97.2	948.5
30.0	94	916.8

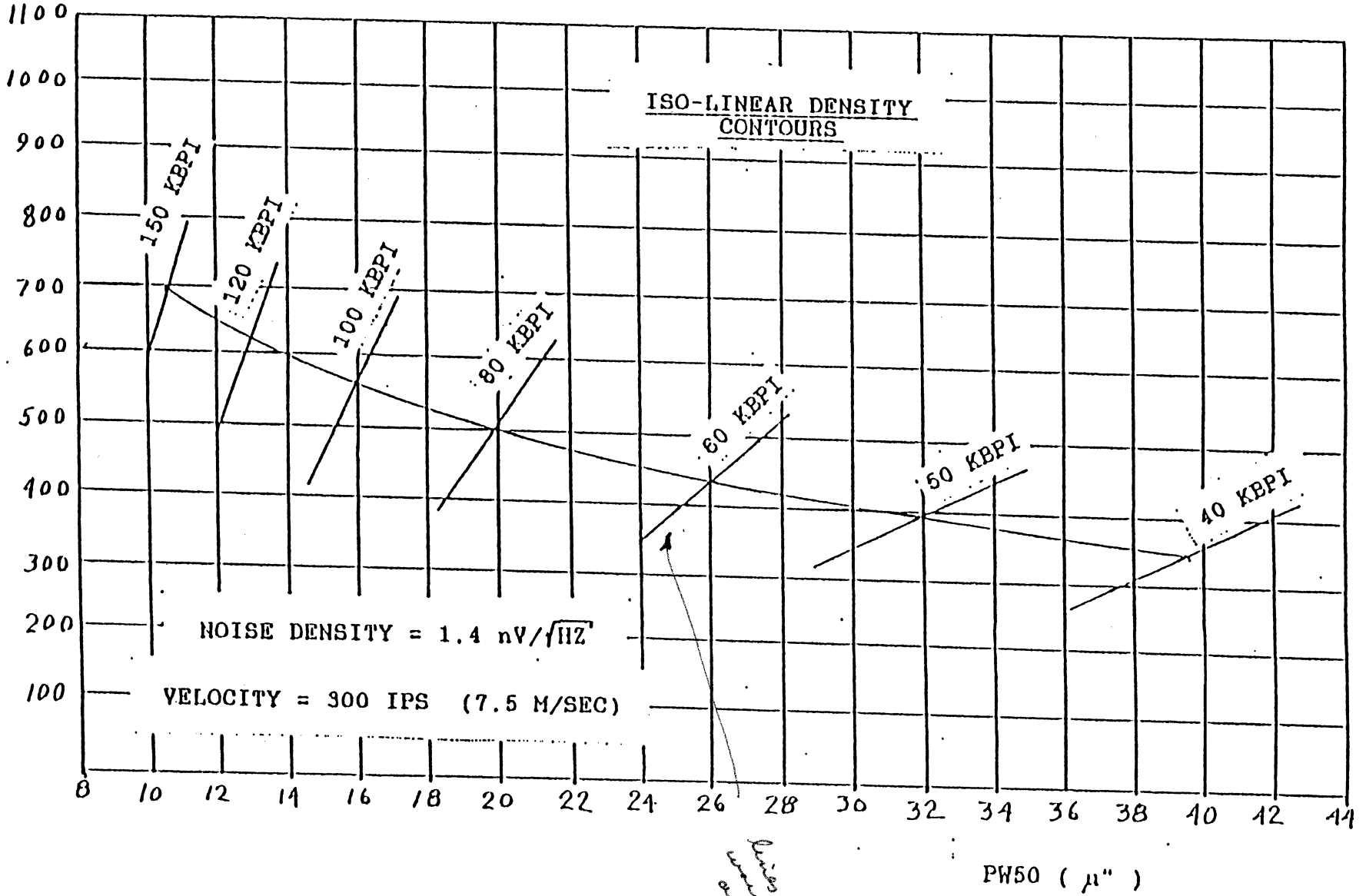
O.V. 33.5 dB @ 4/8MHz

OPR. INIT. PO #1

240M
53

PERFORMANCE
AND
IMPROVEMENTS

TAA (ISOI, PULSE)
μV P-P



TAA
(ISOL PULSE)

600
($\mu\text{V pp}$)

550

500

450

400

350

300

250

200

150

100

50

VELOCITY = 150 IPS

ISO-LINEAR DENSITY
CONTOURS

NOISE DENSITY
= $1.4 \text{ nV}/\sqrt{\text{Hz}}$

NOISE DENSITY
= $1.0 \text{ nV}/\sqrt{\text{Hz}}$

200 KBPI

150 KBPI

120 KBPI

100 KBPI

80 KBPI

200 KBPI

150 KBPI

120 KBPI

100 KBPI

80 KBPI

60 KBPI

60 KBPI

50 KBPI

50 KBPI

PW50 (μin)

56

48mm
(1.8")

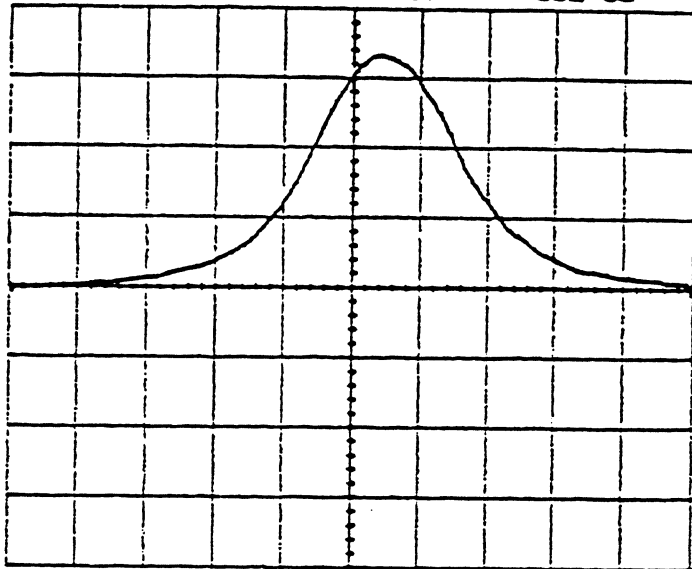
CENSTOR

WED 08/13/92 11:09:26 Pg.

-97.05E-03

41.4 uV

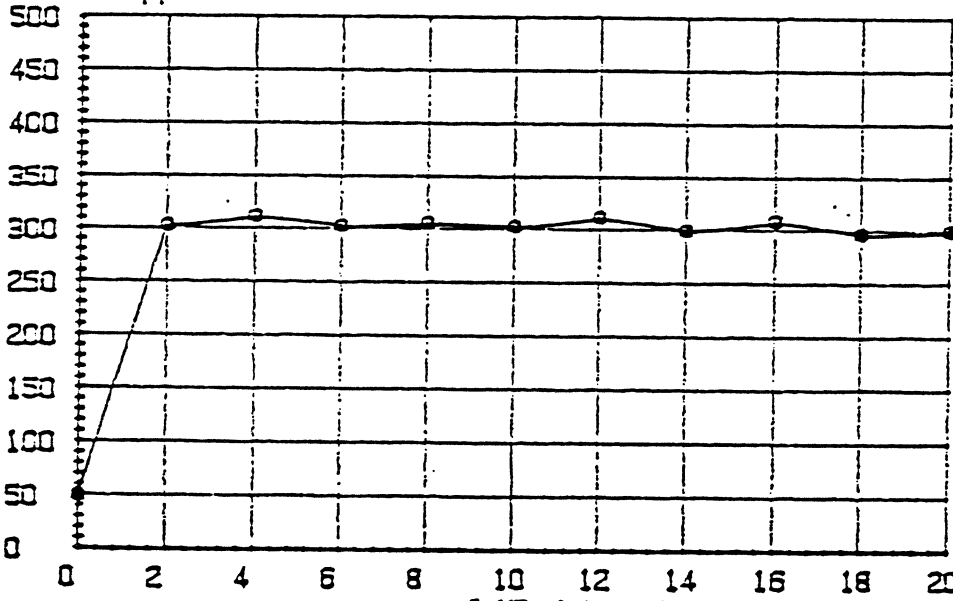
50E-09



DISK S/N STD 621 7 10 A
 HEAD S/N 1922 C 17 (6.5) (HELIX)
 F.H. = uIn. TPI = 6.5 μm
 I. WR. 10 mA FREQ. .5 MHz
 SPEED 1195 RPM 150.2 IPS
 RADIUS 1.2 In

TAA (pp) 305.2 uV MOD. 36.3 %
 Epp 283.9 uV
 PY-50 125 nS 18.8 uIN
 PY-20 214.8 nS 32.3 uIN
 SYM-AREA -3.7 %
 NOISE Elec. 6.4 uV, Mod. 1.6 uV
 (20 MHz) Total 6.6 uV

TAA (uV, pp)

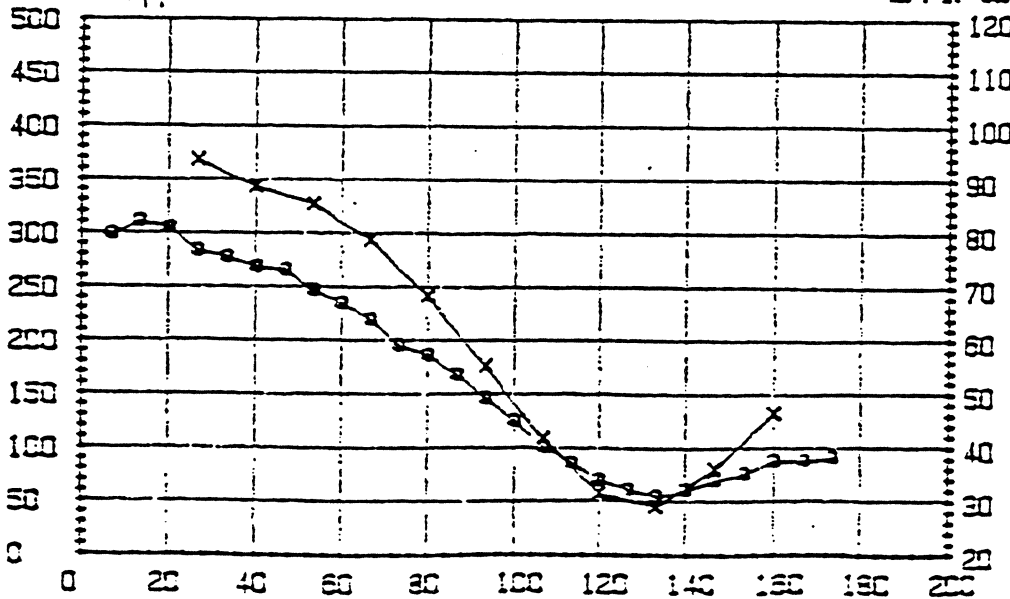


—SAT. CURVE—

FREQ. WR. .5 MHz
 SPEED 150.2 IPS
 RADIUS 1.2 IN

EST Linear Density
 ~ 90 KBPI

TAA (uV, pp)



—RESOL. CURVE—

o - Epp. x - Res. %
 I. WR. 10 mA
 SPEED 150.2 IPS
 RADIUS 1.2 IN
 KFCI. RES. % TAA (pp)

D.W. 35.3 dB @ 4/8MHz

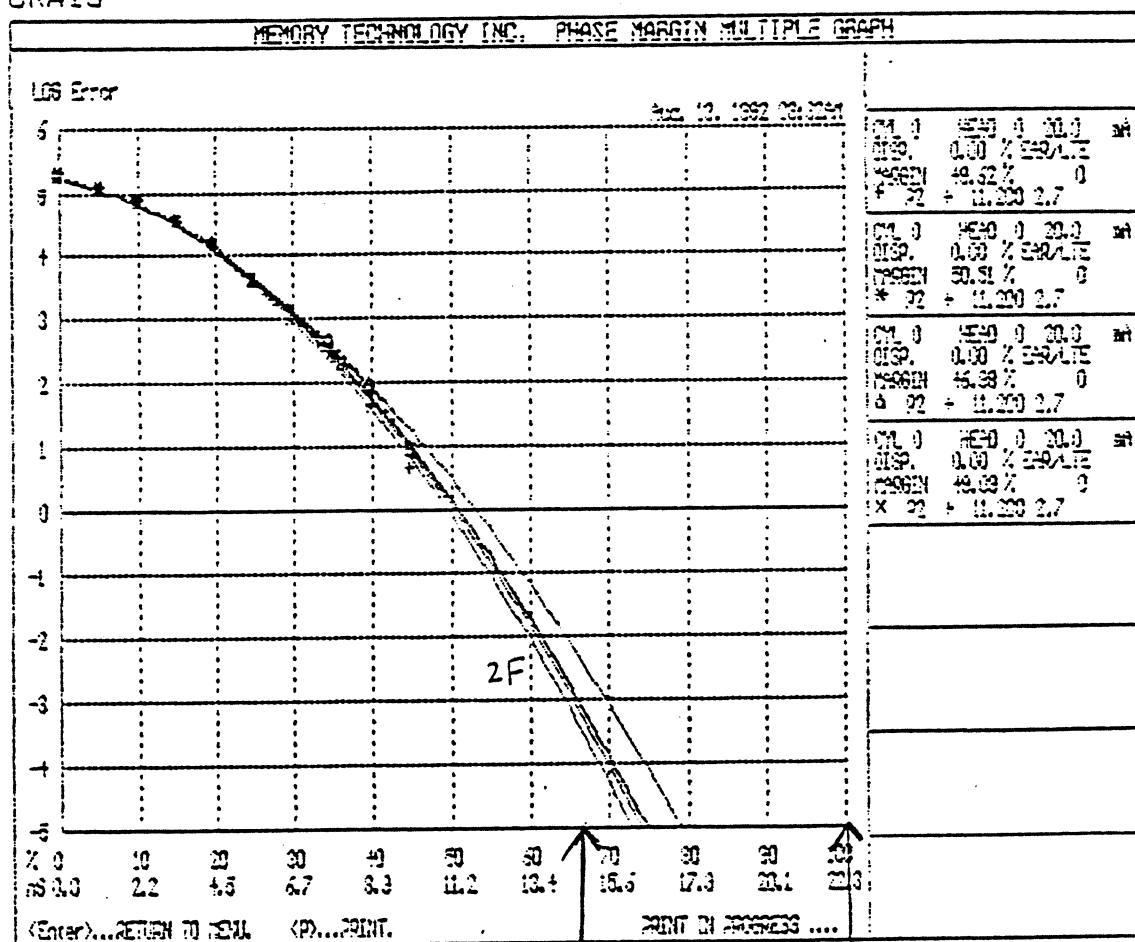
OPP. INIT. DALC #1

PHASE MARGIN ANALYSER II

DISK: 95mm = STD 621 7 10 A
 HEAD: CONTACT = 1922 C 17 (8)
 VELOCITY (IPS) = 150
 RPM = 1194
 RADIUS = 1.20
 PERIOD = 50.3
 MIC. READ. = 2.75
 DETENT = 200mm
 FREQ. VFO CARD = 11.2 mb/sec
 READ CH. = 11.2 mb/sec
 6.3 MHZ B.W.

NOTE(S):
 P3 (B6D) = (OVER SHOT) NO GRAPH
 TAA= 139 mV
 PATT.RLL = 13CODE.RLL
 75 KFCI 112 KBPI (2,7)
 I = 20 ma po
 PRECOMP K =

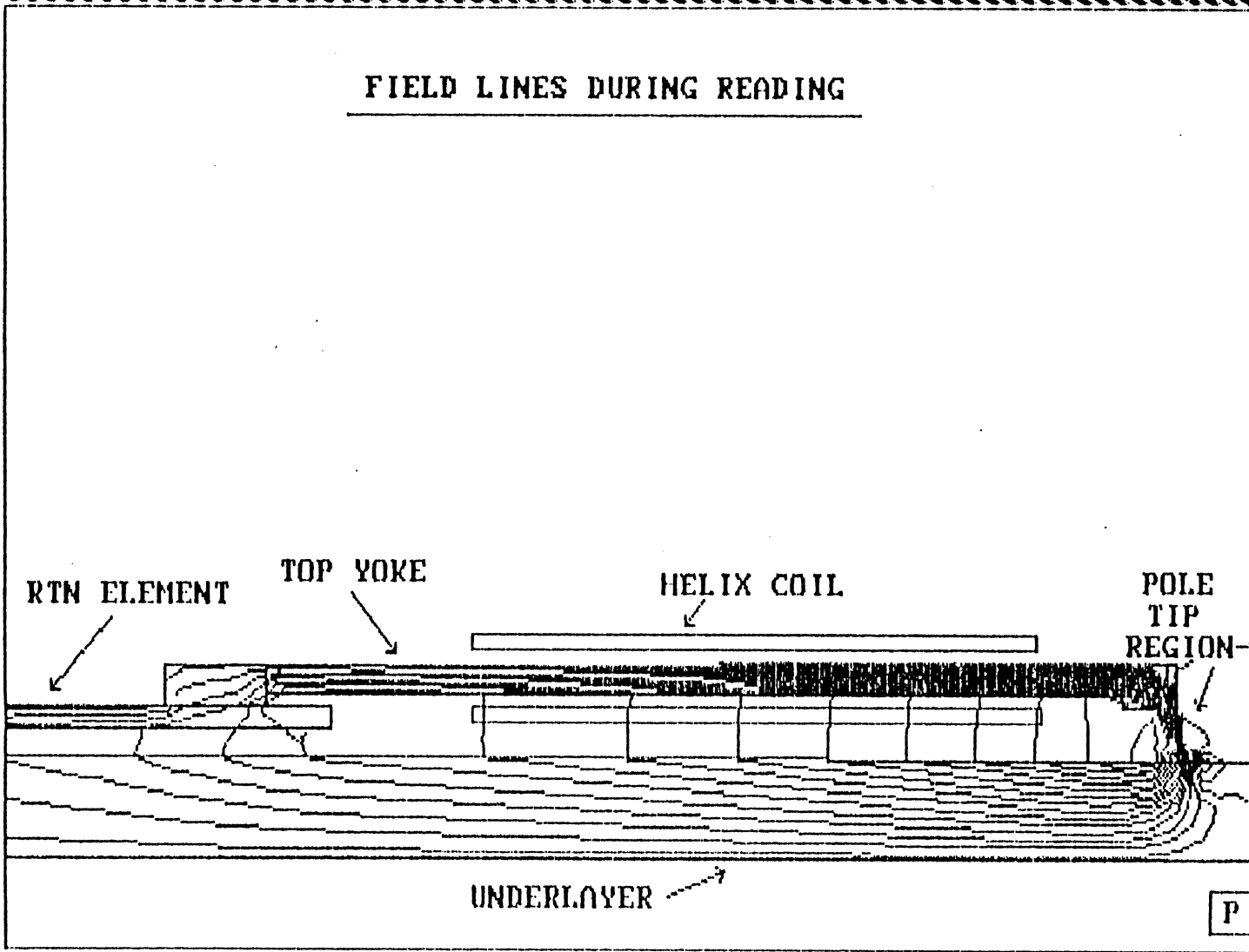
TECH: P. ORAIS



(Parametric performance → ~ 90 KBPI)

DATE = 03/26/1992
Current file: HELIX1
Mode of analysis: MAGNETO_2D Field analysis
Analysis type: Static mode
TIME = 10:31:52.10
dbasa.ies

FIELD LINES DURING READING

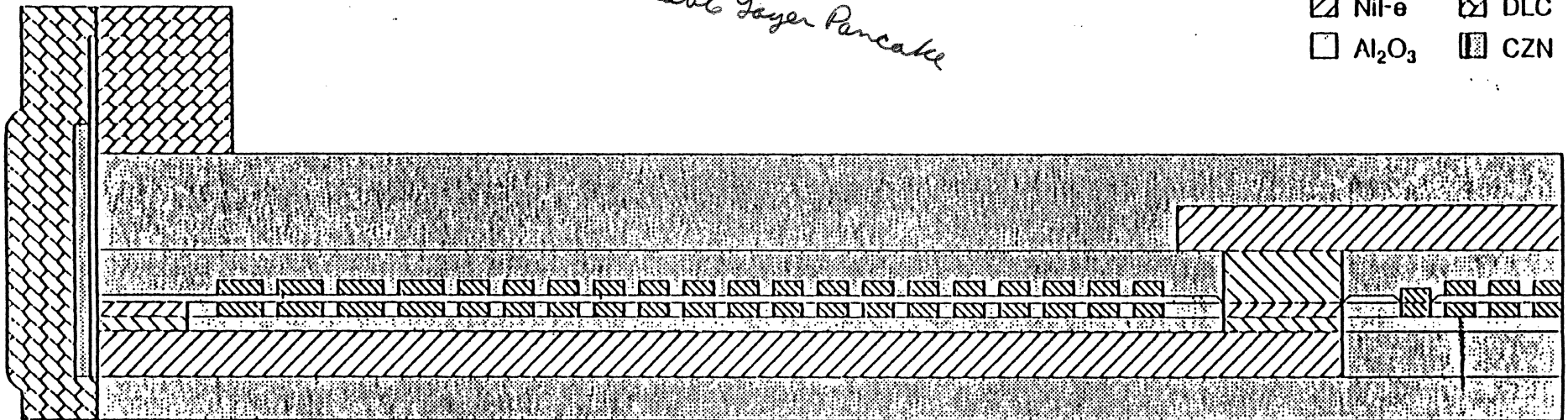


*Early design
leaky
flux lines*

DLP DEVICE

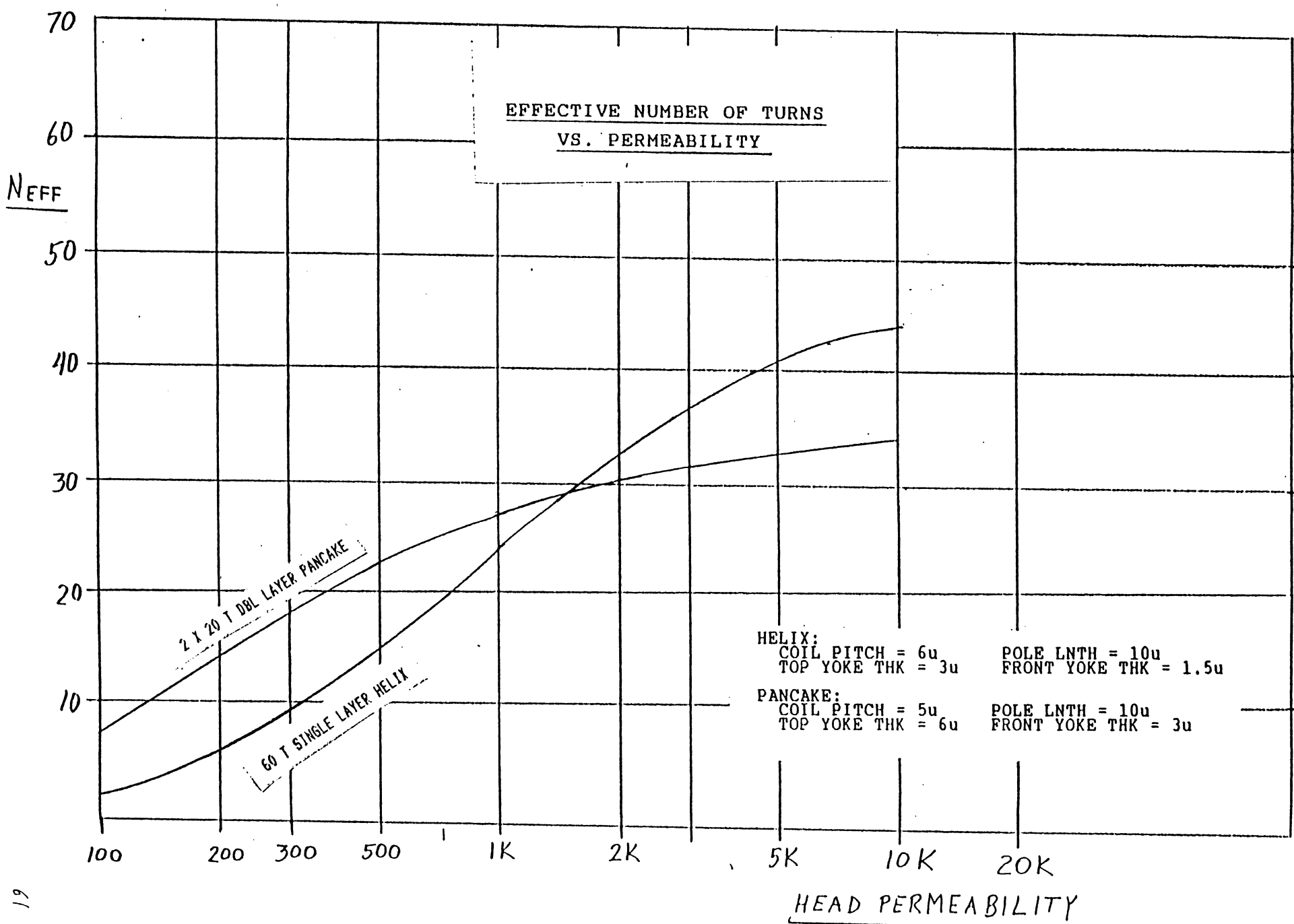
Double Layer Pancake

 Cu	 DLC
 NiFe	 CZN
 Al ₂ O ₃	



7.1ms

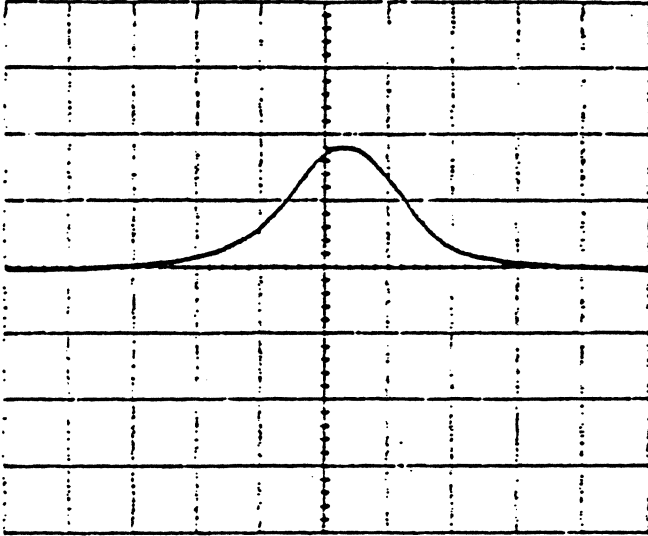
- 2.5 μm THICK COILS
- 6.0 μm PITCH (16 OF 20 TURNS)
- 40 TURNS (2 LAYERS OF 20)
- 35 μm BEAM
- 6 μm CORE



CENSTOR

WED 09/02/92 07:49:52 Pg.

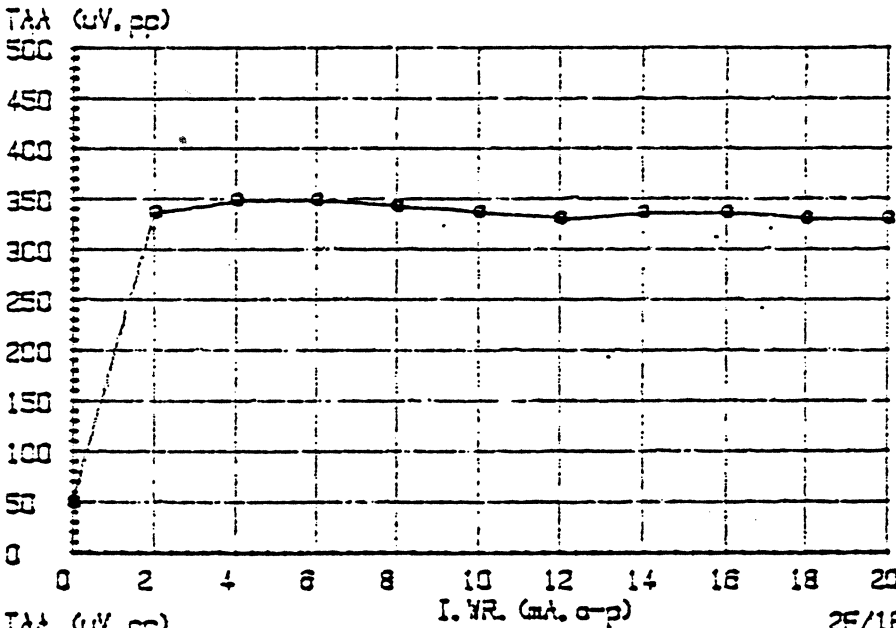
-30.33E-03 82.9 uV 50E-09



DISK S/N (48MM) 15 B
 HEAD S/N OLP 2127 E 47 DLP
 F.H. = uIn. TPI = 6.5 μm
 I. YR. 10 mA FREQ. .5 MHz
 SPEED 2000 RPM 150.8 IPS
 RADIUS .72 In

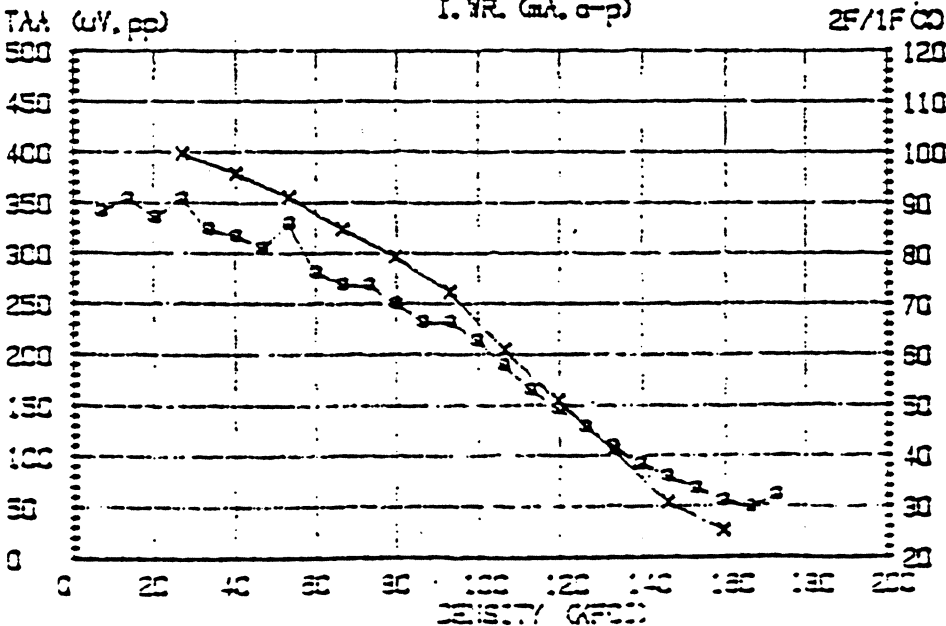
3-3200
 101

TAA (pp) 341.8 uV MOD. 8.8 %
 Epp 313.5 uV
 PV-50 105.5 nS 15.9 uIN
 PV-20 175.8 nS 26.5 uIN
 SYN-AREA 3.2 %
 NOISE Elec. 6.9 uV, Mod. 1.3 uV
 (20 MHz) Total 7 uV



—SAT. CURVE—
 FREQ. YR. .5 MHz
 SPEED 150.8 IPS
 RADIUS .72 IN

EST Linear Density
 ~ 105 KBI



—RESOL. CURVE—
 o - Epp. x - Res. %
 I. YR. 10 mA
 SPEED 150.8 IPS
 RADIUS .72 IN

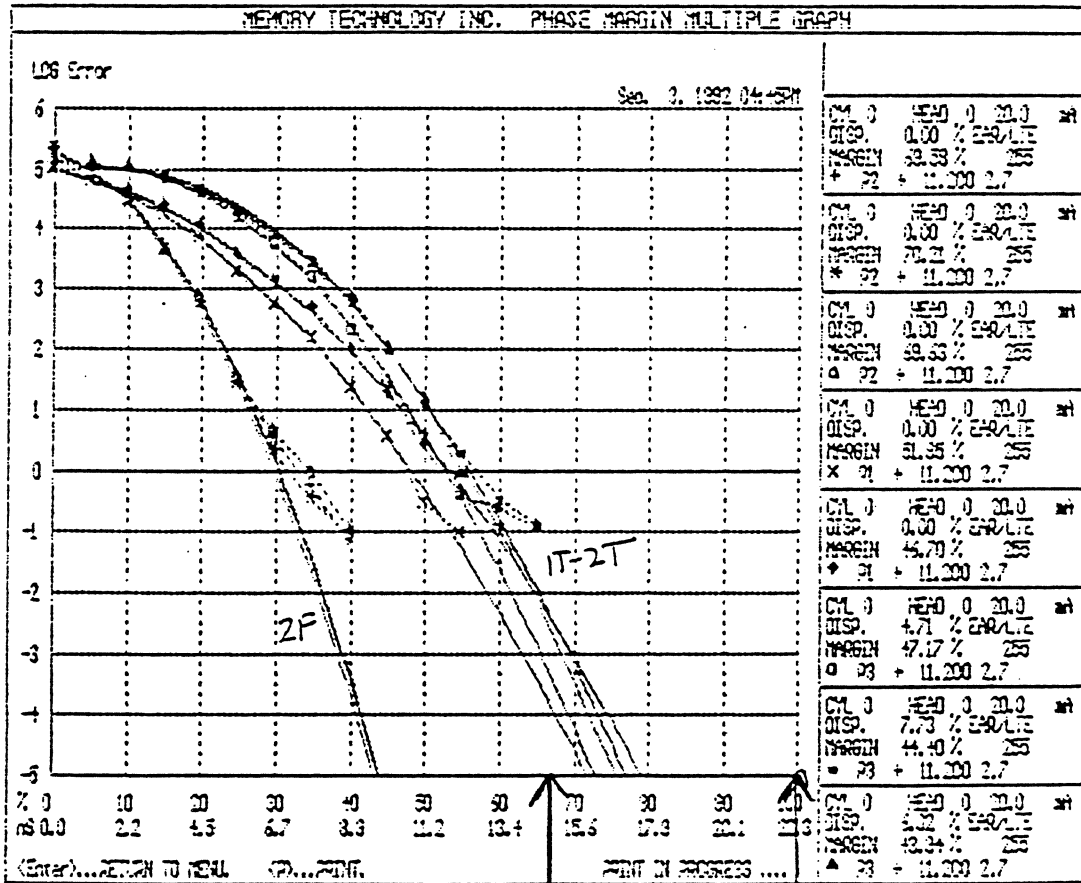
KFCI. RES. % TAA (pp)

D.Y. 31.3 dB @ 3 3/4 MHz

OPR. INIT. _____ #1

PHASE MARGIN ANALYSER II

DISK: (48mm) = 15 B NOTE(S): DLP
 HEAD: = 2127 E 47 3X 2F
 VELOCITY (IPS): = 150 2X 1F
 RPM: = 1790 3X 1T-2T
 RADIUS: = 0.80
 PERIOD: = 33.5 TAA:(uV) = 273
 MIC. READ.: = 12.91
 DETENT: = 200mm PATT.RLL = 13CODE.RLL
 FREQ. VFO CARD: = 11.2 mb/sec 75 KFCI 112 KBPI (2,7)
 READ CH.: = 11.2 mb/sec I WR = 20 ma pp
 = 6.3 MHZ B.W. PRECOMP K = 255
 TECH. NAME: = PAUL ORAIS FILE NAME: P1



(Parametric performance → 105 KBPI)

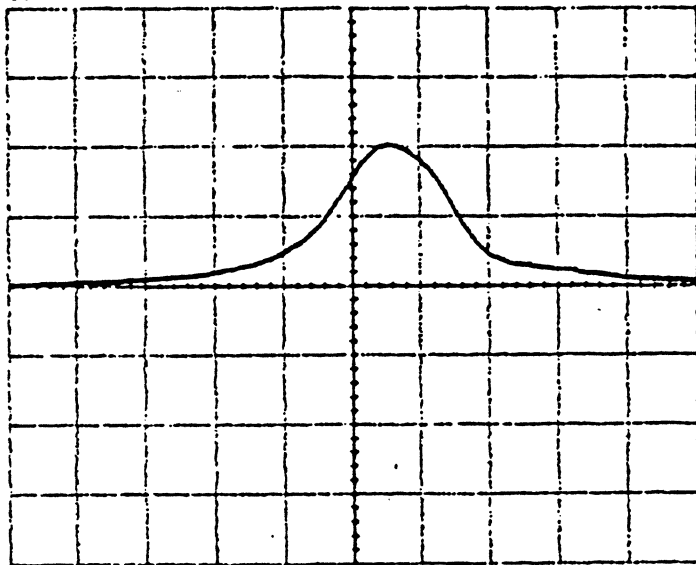
CENSTOR

FRI 09/04/92 13:39:17 Pg.

1.831E-03

82.9 uV

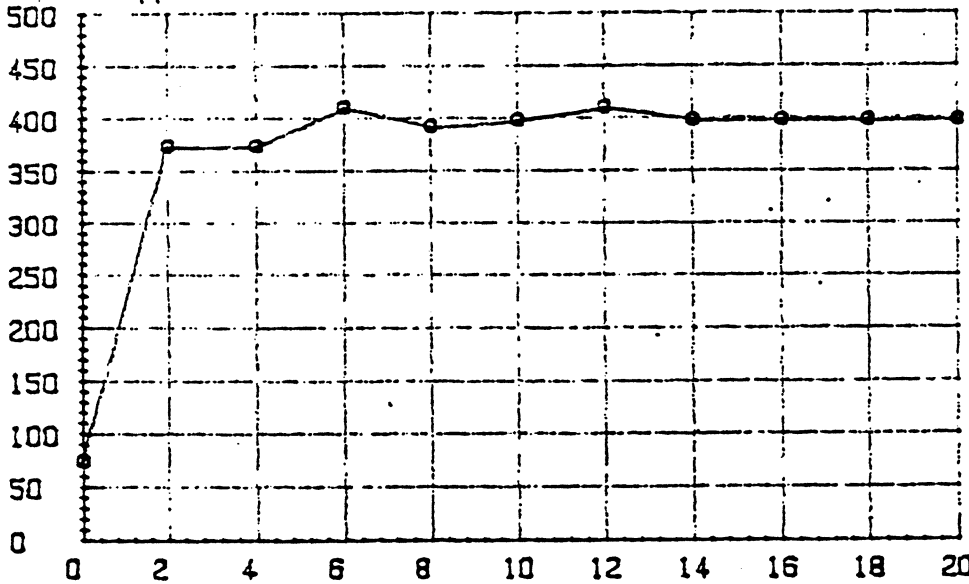
50E-09



DISK S/N (48MM) 15 B
 HEAD S/N 2127 C 64 (DLP)
 F.H. = uIn. TPI = 615 μ m
 I. WR. 10 mA FREQ. .5 MHz
 SPEED 2000 RPM 150.8 IPS
 RADIUS .72 In

TAA (pp) 402.9 uV MOD. 16.2 %
 Epp 335.5 uV
 PW-50 93.75 nS 14.1 uIn
 PW-20 162.1 nS 24.4 uIn
 SYM-AREA .1 %
 NOISE Elec. 6.9 uV, Med. 1.2 uV
 (20 MHz) Total 7 uV

TAA (uV. pp)



—SAT. CURVE—

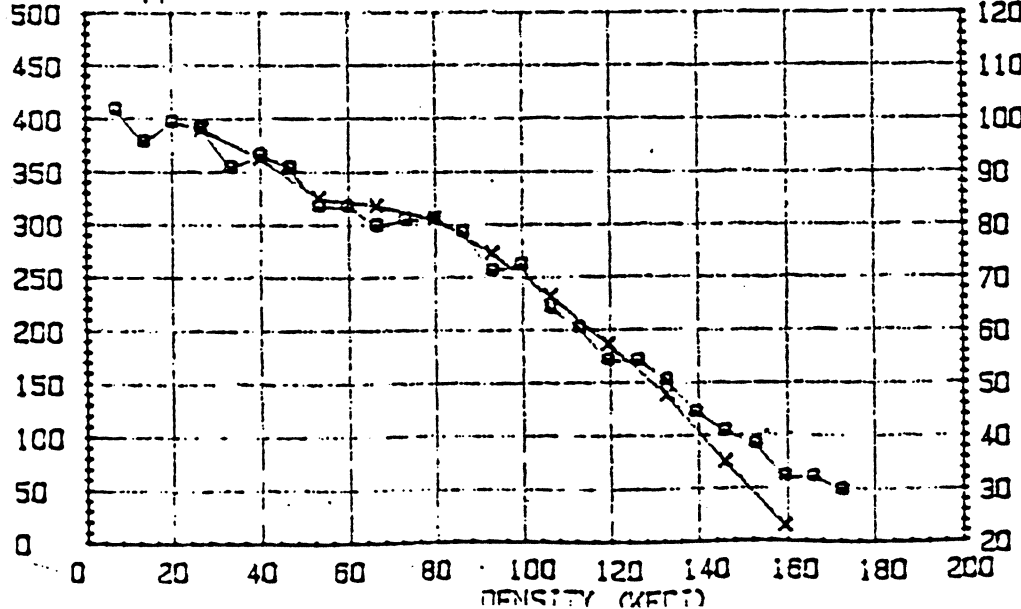
FREQ. WR. .5 MHz
 SPEED 150.8 IPS
 RADIUS .72 IN

EST LINEAR DENSITY

~ 120 KBPI

350 MB/IN²

TAA (uV. pp)



—RESO. CURVE—

o - Epp. x - Res. %
 I. WR. 10 mA
 SPEED 150.8 IPS
 RADIUS .72 IN

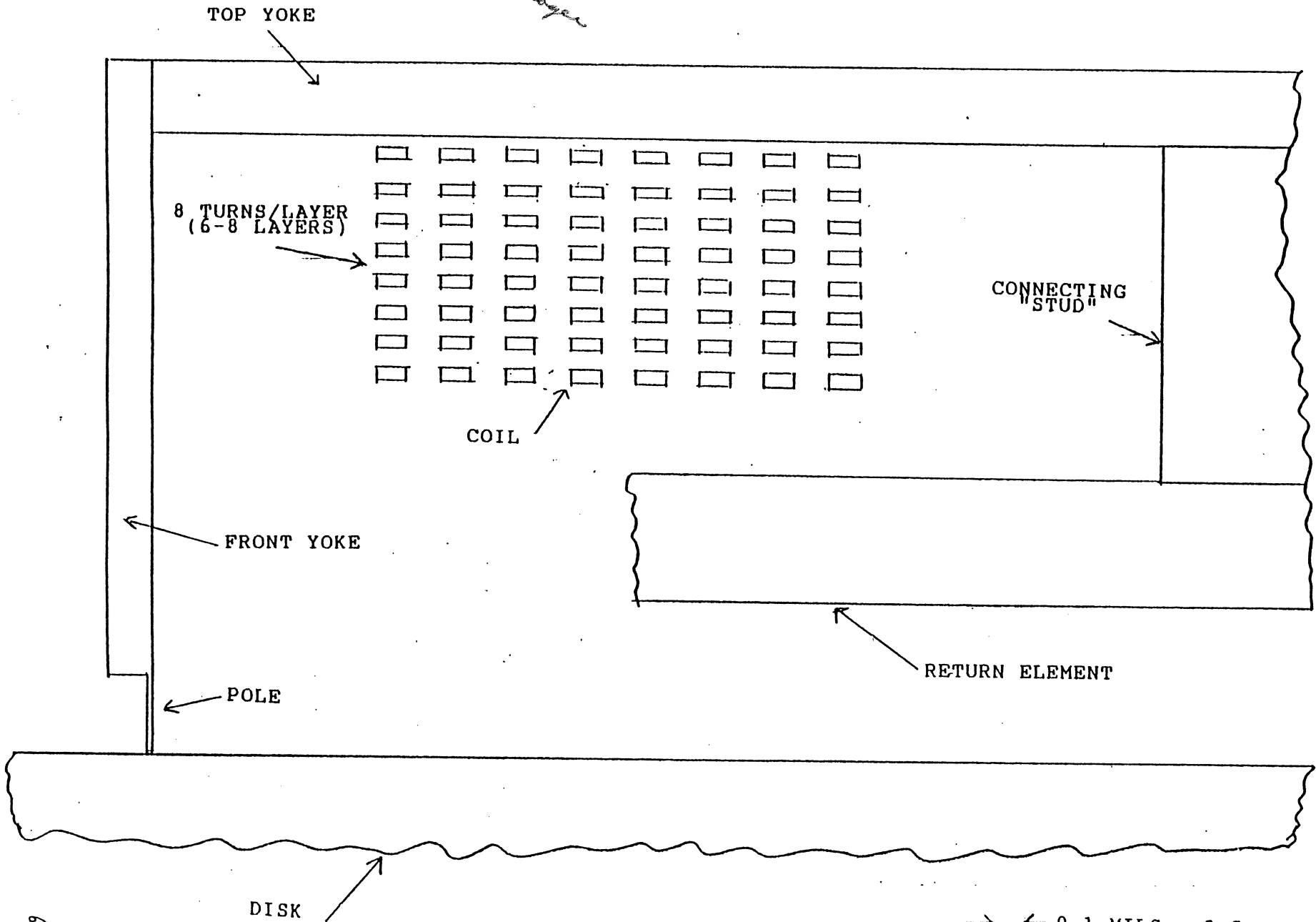
KFCI. RES. % TAA (pp)

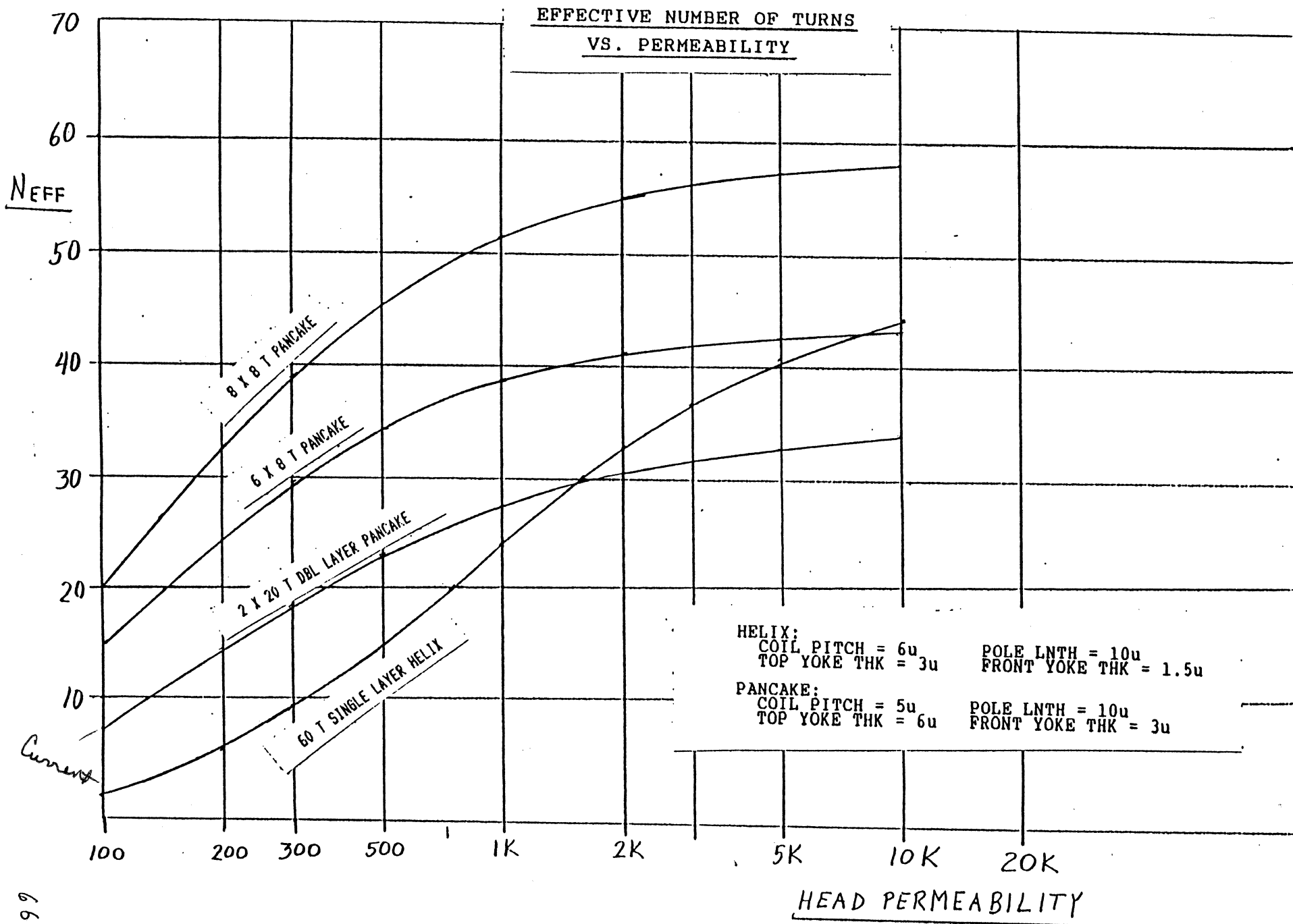
O. W. 31.7 dB @ 4/8MHz

OPR. INIT. PAUL #1

MULTI-LAYER PANCAKE COIL CONTACT HEAD

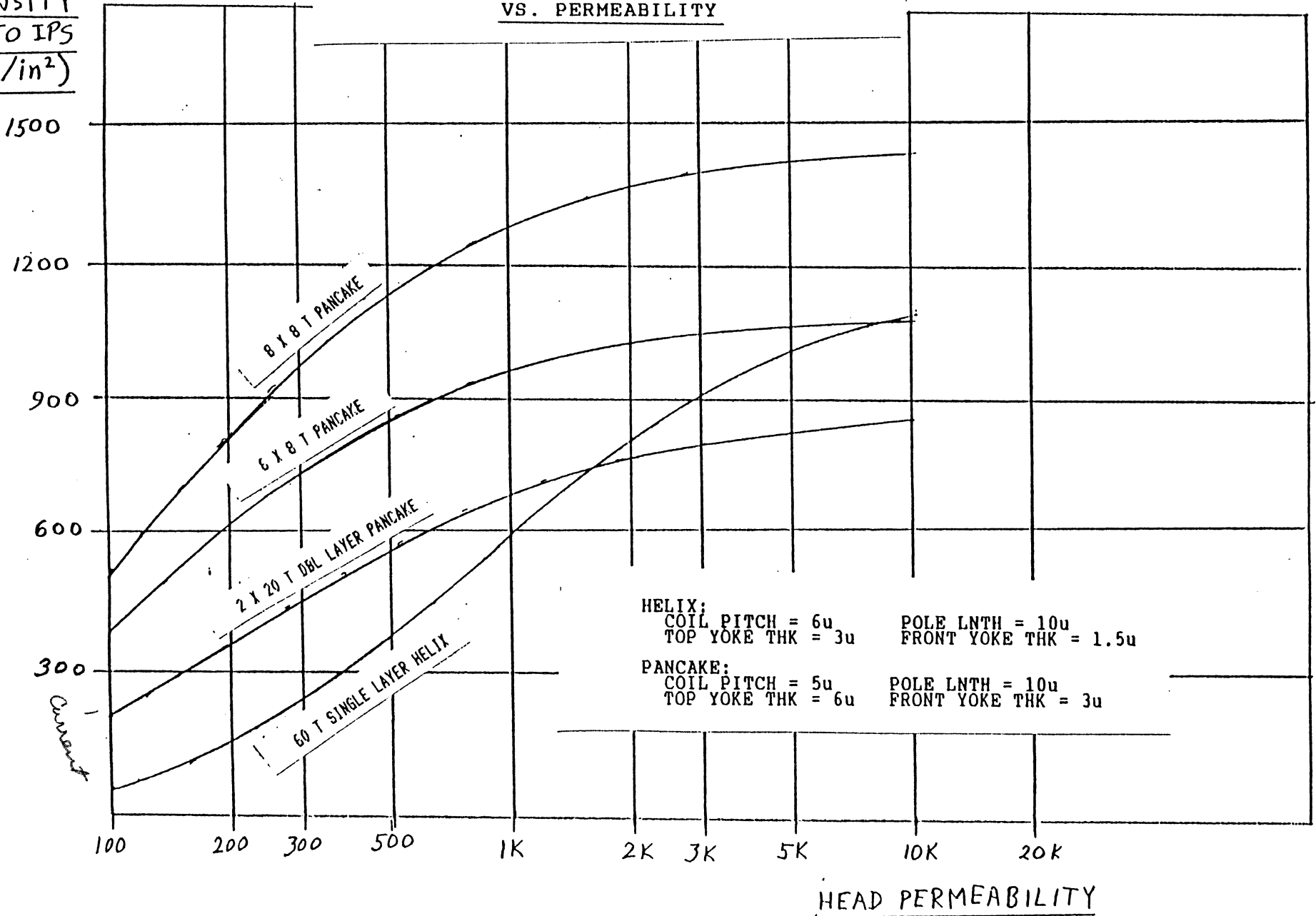
*Features
Lead
6-8 layers*



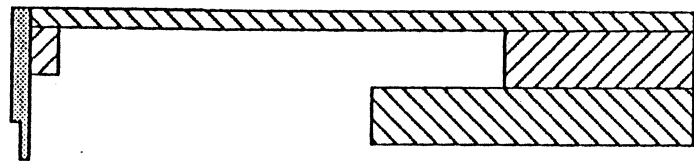
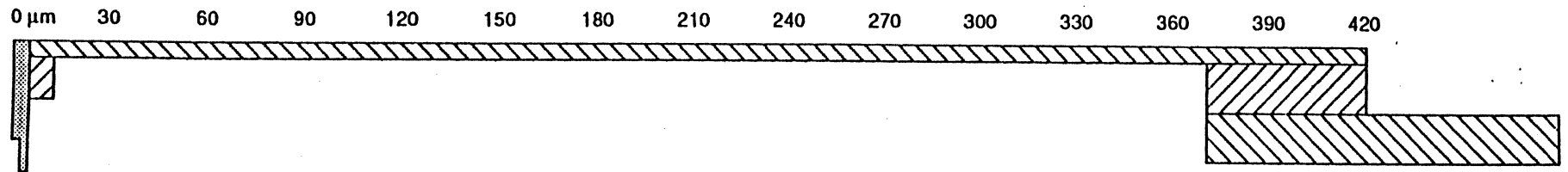


EST
AREAL
DENSITY
@150 IPS
(Mb/in²)

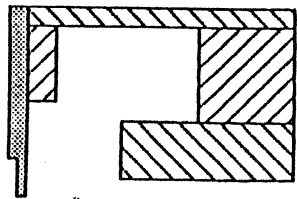
ESTIMATED AREAL DENSITY CAPABILITY
VS. PERMEABILITY



HELIX



PANCAKE 2 LAYERS



PANCAKE 4 LAYERS

64 turns
↑

67.5

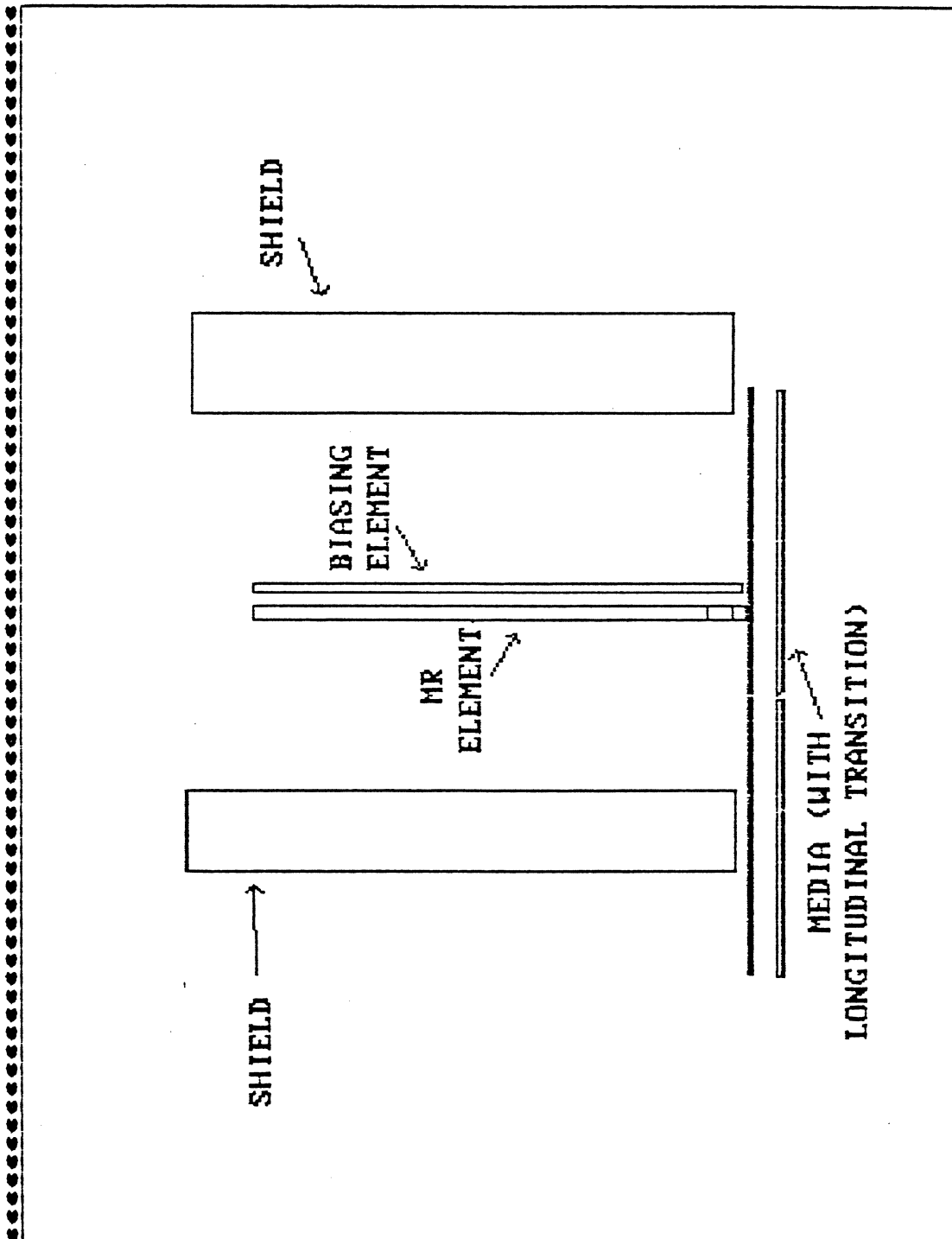
MAGNETO-RESISTIVE
HEADS

MR HEADS - ADVANTAGES

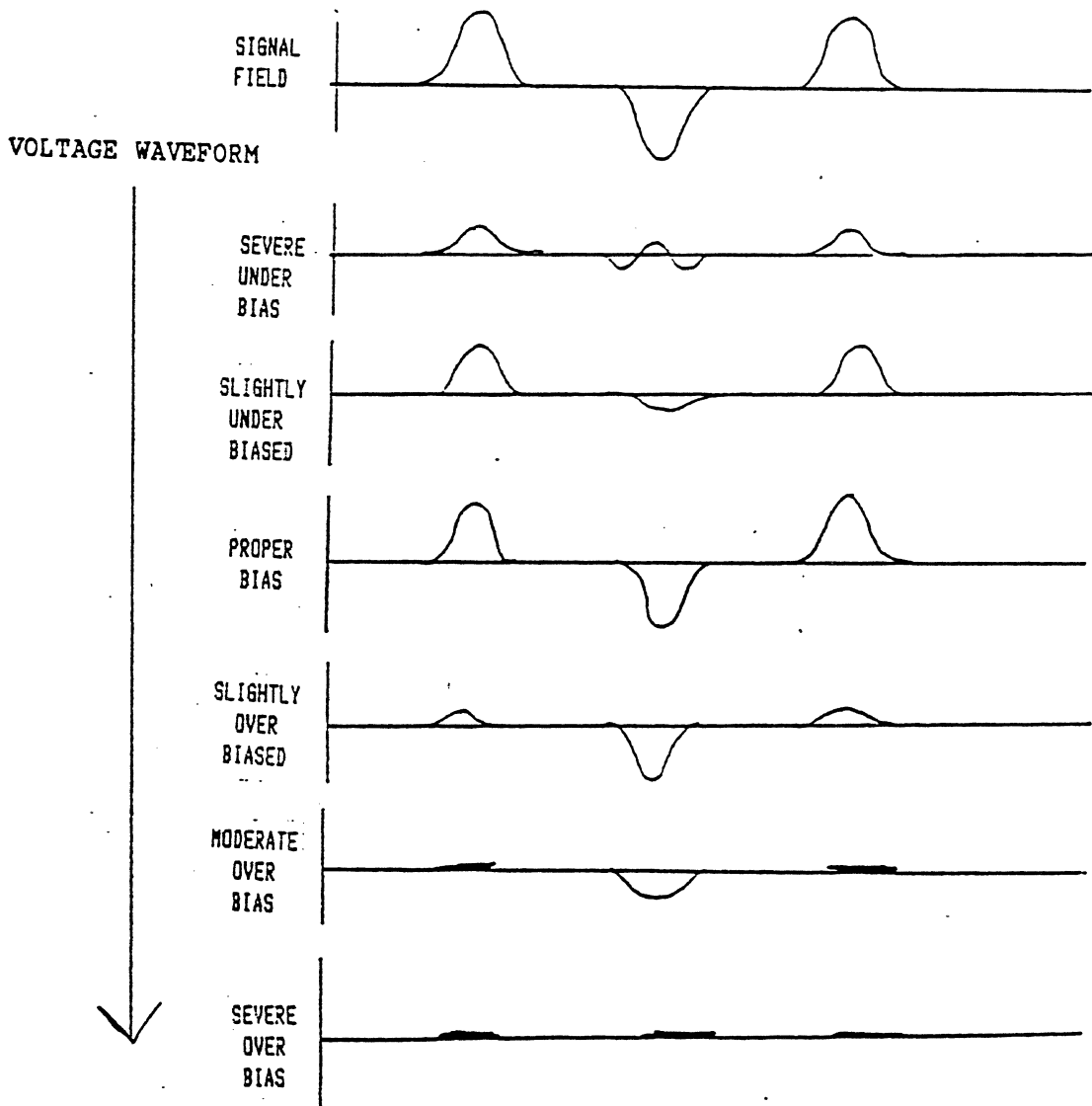
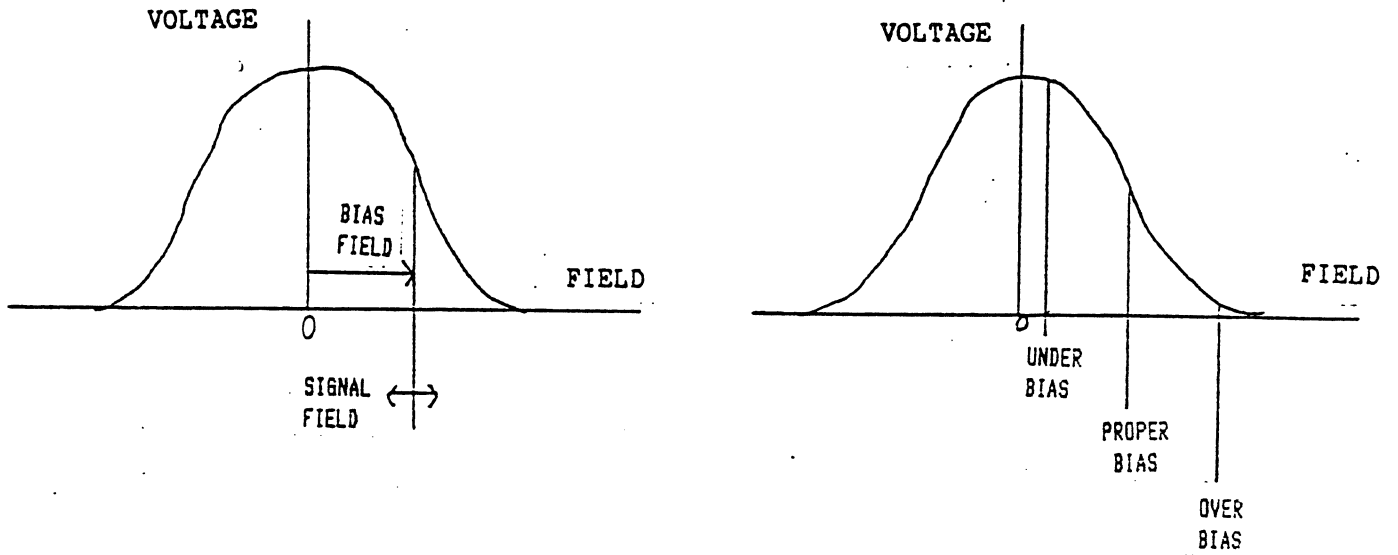
1. WRITE-WIDE READ-NARROW CONFIGURATIONS POSSIBLE.
2. CAN SIMULTANEOUSLY OPTIMIZE WRITE ELEMENT FOR OVERWRITE PERFORMANCE, AND READ ELEMENT FOR RESOLUTION PERFORMANCE.
3. VELOCITY INDEPENDENCE OF SIGNAL PROVIDES LARGE SIGNALS AT LOW MEDIA VELOCITIES IN SMALLER FORMS FACTORS.
4. VERY HIGH SIGNAL AMPLITUDES PER UNIT OF TRACKWIDTH ALLOW HIGH TRACK DENSITIES.
5. DESIGNS FOR HIGH RESOLUTION ALLOW HIGH LINEAR BIT DENSITIES.
6. VERY LOW IMPEDANCE - MINIMIZES ELECTRICAL NOISE.
7. HIGHER SNR'S CAN BE USED TO INCREASE AREAL DENSITY:
 TRACK DENSITY - USING NARROWER TRACKS
 BIT DENSITY - USING CODES WITH MORE "DETENTS" PER
 MINIMUM PULSE SPACING (MORE USERBITS PER FCI).

MR ELEMENT
ON
LONGITUDINAL MEDIA

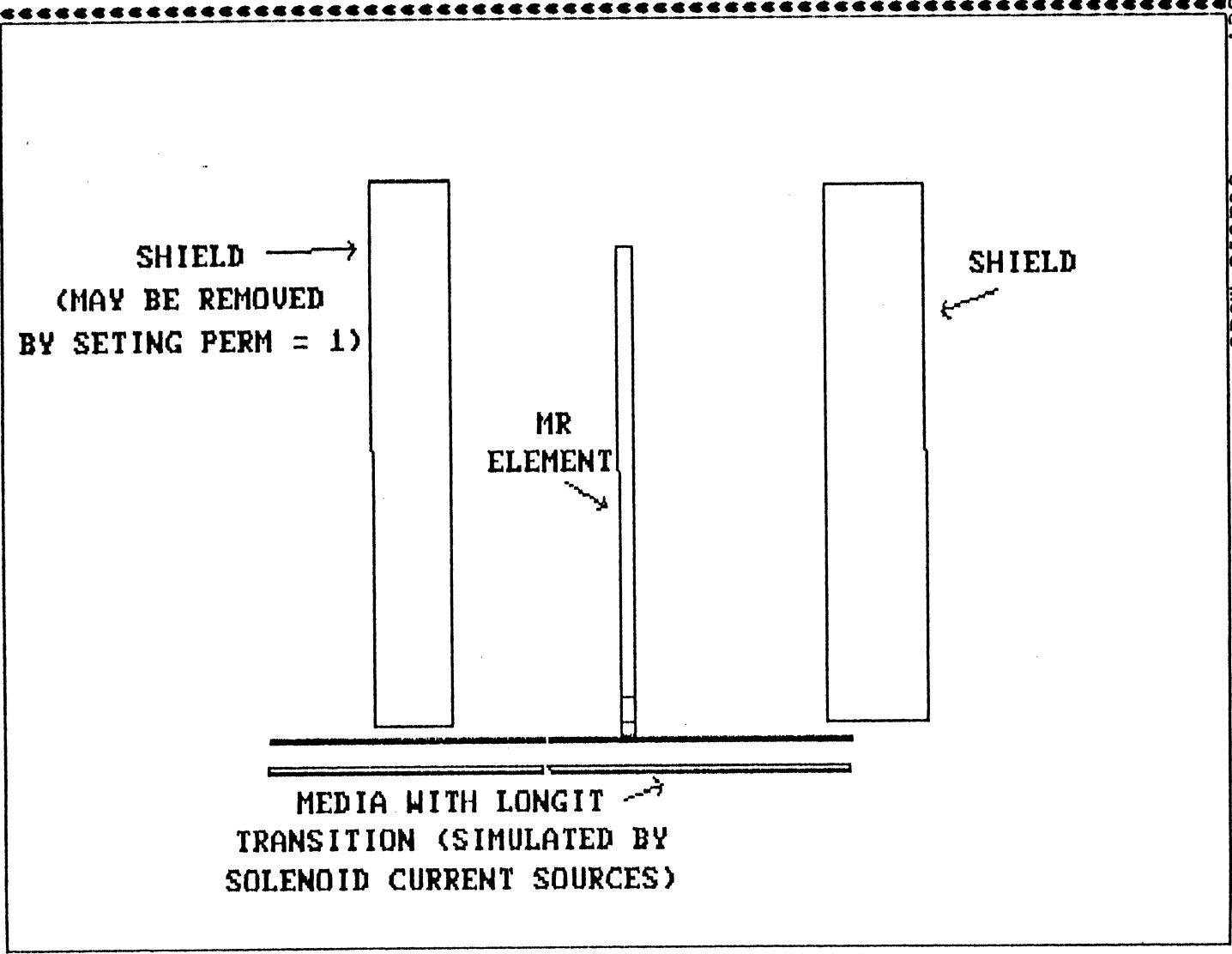
DATE = 11/09/1992 TIME= 13:48:57.34
Current database: MRHEADS.DBS
Current file: MRLONG3
Mode of analysis: MAGNETO 2D Field analysis
Analysis type: Static mode



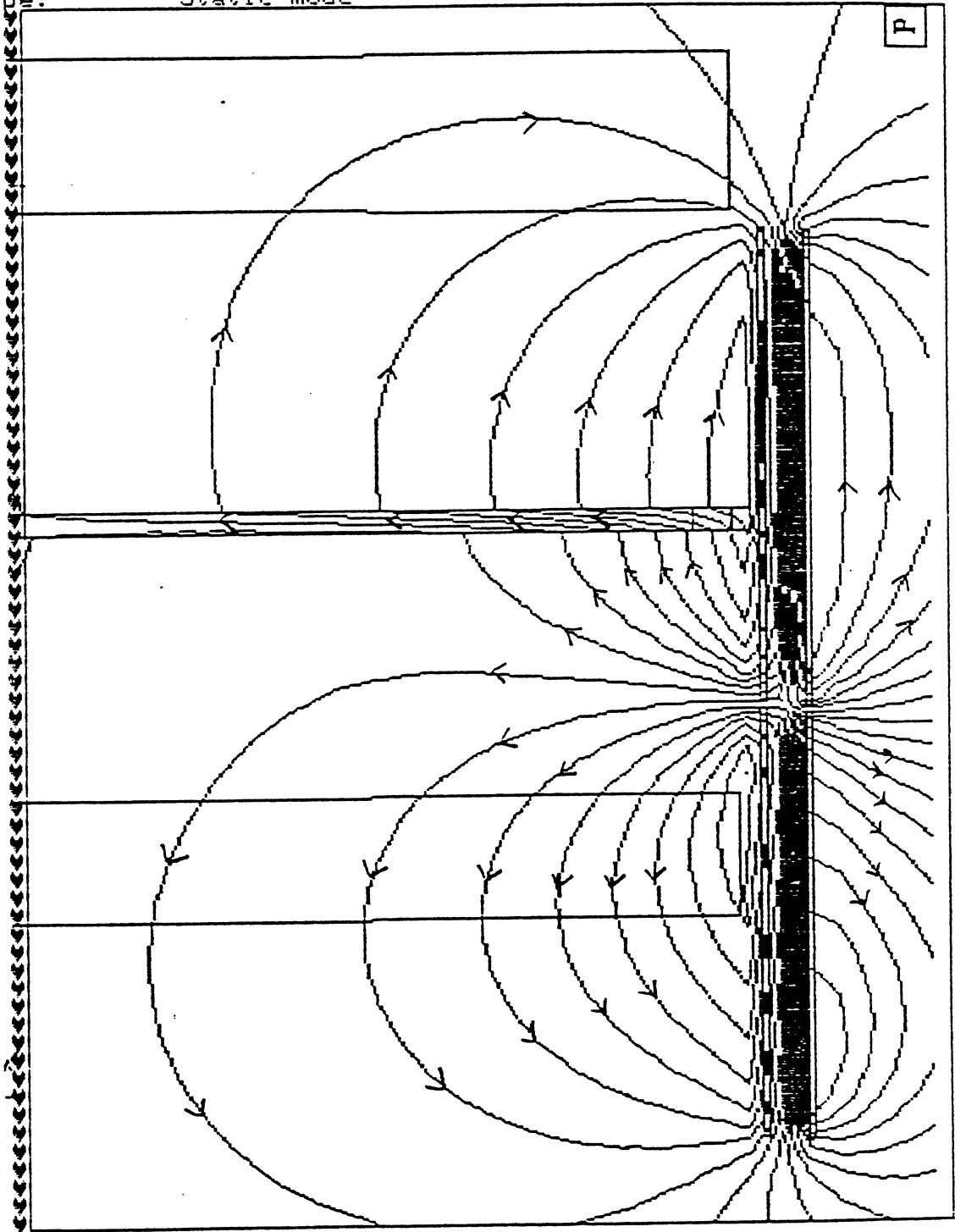
USE OF BIAS TO LINEARIZE MR HEAD RESPONSE



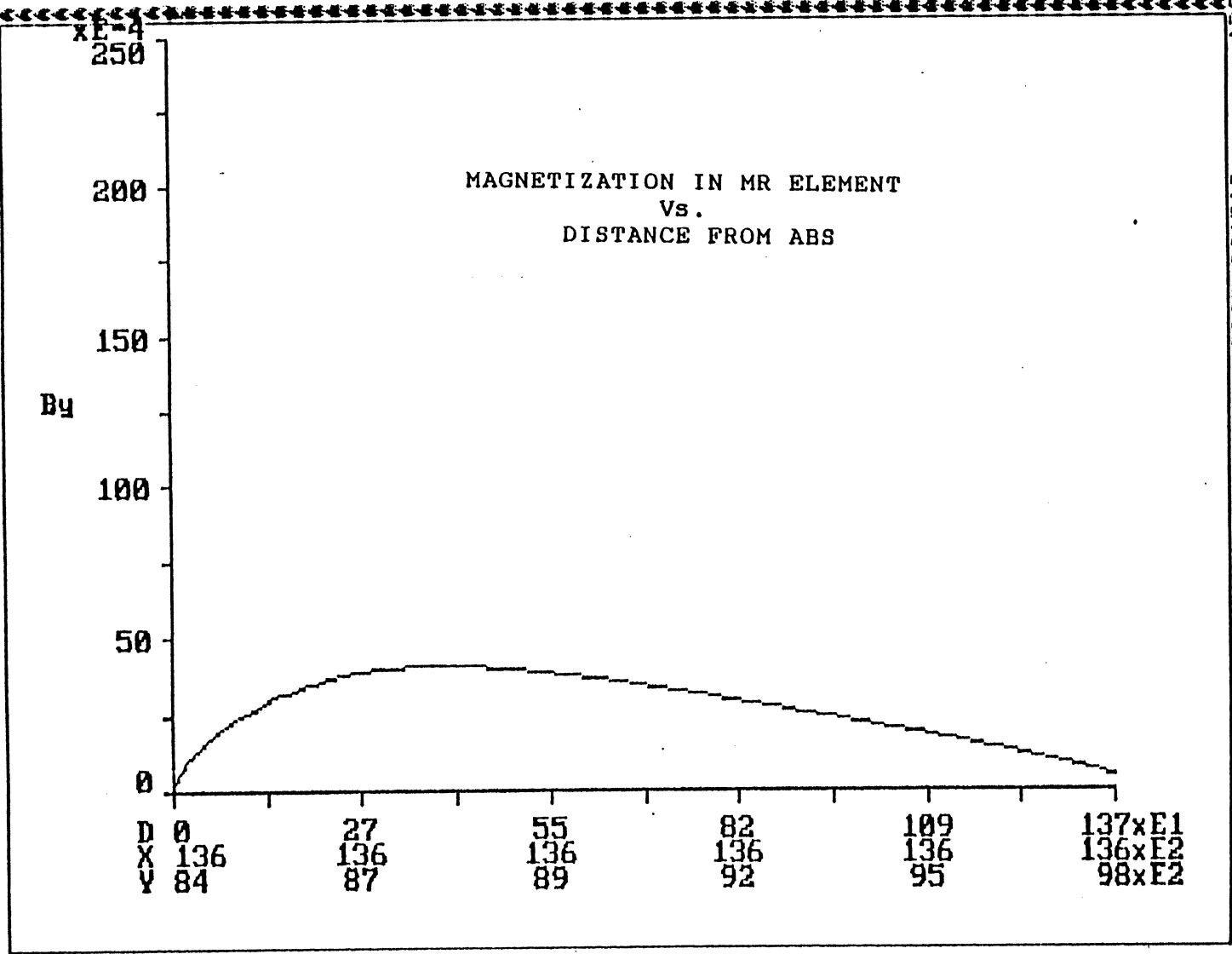
DATE = 10/03/1992 TIME = 10:02:43.43
Current database: MRHEADJ.DBS
File: MRLONG3
Mode of analysis: MAGNETO 2D Field analysis
Analysis type: Static mode



DATE = 03/29/1992 TIME= 16:51:44.75
Current database: mrheads.db
Current file: MRLONG3
Mode of analysis: MAGNETO 2D Field analysis
Analysis type: Static mode

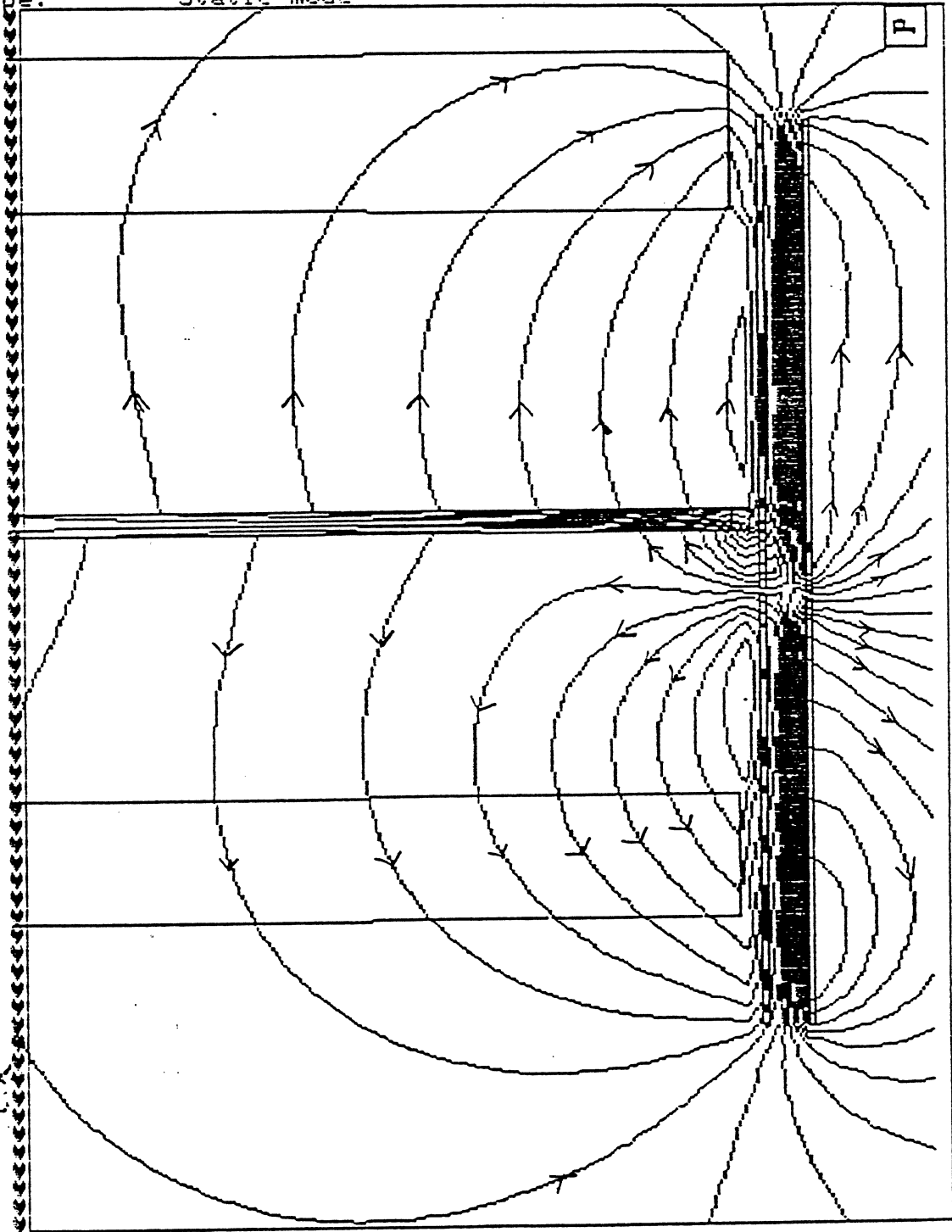


DATE = 09/29/1992 TIME = 16:55:12.42
 Current database: mrheads.dbs
 Current file: MRLONM33
 Mode of analysis: MAGNETO 2D Field analysis
 Analysis type: Static mode

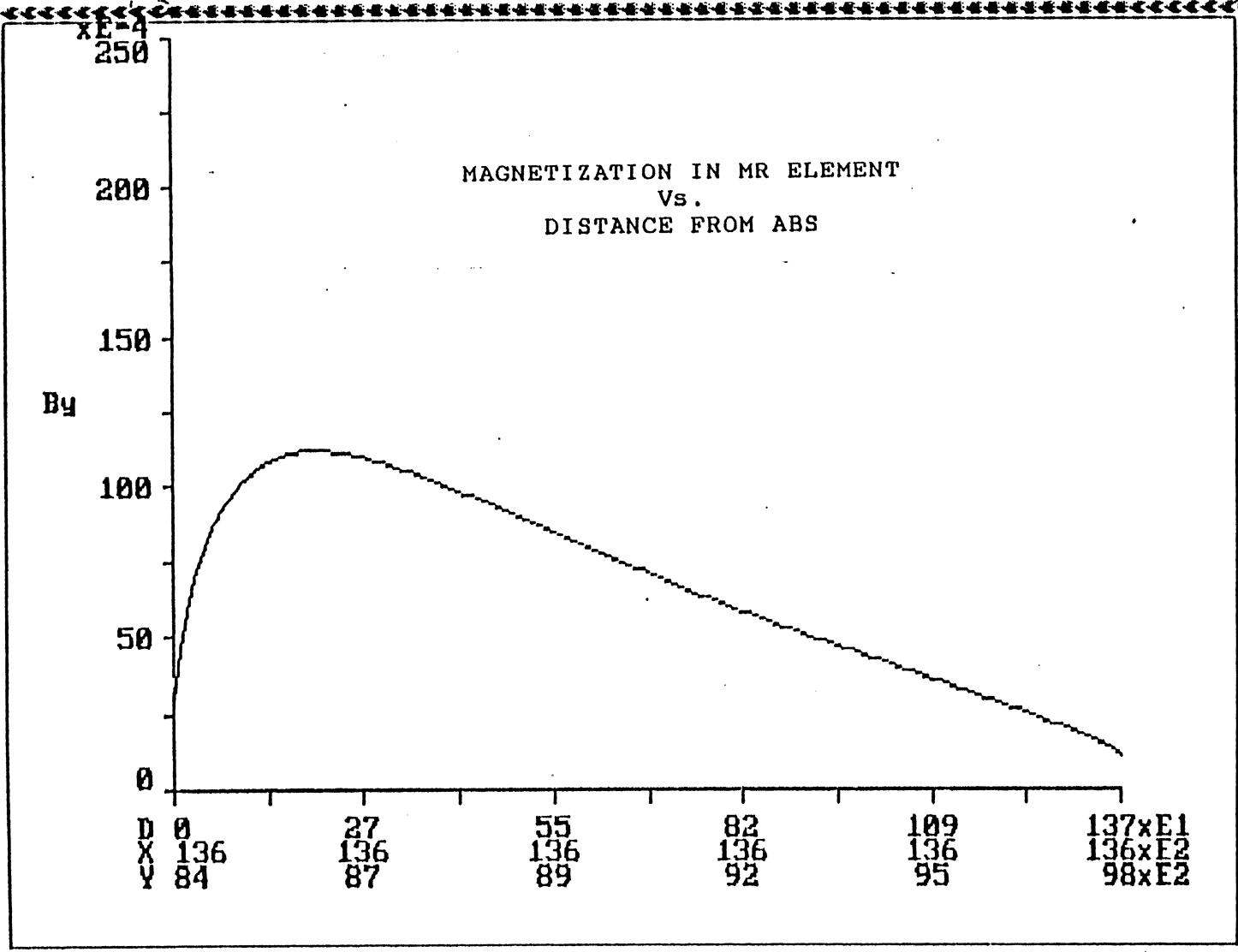


D	0	27	55	82	109	137xE1
X	136	136	136	136	136	136xE2
Y	84	87	89	92	95	98xE2

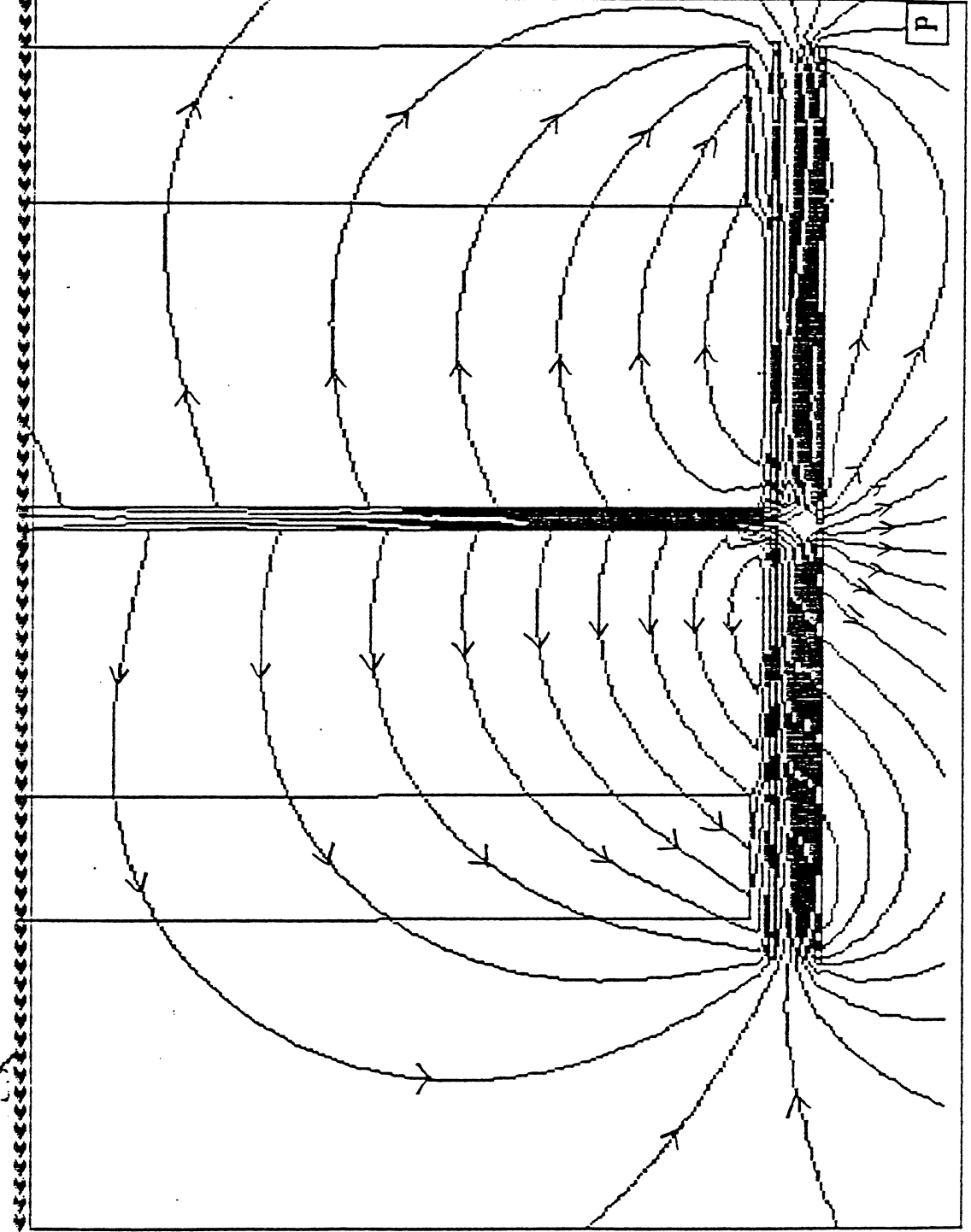
DATE = 09/29/1992 TIME= 16:33:13.33
Current database: mrheads.dbs
Current file: MR.LONG3
Mode of analysis: MAGNETO 2D Field analysis
Analysis type: Static mode



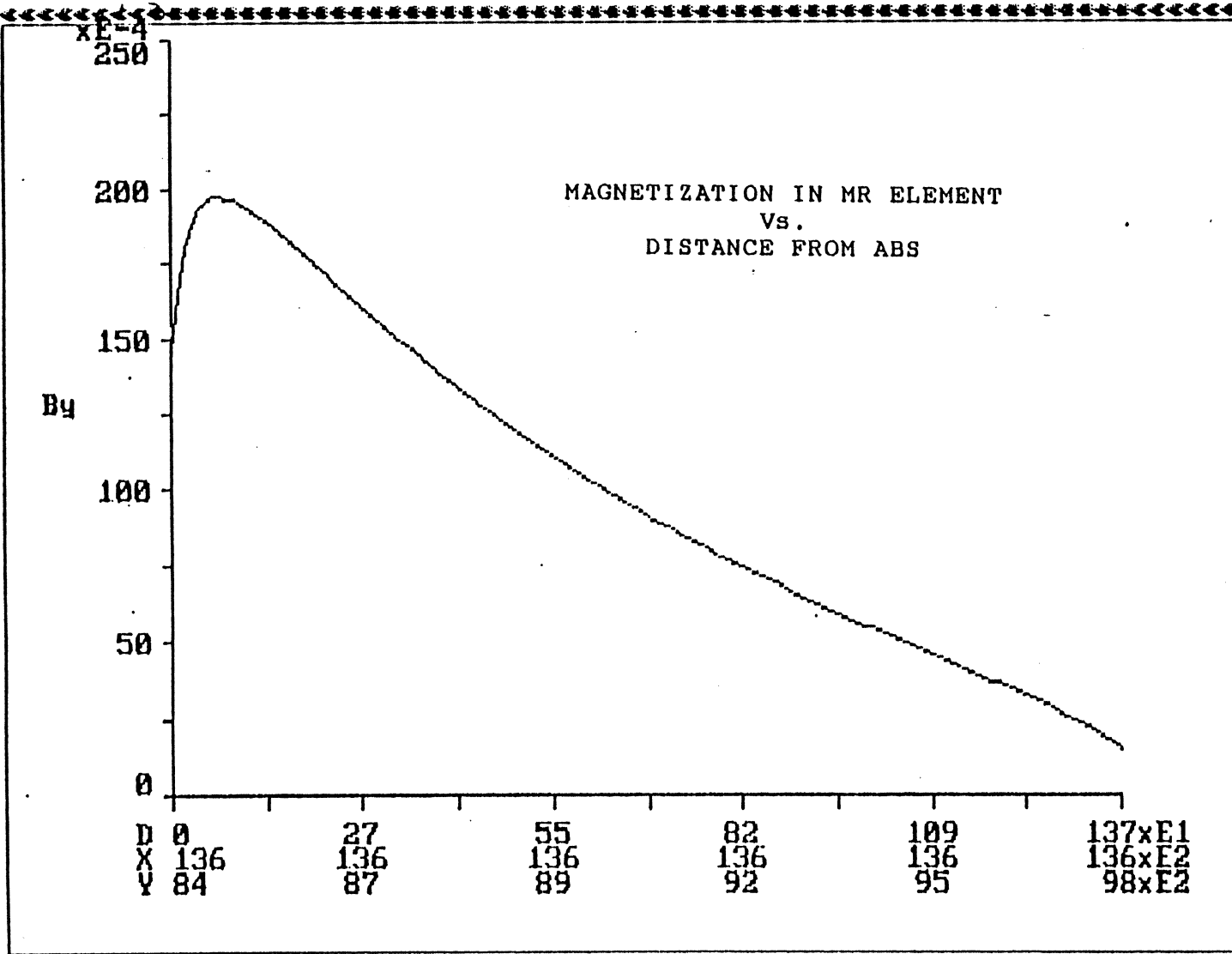
DATE = 09/23/1992
 Current database: mrheads.dbs
 Current file: MRLOM33
 Mode of analysis: MAGNETO, 2D Field analysis
 Analysis type: Static mode
 TIME = 16:36:55.07



DATE = 03/29/1992 TIME= 16:22:17.74
Current database: mrheads.dbs
Current file: MRLONG30
Mode of analysis: MAGNETO 2D Field analysis
Analysis type: Static mode

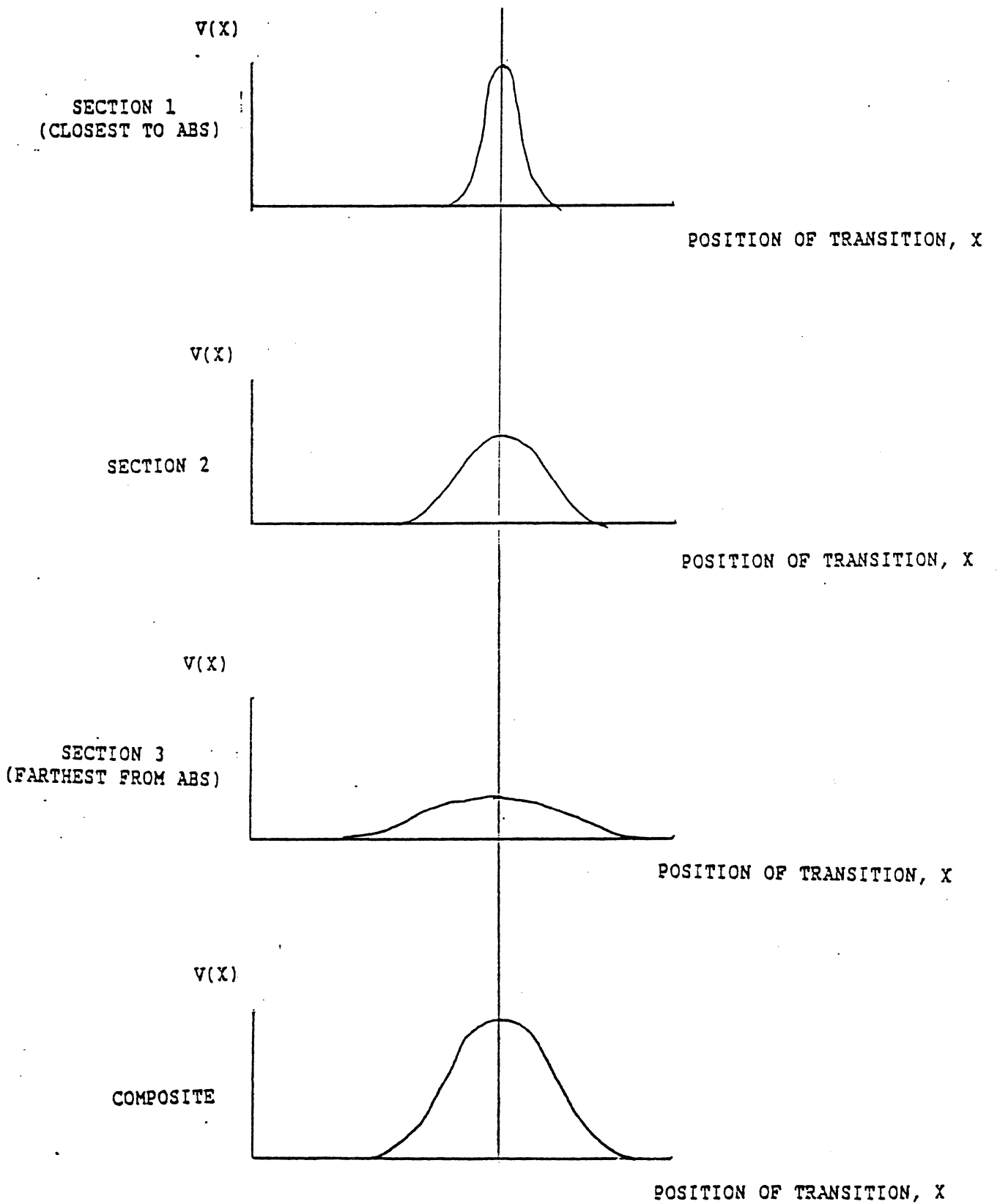


DATE = 09/29/1992
 Current database: MRheads.dbs
 Current file: MKLON33
 Mode of analysis: MAGNETO 2D Field analysis
 Analysis type: Static mode
 TIME = 16:26:41.49

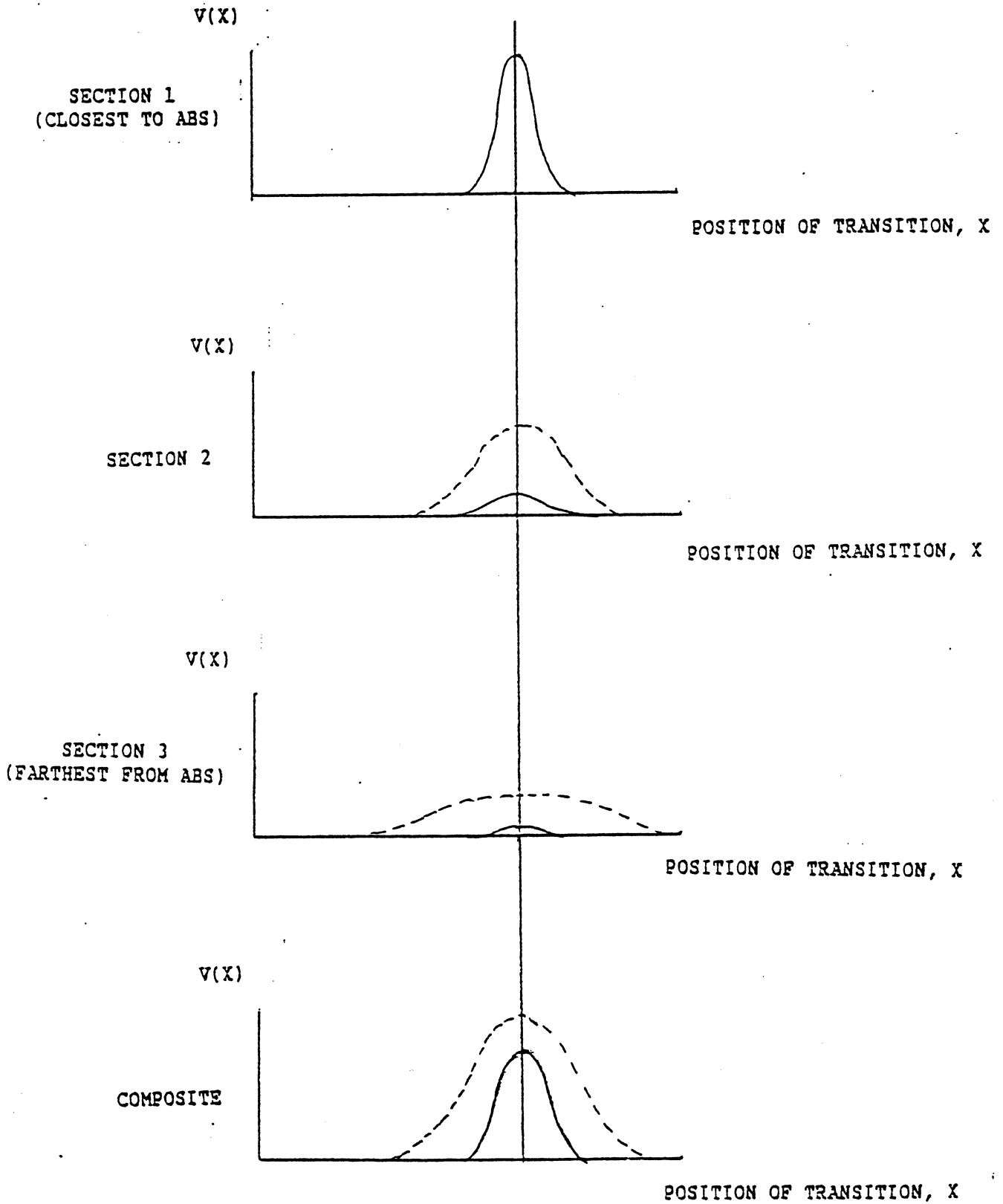


D 0
 X 136
 Y 84
 27
 136
 87
 55
 136
 89
 82
 136
 92
 109
 136
 95
 137xE1
 136xE2
 98xE2

RESPONSE OF MR SENSOR TO LONGITUDINAL MEDIA

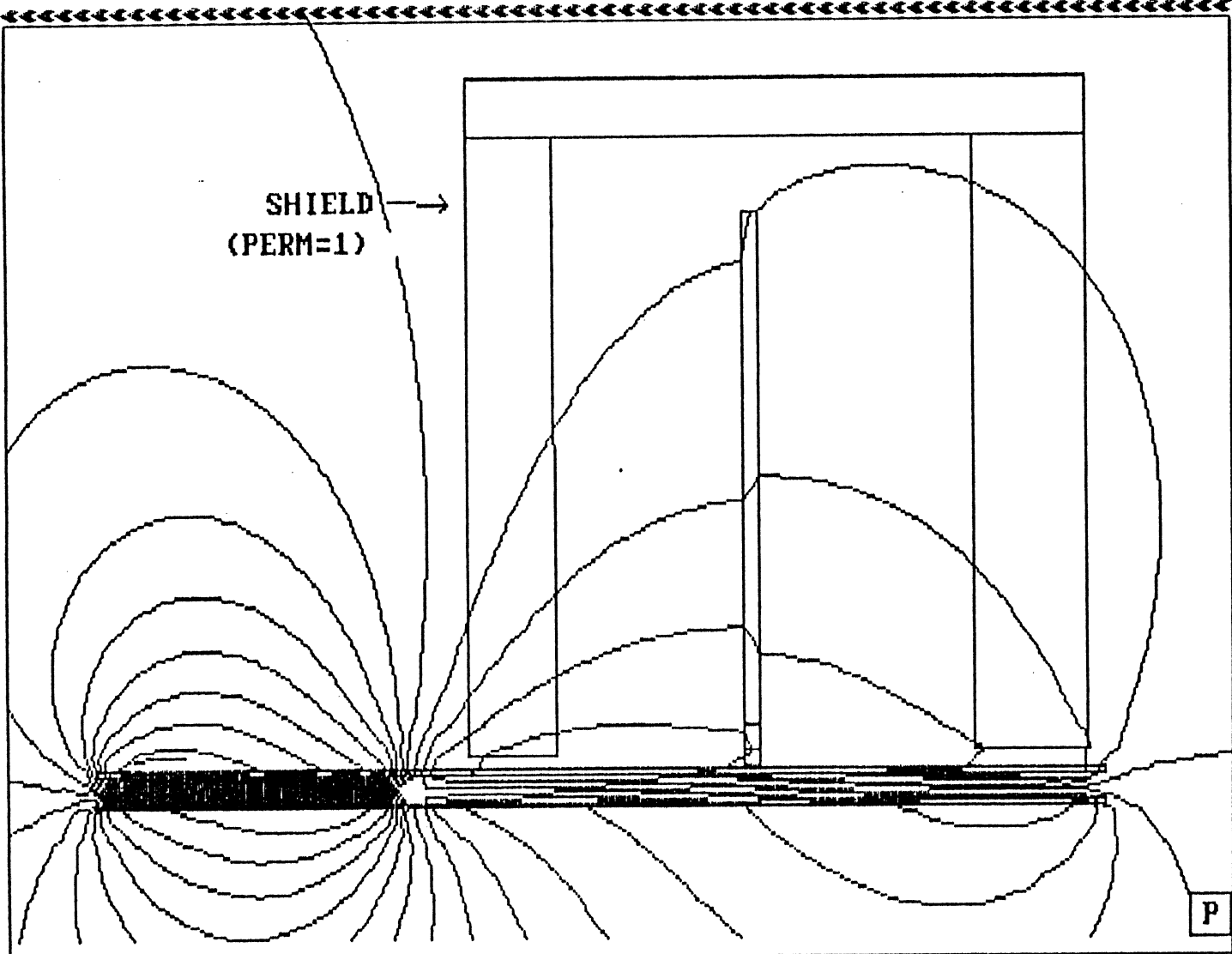


RESPONSE OF OVERBIASED (EXCEPT NEAR ABS) MR SENSOR
TO LONGITUDINAL MEDIA

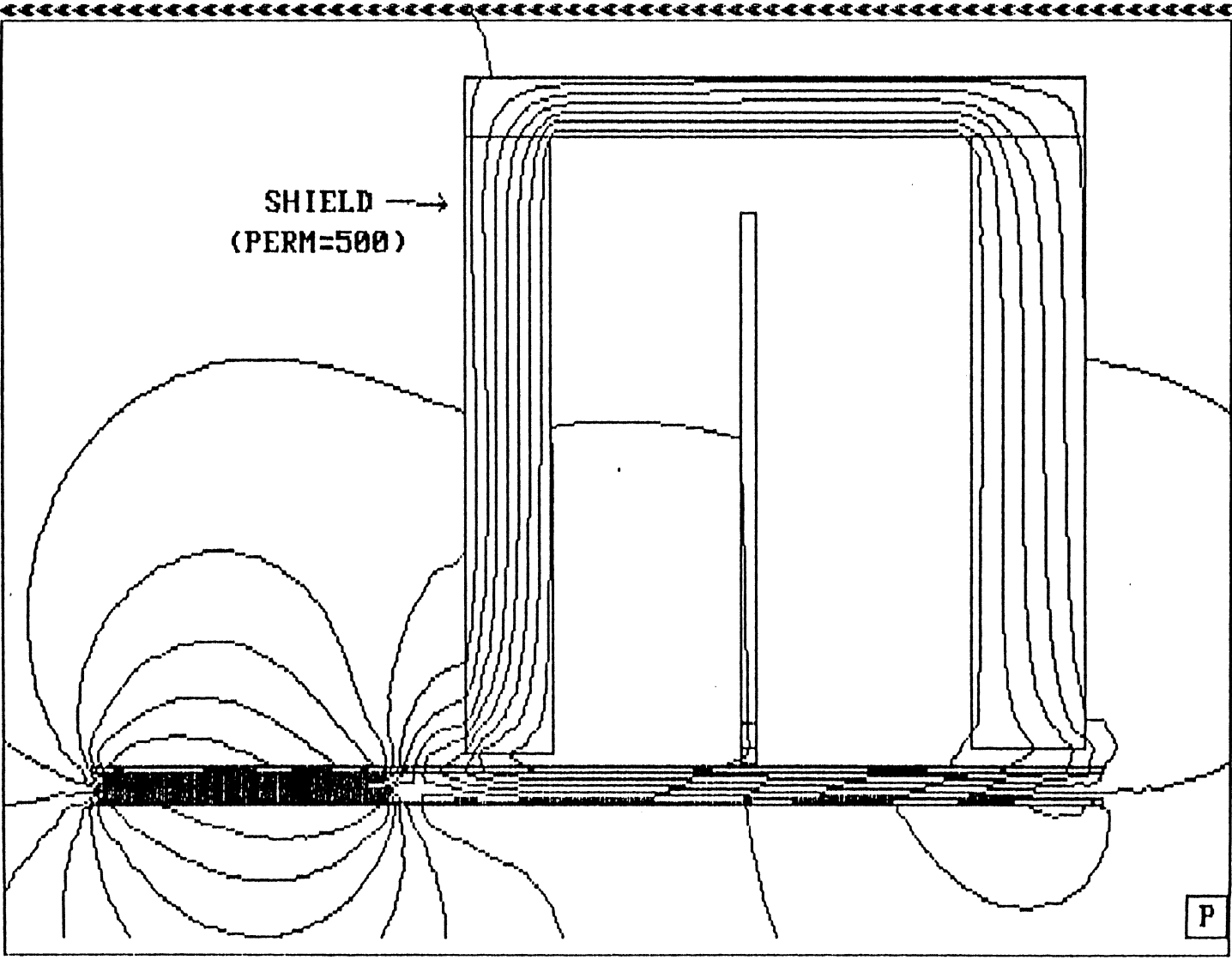


EFFECT OF SHIELDS

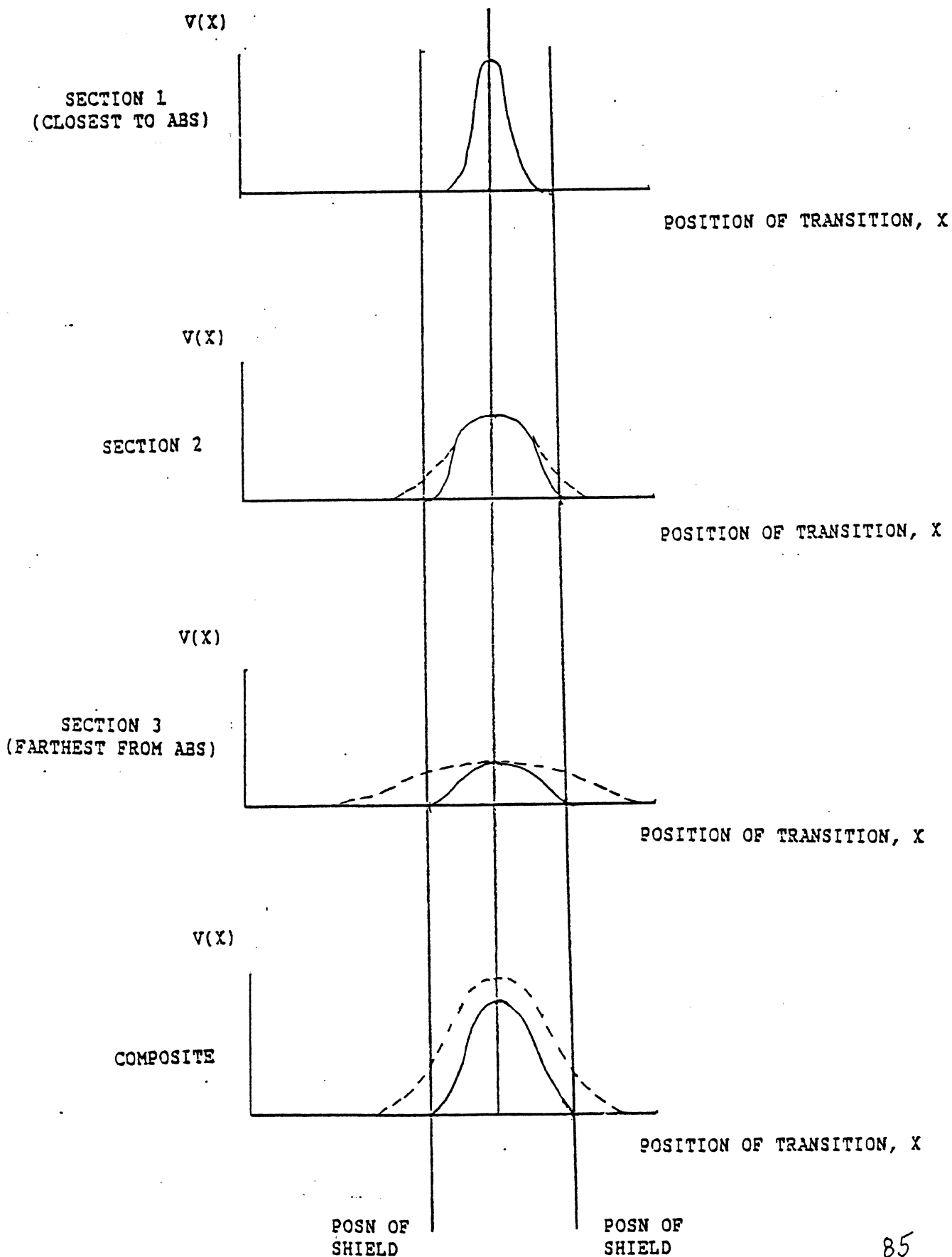
DATE = 10/06/1992 TIME = 11:05:34.34
Current database: MRHEADS.DBS
Current file: MRLOM33
Mode of analysis: MAGNETO 2D Field analysis
Analysis type: Static mode



DATE = 10/06/1992 TIME = 10:58:47.68
Current database: MRHEADS.DBS
Current file: MFLONG
Mode of analysis: MAGNETO 2D Field analysis
Analysis type: Static mode

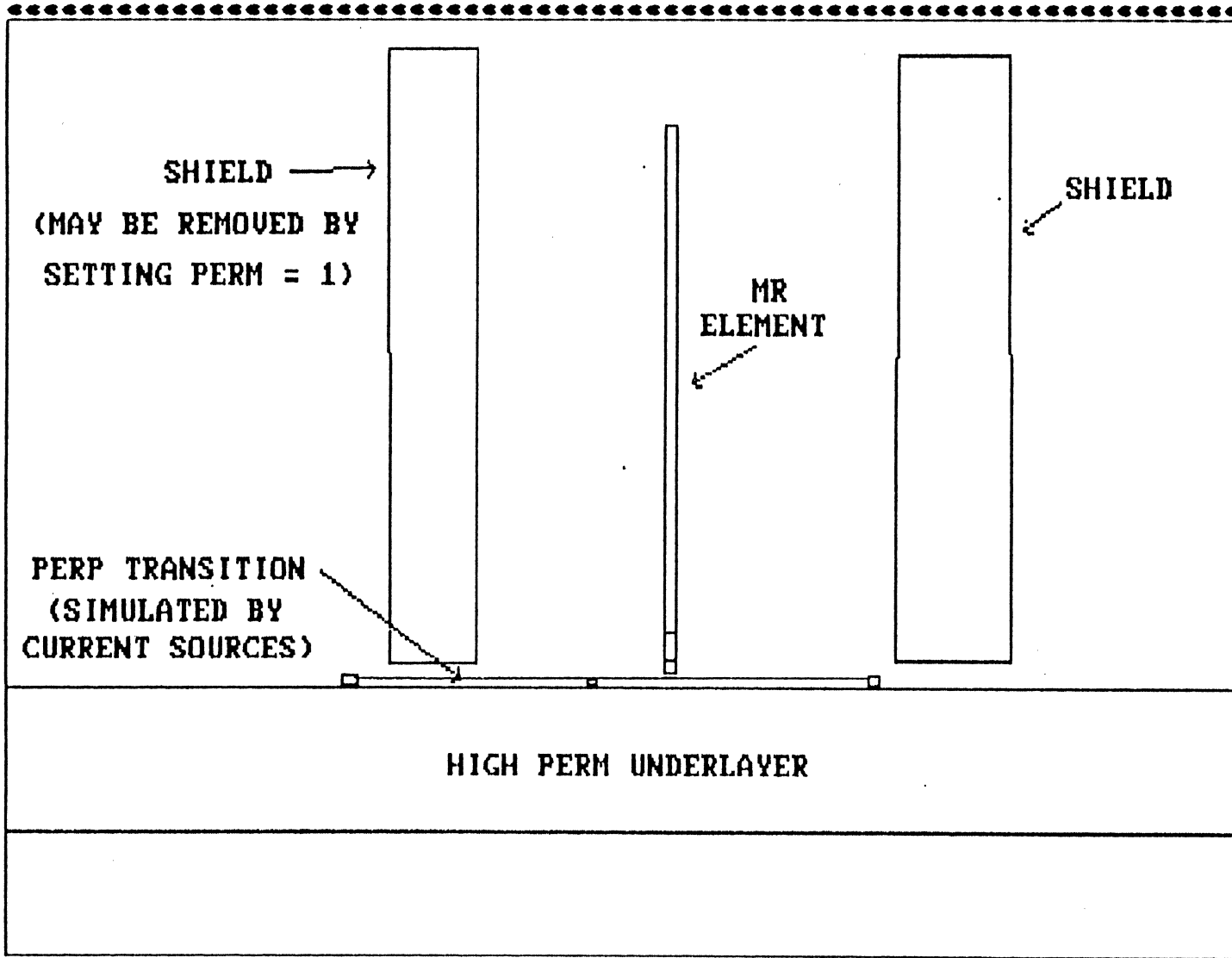


RESPONSE OF SHIELDED MR SENSOR TO LONGITUDINAL MEDIA

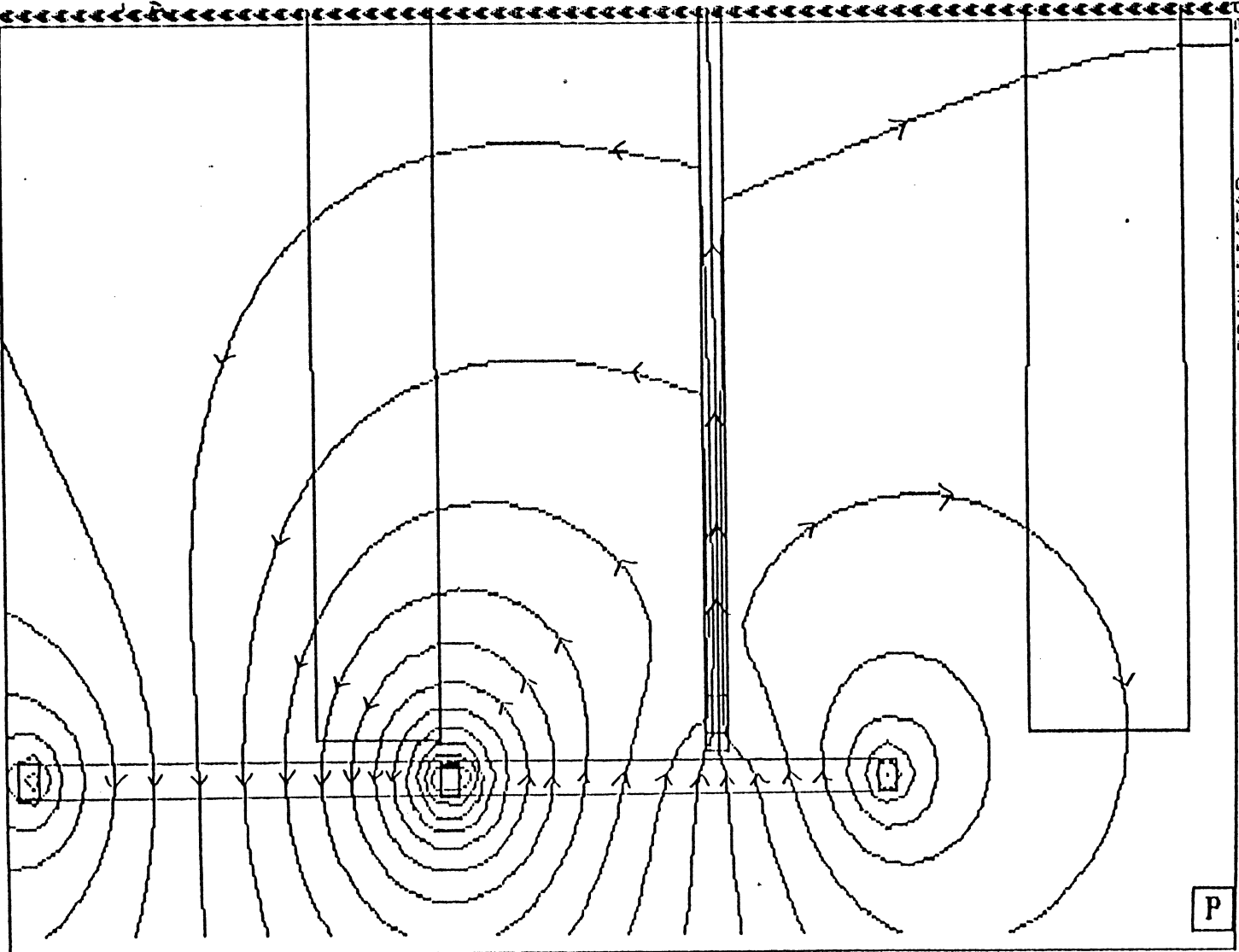


MR ELEMENT
ON
PERPENDICULAR MEDIA

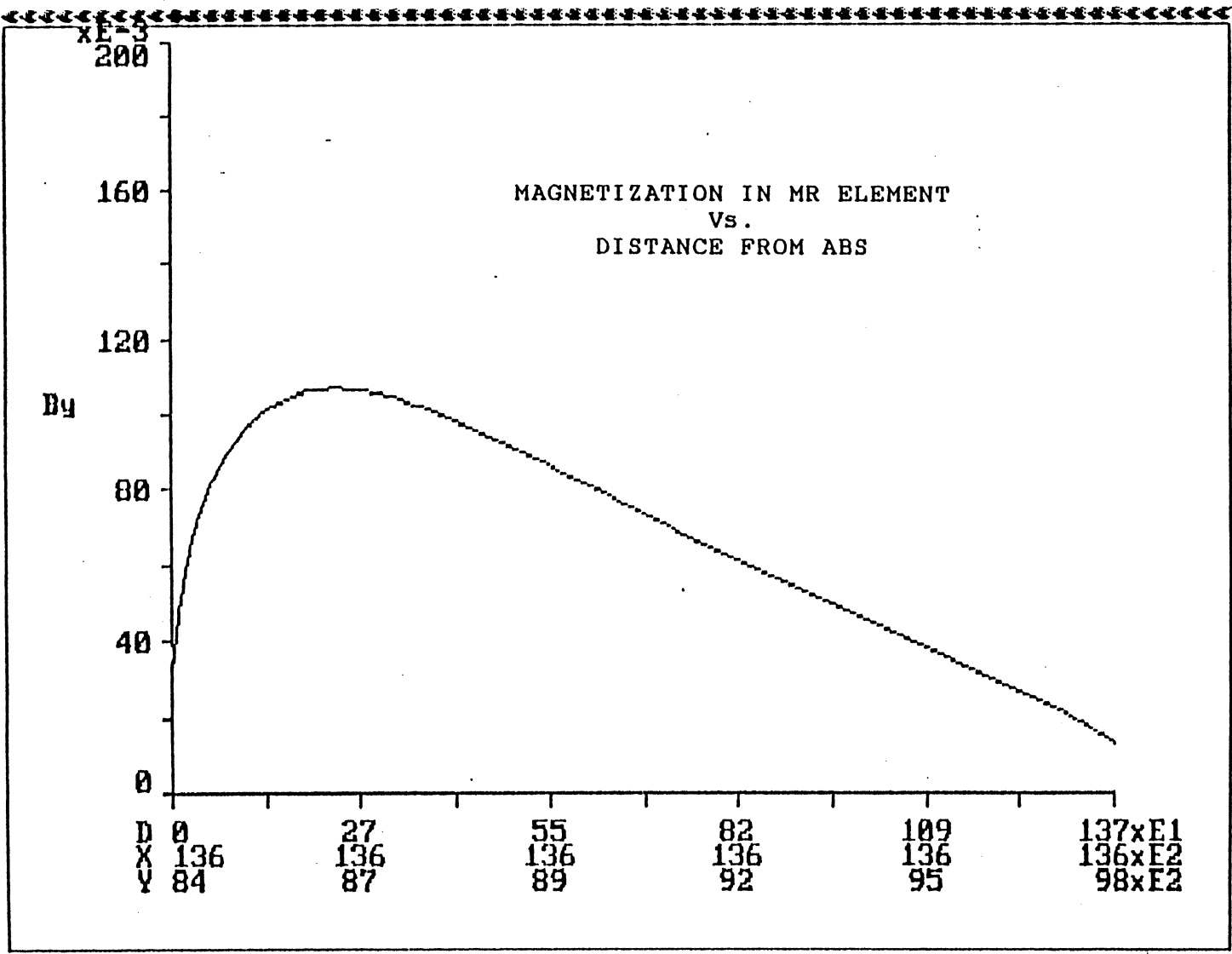
DATE = 10/03/1992
Current database: MRHEADS.DBS
Current file: MRHEAD7A
Mode of analysis: MAGNETO 2D field analysis
Analysis type: static mode
TIME= 11:16:58.83



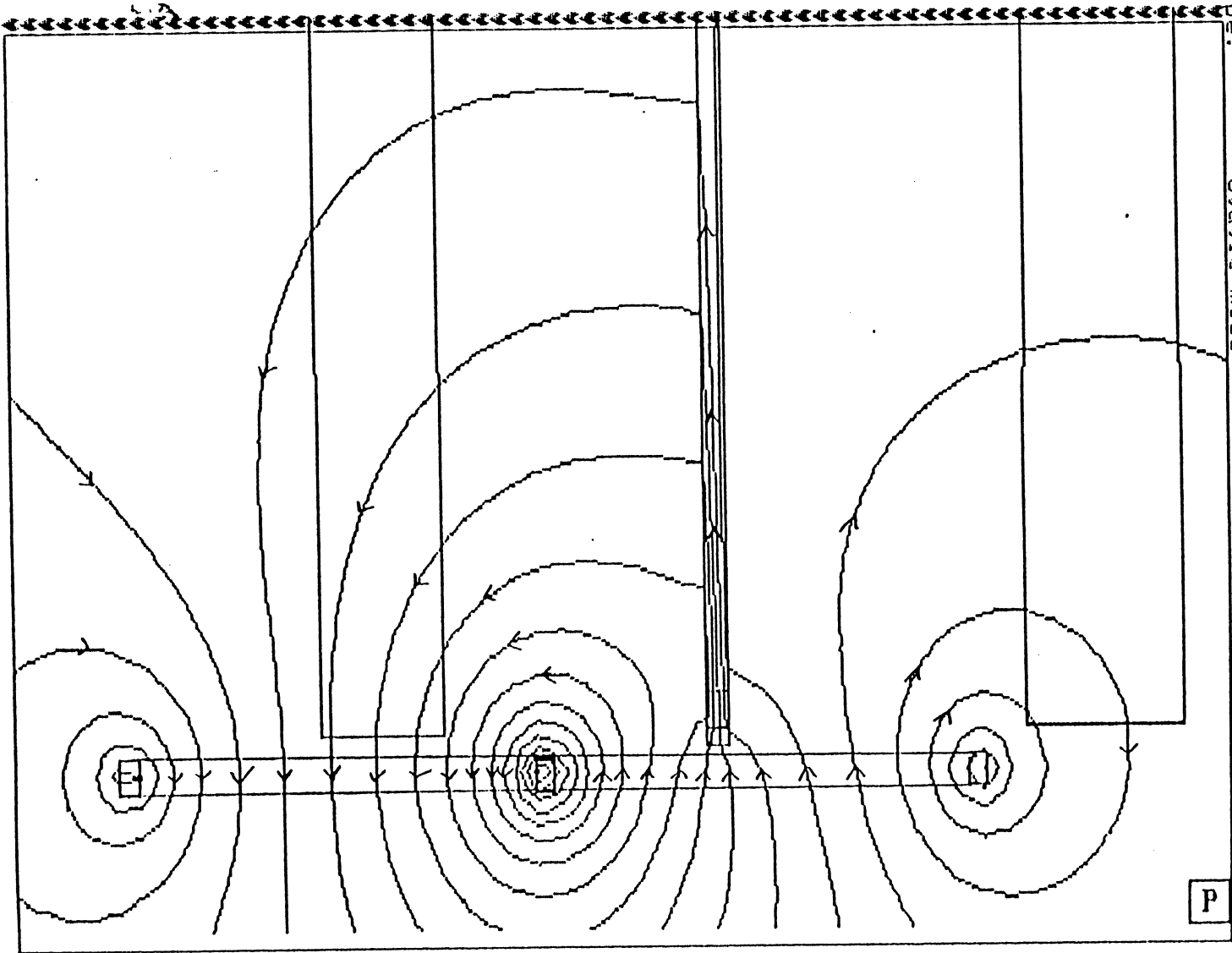
DATE = 09/29/1992 TIME = 14:50:36.24
Current database: MRheads.db
Current file: MRVEPT1
Mode of analysis: MAGNETO 2D Field analysis
Analysis type: Static.mda



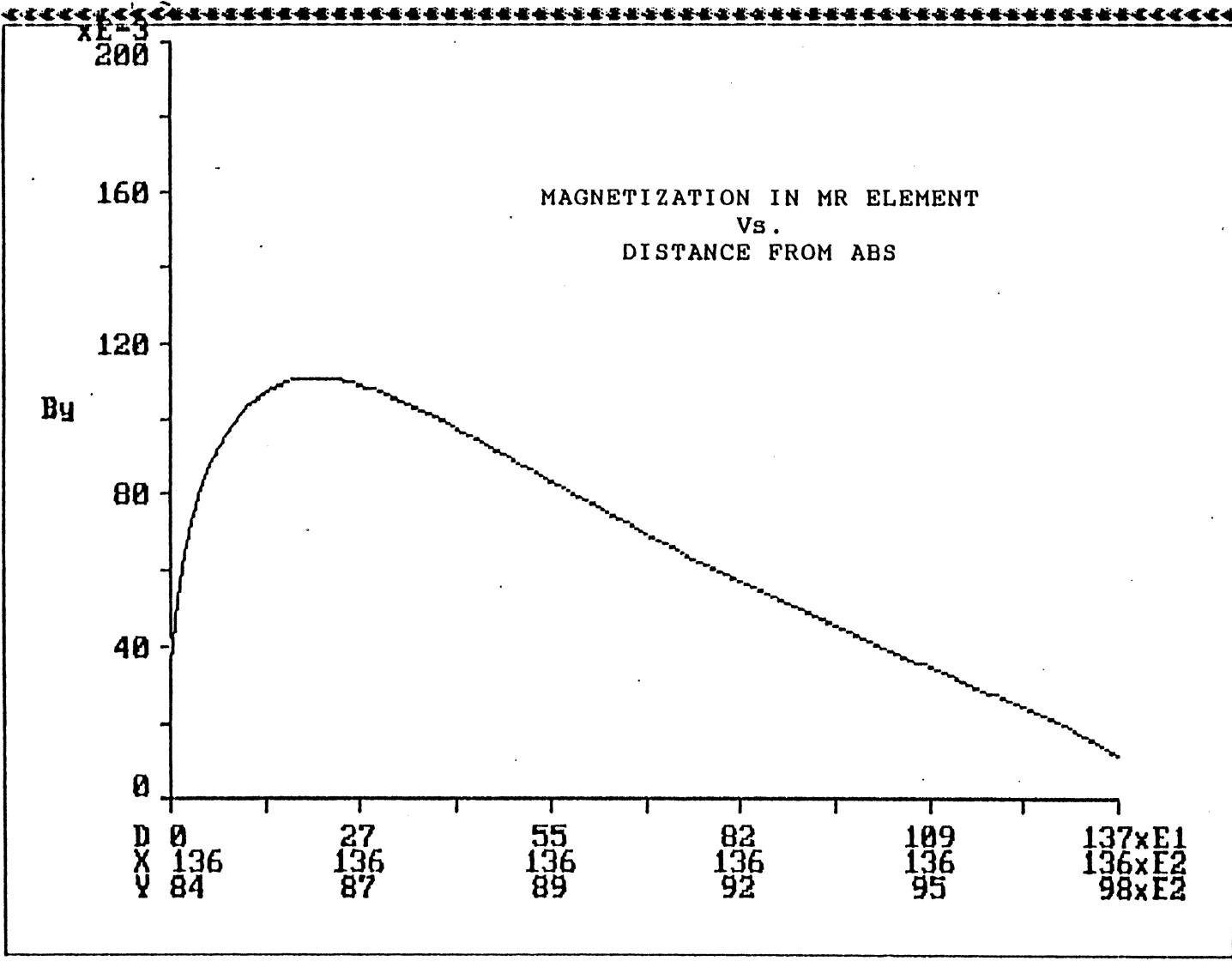
DATE = 09/29/1992 TIME = 14:54:10.34
 Current database: mrheads.dbs
 Current file: MRVERT1
 Mode of analysis: MAGNETO 2D field analysis
 Analysis type: Static mode



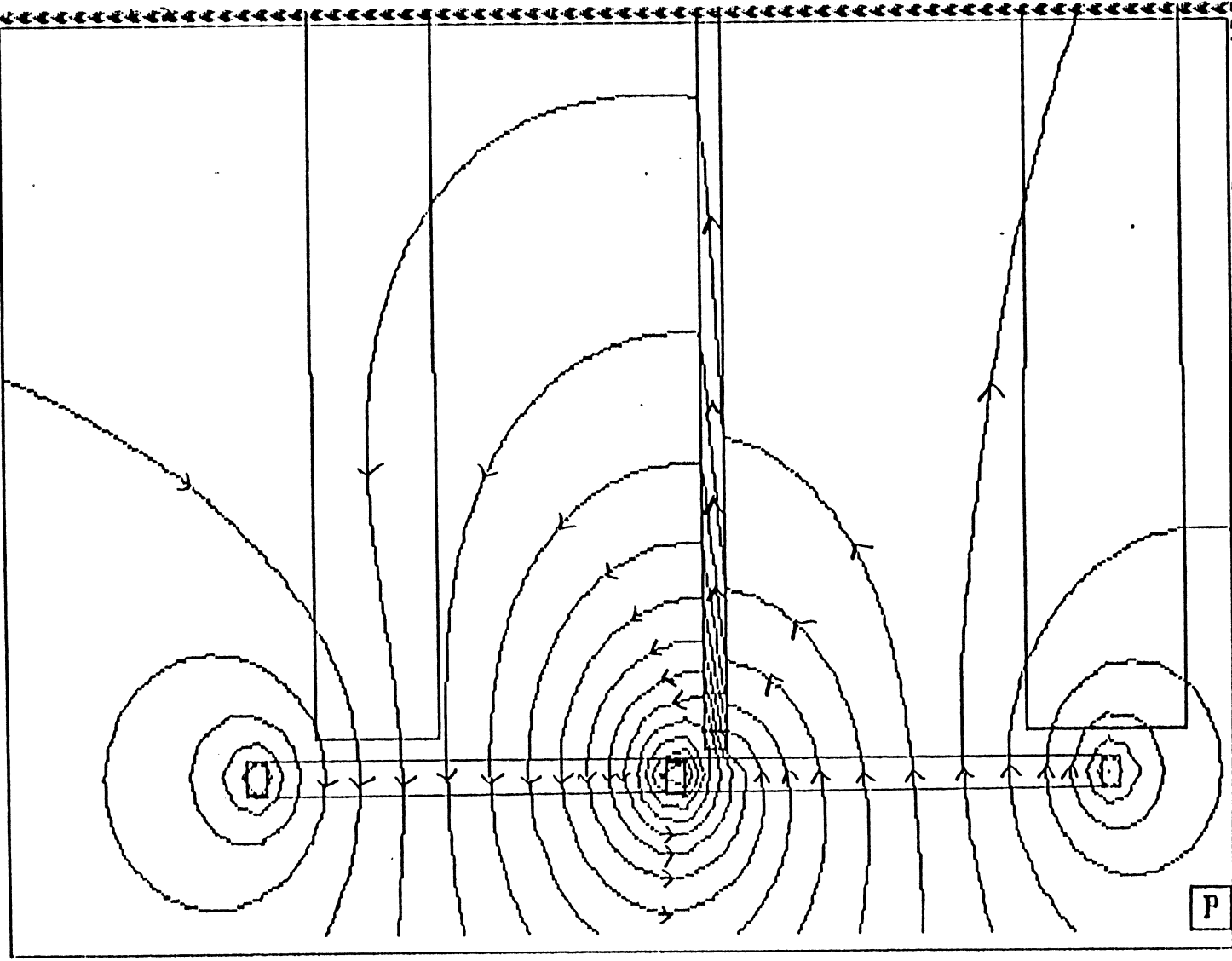
DATE = 09/29/1992 TIME = 14:42:04.06
Current database: mrheads.dbs
Current file: MRV EPTI
Mode of analysis: MAINNETO 2D Field analysis
Analysis type: Static mode



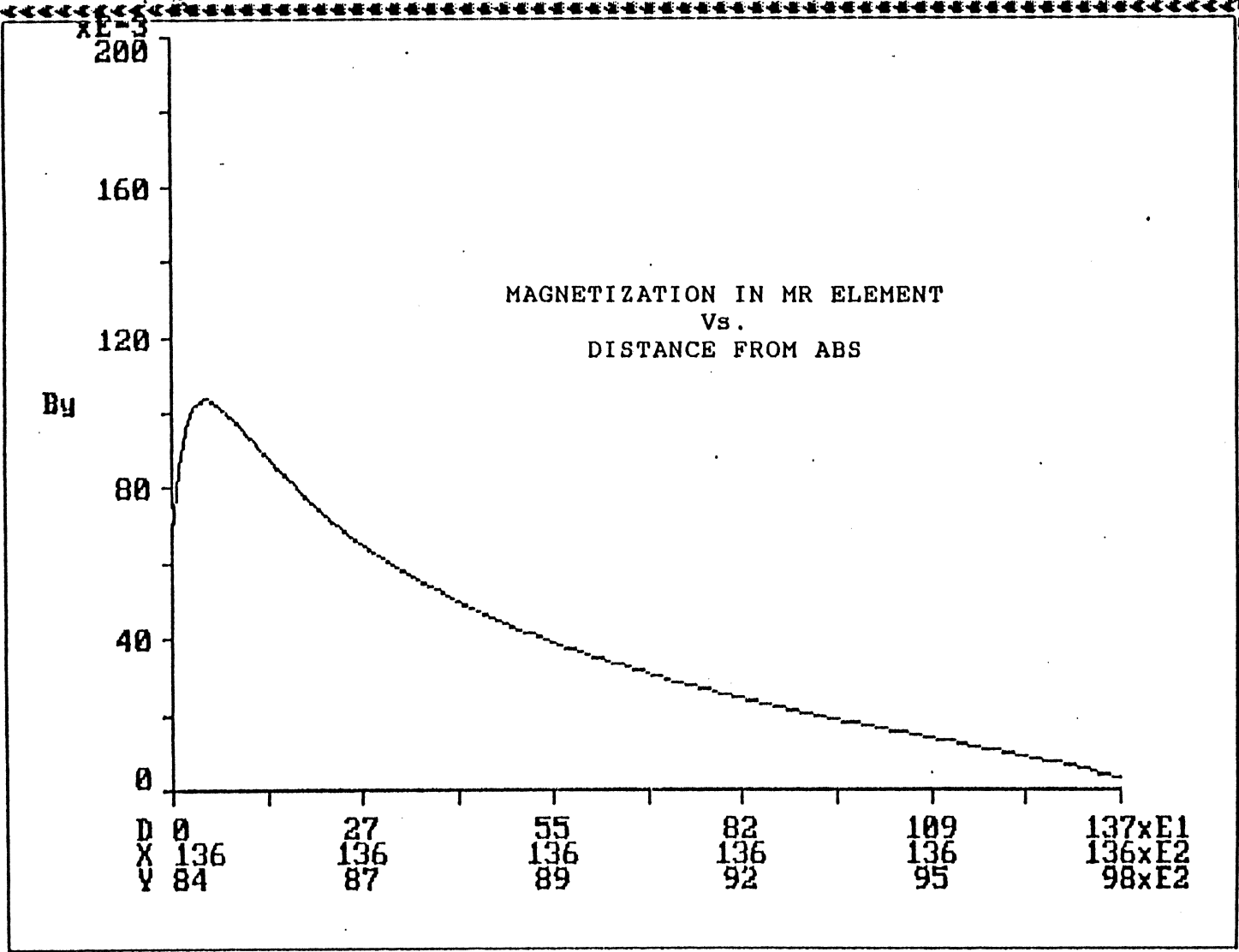
DATE = 03/23/1992
 Current database: mrheads.dbs
 Current file: MRVEPT1
 Mode of analysis: MAGNETO 2D Field analysis
 Analysis type: Static mode
 TIME= 14:45:30.30



DATE = 03/23/1992 TIME = 15:36:01.26
Current database: MRHEADS.DBS
Current file: MRVERT1
Mode of analysis: MAGNETO 2D Field analysis
Analysis type: Static mode

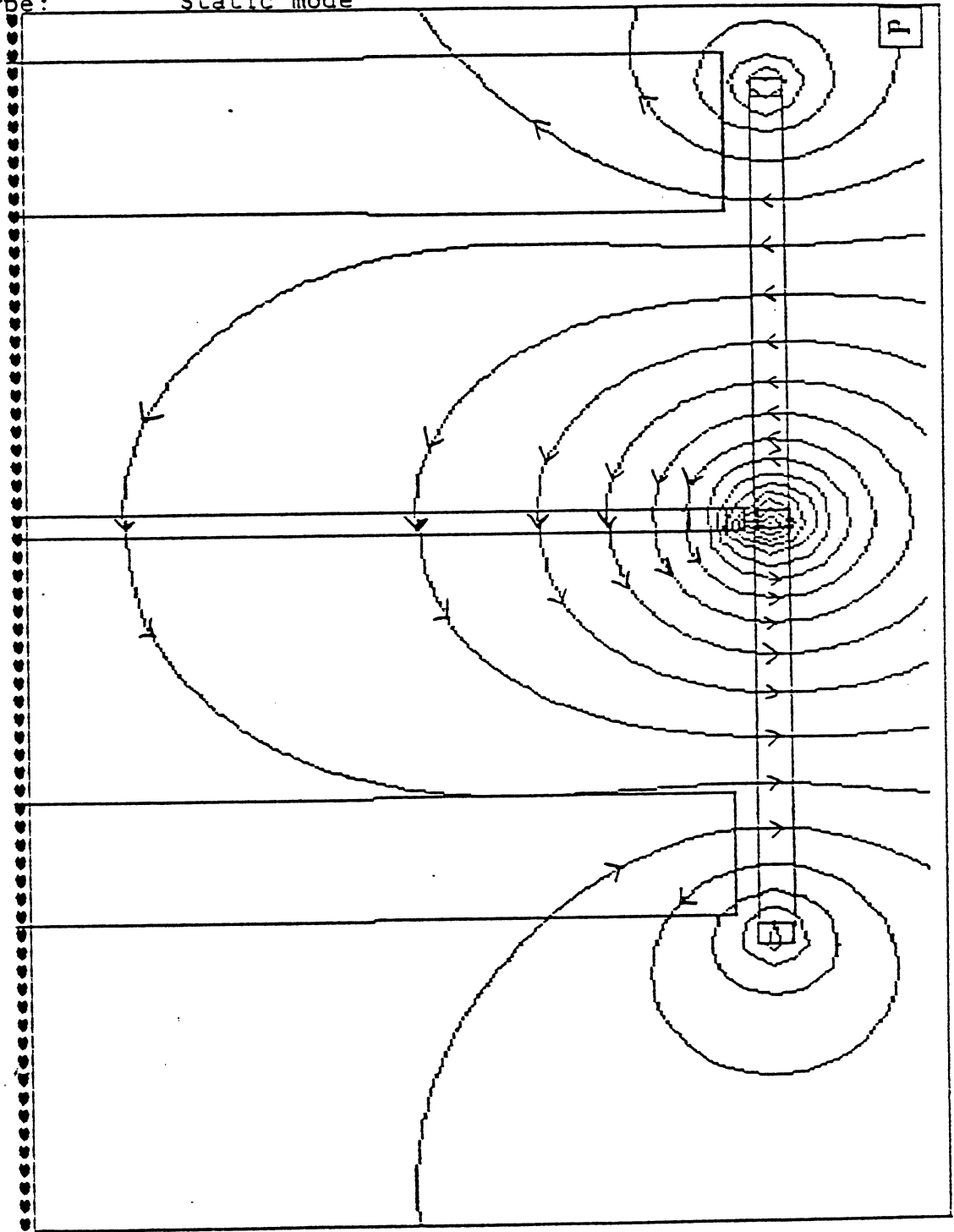


DATE = 09/23/1992 TIME = 15:40:16.77
 Current database: mrheads.dbs
 Current file: MRVERT1
 Mode of analysis: MAGNETO 2D Field analysis
 Analysis type: Static mode

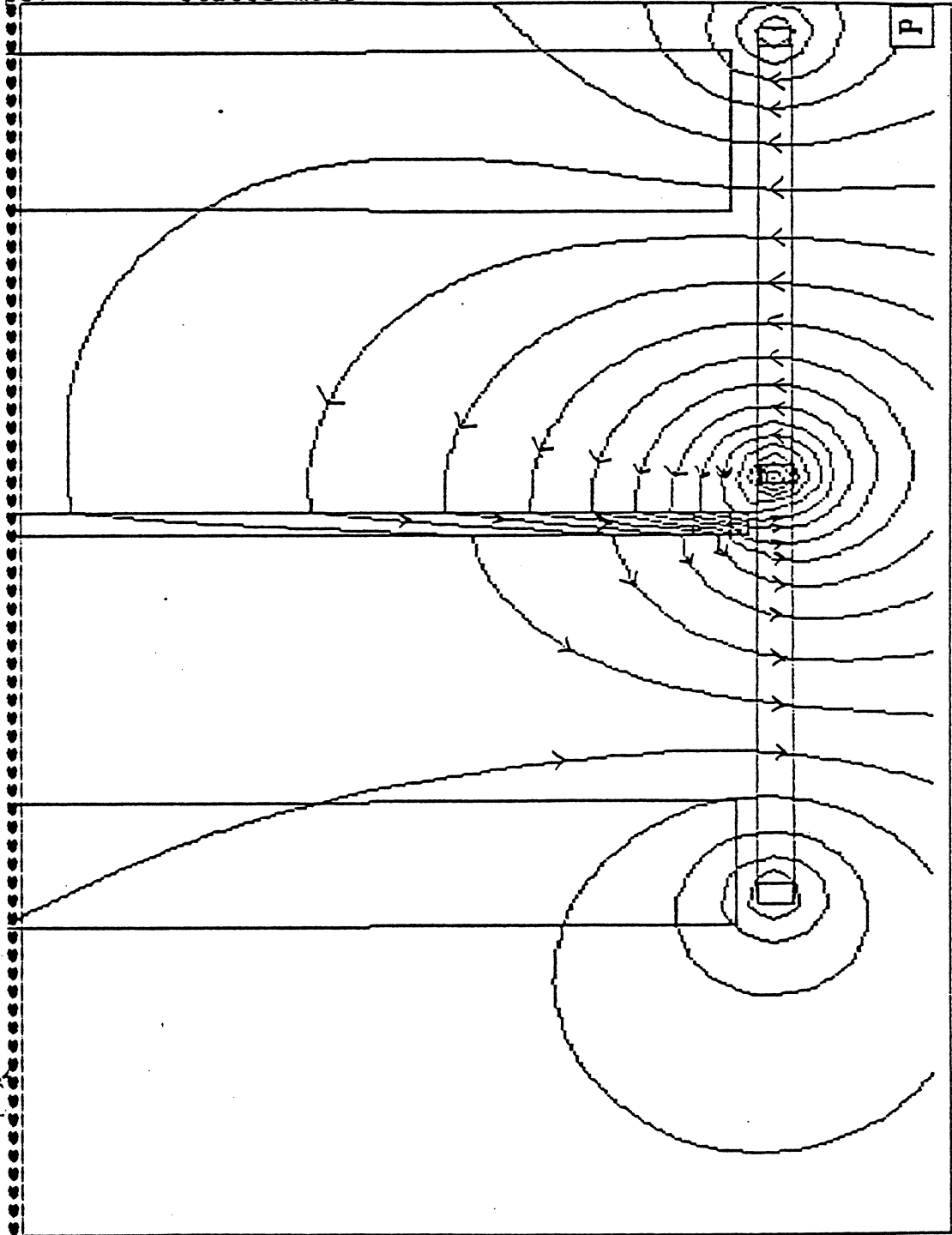


D	0	27	55	82	109	137xE1
X	136	136	136	136	136	136xE2
Y	84	87	89	92	95	98xE2

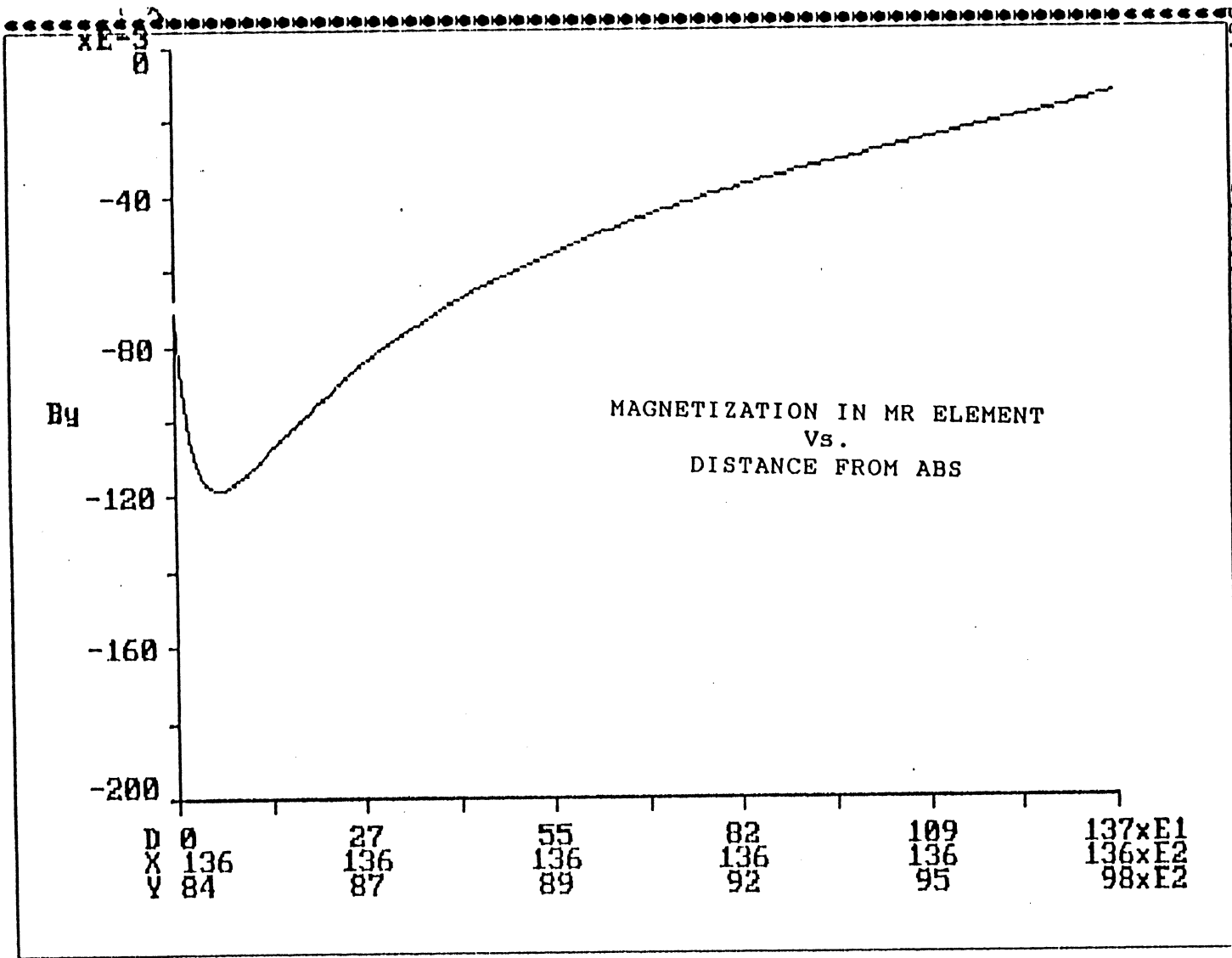
DATE = 09/29/1992 TIME= 13:55:56.42
Current database: mrheads.dbs
Current file: MRVERT1
Mode of analysis: MAGNETO 2D Field analysis
Analysis type: Static mode



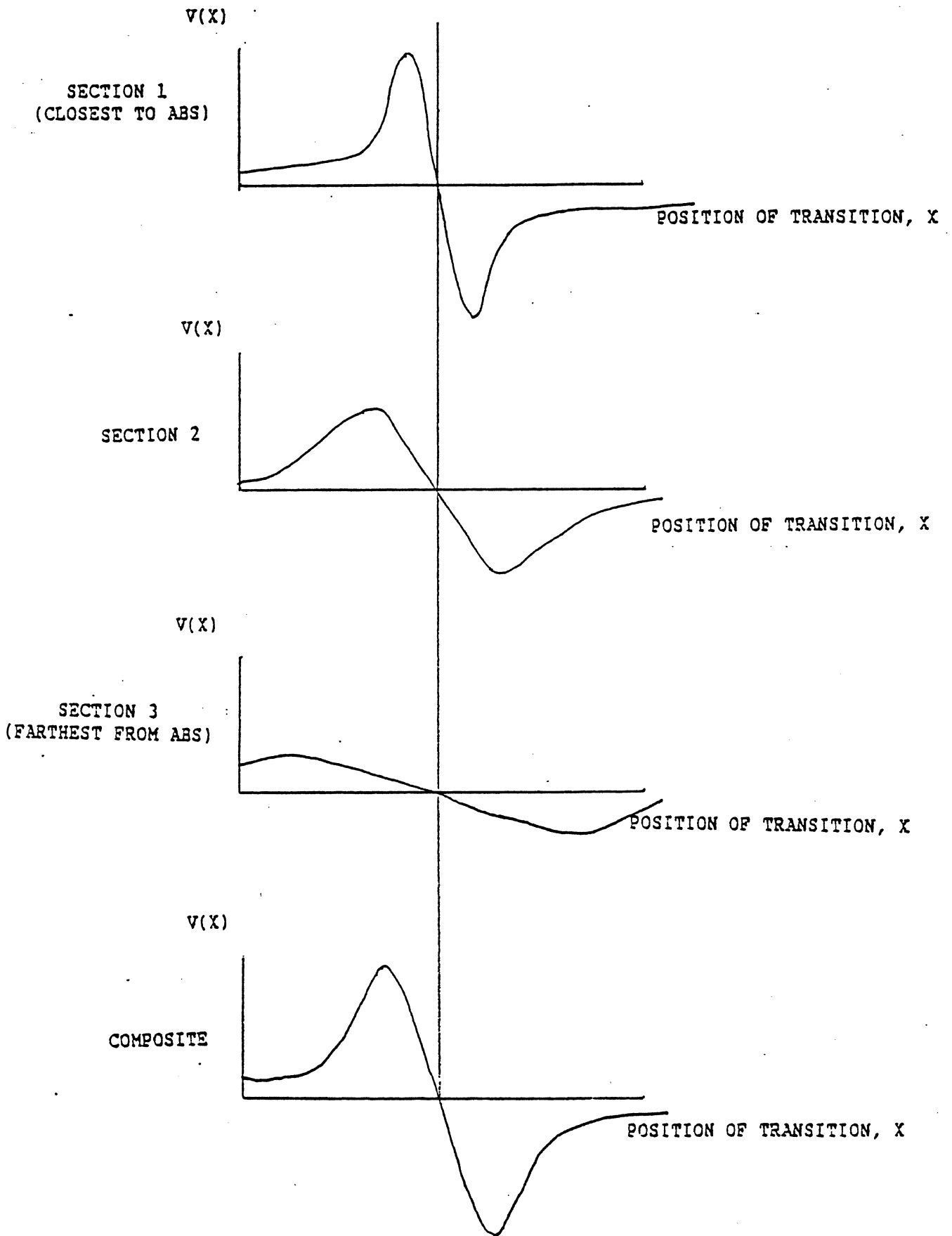
DATE = 09/29/1992 TIME= 14:00:38.35
Current database: mrheads.dbs
Current file: MRVERT1
Mode of analysis: MAGNETO 2D Field analysis
Analysis type: Static mode



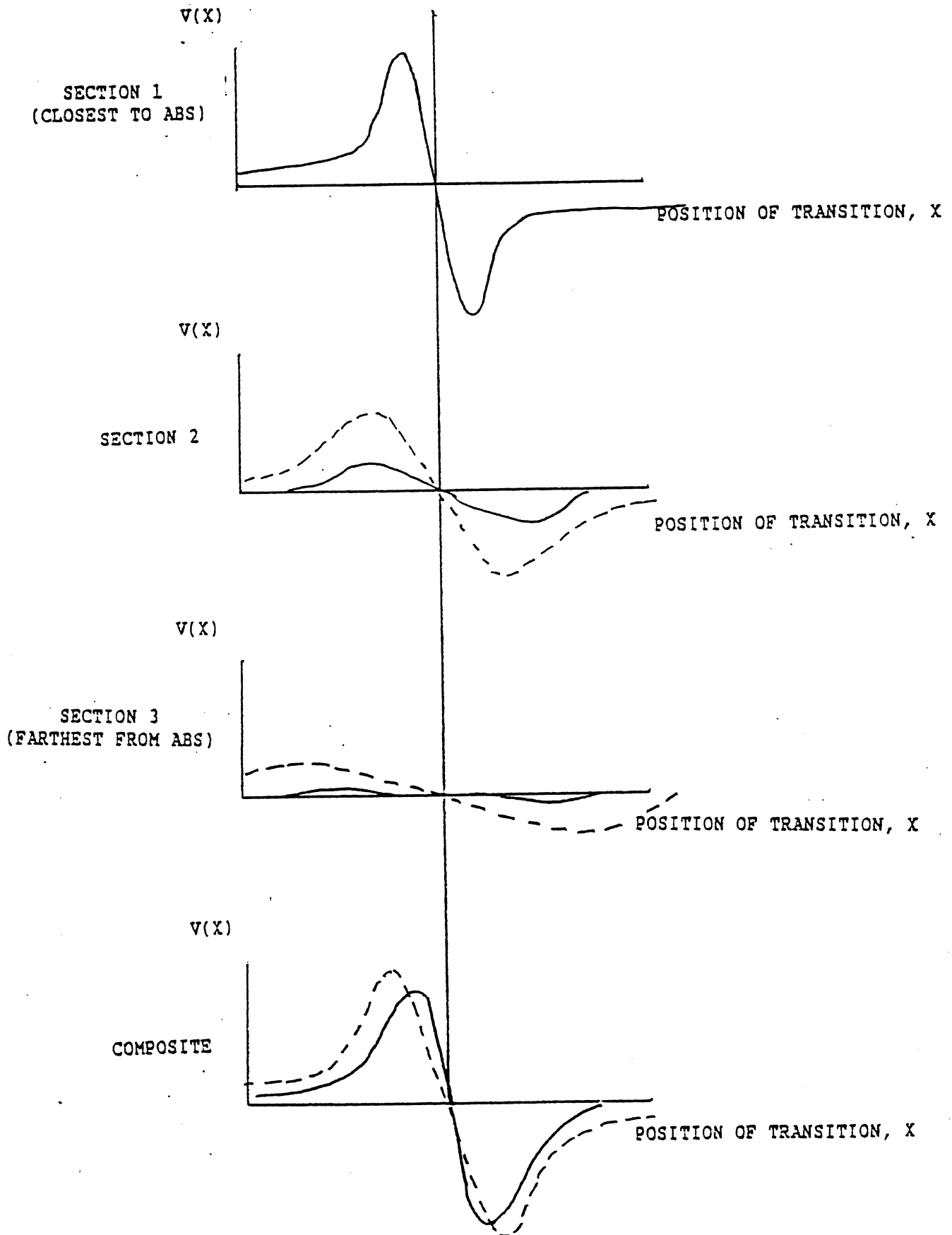
DATE = 09/29/1992
 Current database: MRheads.dbs
 Current file: MRVERT1
 Mode of analysis: MAGNETO 2D field analysis
 Analysis type: Static mode
 TIME = 14:05:14.84



RESPONSE OF MR SENSOR TO PERPENDICULAR MEDIA

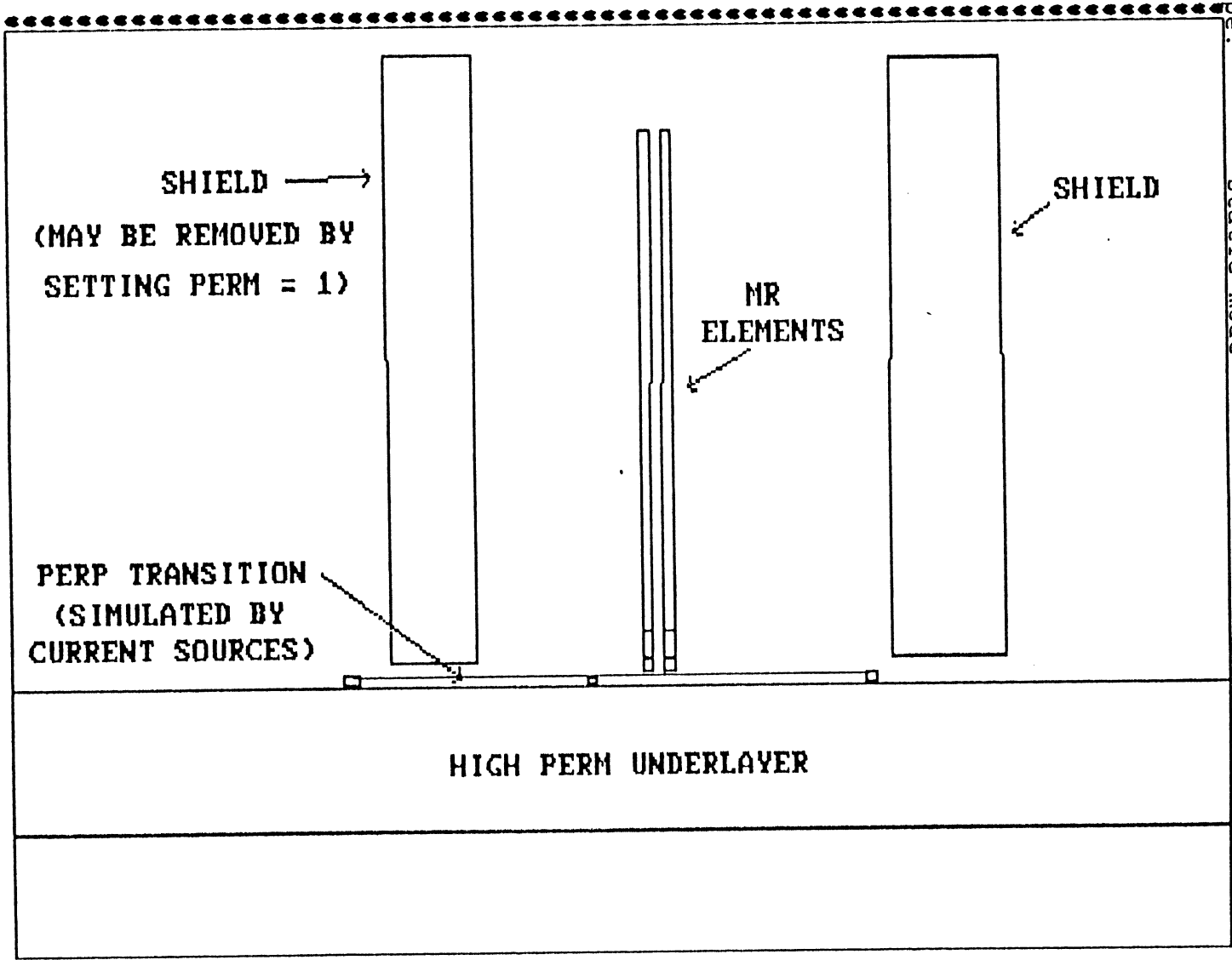


RESPONSE OF OVERBIASED (EXCEPT NEAR ABS) MR SENSOR
TO PERPENDICULAR MEDIA

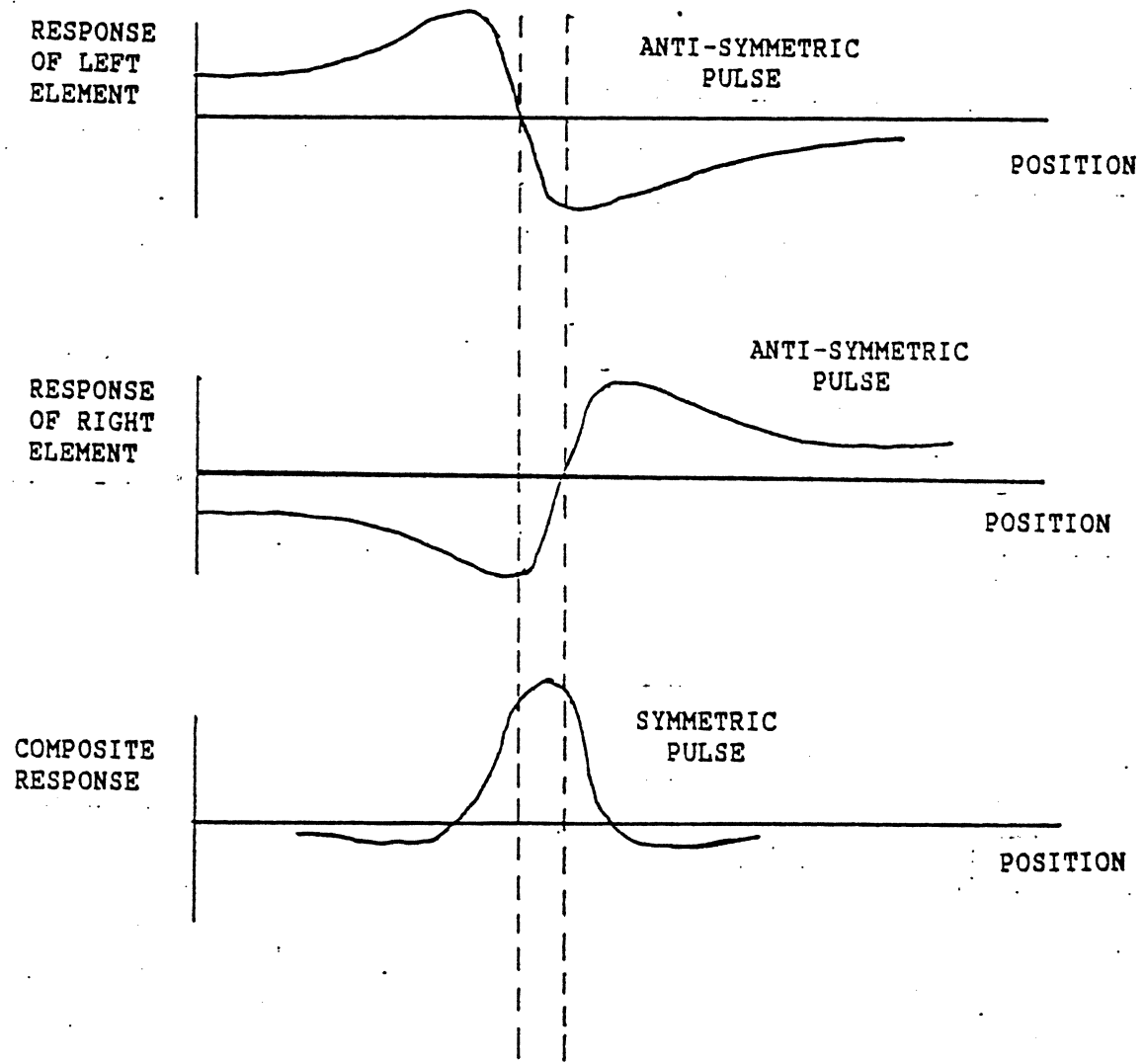


DUAL MR ELEMENTS
ON
PERPENDICULAR MEDIA

DATE = 10/03/1992 TIME = 11:10:07.98
Current database: MRHEADS.DBS
Current file: MRHEAD7A
Mode of analysis: MAGNETO_2D Field analysis
Analysis type: Static mode

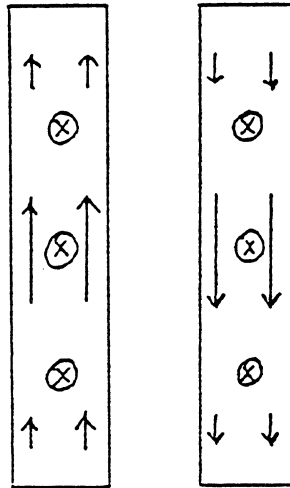


COMPOSITE RESPONSE OF DUAL ELEMENT MR SENSOR

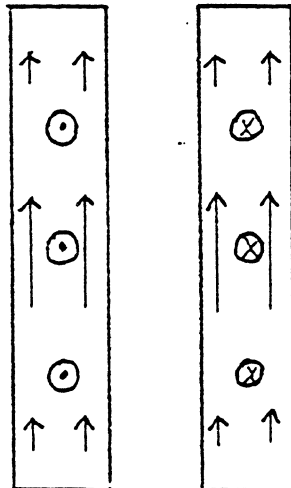


MUTUALLY BIASED ELEMENTS

RESISTANCE-SENSOR CURRENT IN EACH ELEMENT ALSO
USED TO BIAS THE ALTERNATE ELEMENT



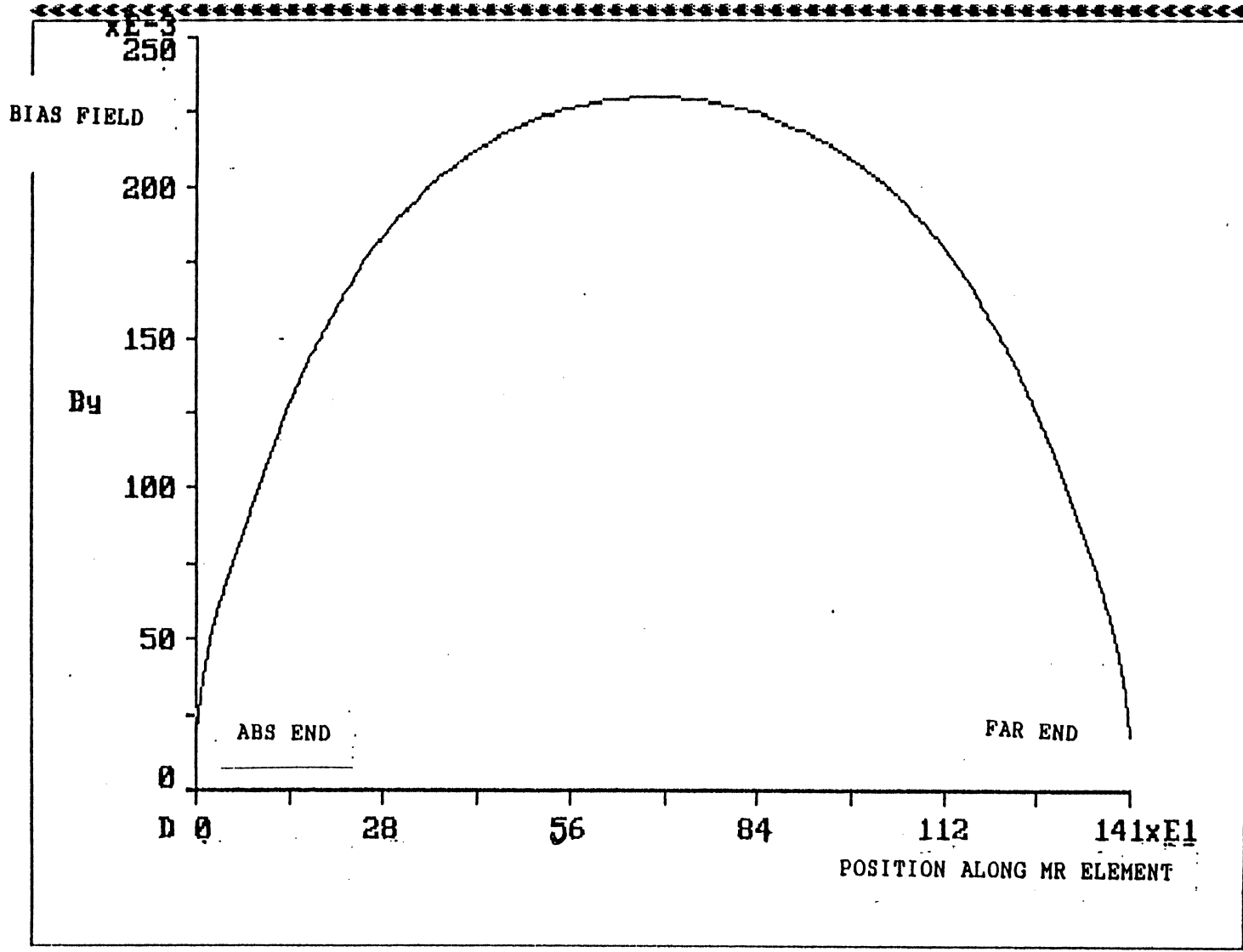
CURRENTS IN SAME DIRECTION
SIGNAL VOLTAGES HAVE OPPOSITE POLARITY



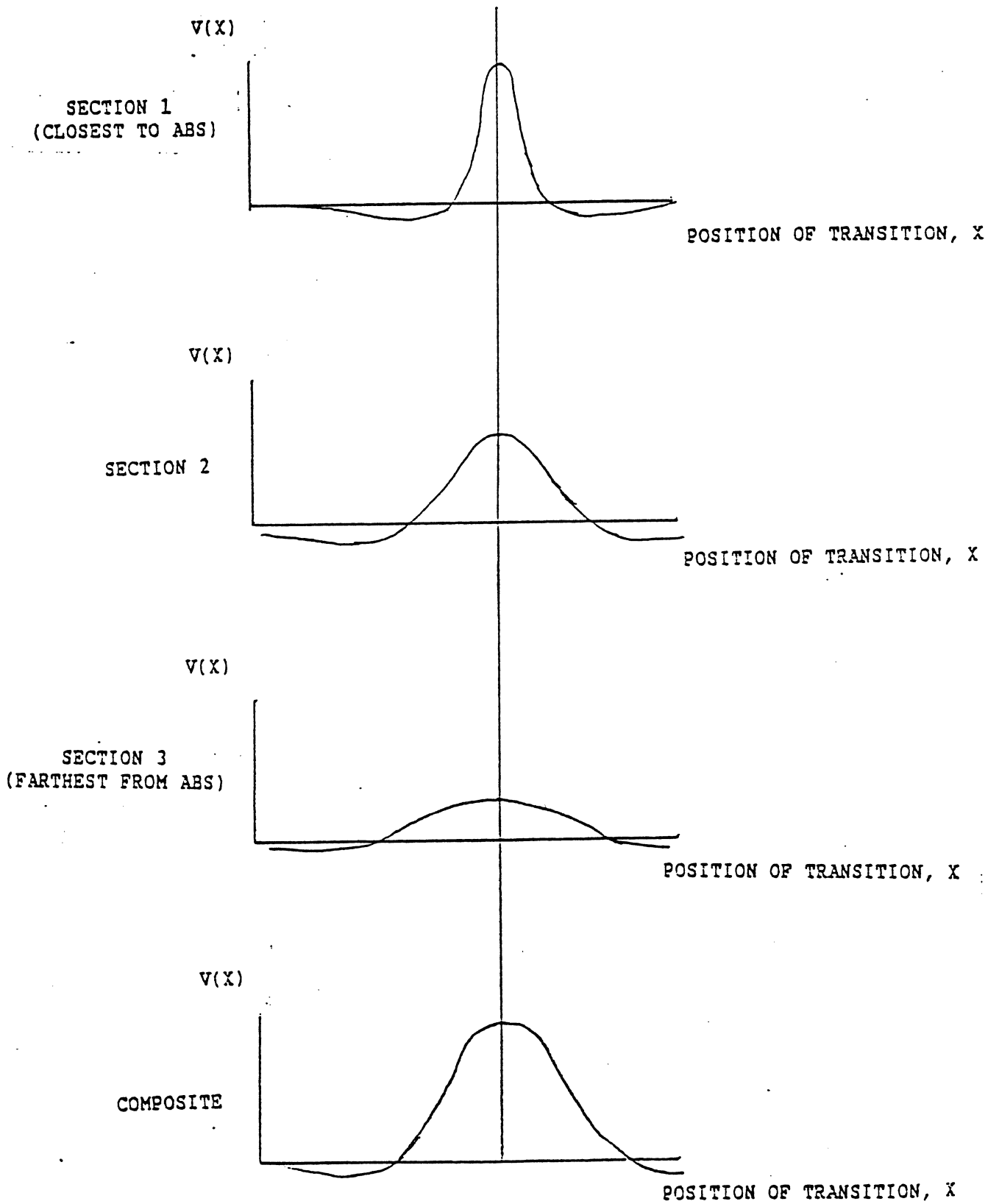
CURRENTS IN OPPOSITE DIRECTION
SIGNAL VOLTAGES HAVE THE SAME POLARITY

BIAS FIELD VS POSITION ALONG LENGTH
OF MUTUALLY SELF-BIASED DUAL ELEMENT
MR SENSOR

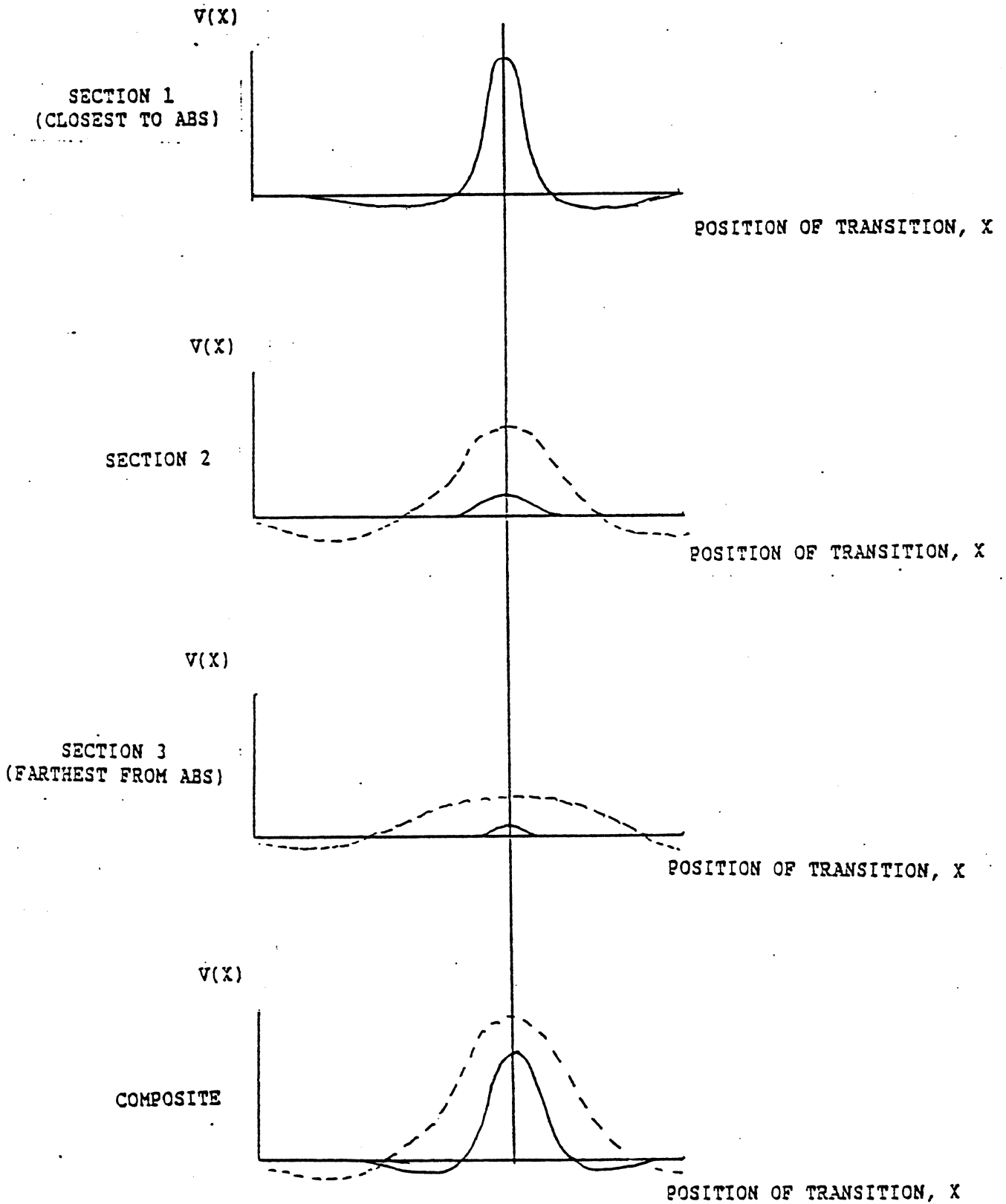
DATE = 10/04/1992
Current database: MRHEADS.DBS
Mode of analysis: MRHEADS
Analysis type: MAGNETO 2D Field analysis
TIME = 13:47:42.47
Static mode



RESPONSE OF DUAL ELEMENT MR SENSOR TO PERPENDICULAR MEDIA



RESPONSE OF OVERBIASED (EXCEPT NEAR ABS) DUAL ELEMENT
MR SENSOR TO PERPENDICULAR MEDIA



ADVANTAGES OF DUAL ELEMENT MR HEAD FOR PERPENDICULAR
RECORDING MEDIA

1. GENERATES SYMMETRIC, RATHER THAN ANTISYMMETRIC PULSE
2. COMMON MODE NOISE REJECTION, INCLUDING THERMAL NOISE SPIKES FROM CONTACT OF HEAD WITH MEDIA ASPERITIES.
3. VERY HIGH SPATIAL RESOLUTION POSSIBLE BY USING THE 2 ELEMENTS CLOSE TOGETHER, AND USING OVERBIAS TO LIMIT RESPONSE TO PORTIONS OF THE SENSOR VERY CLOSE TO THE MEDIA.
4. OPPORTUNITY TO USE THE VERY HIGH RESOLUTION POTENTIAL OF PERPENDICULAR RECORDING MEDIA.

SUMMARY

1. PRESENT DENSITIES OF INDUCTIVE PERPENDICULAR RECORDING HEADS (IN-CONTACT) IS ~ 300 Mb/SQ IN
 - 1.1 SMALL "SLIDER" SIZE ALLOWS USE OF MORE DISK AREA
 - 1.2 CONTACT MODE ALLOWS MORE GAINS FROM ZONE-BIT RECORDING
 - 1.3 LESS SEVERE TOLERANCE ON THROAT HEIGHT IMPROVES EASE OF MANUFACTURING

2. EVOLUTIONARY IMPROVEMENTS OF INDUCTIVE HEADS ~ 1 Gb/SQ IN
 - 2.1 INCREASE NUMBER OF TURNS AND TURNS LAYERS
 - 2.2 DECREASE PROBE THICKNESS AND USE HIGHER Ms POLE MAT'L

3. FOLLOW-ON WITH MR HEADS AND PERPENDICULAR RECORDING MEDIA $\sim 3-5$ Gb/SQ IN

"Scaling Suspension System Designs"

Celia Yeack-Scranton

~~IBM Corp.~~

Ad STAR

Institute for Information **S**torage **T**echnology

Santa Clara University, California

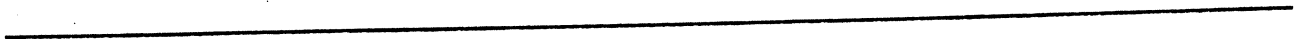
December 14 - 16, 1992

Scaling Suspension System Designs

Celia E. Yeack-Scranton

AdStaR

December 15, 1992



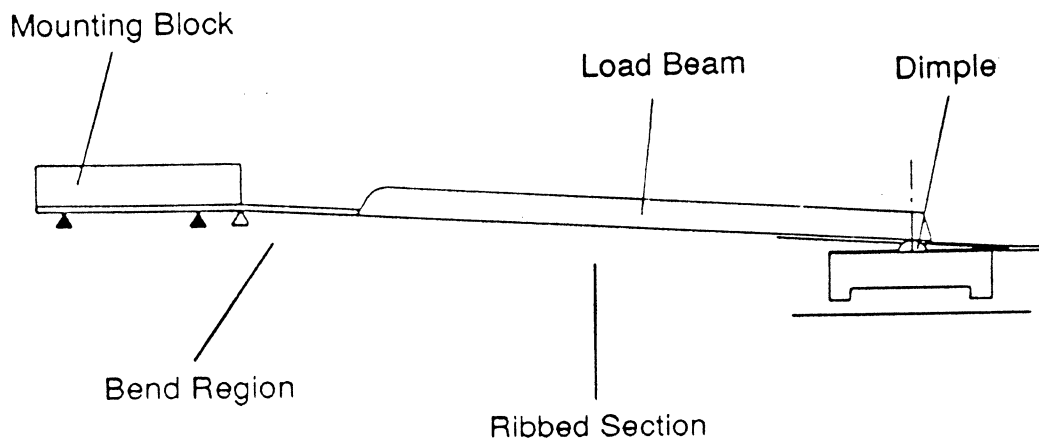
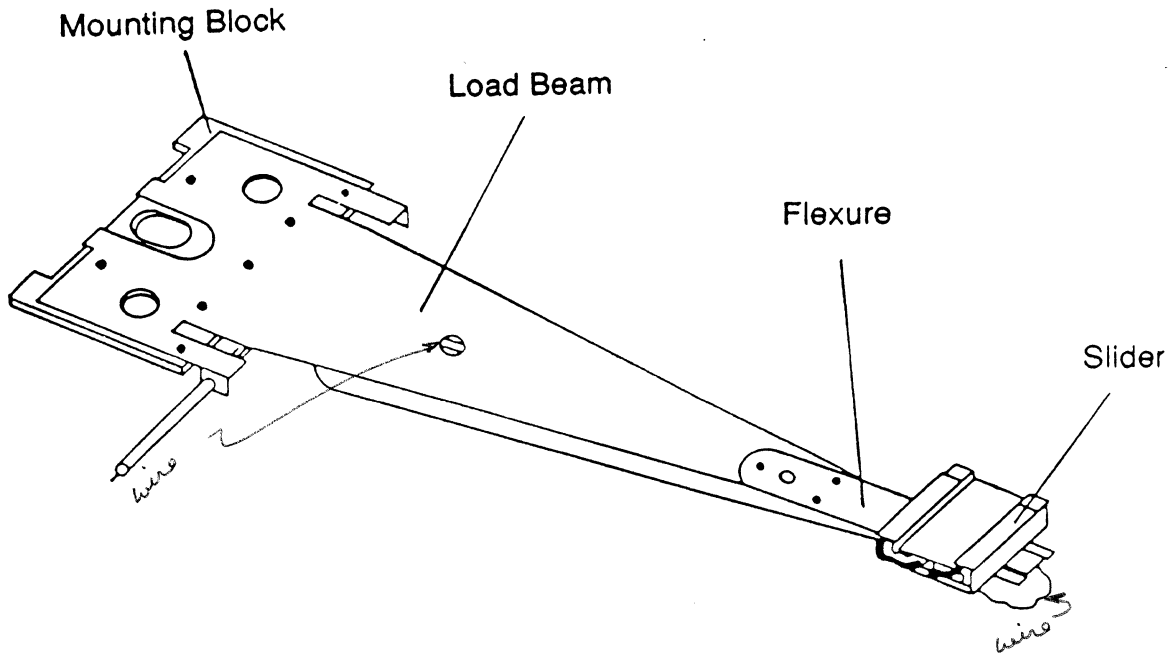
Scaling Suspension System Designs

- Suspension Basics
- Slider and Air Bearing Trends
- Suspension Scaling Exercise
- Inertia
- Design Examples
- Where are We Headed?
- Summary

A Few Basics

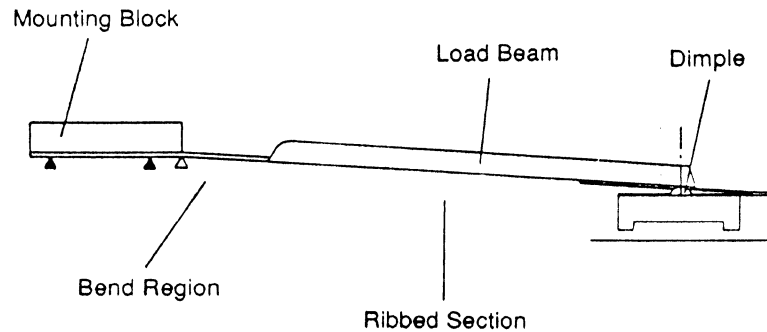
- Scaling
 - Shrinking All Dimensions by N
 - Usually a Theoretical Exercise
- Downsizing
 - Decreasing Dimensions, But Not All By Same Factor
 - Usually Determined by Practical Constraints
- Observations
 - Understanding Details of Suspension Design Requires Sophisticated Modeling Tools and Well Understood Boundary Conditions
 - Understanding Trends and Challenges Can Be Accomplished by Scaling Relatively Simple Structures

Typical Suspension

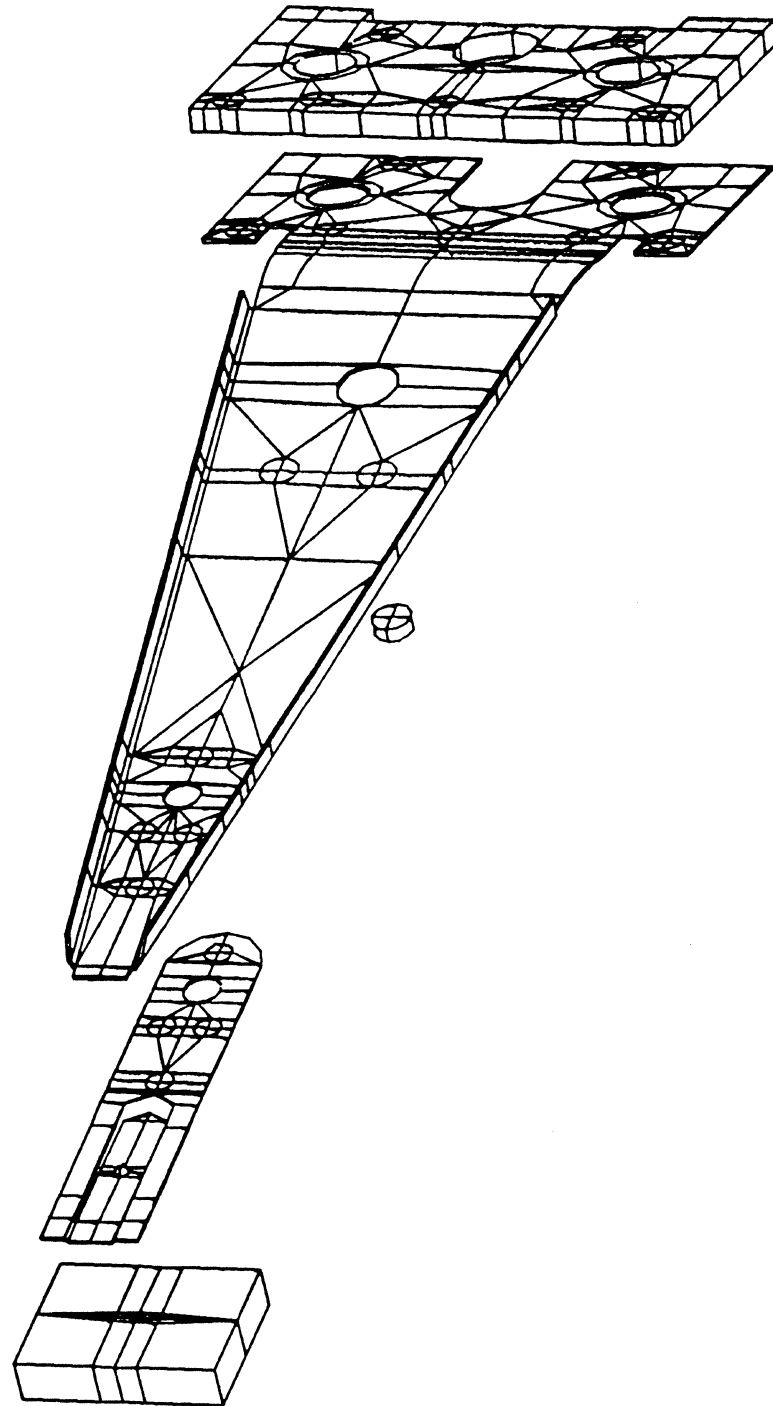


(from Wilson and Bogy, 1992)

Important Suspension Design Parameters



- Load Force
- Pitch and Roll Compliance
- Pitch and Roll Static Attitude
- Lateral Stiffness
- Lateral Strength
- Low Profile
- Load/Unload Compatibility
- Inertia
- Resonant Frequency
- Lead Routing
- Cost

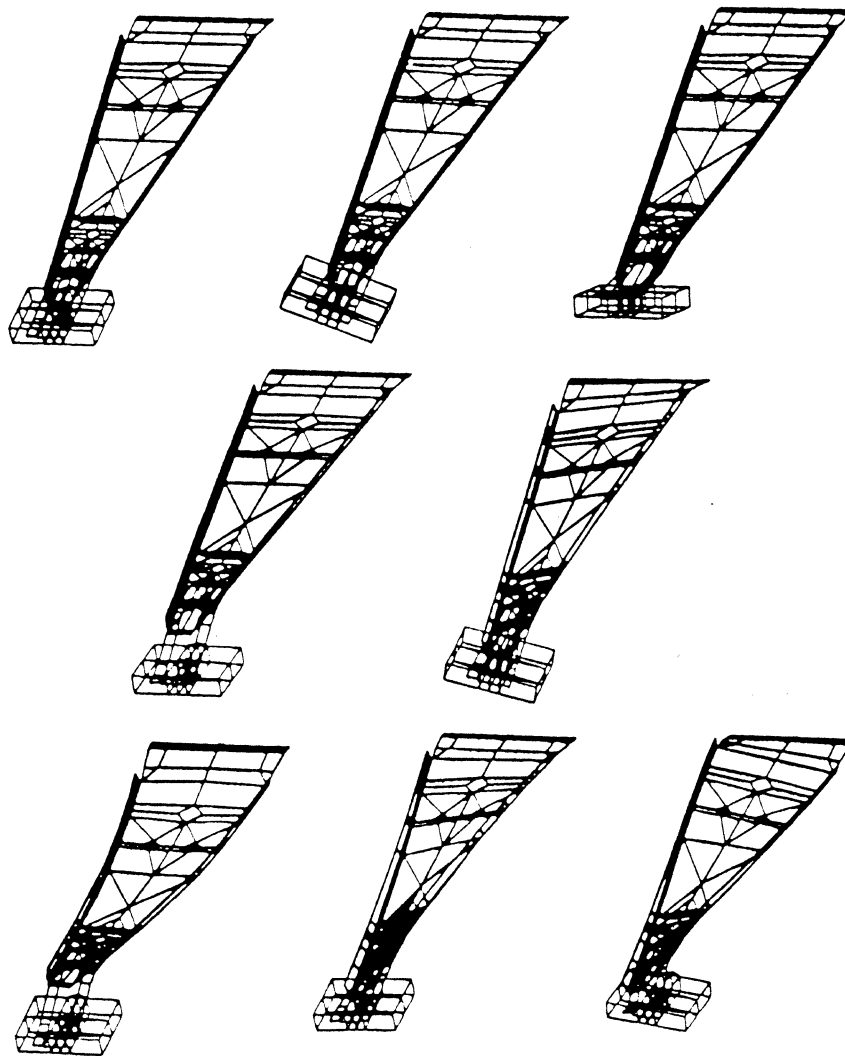


Finite element model of the suspension assembly.

Typical Suspension Resonance Modes

Numerous Modes

Off-Track Most Troublesome



Historical Suspension Trends

- IBM 3350 - IBM 3380 Design Evolution
 - Create Hinge Section for Bending
 - Reduce Flexure Width at Slider
 - Significant Overall Size Reduction
- Inline Suspension
 - First Offtrack Mode is Torsional or Yaw, NOT (Lower) Bending Resonance
- Reduce Offset Angle
 - Decreases Out of Plane Excitation

New News

- Shock Requirement for Laptop, Palmtop is
 - > 1000g's for Small Form Factor
 - Possible Significant Disk Deflection
 - Slider to Disk Separation When
 - Mass × Shock Acceleration > Load Force
 - Improvement Requires Increased Load Force or Reduced Mass
- Reduced Disk to Disk Spacing
 - Increases Shock Exposure
 - ^{load unloads} L/UL More Difficult
 - Requires Better Stacking Tolerances
 - Requires Lower Profile Suspensions

New Solutions

- *transverse pressure contour*
TPC Sliders
 - Uniform Fly Height
- *aka Seagate*
Shock Sensing/Write Inhibit
- Load/Unload
 - Integral Example
- Sleep Mode

TPC (Transverse Pressure Contour) Sliders

- Uniform Fly Height for Disk Velocity, Skew Range
- Potential Suspension Tolerance Relaxation
- Requires Air Bearing Patterning

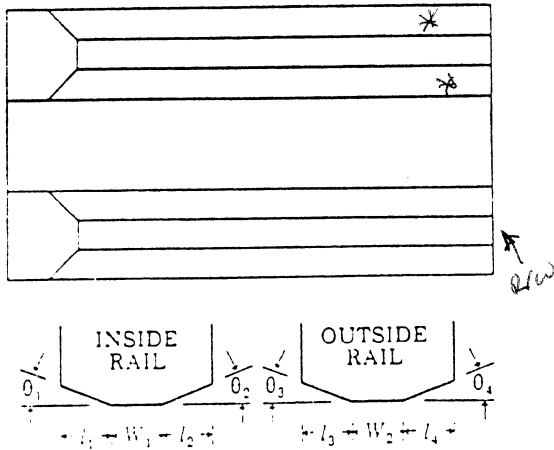


Fig. 5—The transverse pressurization contour (TPC) slider

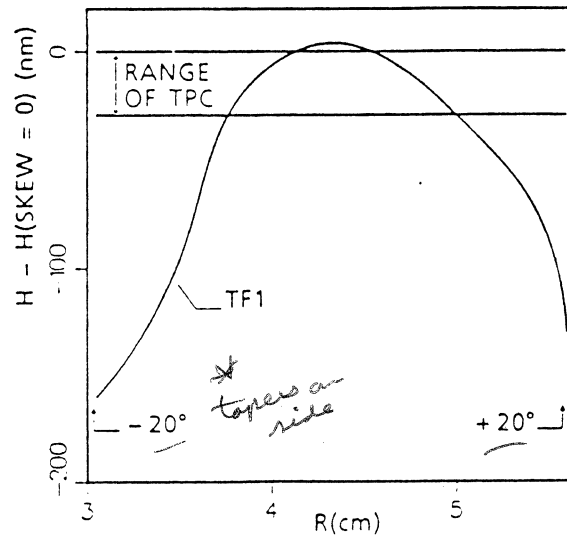
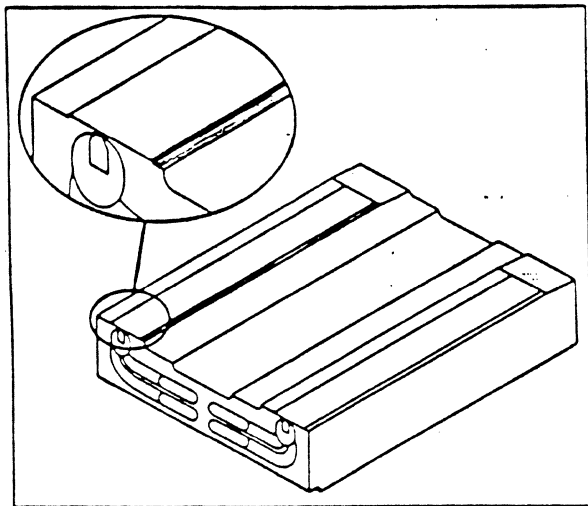


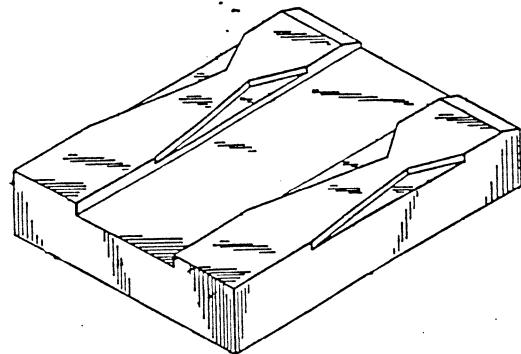
Fig. 4—Flying height radial profile for TPC and TF1 sliders

(J. W. White)



Applied Magnetics has developed a proprietary process to fashion steps for TPC air bearings in thin-film disk head sliders.

(Applied Magnetics)



(Seagate)

Slider Downsizing

- Dimensional Scaling By $N = \frac{1}{2}$ ($N = .7$) is Recent Industry Trend
- Performance Changes Do Not Simply Scale But Trends Observed in Literature:
 - Enhanced Impact Stability From Sliding to Flying (Shown for 50% Sliders at Normalized Fly Height by Kumaran, Lue, and Talke) Due To:
 - Smaller Slider Length, Width (Reduced Impact Moments)
 - Reduced Height (Reduced Moments from Friction)
 - Increase in Pitch Angle
 - Increased Air Bearing Resonant Frequencies (Briggs and Talke, 1990)

	100% slider	70% slider	50% slider
Vertical	16 kHz	22 kHz	47 kHz
Pitch	14 kHz	18.5 kHz	30 kHz
Roll	28 kHz	42 kHz	? 58 kHz ?

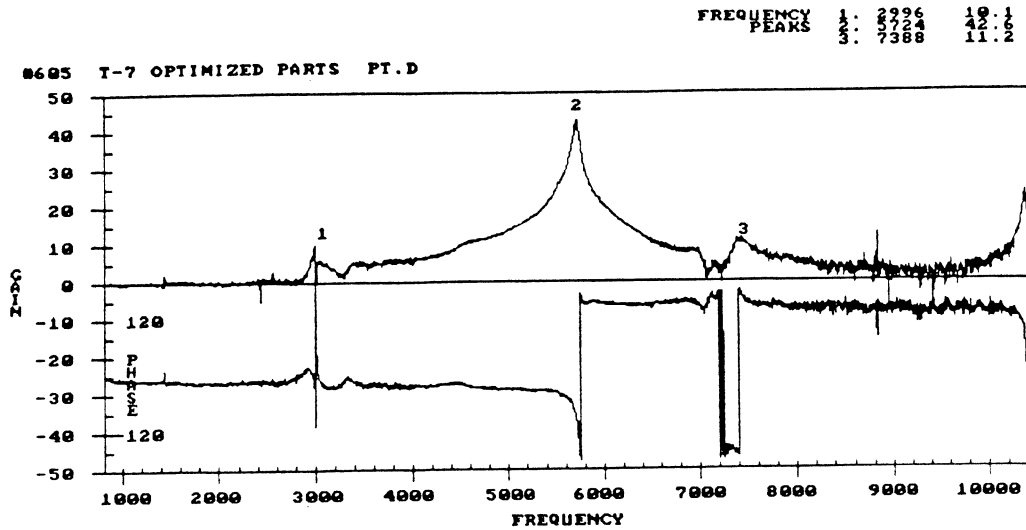
Consequences of Slider Downsizing

(Suspension - Related)

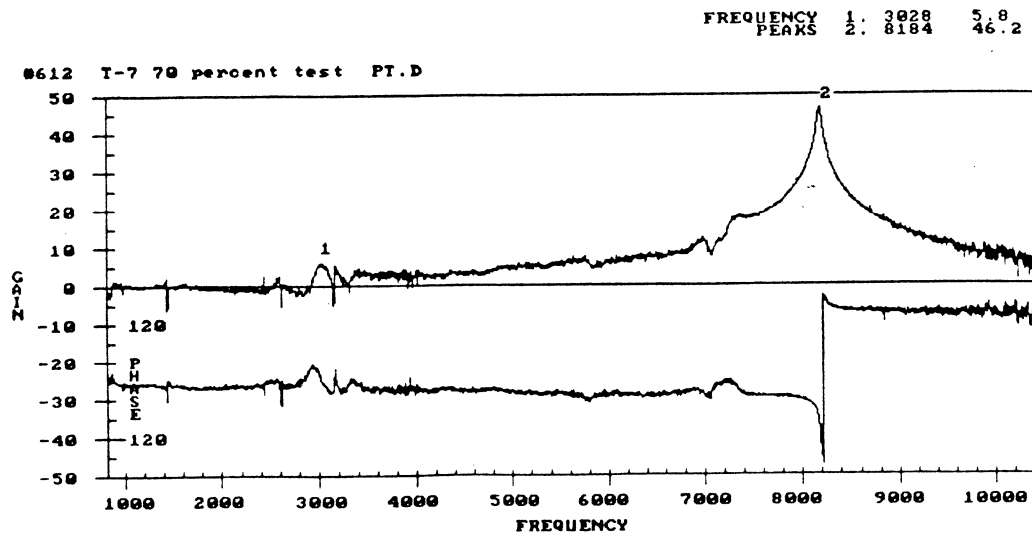
- Potential Improvements
 - Reduced Inertia Component from Slider
 - Increased Shock Resilience, If Mass Decreases More Rapidly Than Load
 - Allows Some Flexure Thickness Reduction
- Challenges in Manufacturing Tolerance Control
 - Suspension Attach
 - Lead Attach Effects

Example - Slider Size Effect on Suspension Resonances

Full Size Slider

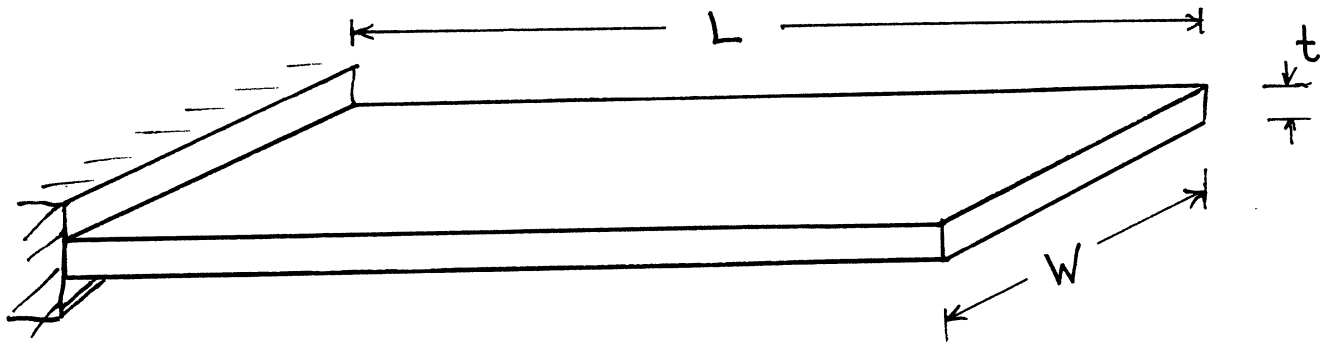


70% Slider



(From Hutchinson Technology Inc. Product Literature)

Suspension Scaling



Key Scaling Equations

$$f \propto \frac{t}{L^2} \sqrt{\frac{E}{\rho}} \quad (\text{resonant frequency})$$

$$K_t = \frac{EtW^3}{4L^3} \quad (\text{transverse stiffness})$$

$$K_v = \frac{EWt^3}{4L^3} \quad (\text{vertical stiffness})$$

$$F = K_v \delta \quad (\text{loading force, deflection})$$

$$K_T \propto \frac{t^3 W G}{L} \quad (\text{torsional stiffness})$$

If all dimensions scale by $N = 1/2$

$$f' \rightarrow 2f$$

$$K_t' \rightarrow 1/2 K_t$$

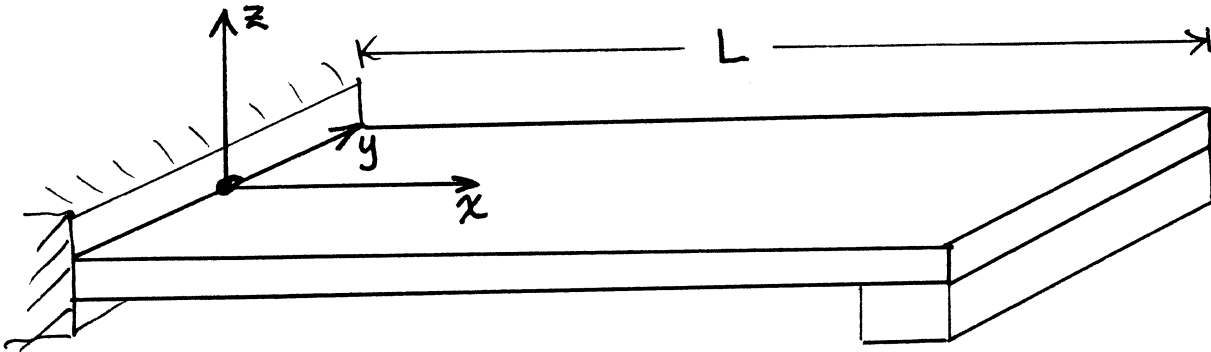
$$K_v' \rightarrow 1/2 K_v$$

$$F' \rightarrow 1/4 F \quad \text{if} \quad \delta' \rightarrow 1/2 \delta$$

$$K_T' \rightarrow 1/8 K_T$$

(E is Young's Modulus, G is Shear Modulus, ρ is Density)

Scaling - Moments of Inertia



$$I_{ij} = \rho \int_V (\delta_{ij} \sum_k x_k^2 - x_i x_j) dV$$

Thus for Rotation Around Z Axis,

$$I_{33} = \rho t \iint dx dy (x^2 + y^2) + M_{\text{slider}} L^2$$

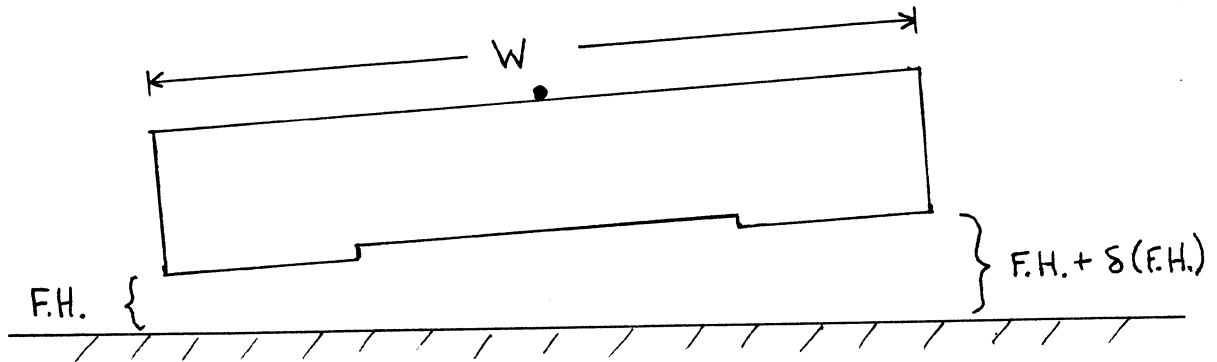
For a Simple Rectangular Plate, $t \times W \times L$, With Slider of Mass M ,

$$I_{33} \approx \frac{M_{\text{plate}}}{3} L^2 + M_{\text{slider}} L^2$$

If All Dimensions Scale by $N = 1/2$,

$$I_{33}' = \frac{1}{32} I_{33}$$

Head/Suspension Scaling - Roll



- Air Bearing Forces on Each Rail Provide a Torque Against Suspension Torsional Stiffness to Correct Roll Static Attitude, Keeping $\delta(\text{F.H.})$ Within Spec.

- Air Bearing Torque is $\cong \underbrace{\frac{\partial(\text{Load})}{\partial(\text{Fly Height})}}_{\text{stiffness, } K_A} \bullet \delta(\text{F.H.}) \bullet W$

- If θ_R is Max Allowable Suspension Roll Static Attitude,

$$K_T < \frac{K_A \delta(\text{F.H.}) W}{\theta_R}$$

- If Dimensions and F.H., $\delta(\text{F.H.})$ Scale by 1/2,

$$K_T' < 2 \frac{K_A \delta(\text{F.H.}) W}{\theta_R}$$

- (Assumes $K_A \propto 1/(\text{F.H.})^3$)

Typical Frustrations to Scaling

- Finite Practical Thickness For Stainless Steel
 - Warp
 - Buckling
 - Fragility $\sigma \approx \frac{GL}{wt^2}$
- Stiction Increases With Smoother Surfaces
 - Reduced Rail Size Only Partially Helps
- Customer Shock Requirements Increasing Very Rapidly As Portable Applications Emerge
- Some Things Simply Don't Scale Well
 - Load/Unload Devices
 - Wire Size
 - Bearings
 - Electronics
 - People Who Assemble Files
- Disk Diameter Decreasing Only By $1/\sqrt{2}$ Per Generation
- Tolerances Must Improve With Dimensional Reductions

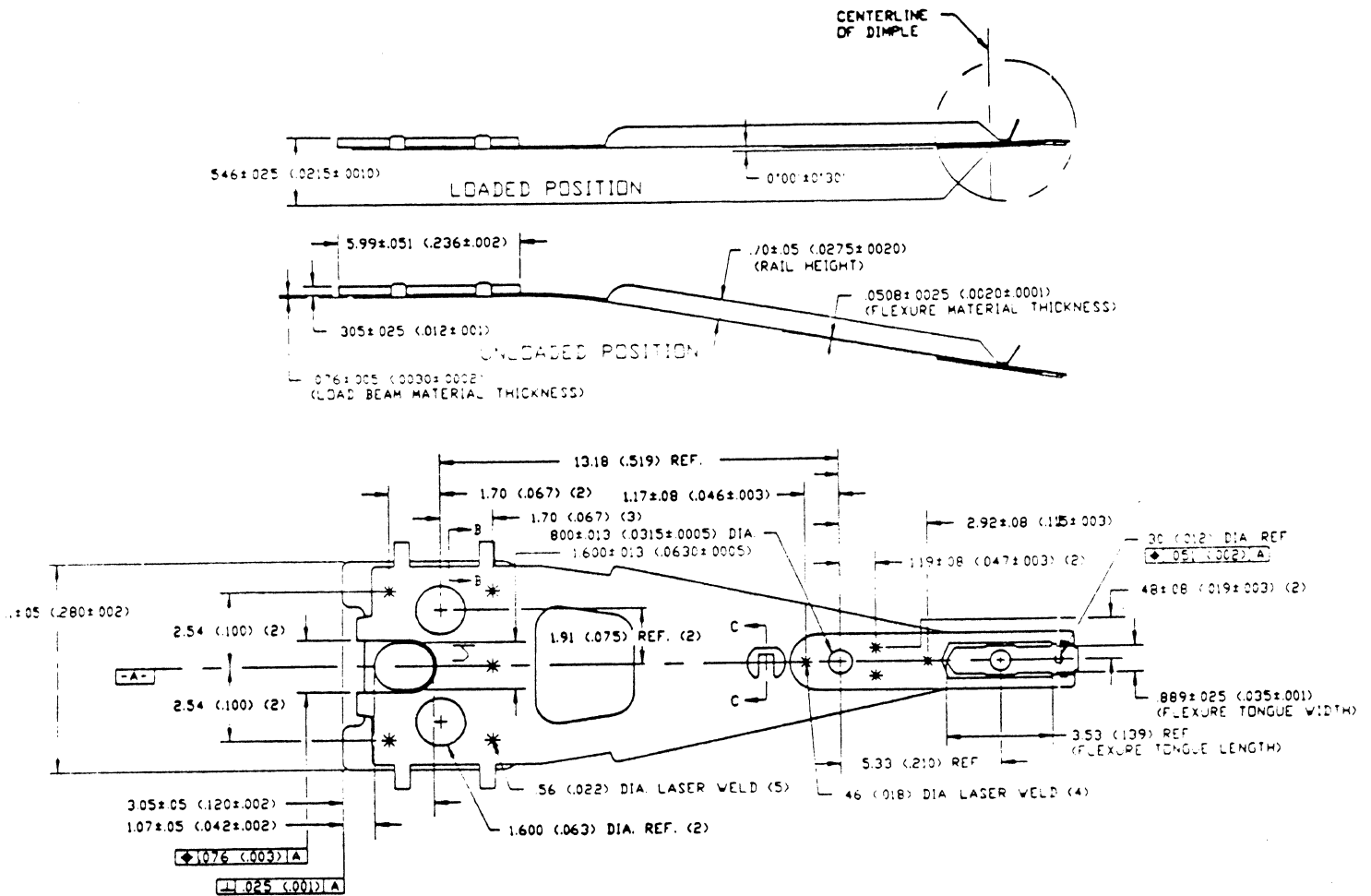
Example - Hutchinson Type 7 Suspension

≈24 mm Overall Length

No Offset Angle (Loaded)

3 gmf - 14 gmf Load

Modified Hinge Region



(From Hutchinson Technology Inc. Product Literature)

Example - Hutchinson Type 14 Suspension

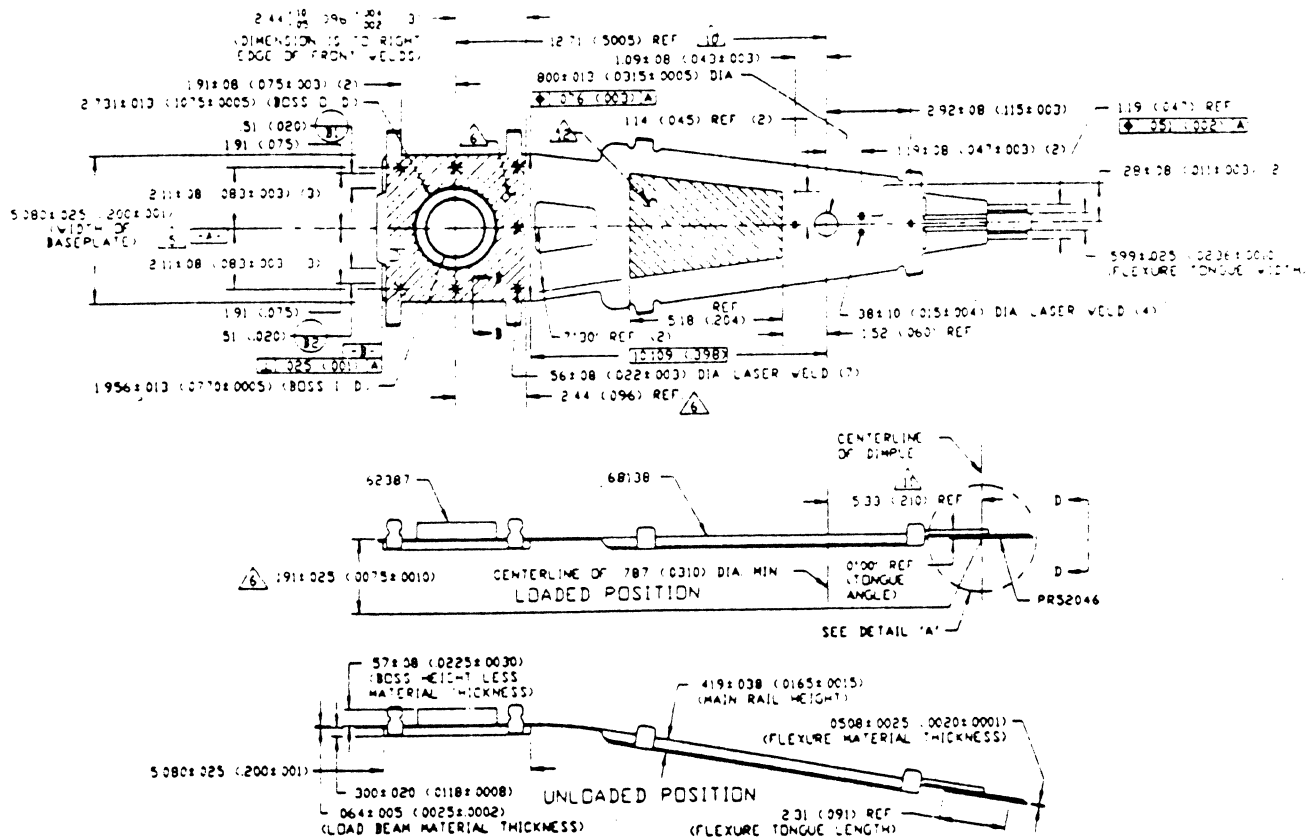
≈24 mm Overall Length

No Offset Angle (Loaded)

3.5 gmf - 7 gmf Load

Reversed Rails for Low Profile

L/UL Optimizations (Debris and Shaping)



(From Hutchinson Technology Inc. Product Literature)

Example - Hutchinson Flexure Stiffnesses

Stiffnesses in N-mm/deg (lbf-in/deg)

Types 2, 7 (Thicknesses = .051 mm, .038 mm)

	Pitch	Roll
FEA	.0062 (5.5×10^{-5})	.0108 (9.6×10^{-5})
Experiment	.0073 (6.5×10^{-5})	.0087 (7.7×10^{-5})

Reduced Thickness

	Pitch	Roll
FEA	.0026 (2.3×10^{-5})	.0043 (3.8×10^{-5})
Experiment	.0028 (2.5×10^{-5})	.0036 (3.2×10^{-5})

Type 14 (Thickness = .051 mm)

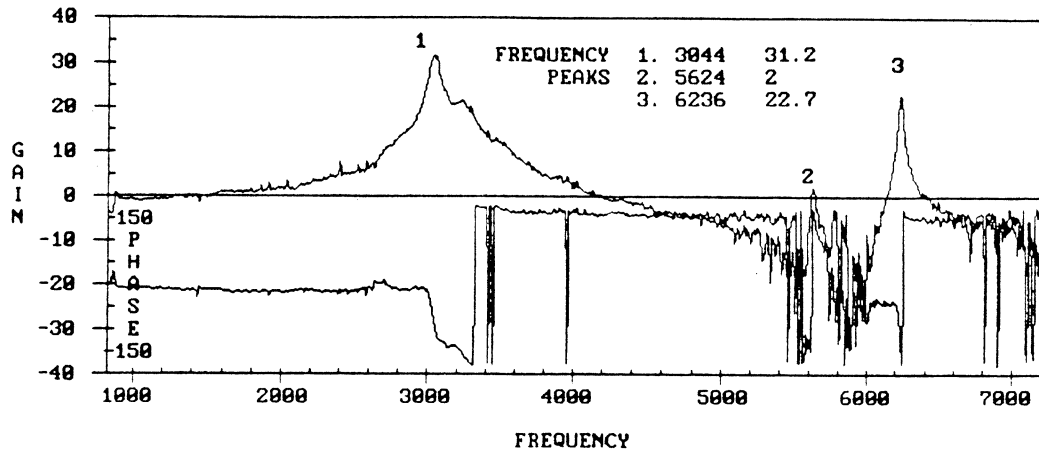
	Pitch	Roll
FEA	.005013 (4.4×10^{-5})	.007364 (6.5×10^{-5})
Exper	.005498 (4.9×10^{-5})	.005764 (5.1×10^{-5})

NOTE that Stiffnesses for Flexures DO Scale as t^3

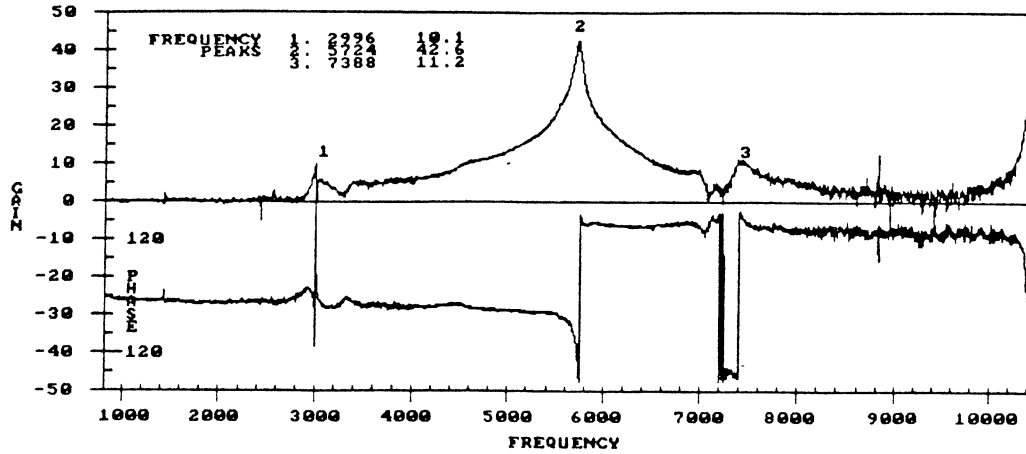
(From Hutchinson Technology Inc. Product Literature)

Example - Hutchinson Suspension Resonances

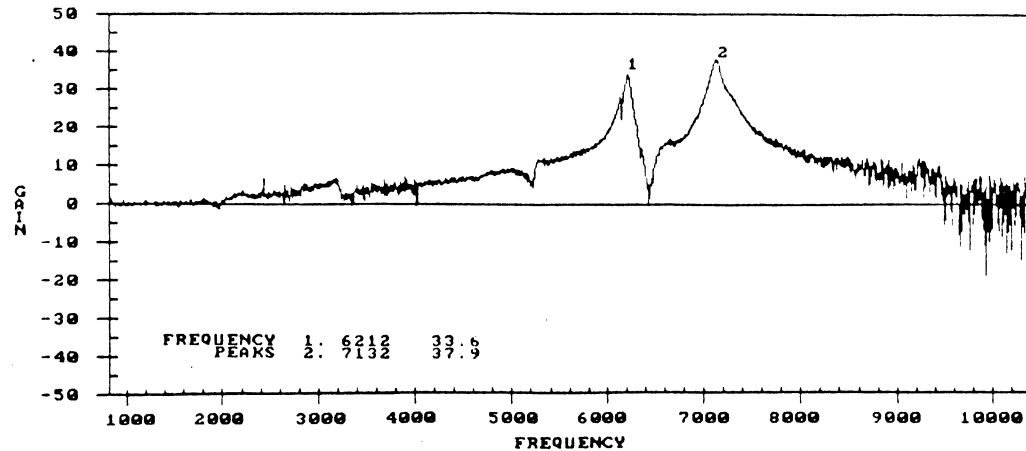
Type 2



Type 7



Type 14



(From Hutchinson Technology Inc. Product Literature)

Summary

- If Suspensions Simply Scaled (Down in Size) Most Suspension Performance Parameters Would Improve
- Practical Limits Prevent Simple Scaling, but Downsizing Trends and Design Improvements Give Performance Gains
- New Requirements Present New Challenges
 - Shock
 - Load/Unload
 - Tight Disk Spacing
 - Ultra Low Fly Heights

**"Head Positioning and Tracking
for High Track Densities"**

John S. Heath

IBM Corp.

Institute for Information **S**torage **T**echnology

Santa Clara University, California

December 14 - 16, 1992

Introduction

The purpose of tracking control in a disk drive is not simply to follow the data, it is to follow it well enough that the best possible density can be obtained in the product. To understand the link between tracking accuracy and the track density we have to consider the recording and reading process from the point of view of the noise introduced by mis-positioning, as well as the various mechanical causes of mis-positioning themselves. And to understand the causes we have also to look at one of the cures, the servo. So these notes cover the recording process, the servo and the mechanics of the disk file. Only the interface is ignored. An understanding of servo theory is not required.

Noise sources due to mis-positioning

Density is limited by Noise

The development of disk drives has been primarily concerned with minimisation. First of the head magnetics, then of the media thickness, and recently of the drive itself. The process of minimisation has only been possible as far as has been permitted by reductions in noise. Smaller parts may mean less noise in some cases but not all. As the head is narrowed, noise is certainly increased if nothing else is changed. Noise is the limitation of track density so this is where we start.

Old Information

Any write operation leaves old information on either side of the newly written track. This is because of three effects.

Side writing

Mis-positioning at time of writing

Mis-positioning at time of reading.

The capability to read in the presence of Old information is referred to as OI capability. OI tests produce curves of error rate vs distance the head is off-track. The test is done on a precision test stand and the results are called Bathtub curves named for the shape. (Figure 1) OI capability is rated as the off-track distance where the error rate falls to $8E-5$ per byte.

Adjacent track interference

Data written on an adjacent track after the current track was written may improve signal to noise by overwriting other noise, but it will more likely degrade the signal by over-writing the data being read (Squeeze)

Squeeze is defined as the amount of track overlap. (figure 2).

The capability to survive squeeze is rated by the 747 test method .

747 Curve

Named for its shape which resembles a 747 cockpit (figure 3 taken from reference 1.) The curve results from a test to find the off-track capability when reading over previously written data, and with an adjacent track written at a variable distance. Figure 2 shows the pattern of data for this test, OI is the Old Information distance and SD is the squeeze. The test determines how squeeze changes the OI capability. There are 5 significant points on the curve figure 3.

1. Adjacent track far removed. No effect on OI.
2. Adjacent track starts to reduce coherent noise. OI starts improving.
3. Adjacent track erase band butts read track erase band. OI at peak.
4. Erase bands overlap. OI same as with Old information noise.
5. Further squeeze reduces OI to point of on-track failure. $OI = 0$.

Optimum noise rejection is close to the point at which the 747 curve peaks, but depends on having a balance between Old Information interference and squeeze.

Position error defined

Write to read TMR

This is the mis-positioning of the head over the track as a probability density function (PDF or histogram). This is known as the Write to Read Track Mis-Registration or Write to Read TMR. It is due to errors in the positioning system of the drive. It is the convolution of the mispositioning of both the head and the track so it is root of 2 wider than the mispositioning of the head alone.

Write to write TMR

This is the mis-positioning of the adjacent track from the nominal position of the read track. Also a PDF, this is known as the Write to write TMR. It includes errors in the servo-written track spacing as well as positioning errors due to the drive. Again this is the convolution of two PDFs.

Optimum track density

The optimum track density for a head is the density at which the error rate will be adequate for the product applications. This can be computed from the bathtub (Old Information) curve for the head and the TMR of the product again as described in reference 1.

Square bits ?

If there were perfect tracking (no TMR) then how much narrower could the tracks be made, and how much closer could they be packed. Not an easy question to answer. The *status quo* today is that all drives have plenty of TMR under adverse conditions and consequently need wide heads. So under nominal conditions the heads are on-track, the signal/noise ratios are very good, and consequently uncorrected soft error rates are good too. The customers demand good uncorrected error rates for reasons of their own (maybe habit). If tracking was always perfect then recording would be possible at much higher track densities limited only by the on-track error rate. So what error rate would be acceptable on that different planet, and what ECC power might be applied?

Maybe not a very important question to answer as TMR is not likely to go away at more than a steady pace comparable with improvements in bit density.

Servo Systems

Servo theory

Servos can be rigorously analyzed by linear control theory of various flavors. The theories give guidance and insight to servo designers, but seldom give a complete analysis of a disk drive servo as there are several non-linearities in disk drive mechanisms that defy closed form solution. Control theory which is a complex and specialized math-problematical topic can also present a barrier to understanding disk drive operation by engineers lacking a rigorous mathematical background. An intuitive treatment of the subject is given here to avoid these problems. This treatment can be the basis for an appreciation of system design options. The distinction between analog and digital servos is not of great importance to the tracking ability so it is not dealt with here.

It is important to recognize that the servo is not just the electronics and the control functions implemented within it. The servo is the whole system and all that affects it and is affected by it. This includes the actuator, aspects of the spindle, and in many cases the structure of the drive as well. This is important in understanding the response of the system to the major disturbances.

Figure 7 is a diagram of the system that is treated here.

The function of the servo

The job of the servo is to move the heads from one track to another (positioning), and to keep it on track as well as possible (tracking). The positioning function is not strongly linked to track density, since there are many algorithms that can control the seek motion even crossing tracks at very high rate. We have no need to fear that high track densities will limit access performance. The tracking function however determines the Write to read TMR and much of the Write to write TMR. It therefore determines what track density can be obtained from a given set of mechanics.

The quality of design and manufacture of the mechanics is equally important in determining the track density, and this is described in detail later.

The servo characteristic that describes the ability of a given servo system to give close tracking is Gain or band-width. In these notes Gain is defined as a ratio rather than as dB figure. Apologies to A G Bell.

Figure 8 shows the relation between gain and bandwidth of an ideal system.

Gain and frequency

The actuator is a limp "straw in the wind" that will drift around under the influence of bias forces, wind, vibration etc, The servo, fed with information about the error in position of the head to the selected track, drives the head toward the correct position over the track.

If the head is pushed off track by some influence, then over a wide band of frequencies the servo generates a force proportional to the error that tries to restore the head to the track center. Thus the servo acts as a spring, linking the head to the track. Just like any mass spring system this one has a resonant frequency and an unfortunate tendency to oscillate. The servo system includes phase and amplitude compensating function that damp this resonant behavior. With this compensator the response is similar to, but not the same as, a simple mechanical resonance. Its frequency response is shown in figure 8 in several ways. Probably the most helpful is the error rejection function. This is the reduction in amplitude by the servo of the tracking error caused by disturbing forces at any frequency. The other frequency responses are shown including that of the mechanics. The mechanics and the compensator response together give the open loop response. This has unity gain at what is called the crossover frequency. Below this frequency the servo system can be regarded as a spring resisting any disturbance attempting to cause an error. So the spring stiffness is the servo gain. The more stiffness or gain, the less the error. And the higher the stiffness, the higher the frequency that the gain extends to. Above the crossover frequency the actuator is an inertia. There is no servo gain (actually errors are slightly amplified over frequency range above the crossover frequency.) Clearly greater servo stiffness can resist disturbances more strongly and therefore reduce TMR. It also reduces TMR disturbances at higher frequencies. So we must understand what limits the gain that can be applied.

Limits to gain

Resonances

Gain is frequently limited by mechanical resonances which are often in the head suspension. The second order torsional resonance of the load beam is often the critical resonance. The effect of this on the servo is to cause instability at the offending frequency. The servo oscillates consuming power, making noise, effecting gain at other frequencies, and possibly producing significant TMR at the resonant frequency. As sliders have become lighter, suspensions shorter, and with improved understanding of suspension design, this limitation of servo gain is receding to higher frequencies. 1 kHz crossover would probably be attainable today if this were the only limitation. Figure 8 and see references 2 3 and 4.

Sample rate

In sector servos, and some embedded servos, the position error is only measured at discrete time intervals called samples. The lack of a continuous signal represents a loss in phase from the position error signal at frequencies approaching the sampling frequency (reference 2.) This makes it difficult to apply a high gain without causing the system resonance at the crossover frequency to become under-damped which in turn makes settle times after a move become too long.

It turns out to be difficult to make the crossover frequency much higher than one tenth of the sample frequency, and it has to be even lower for really good settle performance. See reference 4.

Pivot bearing stiffness

It requires a small torque to move a ball race actuator pivot. Smaller torques cause proportional but miniscule rotation of the actuator arm, but the arm returns when the torque is removed. So the bearing is acting like a spring as described in reference 5 The effect on the mechanical transfer function and the gain is shown chain dotted in figure 8. A very significant loss in gain can be caused by this effect.

Ways of boosting gain

Integrator.

Given a system as described previously, the gain at low frequencies can be increased by adding one or more integrators to the control function. An integrator accumulates the error over time and applies a proportional correcting current to the voice coil. This can strongly reduce the position error due to bias forces, but is also effective in reducing other low frequency disturbances such as external vibration. As with other gain enhancing measures, integrators lose phase and can not be applied without limit. The effect of an integrator on the error rejection function of a typical response is shown in figure 8. figure It has gain falling proportional to frequency and is asymptotic to unity at some frequency referred to as the pole. One problem with an integrator is that it requires time in order to become effective. This is a particular problem when arriving on a new track. A solution can be to set a known initial value into it after a seek. This can be effective

in reducing offsets from time zero, but can only be applied if the offsetting force is known ahead of time when arriving at a new track. A similar solution to bias force can be obtained by storing a table of values from which the offset force required at a given track can be computed. A current to correct the offset can then be added to the driver output at the time of arrival at a new track. See reference 7.

Adaptive run-out correction systems.

For the case of a disturbance that is accurately predictable in both amplitude and phase with respect to the disk rotation, it is possible to correct it more or less completely by determining the magnitude from prior revolutions and applying a current waveform to reduce it to zero.

This is called feed forward and is used in high density floppy disk drives to cancel disk run-out and also the ovality caused by floppy media anisotropy. (Reference 8). It is also used in some hard disk drives to reduce the effect of changes in disk run-out. (Run-out is not a problem when it remains constant, but only when it changes.) (Reference 7 and figure 10.) The gain enhancement of feed forward can be high (strictly it is not gain in the control theory sense) and it has no destabilising influence on the regular servo function. The achievable gain has not been described.

Types of servo architecture

Dedicated Servo

One head in the drive is dedicated to providing position error information for the servo. There are drives where an optical encoder system provides the same function. All other heads dependant on the relative accuracy of the actuator to maintain their positioning. (figure 12.) In a drive with many heads, a dedicated servo head has the advantage of wasting less disk area in servo position information than a sector servo, but this advantage goes away with smaller numbers of disks. The dedicated servo head is found mainly in older large drives where it was favoured for its simplicity and efficient use of disk space. High end drives use a dedicated head as it enforces the situation where all the heads in a cylinder of tracks are positioned correctly over data all of the time. This is not so with embedded servos as a correction may have to be made each time the head is switched. The cylinder concept is used strongly by high end operating systems to gain performance advantages way beyond that obtained in low end operating systems.

The disadvantage of dedicated servos is that disturbances which are different between the servo head and the data heads cannot be corrected or even detected. The worst such disturbance is static distortion of the actuator or base. As track density has increased this has become an unmanageable problem despite the decrease in the size of drives and consequent reductions in distortion. Various augmented dedicated servo systems are able to minimize this problem. Most gain some limited amount of position information from the data tracks ranging from a single servo track per disk, through a single burst per track (Wedge servo), to a combination of embedded sectors and dedicated signals (Hybrid servo). These solutions are able to respond to disturbances that vary from very slow (single track per surface) through to medium speed (hybrid servo). These solutions can retain much of the capacity advantage of dedicated servos but all loose the cylinder concept.

Embedded servos

All the servo information is encoded on the data disk either distributed among the data dividing it into sectors (sector servo), or encoded transparently to the transfer of data.

Sector servo

Position information is encoded at regular intervals on all tracks in the drive. Data cannot be stored in these locations so they are made as small as possible while ensuring that noise is not significant. For the same reason there is a strong motivation to minimize the number of position information samples. The reduced sample rate however makes difficulties in achieving a high gain for the reasons described previously. This compromise of loss of data recording area vs reduced gain is one of the main reasons for the adoption of transparent embedded servo systems in some products. As the speed of circuitry and data rate capability of heads improves the duration of the servo samples can be reduced without increasing noise. This increases the attractiveness of sector servo.

Buried servo

Servo information is encoded in a separate magnetic layer below the data magnetic layer. It is encoded in a frequency range below that used to encode the data so it can be read concurrently with the data. (Brier reference 9 and figure 13).

Optical servo

The disk is embossed to provide encoding for an optical sensor which is mounted on the slider or near to it. (Hitachi, reference 10 and 11 and figure 14. Also Insite, reference 12) The encoding and detection methods are derived from the optical recording product technologies.

Tracking disturbances

Tracking error (TMR) as a sum of servo response to disturbances

We have seen that the achievable track density can be predicted from the head characteristics and the tracking errors of the drive represented as a TMR probability distribution function (histogram). Each individual disturbing influence on the tracking can be estimated by quantifying the disturbance, and determining the response of the servo and mechanics to that disturbance. These separate contributions to TMR can then be summed by the Root mean square method to give a total. The total TMR defines the ability of a given drive or design point to support high track density. The disturbances fall into two groups, Static shifts, and vibrations. The distinction is important since as we have already seen the static shifts can be the prime tracking error with a dedicated servo system, but are only of secondary significance with a sector servo.

Static shifts

Arm shifts

Distortions of the arms can be caused by temperature changes, by ageing, and by shock. With an uncorrected dedicated servo the shifts are not reduced by the servo at all. They are then often the main contribution to TMR. With linear actuators, run-out of the carriage bearings also contribute significant shifts that vary with time. The augmented dedicated servo systems described previously are able to reduce static shifts to very small residuals, and the embedded servos reduce shifts to zero.

Disk shifts.

Disk shift can be caused by shock or by temperature or by changes in the shock mount stiffness of drives with poor spindle balance. Drives with steel hubs and aluminum disks are obviously prone to disk shift due to temperature changes. (reference 13.) A regular servo will reduce disk shift to around 10% of its UN-corrected amount, but this is may not be sufficient for high track density. In this case the adaptive run-out corrections systems described previously can be used.

Vibrational tracking disturbances

Any drive will have at least some tracking disturbance from the following.

- Settle after seek (arrivals)
- Spindle bearing non-repeatable run-out
- Motor excited spindle vibration
- PES noise.
- External vibration
 - Rotating the actuator arms,
 - Rotating the Drive
 - Distorting the drive

Disk shift caused by temperature and by shock.

A drive with contact recording heads may also have a disturbance due to variations in the friction force between head and disk.

Vibration and servo response

The vibrational disturbances are best described and analyzed by the methods of Random Vibration Analysis (Reference 12). Some drives are specified for operation under sinusoidal external vibration, but random vibration is more likely to represent real life for a drive living a rough life. To determine the TMR with given vibrational input, the power spectrum of the motion of the head over the disk can be computed assuming that there is no servo. The product of this spectrum with the servo error rejection function can be integrated to determine the TMR. This standard method of vibration Analysis is illustrated diagrammatically in figure 9 for the case of non-repeatable bearing run-out..

HDA Vibration mechanics

Vibration input to the drive disturbs the TMR by both rigid body and elastic mechanisms. The rigid body components are easily calculated by simple mechanics theory from the inertia, mass and geometry of the actuator for given translational and rotational acceleration of the HDA.

An actuator with its mass located at the pivot is entirely insensitive to translational vibration input. Rotational vibration of the HDA is best avoided, but can be produced by unsymmetrical mounting of the HDA. Some industry standard mounting hole positions are not well chosen in this respect.

Elastic mechanisms (deflection of the HDA structure between disk and actuator) can be determined by finite element modelling, or by direct measurement. Spindle bearing elasticity is an unavoidable elastic contributor to TMR, but deflection of the HDA can be made small by suitable choice of HDA construction.

The HDA has its own internal sources of vibration. Spindle imbalance, disk run-out, spindle bearings, spindle motor, and actuator seek. Spindle balance will (or should) be always the same from one revolution to another and so should disk run-out. If there is no change then there should be no TMR resulting. If there is any change then that is a good reason to adopt some adaptive run-out correction system.

More vibrations

The spindle bearings can be a very significant source of TMR. Ball races generate random vibrations due to imperfections of the balls and raceways. The frequency spectrum of bearing run-out is a complex set of fixed frequencies that range from around 0.4x the rotation speed to many kilohertz. Most of the motion is often in the lowest few frequencies and is strongly reduced by the servo. Poor base stiffness can amplify higher frequency components when resonances co-incident with significant bearing run-out frequencies and the servo error function increases these components. The bearing frequencies that contribute most to run-out are those that

Excitation of spindle resonances by motor magnetic forces can occur on larger HDAs or when the spindle structure is weak..

At the time of arrival of the heads onto the destination track, a lot of energy is being applied to the drive by the voice coil. Inconsistent arrivals are major component of TMR in most drives. One solution is to avoid writing data, till the transient dies away (reading is OK on many interfaces that tolerate soft errors.) But to avoid impacting the performance of the drive the problem must be fixed. This is often motion of the HDA induced by the reaction of the voice coil motor during the preceding seek. Smaller drives not requiring shock isolation have much better arrivals as the HDA cannot move when it is screwed direct to the system.

Position Error Signal noise.

The process of decoding the Position Error signal generates noise or error. The servo attempts to follow this erroneous signal so it causes TMR. Some of the noise coming from the medium is repeatable from one revolution to another. This is media noise and increases the error in servo track position so it adds to write to write TMR (track squeeze) but since it is the same on each revolution it does not add to write to read TMR. It was significant with brown disks but tends to be very small with film disks.

The non-repeatable noise comes from electronic sources, and is reduced by increasing the length of the PES encoded burst on the disk. It is therefore a design variable trading disk real estate (capacity) for better TMR (capacity).

Trends

There is no doubt that track positioning can be made sufficiently accurate to support much higher track densities than we have today. The only question is what (is the most cost effective way to do it.. There are several approaches each of which has its proponent.

I don't propose to vote, only identify the candidates which are.

1. More band-width,
2. Much more band-width,
3. Better mechanics,
4. Smarter servos.

More band-width.

More band-width becomes available as bit density rises, since the number of samples per rotation of the disk increases. (Raising the RPM does not help a lot since the important spindle run-out frequencies are then harder to follow.). Higher band-width will be supportable by the mechanical structure as the resonances move to higher frequencies with small size.

Much more band-width.

This approach is to use the technology of the Optical recording business which gains a very high band-width position error signal from a dedicated optical sensor. Even smaller actuators have resonances that limit the servo band-width strongly. The optical industries answer is to have a very small stroke secondary actuator riding piggy-back on the main actuator. This way the resonances of the main actuator structure are not excited. While complex and expensive and seemingly unable to support fast seek times, this technology has been used by Hitachi to demonstrate 5Gb/in² magnetic recording density, (Reference 10 and 11). The bandwidth obtained by Hitachi by this methods has unfortunately not been disclosed. Optical sensing is used by Insite peripherals in their Floptical products. (Reference 12.) In both these cases the magnetic disk medium is embossed with a pattern of optical pits sensed by laser-diode systems.

Better mechanics

Oil journal bearings are the best illustration of this trend. Journal oil bearing technology devised last century has been combined with new insights into long life oil, and new ways of retaining small amounts of oil strictly where it is needed, to provide low run-out spindles for video recorders and Lazer printer scan mirrors. Journal bearings have been tried in disk drives and found to offer better non-repeatable run-out than ball bearings (reference 15.). Ball bearings too have seen continuous improvement through time coupled with the advantages of reducing size.

Smarter servos

Some of the smart servo concepts have been described. Adaptiveness is the key to these, and enhancements of processing power in the drive controller will make this easier to implement. Another direction of smarter servos is Fuzzy logic, a control method that works more like the human mind in deciding what action to take, and which may not use the concepts of conventional servo theory. There is a wide

belief that fuzzy logic will be able to make improvements in disk drive tracking control (reference 16.)

Limitations ?

Disk drive density has always been regarded as limited in part by tracking accuracy, but despite that, areal density has moved forward by four orders of magnitude in a few decades, requiring a two order improvement in TMR. It has taken ingenuity, but there is no shortage of that commodity. There are no fundamental limitations., We can confidently expect that by the normal processes of engineering progress in each of the areas that have been outlined, positional accuracy will be available to support the highest densities that improvements in the head, the disk, and their separation can deliver.

References

1. Demonstration of 500 Megabits per square inch with Magnetic Recording. R Jensen, J Mortelmans and R Hauswitzer. IBM Corp MRI. IEEE Trans Mag Vol 26 No 5 Sept 90
2. Data Storage on Rigid disks. R L Comstock and M L Workman. Magnetic recording Handbook Ed C D Mee. Chapter 2. McGraw Hill 1990.
3. Design of a swinging arm actuator for a disk file. J.S. Heath. IBM Journal of R and D. July 76.
4. Digital Control of Dynamic systems, G.F.Franklin, J.D.Powell, and M.L. Workman Addison-Wesley 1990 (pp 703-747)
5. Nanometer positioning and its micro-dynamics. S. Futami A. Furutani and S. Yoshida.
7. Control Systems technology in Digitals Disk Drives. M. D. Sidman Digital Technical Journal No 8 Feb 89.
8. Data storage on flexible disks. S. Yaskawa and J.S Heath. Magnetic recording Handbook Ed C D Mee. Chapter 3. McGraw Hill 1990.
9. Brier technology brochure. Brier Technology 2363 Bering Drive. San Jose CA 95131.
10. M Futamoto et Al. Investigation of 2 Gb/in² recording at a track density of 17kTPI. IEEE trans Mag, Vol 27, No 6, Nov 91
11. K Akagi et al. High density magnetic Recording Tracking method using a Laser diode. IEEE trans mag, Vol 27, No 6.
12. Insite Periferals brochure. tral analysis. D.E.Newland. Longman 1975.
14. US Patent 4,814,652 Disk drive motor with thermally matched parts. H.T. Wright.
15. G Buchard, L Lau, and F Talke. An Investigation of non-repaetable spindle runout. IEEE trans Mag Vol 23, No 5, Sept 87.
17. C.N. Wallis Track following system for a disk file. US patent 4,594,622 1984.
18. T J Chainer and E.J. Yarmchuk. A technique for the Measurement of Track misregistration in disk files. IEEE trans mag. Vol 27. No 6. Nov 1991

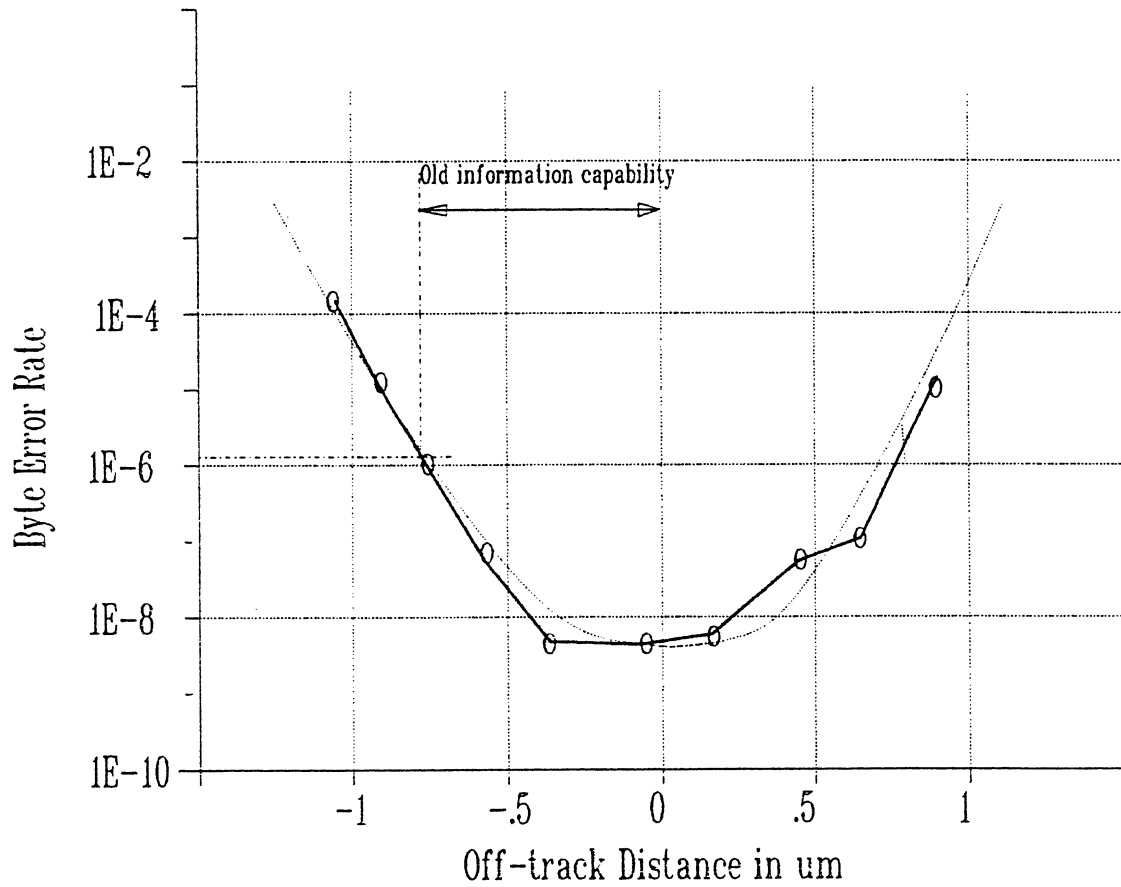


Figure 1. Error rate off-track (Bathtub Curve)

Redrawn from paper Demonstration of 500 Megabits per square inch with Magnetic Recording. R Jensen, J Mortelmans and R Hauswitzer. IBM Corp MRI. IEEE Trans Mag Vol 26 No 5 Sept 90

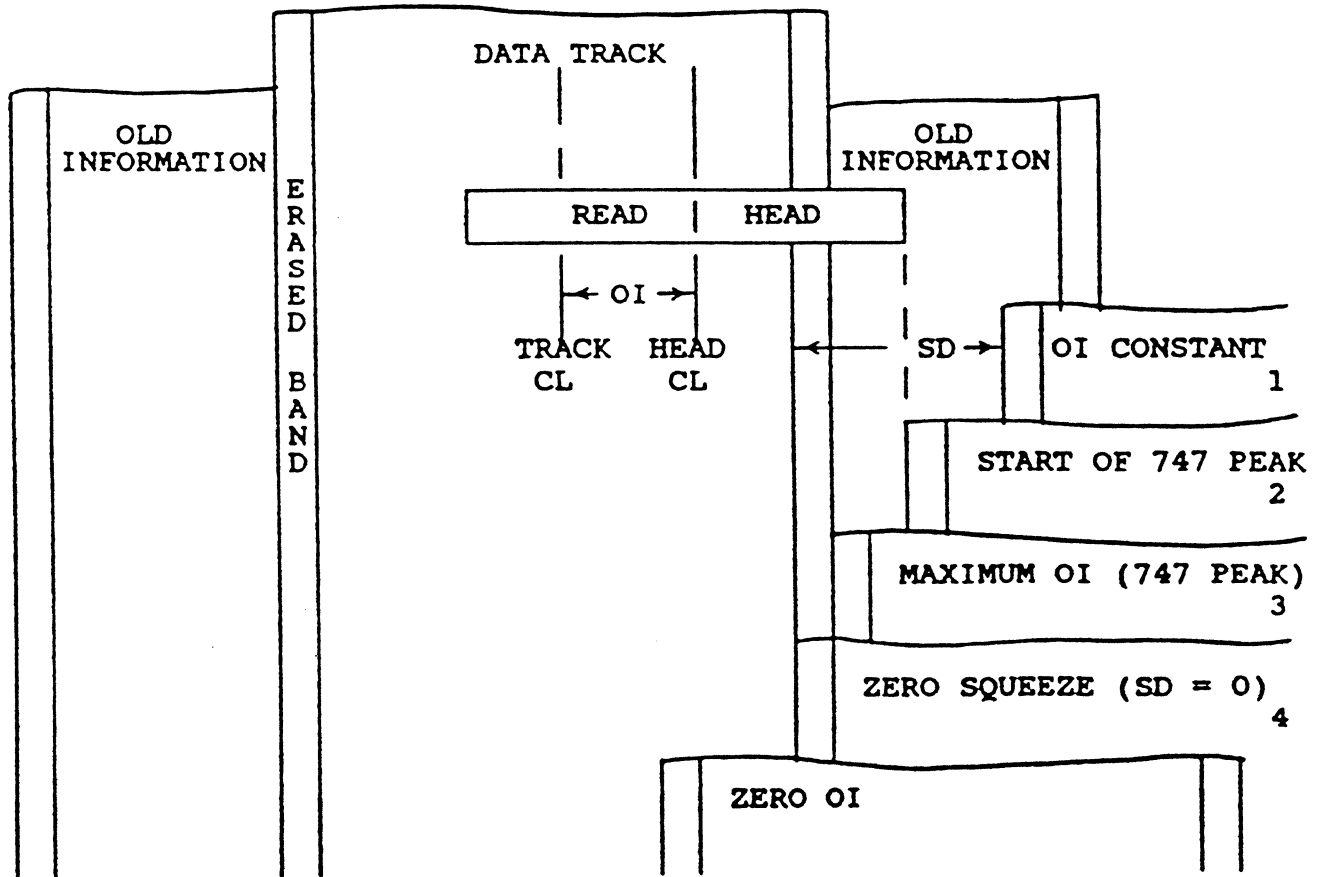


Figure 2. Old information and 747 test schematics.

SD is the squeeze distance.

OI the Old information distance.

Numbers on the left refer to figure 2.

Taken from paper Demonstration of 500 Megabits per square inch with Magnetic Recording. R Jensen, J Mortelmans and R Hauswitzer. IBM Corp MRI. IEEE Trans Mag Vol 26 No 5 Sept 90

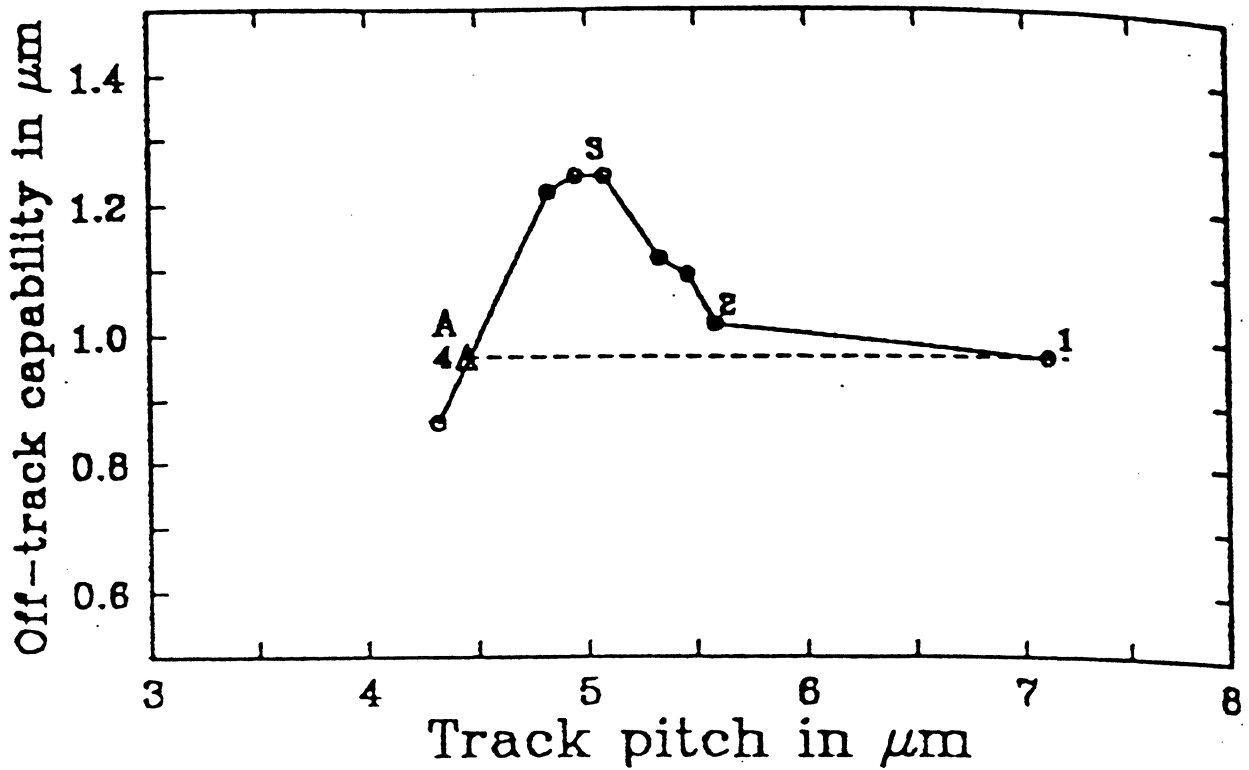


Figure 3. 747 curve for 500 Mb/in²

Point A occurs when the erased bands of the adjacent and center tracks overlap. Numbers refer to figure 2.

Taken from paper Demonstration of 500 Megabits per square inch with Magnetic Recording. R Jensen, J Mortelmans and R Hauswitzer. IBM Corp MRI. IEEE Trans Mag Vol 26 No 5 Sept 90

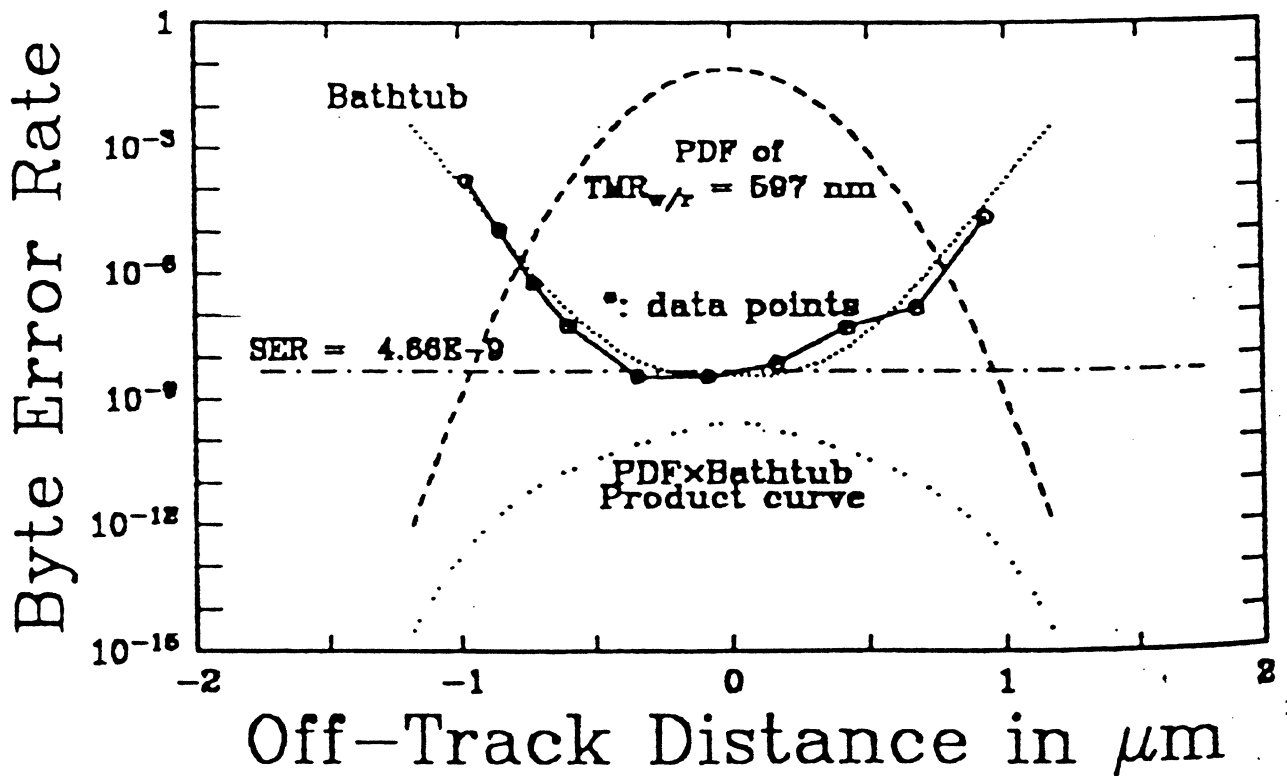


Figure 4. Measured and calc bathtub with PDF of TMR.

No adjacent track is recorded. Alos shown are PDF of TMR w/r, the product curve and its integral value (horizontal line), which yields the expected error rate and point B in figures 5 and 6.

Taken from paper Demonstration of 500 Megabits per square inch with Magnetic Recording. R Jensen, J Mortelmans and R Hauswitzer. IBM Corp MRI. IEEE Trans Mag Vol 26 No 5 Sept 90

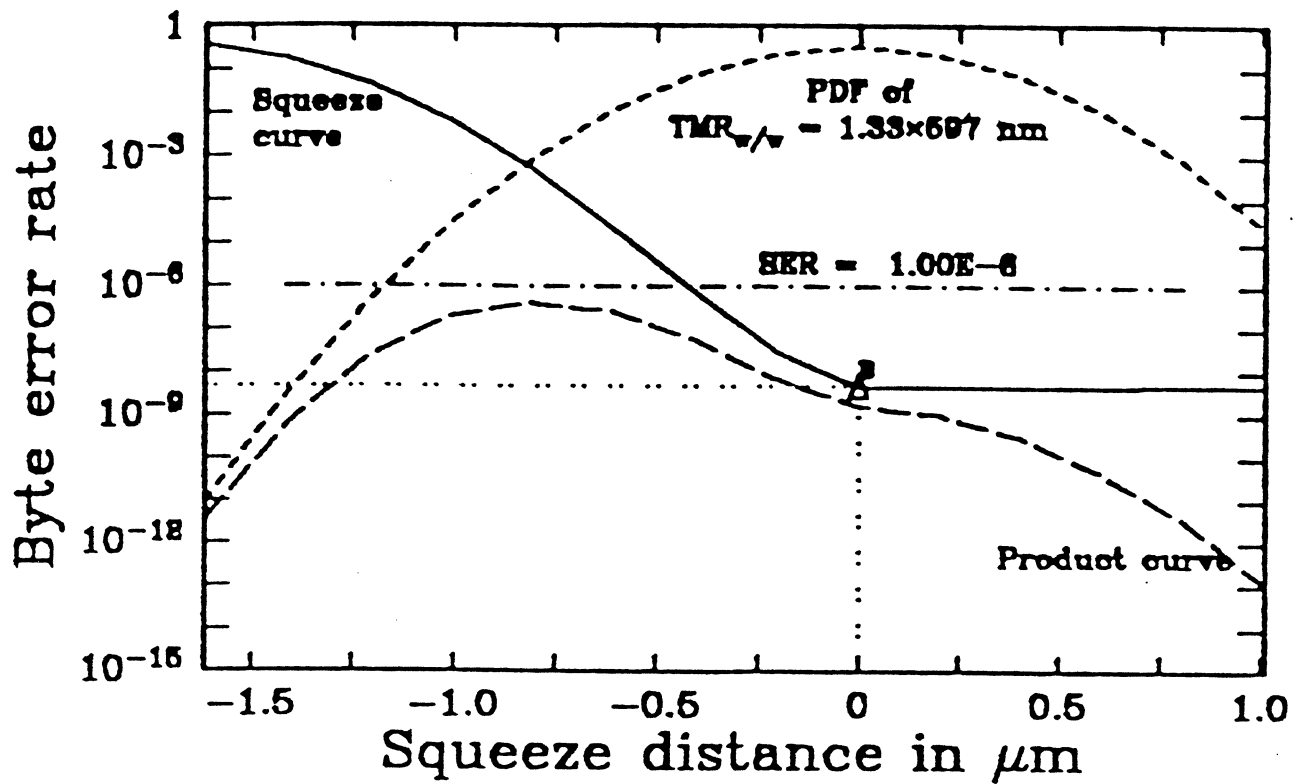


Figure 5. Calculated squeeze.

Also shown is the PDF of TMR w/w , the product curve and its integral value which yields the overall expected error rate.

Taken from paper. Demonstration of 500 Megabits per square inch with Magnetic Recording. R Jensen, J Mortelmans and R Hauswitzer. IBM Corp MRI. IEEE Trans Mag Vol 26 No 5 Sept 90

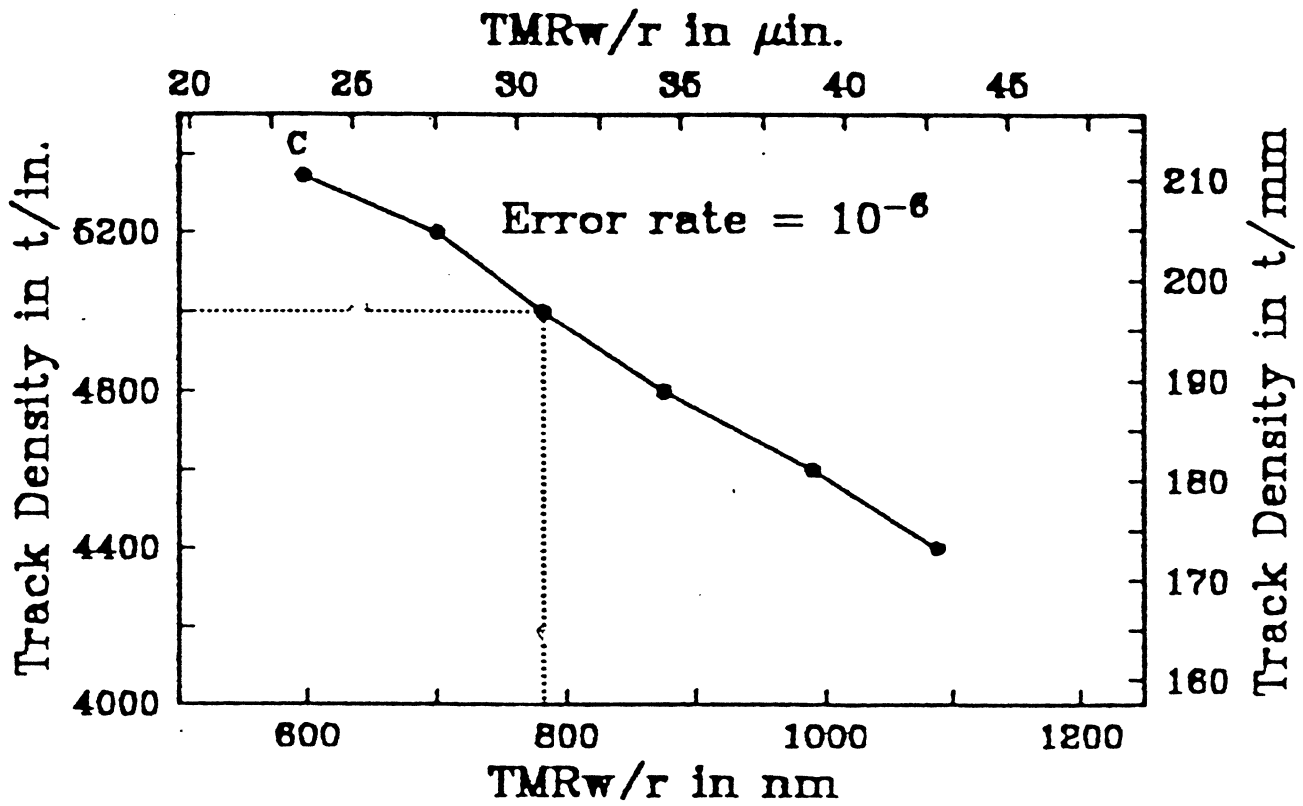


Figure 6. Track density vs TMR

1. Demonstration of 500 Megabits per square inch with Magnetic Recording. R Jensen, J Mortelmans and R Hauswitzer. IBM Corp MRI. IEEE Trans Mag Vol 26 No 5 Sept 90

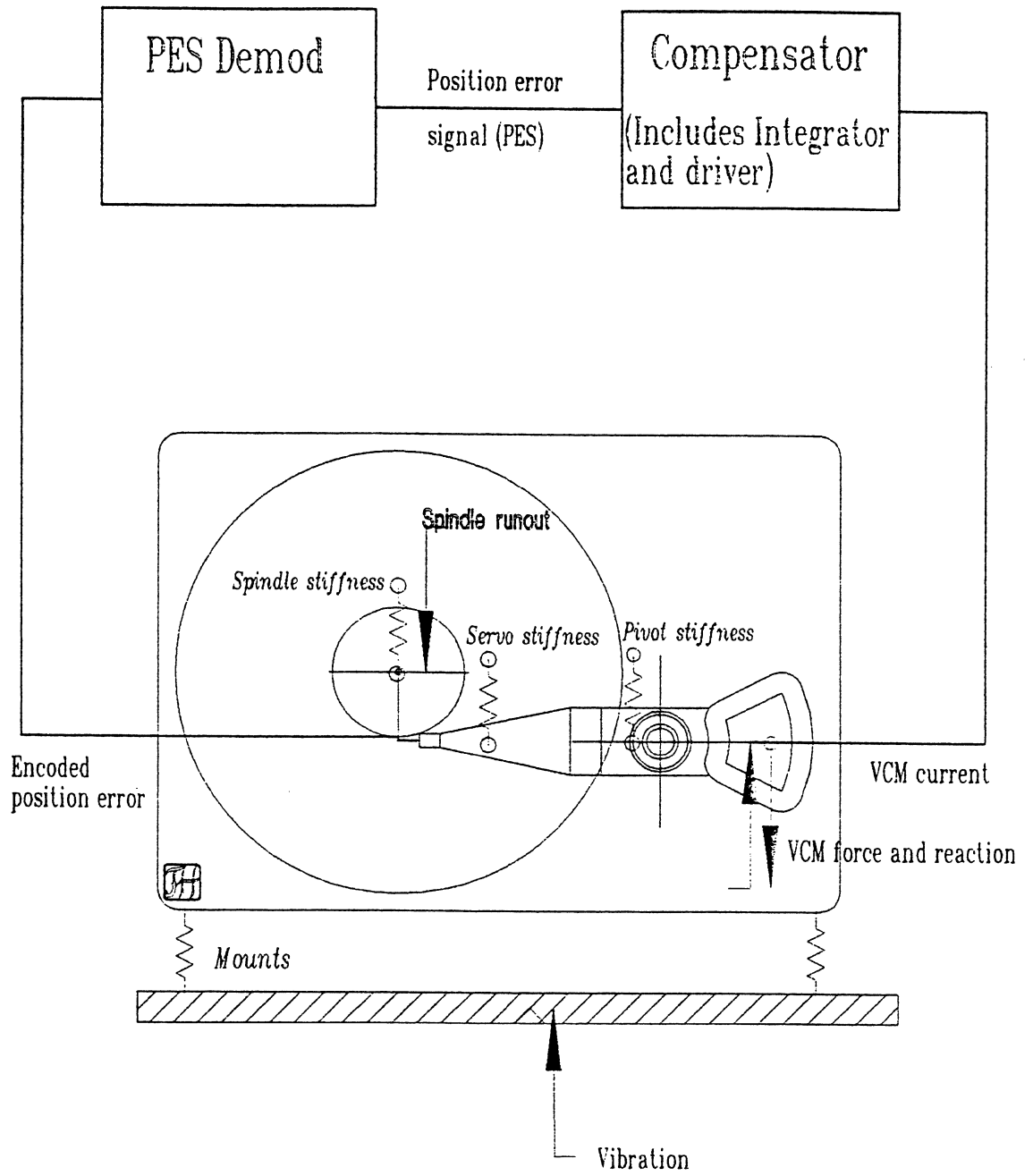


Figure 7. Disk drive mechanical system and servo.

Shows the essential elements needed to understand tracking accuracy (TMR)

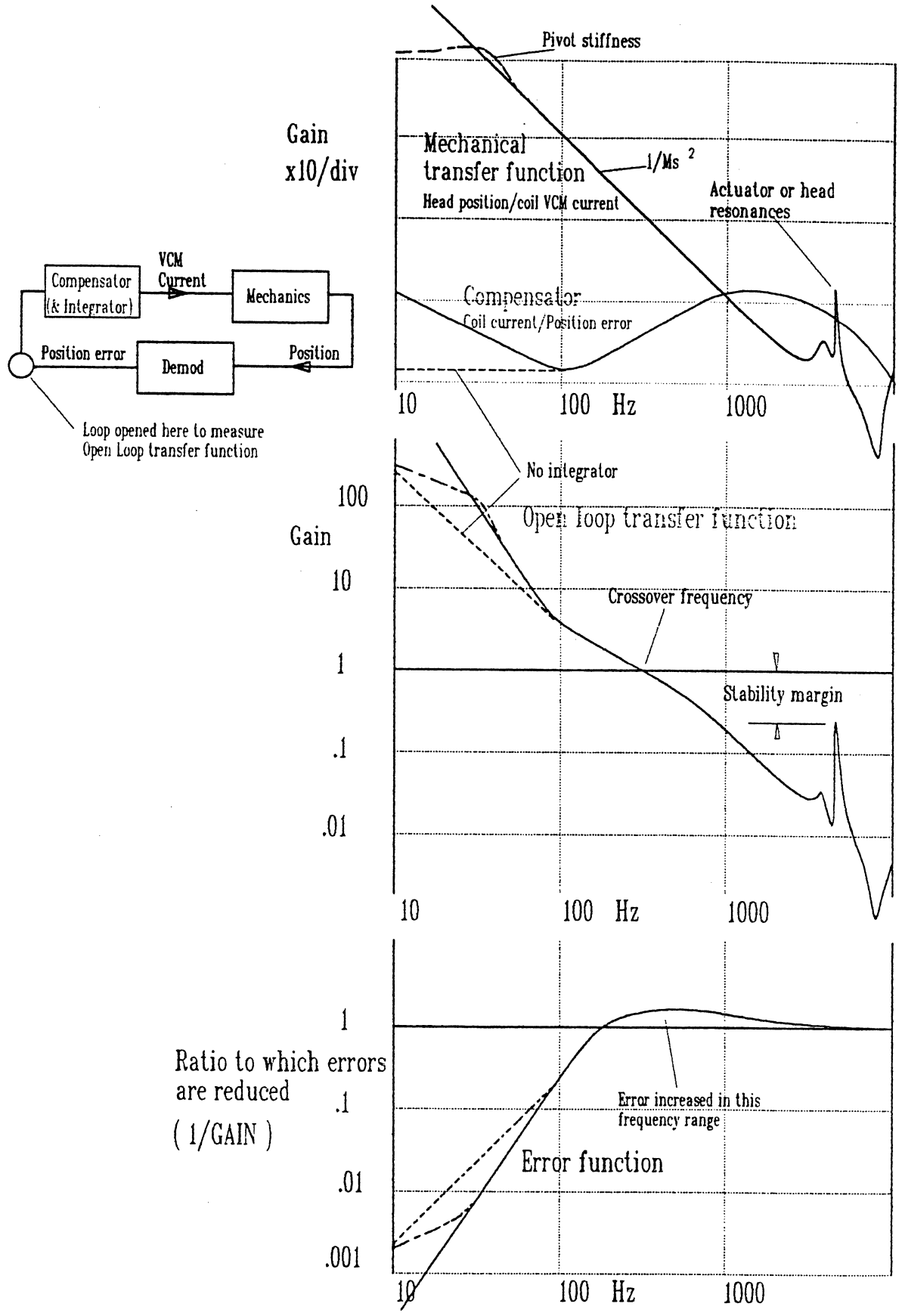


Figure 8. Mechanical and Servo system transfer functions and gain.

Shows mechanical and compensator (electronics) transfer functions.

The product of these two is the open loop transfer function, which is drawn to show the potential gain limit due to resonances.

The error function (inverse of open loop tfn at low frequencies) is also shown in fig 9

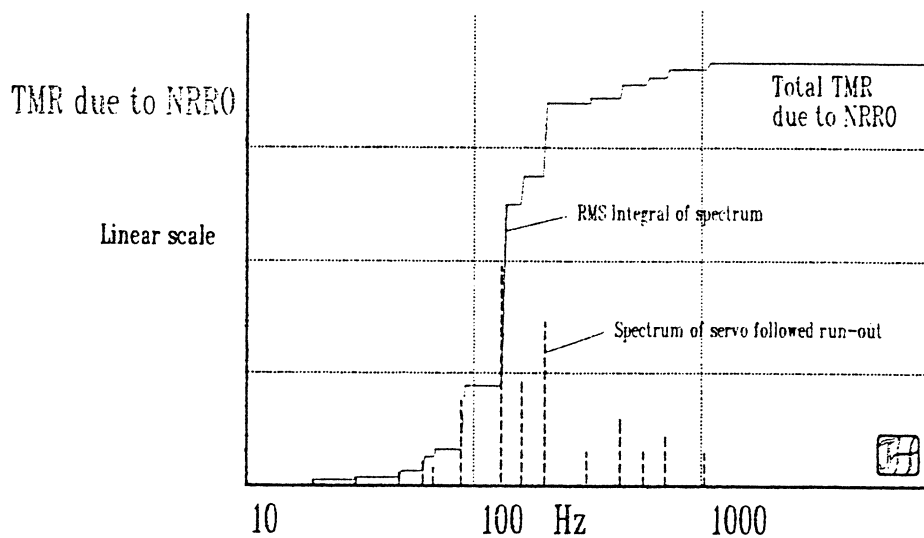
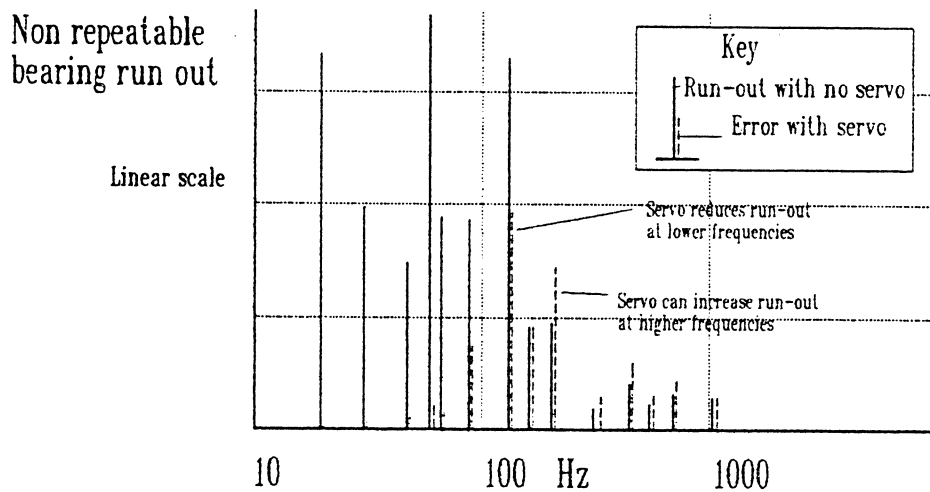
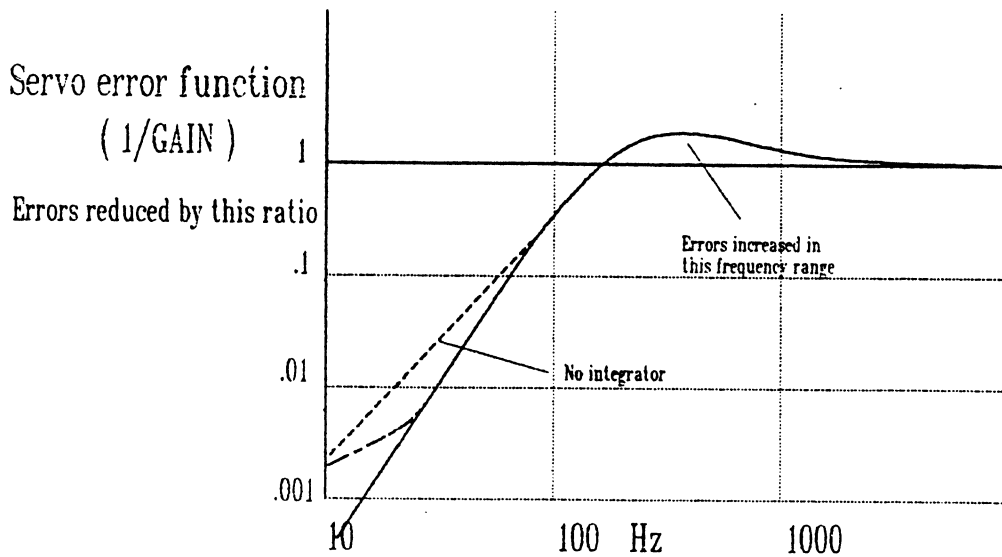


Figure 9. How Gain determines TMR of mechanical disturbances

Bearing non-repeatable run-out is used as an example to show how the servo reduces run-out and also what the limitations are. The same methodology is used to optimise the servo to reduce the other vibrational disturbances of head tracking.

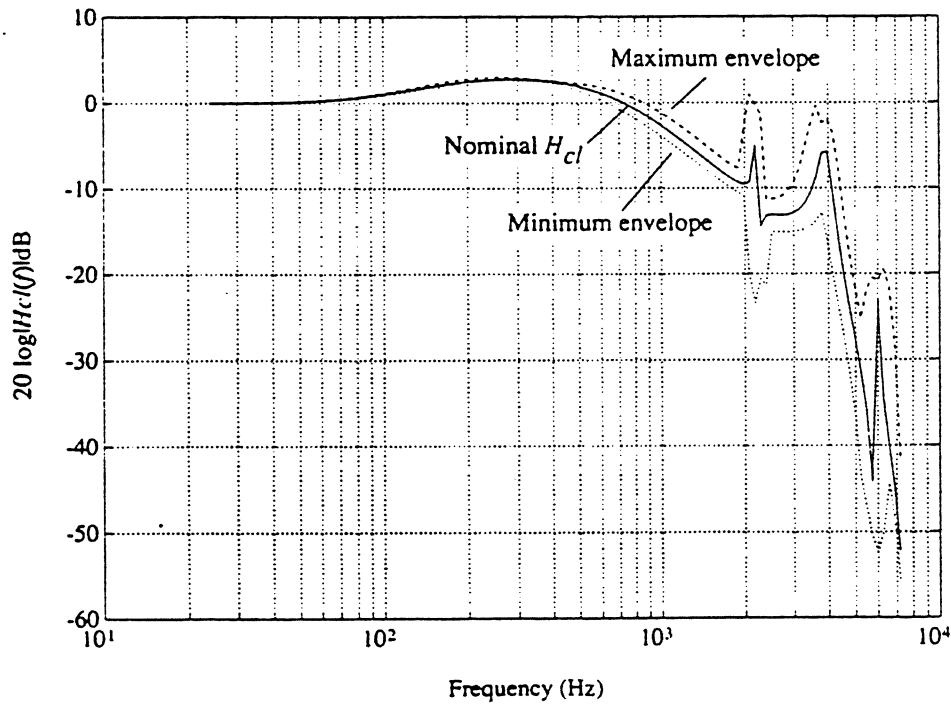
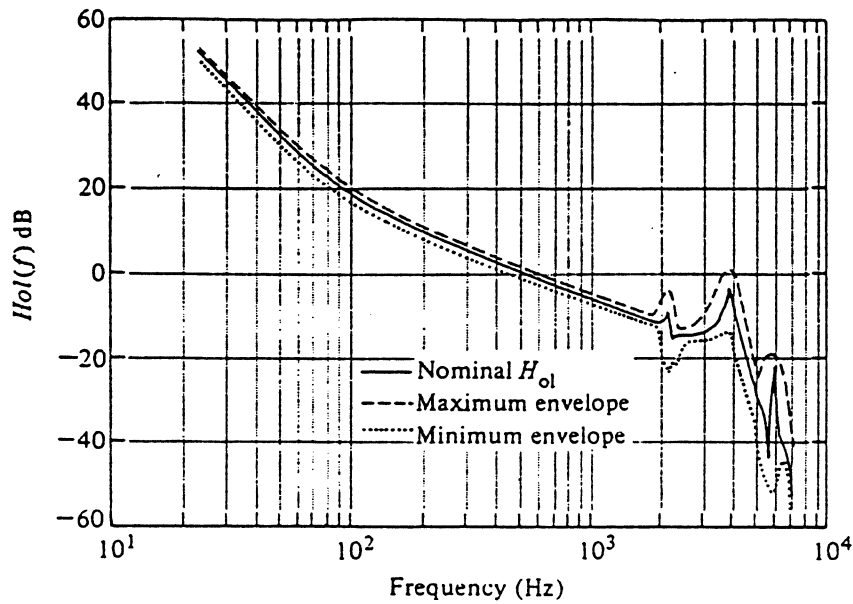


Figure 10. Variation of Mechanical transfer functions

Variability of open loop transfer function in a population of disk drives. Showing why allowance has to be made in servo gain for ~~worse case hardware~~.

Taken from Digital Control of Dynamic systems, G.F.Franklin, J.D.Powell, and M.L. Workman Addison-Wesley 1990 (pp 703-747)

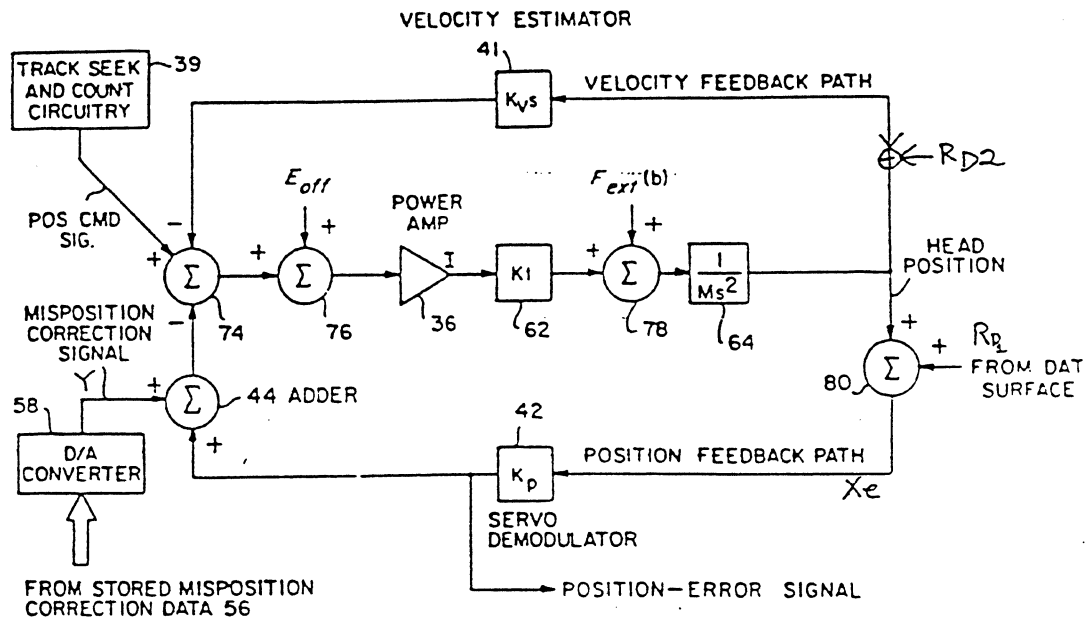
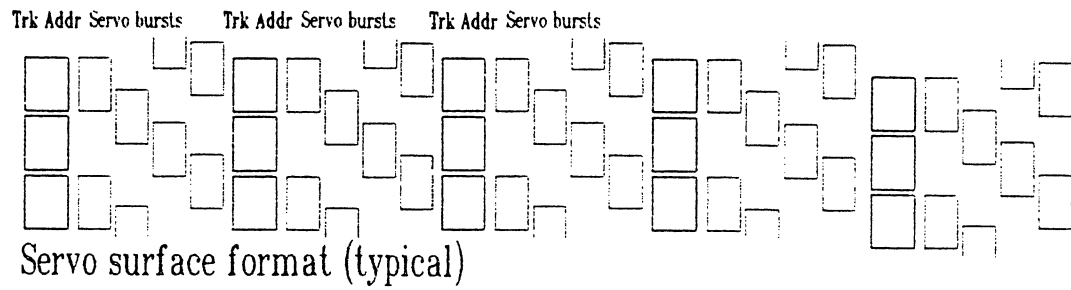
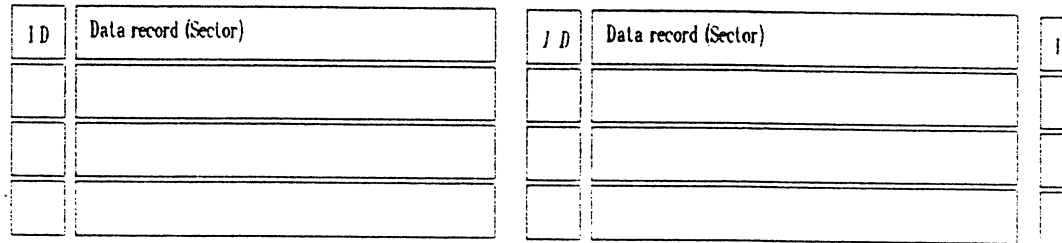
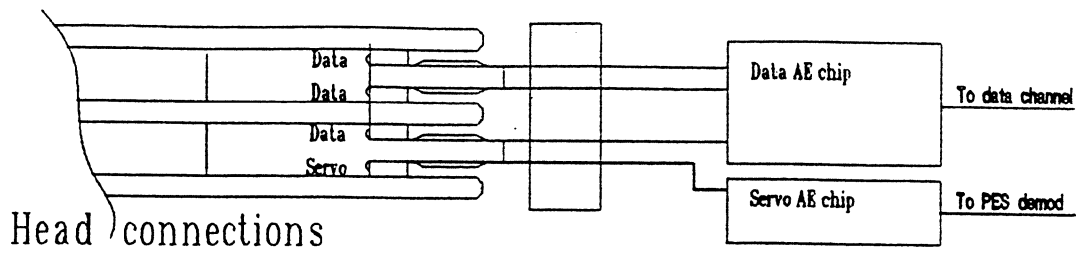
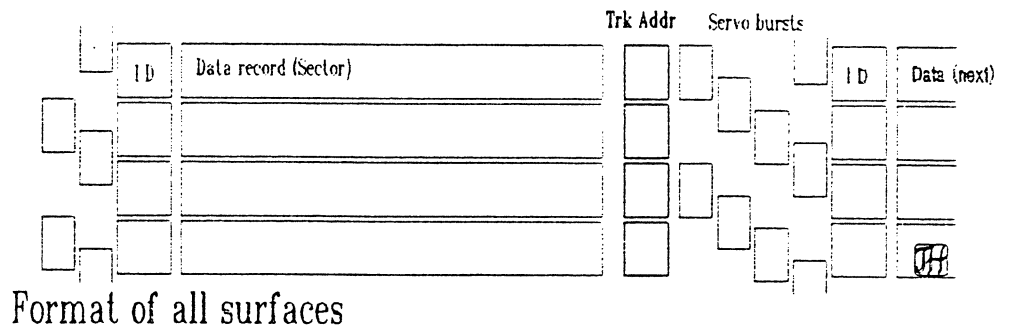
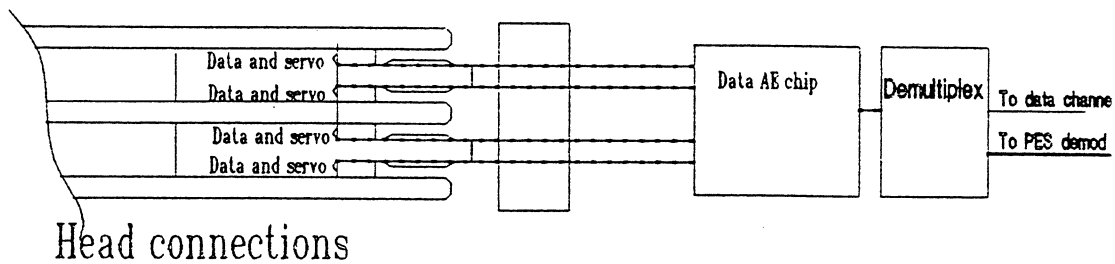


Figure 11. Adaptive runout correction.

Taken from Control Systems technology in Digital Disk Drives. M. D. Sidman
 Digital Technical Journal No 8 Feb 89.



Dedicated servo



Sector servo

Figure 12. Dedicated and sector servos compared.

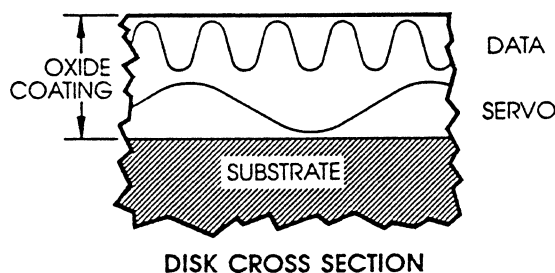
Simplified schematic showing main differences between dedicated and sector servos. Data rate banding makes sector servo surface format much more complex.

Twin Tier Tracking®

The Flextra drives employ a new, proprietary, Twin Tier Tracking (T³) technology that makes ultra high performance floppy disk drives a reality.

Brier's T³ servo technique enables industry standard 3.5" media to store 25 MB of data by creating two distinct, horizontal magnetic layers in the disk media. The lower or positioning tier, consisting of thousands of magnetically embedded, prerecorded positioning tracks, precisely controls the read/write head of the drive.

The upper tier is used for the storage of data. Since no head positioning information is required in the upper tier, Brier's data tracks use the complete upper surface of the disk and achieve maximum efficiency and reliability.



Twin Tier Tracking provides accurate head positioning coupled with precise track following to assure data integrity and cartridge interchangeability.

T³ offers upward mobility to much higher capacities in the future. The magnetically embedded lower tier already contains all the positioning tracks needed to achieve increased capacities.

Figure 13. Brier buried servo

Servo information buried below data saves space normally required for sector servo on a single disk. Sample rate can also be high and not limit the gain.

From Brier technology brochure. Brier Technology 2363 Bering Drive. San Jose CA 95131.

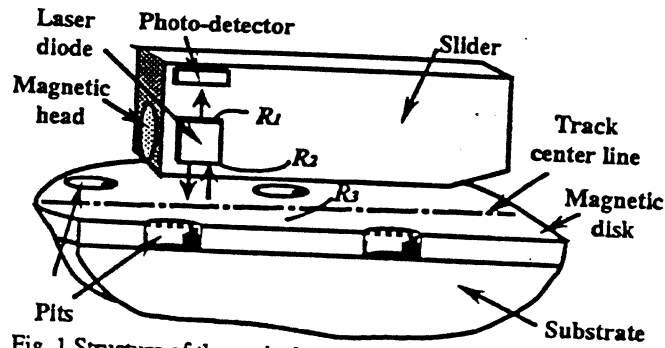


Fig. 1 Structure of the optical servo head where the laser diode is attached on the slider with its active layer parallel to the track line and apart from the disk surface.

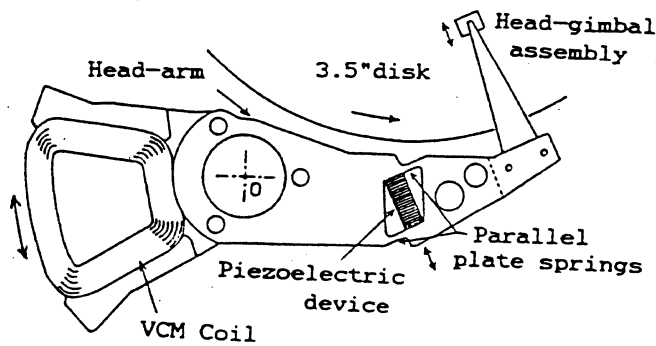


Fig.2 Structure of a dual-stage actuator

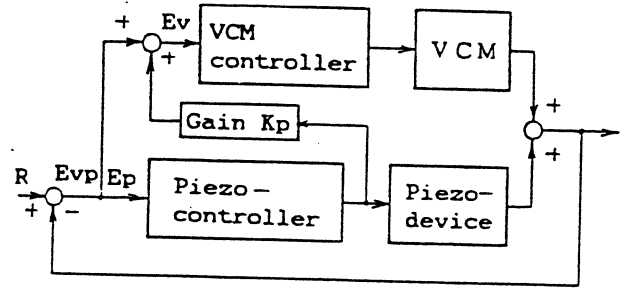


Fig.5 Block diagram of the dual-stage servo system

Figure 14. Hitachi optical sensor and dual servo

Showing optical track position sensing system separate from magnetic recording channel. Two stage actuator provides potential for much higher gain because effect of resonances can be reduced. (Actual gain of this system not disclosed).

From
M Futamoto et Al. Investigation of 2 Gb/in² recording at a track density of 17kTPI.
IEEE trans Mag, Vol 27, No 6, Nov 91

and
K Akagi et al. High density magnetic Recording Tracking method using a Laser diode.
IEEE trans mag, Vol 27, No 6.

"Low Flying/Contact Recording"

James U. Lemke

Recording Physics

Institute for Information **S**torage **T**echnology

Santa Clara University, California

December 14 - 16, 1992

THE IDEAL DRIVE

- HIGH DENSITY (SINGLE, SMOOTH DISK)
- LESS THAN ONE MICRO-INCH HEAD/DISK SPACING
- NO STICTION
- NO CONTACT BETWEEN HEAD AND DISK AT ANY TIME
- STIFF HEAD/DISK BEARING
- SHORT SETTLING TIME
- LOW DRAG (LOW POWER)
- ~~R~~UBUST
- QUIET
- CONTAMINATION-FREE

4.3. Friction Theories

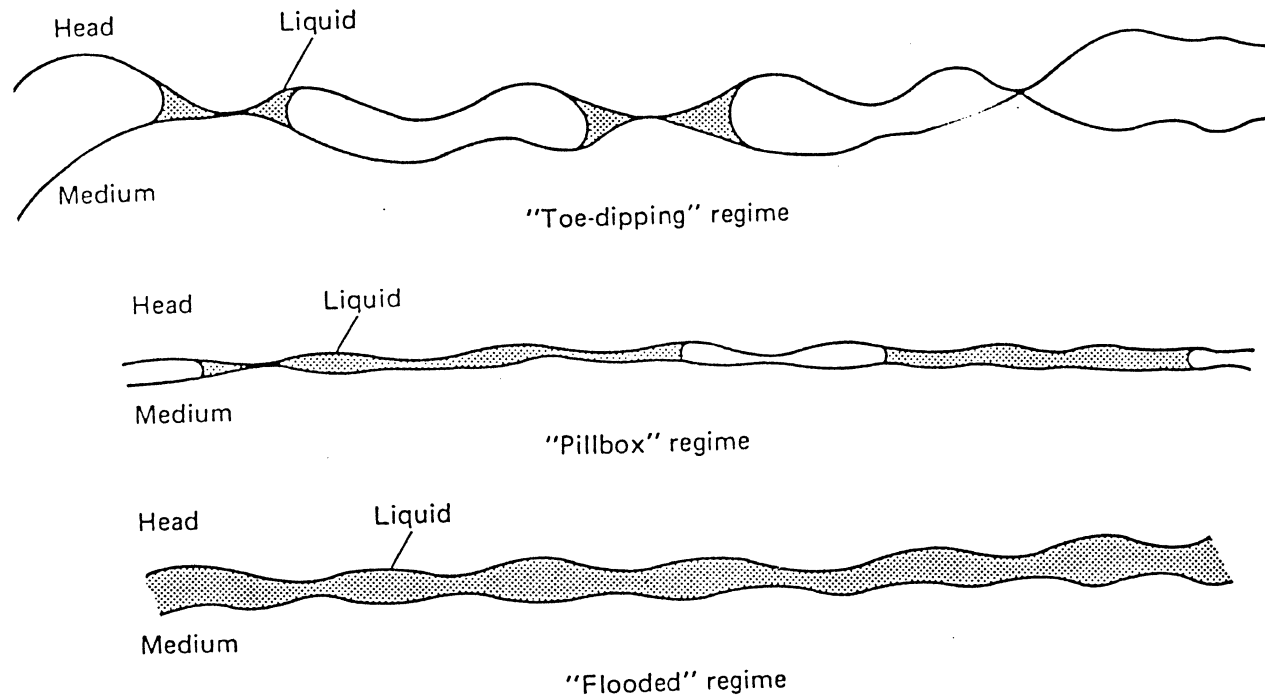
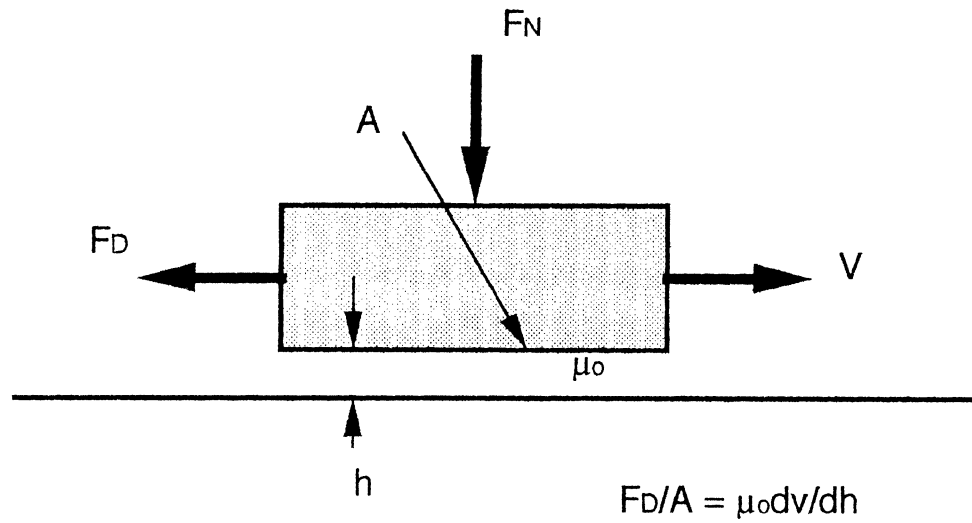


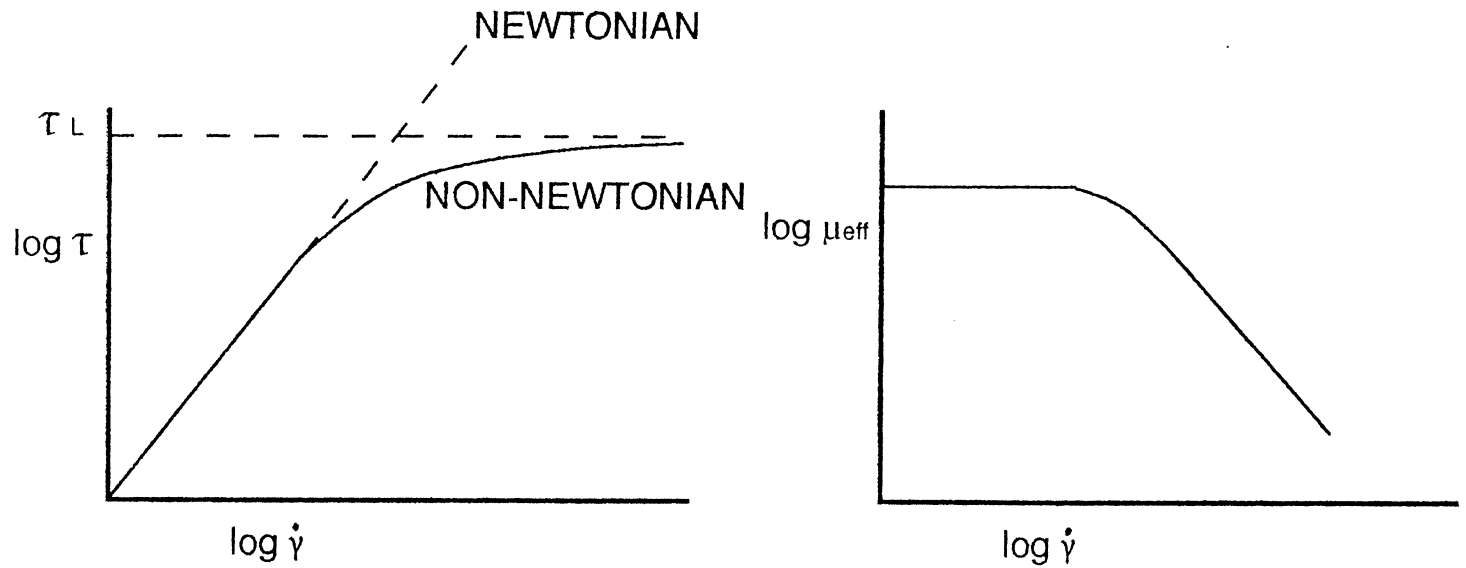
Fig. 4.15. Regimes of different liquid levels in the head-medium interface.

(BHUSHAN)

COUETTE FLOW



$$\tau = \mu_0 \dot{\gamma}$$



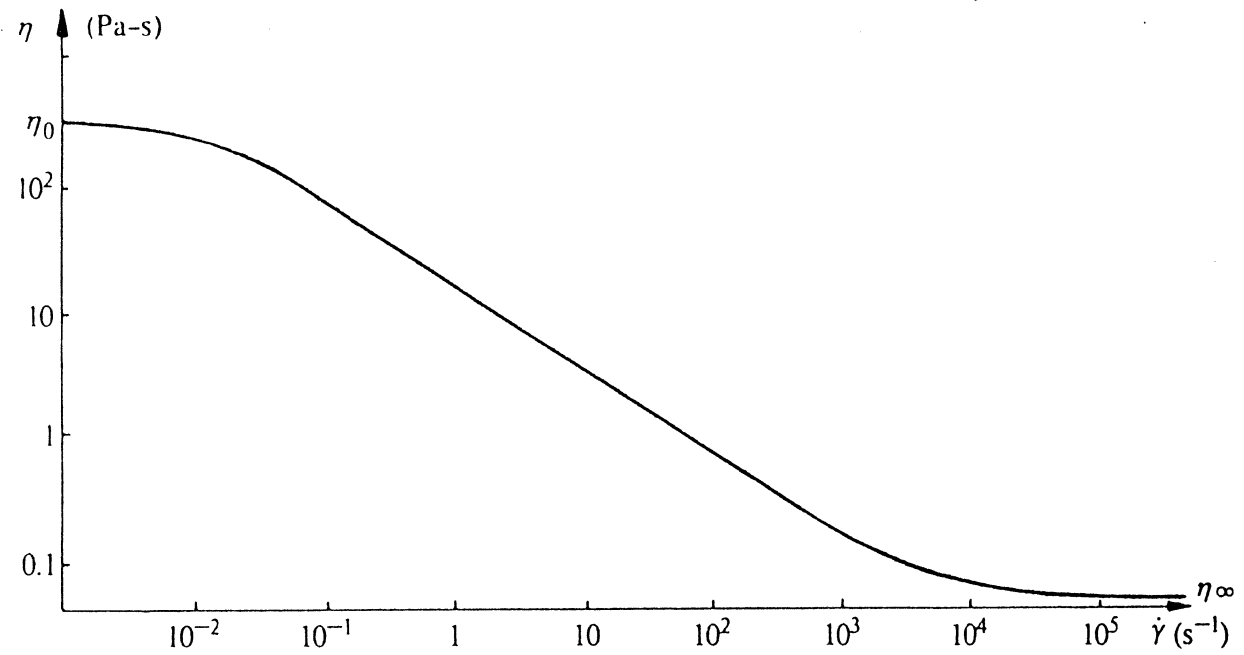


Fig. 1.2. Shear-thinning in a typical non-Newtonian fluid, Separan AP-30 in glycerol/water.

(TANNER)

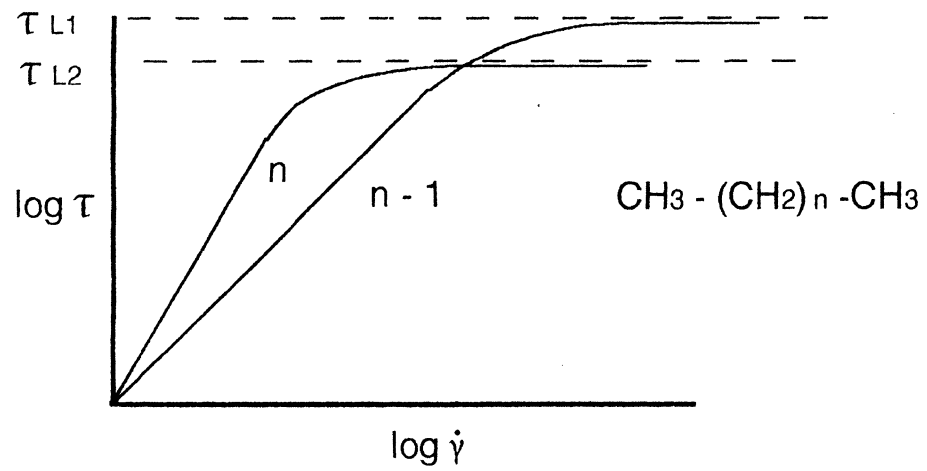
PSEUDOPLASTIC FUNCTIONS

MANY MODELS HAVE BEEN PROPOSED BUT NONE TESTED IN THE SHEAR RATE RANGE OF INTEREST SINCE NO VISCOMETERS EXIST WITH RATES OF EXP 8-9/SEC.

$$\tau = \tau_L(1 - e^{-\mu\dot{\gamma}/\tau_L})$$

THIS WORK WAS DONE FOR SHEAR BANDING AT HIGH PRESSURE AND LOW SHEAR RATE BUT SEEMS TO MATCH OUR RESULTS BEST.

SHEAR LIMITED STRESS AND MOLECULAR LENGTH



FLUID

- LOW INITIAL VISCOSITY (PART OF THE SYSTEM IS NEWTONIAN)
- HIGH VISCOSITY INDEX
- LOW FREEZING POINT
- PSEUDO-PLASTIC BEHAVIOR IN THE SHEAR-RATE OF INTEREST
- μ_{eff} OFFSET FOR INNER/OUTER SPEED RANGE
- LUBRICITY
- SPINDLE BEARING COMPATIBILITY

NON-NEWTONIAN FLUIDS

PERFLUOROCARBONS

(e.g., PERFLUOROETHERS, FLOURINE SUBSTITUTED PARAFFINS)

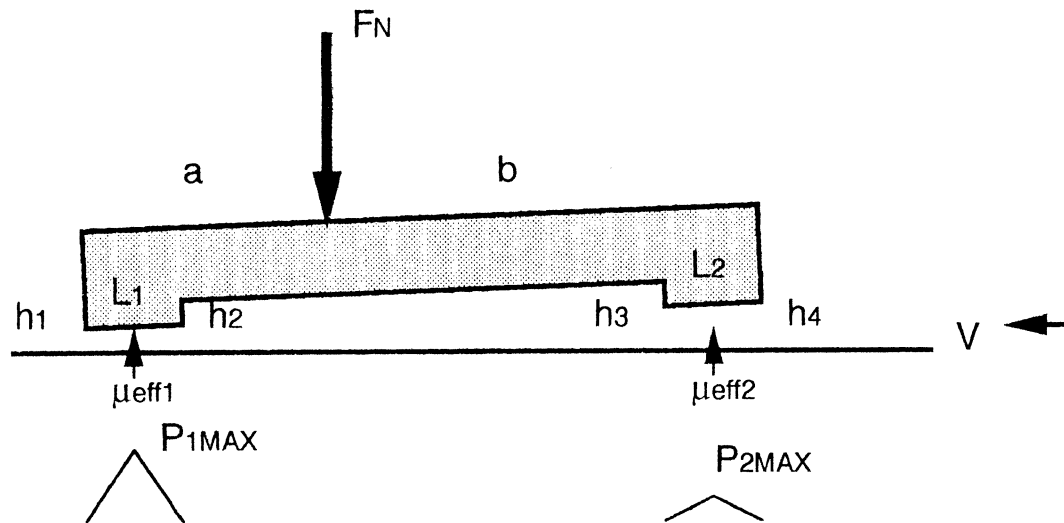
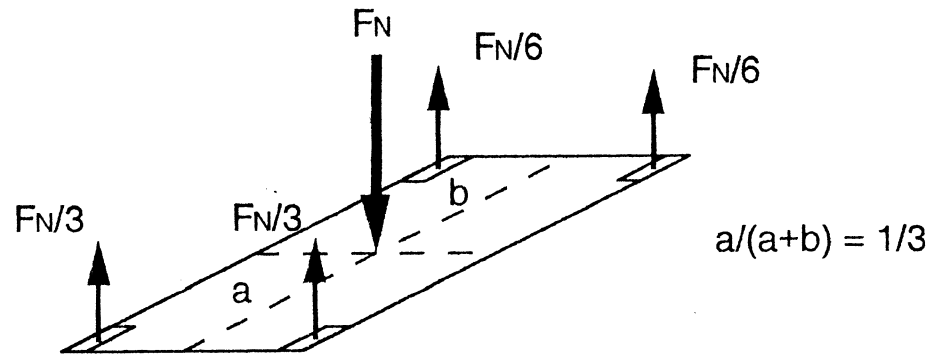
- HIGH DENSITY
- STABLE
- INERT
- POOR SOLVENTS

HYDROCARBONS

(e.g., n-HEXADECANE, BLENDED PARAFFINS, BRANCHED HYDROCARBONS)

- LOW DENSITY
- STABLE
- GOOD SOLVENTS

FORCES AND PRESSURES ON A 4 PAD HEAD



THE EFFECTIVE VISCOSITY CAN BE DETERMINED FOR EACH PAD BY MEASURING THE PAD HEIGHTS THROUGH INTERFEROMETRY AND THEN USING THE NAVIER-STOKES EQUATION TO BALANCE THE TORQUES AROUND THE LOAD POINT.

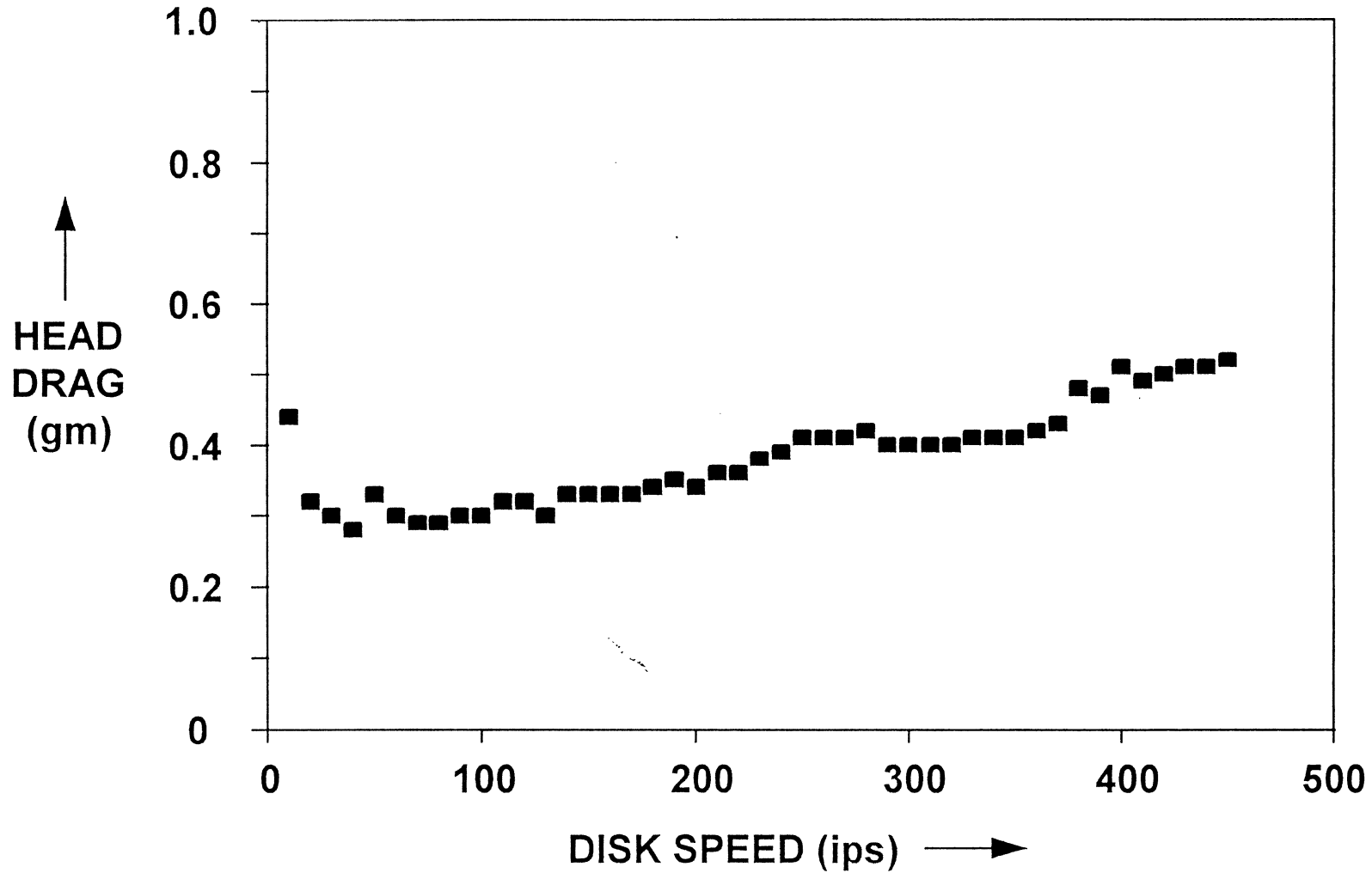
$$P_{1\max} = \frac{6L_1 v \mu_{1\text{eff}} (h_2 - h_1)}{2(h_1^3 + h_2^3)}$$

DRAG/POWER CONSIDERATIONS

- IN THE PLASTIC SHEAR REGION, THE EFFECTIVE VISCOSITY DECREASES WITH SHEAR RATE. THIS RESULTS IN A CONSTANT SPACING AND A CONSTANT DRAG HEAD DRAGS ARE A FRACTION OF A GRAM.
- THE WICK DRAG IS PRESSURE DEPENDENT. USE STIFF APPLICATOR WICKS AND LOW PRESSURE. WICK DRAGS ARE LESS THAN HEAD DRAGS.
- HYDRODYNAMIC BEARING POWER LOSSES ARE TYPICALLY TWICE WINDAGE LOSSES.
- A HIGH-PERFORMANCE 500 MEGABYTE DRIVE AT LESS THAN 500 mW IS FEASIBLE.

VISqUS LIQUID INTERFACE

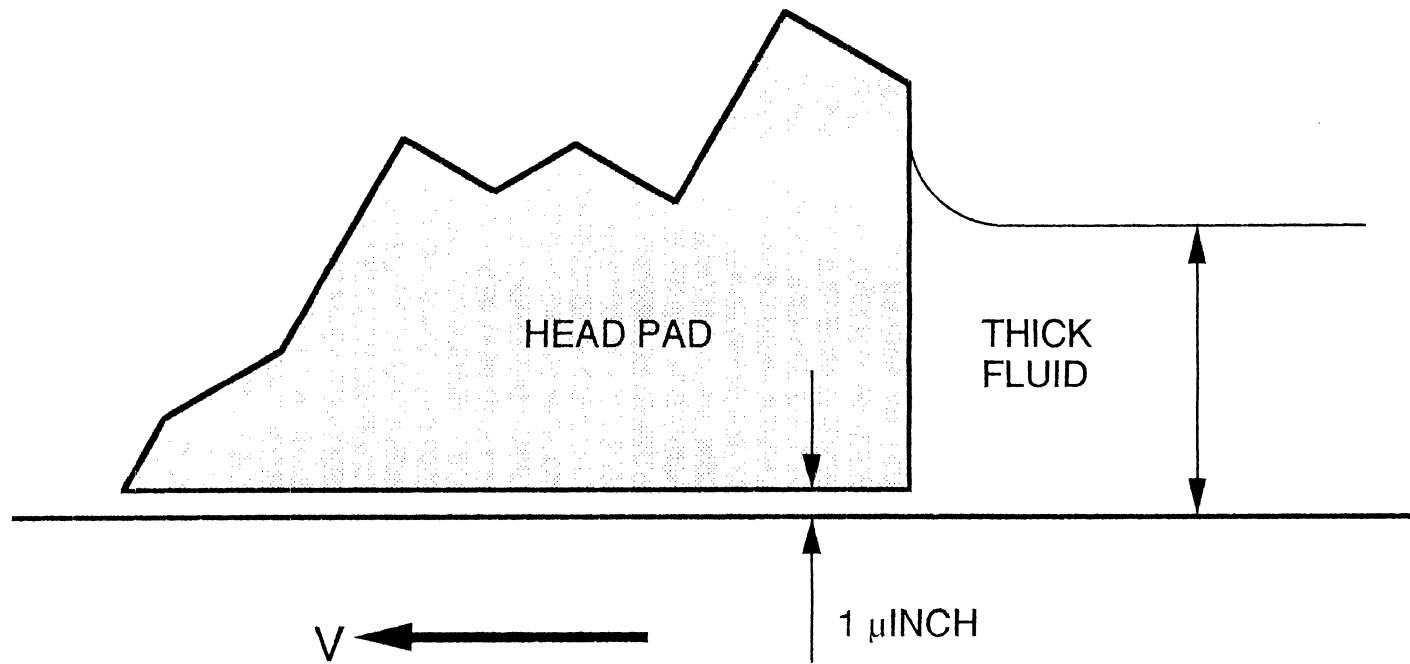
Head Drag - No Stiction

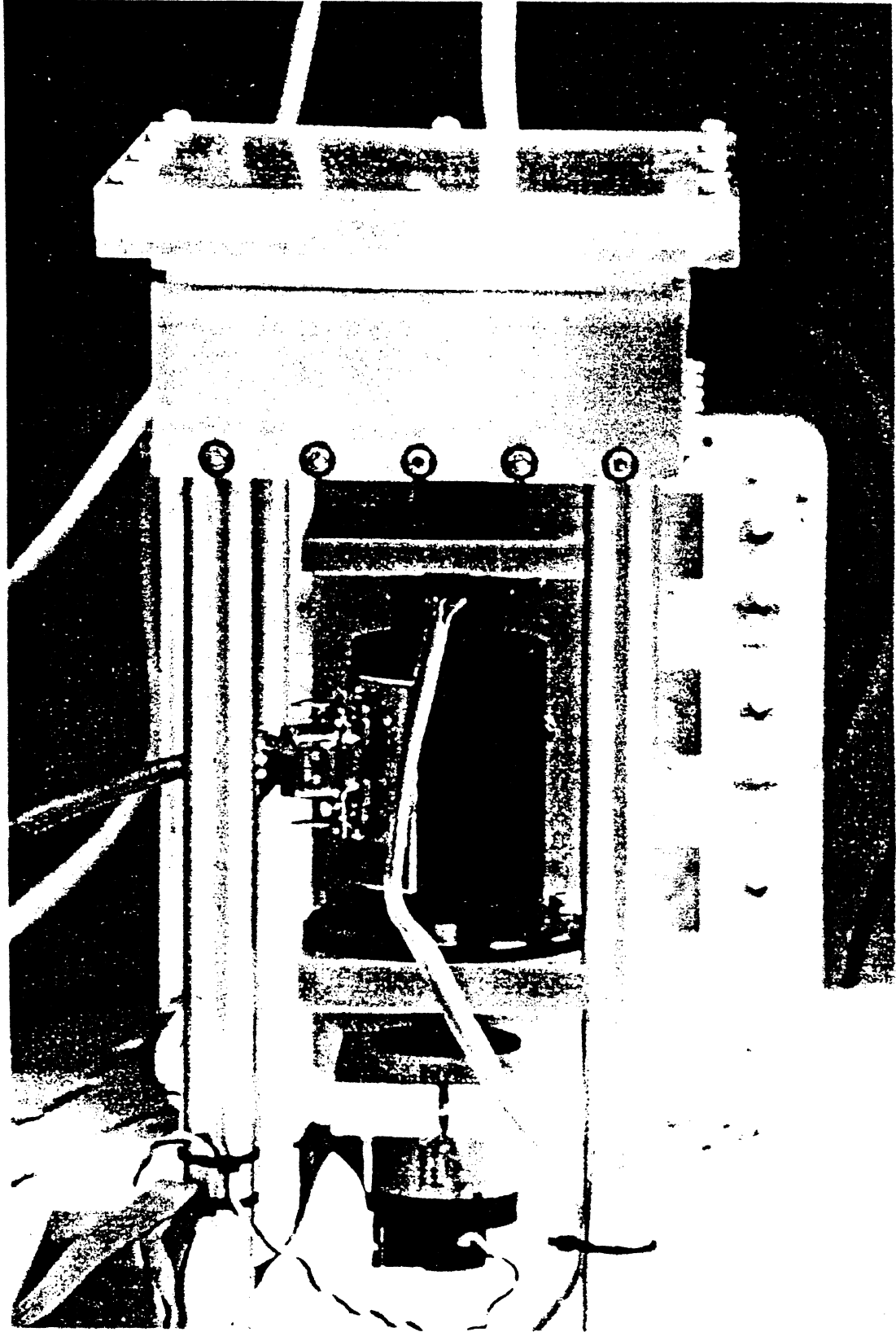


CONNER

NON-CRITICAL FLUID THICKNESS

THE HEAD SHEARS FROM THE BOTTOM OF THE POOL
A NON-NEWTONIAN LAYER OF THE REQUISITE THICKNESS





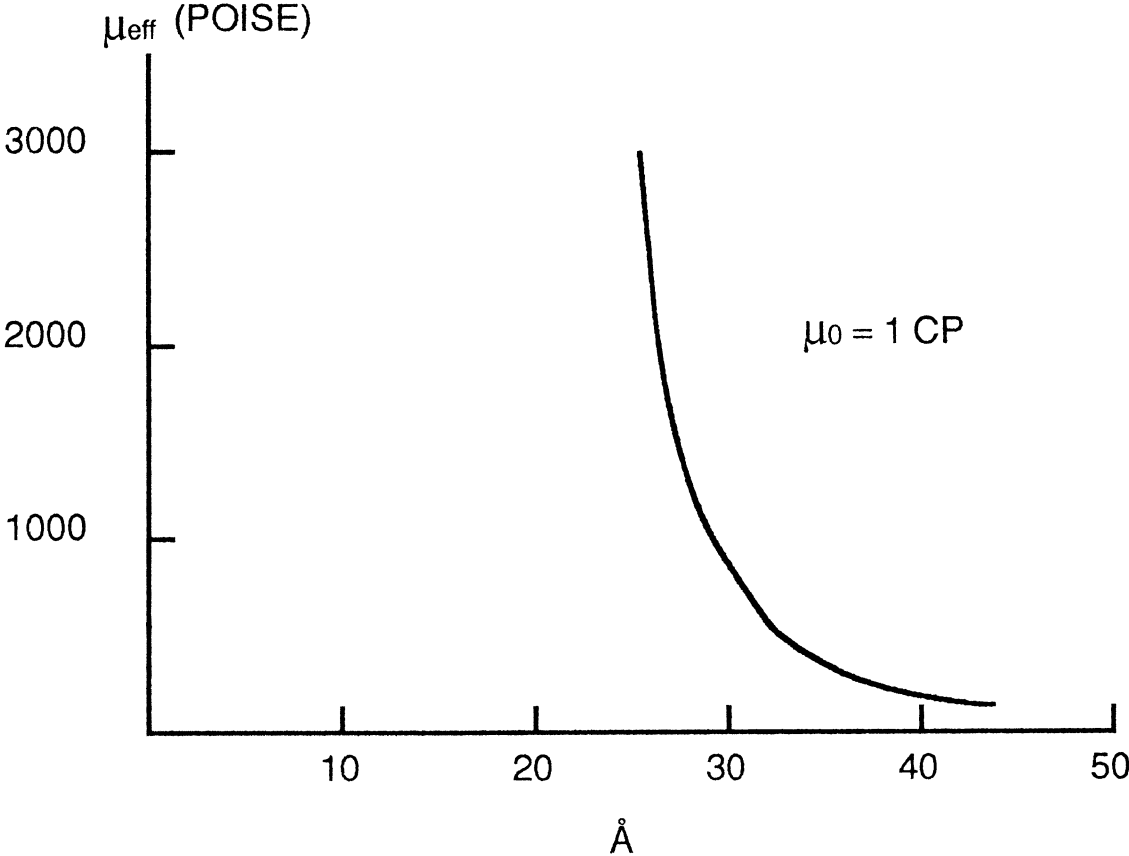
SPACING AT $V = 0$

RECENT LITERATURE (GRANICK, ISRAELACHVILI, AND OTHERS) HAVE SHOWN THAT CONFINED LIQUIDS ON VERY SMOOTH SURFACES ORDER INTO A SOLID PHASE WITH VERY HIGH APPARENT VISCOSITIES.

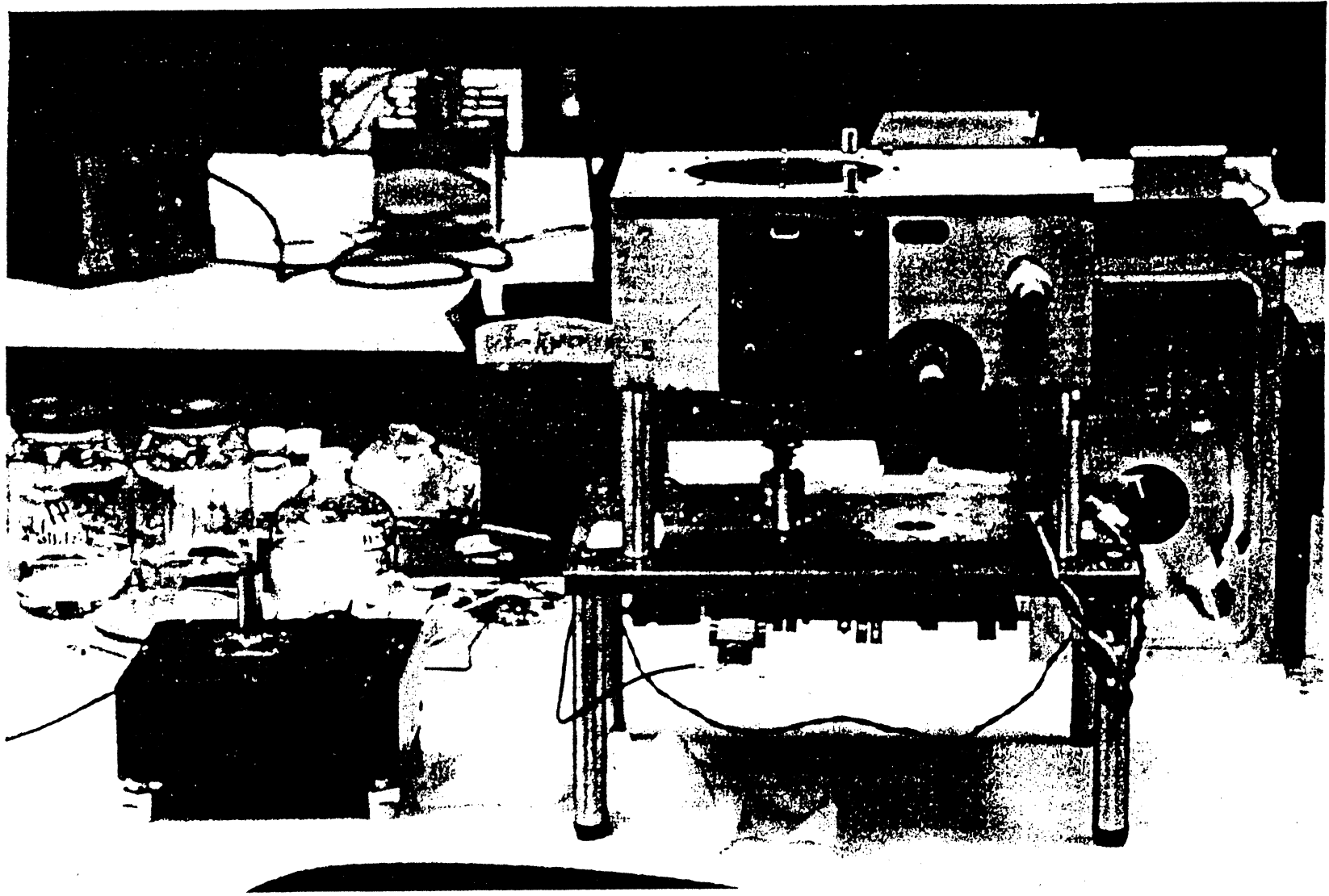
THIS MOLECULARLY THIN CRYSTAL MELTS UNDER SHEAR AND RETURNS TO NORMAL VISCOSITY FROM A SHEAR STRESS IMMEASURABLY SMALL IN A DISK DRIVE.

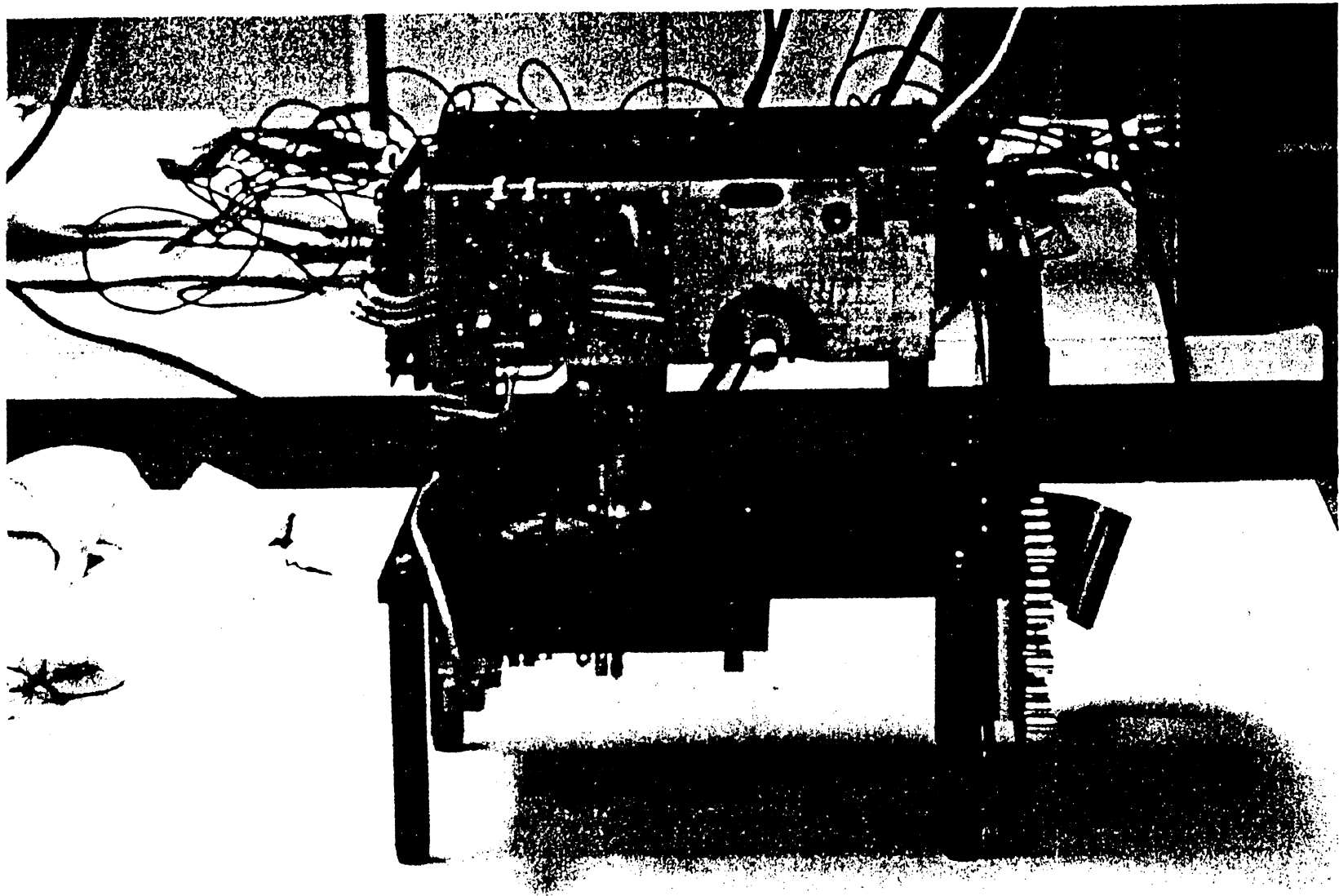
THE HEAD NEVER TOUCHES THE DISK.

FLUID ORDERING AT SMALL DIMENSIONS



FROM GRANICK, SCIENCE SEPT. 20, 1992



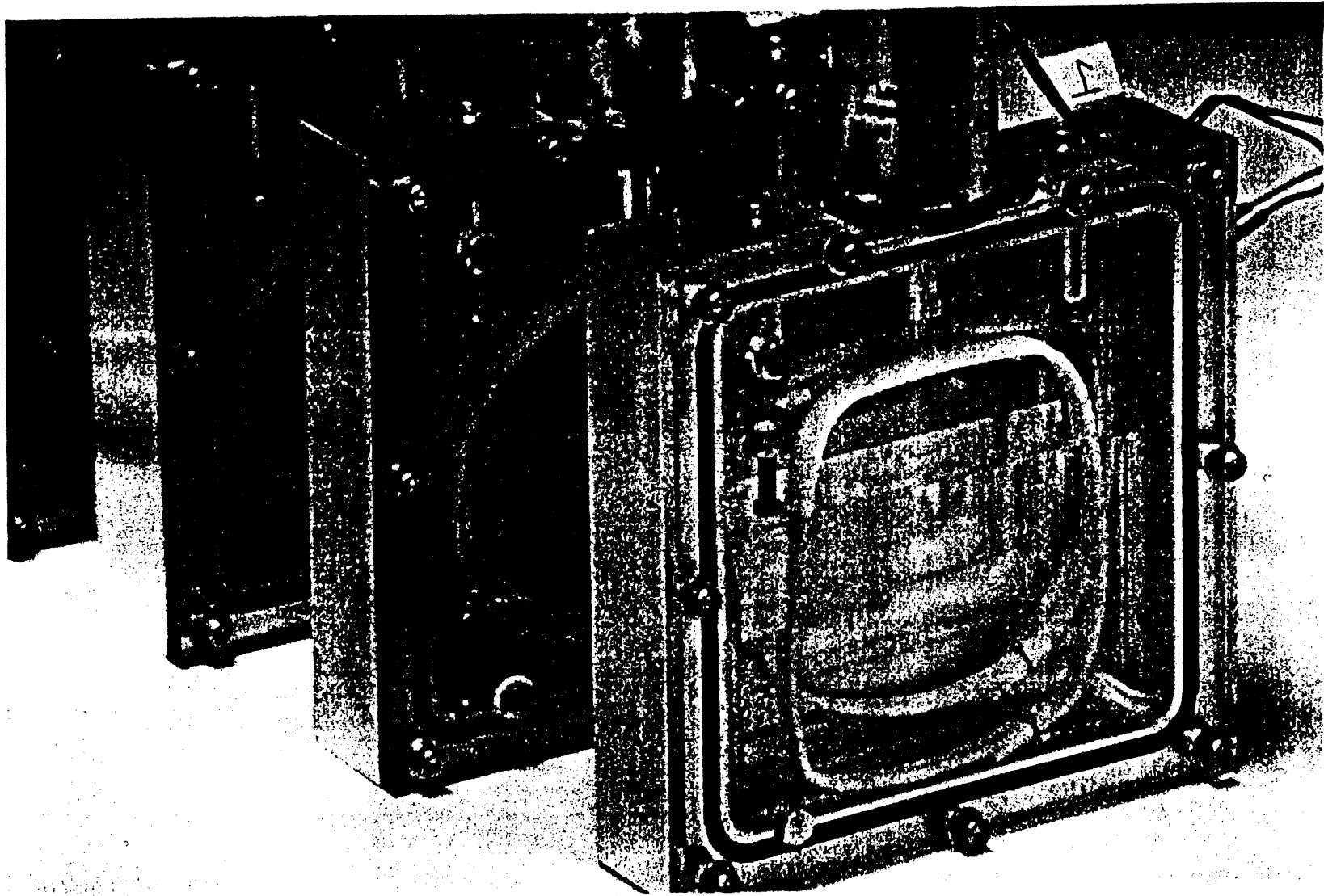


WICKING

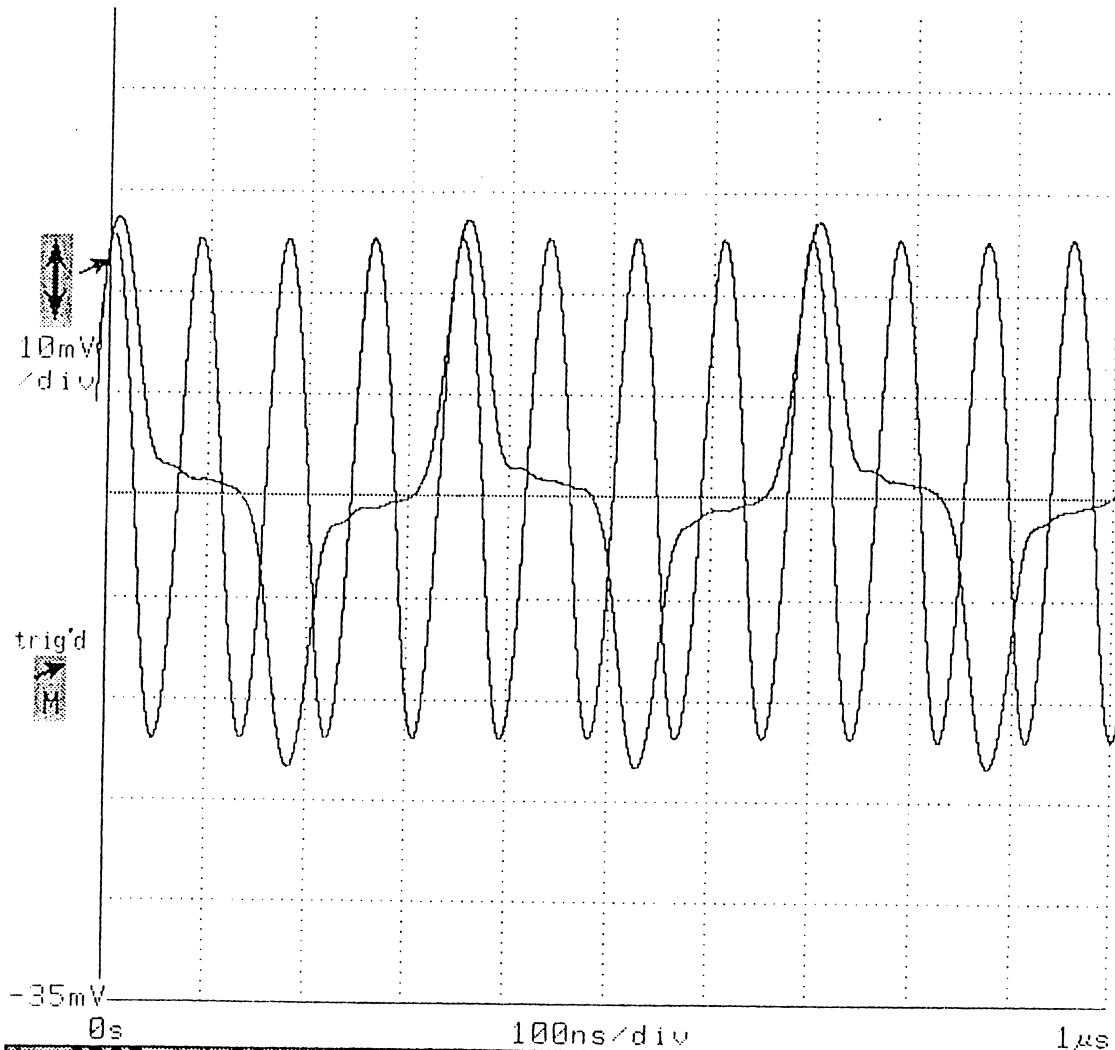
- SURFACE TENSION
- WETTING ANGLE
- FLUID DENSITY
- PORE SIZE
- DURABILITY
- STIFFNESS

$$h = \frac{2\sigma\cos\theta}{\rho r g}$$

THE WICK IS THE RESERVOIR, TRANSPORTER, FILTER, AND APPLICATOR FOR THE FLUID.



DSA 602 DIGITIZING SIGNAL ANALYZER
 date: 7-FEB-91 time: 12:46:42



INDUCTIVE HEAD
 70 KFCI
 92% RESOLUTION

400MB/SQ. IN.
 EPR-IV

0s		100ns/div		1µs	
GPIB	RS-232-C	Hardcopy	Ident	Page to	Rem
Talk Only	9600 baud	Alt.		Utility 1	Wfm 2
14		HiRes			ST018
Extended	Self		Horizontal	Horizontal	
Diagnostic	Test		Magnify	Zoom	Pos Gr
			1	On	0
			x		pts

PW₅₀ AT 1 μINCH

FOR A KARLQUIST HEAD, THE MINIMUM ARCTANGENT TRANSITION LENGTH, a , IS GIVEN BY:

$$a = \frac{4\pi M_R \delta}{2\pi H_C}$$

FOR A REMANENCE OF 7000 GAUSS, THICKNESS OF 2 μINCH, AND COERCIVITY OF 1300 OERSTEDS,

$$a(\text{MIN}) = 1.7 \mu\text{INCH}$$

THE MEASURED PW₅₀ AT 1 μINCH IS 12.7 μINCH ($G' = 10 \mu\text{in}$, $\delta = 2 \mu\text{IN}$)

$$PW_{50} = (G^2 + 4(d + a)(d + a + \delta))^{1/2}$$

$$PW_{50} = 12.3 \mu\text{IN}$$

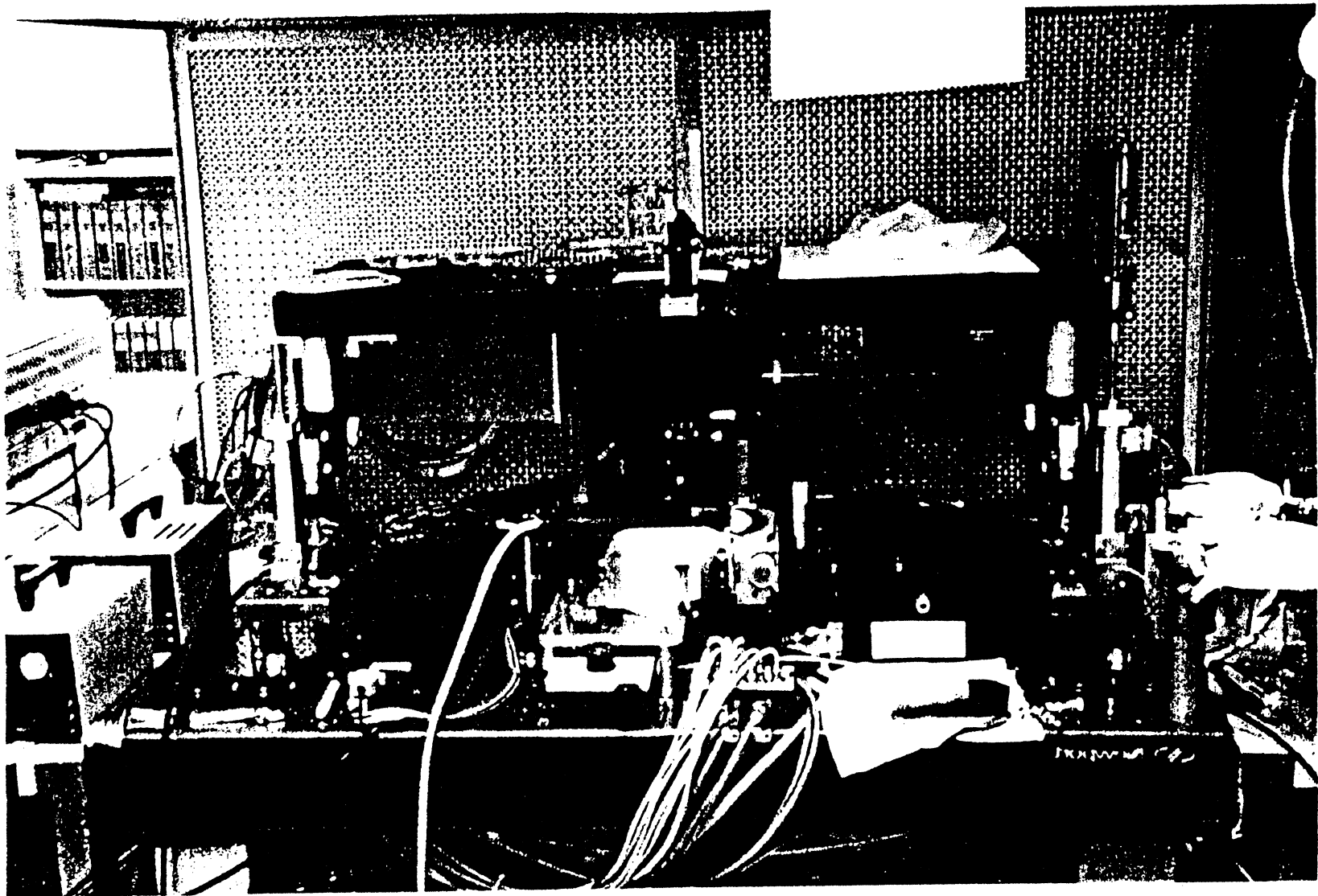
THE CLOSE PROXIMITY OF THE HEAD IMAGES OUT THE DEMAG FIELDS FOR MINIMAL a

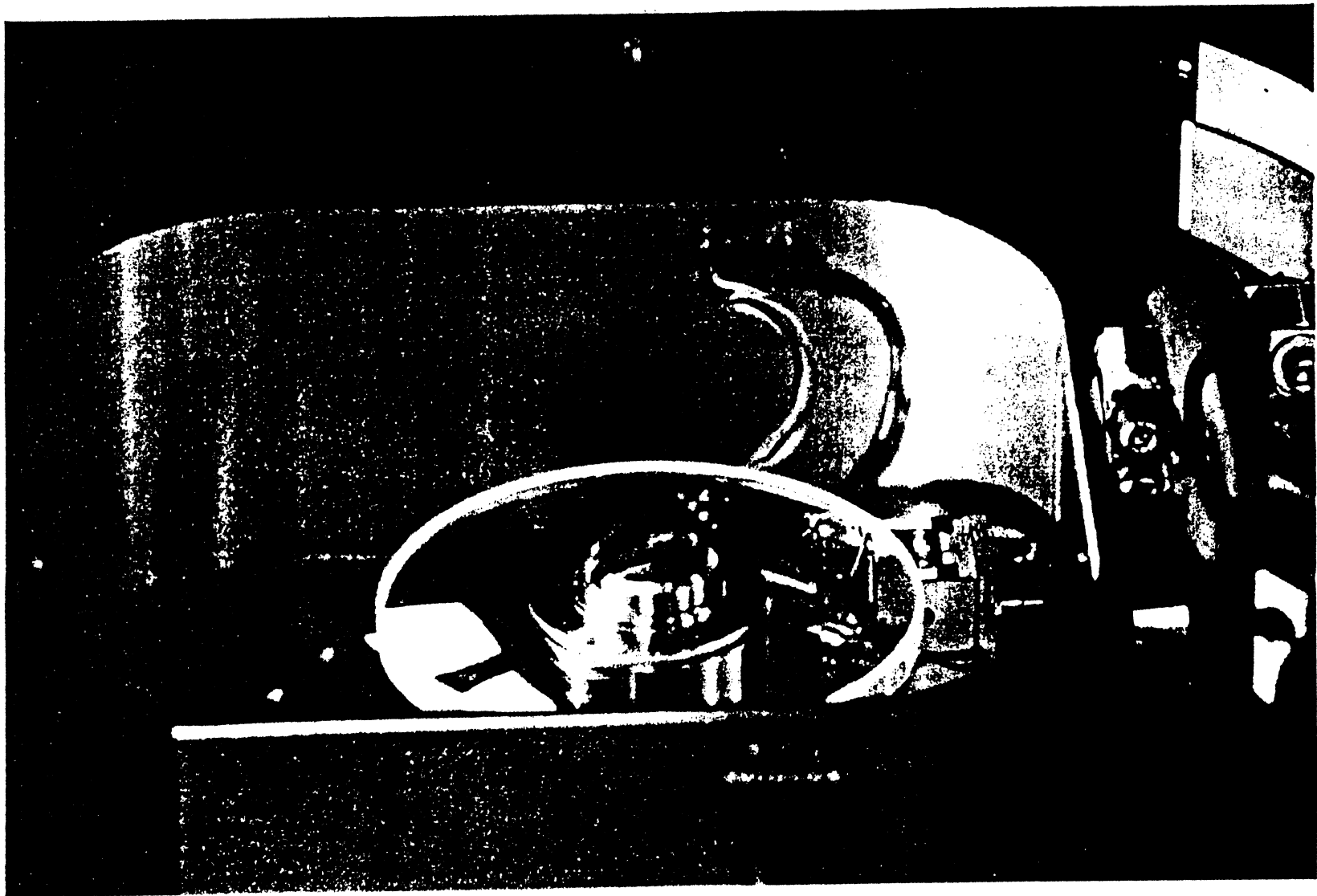
MEASUREMENT TECHNIQUES AND PROBLEMS

MAGNETIC SPACING LOSS

- WALLACE EQUATION NOT VALID DUE TO NON-UNIFORM MAGNETIZATION
- RECORD SPACING LOSS INDETERMINATE (BEARDSLEY AND JEFFERSON '88 UNPUBLISHED)
- CALIBRATE MAGNETIC SPACING FOR DISK AND HEAD WITH INTERFEROMETER
- DETERMINE a PARAMETER FROM PW_{50}
- REVERSE HEAD TO MEASURE FRONT AND REAR MAGNETICALLY
- CORRECT FOR a PARAMETER AND CORRELATE WITH OPTICAL

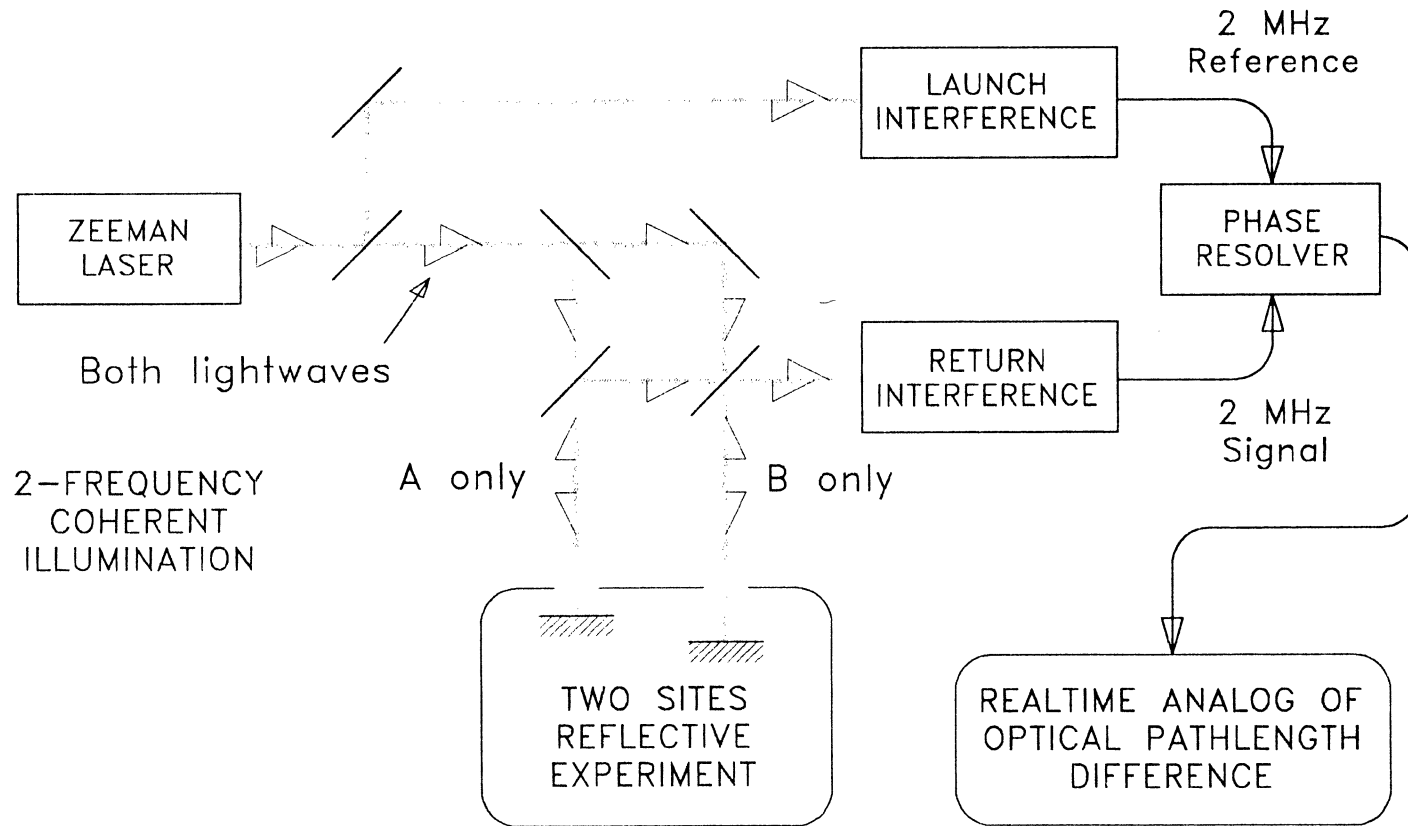






OPTICAL TRACKING OF THE HEAD-DISK SEPARATION

INSTRUMENTATION CONCEPT



RESOLUTION: $\lambda/512$ (.05 microinch)
REFRESH RATE: 32,000 Samples per second.

TRACKING HEAD-DISK SEPARATION THROUGH THE DISK MEASUREMENT ALGORITHM

STEP ONE:

Slider out of the way,
Acquire reference.

R1 only.

Glass

Liquid

Simple echo, from high
index to low index,
no phase reversal.

STEP TWO:

Slider intercepts beam,
Acquire signal.

Vector sum, $R1+R2$

Glass

Liquid

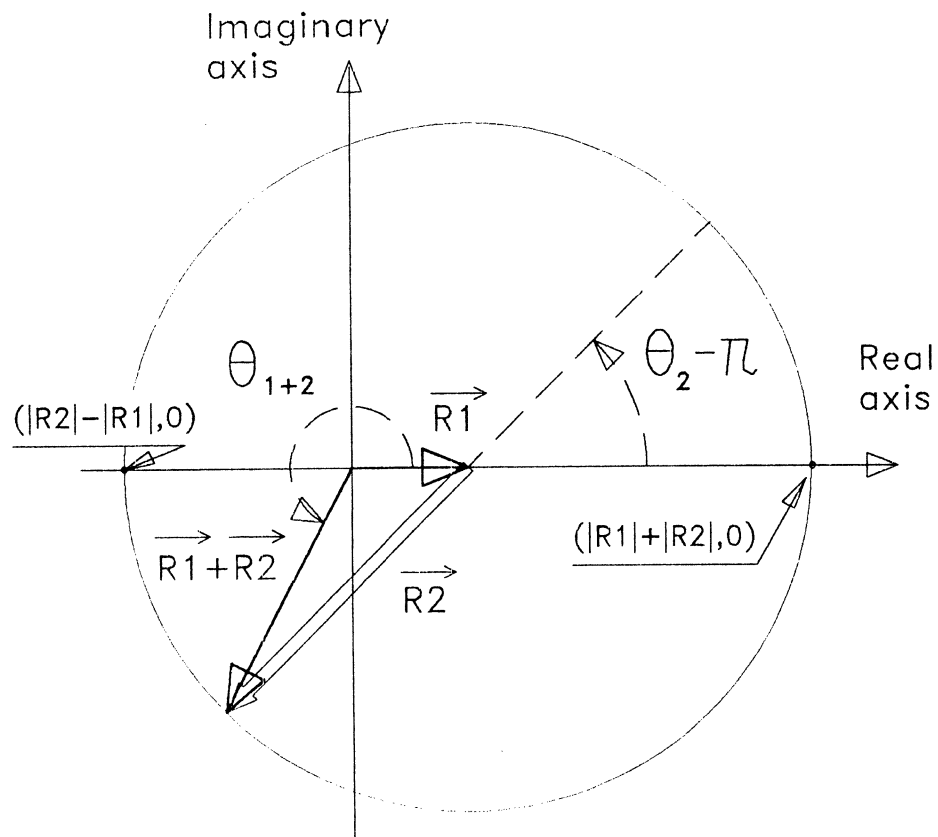
Slider

Two-component echo:
1. Same as step one, plus
2. Slider echo (stronger in
amplitude, with 180 deg.
phase reversal.)

STEP THREE: Calculate separation. (next slide)

OBTAINING SEPARATION FROM THE LIGHTWAVE DATA

VECTOR REPRESENTATION



The angle θ_2 is proportional to the separation.

The vector R_1 was acquired in step 1, and $R_1 + R_2$ (vector) was acquired in step 2.

Simple trigonometry will resolve θ_2 as a function of the two data vectors.

$$\theta_2 = \theta_{1+2} - \pi + \arcsin \left[\frac{|R_1|}{|R_2|} \sin(\theta_{1+2}) \right]$$

"Magnetic Head Testing"

Ralph Simmons

Hewlett Packard

Institute for Information Storage Technology

Santa Clara University, California

December 14 - 16, 1992

OUTLINE

Why Test Heads ?

Characterization of Tester

Head Tests for Advanced Channels

MR Head Tests

Case Study:

Sensitivity to Write Current

Summary

WHY TEST HEADS ?

Head Manufacturing Process Control

Pass/Fail to Head Customer Specifications

Failure Analysis

Head Design/Process Changes

Product Development

Customer Incoming Inspection

Drive Line Failure Analysis

Technology Development

3

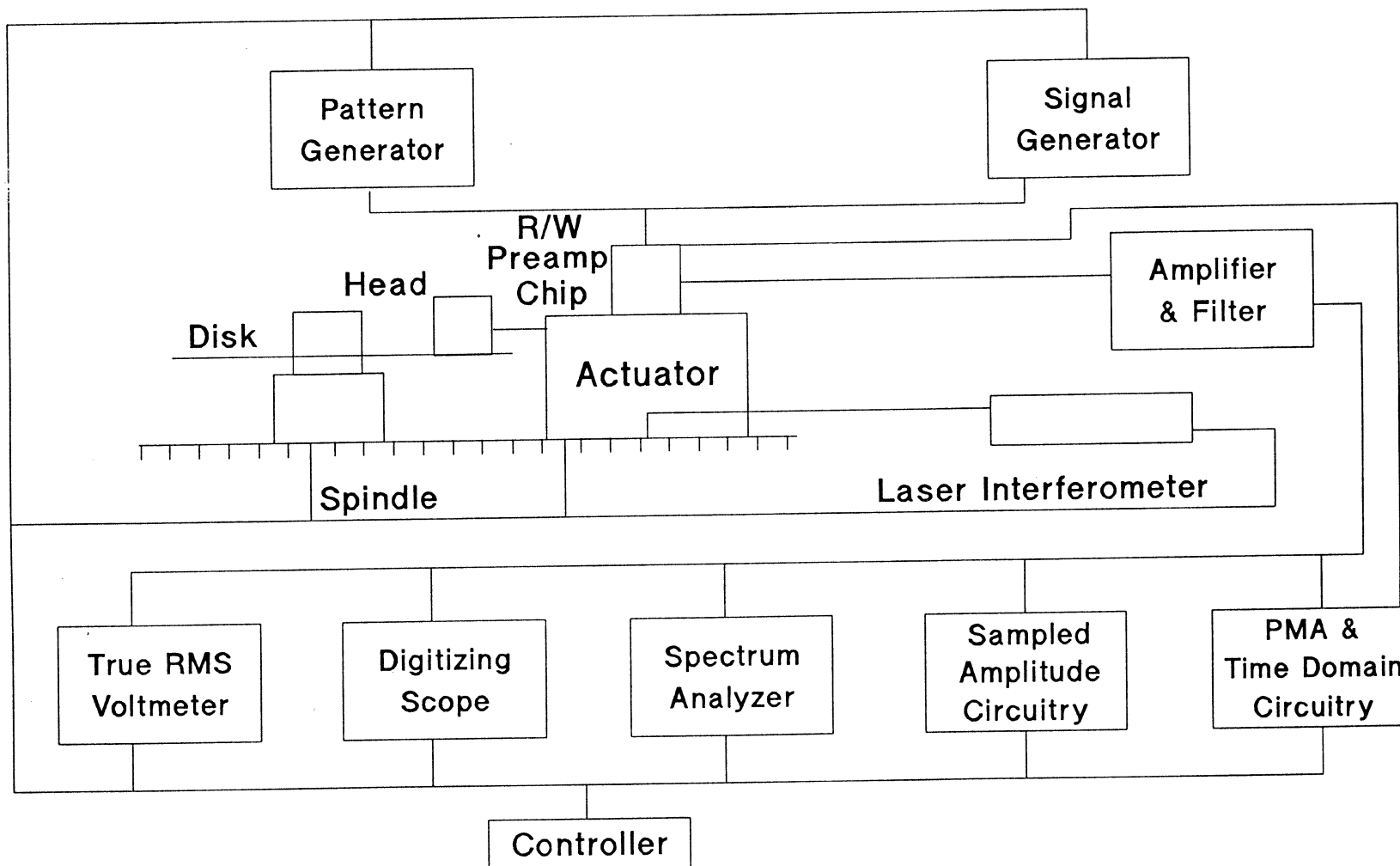
Research and Development Tester Requirements

Voltage versus Time: 8 Bit Amplitude Resolution
 1 GigaSample/sec Timing
 64 kSample Record Size

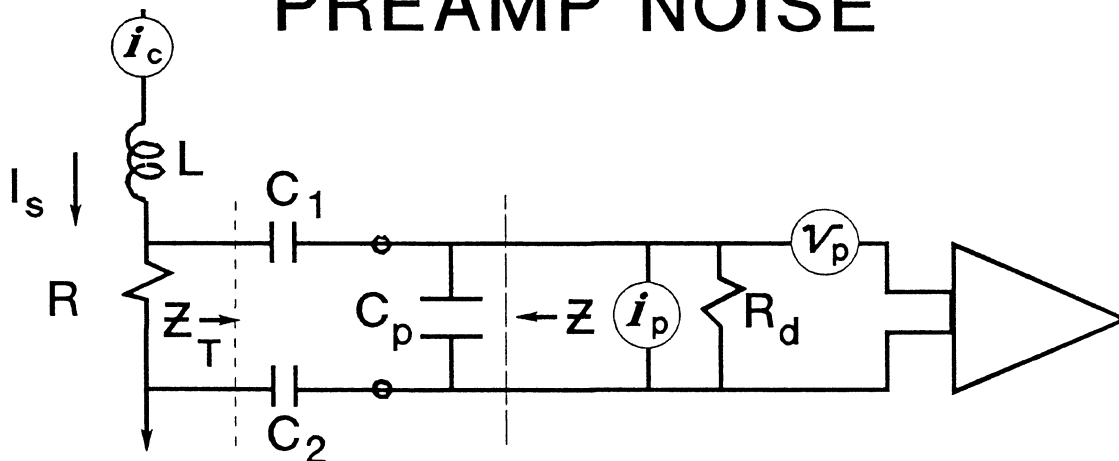
4 Time Interval Tests: 150 psec Resolution
 135 nsec Rearm

Radial Positioning: 0.1 mm Absolute
 0.1 um Relative

Typical Head Tester



PREAMP NOISE



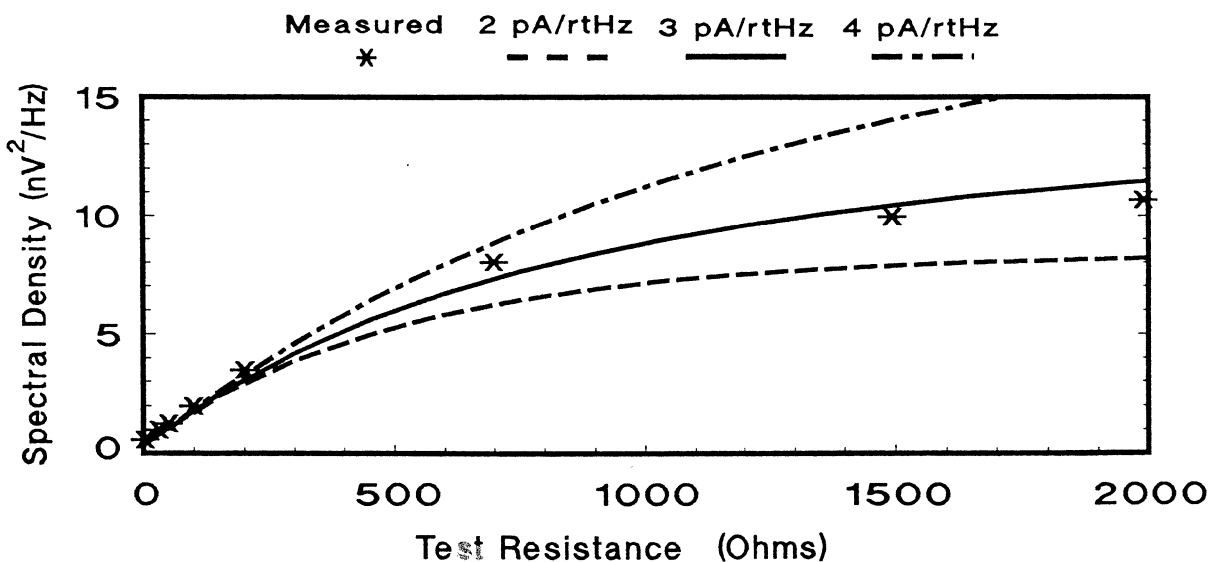
- Resistor Noise Density

$$V_R^2 = 4kT \operatorname{Re}(Z) \left| \frac{R_d}{R_d + Z} \right|^2$$

- Total Noise Density

$$V^2 = V_p^2 + V_R^2 + i_p^2 \left| \frac{R_d Z}{R_d + Z} \right|^2 + i_c^2 \left| \frac{R Z_T}{R + Z_T} \right|^2$$

- Measured and Calculated Power Spectral Density

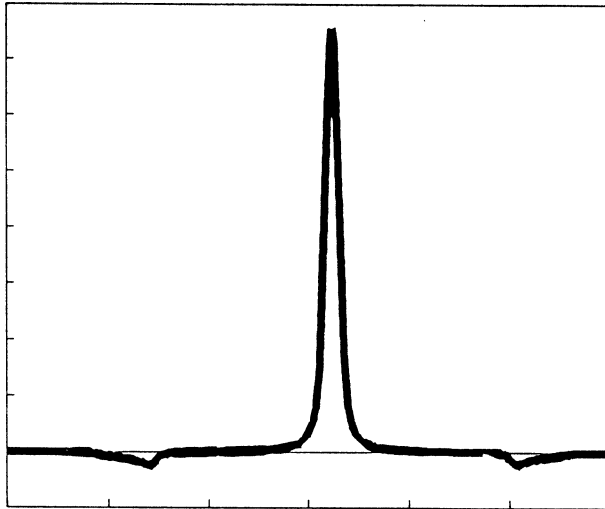


HEAD TESTS FOR ADVANCED CHANNELS

- Isolated Pulse Characterization
- Matched Filter SNR Limit
 - * Definition
 - * Examples

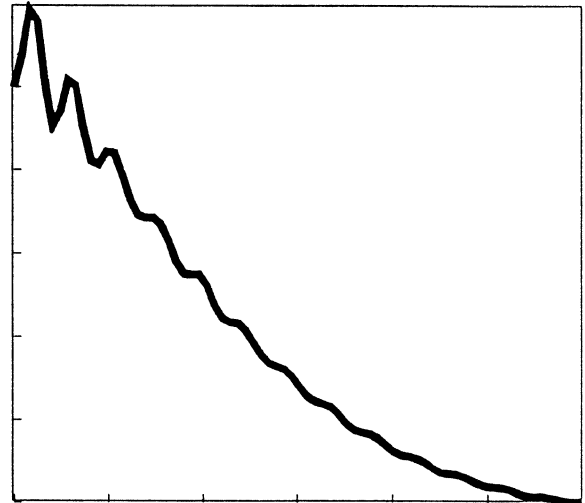
Matched Filter SNR Limit

Isolated Pulse



Time

Filter Transfer Function



Frequency

Peak Signal to rms Noise

$$\frac{V_{op}}{N} = \frac{\left| \int_{-\infty}^{\infty} F(\omega) H(\omega) e^{j\omega t_0} d\omega \right|}{\left\{ \int_{-\infty}^{\infty} n^2 |H(\omega)|^2 d\omega \right\}^{\frac{1}{2}}}$$

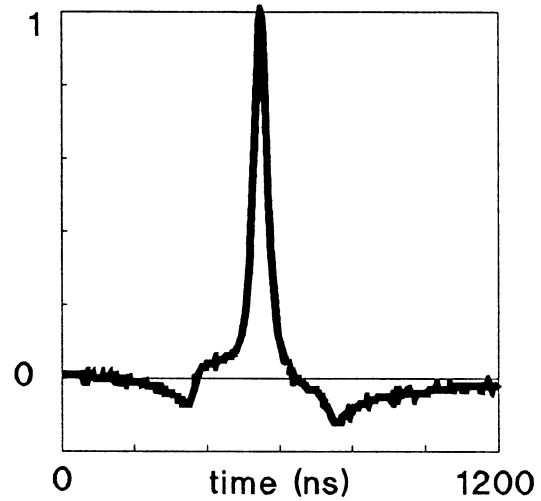
$$\frac{V_{op}}{N} \text{ is Maximum for } H(\omega) = c F^*(\omega)$$

Norman L. Koren, "Matched Filter Limits and Code Performance in Digital Magnetic Recording" IEEE Trans Mag, v27, n6, Nov.1991.

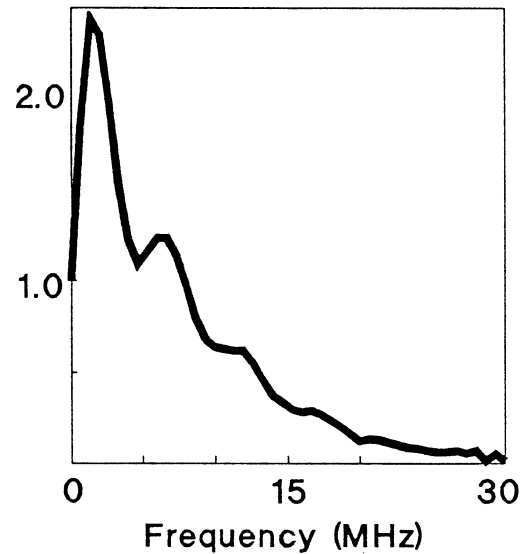
Matched Filter SNR Limit

Inductive: High Velocity

Isolated Pulse



Filter Transfer Function



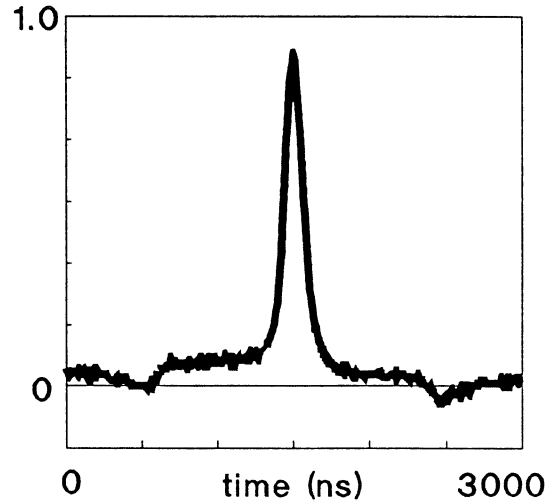
Peak Signal to rms Noise

$$\frac{V_{op}}{N} \longrightarrow 35.3 \text{ dB}$$

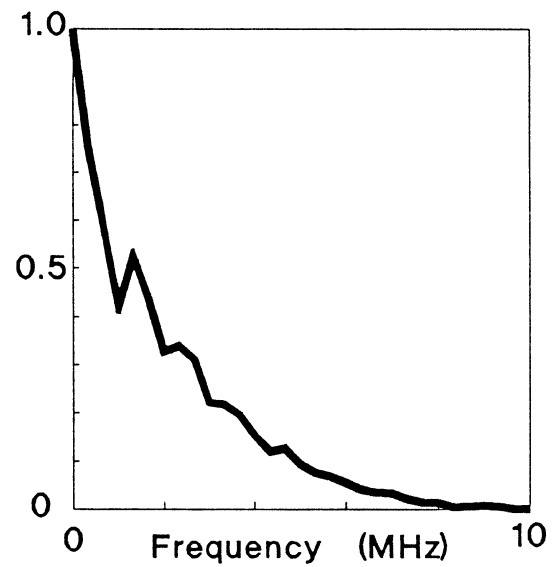
Matched Filter SNR Limit

Inductive: Low Velocity

Isolated Pulse



Filter Transfer Function



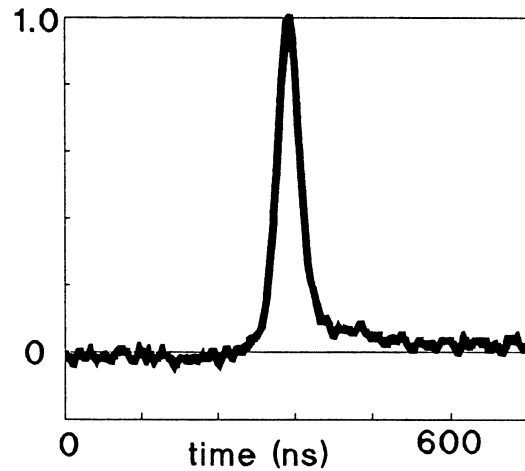
Peak Signal to rms Noise

$$\frac{V_{op}}{N} \longrightarrow 29.3 \text{ dB}$$

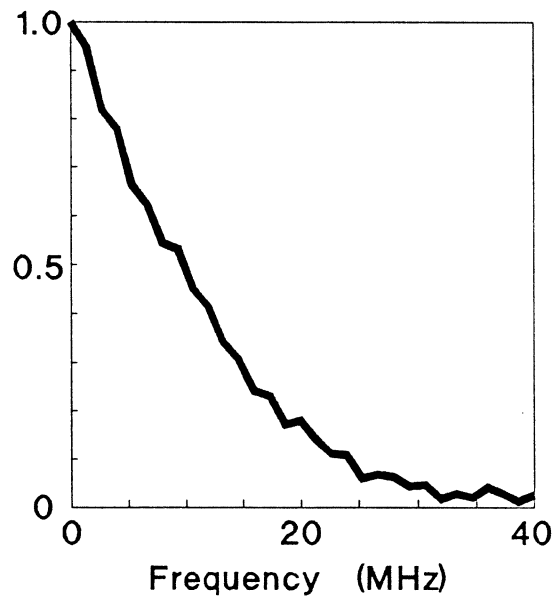
Matched Filter SNR Limit

Magnetoresistive

Isolated Pulse



Filter Transfer Function



Peak Signal to rms Noise

$$\frac{V_{op}}{N} \longrightarrow 34.8 \text{ dB}$$

MR HEAD TESTS

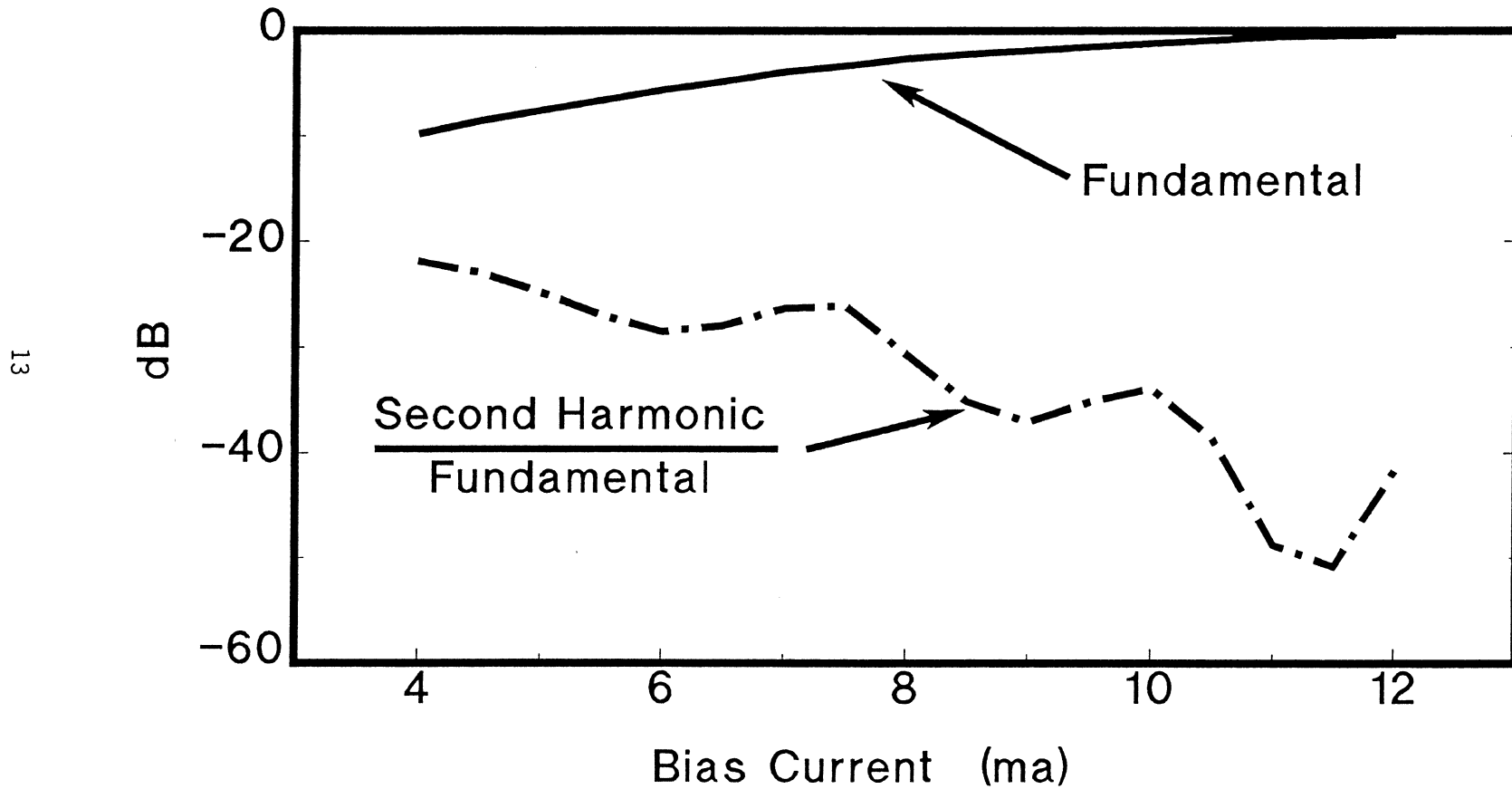
- Bias Current Choice
 - * Second Harmonic Distortion

- Track Density Capability
 - * Data
 - * Servo

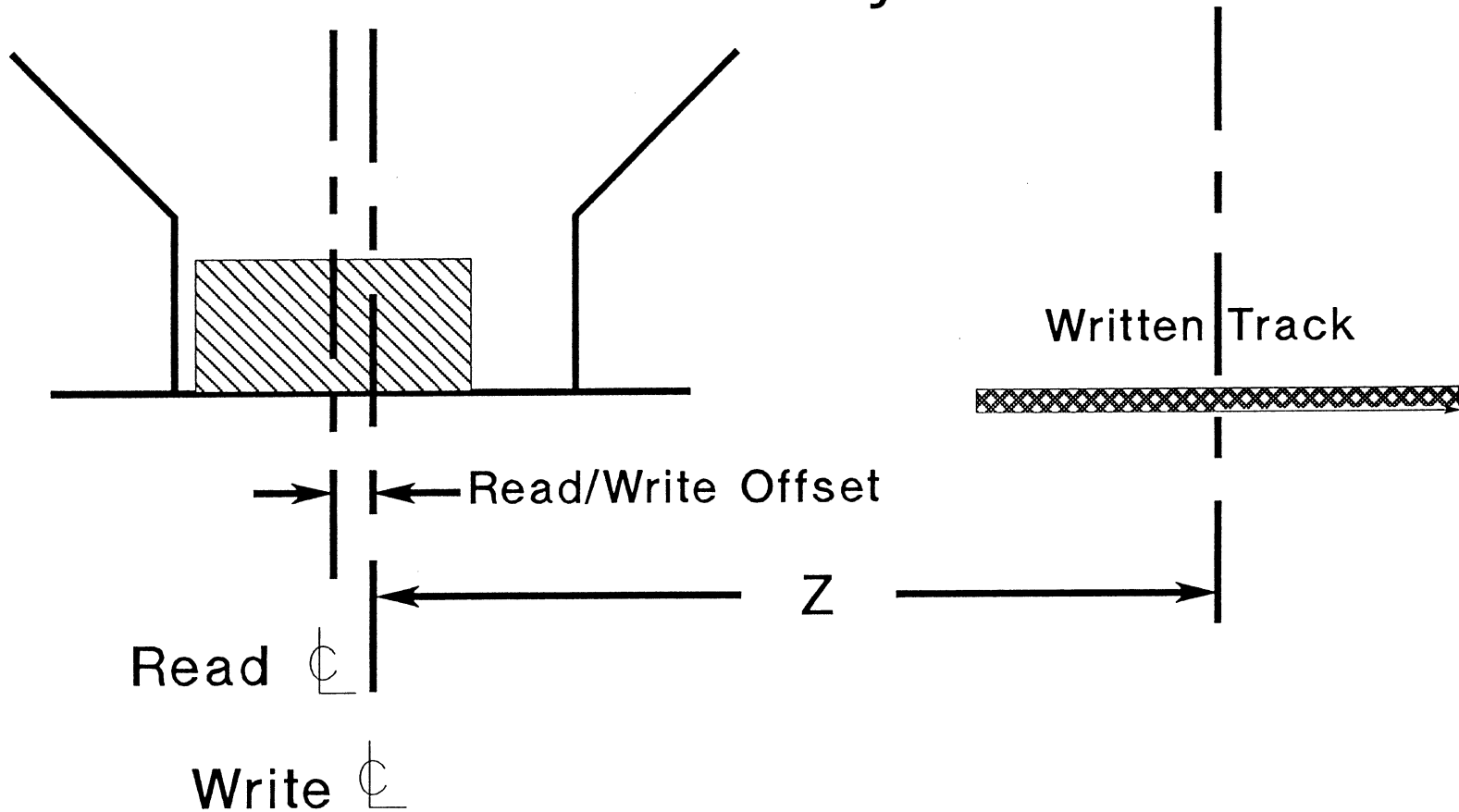
- Case Study:
 - * MR Head Write/Read Stability

Second Harmonic versus Bias Current

Dual Stripe MR Head

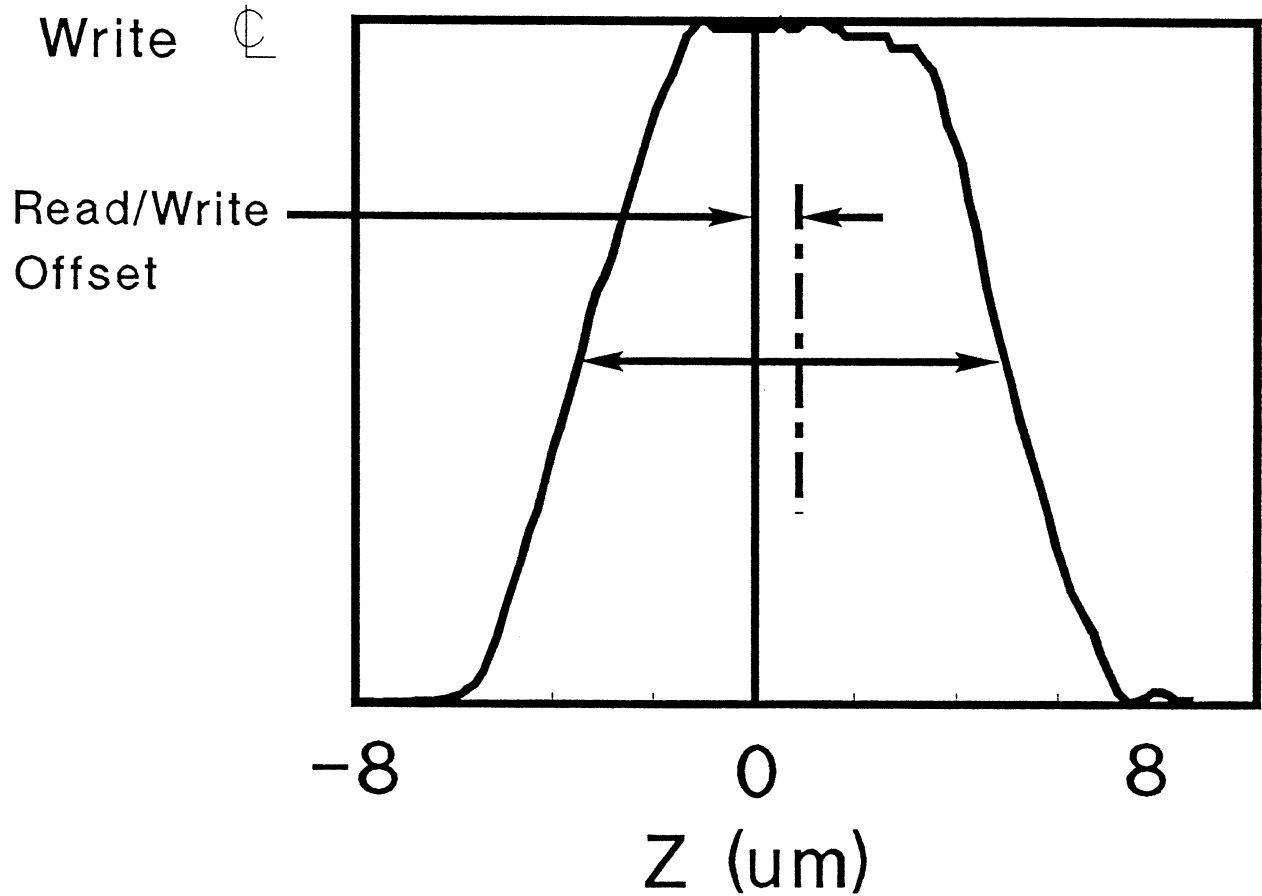
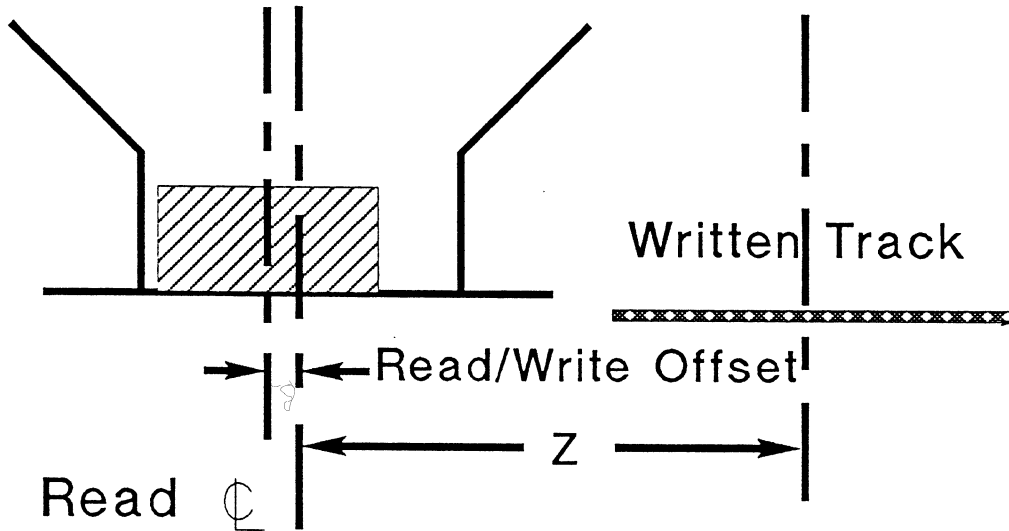


Read/Write Cross Track Capability Geometry

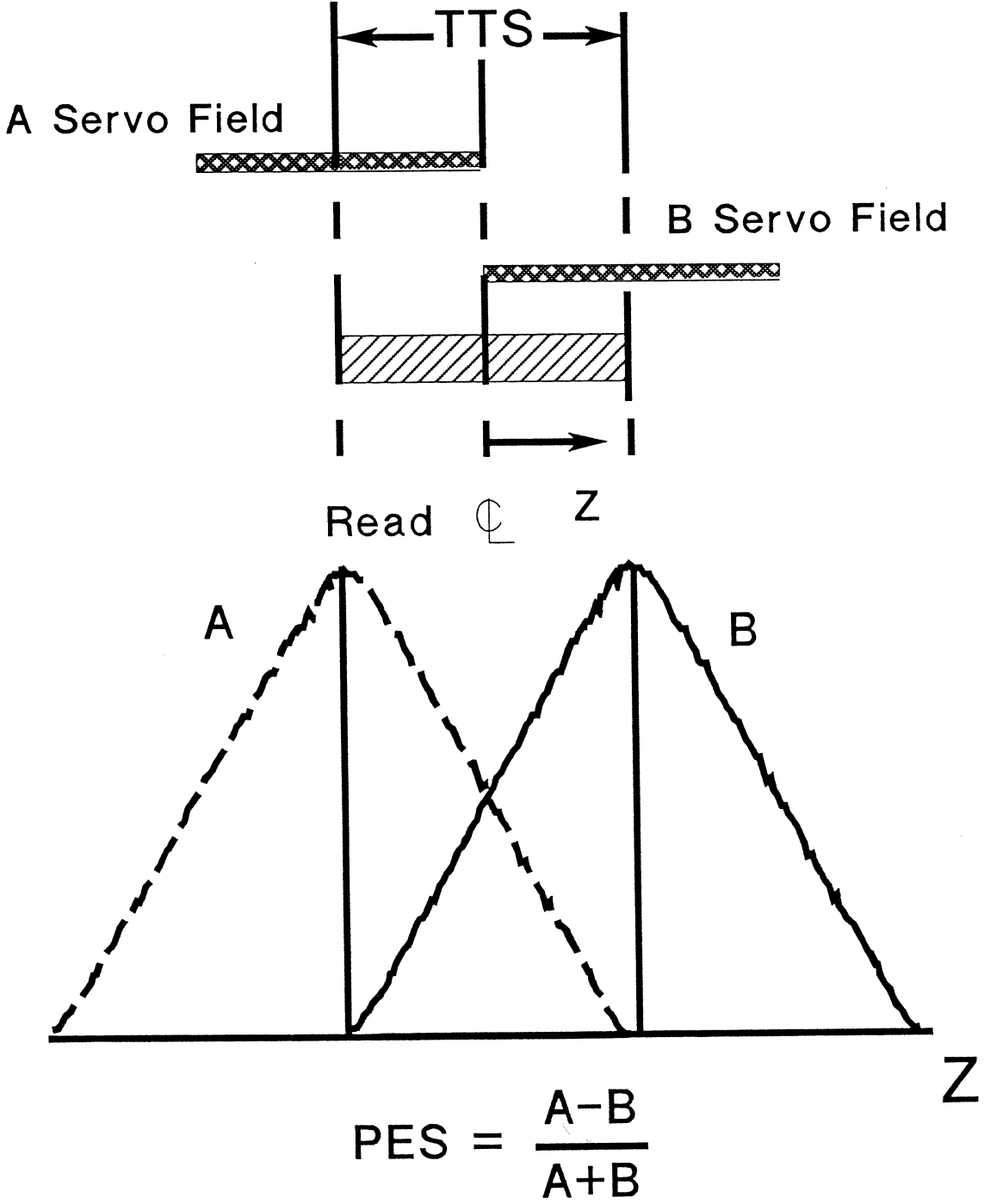


14

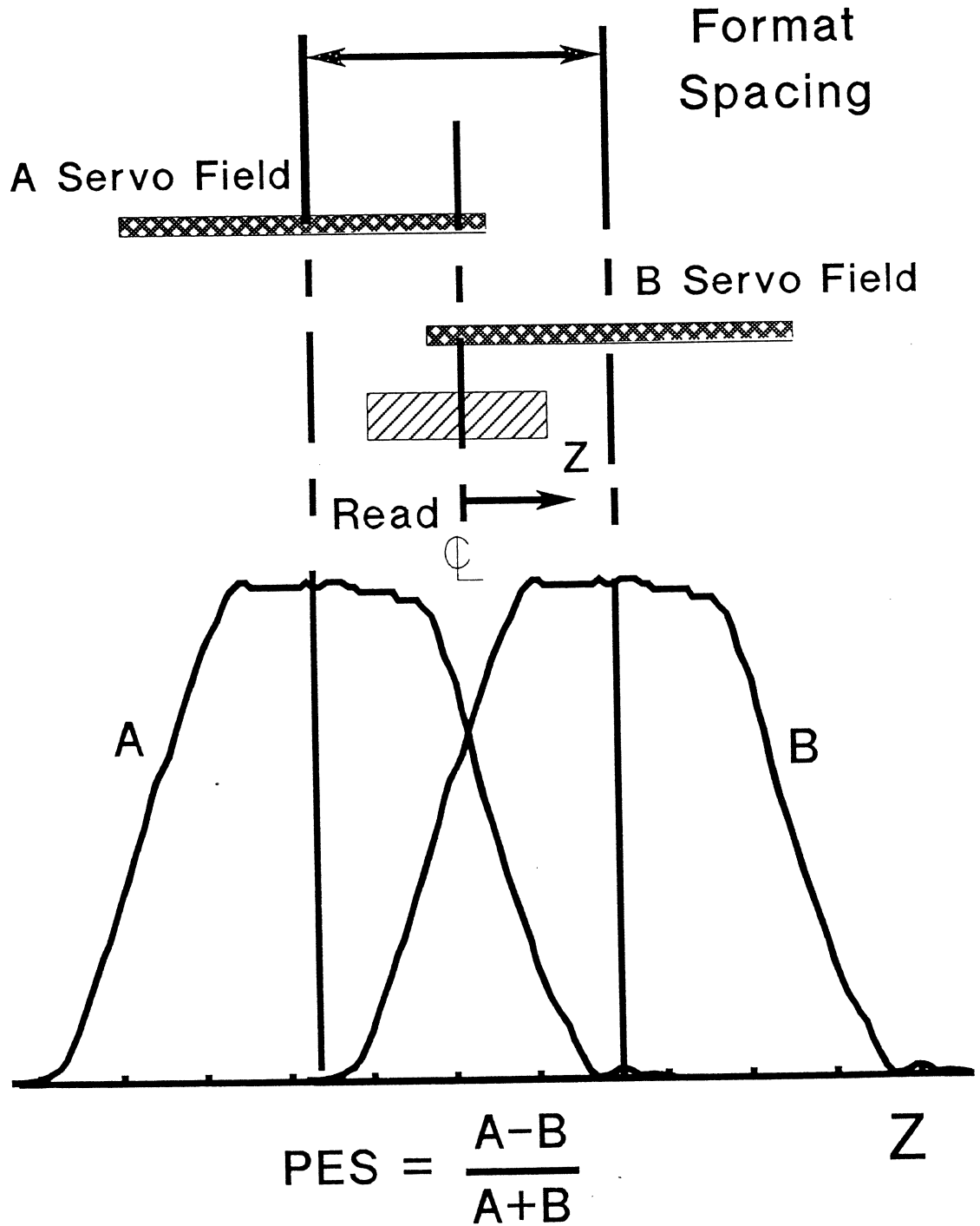
Read/Write Cross Track Capability Track Scan



Read/Write Cross Track Capability Servo

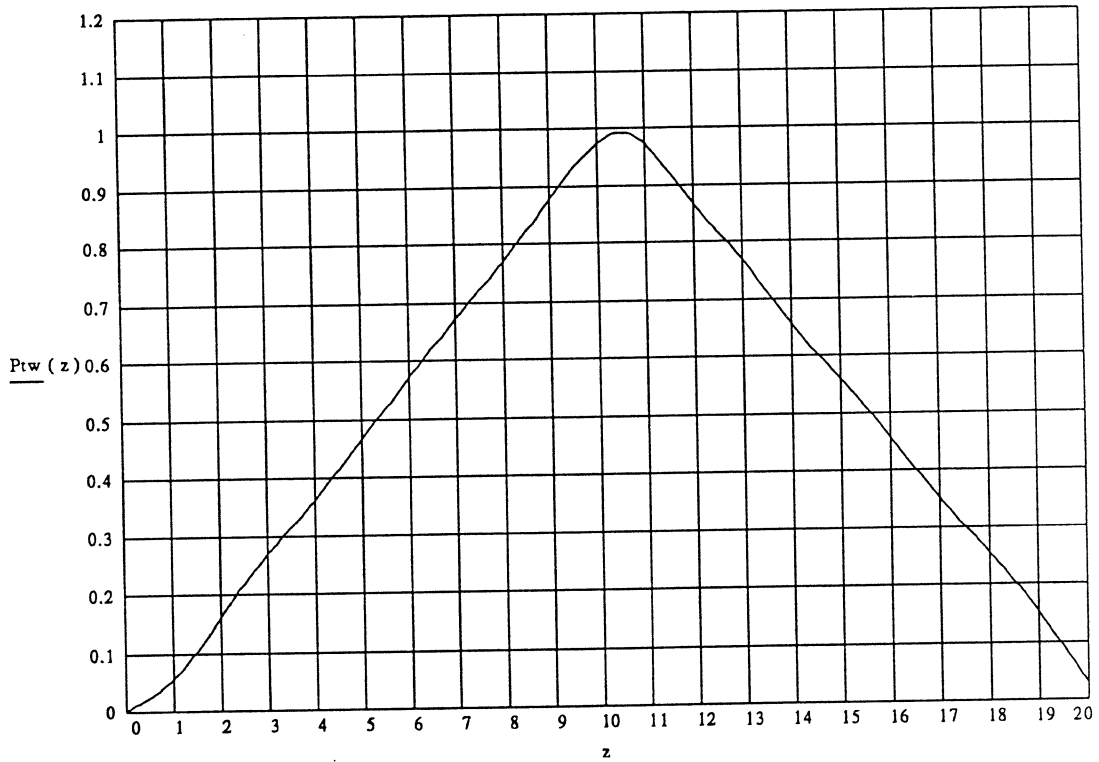


Read/Write Cross Track Capability Servo



Cross Track Scan

Thin Film Inductive Head



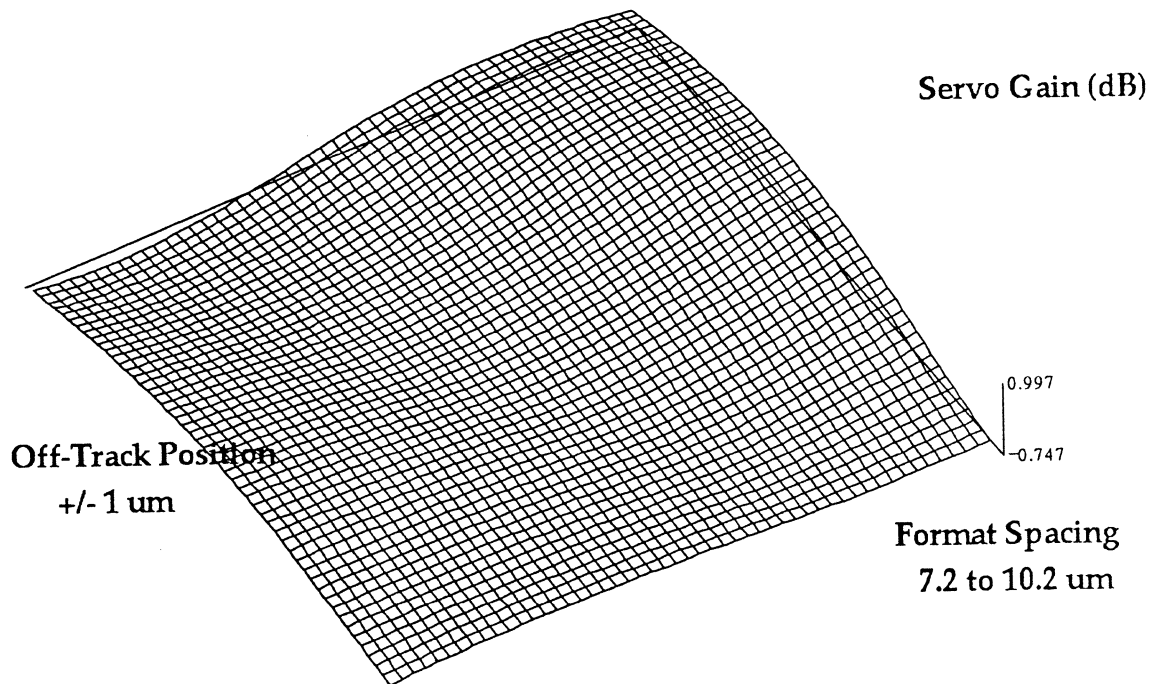
Disk Memory Division
VIST92I.GAL

R. Simmons
11/14/92



Servo Gain Surface Plot

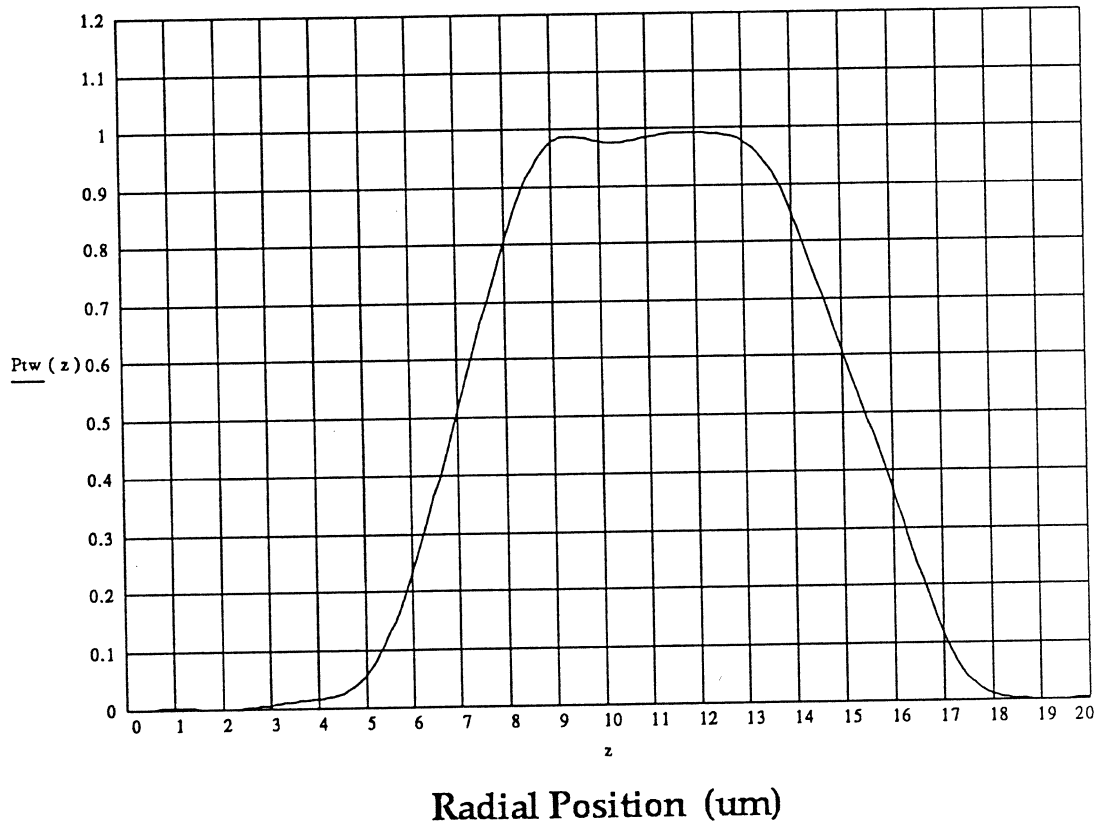
Servo Gain versus Format Spacing and Off-Track Position
Thin Film Head 80 tracks/mm



SurfGain

Cross Track Scan

Dual Stripe Magnetoresistive Head



Disk Memory Division
VIST92L.GAL

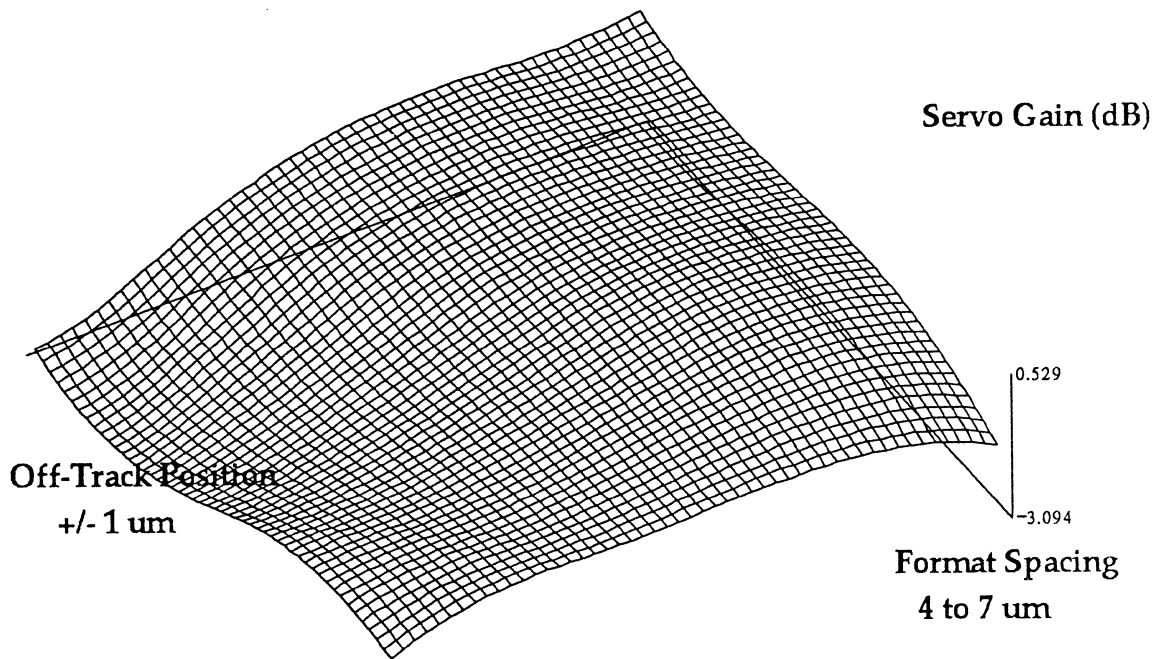
R. Simmons
11/14/92



Servo Gain Surface Plot

Servo Gain versus Format Spacing and Off-Track Position

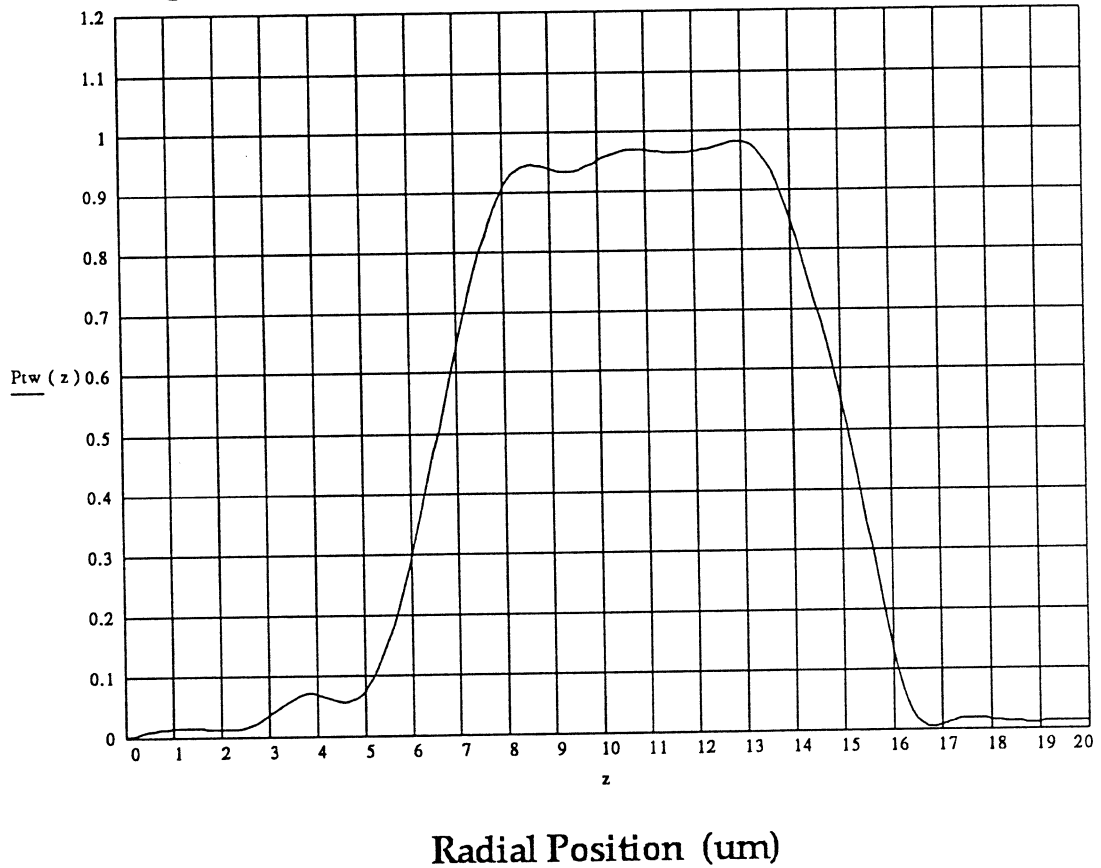
Dual Stripe Magnetoresistive Head
160 tracks/mm



SurfGain

Cross Track Scan

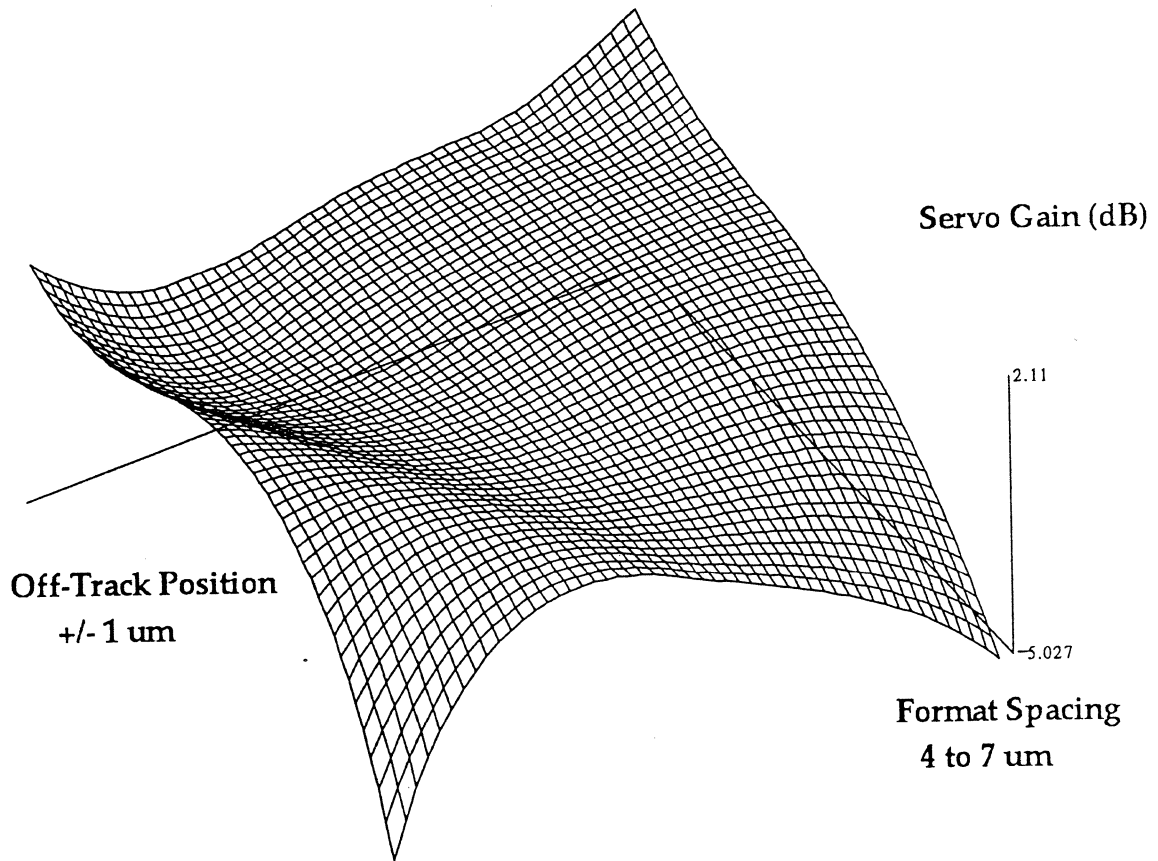
Single Element Magnetoresistive Head



Servo Gain Surface Plot

Servo Gain versus Format Spacing and Off-Track Position

Single Element Magnetoresistive Head
160 tracks/mm



SurfGain

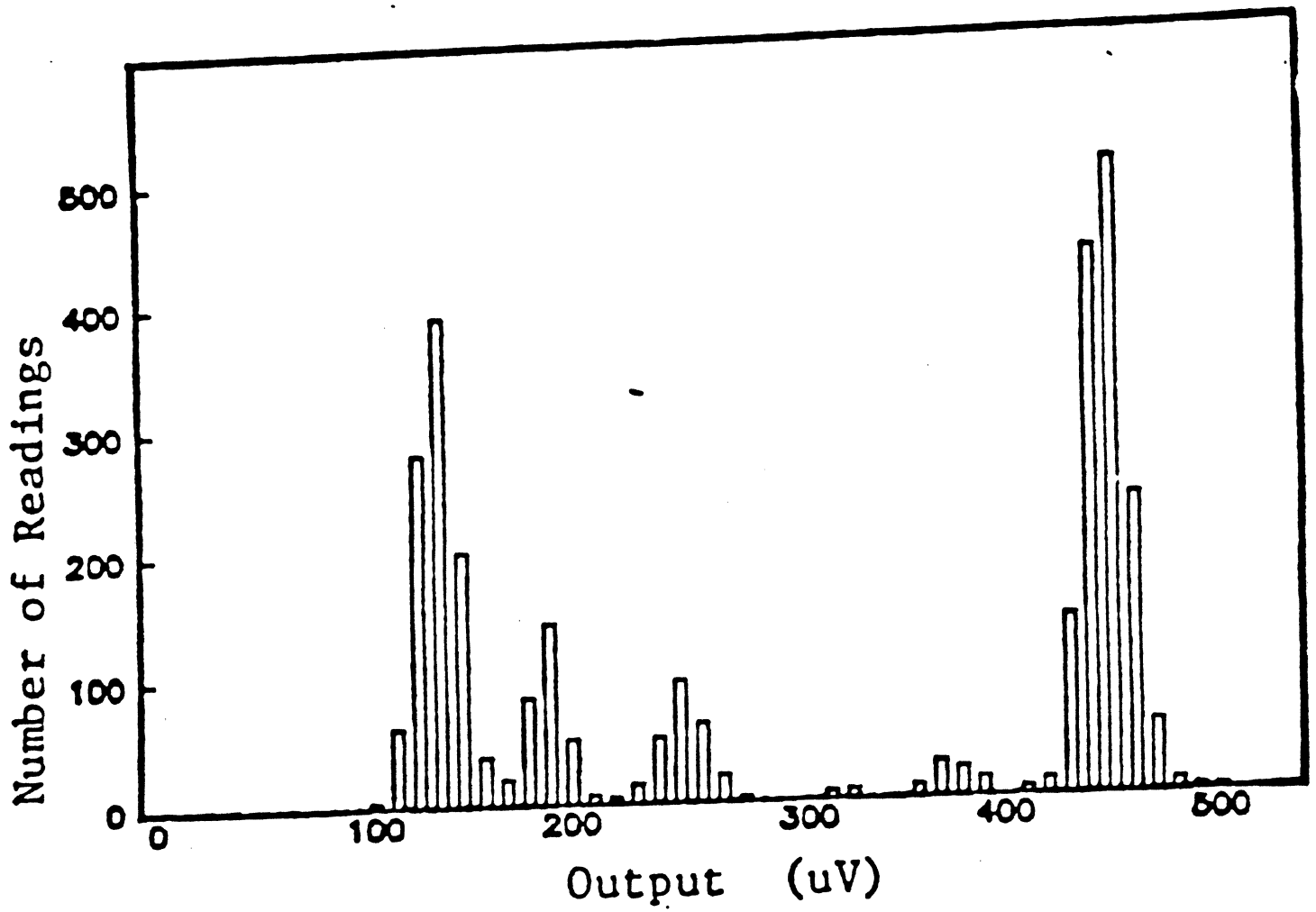
Case Study - Multidomains In Magnetoresistive Heads

- Recording System
 - . Barber Pole Bias Magnetoresistive Head
 - . 1000 TPI
 - . 12000 BPI

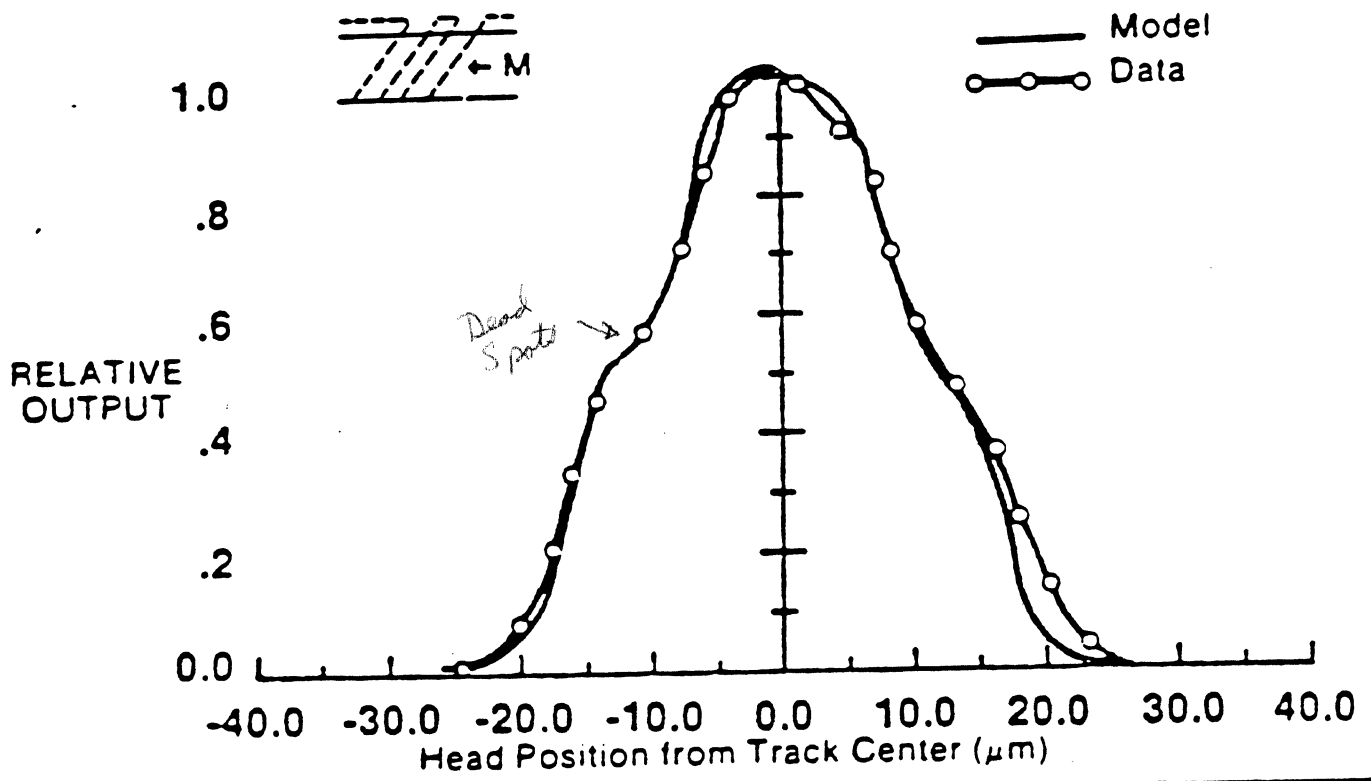
- Failure Symptom
 - . TAA Values in Write/Read Tests Form A Discrete Spectrum

 - . Displacement Curves are Distorted

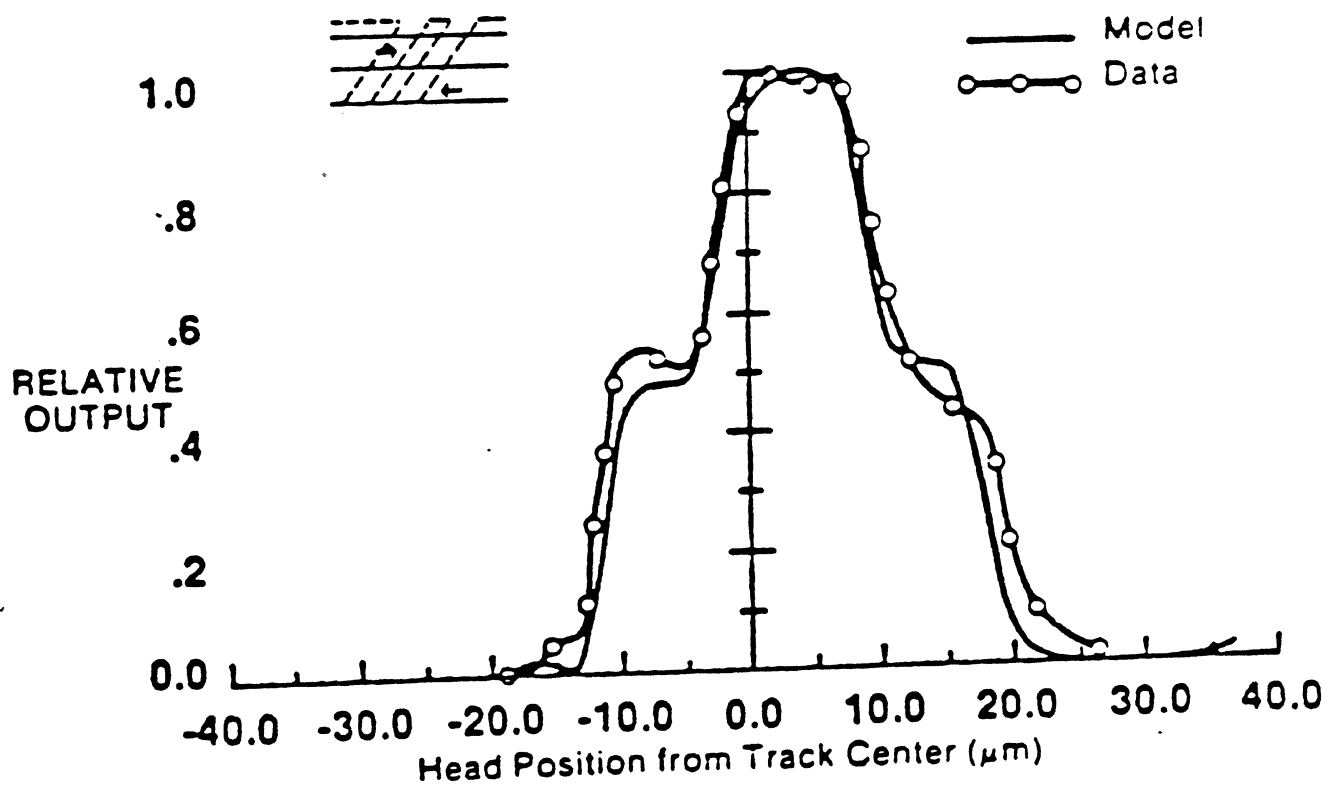
- Cause of Failure
 - . Stripe Domains Created in MR Film By Fields Applied During Write Cycle



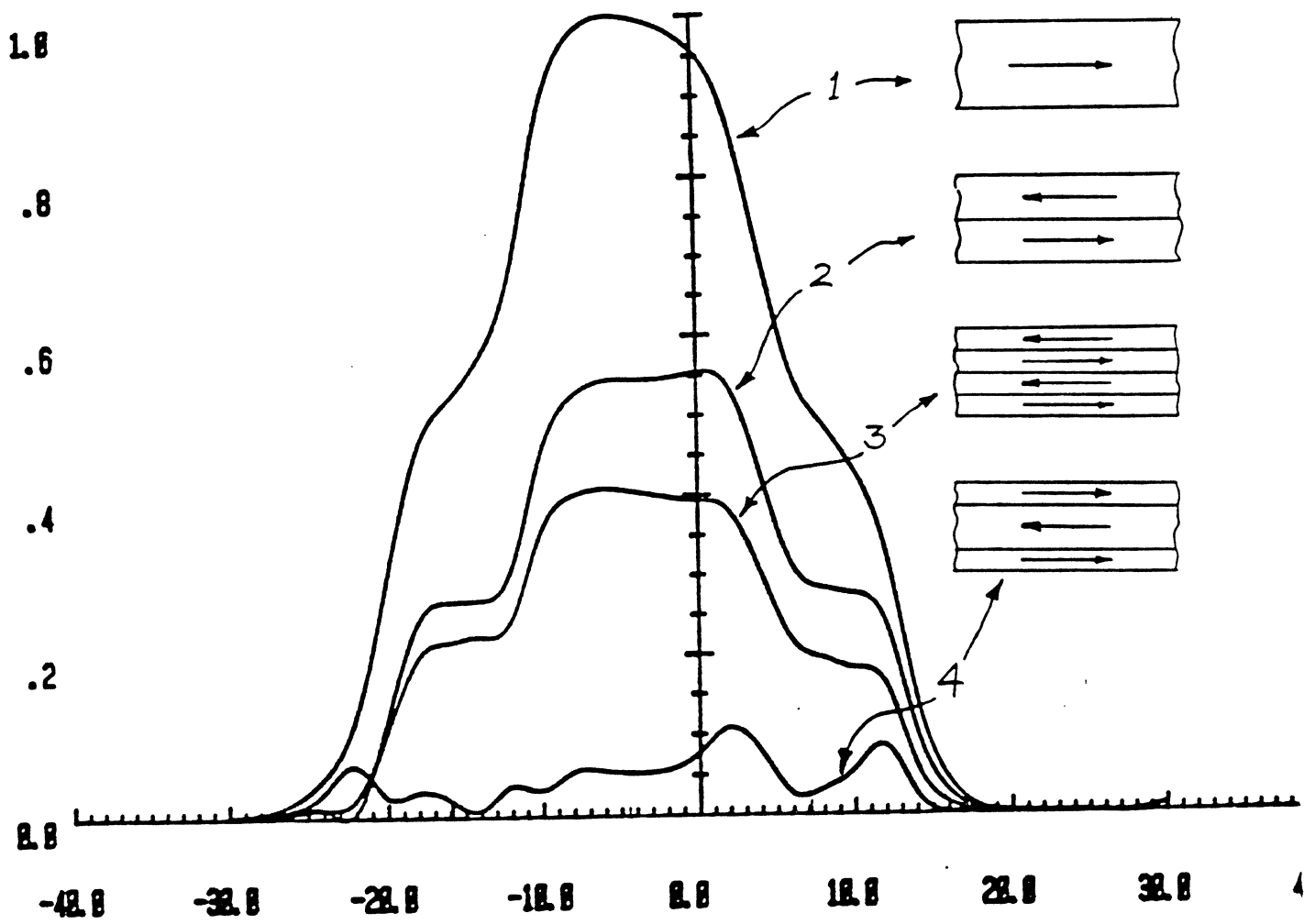
3000
 R/W
 Squares



Displacement Curve — Single Domain



Displacement Curve — Two Domains

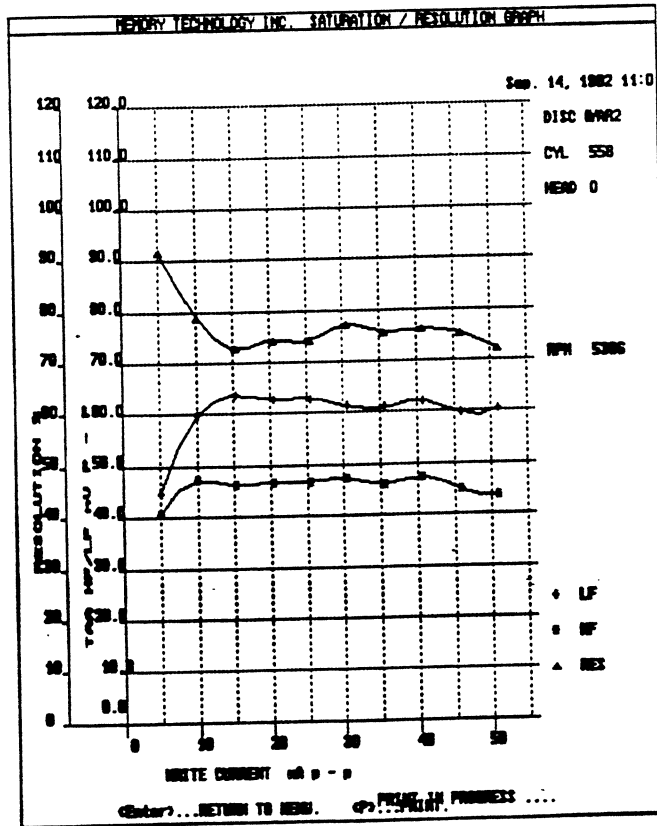
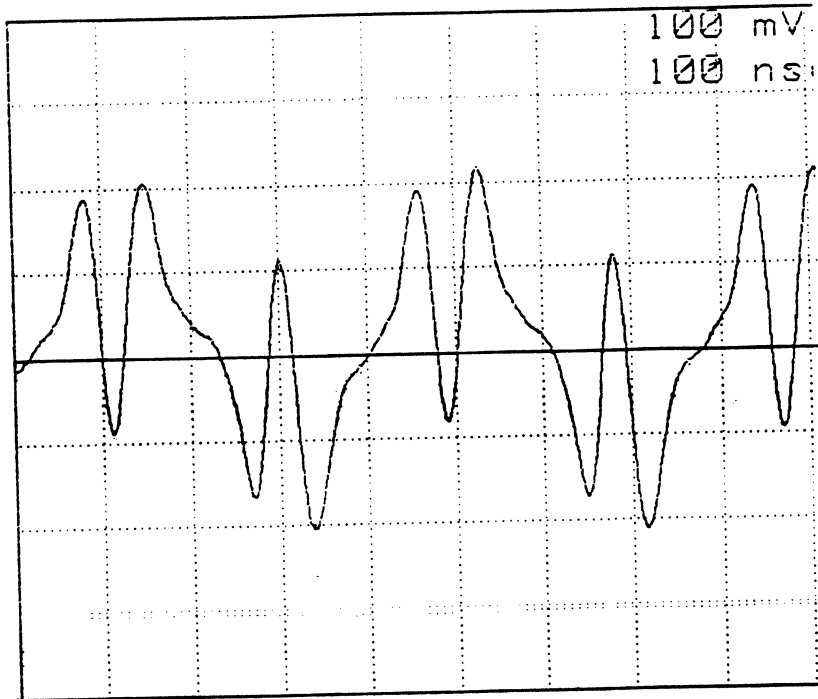


(volts) vs. X (microns) -- PTW37

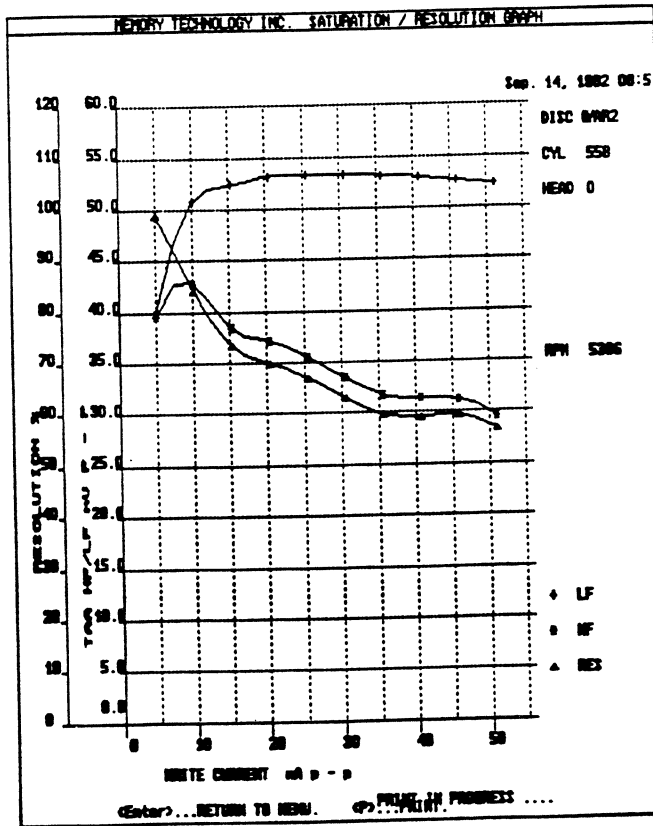
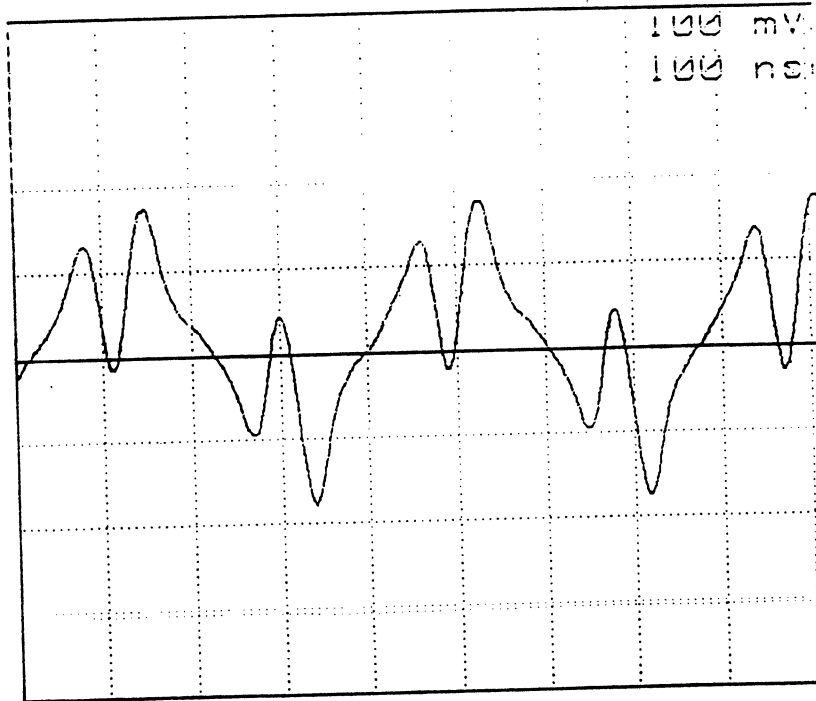
CASE STUDY: WRITE CURRENT SENSITIVITY

- Recording System
 - Inductive Thin Film Head at
52 kbp
- Failure Symptoms
 - Error Rate Failure in Drive
Top Level Testing
- Cause of Failure
 - Pole Tip Saturation at High
Write Current

Typical Head



Failed Head



Write Current Sensitivity

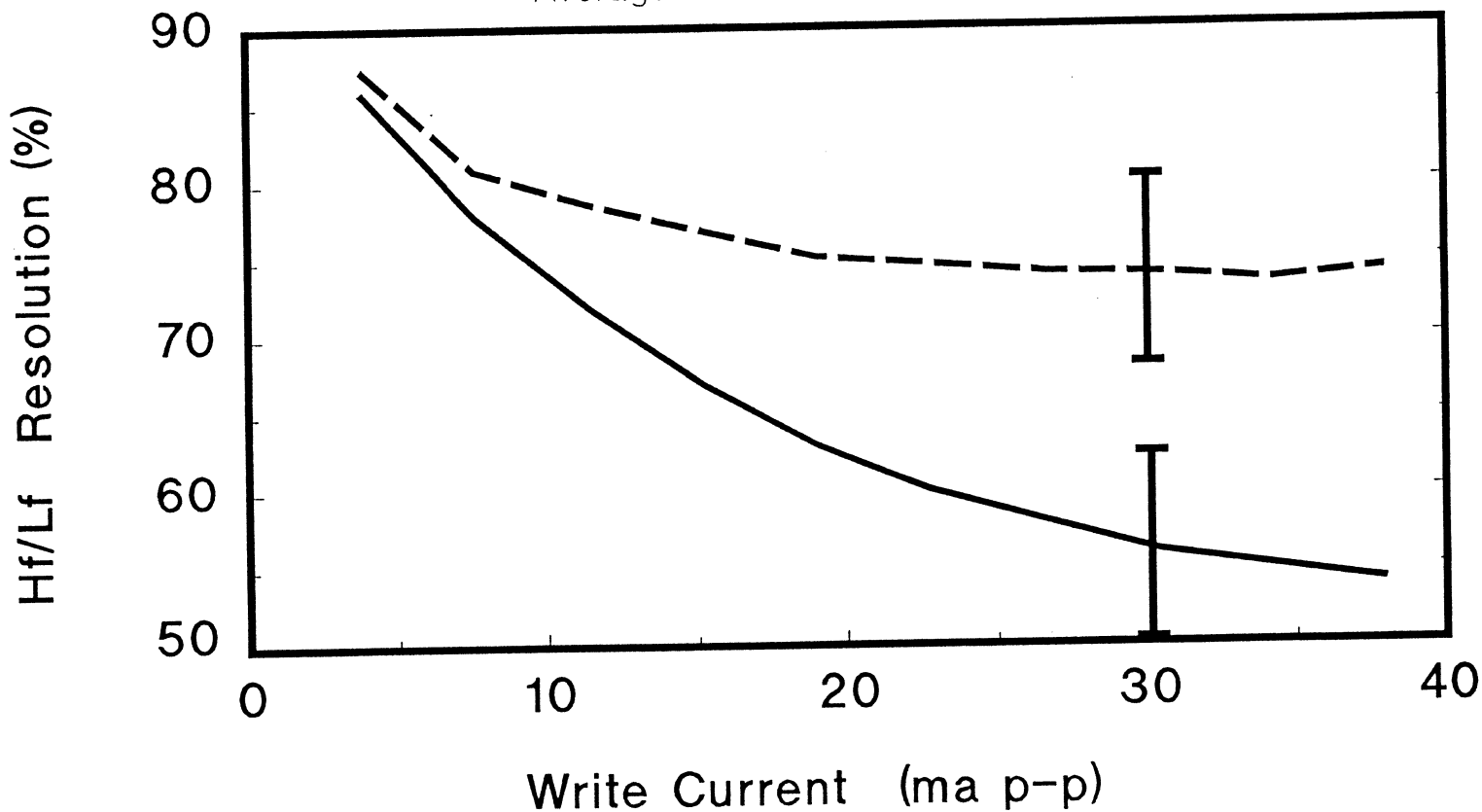
Fail Drive Error Rate

Pass Drive Error Rate

—

- - -

Average of 45 Heads Each



31

SUMMARY

* R & D Tester

* Matched Filter SNR

* MR Head Tests

Read Narrower Than Write

Servo Gain Linearity

* Nonlinear Writing Due to
Pole Tip Saturation

Signal to Noise and Equalization Issues

Tom Howell

Quantum Corp.

Institute for Information **S**torage **T**echnology

Santa Clara University, California

December 14 - 16, 1992

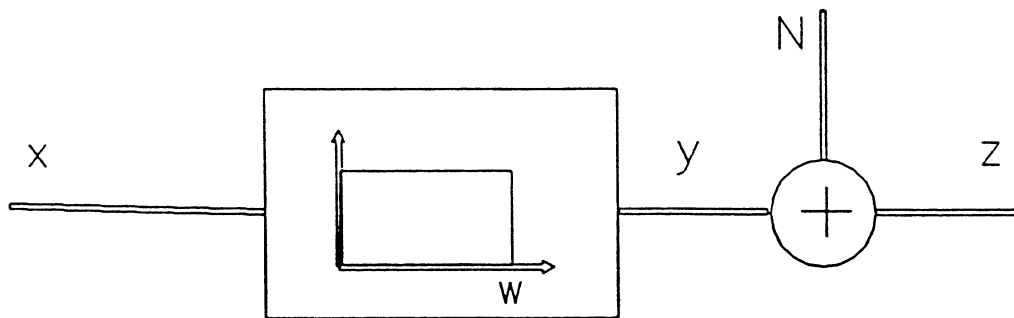
Signal to Noise and Equalization Issues

1. SNR Scaling
2. Signaling and Detection
3. Write Precompensation
4. Adaptive Equalization
5. Trellis Codes

1. SNR Scaling

- The Capacity of a Magnetic Recording System as a Function of Track Width

Simple Channel Model



$$C = W \log_2 \left(1 + \frac{\overline{y^2}}{\sigma_N^2} \right)$$

mean squared
noise

Simple Scaling (Eldridge, 1962)

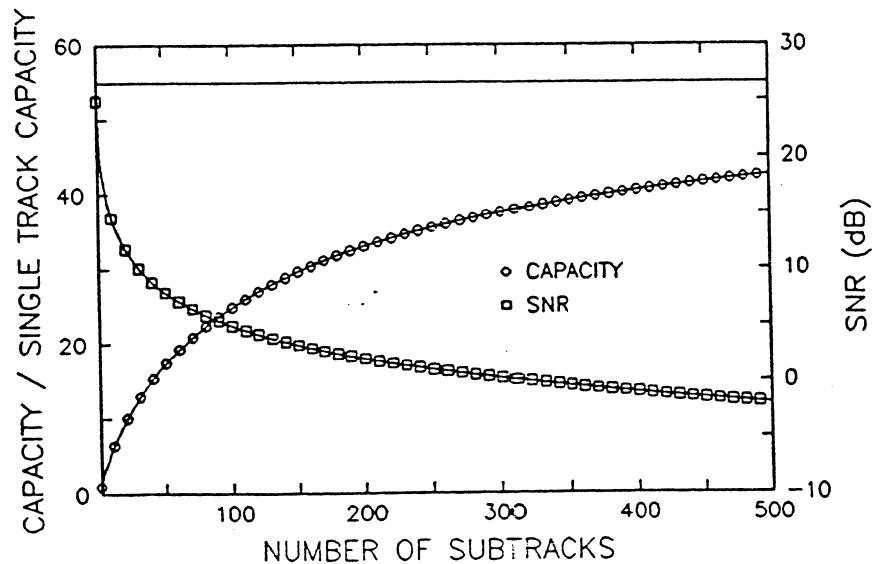
Make track n times narrower

$$\bar{y}^2 \rightarrow \frac{1}{n^2} \bar{y}^2$$

$$\sigma_N^2 \rightarrow \frac{1}{n} \sigma_N^2$$

$$C_n = nW \log_2 \left(1 + \frac{\bar{y}^2 / n^2}{\sigma_N^2 / n} \right)$$

$$C_\infty = \lim_{n \rightarrow \infty} C_n = \frac{W}{\ln 2} \frac{\bar{y}^2}{\sigma_N^2}$$



Some Noise Does Not Scale

Make track n times narrower

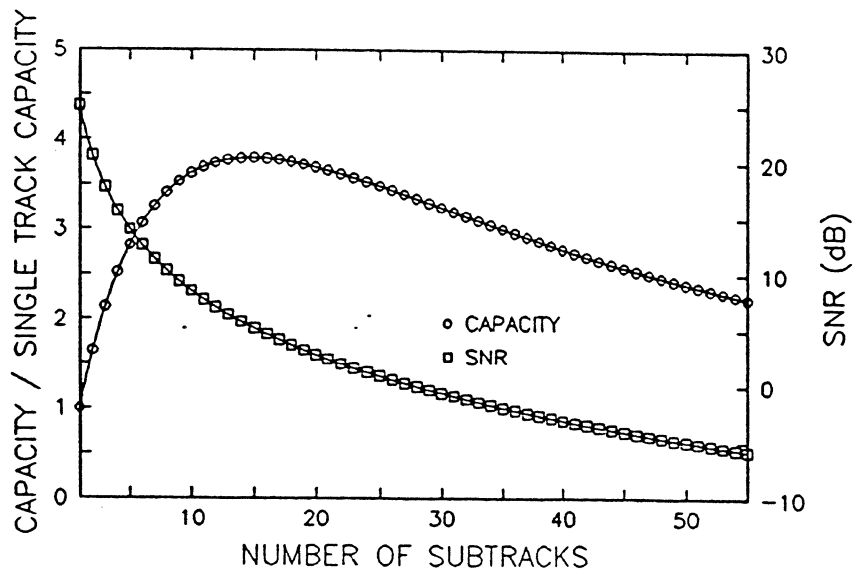
$$\overline{y^2} \rightarrow \frac{1}{n^2} \overline{y^2}$$

$$\sigma_d^2 \rightarrow \frac{1}{n} \sigma_d^2$$

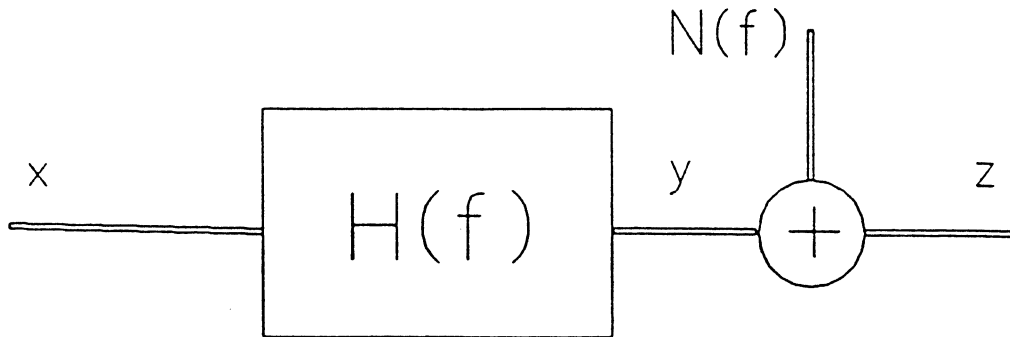
$$\sigma_e^2 \rightarrow \sigma_e^2$$

$$C_n = nW \log_2 \left(1 + \frac{\overline{y^2} / n^2}{\sigma_e^2 + \sigma_d^2 / n} \right)$$

$$C_\infty = 0$$



Water-Filling Calculation



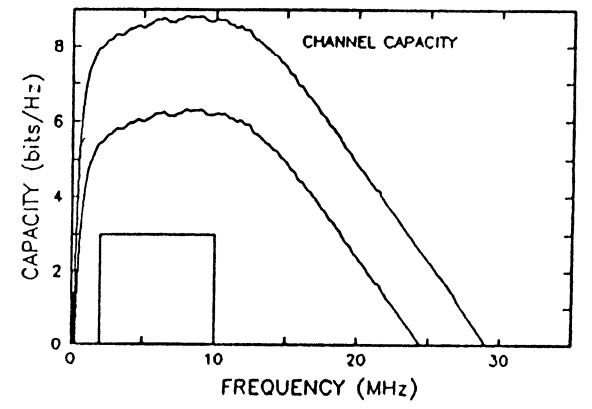
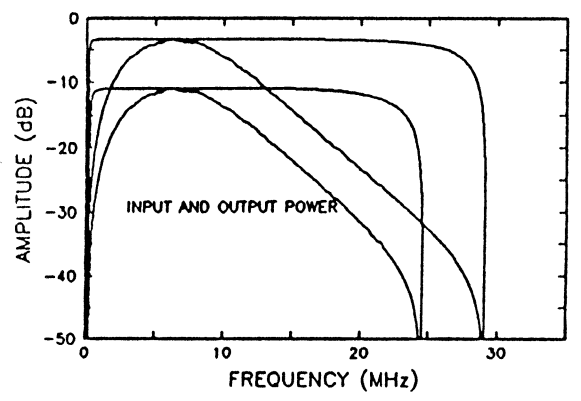
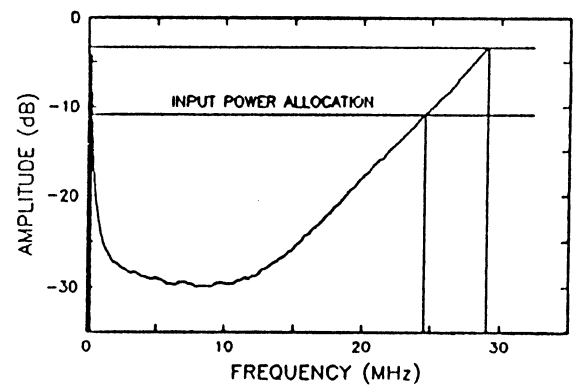
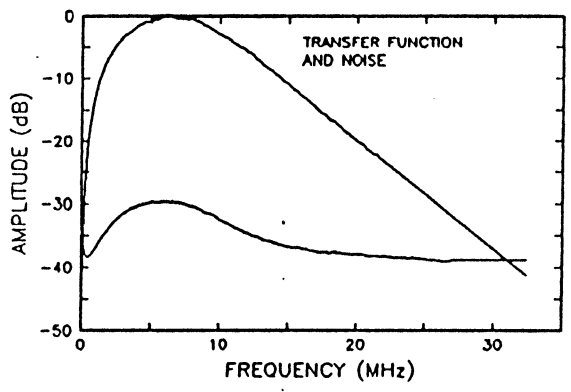
$$\overline{x^2} \leq P$$

$$|X_B(f)|^2 = \max\left\{0, B - \frac{N(f)}{|H(f)|^2}\right\}$$

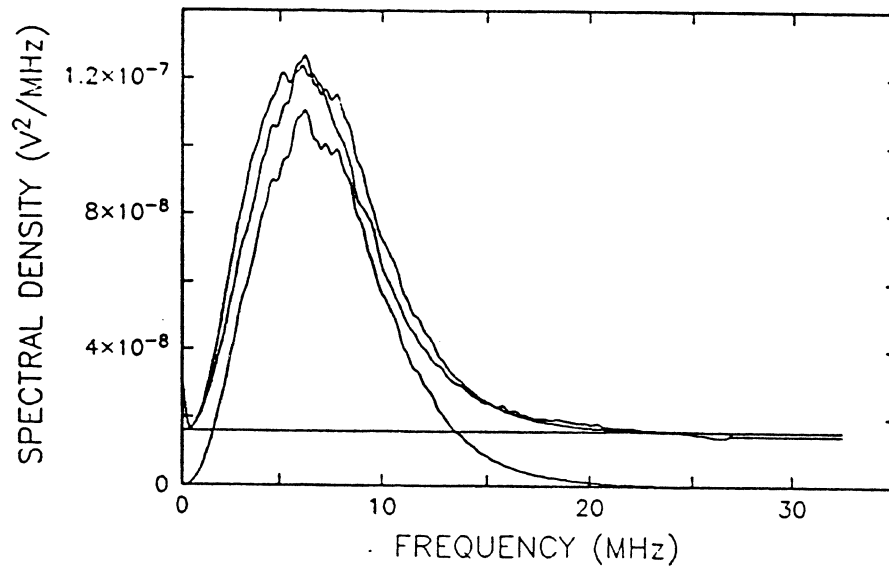
$$\text{where } B \text{ solves } P = \int_0^\infty |X_B(f)|^2 df$$

$$C = \int_0^\infty \log \frac{B |H(f)|^2}{N(f)} df$$

Water-Filling Calculation (cont.)



Scaled Water-Filling Calculation

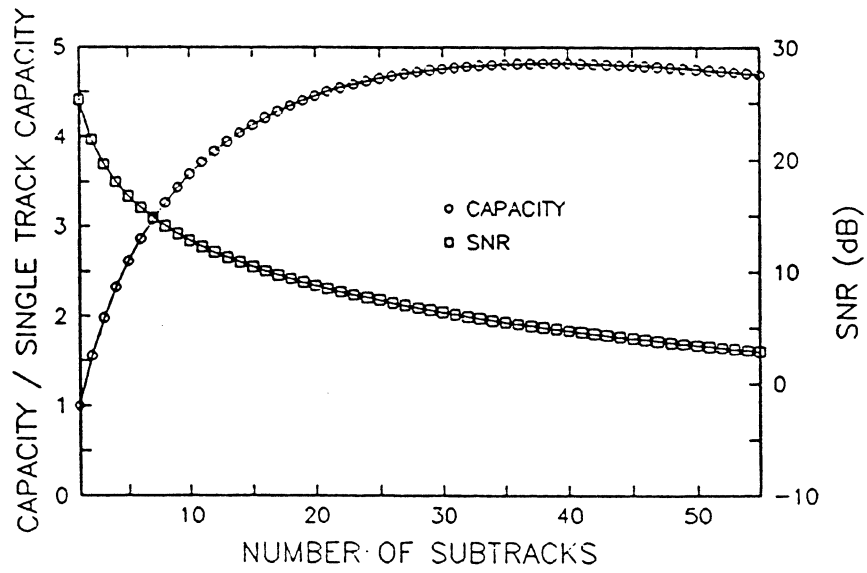


Assume:

white component does not scale $\rightarrow N_e(f)$

colored component scales $\rightarrow N_d(f)$

Capacity versus Track Density



$$\sigma_e^2 = .63 \sigma_d^2$$

$$\frac{\overline{y^2}}{\sigma_e^2 + \sigma_d^2} = 25dB$$

SNR Scaling - Conclusion

- **Inconclusion of non-scaling noise is important.**
- **Potential capacity gains are 2-5x, not 50x for the channel studied.**
- **Reducing electronic and other non-scaling noise is the key to larger gains.**
- **SNR at maximum capacity is around 5 dB.**

2. Signaling and Detection

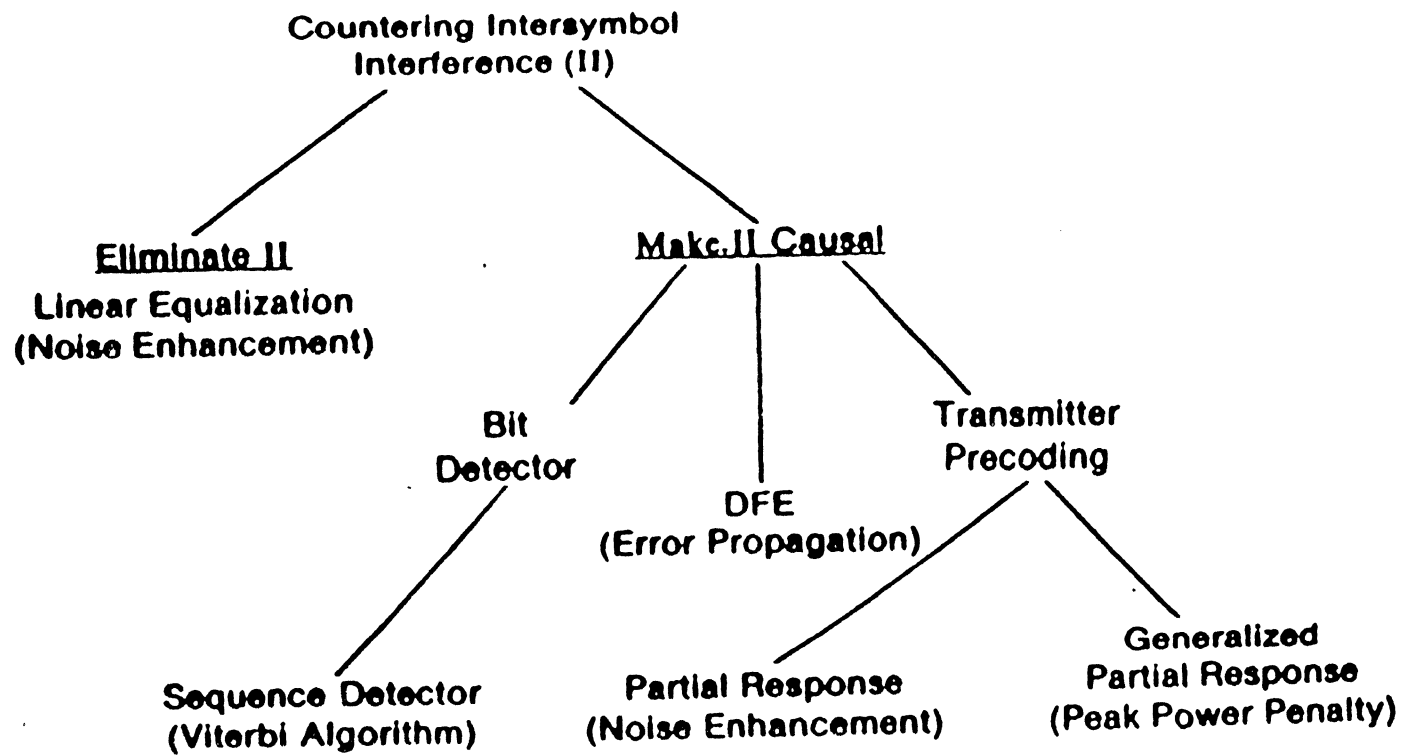
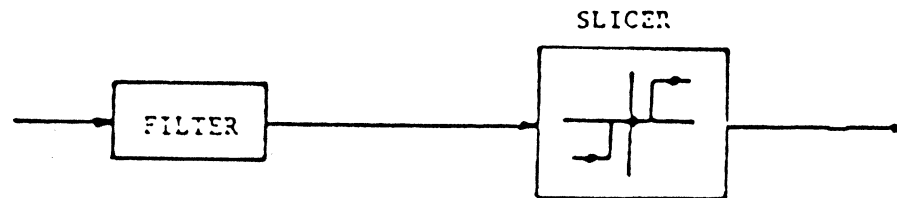
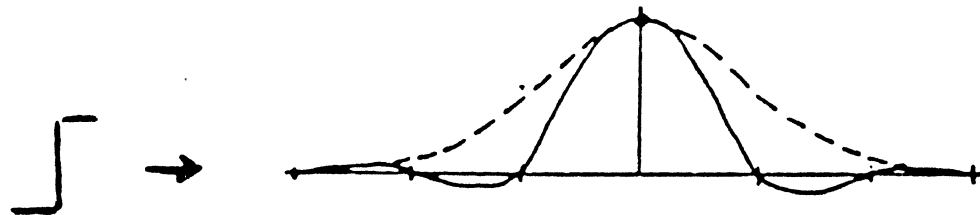


Figure 1. Summary of available methods of countering intersymbol interference in sampling detectors.

Zero-Forcing Equalization

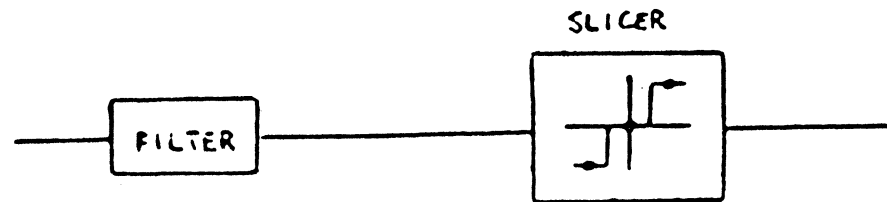
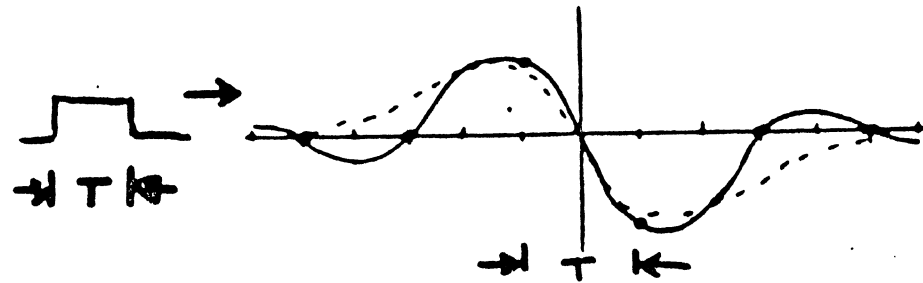
- Equalize step response to:



- limited by noise enhancement

Zero-Forcing Equalization

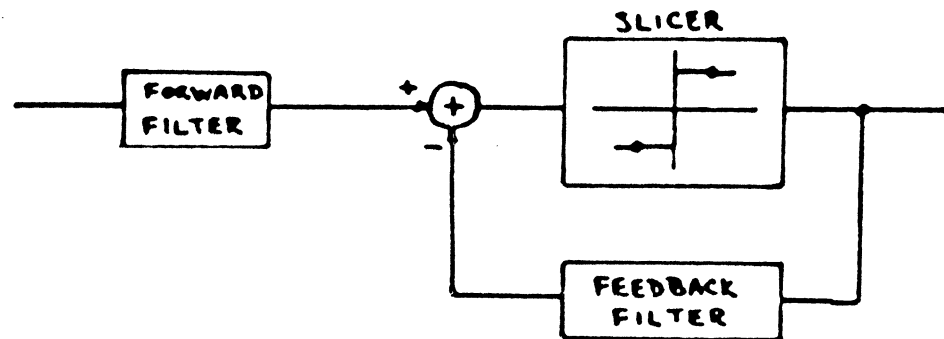
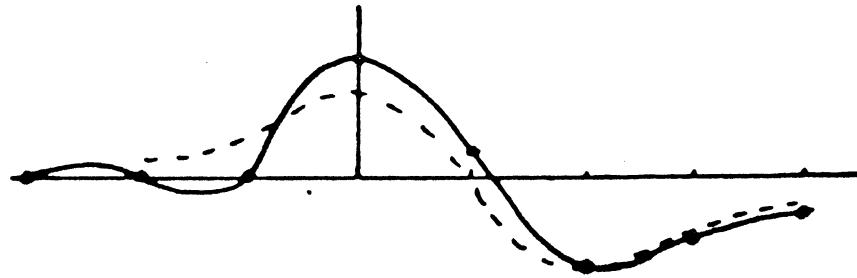
- Equalize NRZ bit response to:



- limited by noise enhancement

Decision Feedback Equalization

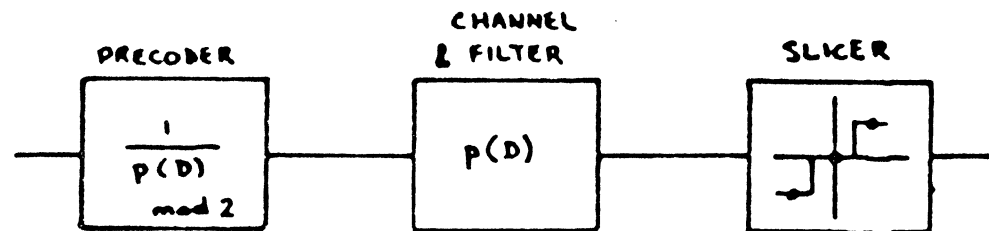
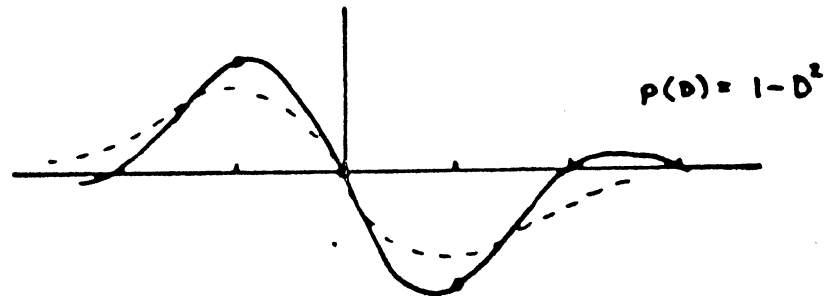
- Equalize NRZ bit response to:



- subject to error propagation

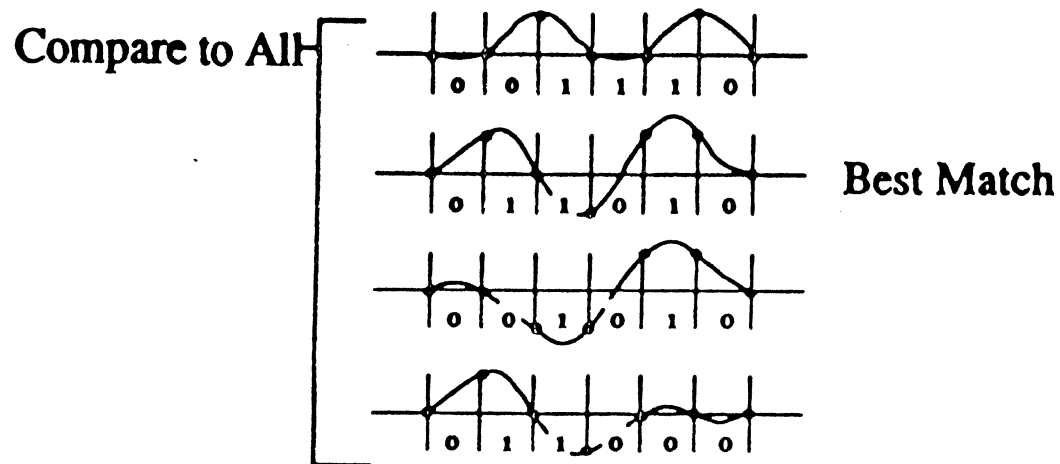
Partial Response

- Equalize NRZ bit response to:



- no error propagation
- less noise enhancement than ZFE or Flat
- more noise enhancement than DFE

Maximum Likelihood Sequence Detector



Most likely information sequence:

... 0 1 1 0 1 0 ...

3. Write Precompensation

Identification of Nonlinear Write Effects Using Pseudorandom Sequences

Thomas D. Howell

*ref: Palmer, et. al., IEEE Trans. Mag., MAG-23,
No. 5, Sept. 1987, pp. 2237-2379*

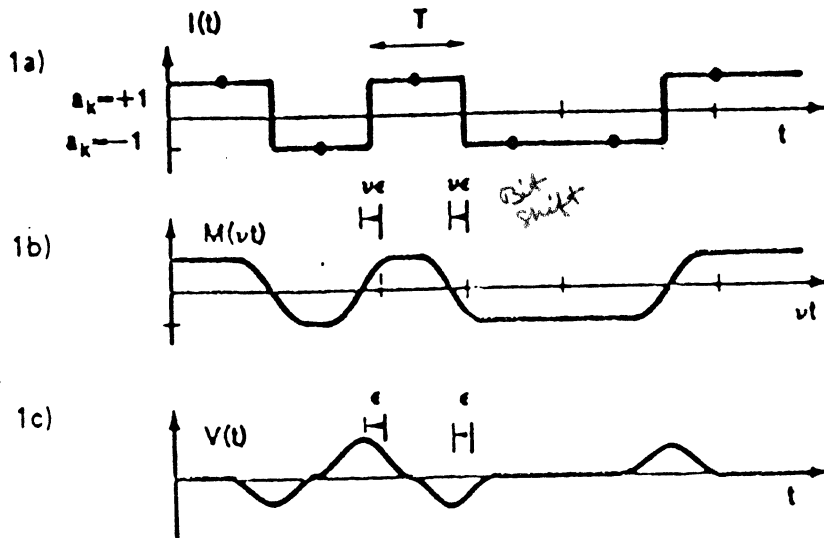


Figure 1a NRZ record current comprising a stream of bits taking values $a_k = \pm 1$.

Figure 1b Recorded magnetization showing transition shifts

Figure 1c Playback voltage with transition shift distortion. The isolated pulse, $h(t)$, due to a transition is shifted earlier in time only if it is immediately preceded by another transition in the NRZ waveform.

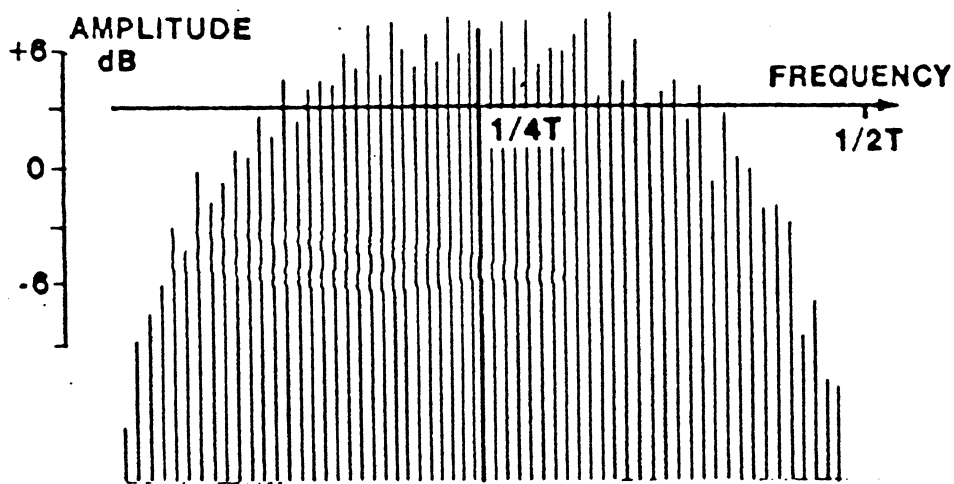
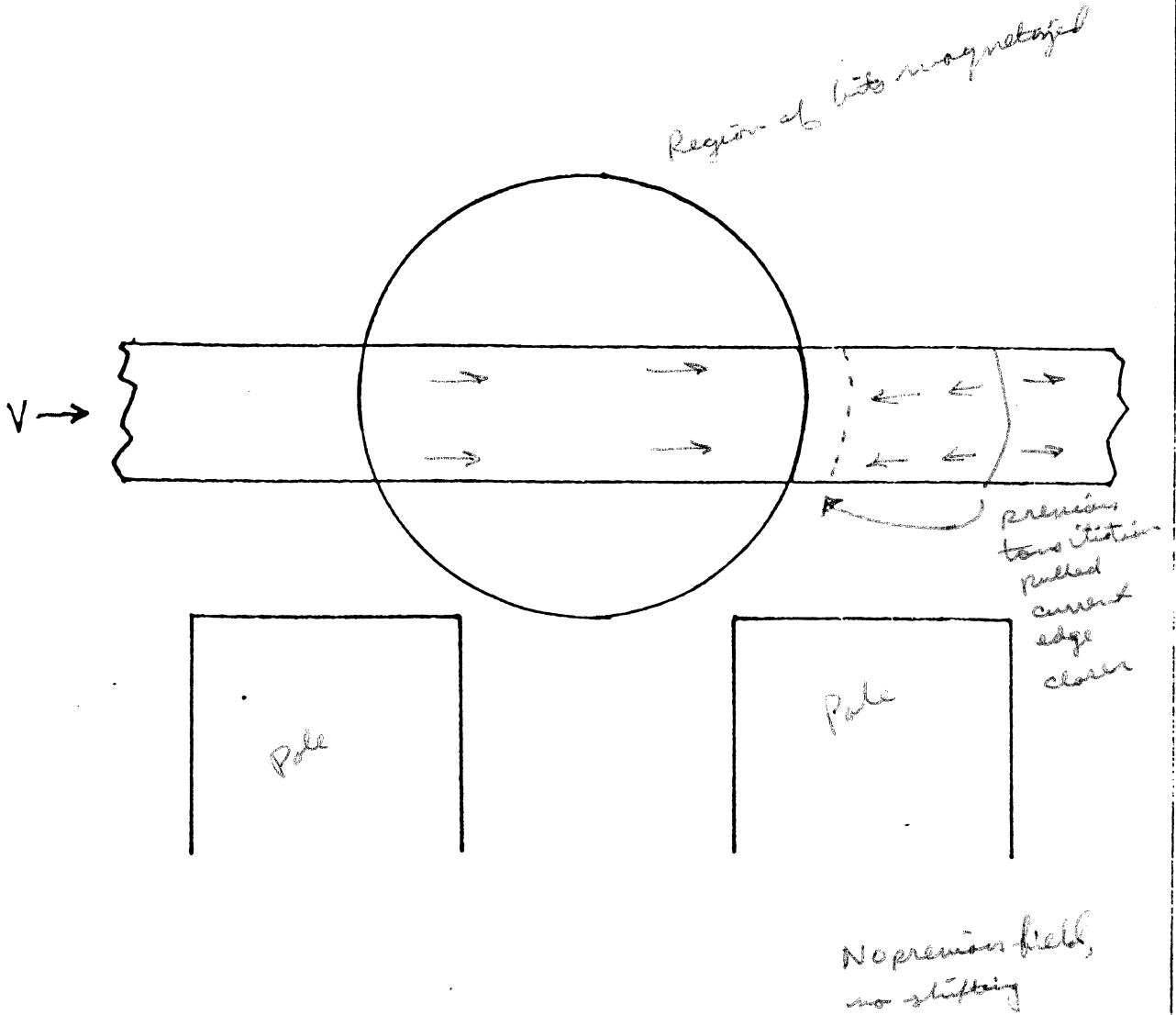


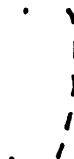
Figure 4 Spectrum from a hard disc transport shaped to Class IV showing nonlinear ripples similar to those shown in Fig. 2.

NONLINEAR TRANSITION SHIFTS

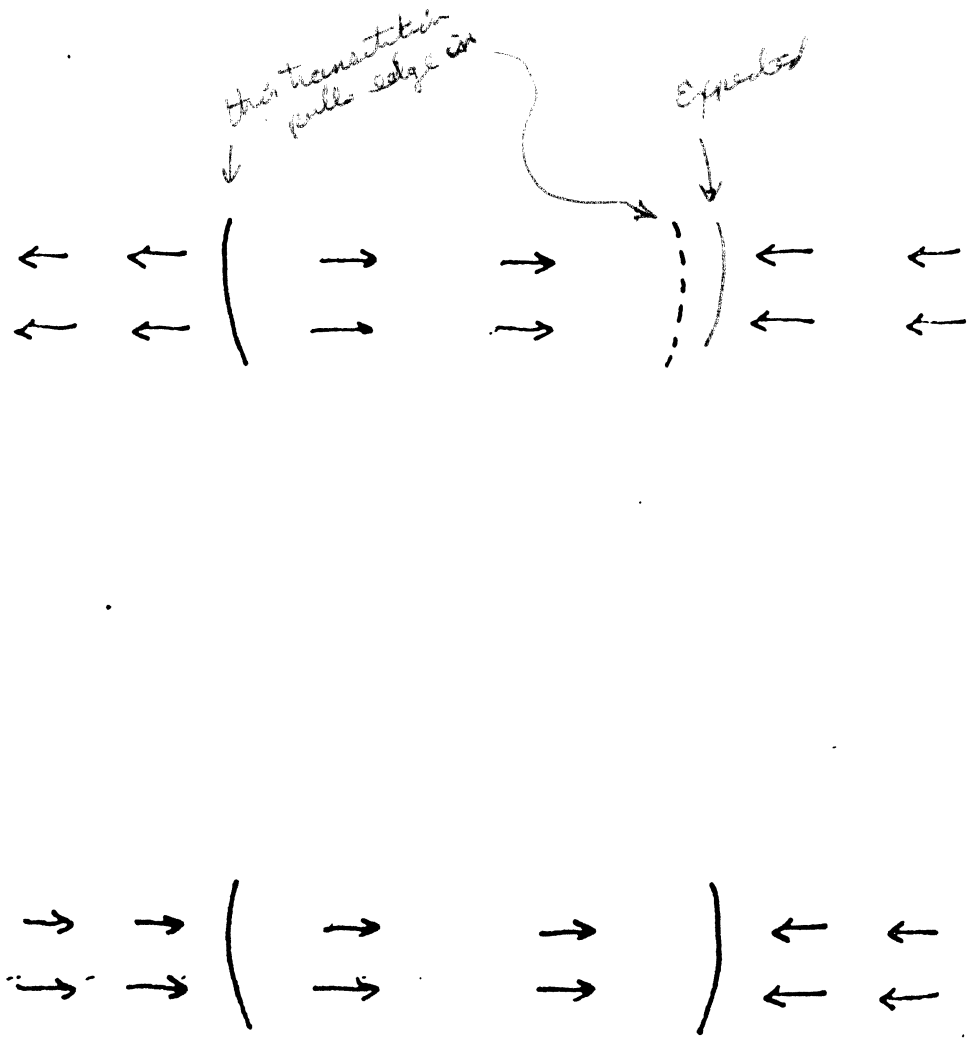
22-141 50 SHEETS
22-142 100 SHEETS
22-144 200 SHEETS



22-141 50 SHEETS
22-142 100 SHEETS
22-144 200 SHEETS



22-141 50 SHEETS
22-142 100 SHEETS
22-144 200 SHEETS



Origin of Echo

$$V(t) = \sum_k \frac{1}{2}(a_{k+1} - a_k)h(t_k), \quad a_k \in \{-1, +1\}$$

$$\tilde{V}(t) = \sum_k \frac{1}{2}(a_{k+1} - a_k)h(t_k - \frac{1}{2}\varepsilon_0 + \frac{1}{4}\varepsilon_0(a_{k+1} - a_k))$$

Taylor series, simplification

$$\tilde{V}(t) = V(t - \frac{1}{2}\varepsilon_0) - \frac{1}{4}\varepsilon_0 \sum_k a_k a_{k+1} h'(t_k - \frac{1}{2}\varepsilon_0)$$

Shift and add property of $\{a_k\}$

$$\tilde{V}(t) = V(t - \frac{1}{2}\varepsilon_0) - \frac{1}{4}\varepsilon_0 \sum_k a_{k+M_0} h'(t_k - \frac{1}{2}\varepsilon_0)$$

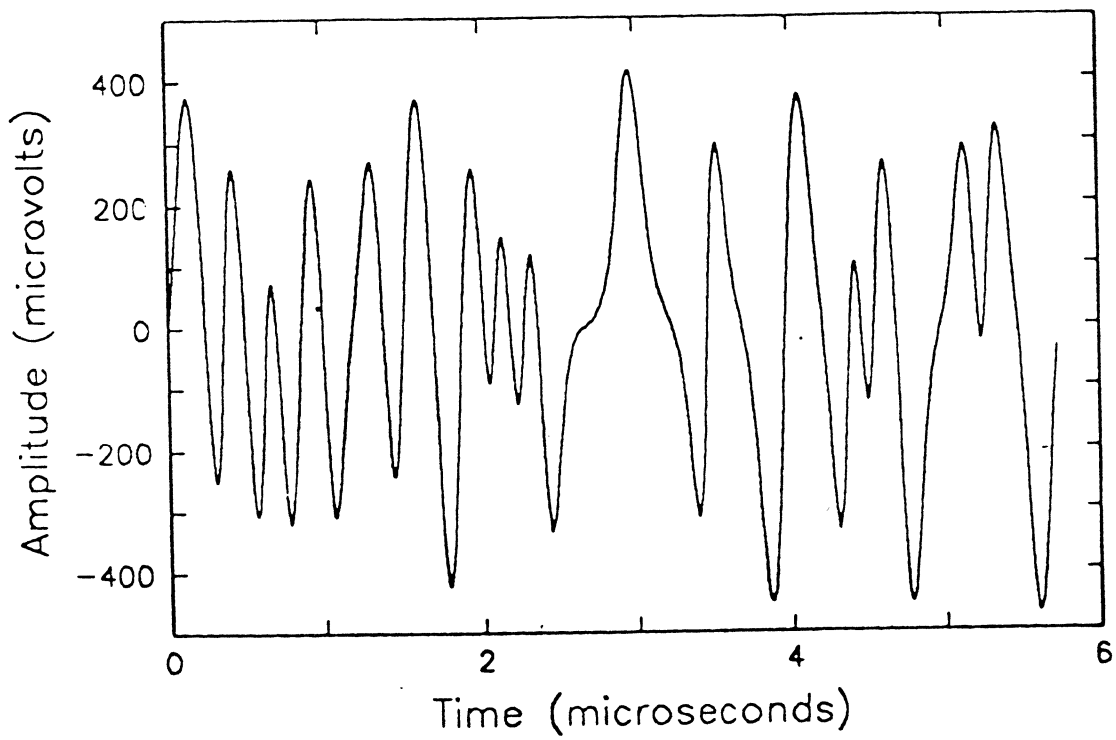
Finite difference for derivative

$$\tilde{V}(t) \simeq V(t - \frac{1}{2}\varepsilon_0) - \frac{1}{2} \frac{\varepsilon_0}{T} V(t - \frac{1}{2}\varepsilon_0 + (M_0 - \frac{1}{2})T)$$

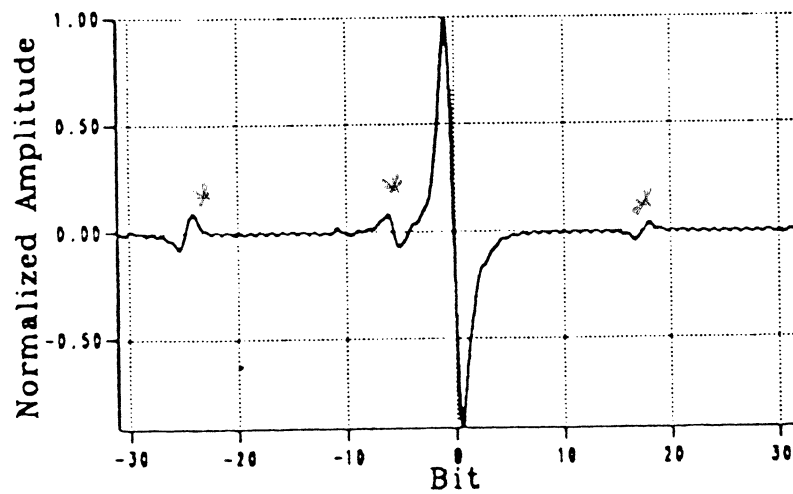
Summary of Echoes

- | | |
|--------------------------------|-----------------------|
| 1. Initial magnetization | $a_k a_{k+1}$ |
| 2. Adjacent transition | $a_{k-1} a_k a_{k+1}$ |
| 3. Next-to-adjacent transition | $a_{k-2} a_k a_{k+1}$ |
| 4. Transition broadening | add first derivative |
| 5. Interaction of 1 and 2 | $a_{k-1} a_{k+1}$ |

*Pseudo-random
sequence. 63 bits*



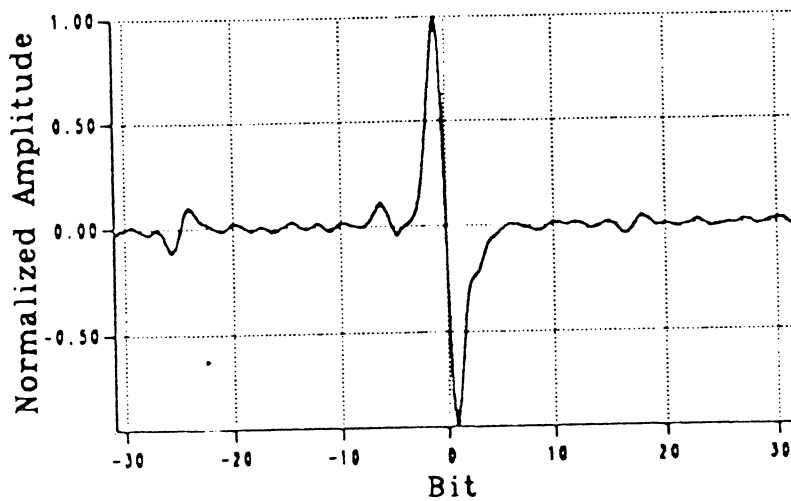
Simulated Result



* Echo effects from non-linear effects (bit shifts)

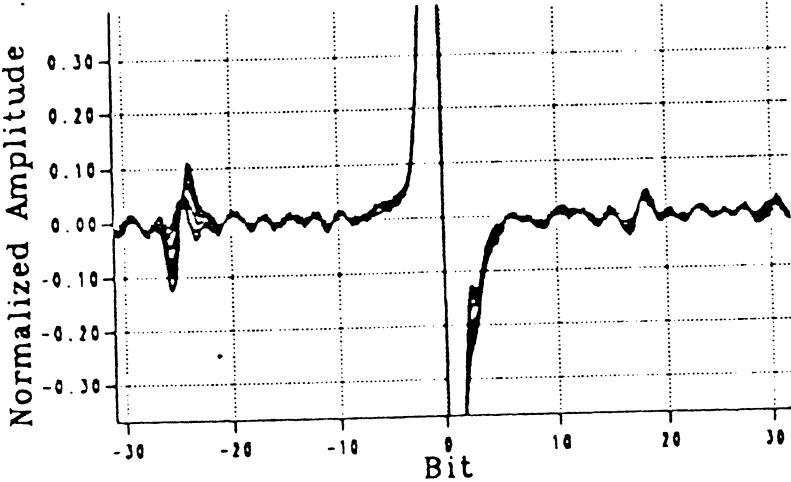
Simulated Inverse Transform with $\varepsilon_0 = \frac{T}{8}$, $\varepsilon_1 = \frac{3T}{16}$,
 $\varepsilon_2 = \frac{7}{16}$, with Selected Pulses Broadened by a Factor of
 $\frac{1}{16}$.

Derived Dipulse Responses



Response obtained by first dividing the Fourier Transform of the measured readback waveform by the Transform of the binary discrete-time input sequence and then taking the Inverse Transform of the result. Characteristic polynomial for the sequence is $x^6 + x + 1$.

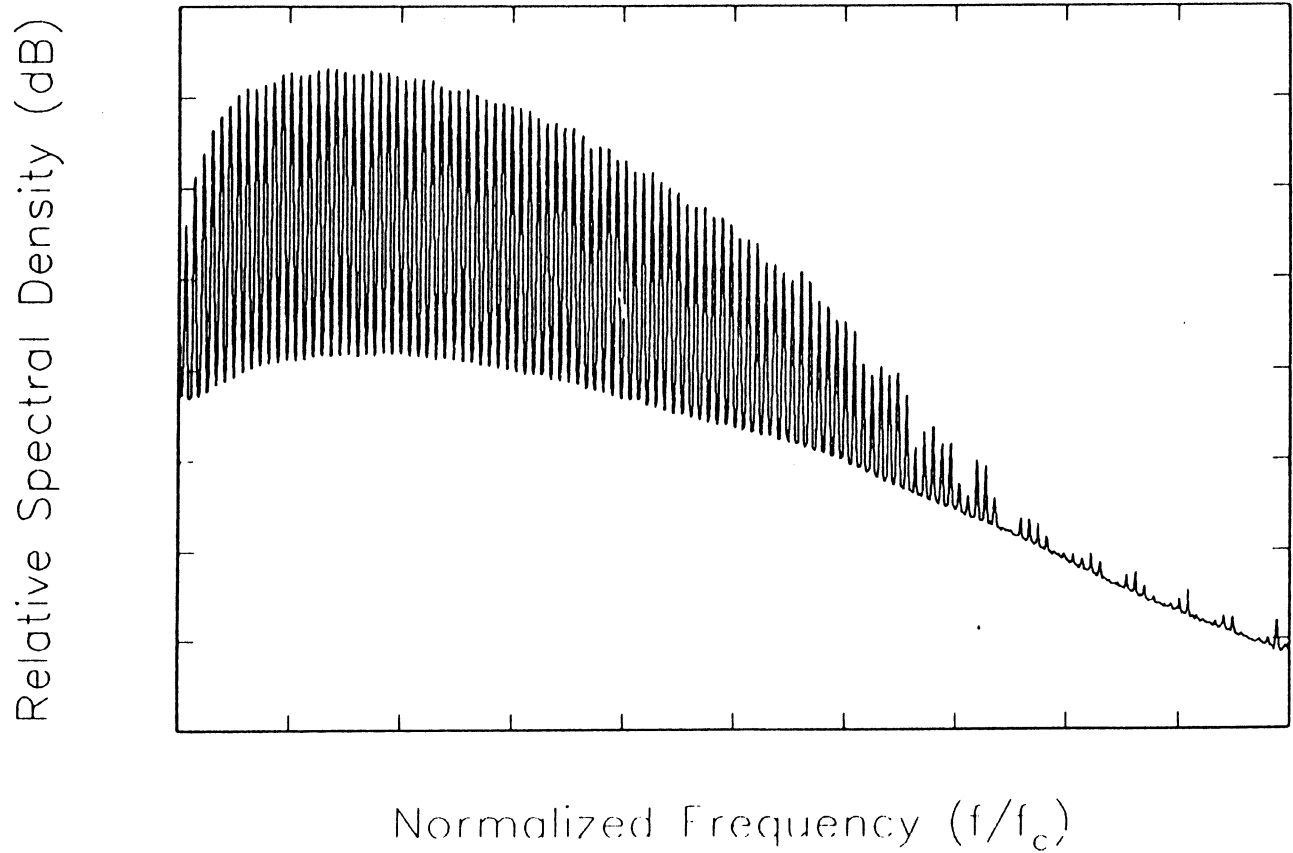
Controlling the Echoes



Effect of Timing Precompensation.

4. Adaptive Equalization

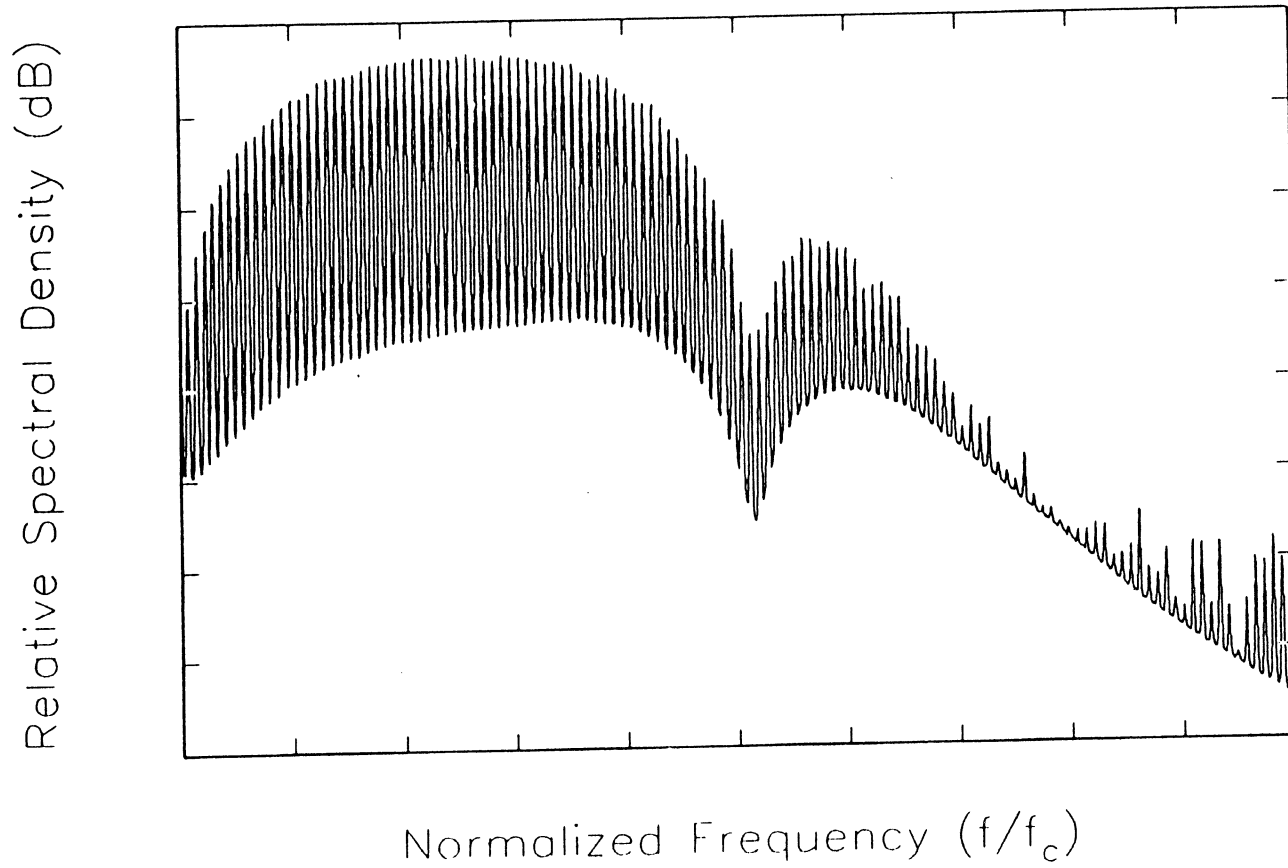
HOWELL D UNEPRBS3 January 24, 1990 at 17:48:00 by GDFTRN (V-88.322)



1227-2000
power
power

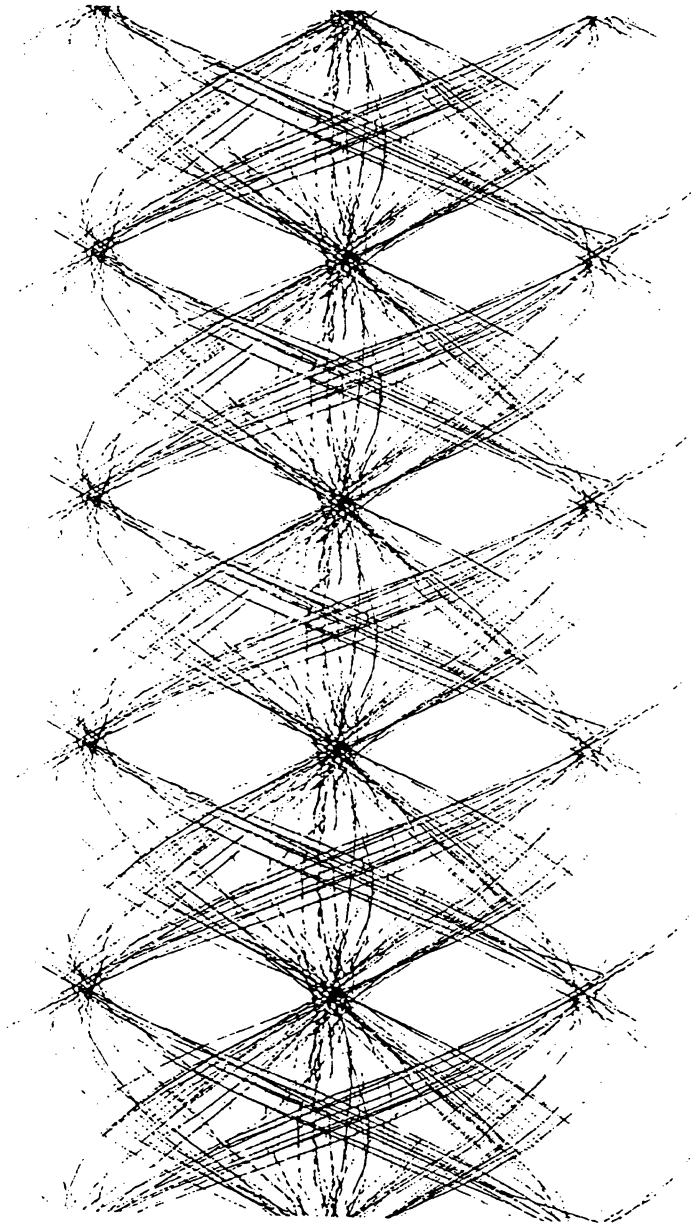
Unexplained
power
power

HOWELL D EQU PRBS3 January 24, 1990 at 17:48:16 by GDFTRN (V-88.322)

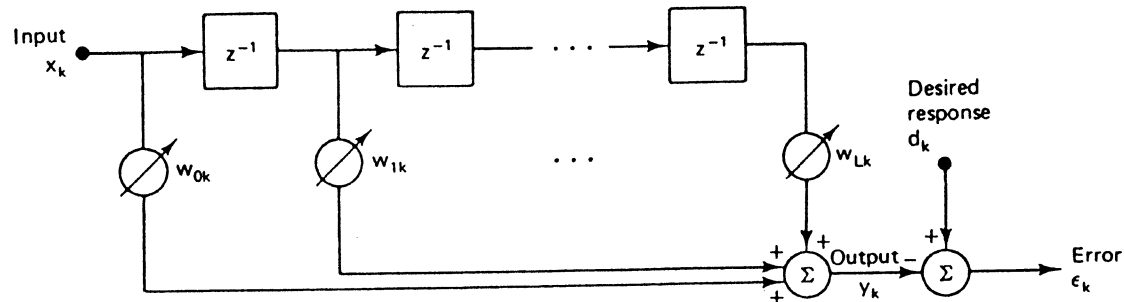


*Equivalent to
equation 10
with $\theta = 0$
and $\omega = 0$*

Time
Domain
of
Equatorial
Response.



The LMS Algorithm



$$\epsilon_k = d_k - \mathbf{X}_k^T \mathbf{W}_k$$

$$\begin{aligned} \mathbf{W}_{k+1} &= \mathbf{W}_k - \mu \hat{\nabla}_k \\ &= \mathbf{W}_k + 2\mu \epsilon_k \mathbf{X}_k \end{aligned}$$

from Widrow & Stearns *Adaptive Signal Processing*, Prentice Hall 1985

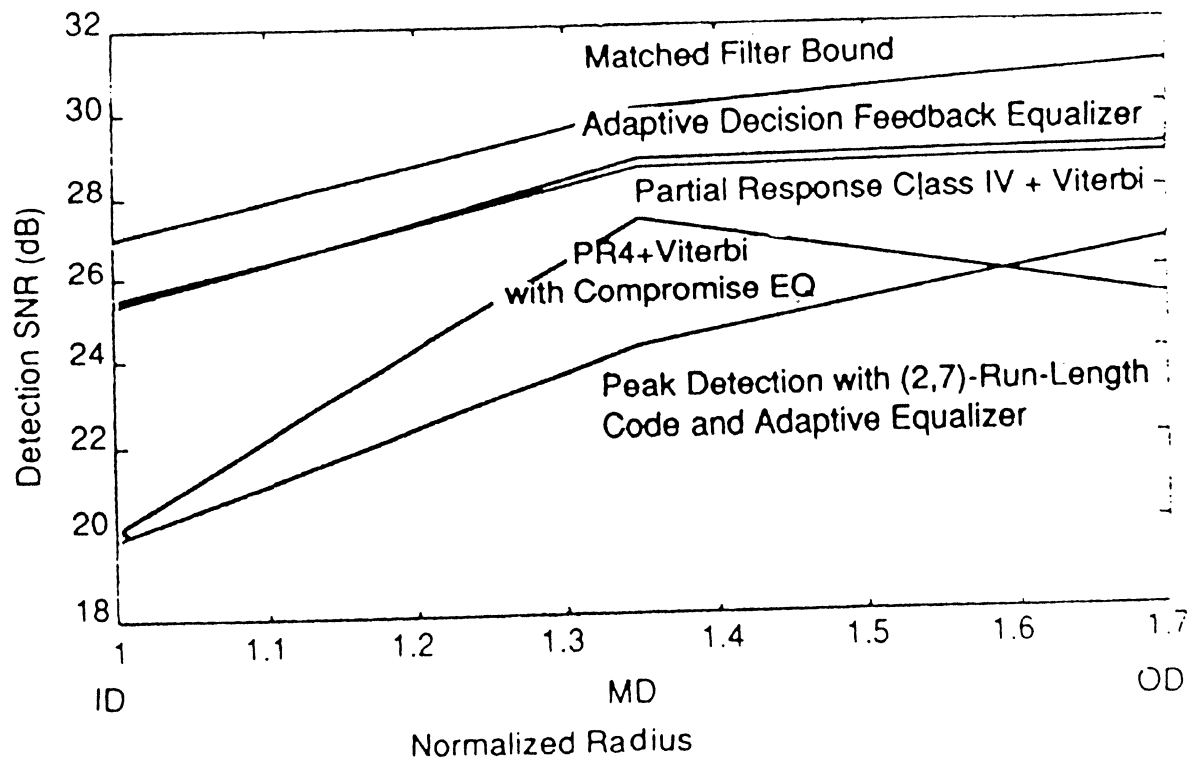


Fig. 17. Equalizer performance vs. disk radius.

5. Trellis Codes

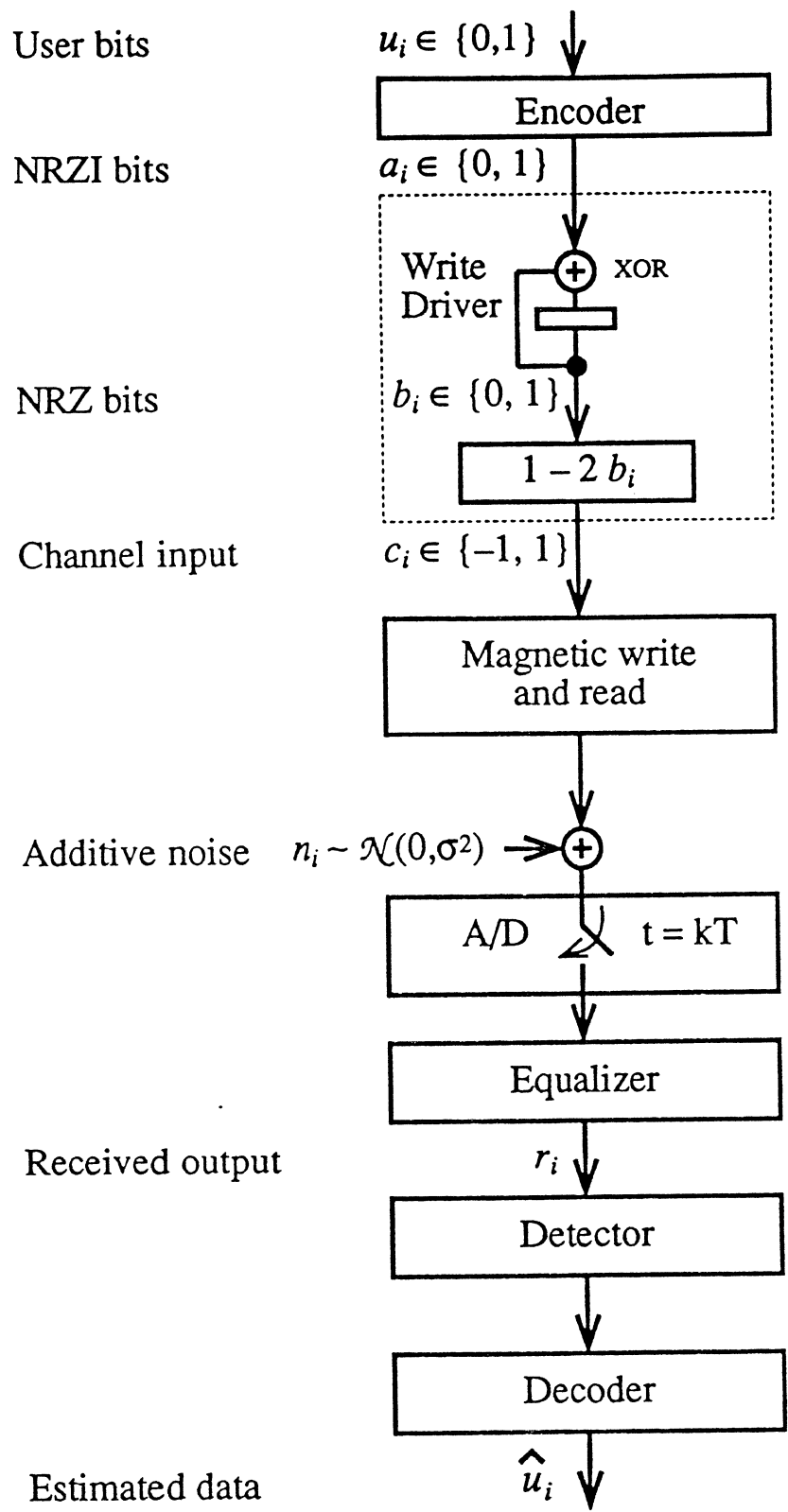


Fig. 1. System Model.

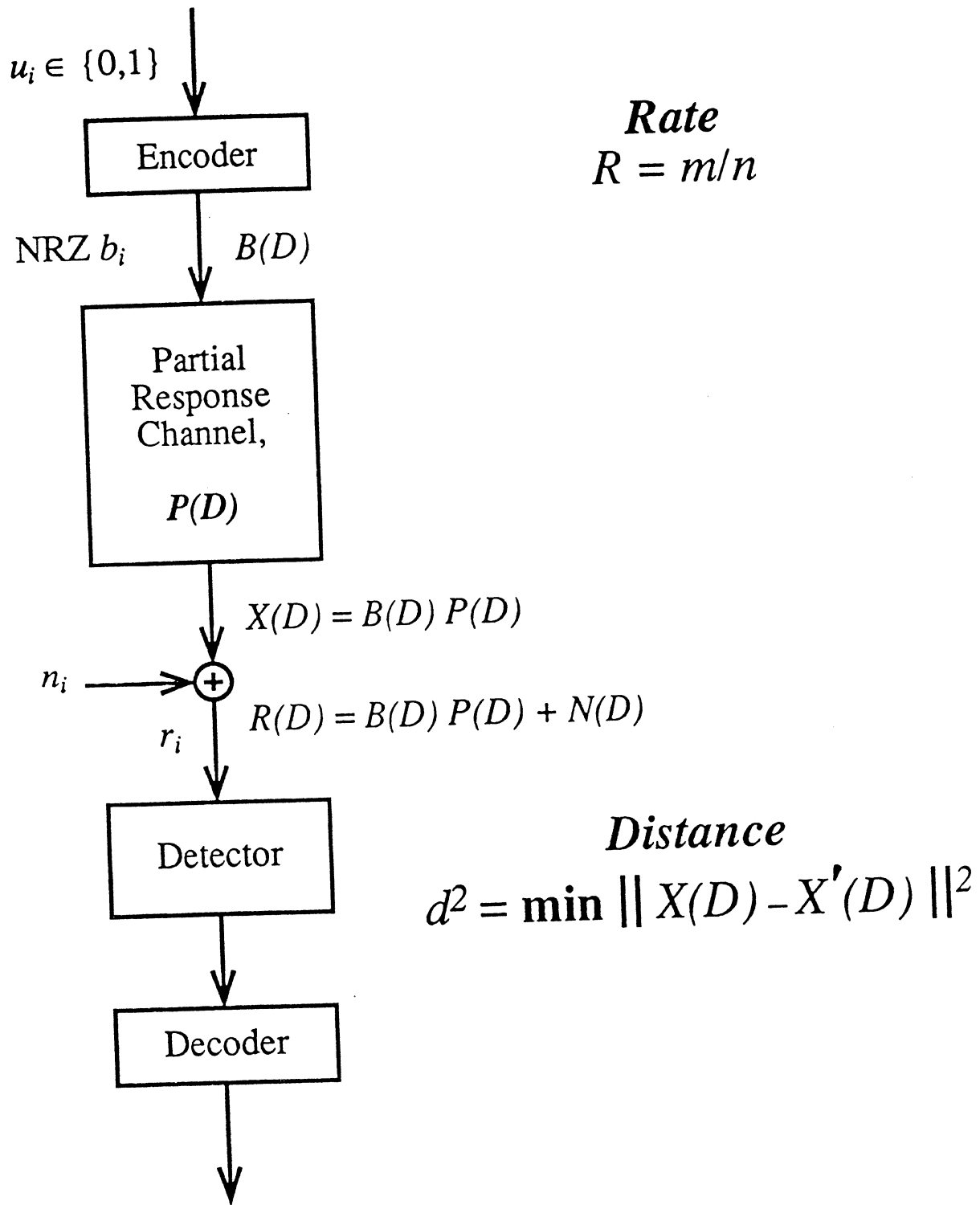


Fig. 2. Simplified Partial Response System Model.

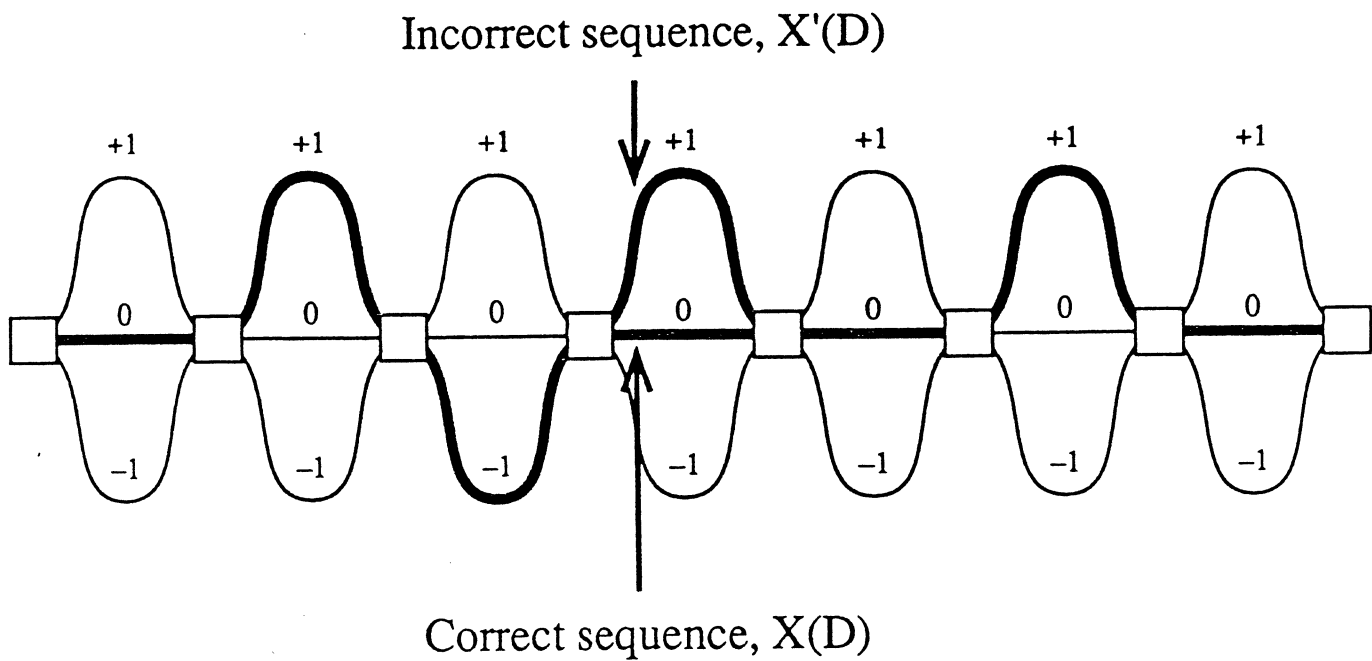


Fig. 3. Threshold detection, $d^2 = \text{Min} \| X(D) - X'(D) \|^2 = 1$.

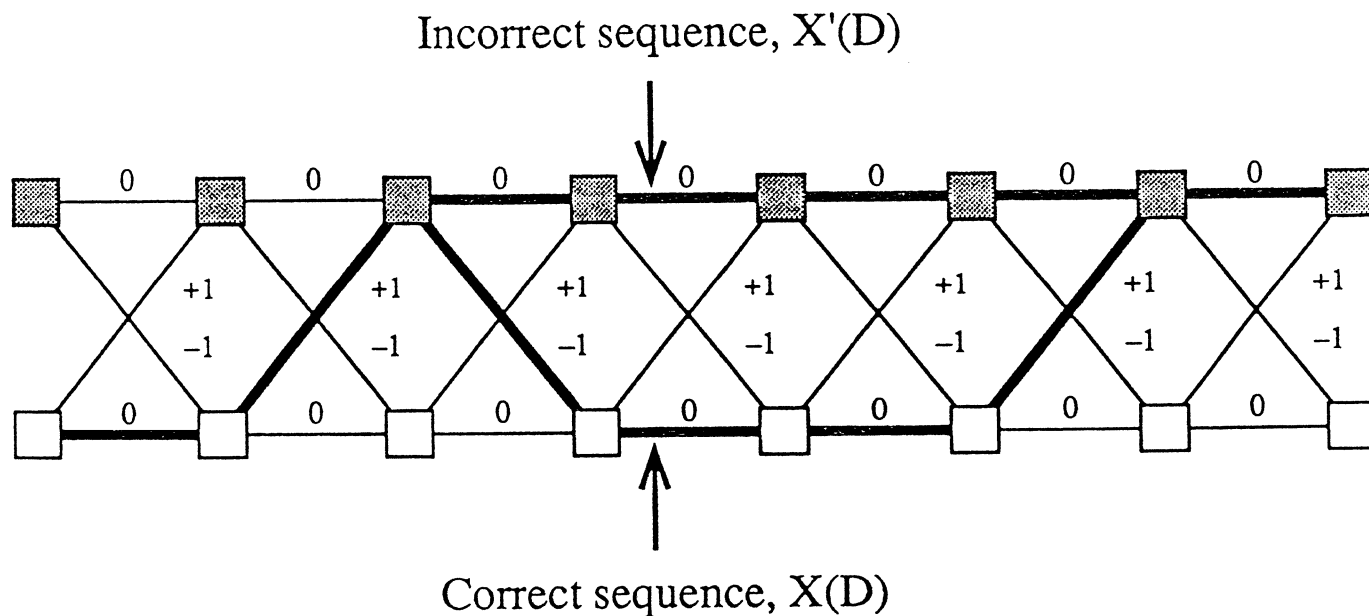


Fig. 4. PRML detection, $P(D) = 1-D$, $d^2 = \text{Min} \| X(D) - X'(D) \|^2 = 2$.

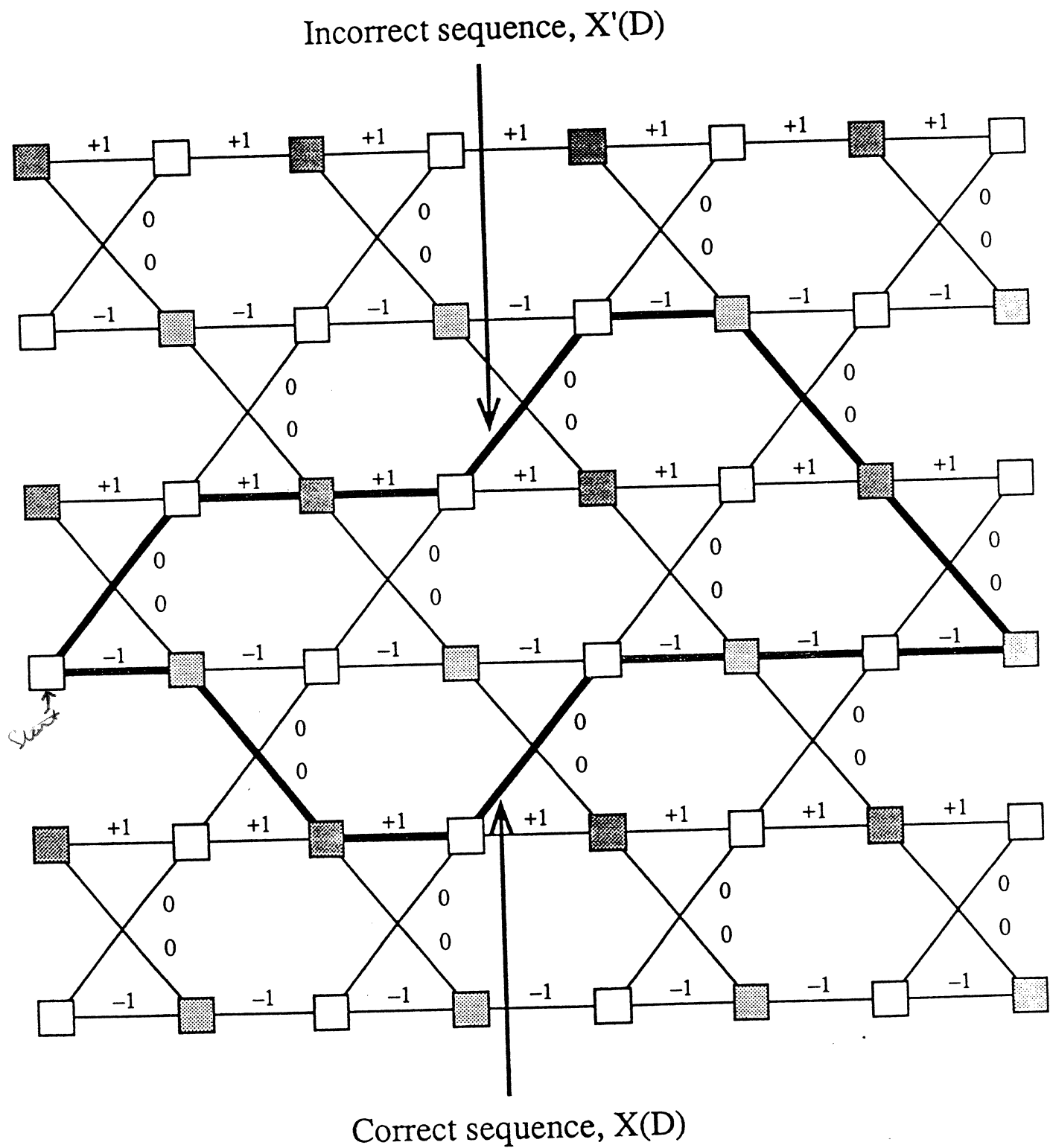


Fig. 4. TCPR detection, $P(D) = 1-D$, $d^2 = \text{Min} \|X(D) - X'(D)\|^2 = 4$.

Summary

- 1. Track Width and SNR will decrease;**
- 2. Efficient signalling allows intersymbol interference;**
- 3. Detection by maximum-likelihood sequence estimation;**
- 4. Write precompensation alleviates nonlinear transition shifts;**
- 5. Adaptive equalization improves performance when conditions vary;**
- 6. Trellis codes allow reliable detection even with low SNR.**

**"Small Form Factor
Drive Design Tradeoffs"**

Bob Kobliska

Aura Associates.

Institute for Information **S**torage **T**echnology

Santa Clara University, California

December 14 - 16, 1992

MARKET (1.8" AND SMALLER)

NOTEBOOKS
SUB-NOTEBOOKS
PALMTOPS
"MOBILE COMPUTING"
REMOVABLE STORAGE
NEW MARKETS:
 FAX
 TELEPHONE
 AUDIO
 DATA LOGGING

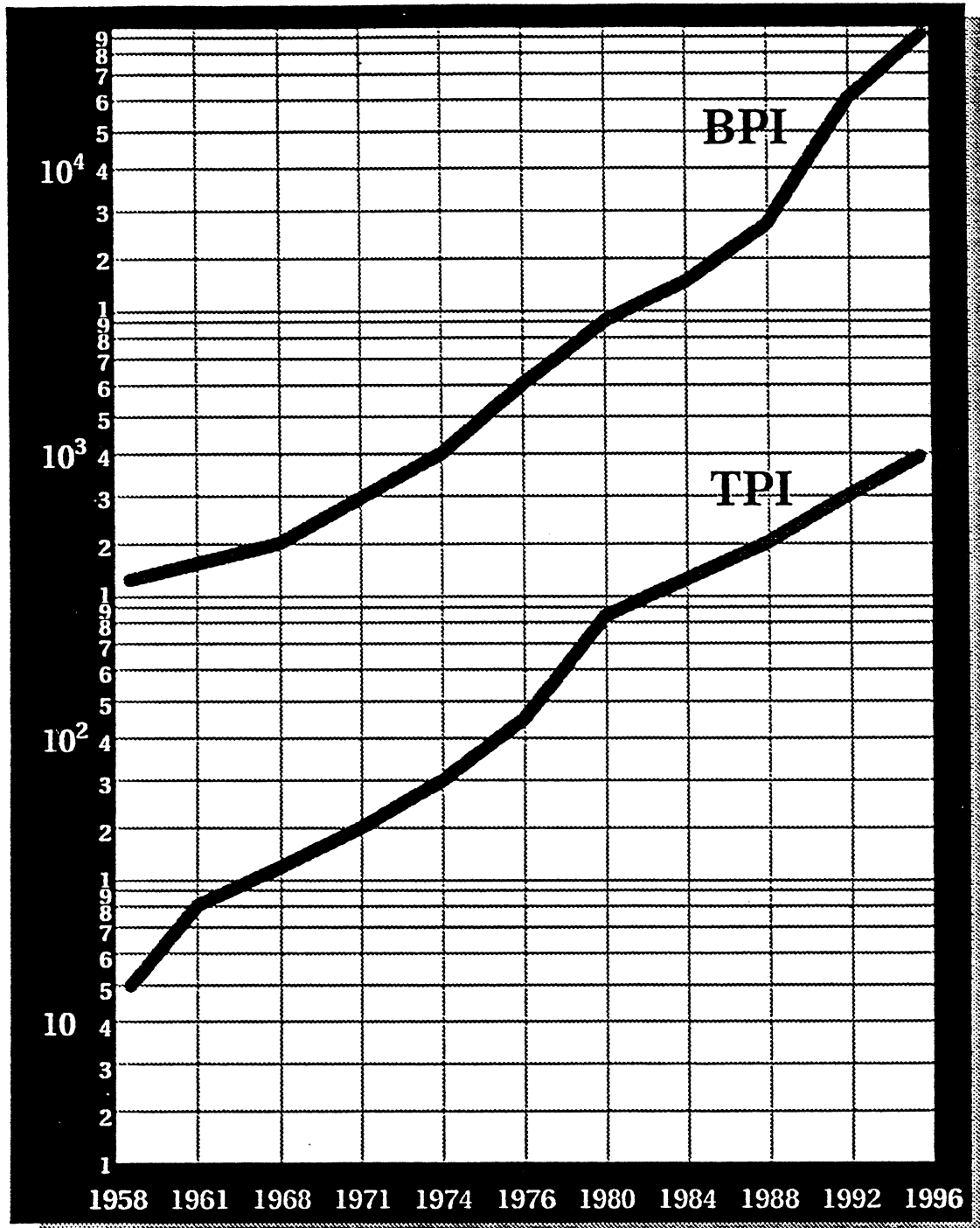
REQUIREMENTS

ADEQUATE STORAGE CAPACITY
LOW COST
LOW POWER
SMALL AND LIGHTWEIGHT
PCMCIA FOR REMOVABILITY
SHOCK RESISTANCE

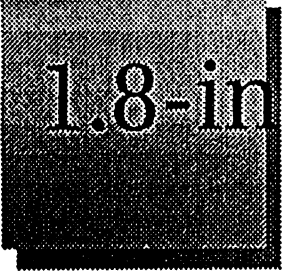


AURA ASSOCIATES

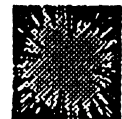
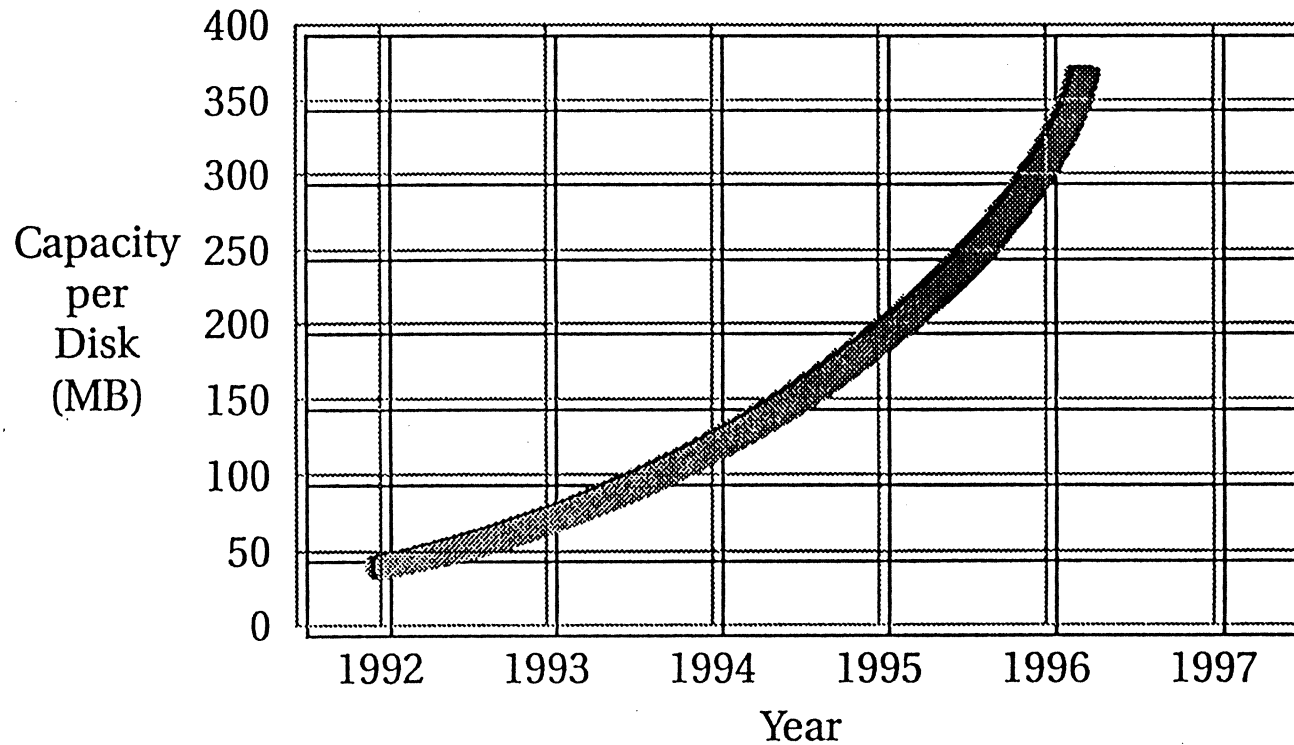
TPI/BPI Curve



AURA Associates



1.8-inch Disk Capacity Growth



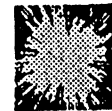
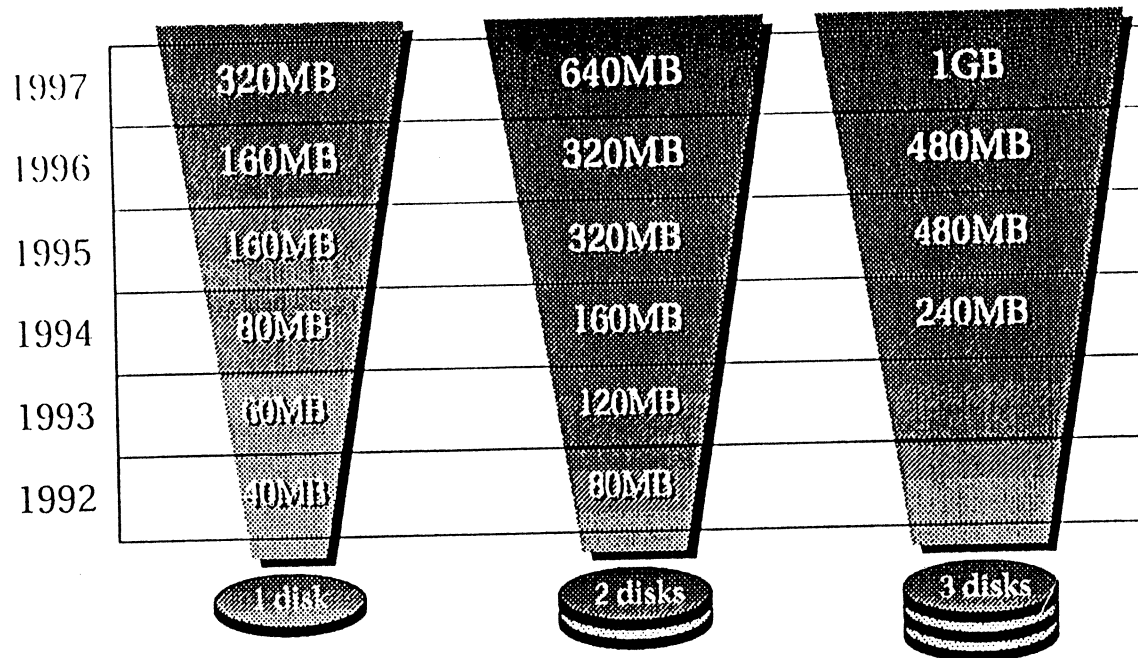
AURA Associates





Aura Product Evolution

1.8-inch Fixed Products



AURA Associates

TECHNICAL OPTIONS

READ/WRITE

INDUCTIVE HEADS
MAGNETO-RESISTIVE HEADS
VERTICAL RECORDING
PLANAR Si HEADS

CHANNEL

PEAK DETECTION
ZONE BIT RECORDING
MODULATION CODE
ERROR DETECTION CODE
PRML
ADAPTIVE EQUALIZATION

SERVO

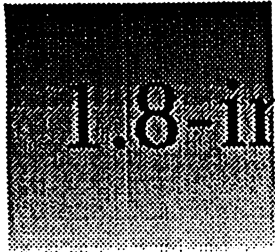
DIGITAL VERSUS ANALOG
EMBEDDED SECTOR VERSUS DEDICATED

MECHANICAL

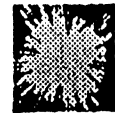
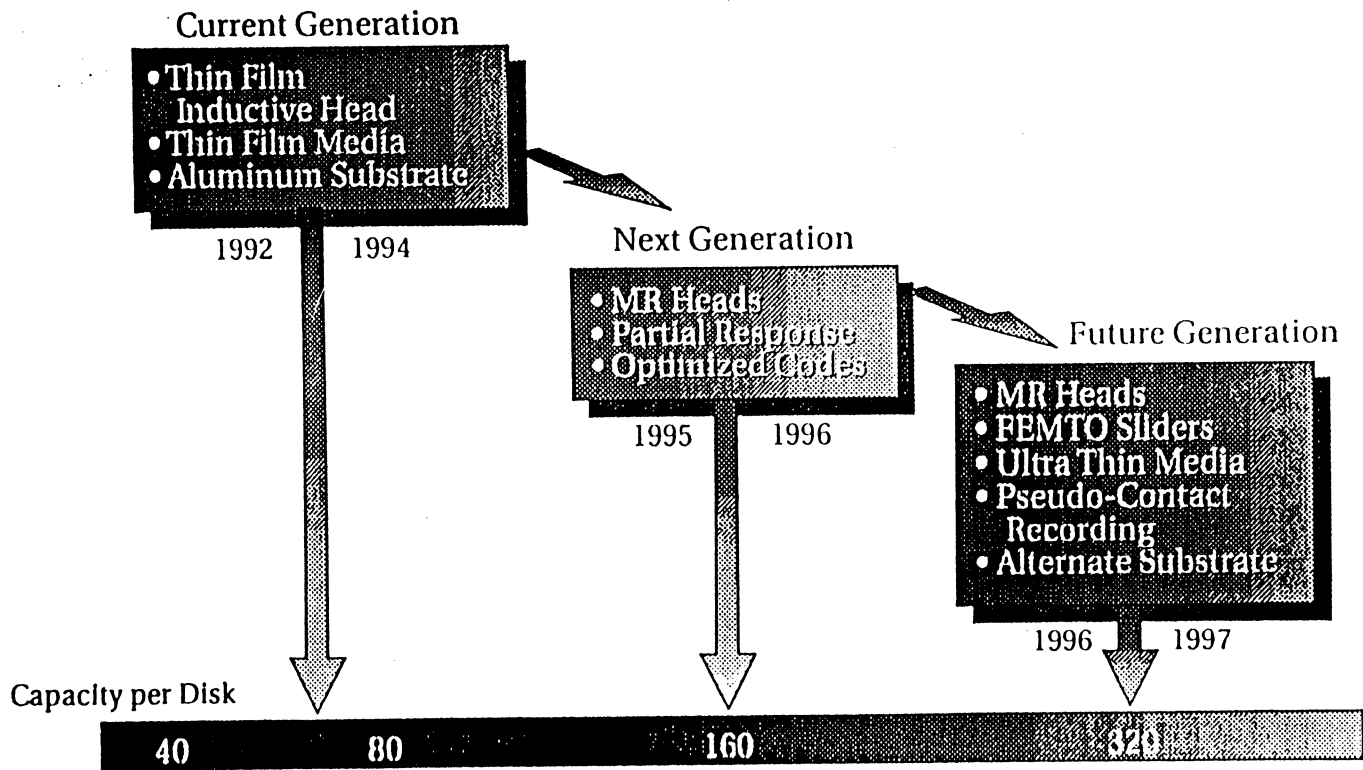
C.S.S. VERSUS HEAD LIFTERS/RAMPS
CONTACT RECORDING
KEY ISSUES:
DURABILITY, STICTION
SHOCK, VIBRATION



AURA ASSOCIATES



1.8-inch Technology Evolution



READ/WRITE INTERFACE DESIGN

GOAL: MAXIMIZE CAPACITY PER DISK

CONSTRAINTS:

LIMITED SURFACE AREA
LOW LINEAR VELOCITY
FLYING HEIGHT (RELIABILITY) - 4 μ "
CHANNEL DATA RATE - Chips aren't available
SERVO TRACKING CAPABILITY

*20-40 mb/s
Best for
integrated
chip sets.*

DESIGN OPTIONS:

RPM
HEAD DESIGN
FLYING HEIGHT PROFILE - large skew ID vs OD
DISK DESIGN
ZONE BIT RECORDING Done in software - 10% of zones
PROGRAMMABLE FILTERS FOR EQUALIZATION



AURA ASSOCIATES

HEAD DESIGN ISSUES
(INDUCTIVE)

READ/WRITE

NOMINAL FLYING HEIGHT

OF TURNS *42 min 50-60 better*

RESISTANCE/INDUCTANCE *.5/6 W/A*

GAP LENGTH

POLE TIP GEOMETRY

POPCORN/BARKHAUSEN NOISE

MECHANICAL

REQUIRED FLYING HEIGHT PROFILE

AIR BEARING DESIGN SELECTION

2 RAIL TAPER FLAT

TPC

TRI-RAIL

TAPER FLAT DESIGN - 2 RAIL

SLIDER SIZE

RAIL-WIDTH

GRAM LOAD

SUSPENSION DESIGN

Z-HEIGHT

OFFSET

CROWN

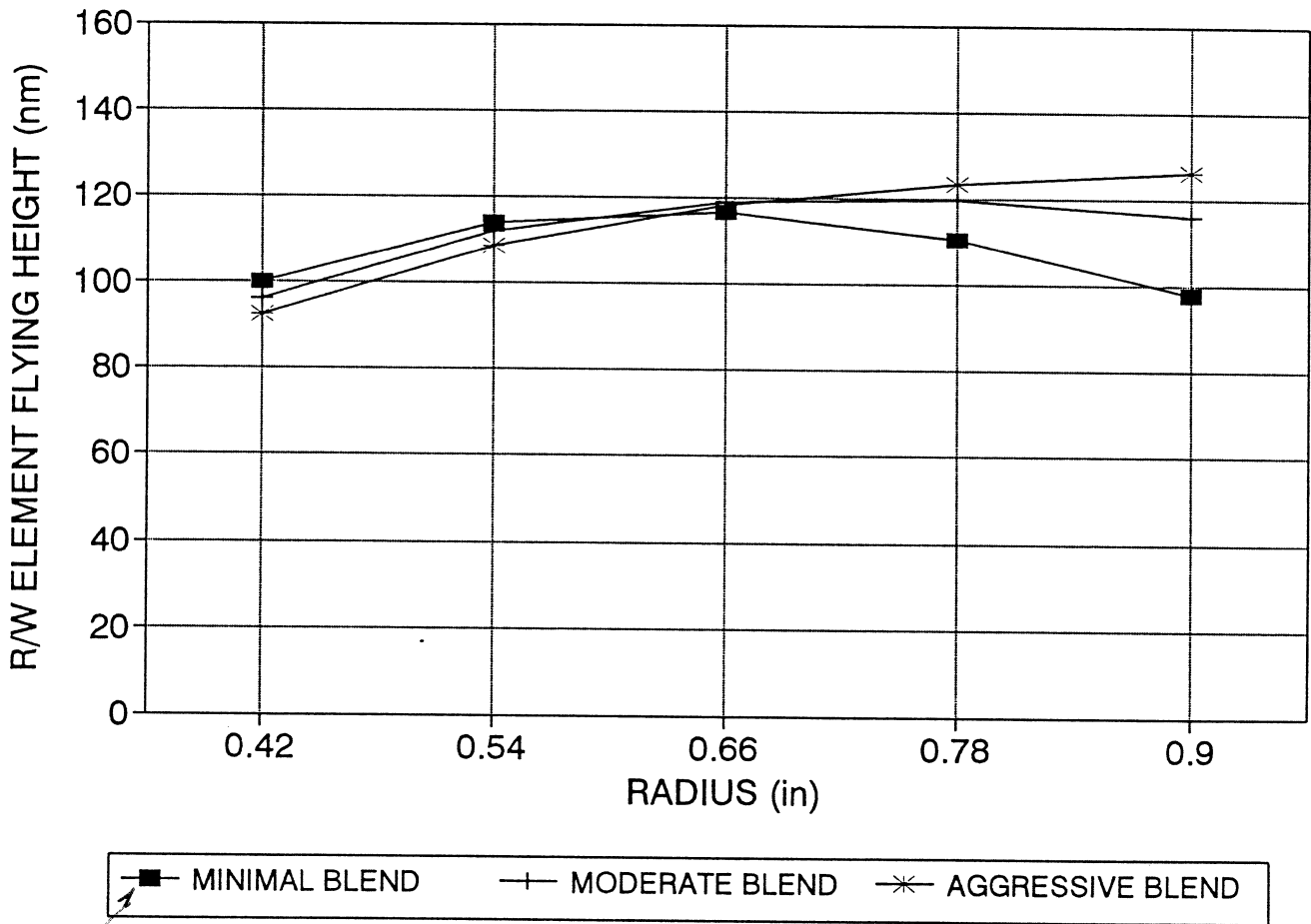
CAMBER

BLEND



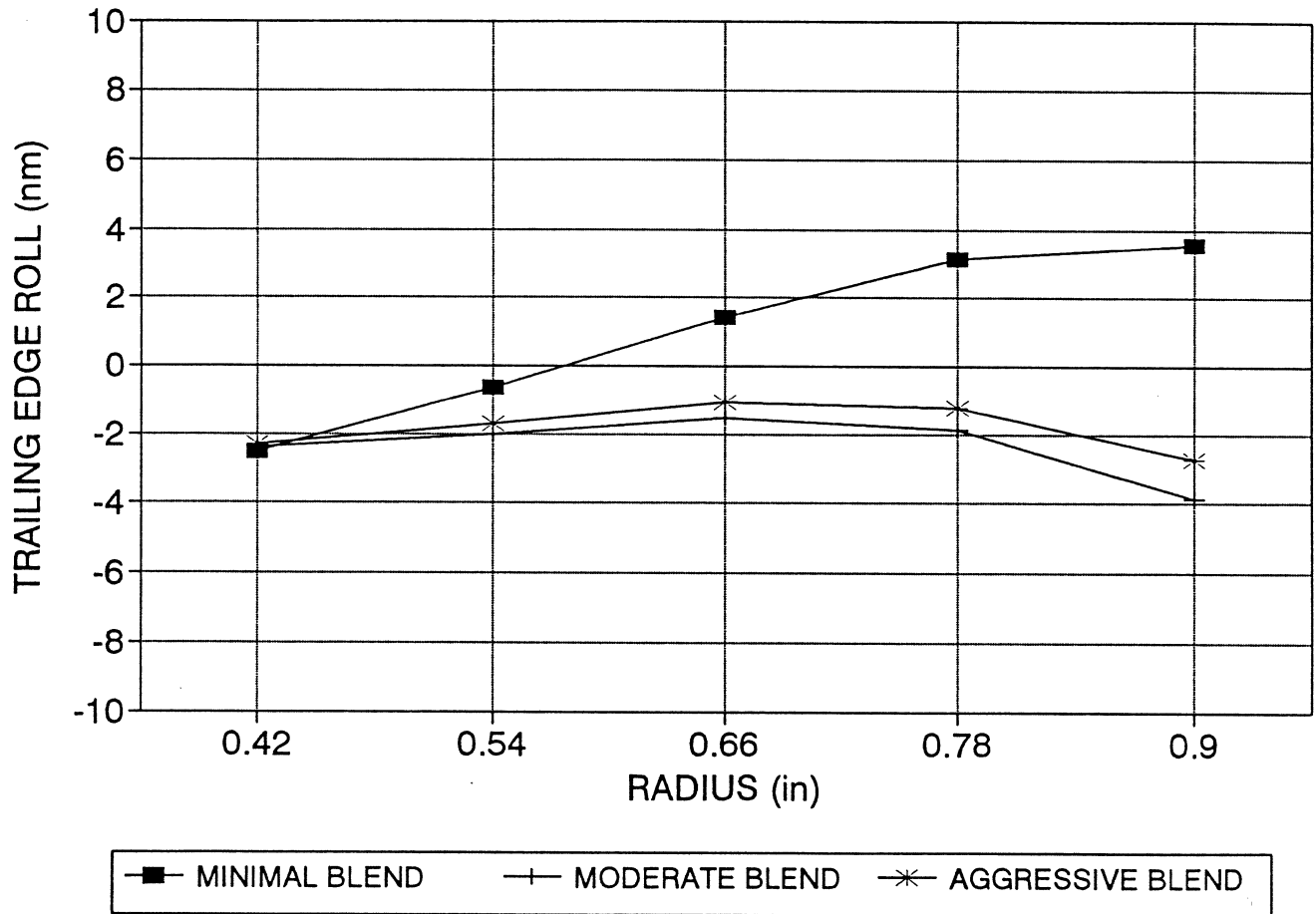
AURA ASSOCIATES

RADIAL DEPENDENCE OF FLYING HEIGHT FOR DIFFERENT SLIDER BLENDS



*lowest at 0.42 inches
best density of bits.*

RADIAL DEPENDENCE OF SLIDER ROLL FOR DIFFERENT SLIDER BLENDS



MAGNETIC DISK ISSUES

READ/WRITE

READBACK SIGNAL

MrT

COERCIVITY

SQUARENESS

NOISE

SINGLE VERSUS MULTILAYER

- lower noise

MODULATION

DEFECTS

ANALOG VERSUS DIGITAL

UNIFORMITY

RADIAL

CIRCUMFERENTIAL

TRIBOLOGY

GLIDE

STICTION

DURABILITY (>100 K CSS CYCLES)

MECHANICAL

FLATNESS

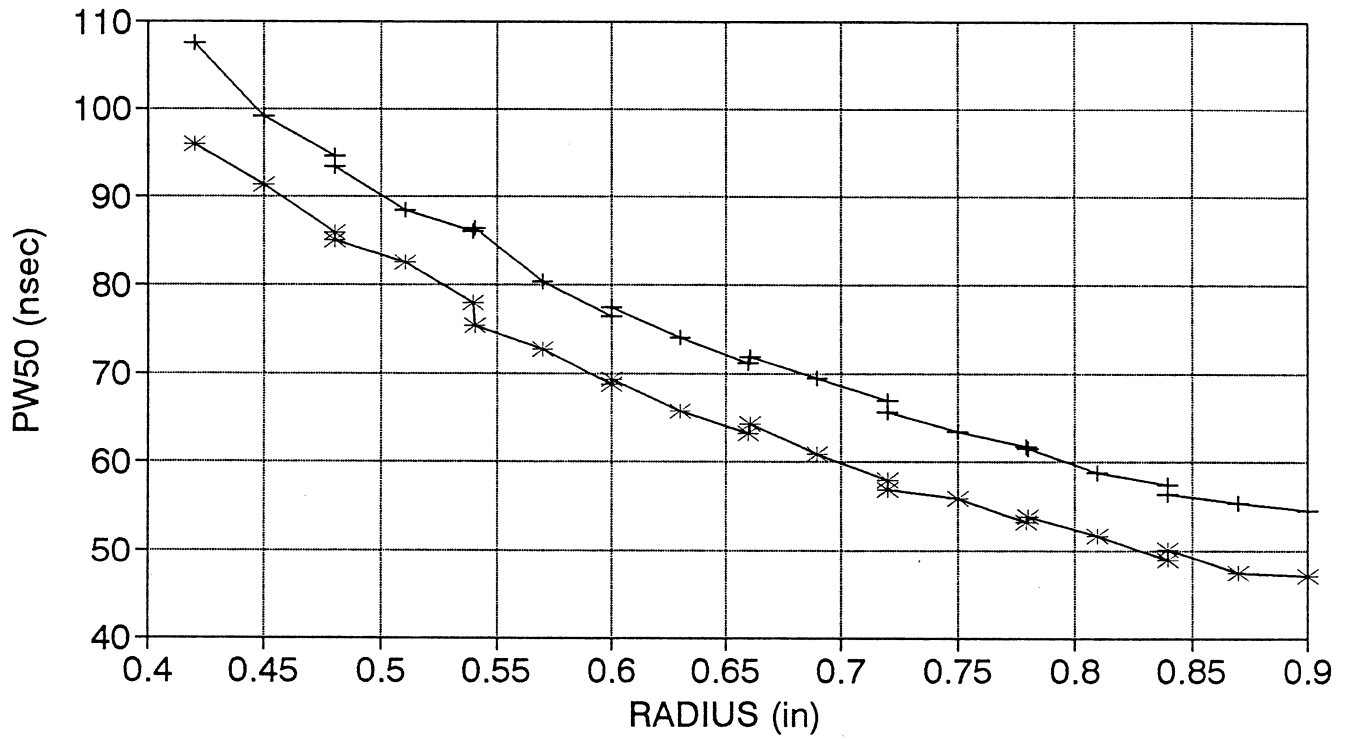
IMPACT RESISTANCE

DUBOFF



AURA ASSOCIATES

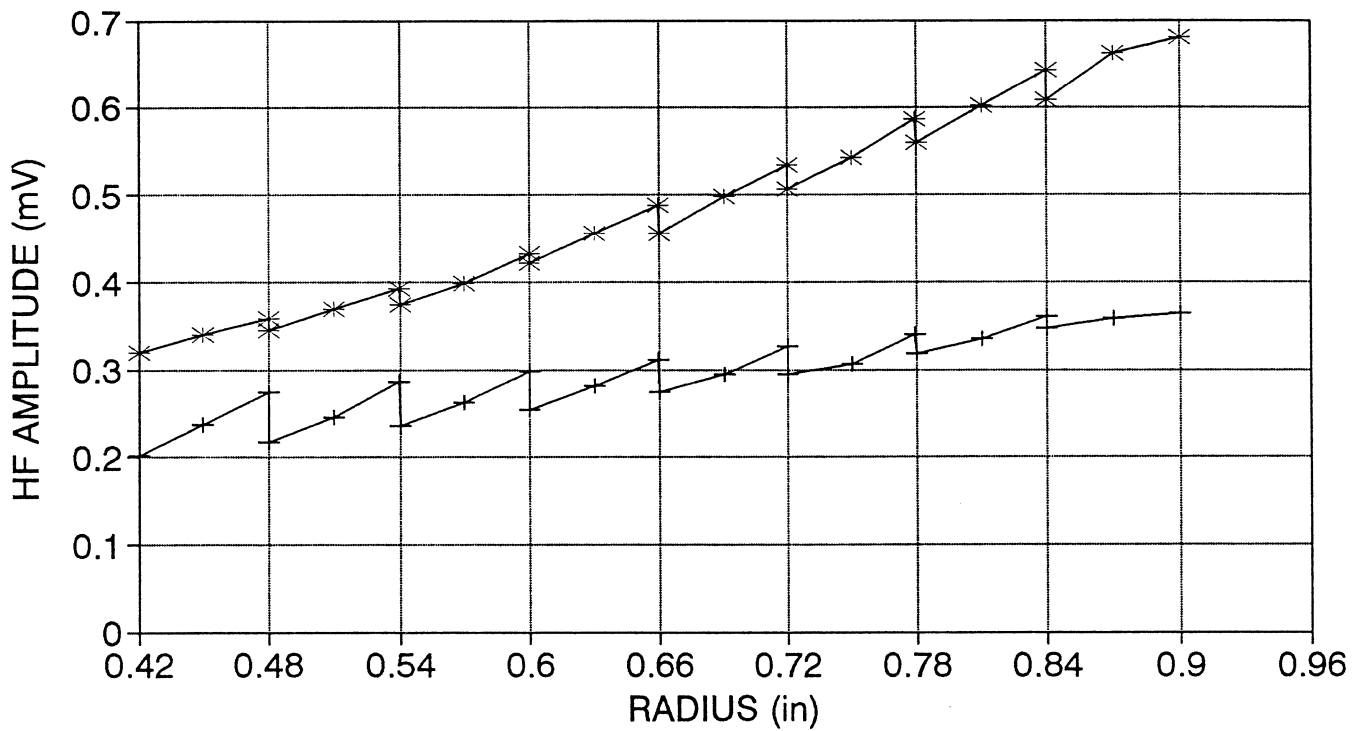
PW50 VERSUS RADIUS TWO HEAD GEOMETRIES



—+— GAP = .35 MICRON —*— GAP = .30 MICRON

HF AMPLITUDE VERSUS RADIUS

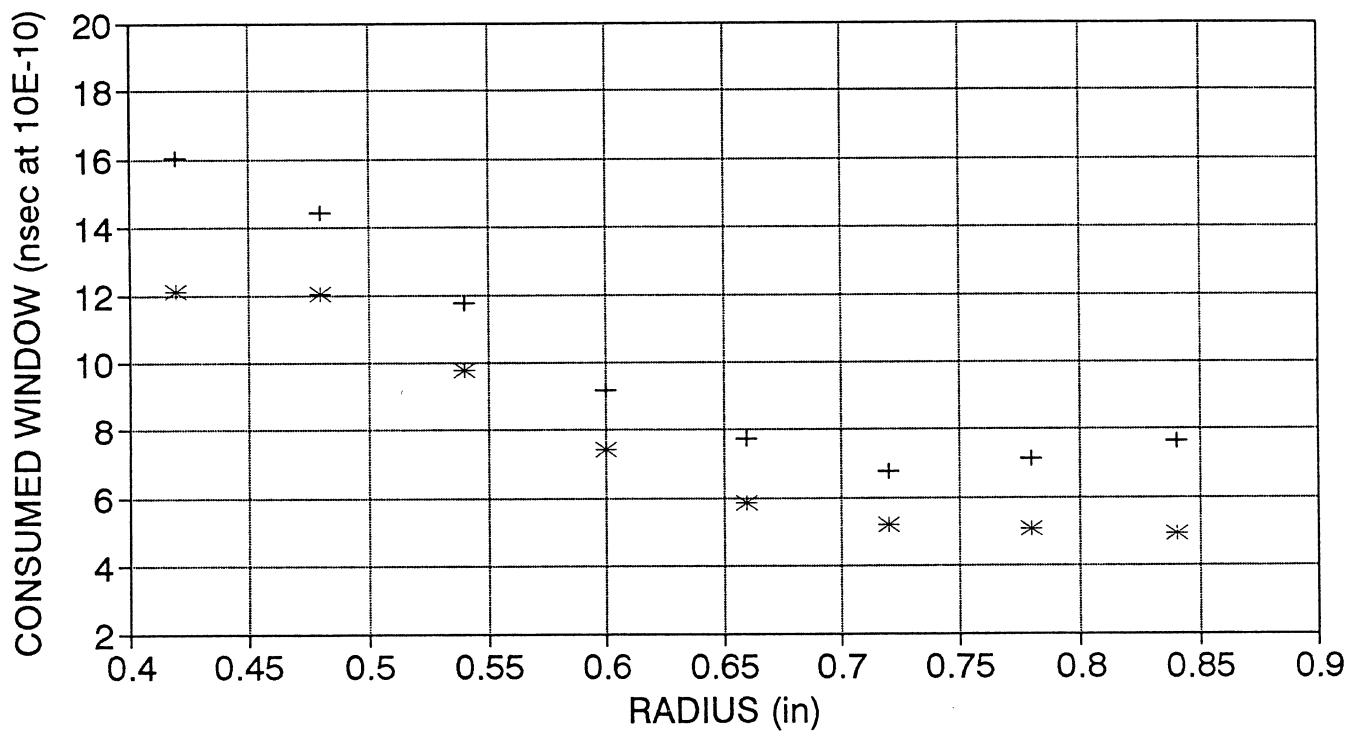
8 ZONES, TWO HEAD TYPES, 38 KFCI MAX



—+— 42 TURNS, GAP=.35 —*— 50 TURNS, GAP=.30

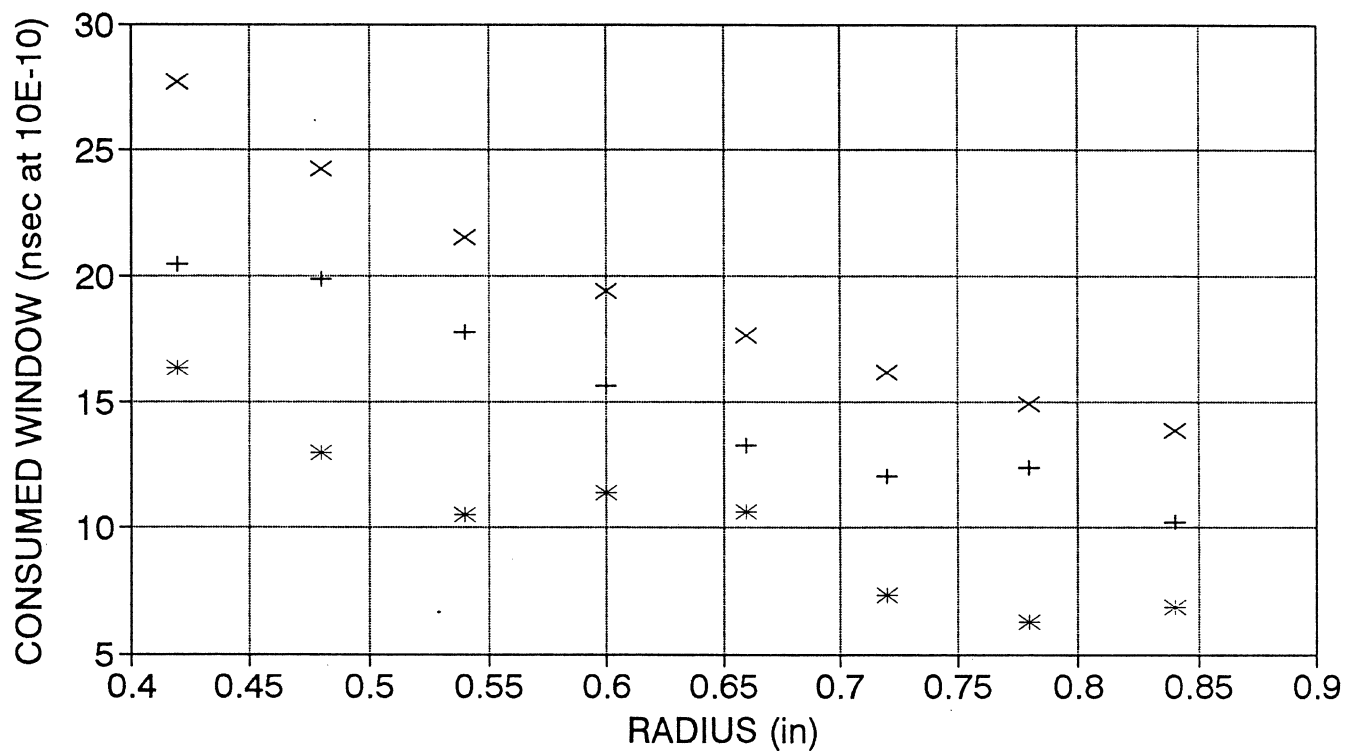
RADIAL DEPENDENCE OF JITTER

TWO HEAD TYPES, 38 KFCI



+ 42 TURNS, GAP=.35 * 50 TURNS, GAP=.3

RADIAL DEPENDENCE OF BITSHIFT TWO HEAD TYPES, 38 KFCI



+ 42 TURNS, GAP=.35 * 50 TURNS, GAP=.3 x HALF WINDOW

SEMICONDUCTOR CHIP REQUIREMENTS

FUNCTIONS TO BE PERFORMED:

- ✓ READ/WRITE PREAMP
- ✓ READ/WRITE CHANNEL
 - PULSE DETECTOR
 - PLL
 - ENDEC
 - FREQ. SYNTH.
 - FILTER/EQUALIZER
 - WRITE PRECOMPENSATION
 - SERVO DEMODULATOR
- ✓ SERVO CONTROLLER
- ✓ MICRO-CONTROLLER
- VCM/SPINDLE/LATCH DRIVERS
- ✓ MASS STORAGE CONTROLLER
 - ECC
 - BUFFER
 - INTERFACE

5 major chips

KEY ISSUES:

SPEED/DATA RATE

24 => 40 Mb/sec

POWER

VOLTAGE, 5 => 3.3 VOLTS

POWER SAVING, SLEEP/IDLE MODES

RELIABILITY

COST

*chip cost
is most
expensive
part of drive*

*data rates too low
40 good for 1 year*



AURA ASSOCIATES

SUMMARY

THE AREAL DENSITIES WHICH WILL BE ACHIEVED IN SMALL FORM FACTOR DISK DRIVES WILL BE COMPARABLE TO THOSE OBTAINED IN LARGER DRIVES

THE HEAD/DISK INTERFACE MUST BE CAREFULLY DESIGNED TO OBTAIN ADEQUATE MECHANICAL AND MAGNETIC RECORDING PERFORMANCE

THE SEMICONDUCTOR CHIPS ARE A GATING FACTOR IN THE DESIGN OF SMALL FORM FACTOR DRIVES

Key factor

FORTUNATELY, THE HIGH DATA RATES OF LARGER DRIVES REQUIRE THE DEVELOPMENT OF CHIP TECHNOLOGY THAT CAN BE LATER INTEGRATED INTO SINGLE CHIP SOLUTIONS FOR SMALL DRIVES

MECHANICAL RESONANCE PROBLEMS ARE LESS SEVERE FOR SMALL FORM FACTOR DRIVES, HOWEVER THE SHOCK AND VIBRATION ISSUES CONTINUE TO PROVIDE MECHANICAL DESIGN CHALLENGES



AURA ASSOCIATES

Case Study:
1.3 Inch "Kittyhawk" Drive

Carol Schwiebert

Hewlett Packard

Institute for Information Storage Technology

Santa Clara University, California

December 14 - 16, 1992

HP Kittyhawk Personal Storage Module

Product Description

- Stores 21.3 Mbytes of Data (Formatted)
- Module is 10.5 mm High, 36.5 mm Wide and 50.8 mm Long
- Weighs about 28 grams
- Supports AT and PCMCIA Interfaces
- Industry-Leading 100 g Operating Shock
- MTBF of 300,000 Hours
- Average Start Peak: 2.2 W
- Average Read/Write: 1.5 W
- Sleep Mode of 15 milliwatts

Kittyhawk Design Decision Criteria

- Size
- Schedule
- Cost
- Ruggedness
- Low Power

July 1991 - What's Available?

■ Heads

- **Suspensions** HTI Starting to Announce that They will Soon Have Prototype Samples of their New T-16 Integrated Gimbal Small Drive Suspension for 70% and 50% Heads

- **42-Turn 70% TF Available**

Head Companies Talking About: Proto Mechanical Samples for 50%

>50-Turn TF

■ Disks

- **No Vendor even Working on this Size**

Media Design

- **Glass**
 - **Flatter and Smoother**
 - ◆ **Lower Flying Height**
 - ◆ **Lower Friction**
 - **More Impact Tolerance**

- **34 mm OD**
 - **Largest Size that can Fit in the Form Factor**

- **15 mil Thickness**
 - **Thinnest We Thought We Could Get**

Ruggedness / Reliability

- MTBF: 300,000 Hours
- Start/Stops: >100,000

	Operating	Non-Operating
■ Temperature	-5° C to 55° C	-40° C to 70° C
■ Humidity	8% to 80%/28° C	5% to 85%/28° C
■ Altitude	-30.5m to 3046m	-305m to 15,240m
■ Shock	100g/3ms	225g/3ms
■ Tilt	Any Orientation	

Kittyhawk Ruggedness Philosophy

■ The Three Critical Parameters

- **Motion** *Head Slap, Bernelling & Off-track*
- **Wear** *Head & Media Wearout, &
Stiction/Friction*
- **Environment** *Temperature Cycling, Humidity &
Altitude*

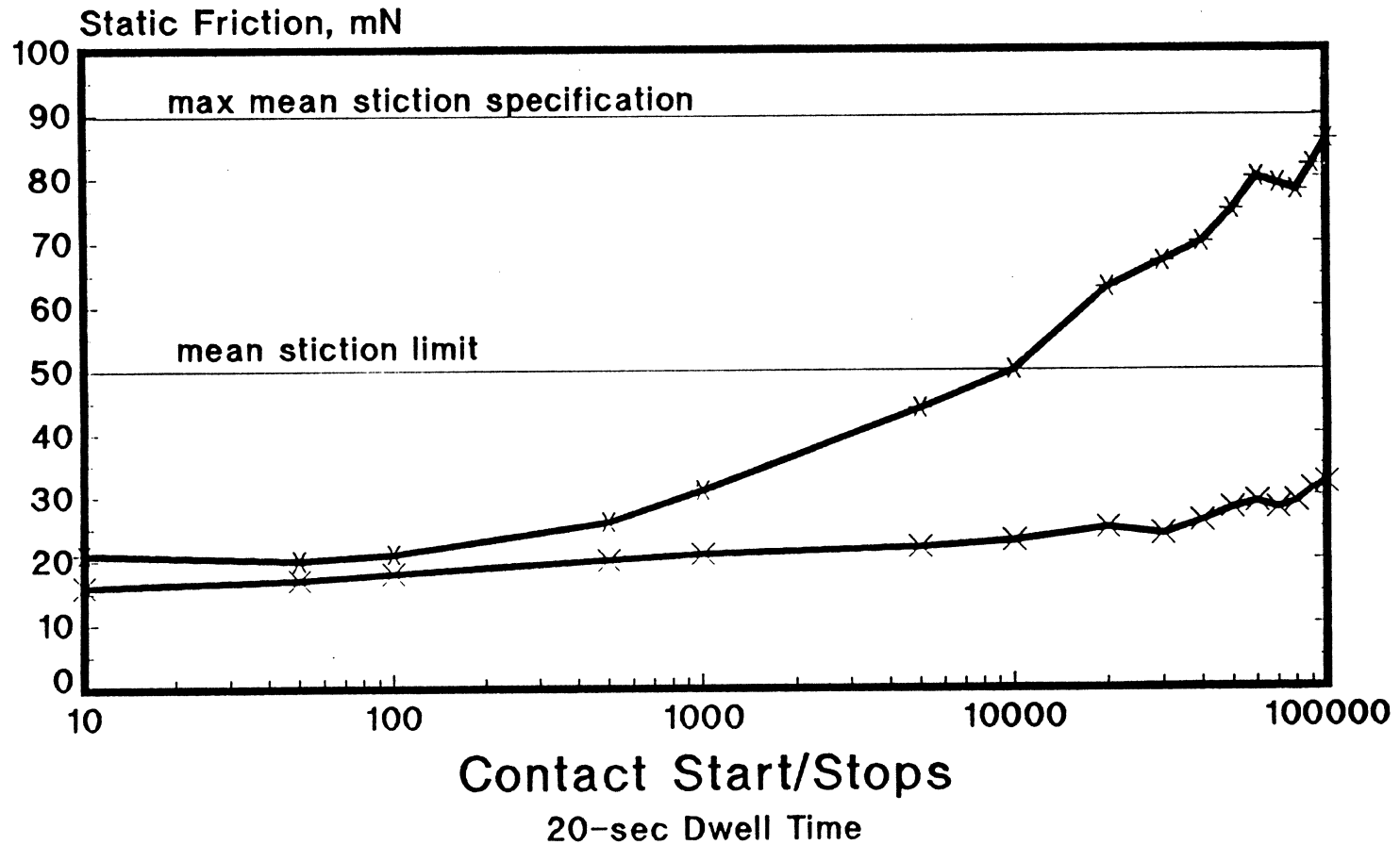
Ruggedness Impact on Head/Media Design

- Very Low Stiction/Friction over Entire Temperature and Humidity Range
- Need to Minimize Damage due to Head Slap and Head Skating
- Higher Corrosion Requirements
- Severe Requirements on Media Flatness and OD Rolloff
- Robust Servo Design

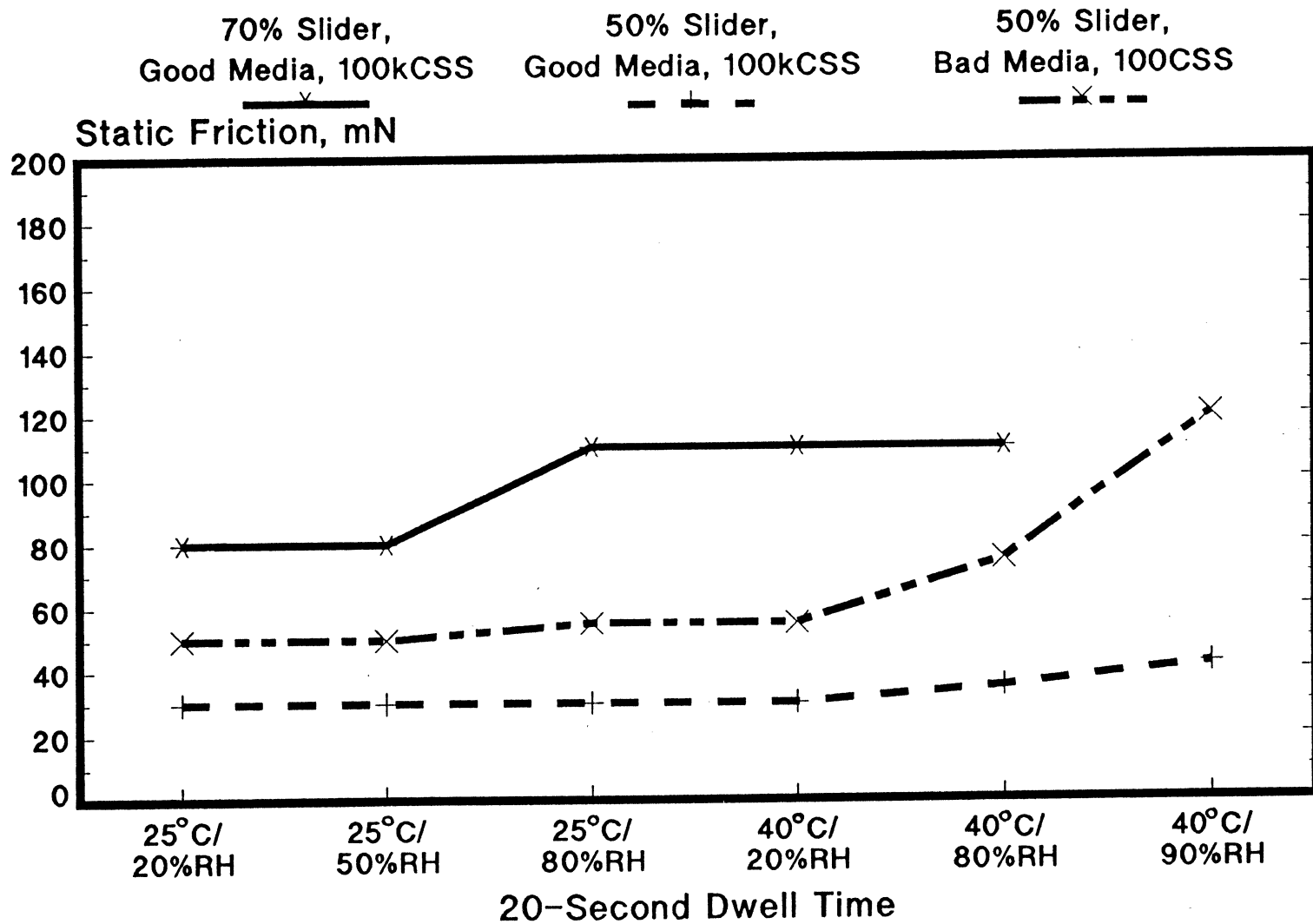
Static Friction During CSS Wear

70% Slider
Mean

50% Slider
Mean

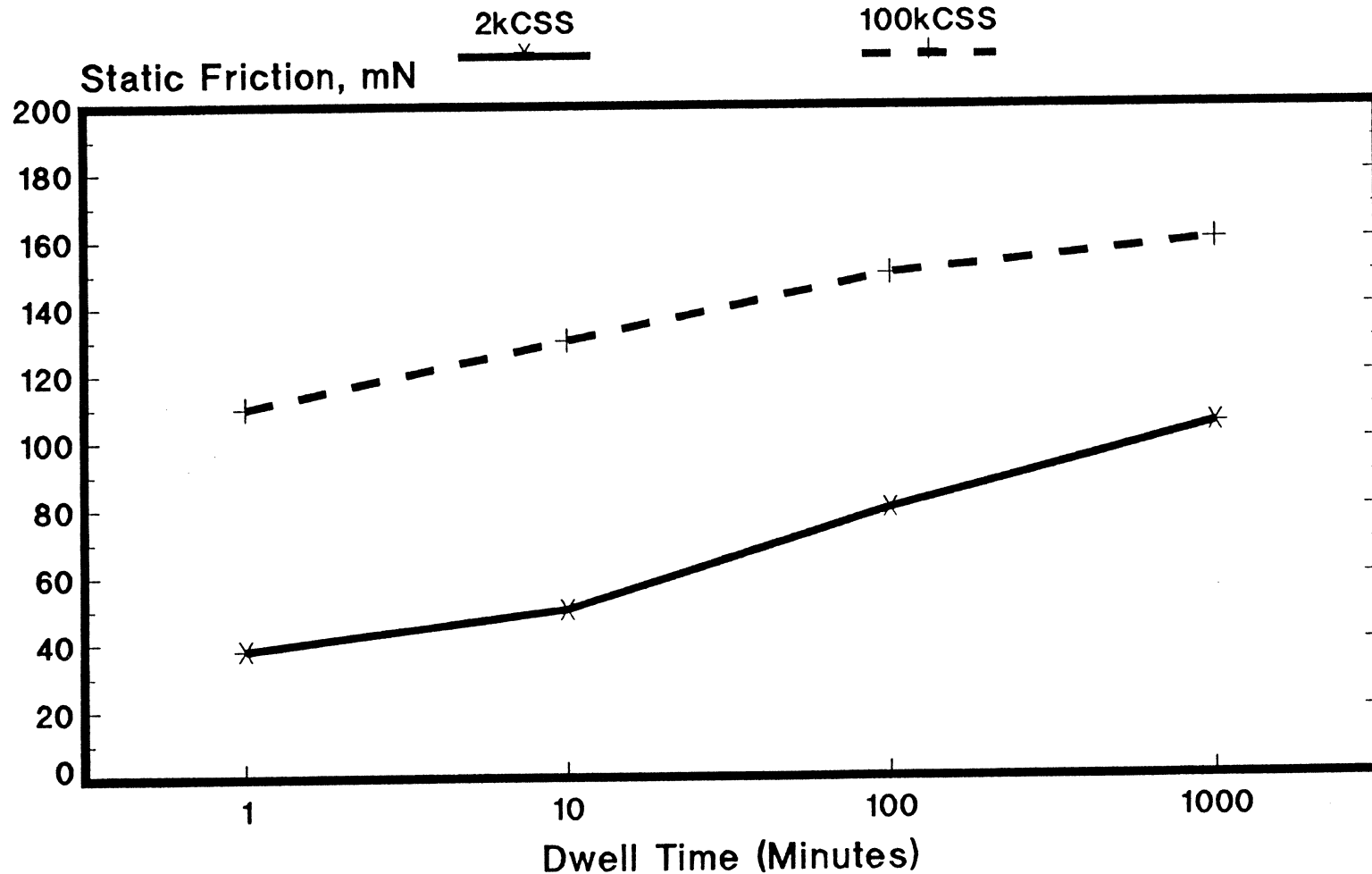


Static Friction: Effect of Temperature and Relative Humidity

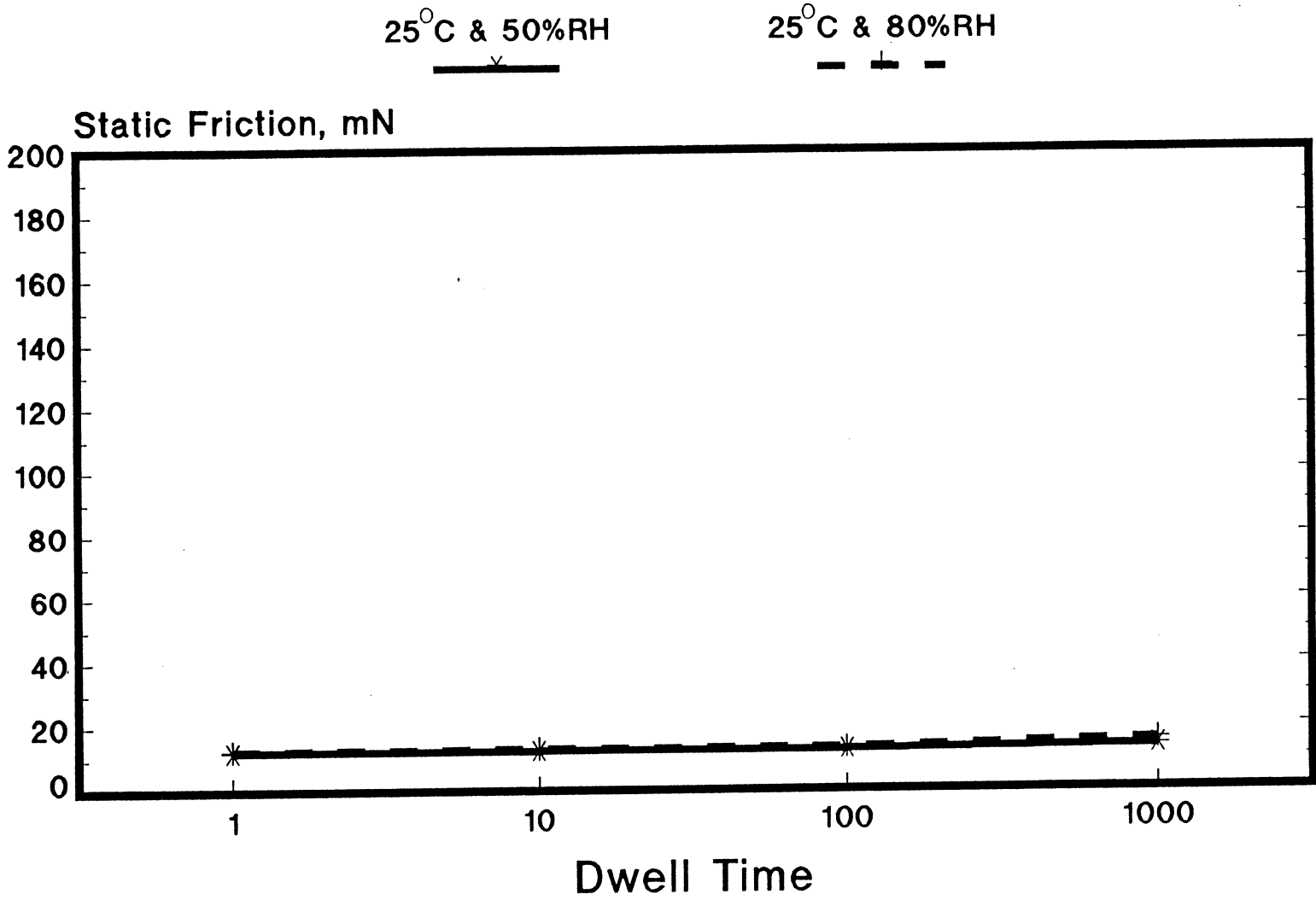


Static Friction: Effect of Dwell Time at 80% Relative Humidity

70% Slider, 6.5 gm Load

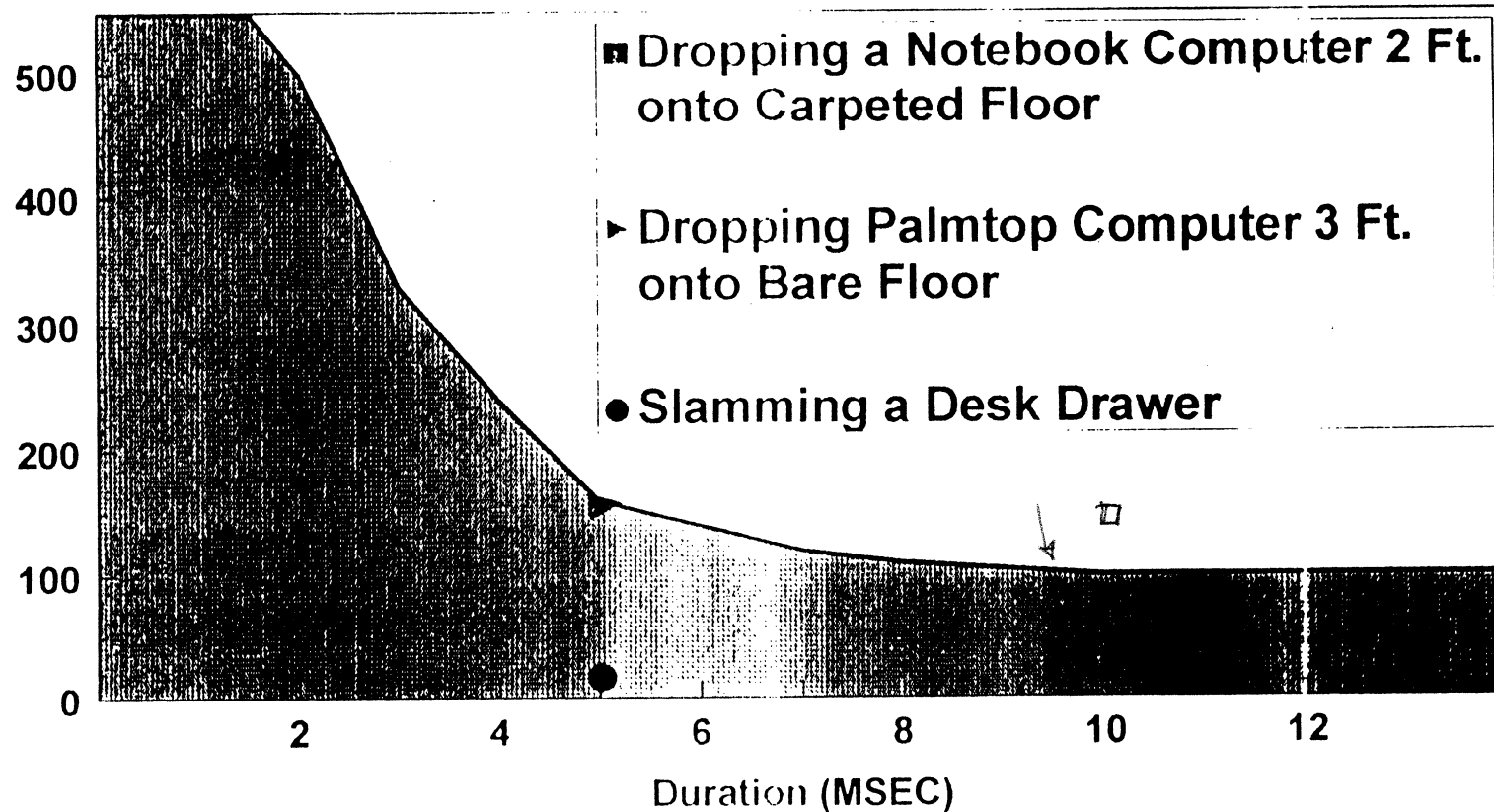


Static Friction: Effect of Dwell Time at 100kCSS



Mobile Computing Shock Tolerance Envelope

Peak Acceleration (G)

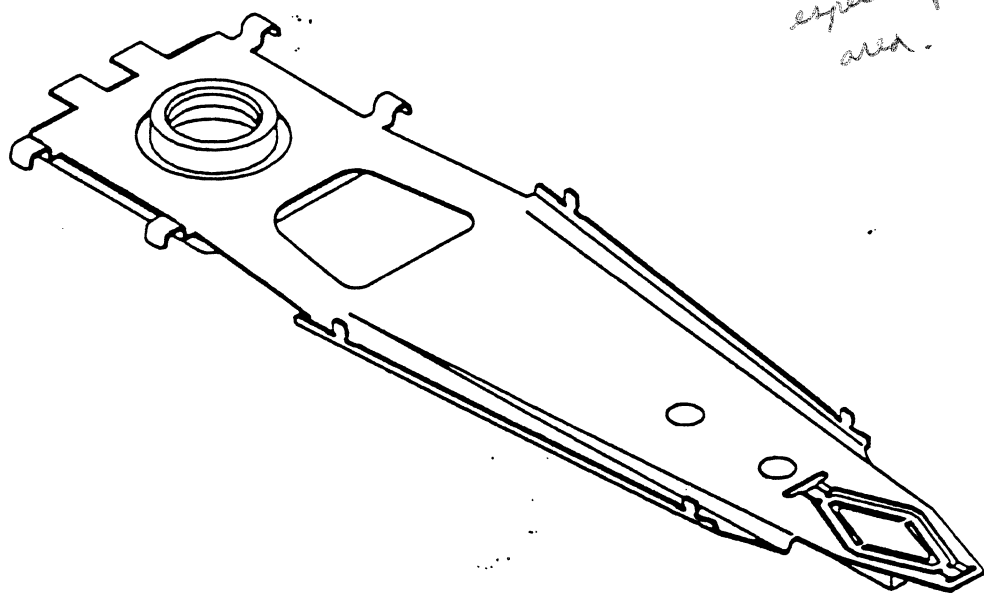


Head/Media Mechanical Parameters Impacting Ruggedness

- HGA Roll and Pitch Static Angle
- Drive Build Tolerances
 - Z-Height
 - Angular Misalignment
- Edge Blend
- Low Inertia
 - Slider
 - Suspension
- Gimbal Design
- Impact-Tolerant Media

**Type 16 Suspension Assembly
Characteristics Summary**

*Problems at
high G's.
HP totally redesigned,
especially in gimbal
area.*



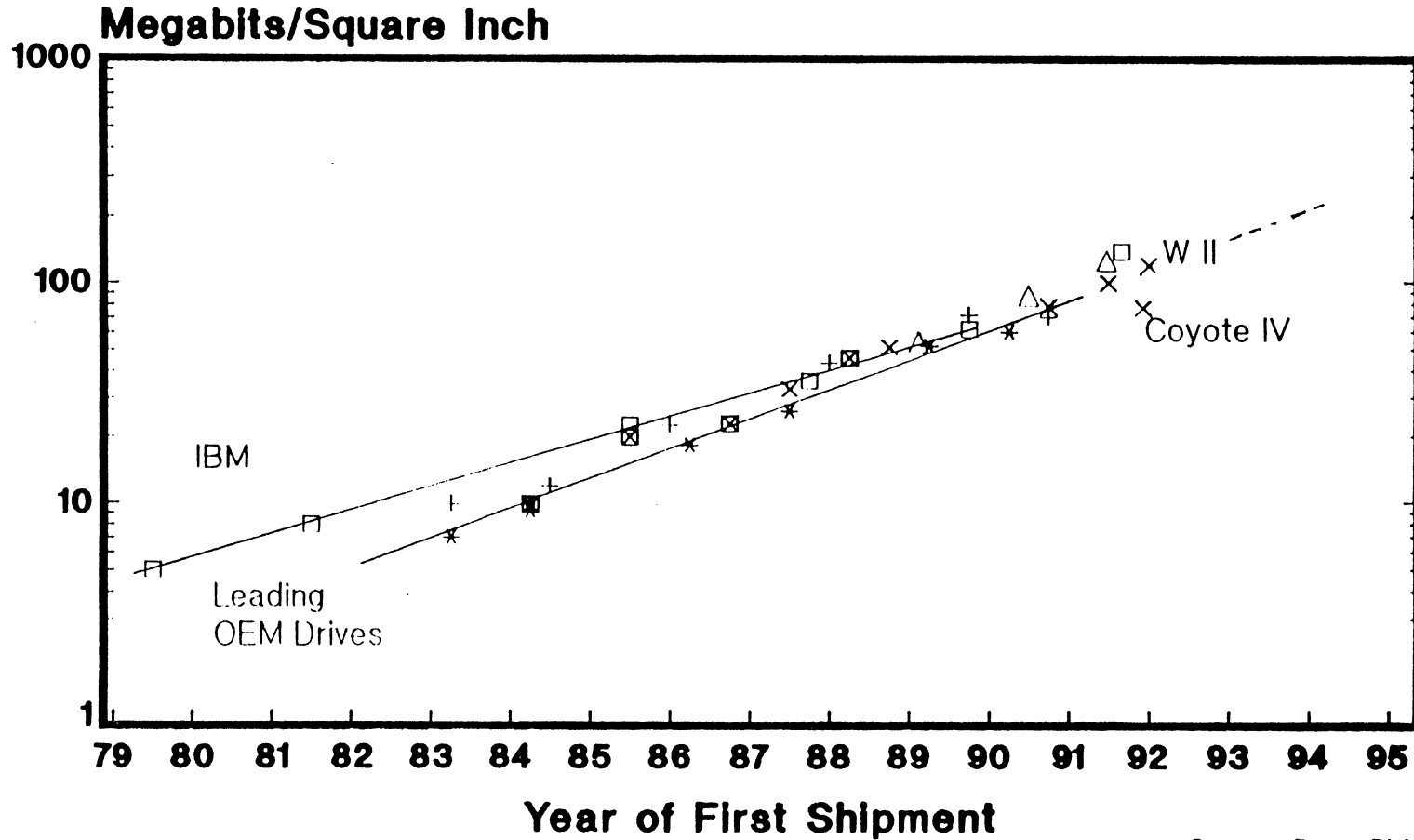
20 MB and 40 MB Designs

	20 MB			40 MB		
# of Heads	2	3	4	2	3	4
~ Areal Density (Mbits/in ²)	170	115	85	335	225	170
Head Size	70%, 50%	50%	50%	70%, 50%	50%	50%
Disk to Disk Spacing (mm)	-	1.93	1.13	-	1.93	1.13
Media Thickness (mm)	?	.381	.381	?	.381	.381
Flying Height (μin)	2.5 μin AAB	3.0 μin	4.0 μin	3.0 μin	2.0-2.25 μin AAB	2.5 μin
Suspension	Type 13	T-16	New Design	Type 13	T-16	New Design
# Turns	54	42	42	MR	54	54

*Selected devices
not in scope
are in scope*

Areal Recording Density

Seagate * **Maxtor** + **HP** ×
Micropolls ☒ **Conner** △ **IBM** □



Source: Porter Disk Trends

Kittyhawk I

- 3 Heads, Thin Film, 50% Slider
- Areal Density: 117 Mbits/sq. in.
- Track Density: 95 trk/mm
- Linear Density: 1456 fc/mm
- Conventional Rail, 2.7 μ in Flying Height
- Modified HTI T-16 Suspension
- 5400 RPM

Design Risk Assessment

	High	Medium	Low
Schedule	34mm Glass Media 50% Slider	Suspension	Areal Density Error Rate Conventional Rail Design
Cost	34mm Glass Media 50% Slider	Suspension Areal Density	Error Rate Conventional Rail Design
Ruggedness	Suspension	Conventional Rail Design	TF Head, 50% Glass Media Areal Density
Low Power			Glass Media 50% Sliders
Size			3-Head Design